Assessing Stratigraphic Controls on the Secondary Detrital Footprint from Buried Mineralization and Alteration at the Highland Valley Copper Mine, British Columbia

by

Andrea Reman

A thesis
presented to the University of Waterloo
in fulfilment of the
thesis requirements for the degree of

Master of Science
in
Earth Sciences

Waterloo, Ontario, Canada, 2019

Author's Declaration

I hereby declare that I am the sole author of this thesis. This is a true copy of the thesis, including any required final revisions, as accepted by my examiners.

I understand that my thesis may be made electronically available to the public.

Statement of Contributions

Alain Plouffe of the Geological Survey of Canada provided data in the form of photos and descriptions of several sections of the Valley pit walls.

Dong Shi processed the seismic data and provided the seismic cross-section for this thesis.

Petrophysical property measurements and photos were made by Randy Enkin of the Geological Survey of Canada.

Hyperspectral data and photos were provided by Philip Lypaczewski and Dr. Benoit Rivard at the University of Alberta.

Heavy mineral analysis data and photos were done by Overburden Drilling Management Limited.

Geochemical analysis data was provided by ACME Analytical Laboratories (Bureau Veritas Company) in Vancouver.

Abstract

Mineral exploration is progressively shifting to deeper targets, including those buried under thick unconsolidated sediments. It is thus becoming increasingly important to understand the sedimentary successions of the shallow subsurface (0-200m) in order to enhance exploration strategies to locate and characterize buried targets. One strategy is to investigate the sedimentary sequence overlying known mineralized and altered zones. As such, this study aims to characterize stratified unconsolidated sediments overlying mineralized as well as altered zones at the Highland Valley porphyry copper system (HVC), in south-central British Columbia, and investigate their effects on dispersion patterns of indicator minerals and geochemical pathfinders.

Stratigraphic logging and sedimentary facies analysis of ten drillcores have produced a new stratigraphic framework of the unconsolidated sediment cover and a refined depositional environment interpretation. Four geological cross-sections and an interpreted seismic profile improve our understanding of the stratigraphic architecture of the valley fill sediments in the vicinity of the Highland Valley Pit, as well as across the J.A. target, located four km to the east. Two new, previously unreported units are described from this study: a deeper, older till unit as well as a deglacial sequence overlying the older till unit. This study also reveals important lateral stratigraphic and sedimentary facies changes over relatively short distances. Two major ice advance and retreat cycles, the 1st one being older than 50 ka, and additional minor oscillations of ice margins during the last deglaciation of the area, are recognized in the stratigraphic record.

Petrophysical (density, porosity, magnetic susceptibility, resistivity, and chargeability) and sedimentological (grain size) property measurements are presented for the major cover units, which can help better resolve the geophysical footprint of buried targets.

Stratigraphic units interpreted to have formed by meltwater related processes and deposited in ice-marginal or proglacial settings generally have a higher proportion of locally-derived lithologies relative to other units, while tills have a more dominantly distal signature.

Several porphyry copper indicator minerals, such as pyrite, chalcopyrite, and jarosite, are found in each of the Quaternary sediment cover sub-units analyzed. The

strongest overall footprint of mineralization is found in two deep, poorly-sorted outwash and two deeper subglacial tills. They contain variably abundant indicator minerals (e.g. pyrite, chalcopyrite, Mn-epidote, chromite) and elements (Cu, Mo, W, As) that are indicative of porphyry copper mineralization. The source of most of these indicators is predominantly the Guichon Creek batholith that hosts the mineralization, but some indicators may be derived from distal volcanic rocks and volcanogenic sediments outside of the batholith. Coarse grain size and felsic lithology distinguished Guichon Creek batholith material from the others.

Hyperspectral techniques were applied to determine the abundance of prehnite (distal alteration footprint) and kaolinite (proximal alteration footprint) in large (>2 mm) clasts. Overall, results are consistent with the abundance of clasts sourced from Guichon Creek batholith (lower prehnite content and higher kaolinite content = higher GCB clast abundance). This finding suggests the technique may be used to get insights into the proximity of the source of clasts relative to buried HVC-type mineralization.

Subsurface till units also appear to have higher abundances of several indicator minerals (e.g. pyrite, chalcopyrite, jarosite) and geochemical pathfinders of mineralization (e.g. Cu, Mo, W, As) and alteration (e.g. Mg, Te, Bi) compared to previously published surficial till data. Oxidation of the surficial till and water-mineral interactions in the deeper (water-saturated) tills may explain some of the observed differences (esp. for mobile elements); however, re-entrainment of pre-existing sediments is another important mechanism to consider. The strongest footprint signal occurs in the deepest tills. Mineralized and altered bedrock thus appears to have been more accessible to glacial erosion during the older glacial phases due to less preserved sedimentary cover in depressions. Indirect sources (sediment re-entrainment) may have contributed to the footprint signal in the surficial till, perhaps more than shallow mineralized sources in some places.

Overall, this study provides several refinements to the stratigraphic framework of the sedimentary cover at HVC, as well as new insights into the occurrence and abundance of HVC-related indicator minerals and pathfinders in these units. One important implication of this study is that dilution up the stratigraphy is clear but limited at HVC; however, it could be greater in other prospective thick drift areas; stronger dilution in surficial units is possible, which could mask a clear subsurface footprint and buried sources of importance.

Acknowledgements

I would like to thank my primary supervisor Dr. Martin Ross for guidance and insightful evaluations of my work. I would also like to thank my other supervisor Dr. Robert G. Lee for much appreciated direction and advice, as well as logistical support while in the field. Thank you to my committee member Dr. Chris Yakymchuck for assistance with identifying lithologies and very helpful comments for the rest of the data collection and interpretation. I would also like to thank Alain Plouffe of the Geological Survey of Canada for providing advice on the stratigraphy portion of this thesis.

This project would not have been possible without the access to cores and into the Valley pit that Teck provided. The generous support of staff at Teck's Highland Valley Copper mine was greatly appreciated.

Thanks to Darius Kamal for his assistance collecting many samples and doing other fieldwork. Samples were disaggregated and sieved in the lab by Jeremy Kamutzki. I would like to particularly thank Dong Shi and Shawn Scott for their active role in completion of the seismic survey for this project, and Dong Shi for the processing of the data. Thanks to Kevin Byrne and Guillaume Lesage for their assistance identifying lithologies and insights into bedrock composition in the area.

This project was funded by the NSERC-CMIC Footprints research project, for which I am very grateful. This thesis is NSERC-CMIC Footprints contribution #219.

Table of Contents

List of Figures

List of Tables

Introduction

1.1 Rationale for this Study

Most mineral resources at the surface have been mined or are already accounted for in global mineral reserves (e.g. Doggett, 2000). As a result, mineral exploration is progressively shifting to areas where prospective bedrock is located at greater depths. Many areas in Canada have several meters of relatively young unconsolidated (non-lithified) sediments at the surface. Every province and territory has a significant amount of area covered by sediment (**Figure 1.1**). A thick unconsolidated cover can make exploration for new mineral deposits challenging (Mihalynuk, 2007; Andrews et al., 2011). This difficulty has increased interest in surficial geology research. Two problems are considered herein: 1) The effect of heterogeneous sediment cover on geophysical characterisation of buried bedrock and; 2) the distribution of compositional indicators of the buried mineralization throughout the sediment cover. More specifically, the first topic focuses on the effect surficial sediments may have on geophysical response of underlying buried mineralization and its alteration zones, particularly if the cover is thick and stratified (heterogeneous). Geophysical surveys, such as magnetic and gravity surveys, are conducted to identify the physical properties of underlying bedrock, but results are variably affected by the overlying cover (Enkin et al., 2008). The unconsolidated cover has its own physical properties, and these may partly overprint those of the targeted underlying bedrock. The stratigraphy of the cover material and physical properties of individual units contained within need to be accounted for during geophysical survey processing. Having data on the geometry and physical properties of the cover where it is of significant thickness helps better constrain geophysical inversion (Pears et al., 2017) which leads to a more accurate outline of buried bedrock and identification of potential targets during mineral exploration.

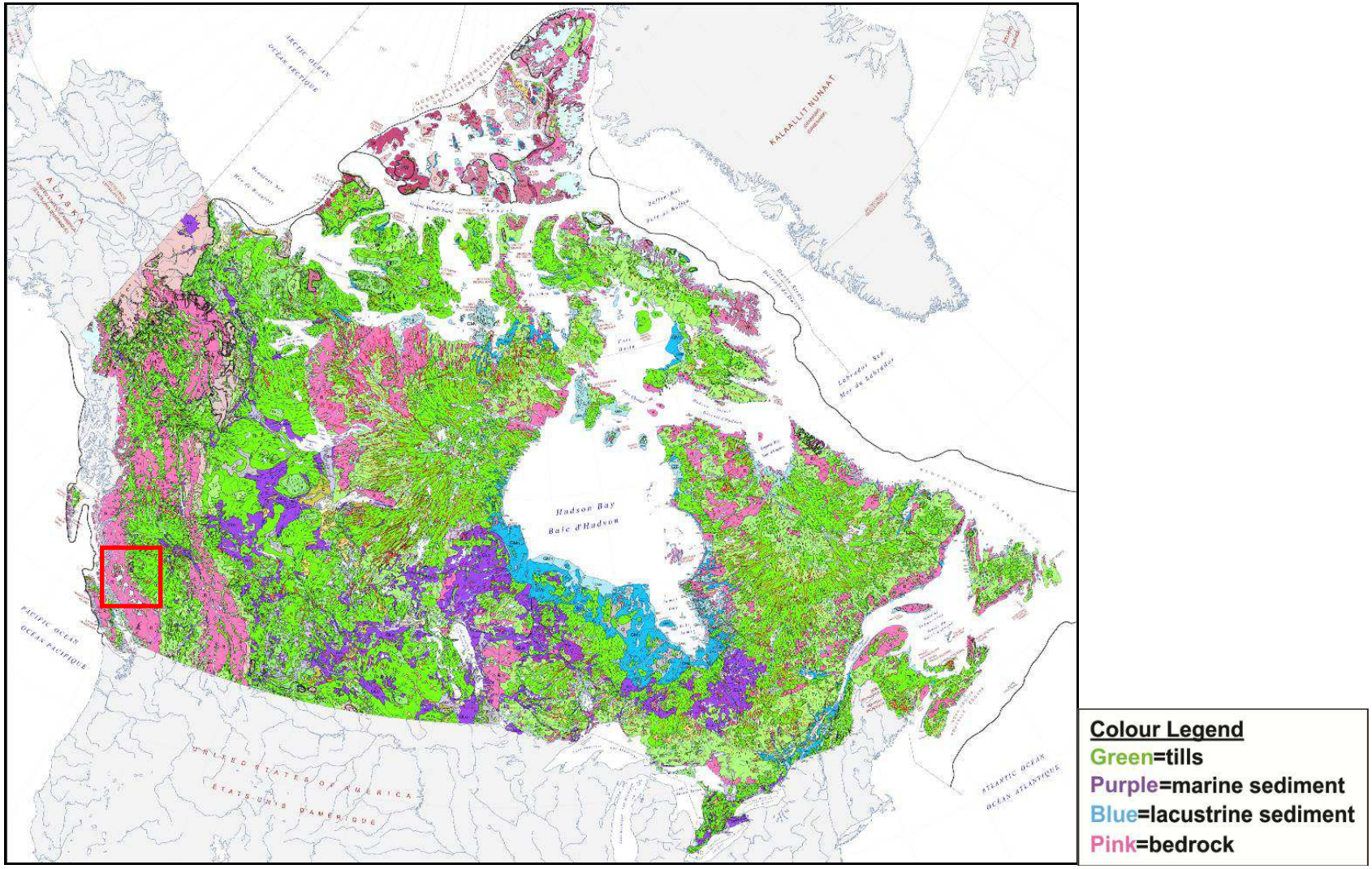

Figure 1.1 Surficial geology map of Canada, showing areas covered by unconsolidated sediment. Greens colour outlines tills, while blue and purple show lacustrine or marine sediment. The red box shows the outline of Figure 1.3. Modified after the Geological Survey of Canada (2014).

The second problem is related to provenance of the sediment cover and its compositional properties. The regolith in Canada typically consists of transported sediments (e.g., glacial sediments) (Geological Survey of Canada, 2014). The compositional makeup of this transported regolith may reflect the underlying bedrock, especially in areas of thin cover, but may also consist of rock fragments and minerals whose source may be several kilometres up paleo-ice flow or paleocurrent direction (Butt et al., 2000). These transported sediments may also contain minerals of interest for exploration due to erosion of mineralized and/or altered bedrock. The sediment transport and deposition processes may have created detectable detrital dispersal patterns of these indicator minerals and the size of these patterns may be several orders of magnitude greater than the surface area of their buried source (e.g., McConnell and Batterson, 1987; Snow and Coker, 1987; McClenaghan et al., 2015). In glaciated terrains, such as in Canada, glacial processes during the Quaternary glaciations have created several such patterns in both thin (e.g., McClenaghan et al., 2017) and thick sediment cover (e.g., Bird and Coker, 1987) areas (**Figure 1.2**). The mineral exploration method of drift prospecting traces these indicators found in the material of glacial origin up the ice-flow directions back to their mineralized bedrock source (e.g., Kujansuu and Saarnisto, 1990; Shilts, 1996; Paulen and McMartin, 2009). However, the processes involved in the formation of unconsolidated sediments are complex, and sediments may have been eroded, transported and deposited in different ways and at various distances from their source. As the overburden becomes thicker, indicators of underlying bedrock mineralization are increasingly attenuated at the surface (Proudfoot et al., 1995).

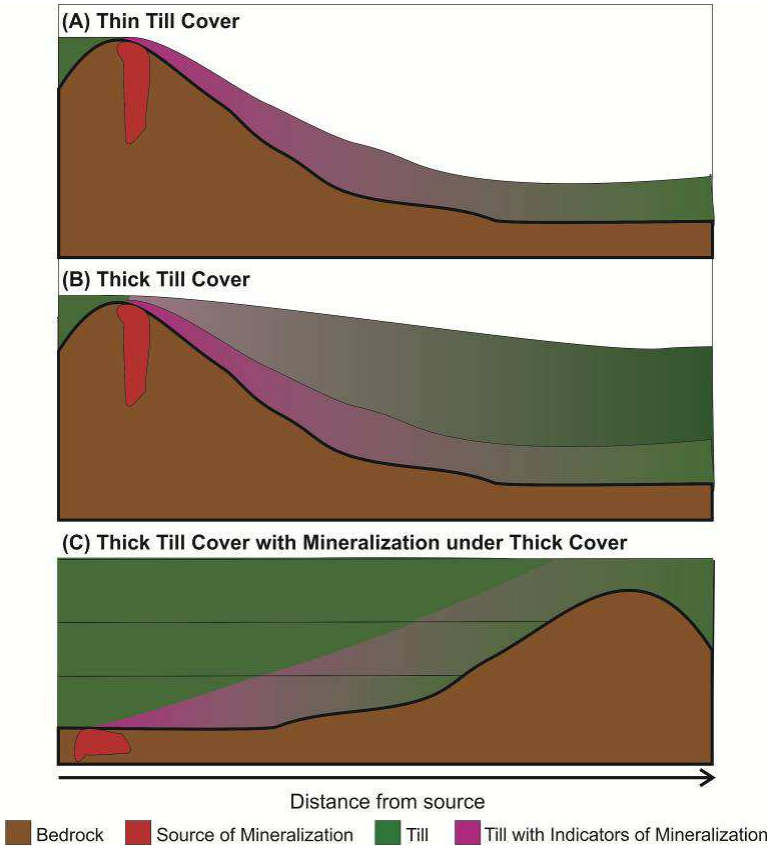

Figure 1.2 Simplified dispersal pattern of indicators of mineralization in areas of thin (A) and thick (B) drift, as well as thick drift with mineralization under thick cover (C).

Consequently there is interest in characterizing the physical and compositional properties of stratified unconsolidated sediments overlying mineralized and/or altered zones. An understanding of the characteristics of these sedimentary units is necessary in order to conduct more effective exploration in areas of thick post-mineralization cover. As Canadian mineral exploration is shifting to more deeply buried targets, the need for better tools and methods of detecting the subtle traces of buried mineralization systems is essential. Being able to interpret the geological history of the cover can provide several useful insights into how weathering, transport and deposition may have affected the buried deposit itself and how potential indicators of the mineralization have moved within the cover material (i.e. surface to depth or down flow directions). It is important to understand these processes in order to make exploration of concealed mineral deposits more efficient and effective.

The Highland Valley Copper district is a large porphyry copper system located in south-central British Columbia (**Figure 1.3**). Porphyry copper deposits are a major global source of copper and molybdenum and many are also a significant resource of gold, silver and other metals. Porphyry copper deposits yield about 43% of the copper and 100% of the molybdenum produced in Canada (Sinclair, 2007). Most known Canadian porphyry deposits are in the Cordillera region of B.C. and Yukon (Sinclair, 2007). This region includes many large mining operations as well as those that have been in production for over one hundred years. The Highland Valley district lies within a region of thick glacial and pre-glacial sedimentation. Many intermontane valleys in B.C. are partly filled by a thick and continuous sediment cover (Geological Survey of Canada, 2014). It is important to further our understanding of the characteristics and effects of this cover because many such regions are rich in economic mineralization. Highland Valley is a good option as a site for this research due to its thick layer of unconsolidated sediment overlying mineralized bedrock (**Figure 1.4**), access to exposures and drillcores and a wealth of geological information about its ore and host rock (e.g., McMillan, 1976; Casselmen et al., 1995; Byrne et al., 2013; D'Angelo et al., 2017). Petrophysical properties as well as geochemical and mineralogical indicators from a thick, mostly glacial cover sequence can be analyzed very close to sites of mineralized bedrock.

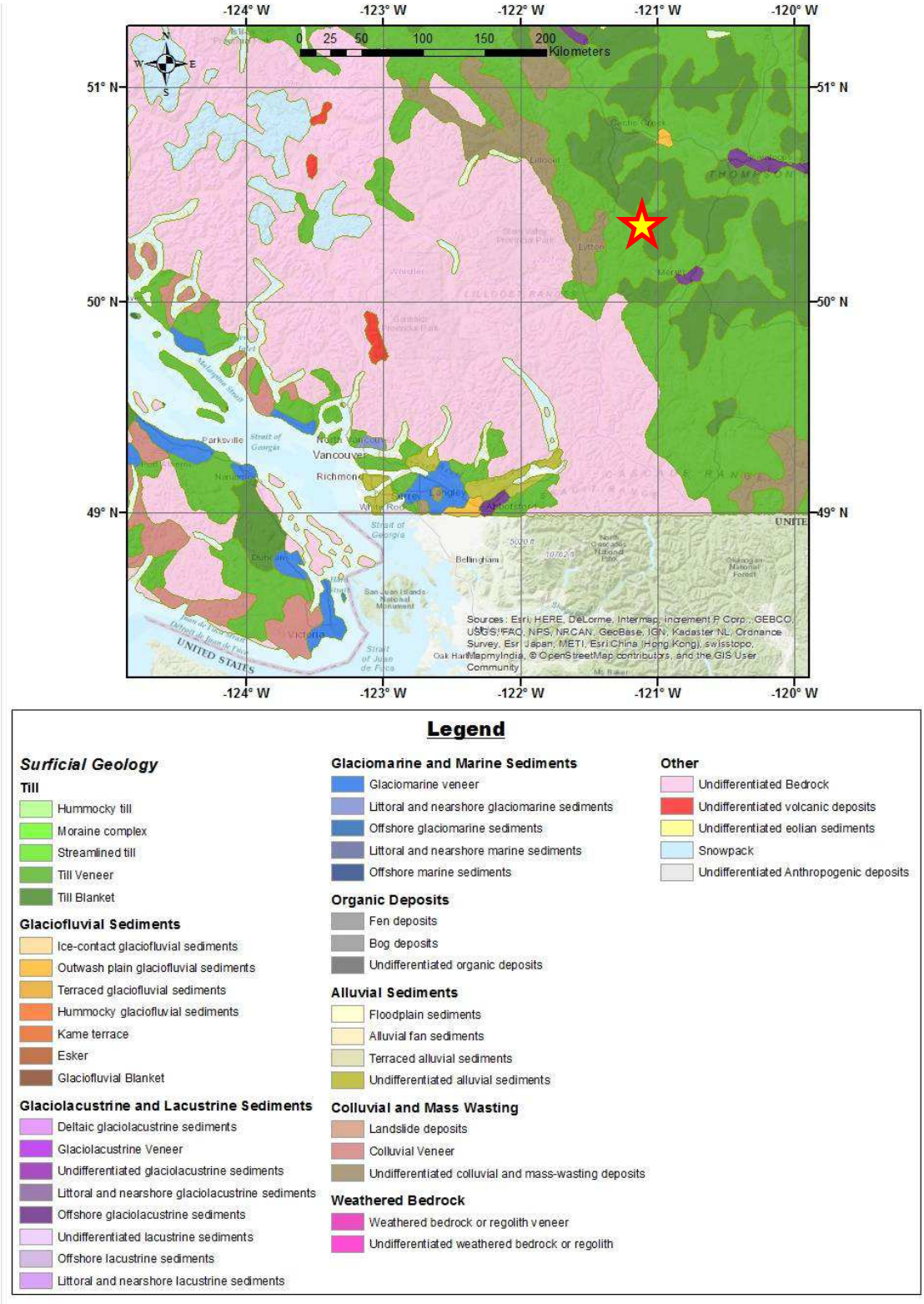

Figure 1.3 Location of Highland Valley Copper Mine in south-central British Columbia. Surficial geology is shown (modified after Fulton (1995) and Plouffe and Ferbey (2018). See also Figure 1.1 for general location in Canada.

Figure 1.4 View of one of the open pits (Valley) at the Highland Valley Copper Mine, viewed towards the southeast. The thick (~200m in this photo) layer of unconsolidated sediments is shown.

1.2 Study Location and Physiographic Setting

The study site is located in the Interior Plateau of British Columbia between the Coast and Caribou Mountains. It is 81 kilometres west-southwest of Kamloops and the nearest town is Logan Lake, 15 kilometres to the east. The topography consists of rolling hills and deep valleys, and is dotted with lakes. Paleovalleys formed by drop normal faulting are filled with glacial and pre-glacial material in the region. The Witches Brook valley is the largest of these infilled paleovalleys and runs from NW to SE before hitting the Valley pit at the Highland Valley Copper Mine, and then continues to the east (**Figure 1.5**). Another infilled paleovalley occurs several kilometres to the east and runs from north to south.

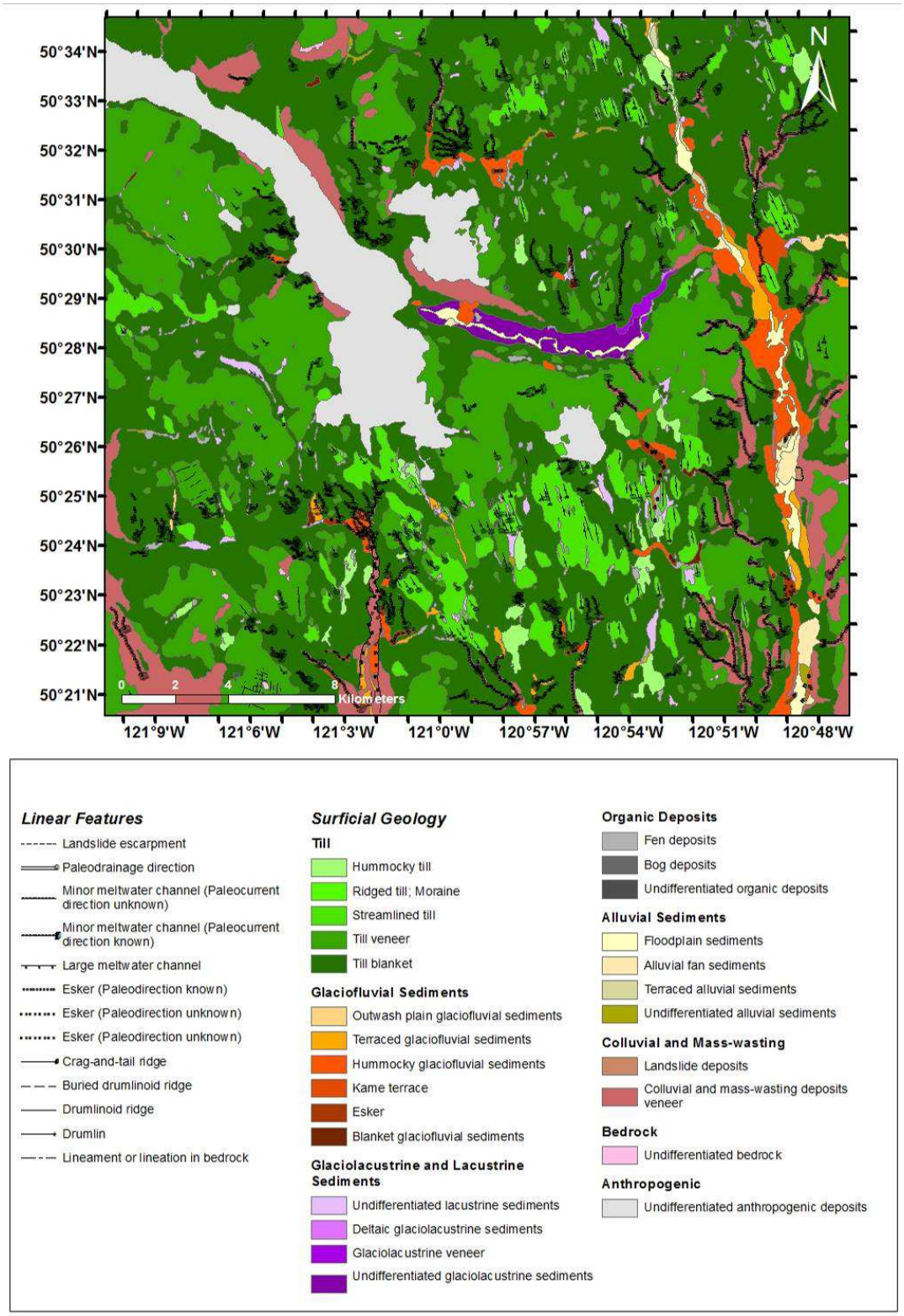

Figure 1.5 A surficial geology map showing the unconsolidated cover at Highland Valley (modified after Plouffe and Ferbey (2018)). The paleovalleys occur along the glaciofluvial (peach to orange to red) and glaciolacustrine (purple) units.

1.3 Igneous Bedrock and Mineralization

The major mineralized zones of the Highland Valley porphyry system occur within the core of the Guichon Creek batholith (GCB) (McMillan et al., 2009; Byrne et al., 2013; D'Angelo et al., 2017). This batholith is granitic and geochemically calc-alkaline (McMillan, 1985). It is late Triassic, having formed about 218-207 Ma ago (D'Angelo et al., 2017; Lee et al., 2017). Its different intrusive facies formed from at least three to four magma pulses that form as concentric zones in the batholith; the older margins are mafic in composition and transition to younger more felsic granodiorite to monzonites in the core (D'Angelo et al., 2017).

The GCB intruded into the Nicola Group, a series of volcanic strata and associated sedimentary rocks formed during the Carnian to Norian ages (230-208 Ma) of the Late Triassic (Casselman, 1995; **Figure 1.6**). The Nicola Group represents a magmatic island arc in a rifted sea basin over a subduction zone, and was metamorphosed to the "albite-epidote-hornfels" facies. It is part of the Quesnellia Terrane of the Intermontane Belt (Eyles and Miall, 2007).

The GCB is unconformably overlain by volcanic sediments of the Jurassic Ashcroft Formation and the Eocene Kamloops Group which were deposited over the north end of the batholith (McMillan et al., 2009; **Figure 1.6**). The Kamloops Group is composed of basaltic to rhyolitic dikes, sills, lava flows and tuffs from numerous volcanic vents in the region. The flows and interbedded sediments follow northeast-southwest oriented faults & fractures formed during a period of crustal extension (Eyles and Miall, 2007). Over the south-west part of the GCB, the Spences Bridge Group was deposited during the Cretaceous (McMillan et al., 2009; **Figure 1.6**). These are felsic volcanic rocks (Eyles and Miall, 2007).

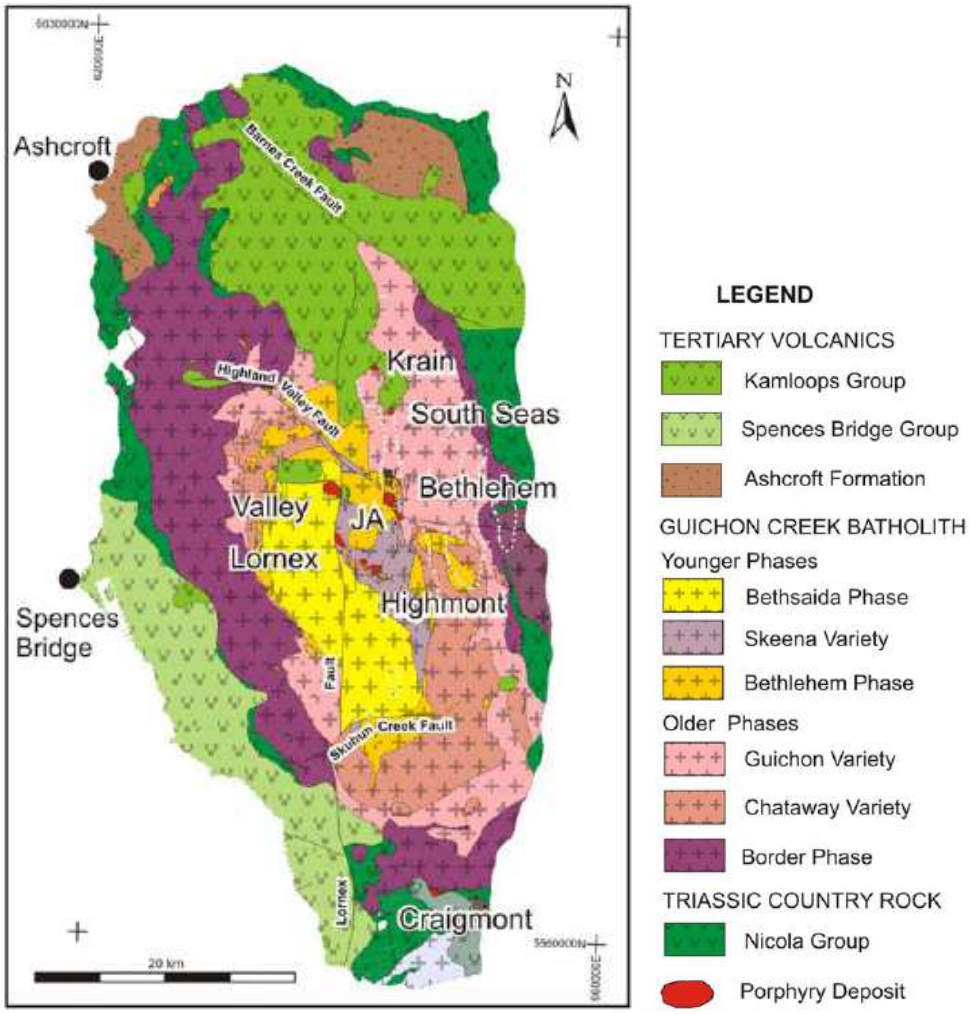

Figure 1.6 A bedrock map showing the mineralized zones of Highland Valley that are found in the Guichon Creek Batholith, which is in turn hosted by the Nicola Group (McMillan et al., 2009; McMillan, 1985). The major faults are also shown in grey.

Highland Valley Copper Operations is fully owned and operated by Teck Resources Limited. Large-scale open pit mining commenced in 1962, and it has been in production discontinuously ever since (Byrne et al., 2013; Teck Resources Limited, 2017). There are five major mineralization locations belonging to the porphyry copper system at Highland Valley (**Figure 1.6**). Three of them are deposits that are currently mined as open pits; these are the Valley, Lornex and Highmont Pits. The J.A. mineral target has never been mined or uncovered, while the Bethlehem deposit has been mined historically. These mineralized zones and others at Highland Valley are covered by a thick (>240m in some areas) blanket of unconsolidated sedimentary material.

Mineralization occurred 207 Ma ago (D'Angelo et al., 2017) at the Valley-Lornex deposit with an older mineralization event occurring at the Bethlehem deposit (Byrne et al., 2013).The first event took place shortly after the formation of the GCB's Bethlehem phase, and produced the Bethlehem mineralized zone among others (Byrne et al., 2013). The second and largest mineralization event occurred after the intrusion of the Bethsaida facies, and resulted in the Valley, Lornex, Highmont, J.A. and many smaller mineralized zones (Byrne et al., 2013). These major mineralizations occurred at the centre of the batholith. Propylitic, argillic, potassic and phyllic alteration zoning as well as silicization surrounds the main mineralized zones of Highland Valley (Lesage et al., 2016; Byrne et al., 2017; D'Angelo et al., 2017). Epidote veins with sodic-calcic haloes of albite, propylitic alteration controlled by fractures and illite, prehnite and vermiculite also controlled by fractures commonly surround the inner alteration and grade outward throughout the batholith's core (Byrne et al., 2017). The sodic-calcic outermost alteration zone at Valley, Lornex and Highmont consists of regularly occurring epidote, albite and actinolite (D'Angelo et al., 2017).

Most sulphide mineralization at Highland Valley occurs in veins, fractures, or as breccia fill and along syn-mineral faults (Casselman et al., 1995). The main metallic hydrothermal minerals are bornite, chalcopyrite, pyrite and molybdenite (Casselman et al., 1995). Specular hematite, magnetite and chalcocite are locally important, while sphalerite, galena, tetrahedrite, pyrrhotite, enargite and covellite are found as traces (Casselman et al., 1995).

The Valley deposit occurs at an intensely fractured area near the intersection of the Lornex and Highland Valley faults (Casselman et al., 1995) (**Figure 1.6**). The post-mineral left lateral strike slip Lornex fault is situated against the south-east side of the Valley ore body. It strikes north and runs between the Valley and Lornex deposits, offsetting the stratigraphy and alteration between the two. It created an escarpment over 280m tall running 70-80° from north and facing east (McMillan, 1976; Waldner et al., 1976; Osatenko and Jones, 1976). Eroded bedrock (including that containing mineralization) was transported by gravitational processes from the Lornex fault escarpment onto Tertiary volcanic rocks below it (McMillan, 1976; Waldner et al., 1976; Osatenko and Jones, 1976).

1.4 Geology of the Sediment Cover

The igneous rocks described in the previous section are partly covered by Late Cenozoic sediments, essentially thin and discontinuous Quaternary units (Plouffe and Ferbey, etc.), except along narrow paleovalleys where sediment thickness can exceed 240m and include Neogene strata at the base of the valley fill sequence (Bobrowsky et al., 1993). This study focuses on one paleovalley in particular, which runs from NW to SE before turning to the east (**Figure 1.5**). The valley-fill stratigraphy is partly exposed within the Highland Valley pit (**Figure 1.4**) and was first documented and interpreted by Bobrowsky et al. (1993). The following sub-section is a summary of the regional and local stratigraphy, with a focus on the one reported by Bobrowsky et al. (1993). It is followed by a description of the surficial geology of the study area and of the related glacial history based on previous work, as well as by previous work on tracing indicator minerals in the regional surficial till.

1.4.1 Late Cenozoic Stratigraphy

Several aspects of the regional stratigraphy and glacial history were first reported in the 1960s (Fulton, 1965; 1967; 1969). More recently, Fulton et al. (1992) described the Quaternary stratigraphic succession in the Merritt area and based on that record interpreted four different glaciations and two interglaciations. In the study area, the stratigraphy was investigated by Bobrowsky et al. (1993). They described the exposed sequence in the Valley pit in which they recognized nine stratigraphic units (**Figure 1.7**). From oldest to youngest, the units are in-situ weathered or eroded bedrock (unit 1), glaciolacustrine silt and clay (unit 2), deltaic sand and gravel (unit 3), glacial outwash with subaqueous debris flows (unit 4), subglacial outwash sands and gravels (unit 5), basal till (unit 6), supraglacial sands with gravel and diamictons (unit 7), in-situ ice decay sands with gravel and diamictons (unit 8) and a lacustrine deposit (unit 9; Bobrowsky et al., 1993).

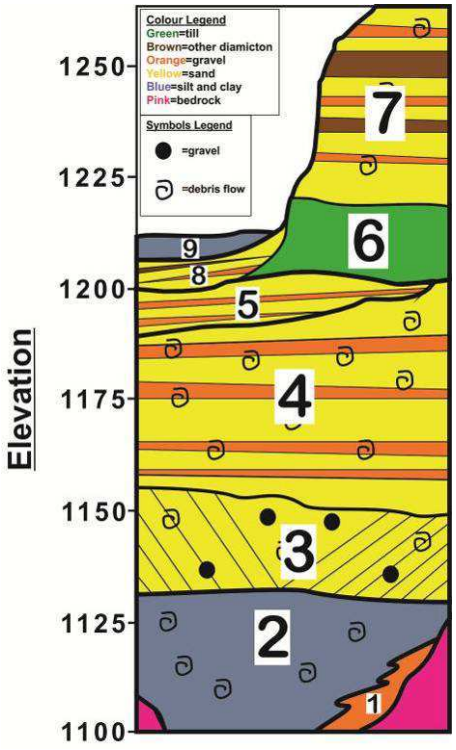

Figure 1.7 The stratigraphic framework of Quaternary sediments at the Valley Pit at Highland Valley (modified after Bobrowsky et al. (1993)).

1.4.2 Ice-Flow History and Surficial Geology

Ice-flow indicators have been previously reported and used to reconstruct ice-flow history in the region. During the last glaciations, an ice divide belonging to the Cordilleran Glacial Complex was located to the north of Highland Valley (**Figure 1.8**). Ice flowed southward from this ice divide and south-southeast across the Highland Valley area during the Last Glacial Maximum about 21ka ago (Ryder et al., 1991). Younger flow indicators on the plateau record a minor shift to a more southeastern direction (Ferbey et al., 2016a). During drawdown, the dynamics of a glacier generally becomes increasingly influenced by the landscape topography and valley lobes between uplands may have formed in the study area blocking drainage and forming elongated glacial lakes (Fulton, 1967). Deglaciation in deep valleys formed terraces with kettles, while deglaciation where open slopes with free drainage were found formed meltwater channels and deposited rill complexes (Fulton, 1967). Deglaciation where valley walls were uneven and meltwater drainage irregular (fluctuating gradient & local ponding) formed deltaic and stream terraces with kettle holes

(Fulton, 1967). In the southern Interior Plateau of British Columbia, deglaciation was fully underway by 9,750 years ago and there was no more ice or glacial lakes remaining as of 8,900 years ago (Fulton, 1969).

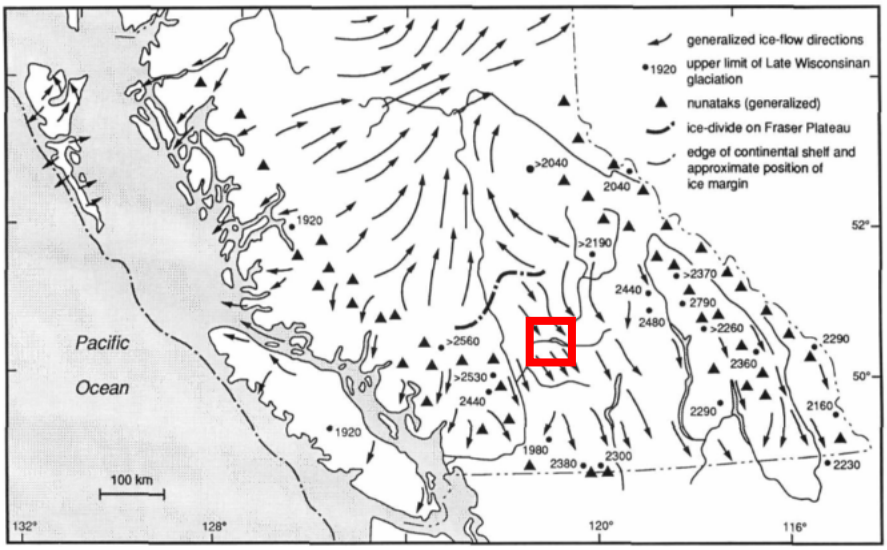

Figure 1.8 Movements and positioning of the Cordilleran Ice Sheet during the last glaciation in south-central British Columbia, with the box outlining the study area (modified after Ryder et al., (1991)).

There are four main Quaternary sediment units distributed at the surface at Highland Valley and its vicinity (**Figure 1.5**). The glaciofluvial (peach to orange to red) and glaciolacustrine (purple) units occur along the main paleo valleys of the study area. Glaciofluvial sediments typically consist of poorly-sorted gravel and sand, whereas the glaciolacustrine unit contains massive to laminated fine-grained sediments. Outside of these valleys, at higher elevation, blanket and veneer till (dark green) and ridged till (light green) occur at the surface. Till typically consists of boulders and pebbles within a compact sandy-silty matrix forming a very poorly-sorted sediment. Primary till is deposited directly by glacial ice processes with little reworking by water. Surficial till in the study area was deposited during the last glaciations (Wisconsinan Episode; ~80-10ka ago). Organics are found at the surface in soils (see Luck et al., 2019 for details) and as small pieces of charcoal. Finally, the light grey areas in the surficial geology map of Figure 1.5 represent sediment with anthropogenic influence, including the open pits and other areas where various fill materials may cover Quaternary sediments.

1.4.3 Indicators of Mineralization and Alteration in Unconsolidated Sediments

Studies on the nature and distribution of geochemical and mineralogical traces of mineralization in the overlying unconsolidated sediments at Highland Valley have only recently begun (Ferbey et al., 2016a). Studies have so far focused on the surficial distribution and dispersion of mineral indicators and geochemical pathfinders. Analyses of surficial till samples at Highland Valley and other sites in the region have identified indicators of porphyry copper mineralization and associated alteration minerals (Bouzari et al., 2011; Ferbey et al., 2014; Ferbey et al., 2016a; Kerr et al., 1993; Pisiak et al., 2015; Plouffe and Ferbey, 2016; Plouffe and Ferbey, 2017; Plouffe et al., 2012; Plouffe et al., 2010; Rogers, 2015). These include grains of chalcopyrite, apatite, rutile, magnetite, titanite and titanomagnetite, as well as elevated copper in C-horizon of till and in rabbitbush plants.

In most of these studies, indicator minerals and geochemical anomalies in glacial sediments have been traced back to their shallow sources. This was done by using known ice-flow direction and the locations of known major mineralized bodies and their alteration footprint in the region. They have also been shown to indicate mineralization potential in areas where the bedrock geology is more continuously covered and still not well known (Chapman et al., 2015; Plouffe, 1998; Plouffe et al., 2011; Hashmi et al., 2015). It has been shown that subglacial tills hold relatively large amounts of indicator minerals and geochemical pathfinder elements forming clear dispersal patterns in the region (Ferbey et al., 2016a). A recent study also demonstrated how glacial history, geology, geophysics and geochronology can be integrated to estimate the most likely source of erratic boulders of an unknown origin containing significant gold concentrations in south-central British Columbia (Plouffe et al., 2011). Other techniques involve investigating soils, vegetation, and groundwater to characterize geochemical anomalies related to post-depositional ‘secondary’ dispersal processes (Anderson et al., 2012; Kerr et al., 1993).

1.5 Research Problem

Despite substantial work having been done investigating the glacial geology of the Highland Valley area and mapping traces and indicators of mineralization in the surface till

(see sect. 1.4.3 above) several questions remain. There is a known detrital footprint in the surficial till and this may come from outcropping zones or shallow subcropping zones. It is unclear whether deeper sources under thicker stratified cover have contributed to the surficial detrital footprint. It is also possible that some of the indicators in the surficial till were reworked by the remobilization of older pre-existing Quaternary units. This process is referred to as compositional 'inheritance' (Stea and Finck, 2001; Trommelen et al., 2013). Older tills may have also been deposited under different subglacial conditions and flow directions leading to different dispersal patterns in the subsurface relative to the ones observed at surface. Sediments deposited in depositional environments other than subglacial (e.g., fluvial, deltaic) may also contain different indicator anomalies and dispersal patterns; no previous studies have looked at the composition of these older subsurface units. In summary, the three-dimensional dispersal patterns through the stratified cover from buried sources toward the surface are unknown. Improving our understanding of mineral dispersion through the stratified cover at Highland Valley could have significant implications for mineral exploration in areas where prospective targets are buried under thick stratified cover of variable origin.

Another related knowledge gap is about the control the subsurface patterns may have on the surface distribution of mineral indicators, such as those described in Ferbey et al. (2016a). What are the effects of stratigraphy on the full three-dimensional dispersion patterns and on their surface expression? Insights into these issues and questions could be useful for conducting exploration elsewhere where there is intermontane valley fill partly covering prospective bedrock or in other settings where thick stratified cover exist.

The effect of the thick cover at Highland Valley on geophysical surveys targeting the underlying mineralization is also not well known. The physical properties of the different cover units and their variation vertically throughout the stratigraphy as well as laterally are poorly understood. There is thus a need to better describe these units in terms of their physical properties (e.g., density, conductivity). A more quantitative description of these units will help better constrain geophysical inversions. This would lead to more accurate processing of geophysical survey data and ultimately of the geophysical footprint of the buried mineralization and alteration at Highland Valley.

1.6 Thesis Objectives

The objectives of this thesis are to:

1) Refine and extend the unconsolidated sediment stratigraphy at Highland Valley; Knowledge is augmented on the depositional environments and processes that lead to the erosion, transport and deposition of the different sedimentary units;

2) Characterize the physical properties and investigate the provenance of the main units of the unconsolidated cover;

3) Identify, characterize and map patterns of mineral indicators and geochemical traces of mineralization throughout the sedimentary successions and investigate their possible provenance;

4) Compare results with those of Ferbey et al. (2016a) to determine whether there are important differences or relationships between surface and subsurface unit compositions.

This research thus documents and contributes to the understanding of the spatial distribution of mineral indicators and geochemical pathfinders above and away from the buried mineralization and related alteration. The methods used to achieve these goals are explained in more detail in Chapter 2.

This study aims to help make exploration methods under thick or thin sediment cover more efficient and effective. The ultimate goal in studying the unconsolidated sediments at Highland Valley is to improve exploration methods and approaches applied to exploration through thick transported and stratified cover.

1.7 Thesis Structure

This thesis is composed of an abstract, an introduction chapter (Chapter 1), a methodology chapter (Chapter 2), a chapter presenting, interpreting and discussing the stratigraphy and individual unit properties (Chapter 3), a chapter on provenance and footprint indicators (Chapter 4) and a conclusion chapter (Chapter 5).

The introduction chapter describes the research problem and relevant state of knowledge, and introduces the location and physiographic setting of the study area as well as the geology of the bedrock and overlying cover. This thesis is part of the NSERC-CMIC Footprints research project (Lesher et al., 2017), a study that is characterizing and integrating multiple proximal and distal footprints of three deposit types within Canada, including the Highland Valley deposit. Lithology, structure, mineralization, alteration, geochemistry and geophysics data have been incorporated into a single 3D Common Earth Model that is quantitatively consistent for each parameter. The goal is to increase knowledge of the footprint of each deposit type and to develop methods and tools to help the mining industry in detecting even subtle outer margins and in discovering concealed deposits to expand Canada's resource base.

The methodology chapter describes the procedures undertaken to carry out all the different field and lab work components for this thesis. Stratigraphic logging with sampling was conducted at Teck Resources Limited's core shack by myself, Dr. Martin Ross and Aaron Bustard, and supported by Robert G. Lee, Teck Resources Limited and field assistant Darius Kamal. Description and sampling of roadcuts and shallow excavations were conducted with Dr. Martin Ross and supported by Robert G. Lee and field assistant Darius Kamal. I was ultimately responsible for recording all observations and selecting and taking all photographs and samples. A seismic survey was conducted jointly by myself and Dong Shi with assistance in the field by Shawn Scott. Processing of the seismic survey was done by Dong Shi at the University of Toronto. Sample disaggregation and sieving were done for select samples mostly by myself and also by lab assistant Jeremy Kamutzki. I carried out all laser grain size analysis and all analysis of pebble lithologies. Petrophysical properties of select samples were measured by Randy Enkin of the Geological Survey of Canada. Heavy mineral analysis was done at Overburden Drilling Management Limited. Geochemical analysis on these samples was done by ACME Analytical Laboratories (Bureau Veritas Company) in Vancouver. The same laboratories and procedures were used for both heavy mineral and geochemical analyses as for Plouffe and Ferbey (2016). Hyperspectral analysis was done at the University of Alberta, The measurements and data processing were done by Philip Lypaczewski and overseen by Dr. Benoit Rivard. I was responsible for all sample preparation for these different laboratory analyses.

Chapters 3 and 4 present all the data obtained for this thesis. All descriptions, figures, tables and photographs were done by myself, with the exception of the seismic cross-section. This was modified after the figure generated by Dong Shi.

The interpretations and discussions in Chapters 3 and 4 present an analysis of all the data, for which I was responsible for.

Methodology

2.0 Introduction

The following sections describe the procedures undertaken to achieve the goals of this thesis. Fieldwork was done in order to collect data and samples, and laboratory work was done to further analyze the collected samples. Stratigraphic logging, observation of surface sediments and pit sections and a geophysical survey was done in order to refine and extend the unconsolidated sediment stratigraphy. Dry bulk density, grain density, magnetic susceptibility, chargeability and resistivity were measured or calculated and grain size curves were produced so that the physical properties of the main units of the unconsolidated cover could be characterized. Heavy mineral, hyperspectral and geochemical analyses were done on select samples in order to identify, characterize and map patterns of mineral indicators and geochemical traces of mineralization throughout the sedimentary successions. Pebble lithologies were analyzed so that the possible provenance of indicators of mineralization might be investigated.

2.1 Fieldwork

2.1.1 Stratigraphic Logging

A stratigraphic framework is needed in order to establish the unconsolidated sediment stratigraphy for the study area (objective 1; section 1.3). This was achieved by logging cores from eight boreholes around the Valley pit, one borehole over the J.A. target and an additional borehole twelve kilometres to the northwest of the major mineralized zones (**Figure 2.1**). Cores of Quaternary and pre-Quaternary sediments were recovered in conditions suitable for stratigraphic and sedimentology analyses (**Figure 2.2**). These cores were provided by Teck Resources Limited. and logged using facies analysis (**Figure 2.3**) at the core shack at Highland Valley Copper operations. This technique consists of identifying distinguishable beds and unit contacts, describing unit textures and other sedimentary features (e.g., structures) and describing the features on a plot with a vertical depth/elevation axis. Stratigraphic contacts are plotted first and types of contacts

(sharp erosional, graded or depositional) are specified. The general texture (e.g., clay, silt, fine/medium/coarse sand) and colour (using a Munsell colour chart) of the sediments between the main contacts are then described. The size category (granule, pebble, cobble, boulder...) and maximum dimensions of any clasts were noted for each unit. The overall sorting, shape, angularity or roundness as well as broad lithology of the clasts were also noted. In addition, the cores were inspected for any sedimentary structures. The beds were drawn to scale, and the overall texture of each unit and their sedimentary structures were described and marked on the logs using standard lithofacies coding schemes (Evans and Benn, 2004; **Figure 2.3**). Photos were taken from a stepladder directly above the boxes using a Nikon D5100 with a maximum resolution of 4,928 × 3,264 (16.2 effective megapixels). The cores were about 8.0-8.5cm in diameter. Their total lengths ranged from 118.3-241.5m, and a total of 1838.5m of core (from the ten boreholes) was logged. Recoveries for major units or sections of each log were calculated.

(a)

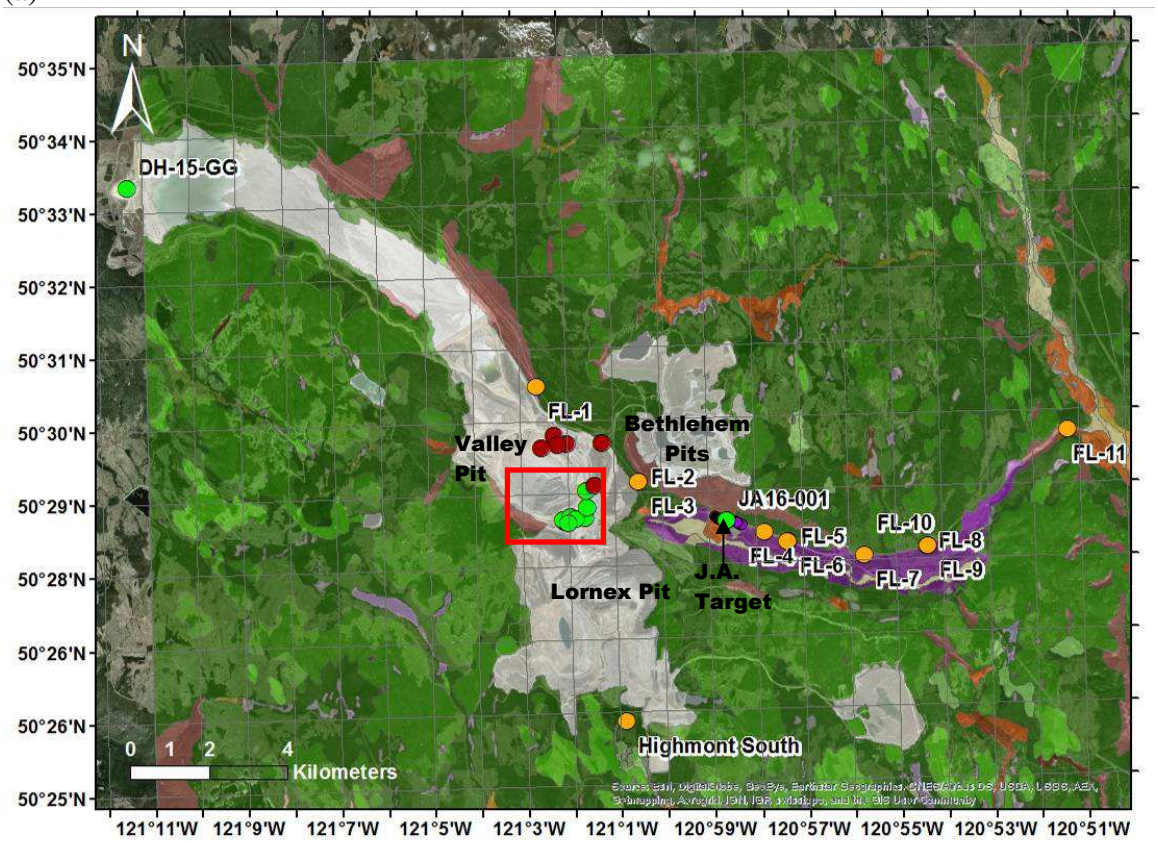

(cont'd next page)

(b)

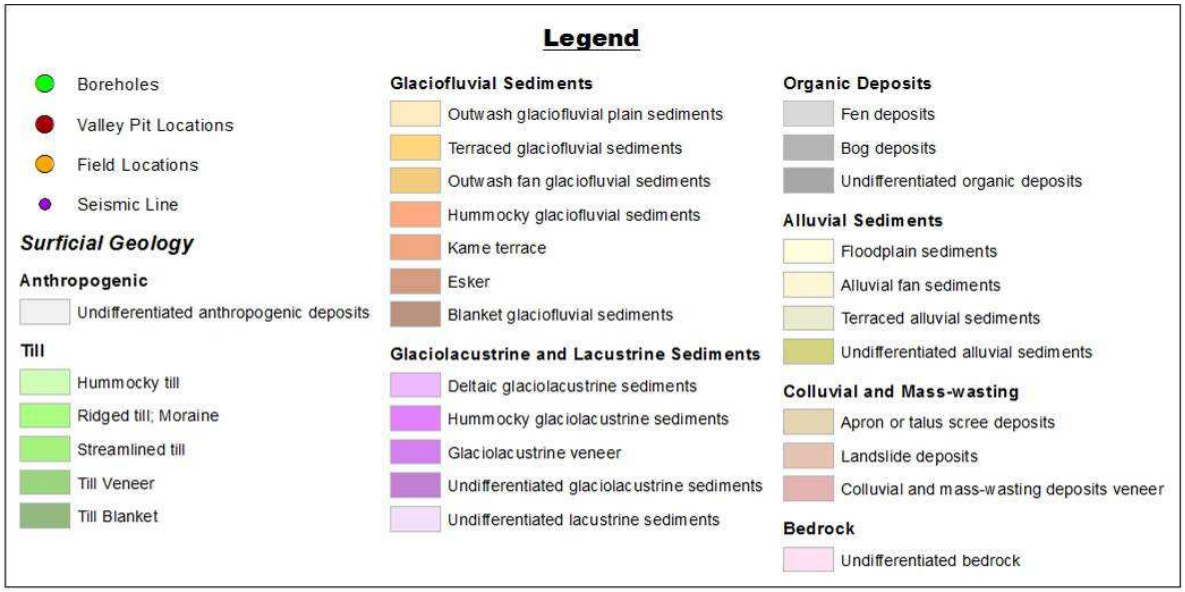

Figure 2.1 The surficial geology of the study area (Plouffe and Ferbey, 2018) as well as the locations of the boreholes and field sites (a). Ice flow during the last glaciation was in a south to south-east direction. The inset map (b) shows the locations of the boreholes around the Valley pit (red squared box).

Figure 2.2 An example of the cores that were logged in order to analyze the stratigraphy of the study area. Each length of core (one row of each box) is 1.5m long.

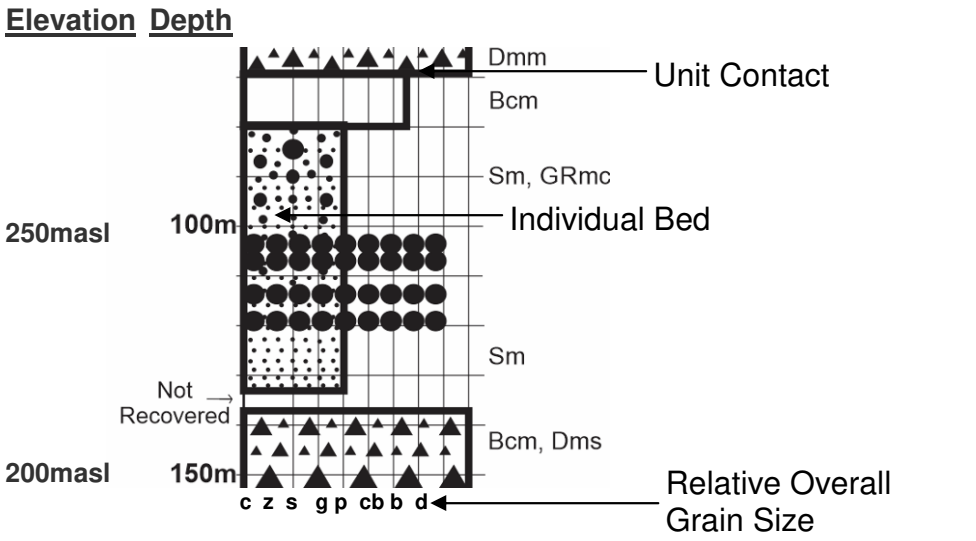

Lithofacies Codes

Dmm=Matrix-supported, massive diamicton
Dcm=Clast-supported, massive diamicton
Dcs= Clast-supported, stratified diamicton
Dms=Matrix-supported, stratified diamicton
Bcm=Clast-supported, massive boulder
Bcg=Clast-supported, graded boulder
Go=Openwork gravel (lacking fine-grained matrix)
Gm=Clast-supported, massive gravel
Gms=Matrix-supported, massive gravel
Gfu=upward fining (normal grading) gravel
Gcu=upward coarsening (inverse grading) gravel
GRh=horizontally bedded (granules)
GRm=Massive and homogeneous granules
GRmc=Massive granules with isolated, outsize clasts
Sh=Very fine to very coarse and horizontally/plane-bedded or low angle cross-laminated sand
Sl=Sand with horizontal and draped lamination
Sm=Massive sand
Suc=Upward coarsening sand
Suf= Upward fining sand
Fl=Finely laminated silts and clays, often with minor fine sand and very small ripples
Flv=Finely laminated silts and clays with rhythmites or varves
Fm=Massive silts and clays
---(d)=with dropstones

Log Symbols

c=clay
z=silt
s=sand
g=gravel
p=pebbles
cb=cobbles
b=boulders
d=diamicton

Figure 2.3 A summary of the logging codes and symbols used to log each core. Standard lithofacies coding schemes are from Evans and Benn (2004).

2.1.2 Surface Sediments and Pit Sections

Fieldwork was also done to map and describe surficial Quaternary sediments in road cuts and excavations (**Figure 2.1**). These observations were used to extend knowledge of the unconsolidated sediment stratigraphy. The road cut field site locations were all along Highway 97c leading to the active mine (where the Valley pit is) that goes over core JA16-001 at the J.A. target. Additional digging was done right before analysis, photographing and sampling to expose fresh sections one to two meters deep. The field sites that consisted of simple excavations were adjacent to the Highmont pit. Visible sections of the eastern wall of the Valley pit were also visited, studied and described (**Figure 2.4**). Photos of sections of the Valley pit wall that were taken in the fall of 2011 by Alain Plouffe of the Geological Survey of Canada allowed study of sections no longer visible or accessible.

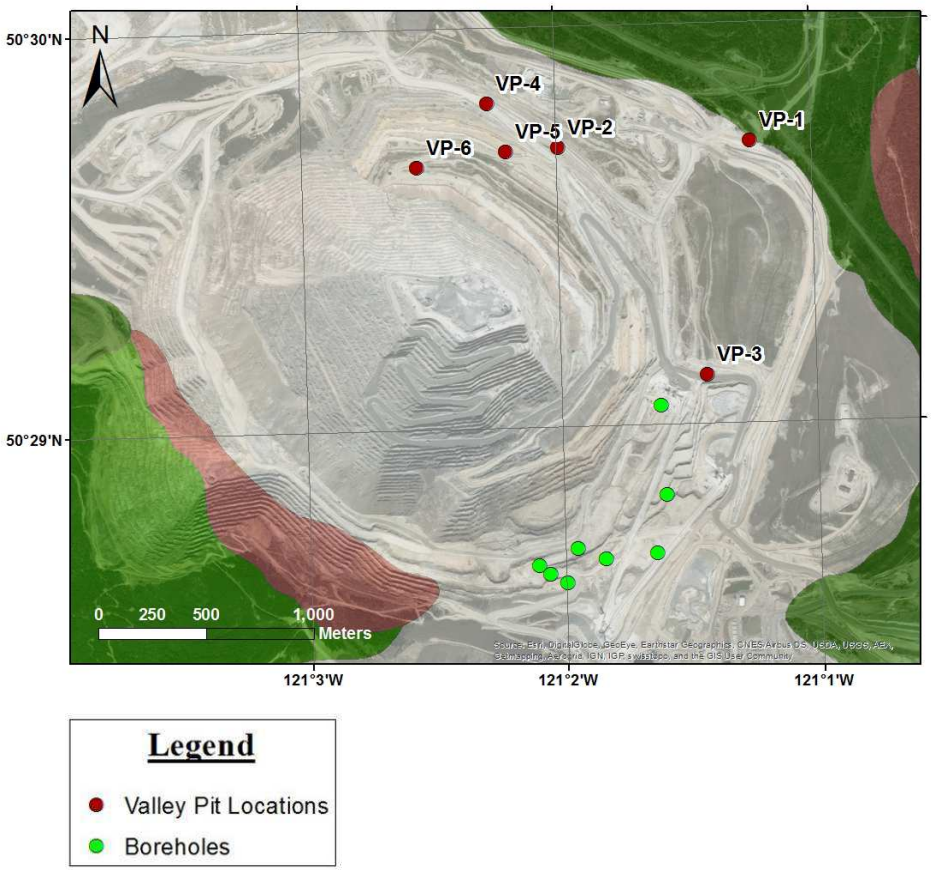

Figure 2.4 The locations of the sections of the Valley Pit walls that were studied. Surficial geology of the study area from Plouffe and Ferbey (2018). The surficial geology legend is the same as Fig. 2.1.

2.1.3 Geophysical Survey

A seismic P-wave reflection survey was done over the J.A. target using a hammer-drop source against a metal plate on the ground (**Figure 2.5**) using typical techniques to image the shallow near-surface subsurface (Bates et al., 1992; Pugin et al., 2004; Zimmer, 2004). An inline spread was used. Two 24-channel Geode seismograph units were connected to 48 vertical geophone (14 Hz) receivers per spread. The geophones were inserted into the ground every 5.0m (takeout), and the plate and hammer were moved to and deployed at every midpoint between two consecutive receivers along the survey line (2.5m offset). The hammer was dropped two or three times at each deployment location and the data stacked each time in order to produce a clear signal at every location. This seismic survey imaged the unconsolidated sediment layers over the 715m long survey line, which passed right by core JA16-001 that was logged and sampled. Downhole geophysical logging of this borehole was partially completed by other workers and included resistivity and porosity. The objective of this survey was to get information on the 2-D stratigraphic architecture along a transect that passes through core JA16-001 (**Figure 2.6**). The stratigraphy determined from logging of the core JA16-001 was extended outwards and provided insights into the general stratigraphic architecture of the valley fill deposits, which was useful for correlating borehole-to-borehole contacts identified in the nearby drillcores at HVC.

Figure 2.5 The hammer drop system, metal plate and line of receivers of the reflection seismic survey done over the J.A. target.

Figure 2.6 The survey line passing by the JA-16-001 borehole (marked by planted wooden stake and surrounded by wide protective metal casing). The pink flags mark the locations of the geophone receivers while the orange ones mark the locations of deployment of the hammer-drop source.

The data processing was done by Dong Shi at the University of Toronto. The raw data went through the following seismic processing steps: 1) Elevation static correction, in order to remove the effect of the variability in elevation of the source and geophone receivers; 2) automatic gain control (AGC), which recovers some of the amplitude lost from waves that arrived late and underwent attenuation or wavefront divergence; 3) frequency-wavenumber (FK) filter, to remove surface waves; 4) deconvolution (inverse filtering), in order to correct the wave shapes and improve the quality of the data made

worse by filtering or natural convolution (filtering of seismic energy by Earth); 5) velocity analysis, or calculation of wave velocity which is used in subsequent seismic processing steps (i.e. stacking); 6) normal moveout (NMO) correction, which is determined from time and offset and used to correct the delay in the arrival time of an event due to the source and geophones being offset from each other; 7) stacking, or adding together the signal from different source deployment instances so that noise is reduced and the overall reflection signal at each location is stronger; and 8) fx deconvolution process, in order to reduce random seismic noise in the data. All these steps are typical data processing procedures and more details about each of them can be found in several books and papers (e.g., Baker et al., 1999; Yilmaz, 2001; Gan et al., 2016). A final 2-D seismic cross-section showing the main reflectors and seismic signal of the subsurface was produced for interpretation of stratigraphy and bedrock contact.

2.2 Sampling and Characterization of Sedimentary Strata

Sampling of the different units in each borehole and road cut and excavation field sites was done for further laboratory analyses. Multiple sample types were collected, however the primary focus was on subglacial tills during petrophysical, provenance and footprint indicator analyses. These till subtypes represent a large proportion of the valley fill sediments, they have a high drillcore recovery (due to being well consolidated), and also because these samples are more likely to have a complete footprint mineral assemblage due to the wide grain size range. A total of 319 samples were collected from the drillcores to characterize the properties and composition of selected stratigraphic units. Each sample consisted of a small cylindrical section of core 5.9 to 8.4cm in diameter and of various lengths up to 110.2cm. A representative number of each of the different unit types was collected; this included 65 till, 41 other diamicton, 75 sand, 66 silt and/or clay and 54 samples of granule- to boulder-sized clasts. See Figure B.1 in Appendix B for each core's stratigraphic log with the sample locations marked. An additional two till samples were collected from a shallow pit at Highmont South. The sub-sections below present the methods applied to samples following the laboratory workflow sequence (**Figure 2.7**).

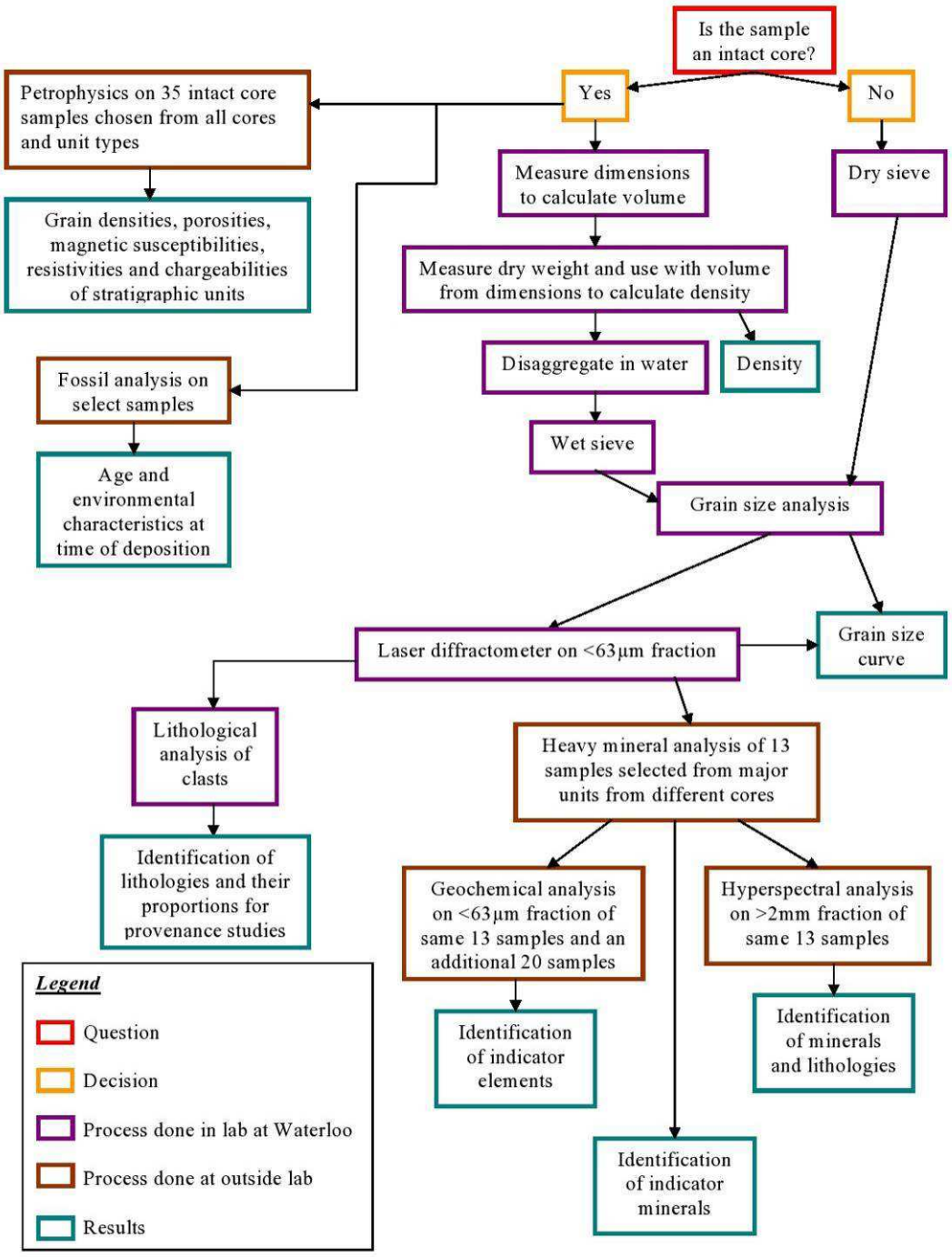

Figure 2.7 Laboratory workflow sequence for collected samples.

2.2.1 Petrophysical Properties

The physical properties of the main units of the unconsolidated cover were characterized (objective 2; section 1.3) by determining certain petrophysical properties for a selection of samples.

Dry bulk density of different units of the overlying sediment cover was calculated at Highland Valley Copper Operations' core shack. This is the mass per unit volume (g/cm^3) of a sample, and is controlled by the sample's mineralogy and porosity. Dry bulk density is a useful physical property for constraining geophysical inversion of gravity surveys targeting underlying alteration/mineralization (Forsberg, 1984; Mitchinson et al., 2013). It is calculated by dividing the mass of a sample by its volume. The weight of the dry sample is used, and the volume calculated using its dimensions. This method was used for determining the density of till, silt and clay units in this study because sufficient core intervals with good cylindrical shapes could be obtained to measure length and core diameter using a calliper (to 0.1 mm). Various regularly shaped pieces of core were weighed and their dimensions measured all throughout each core. This measurement was made for all possible units from every core. A certain degree of error will have been introduced for each one due to the pieces not being perfectly regular. The geometric volume calculation is accurate to about 3% for most samples. This allows estimation of the density of till, silt and clay units, but the densities of several other units were not estimated this way. The density of these other units could not be measured because the original grain packing was not preserved (e.g., dry loose sand). In order to get a bulk estimate that was more representative of long stratified core intervals or the ones that had disintegrated, the overall densities of 3 or 4.5m long sections of core were estimated. This was done by measuring the weight of the entire full corebox and subtracting the weight of an empty corebox, and estimating core recovery and known core diameter to obtain volume. This technique accounted for units that were not preserved as cylindrical cores. In addition, it may provide better estimates of overall density; calculations were able to be made for lengths that may be more representative of the length scale of certain geophysical surveys.

All other petrophysical property analyses were done by Randy Enkin of the Geological Survey of Canada. Grain density (density of just the mineral grains of a sample alone, not including the pores) was determined from the weight of the dry sample and the volume measured using a volume pycnometer. This was done for 30 of the 35 samples, chosen from selected units, representative of sample types from all of the cores drilled over the major mineralized zones (Valley and JA16-001 cores). Consolidated core samples were weighed while dry and the volume of the mineral grains alone for each sample was determined by gas displacement using a pycnometer (Tamari, 2004). The weight was divided by the volume to obtain an average grain density for each sample (Consolmagno et al., 2010). This method assumes that the weight of the air in the pores is zero so only the weight of the mineral grains is considered. Another assumption is that all the pores are interconnected so that when the sample displaces gas inside the pycnometer, only the mineral grains are displacing the gas and not any air-filled pores sealed off from the outside of the sample; only the volume of the mineral grains would be measured, and not of any of the pore space. Despite these simplifying assumptions, grain density values are more accurate than the bulk density ones, because errors accumulated from the assumptions made during the grain density measuring process are insignificant compared to the densities being measured, due to the high compaction and low porosity of the samples measured. Furthermore, deviation of the sample from a perfectly regular cylindrical shape does not affect the measurement of the volume with a pycnometer.

Porosity is a measure of the fraction of a sample made up of pores, and is the volume of the voids of a sample divided by the total bulk volume of the sample. It was calculated for 25 of the 35 samples, chosen from a variety of different units from all of the cores drilled over the major mineralized zones (Valley and JA16-001 cores). Two different methods were employed to do this. One was to use the following equation (**Equation 1**):

Equation 1: $\Phi = [(m_w - m_d)/\rho_{water}] / V_{bulk}$

Φ = sample porosity

m_w = weight of wet saturated sample

m_d = weight of dry sample

ρ_{water} = density of water

V_{bulk} = bulk volume of sample

Sources of error for this technique are that the sample may not become fully saturated during the time it is kept submerged, as well as any errors from calculating bulk volume using the dimensions of the sample (see above). Porosity was determined in an alternative way (**Equation 2**):

Equation 2: $\Phi = 1 - (\rho_{bulk} / \rho_{grain})$

Φ = sample porosity

ρ_{bulk} = bulk density of sample

ρ_{grain} = grain density of sample

Magnetic susceptibility, chargeability and resistivity are means of characterizing differences in mineralogy among core samples (Potter, 2007). Magnetic susceptibility is the ratio of induction of the rock to the small magnetic field applied externally, per volume (Enkin et al., 2012). It is mostly determined by mineralogy, particularly by iron-oxides and sulphides (Mitchinson et al., 2013). Chargeability is influenced by the amount of clay minerals in a sample, as their surfaces have a negative charge and also cause charge to build up (Mitchinson et al., 2013). These three petrophysical properties are measured by subjecting the core sample to a magnetic field or electric current in between two coils placed at opposite ends. The properties of magnetic susceptibility, chargeability and resistivity have been measured for 32 of the 35 intact core samples, representing different sedimentary units and from all the cores drilled over the major mineralized zones (Valley and JA16-001 cores). This was done using the methods outlined in Enkin et al. (2012). The 6cm diameter coil of the SM20 susceptibility meter was used (**Figure 2.8**). These measurements were made across the whole core sample interval, resulting in representative values for the individual units the samples came from. Having representative values of petrophysical properties for individual units of the unconsolidated cover provides a quantitative way of characterizing the signal from the cover and of removing this from geophysical surveys targeting underlying bedrock. The magnetic susceptibility from individual exposed pebbles of eight whole core samples from the

diamicton units was measured with a 10x3mm coil of the high-resolution Bartington MS2E probe. The susceptibility values have been compared with known values for bedrock in the region in order to establish the provenance of the diamicton units.

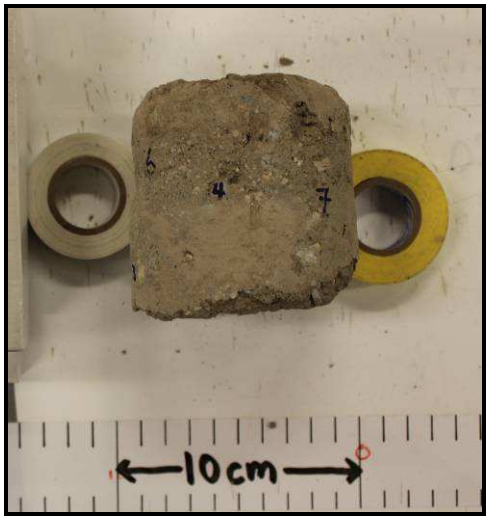

Figure 2.8 The 6cm diameter coils of the SM20 susceptibility meter being used to measure magnetic susceptibility for intact cores. Photo taken by Randy Enkin.

2.2.2 Sedimentological Properties

A selection of all the samples collected for the study were disaggregated for additional sedimentological analyses in order to further characterize the properties of the main units of the unconsolidated cover. These included some of those on which physical properties analyses (see section 2.2.1) were completed, as only half of each core sample was used for the physical property analyses. Samples were disaggregated and sieved into the following different size fractions: <0.063mm, 0.063-0.125mm, 0.125-0.250mm, 0.250-0.500mm, 0.500-1mm, 1-2mm, 2-4mm, 4-8mm, and >8mm. Wet sieving was done beforehand using the 0.063mm and 0.125mm pans if needed, based on the consolidation and difficulty of disaggregation of the individual samples (**Figure 2.9**). Using water helps to break down stiff samples and flush out the small grains from amongst the larger ones, especially the silt and clay particles that tend to form coatings around larger clasts. The dry weight of each size fraction was measured. A small sample was taken from the <0.063mm fraction of each sample and split in two to obtain duplicates which were

analyzed by laser diffractometry in order to provide data on the grain size distribution of grains smaller than 0.063mm. A Fristch Analysette 22 with a full range from 2000 μm to 0.08 μm was used. Despite this wide range, these systems perform better on samples with a narrower range and are ideal for the fine range, especially for silt and clay, which are too small for sieving techniques. The grain size data obtained from both sieving and laser techniques were normalized to weight frequency (%) and combined in order to build full cumulative grain size curves for each sample.

Figure 2.9 Wet sieving a sample using 0.125mm and 0.063mm sieves.

2.2.3 Pebble Lithology and Provenance of Units

As part of the provenance analysis (objective 3; section 1.3), pebbles recovered from till and sorted sediment samples (>4 mm fraction) were washed and classified by broad lithology groups. Clean clasts from select sieved samples, 4-8mm and >8mm in diameter, were examined under an optical microscope. This was done for a range of till and sand samples from all the cores and the Highmont pit. The clasts were grouped based on the following lithological classes: intrusive rocks (mainly Guichon Creek batholith), volcanic and volcanoclastic sedimentary rocks (mainly Nicola Group country rock), and 'others' from various more distal bedrock units up the ice-flow direction. Existing

literature such as Byrne et al., (2013) and D'Angelo et al., (2017), as well as consultation with experts on the geology of the area was used to identify the clasts. The size, shape and angularity/roundness of pebbles, as well as any signs of mineralization were noted. Pebble count results were then plotted on the vertical logs for integration with stratigraphy and other compositional data (see below) for the provenance analysis of the various units.

2.2.4 Heavy Mineral Analysis

Heavy mineral analysis was conducted to collect heavy mineral separates from selected samples. These separates were used to determine whether minerals indicative of the porphyry copper system or its associated hydrothermal alteration are present in selected unconsolidated cover units and the quantity of minerals present (objective 3; section 1.3). Magmatic and hydrothermal systems create high pressures and temperatures and bring fluids favourable for the formation of heavy minerals (Norton, 1984) which can then be concentrated in the sand-size fractions by various sedimentary processes. Several heavy minerals can survive sedimentary transport and be used as indicators of porphyry mineralization (Averill, 2011). The recovery process involved wet sieving to remove the greater than 2mm fraction (**Figure 2.10**). Half of each of the core samples selected for heavy mineral analysis was used; the other half was kept for sedimentological analysis. Visible gold grains were then picked from the less than 2mm fraction of each sample using a shaking table and subsequent micropanning. The table concentrate was dry sieved to 0.125mm. The greater than 0.125mm fraction was then density concentrated: a standard concentrate with a specific gravity of >3.2 as well as an additional concentrate with a specific gravity of 2.8-3.2 specifically for porphyry copper samples was separated using heavy liquids to collect all the indicator minerals. Next, the ferromagnetic portion was removed for each density concentrate. Each non-ferromagnetic fraction, called the heavy mineral concentrate, was then inspected under a microscope for porphyry copper indicator minerals and platinum group minerals. The 0.25-0.5, 0.5-1.0 and 1.0-2.0 mm fractions were picked for these indicator minerals. SEM analysis was used to check the identities of ambiguous grains. Ultraviolet light was employed to help find scheelite in the 1.0-2.0mm fraction. Heavy mineral analysis was done at Overburden Drilling

Management Limited. The same process and the same indicator minerals of copper mineralization were considered as those reported by Plouffe and Ferbey (2016) and Ferbey et al. (2016a) making it possible to compare and integrate the results of the two studies.

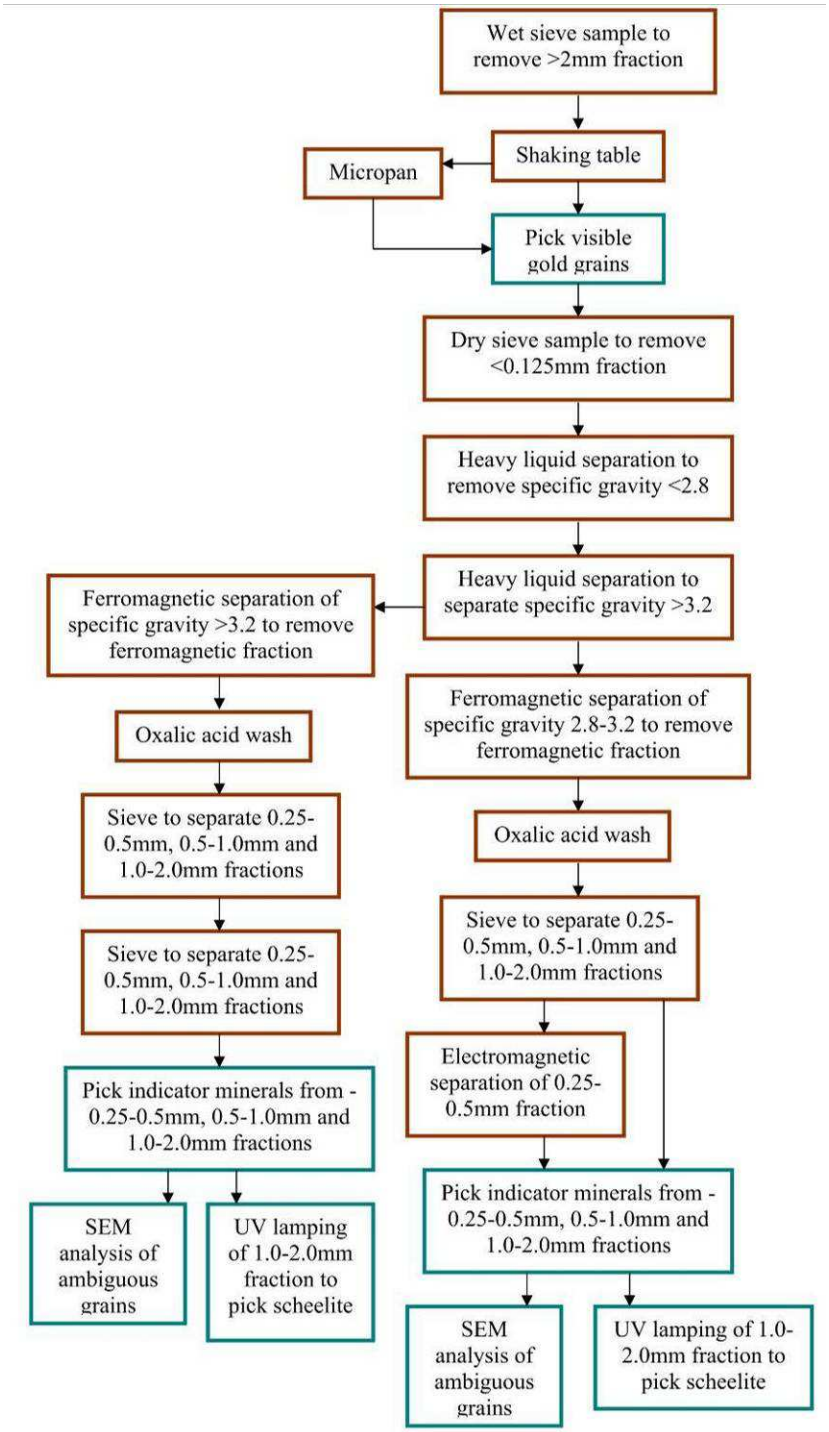

Figure 2.10 Heavy mineral analysis procedure.

Thirteen samples from till and sand units from different cores drilled over the major mineralized zones (Valley and JA16-001 cores) and one sample from the Highmont pit were analyzed. Samples were selected in order to get the best lateral coverage over the area where mineralization was significant (**Figure 2.11**), as well as to sample as many of the major till and sand units as possible over a variety of depths into the sediment cover, with a focus on the thick till units. See Table C.1 of Appendix C for location, depth and elevation intervals and unit description information for these thirteen samples.

The heavy mineral counts are not likely to reflect the true proportions of each mineral in the unconsolidated cover, because 10 to 20 kilograms of sediment are usually required to provide values that are representative (Averill, 2011). The weight of the core samples sent to ODM ranged from only 1.1-3.0kg. Only half of the total volume of the core for these samples were submitted for heavy mineral analysis; the other half was kept for geochemical and grain size analysis. This is a limitation of working with core samples that are needed for a variety of analyses. Nonetheless, heavy mineral results are considered useful herein because the main questions are more about mineral species occurrence and assemblages in the different subsurface units as opposed to sample-to-sample proportions for spatial patterns/trends analysis, which is typically the case with larger surficial samples.

Porphyry copper indicator minerals include chalcopyrite, andradite garnet, apatite, cinnabar, Mn-epidote, visible gold, jarosite, magnetite, pyrite, quartz, rutile, tourmaline and zircon (Bouzari et al., 2011; Kelley et al., 2011; Plouffe and Ferbey, 2016) (**Table 1**). Apatite and magnetite are particularly common indicator minerals at Highland Valley (Bouzari et al., 2011). Indicator minerals need to be heavy (in order to be able to be concentrated and found) (Averill, 2011). Sulphide minerals are sensitive to oxidizing conditions, which can be a problem in certain surficial settings. In this study the core samples were all taken from at least 27.3m below the surface in till samples that do not show any sign of oxidation. However, certain more sandy units that were also sampled showed evidence of oxidation (red colour) which could have altered any sulphide grains to iron oxides. The sample taken from a shallow pit over the Highmont target was at least 45 cm below ground surface. More digging against the side of the pit was done right

before sample collection, in order to remove any recently oxidized layers or anthropogenic debris.

Table 2.1 The main porphyry copper indicator minerals at HVC and some of their identifying characteristics (Bouzari et al., 2011; Ferbey et al., 2016a).

Mineral	Chemical Formula	Colour	Lustre	Transparency
Chalcopyrite	$CuFeS_2$	Brass yellow, sometimes with iridescent purplish tarnish	Metallic	Opaque
Andradite garnet	$Ca_3Fe_2Si_3O_{12}$	Yellow / greenish yellow to emerald-green / dark green / brown / brownish red / brownish yellow / grayish black / black	Adamantine / resinous, dull	Transparent to translucent
Apatite	$Ca_5(PO_4)_3(F,Cl,OH)$	Most often green, sometimes colorless / yellow / blue to violet / pink / brown	Vitreous / subresinous	Transparent to translucent
Cinnabar	HgS	Red to brownish red / lead-gray	Adamantine to dull	Opaque, transparent if as thin

				fragments
Mn-epidote	$Ca_2Al_2(Fe^{3+};Al)(SiO_4)(Si_2O_7)O(OH)$ (Mg rich as impurities)	Pink	Vitreous to resinous	Transparent to somewhat opaque
Gold	Au	Gold	Metallic	Opaque
Jarosite	$KFe^{3+}{}_3(OH)_6(SO_4)_2$	Amber yellow / dark brown	Subadamantine to vitreous	Transparent to translucent
Magnetite	Fe_3O_4	black	Metallic	Opaque
Pyrite	FeS_2	Brass yellow	Metallic	Opaque
Quartz	SiO_2	Colourless / various colours / black	Vitreous / waxy / dull	Transparent to somewhat opaque
Rutile	TiO_2	Reddish brown / red / pale yellow / pale blue / violet / rarely grass-green / black	Adamantine to submetallic	Opaque, transparent if in thin pieces
Tourmaline	$(Ca,K,Na,[])(Al,Fe,Li,Mg,Mn)_3(Al,Cr,Fe,V)_6(BO_3)_3(Si,Al,B)_6O_{18}(OH,F)_4$	Usually black, sometime colorless / brown / red / orange / yellow / green / blue / violet / pink	Vitreous, resinous	Translucent to opaque
Zircon	$ZrSiO_4$	Reddish brown / yellow / green / blue / gray / colorless	Vitreous to adamantine	Transparent to opaque

(a)

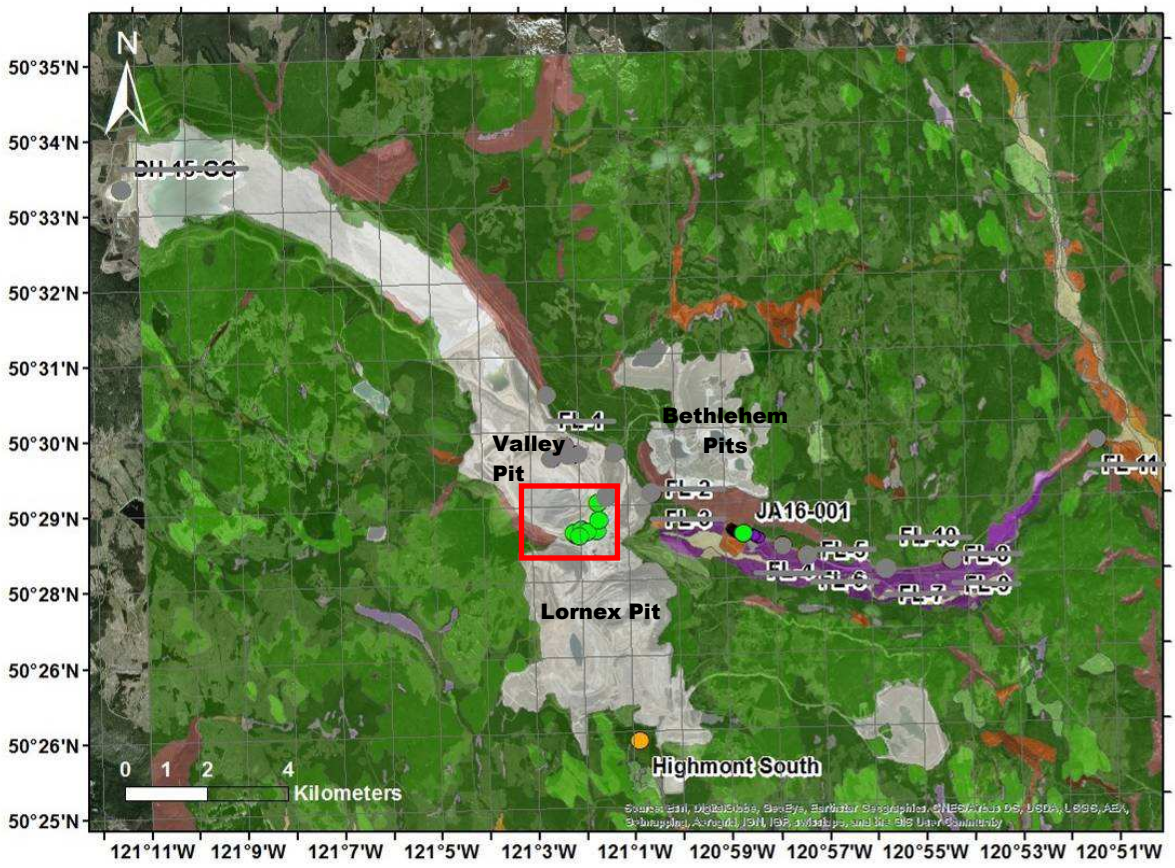

(cont'd next page)

(b)

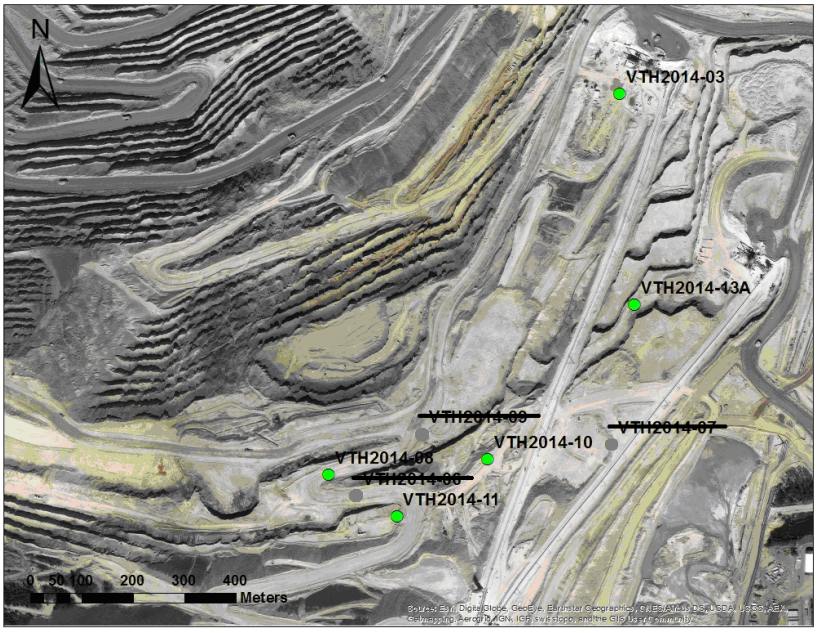

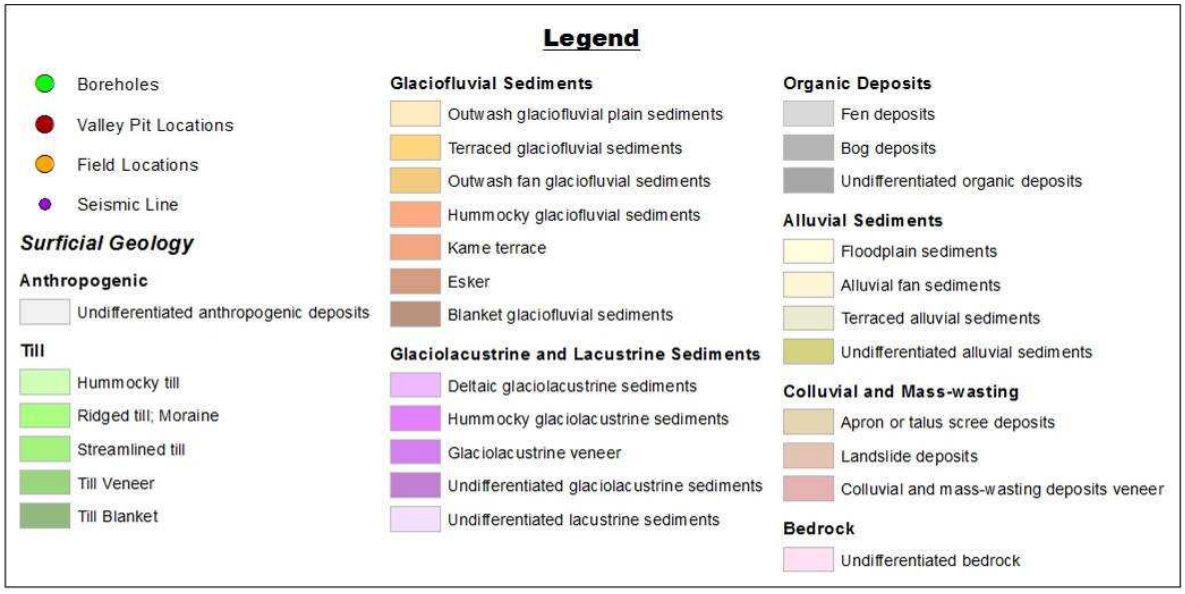

Figure 2.11 The locations of the cores and Highmont pit from which samples were selected for heavy mineral and hyperspectral analyses (a). The bottom map (b) is the inset (red rectangular box) from the top map. The cores and field site locations from which no samples were chosen from for these analyses are crossed and greyed out.

2.2.5 Hyperspectral Analysis

Hyperspectral analysis identified additional mineral indicators in the unconsolidated cover (objective 3; section 1.3). Hyperspectral analysis makes use of an instrument that detects emissivity, radiance or reflectance spectra from a rock sample (Van der Meer et al., 2012). Hydroxyl-bearing minerals, such as most phyllosilicates, as well as carbonate minerals exhibit unique spectral absorption features in the visible to near-infrared wavelength range (0.4–3 µm) and can thus be detected and mapped using hyperspectral instruments (Van der Meer et al., 2012). Since these minerals are often associated with hydrothermal systems, it makes hyperspectral imaging useful to characterize alteration assemblages of such systems (e.g. Tappert et al. 2013). Hyperspectral analysis was conducted on the >2mm (granules and pebbles) fraction of the same thirteen samples analyzed for heavy minerals (see section above; Table C.1 of Appendix C) (**Figure 2.11**). The >2 mm pebbles were analyzed at the University of Alberta Core Imaging Laboratory on a SisuROCK core imaging system (http://www.specim.fi). The granules and pebbles of each sample were spread out on a flat surface so that most of them had their top surface visible from above (**Figure 2.12**). The hyperspectral camera was passed over samples, and spectral data were collected in the visible and near-infrared (0.4-2.5 µm) range (2100 nm bandwidth). The images produced have a spatial resolution (pixel size) of 0.8mm/pixel. The measurements and data processing were done by Philip Lypaczewski and overseen by Dr. Benoit Rivard. **Figure 2.13** shows an example of the type of imagery produced. A pixelated count of coloration was made to determine the fraction of the sample containing the target mineral. This technique assumes that the target mineral content of the top surface of the visible granules and pebbles laid out is representative of the total target mineral content of all the granules and pebbles. Hyperspectral analysis investigated what alteration mineralogy was present in the granules and pebbles of the selected till and sand units, which was then compared with those of the mineralized bedrock. It was done to determine whether the mineral assemblages making up the alteration observed at Highland Valley Copper (Lesage et al., 2016; Byrne et al., 2017) are present in the unconsolidated sediments.

Figure 2.12 The >2mm granule and pebble fraction of selected samples laid out in preparation for hyperspectral analysis.

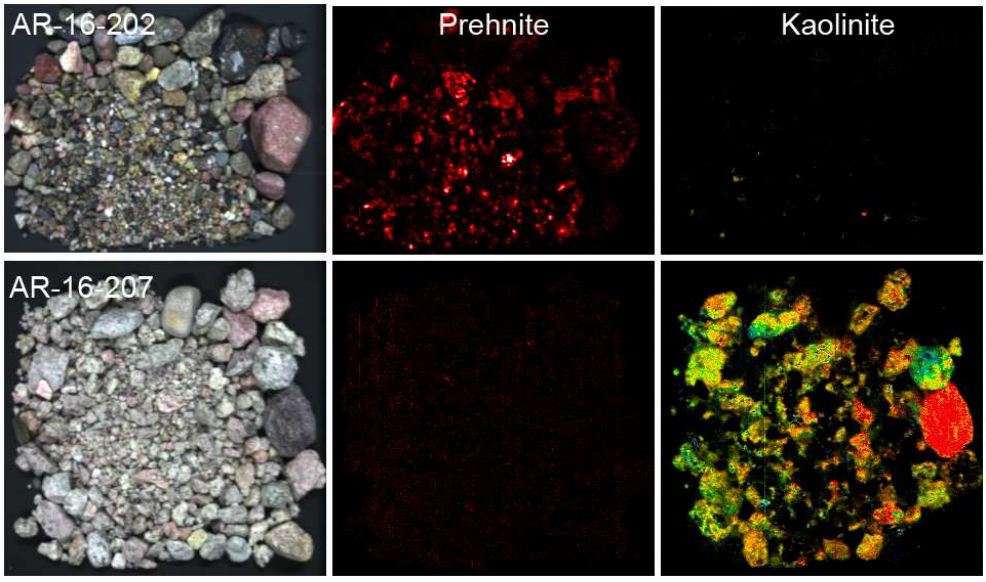

Figure 2.13 Images of the >2mm granule and pebble fraction of two analyzed samples on the left, the samples coloured based on the concentrations of prehnite of the top surfaces in the middle, and the samples coloured based on the concentration of kaolinite of the top surfaces on the right.

2.2.6 Geochemical Analysis

The relative proportions of a wide range of elements were determined for a selection of samples in order to determine if there are any geochemical traces of mineralization (objective 3; section 1.3). Geochemical analysis identifies key elemental composition indicative of the deposit type of interest, as well as the change in composition from alteration, which often results from the interaction between mineralizing fluids and host rocks (McClenaghan et al., 2000). In this study, geochemical analysis was done to determine whether geochemical assemblages indicative of porphyry copper mineralization or alteration footprint are present in one or more subsurface sedimentary 'cover' units and to investigate any potential effects related to stratigraphy and related changes in depositional environments. The less than 0.002 mm (clay-sized) portion is often analyzed for base metals, since elements tend to partition into this size fraction (McClenaghan et al., 2000). The <0.063mm (silt+clay) fraction was sent to the lab, and this was analyzed all together. The method used to perform a geochemical analysis for this study consisted of a near-total digestion with lithium metaborate/tetraborate, fusion at 980°C, dissolving in 5% HNO_3 and then analysis by inductively coupled plasma emission spectrometry (ICP-ES) and inductively coupled mass spectrometry (ICP-MS) on one portion of the sample. Another portion was digested with a modified aqua regia solution of equal parts hydrochloric (HCl) and nitric (HNO_3) acids, and then analyzed by ICP-MS. The first process yields the concentrations of a wide variety of elements and compounds and is usually used for "whole rock" lithogeochemical analysis. The second process targets unstable, mobile and easily soluble species; it is usually used for exploration geochemistry work. This analysis was done on the same thirteen till and sand samples as those on which heavy mineral and hyperspectral analysis were also done, as well as an additional twenty samples chosen from a variety of till and sand samples from all of the cores except core VTH2014-06. Samples were chosen in order to get the best lateral coverage over the mine zone where mineralization is significant (**Figure 21**), as well as to sample as many of the major till and sand units as possible over a variety of depths into the sediment cover. One sample was also chosen from a till unit of the DH-15-GG core several kilometers northwest of the mine area in order to potentially obtain background values of element concentrations away from the major mineralized zone. See Table C.2 of

Appendix C for location, depth and elevation interval and unit description information for these 33 samples. Geochemical analysis on these samples was done by ACME Analytical Laboratories (Bureau Veritas Company) in Vancouver, which is the same laboratory used by Plouffe and Ferbey (2016) to facilitate comparison of results between the two surveys. Two standards (both Reference Sample Till-1 from Canadian Certified Reference Materials Project, Canada Centre for Mineral and Energy Technology; https://www.nrcan.gc.ca/mining-materials/resources/canadian-certified-reference-materials-project/7827) were sent with the samples in order to evaluate accuracy. See Tables C.5 and C.6 of Appendix C for standard results.

(a)

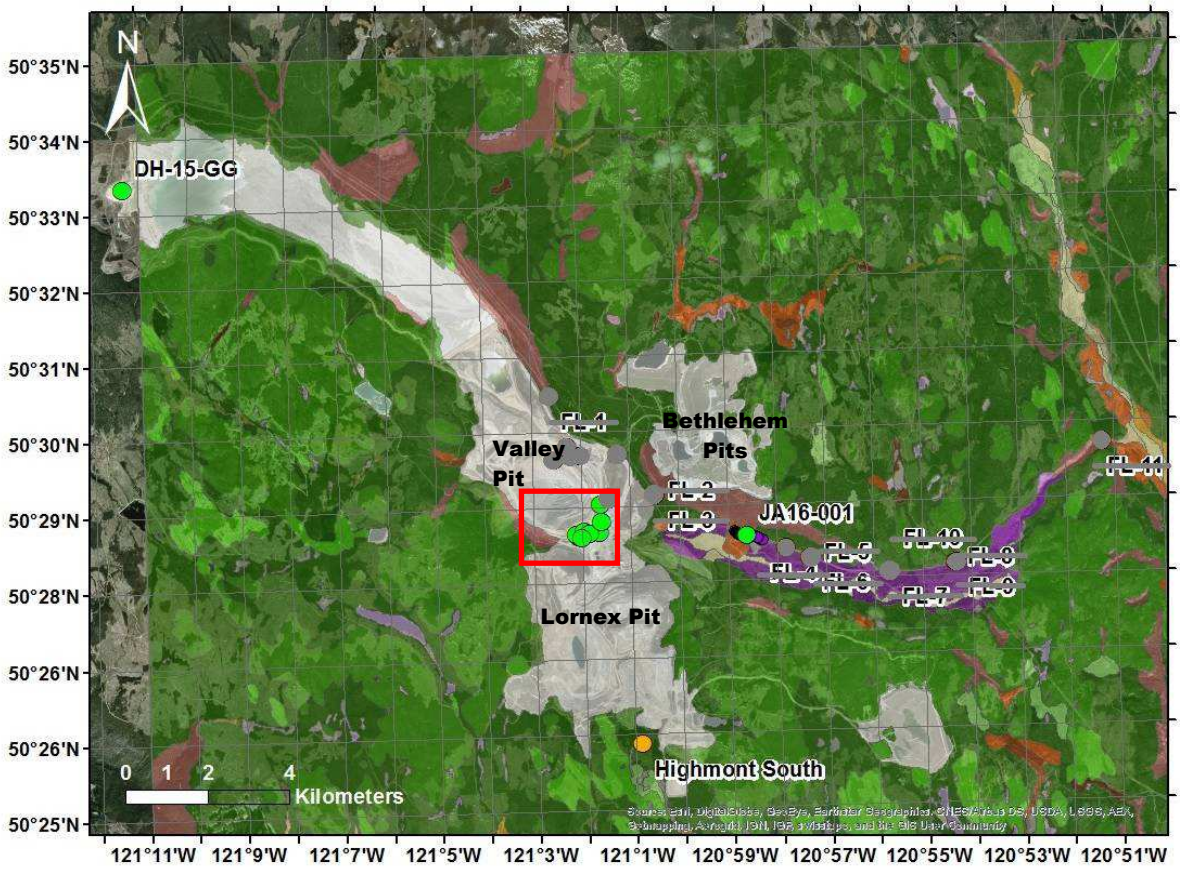

(cont'd next page)

(b)

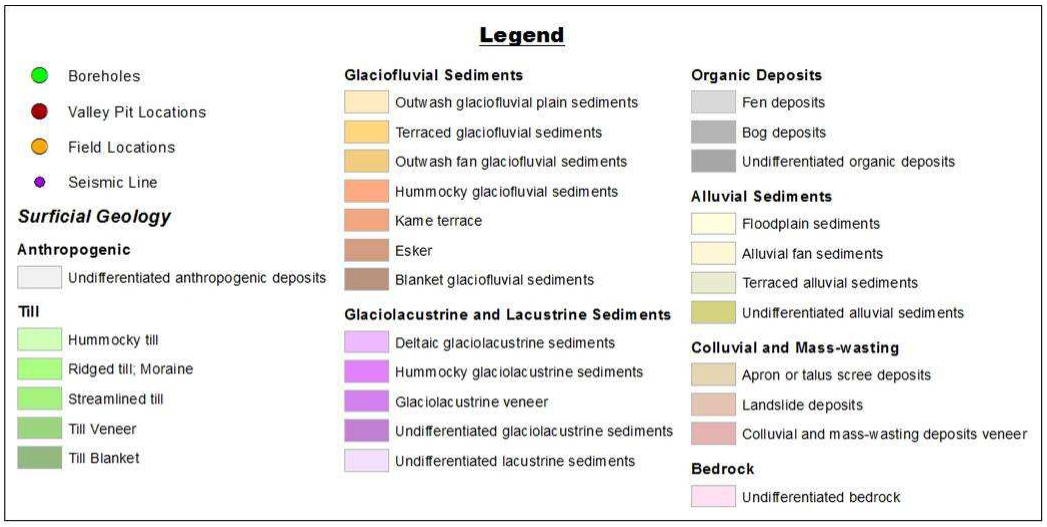

Figure 2.14 The locations of the cores and Highmont pit from which samples were selected for geochemical analysis (a). The bottom map (b) is the inset (red rectangular box) from the top map. The cores and field site locations from which no samples were chosen from for these analyses are crossed and greyed out.

The results of these analyses were examined for stratigraphic variations of mineralogy, hyperspectral signature and geochemistry, and the results were compared to the underlying altered and mineralized bedrock in order to investigate and characterize the secondary (detrital) dispersion of altered/mineralized material and its relationship with the known bedrock sources.

Stratigraphy, Sediment Properties and Depositional Environments

3.0 Introduction

A total of ten drillcores were logged and analyzed using stratigraphic principles and methods (cf. Chap. 2, Sect. 2.1.1 for details). Eight boreholes are from the south and southeastern side of the Valley pit and one is over the J.A. target (**Figure 3.1**). The individual logs for the Valley and core JA16-001 at J.A. are described and interpreted in the following sections. For each drillcore, stratigraphic contacts separating distinctive sediment facies assemblages were logged and the facies described and sampled. Accessible sections of the northeast and east wall of the Valley Pit were also observed and the units described. The first section below provides a description of the stratigraphic units and of their facies, as well as facies interpretation. An additional log, as well as descriptions of sediments at roadcuts, are presented in Appendix A.

Individual logs were first described and their facies interpreted independently of the correlations and cross-section building, which were done later. However, for clarity and consistency, unit numbers on each log follow the nomenclature of the composite (correlated) stratigraphic framework. The 715m-long seismic section running through core JA16-001 with the core log superimposed is also shown and interpreted (cf. Chap. 2, Sect. 2.1.3 for method details). This provided an image of the underlying unconsolidated sediments. The stratigraphic sequence identified in core JA16-001 was extended outward this way, and the general stratigraphic architecture of the cover material over the J.A. target was determined. Correlations between the units identified by different workers and the units observed in this study are also presented. All this is done in order to identify and organize the major facies into a stratigraphic framework and get as much insight into the local stratigraphic architecture as the data allows. The unconsolidated sediment stratigraphy at Highland Valley is thus refined and extended.

(a)

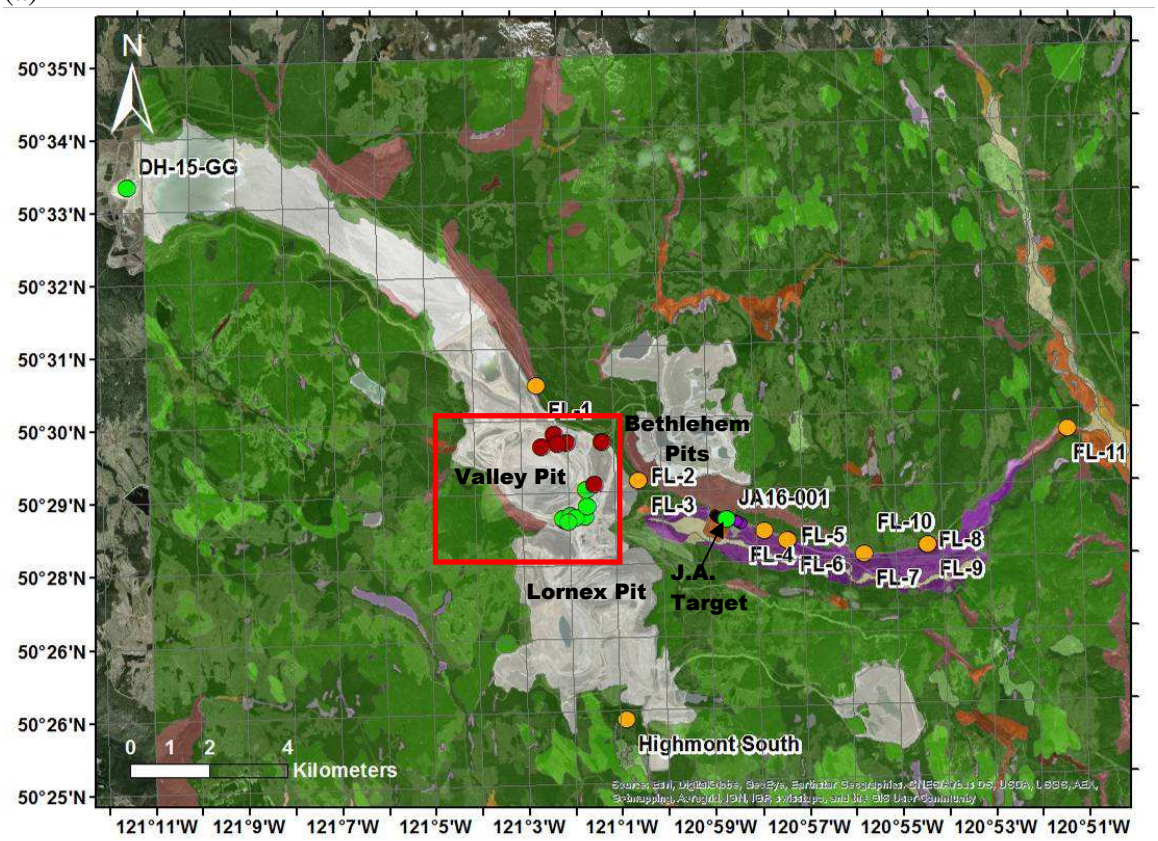

(b)

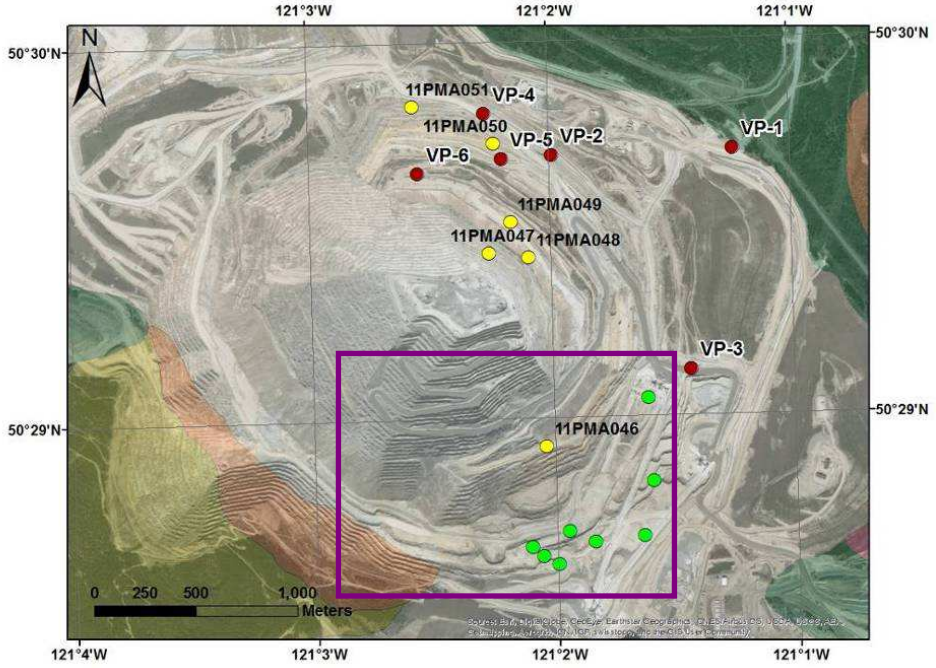

(cont'd next page)

(c)

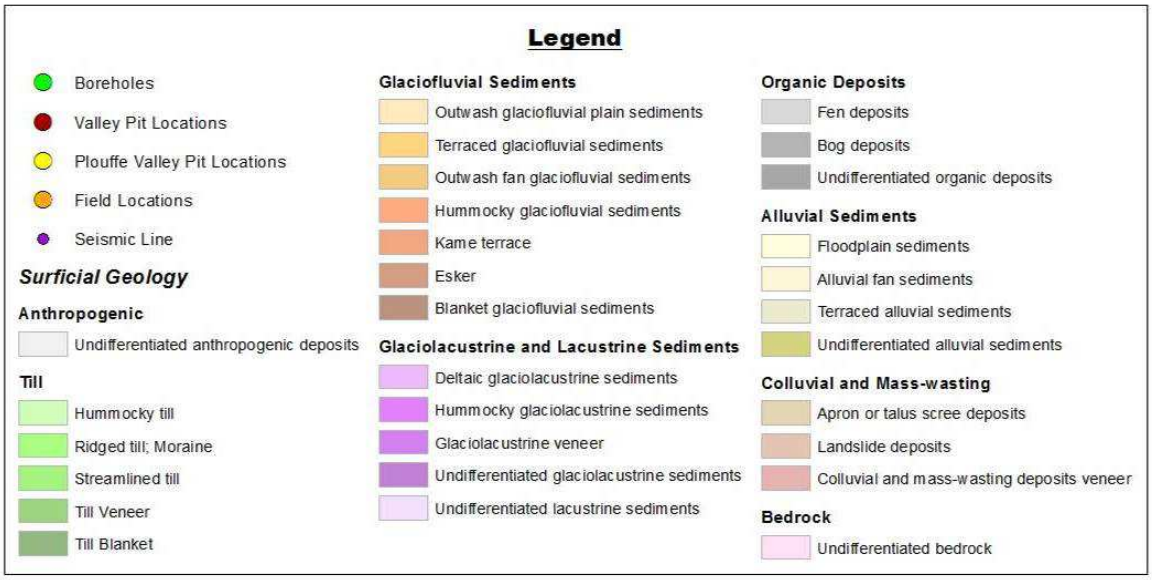

Figure 3.1 The surficial geology of the study area (Plouffe and Ferbey, 2018) as well as the locations of boreholes and field sites (a). The inset map (b) shows the observation locations for this study (red-filled circles), for Alain Plouffe's study (yellow-filled circles) and of the boreholes (green-filled circles) in the Valley pit (red squared box). A second inset map (c) shows the locations of the individual boreholes around the Valley pit (purple squared box).

3.1 Stratigraphic Descriptions of Cores

3.1.1 Core VTH2014-03

Core VTH2014-03 was taken from a borehole southeast of, but immediately adjacent to, the Valley pit (**Figure 3.1c**). A total of four contrasting sub-units were observed throughout the core (**Figure 3.2**). From bottom to top, the first sub-unit (sub-unit 2b; elevation range: 1049.6 to 1057.8 metres above sea level (m asl)) consists mostly of coarse-grained pebbles and cobbles overlying felsic igneous Guichon Creek Batholith bedrock. The clasts have various shapes, and a few are faceted; some are rounded to sub-rounded, whereas others are more sub-angular to angular in shape. On top of this coarse layer is a thin bed (elevation range: 1057.8 to 1058.8 m asl) of medium- to coarse-grained massive sand with faceted, irregularly shaped, subangular to rounded pebbles and granules of various lithologies. This sub-unit is overlain by a thick (~14m), poorly-consolidated sub-unit of laminated silt and clay (sub-unit 3a; elevation range: 1059.8 to 1073.9 m asl). The laminations are about 2 to 3 millimetres thick. This sub-unit is overlain by a thin layer of rounded pebbles, which is in turn overlain by a thick sequence (~65m) consisting mostly of massive and poorly-sorted sand and gravel with minor interbeds of faceted, subangular to rounded pebbles (elevation range: 1073.9 to 1138.8 m asl). This sand and gravel sequence coarsens upward in cycles (sub-units 3b and 3c). It is overlain by thin beds of laminated fines (sub-unit 3d; elevation: 1138.8 to 1140.3 m asl), followed by massive, poorly-sorted sand and gravel (sub-unit 3e; elevation range: 1140.3 to 1161.7 m asl). The top of the stratigraphic sequence consists of two thin massive diamicton layers (sub-units 4a and 4c). The diamicton layers are similar and consist of granules and small pebbles of mixed lithology supported by an abundant clayey silt matrix. They are separated by thin interbeds of massive medium sand with granules and small pebbles and by subangular to subrounded, faceted pebbles and cobbles (sub-unit 4b).

The wide range of shapes and faceted clasts of sub-unit 2b suggest a glacial origin with reworking by water transport; it is thus interpreted as being glaciofluvial. However, it is unclear whether the sediments of this sub-unit (2b) were deposited in an ice-contact setting or a proglacial outwash setting. The laminations of sub-unit 3a form rhythmites that are interpreted to be lacustrine in origin. Sub-units 3b and 3c are interpreted to be a

sediment gravity flow deposit due to their poorly-sorted texture. Sub-unit 3d is interpreted to be glaciolacustrine in origin, while sub-unit 3e is interpreted to be glaciofluvial outwash. The top diamicton and the interbeds (sub-units 4a-c) are interpreted to be subglacial or possibly ice-marginal in origin.

A thin (1.5m) bed of silty clay interpreted to be glaciolacustrine within the sediment gravity flow sub-unit (elevation range: 1138.75 to 1140.25 m asl) was analyzed for macrofossils. The results (moss, shells and charcoal) can be found in Appendix B. Moss from one sample was radiocarbon dated and yielded a non-finite age of >52,800 ^{14}C years before present.

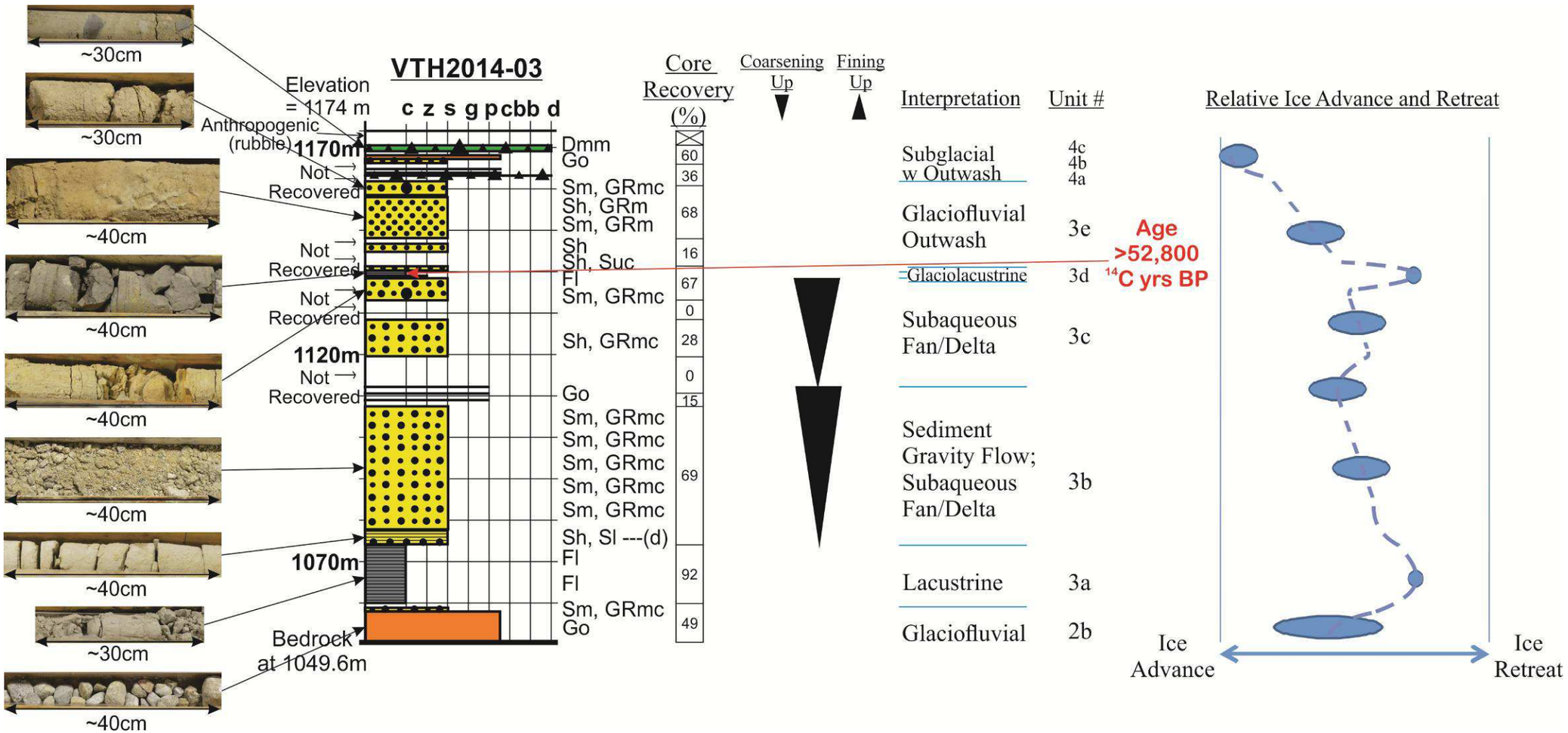

Figure 3.2 Stratigraphic log of core VTH-2014-03, located next to the Valley pit (see Figure 3.1 for location). See Table 3.1 for code descriptions. Stratigraphic unit numbers correspond to the stratigraphic framework (cf. Sect. 3.2.3). Relative ice advance/retreat history is shown to the right; blue circles represent relative uncertainty.

Table 3.1 Codes used in stratigraphic logs and their descriptions. From Evans and Benn (2004).

Code	Description
Dmm	Matrix-supported, massive diamicton
Dcm	Clast-supported, massive diamicton
Dcs	Clast-supported, stratified diamicton
Dms	Matrix-supported, stratified diamicton
Bcm	Clast-supported, massive boulder
Bcg	Clast-supported, graded boulder
Go	Openwork gravel (lacking fine-grained matrix)
Gm	Clast-supported, massive gravel
Gms	Matrix-supported, massive gravel
Gfu	Upward fining (normal grading) gravel
Gcu	Upward coarsening (inverse grading) gravel
GRh	Horizontally bedded (granules)
GRm	Massive and homogeneous granules
GRmc	Massive granules with isolated, outsize clasts
Sh	Very fine to very coarse and horizontally/plane-bedded or low angle cross-laminated sand
Sl	Sand with horizontal and draped lamination
Sm	Massive sand
Suc	Upward coarsening sand
Suf	Upward fining sand
Fl	Finely laminated silts and clays, often with minor fine sand and very small ripples
Flv	Finely laminated silts and clays with rhythmites or varves
Fm	Massive silts and clays
---(d)	with dropstones

3.1.2 Core VTH2014-06

Core VTH2014-06 is from a borehole south of, but immediately adjacent to, the Valley pit (**Figure 3.1c**). The first stratigraphic sub-unit consists of a thick matrix-supported stratified diamicton at the bottom (sub-unit 1a; elevation range from 1006.5 to 1052.7 m asl) (**Figure 3.3**). More specifically, the diamicton is characterized by consolidated silt, abundant granules, and angular small pebbles of a uniform, felsic, coarse-grained igneous lithology, as well as organic-rich horizons. It is interlayered with thin layers of organic-rich fissile clay, consolidated clayey silt and thin coal horizons. Localized slickensides are present in the clay and silt beds. Moving up the stratigraphic sequence is a gradual transition to several layers of coarse sediments,

mostly pebbles and cobbles, increasing in thickness from the base (1054.5 m asl) of the sequence to the top (1120.4 m asl). Sub-unit 1a also contains near the middle (elevation range from 1069.5 to 1095.0 m asl), a few thin layers of chalky, white-to-grey, highly-disintegrated and angular rock fragments. It is overlain by laminated silt and clay couplets resembling varves (sub-unit 3d; elevation range from 1122.0 to 1128.0 m asl), with a few dropstones (**Figure 3.4**) and one thin medium sand laminae. Above this sub-unit is a massive sand layer of varying grain size rich in granules and with small pebbles and at least one cobble, followed by muddy, subangular to subrounded, irregularly shaped, faceted pebbles of mixed lithology (sub-unit 3e; elevation range from 1129.5 to 1147.5 m asl). Overlying it is a fine sand sub-unit with stringers of granules about 2mm thick, laminations at the bottom, and small pebbles in the middle and top (elevation range from 1152.0 to 1156.0 m asl). It is followed by a layer of coarsening upward pebbles and cobbles (elevation range from 1156.5 to 1165.5 m asl). These are faceted, subangular to rounded and of mixed lithology. On top of this are very crude beds of fine to coarse sand in coarsening upward cycles with localized laminations and granules and angular pebbles of mixed lithology at the middle and bottom (elevation range from 1167.5 to 1176.9 m asl). Finally, at the top of the stratigraphic sequence are at least two thin fining upward pebble and cobble layers composed of faceted, subangular, felsic coarse-grained igneous clasts. These two cycles of coarsening-upward sand and gravel are classified as sub-units 3f and 4b.

The heterogeneous stratified layer at the bottom of sub-unit 1a is clearly non-glacial in origin due to the presence of organics. This diamicton and the clasts of sub-unit 1a are interpreted to be altered, weathered bedrock interlayered with sedimentary silts, clays and coals. Sub-unit 3d is interpreted as a distal facies of an ice-contact lake deposit. The sand and gravel of sub-unit 3e is interpreted to be glaciofluvial outwash. The two cycles of coarsening-upward sand and gravel of sub-units 3f and 4b are interpreted to be sediment gravity flows.

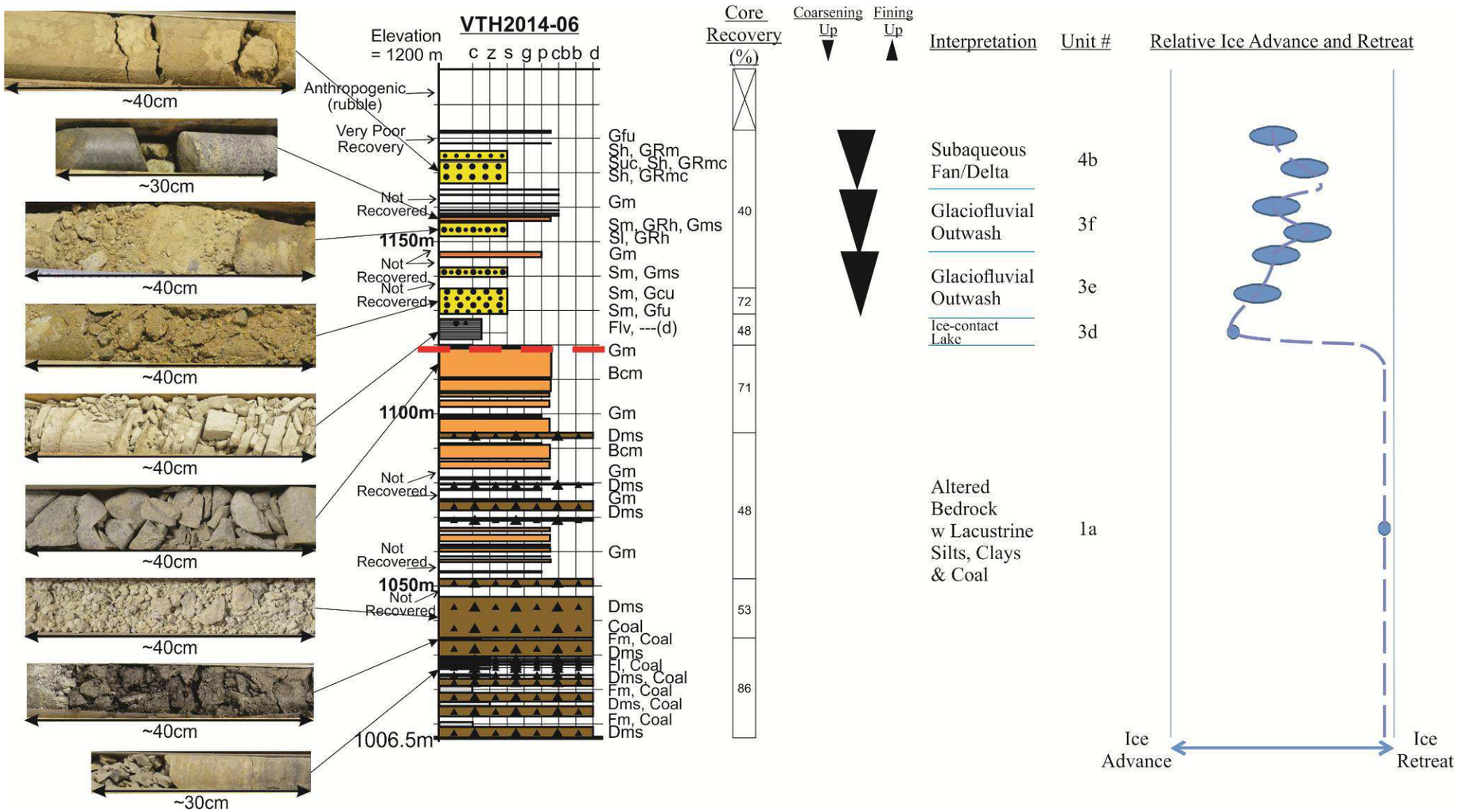

Figure 3.3 Stratigraphic log of core VTH-2014-06, located next to the Valley pit (see Figure 3.1 for location). The red dashed line corresponds to the base of the Quaternary sediments. See Table 3.1 for code description. Stratigraphic unit numbers correspond to the stratigraphic framework (cf. Sect. 3.2.3). Relative ice advance/retreat history is shown to the right; blue circles represent relative uncertainty.

Figure 3.4 Core VTH2014-06 at an elevation of 1127.21 to 1127.06m (sub-unit 3d), showing silt and clay rhythmites with dropstones.

3.1.3 Core VTH2014-07

Core VTH2014-07 is also from a borehole south of the Valley pit (**Figure 3.1c**). From base to top, the stratigraphy (**Figure 3.5**) begins with a matrix-supported, massive diamicton overlying weathered Guichon Creek Batholith bedrock (sub-unit 2a; elevation range: 1089.2 to 1100.7 m asl). The diamicton is clast-rich, mostly granule- to cobble-sized, with a silty matrix. The clasts consist of varied lithology and are angular to rounded and irregular in shape. The diamicton shows some internal structures such as few layers about 18-20 cm in thickness where granules are more abundant, as well as clasts that may have broken apart in-situ (due to the drilling process?). Overlying this is a heterogeneous sub-unit consisting of fine sand (2b) and the same type of clasts as the till below (elevation range: 1100.7 to 1106.4 m asl). Overlying this sub-unit is a ~21m thick clay sub-unit (3d) coarsening upward to silt (elevation range: 1106.4 to 1127.6 m asl). The lower, clay portion has pervasive horizontal breaks throughout, and a few localized clasts. The top of the clay portion is laminated with alternating sand-silt and clay couplets. The top of the sub-unit consists of horizontally bedded silt with oxidized laminations. Following sub-unit 3d is a thin layer of stratified fine sand with granules and small clasts (elevation range: 1127.6 to 1128.5 m asl); these clasts are angular to subangular, some broken in-situ, and increase in proportion, to about two thirds in the top half. Overlying it is a ~4m-thick sub-unit of clean, horizontally bedded sand with oxidized laminations (elevation range: 1128.5.6 to 1132.2 m asl), followed by a ~39m-thick sub-unit of alternating fine and medium bedded sand with a high concentration of granules and angular to subrounded pebbles and cobbles of varied lithology (elevation range: 1132.2

to 1171.6 m asl). Several of these clasts appear to be weathered as they could easily be disaggregated. The horizontally bedded sand and the overlying stratified and poorly-sorted gravelly layers comprise sub-unit 3e. The top of this sandy sub-unit grades into a series of diamictic or poorly-sorted layers including a thin matrix-supported, massive diamicton layer (sub-unit 4a) and a few layers containing sand, gravel, and larger clasts (sub-unit 4b) (elevation range: 1171.6 to 1186.6 m asl). The top portion of the stratigraphy is dominated by massive and matrix-supported diamictons (elevation range: 1186.6 to 1242.0 m asl). These diamictons have a silty fine sand matrix, granules, as well as faceted, irregularly-shaped, angular to rounded pebbles and cobbles of mixed lithology (sub-units 4c, 5b and 5d). They are interstratified with several thin granule-rich sand layers, some of which contain angular to rounded, faceted pebbles and cobbles of varied lithology (sub-units 5a, 5c and 5e). The bottom diamicton of this sequence (sub-unit 4c) is 20.5 m-thick. The uppermost unit (unit 6) consists of thin alternating laminae of fine sand and clay, capped by thin layers of faceted, irregularly-shaped, subangular pebbles and cobbles.

Sub-unit 2a is interpreted as a subglacial traction till, due to the varied lithology and rounded edges of its clasts. Sub-unit 3d is interpreted as a glacial (ice-contact) lake deposit. The alternating sand-silt and clay couplets resemble varves, and the clasts are interpreted as dropstones. The clay and silt sequence of sub-unit 3d records an ice retreat phase with sub-unit 2b possibly representing a subaqueous ice-marginal setting (e.g. grounding line). Sub-unit 3e is interpreted to be glaciofluvial outwash in origin. Sub-units 4a and 4b record an ice advance phase where subglacial till (4a) is interbedded with what appears to be outwash sediment (4b). Sub-unit 4c is interpreted as subglacial traction till, while the overlying stratified diamictons (sub-units 5b and 5d) with interbeds (sub-units 5a, 5c and 5e) are interpreted to record an oscillating ice margin. Unit 6 is interpreted as being deposited in a glacial outwash to fluvial setting.

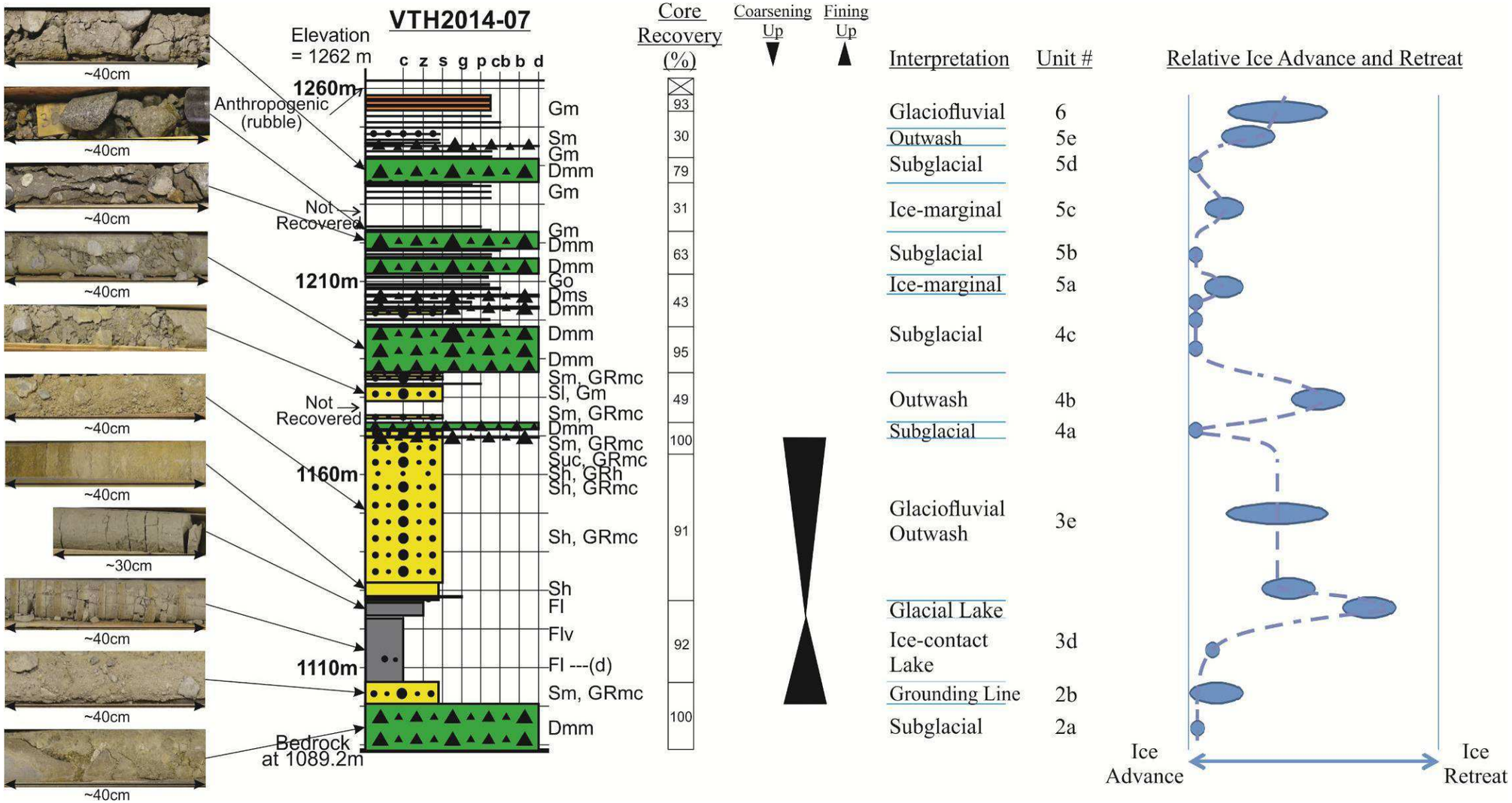

Figure 3.5 Stratigraphic log of core VTH-2014-07, located next to the Valley pit (see Figure 3.1 for location). See Table 3.1 for code descriptions. Stratigraphic unit numbers correspond to the stratigraphic framework (cf. Sect. 3.2.3). Relative ice advance/retreat history is shown to the right; blue circles represent relative uncertainty.

3.1.4 Core VTH2014-08

Core VTH2014-08 is from a borehole south of the Valley pit (**Figure 3.1c**) about 100 metres from core VTH2014-06. The lowermost sub-unit (1a) includes a massive diamicton consisting of highly weathered and altered rock with a poorly-sorted matrix ranging from clay to silt to sand (elevation range from 1023.1 to 1177.4 m asl) (**Figure 3.6**). It has an abundance of granules and pebbles, with most clasts being angular to subangular and monolithologic. This diamicton becomes increasingly crumbly, powdery and dominated by white, greasy argillic alteration going up the sub-unit. It is matrix-supported at the bottom, and clast-supported at the top, with the top consisting of highly disintegrated, fragmented rock similar to the diamicton below. Some thin, steeply-dipping layers of grey or red alteration and localized concentrations of flaky muscovite grains are present. The bottom of the diamicton is interlayered with thin beds of coal, clayey coal, sandy clay, organic-rich clay, hard clay with some smooth, shiny surfaces and silt, all with granule-rich sections and localized pebbles. The lowest clay interbeds of this sequence are friable. The top of the diamicton is interlayered with a significant amount of poorly-sorted, angular, irregularly shaped granules, pebbles and cobbles of a mostly coarse-grained lithology as well as sand with gravel. Sub-unit 1a is overlain by a sub-unit (3f) of granules and angular to subangular, irregularly-shaped pebbles and cobbles. Overlying 3f are thin beds of massive or stratified matrix-supported diamicton (sub-units 4a, 4c, 5b and 5d; elevation range from 1178.6 to 1251.5 m asl). The matrix has a silty-sandy texture with fine sand and silt laminations. The coarser clasts are angular to subrounded, faceted and irregularly-shaped. A few cobbles of various lithology and one boulder were also observed. They are interlayered with massive fine sand with some dark laminations, layered granules and small pebbles, laminated silt, as well as crudely stratified silty sand with granules and pebbles (sub-units 4b and 5c). Sub-unit 5a consists of cobbles and boulders that are subangular to subrounded, of mixed lithology, and either coarsen or fine upward. A number of clothes-iron-shaped pebbles typical of glacial deposits occur throughout. It is overlain by a bed of massive to laminated silt with dropstones (sub-unit 5f; elevation range from 1248.4 to 1252.3 m asl). The uppermost unit (6) contains several thin pebble- to boulder-sized clast layers. The clasts, mostly crystalline igneous rock, are irregularly-shaped with angular to subangular edges and sometimes faceted.

The sand and gravel interlayers of sub-unit 1a are interpreted to be the same altered bedrock as the diamicton; the differences are due to varying degrees of weathering. The friable clay layer at the base of the core is an exception; it is interpreted as lake sediment. This pre-glacial sub-unit 1a thus exhibits a complex stratigraphic succession including lake sediments, organic-rich layers, as well as thick diamictic units with breccia facies. These brecciated layers could record rock slides or falls, possibly earthquake-induced, as they show little evidence of transport (if any) by agents other than gravity. The overlying heterogeneous stratified sequence of sub-units 3f, 4a-c and 5a-d is interpreted as till (sub-units 4a, 4c, 5b and 5d) interlayered with sediment gravity flow (sub-unit 4b) and ice-marginal deposits (sub-units 3f, 5a and 5c). Sub-unit 5f is interpreted as an ice-contact lake. Unit 6 is interpreted as glaciofluvial in origin.

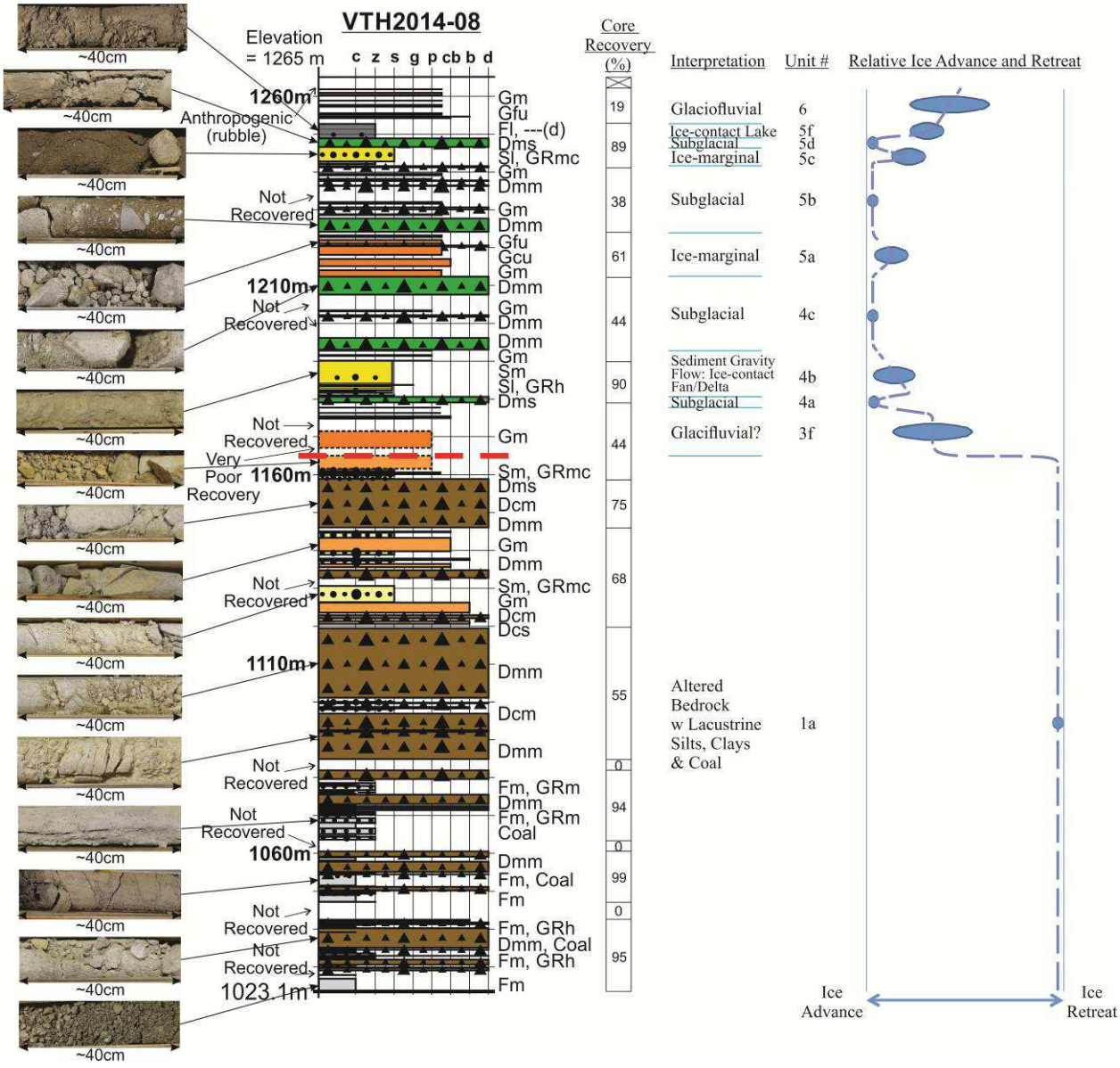

Figure 3.6 Stratigraphic log of core VTH-2014-08, located next to the Valley pit (see Figure 3.1 for location). The red dashed line corresponds to the base of the Quaternary sediments. See Table 3.1 for code descriptions. Stratigraphic unit numbers correspond to the stratigraphic framework (cf. Sect. 3.2.3). Relative ice advance/retreat history is shown to the right; blue circles represent relative uncertainty.

3.1.5 Core VTH2014-09

Core VTH2014-09 is from the same area as cores VTH2014-06 and VTH2014-08 (**Figure 3.1c**). The lowermost sub-unit (sub-unit 1a; elevation range: 1023.8 to 1075.1 m asl) consists of numerous, thin, interlayered beds and lenses of sand, silt, clay, coal and organics (**Figure 3.7**). The sand beds range from fine- to coarse-grained with some containing granules and small pebbles. Laminations, trough cross-beds, and coarsening-upward trends occur within these sand beds. Some localized trough lamination and granules with small pebbles are found in the siltier layers as well. The clay laminations are friable at the bottom of this sequence. It is overlain by a ~46m-thick diamicton (elevation range: 1075.1 to 1121.3 m asl) which is matrix-supported and stratified at its base and transitions upward to massive and clast-supported at the top. The silty clay matrix has dipping, blue-gray, clay lenses, as well as granules and angular, felsic, coarse-grained, igneous pebbles, cobbles and boulders. Some of the larger fragments are particularly angular; the entire diamicton appears to be derived from weathered or altered rock. Flaky muscovite grains occur throughout the sub-unit. This ~40m thick sub-unit (1a) is overlain by a ~68m-thick unit consisting predominantly of sandy layers in a coarsening upward sequence (unit 3; elevation range: 1122.8 to 1190.5 m asl). Granules, pebbles and few cobbles occur within these sand layers. These larger clasts are angular to subangular, mostly irregularly shaped, and of mixed lithology. A few are iron-shaped or faceted. The sandy unit is interstratified with layers containing more abundant pebbles and cobbles, which increase in proportion up the unit. Several of these pebbly layers are oxidized and contain pebbles with more rounded edges. Overlying this is a matrix-supported, massive diamicton (elevation range: 1190.5 to 1228.8 m asl). The diamicton (sub-units 4c and 5b) is characterized by a particularly wide grain size range from a clayey matrix to boulder-sized clasts. The clasts are angular to rounded but mostly subangular, and irregular, iron or bullet-shaped (**Figure 3.8**), with some being faceted. Notably, striations were observed on a few clasts. One thin interval of the diamicton shows clast gradation and textural layering (**Figure 3.9**). Another shows an apparent strong fabric with numerous horizontally aligned clasts (**Figure 3.10**). The upper portion of the till is interlayered with thin coarse-grained intervals containing mostly pebbles, cobbles, and boulders (sub-units 5a and 5c). The uppermost unit 6 consists of thin coarse layers with pebbles, cobbles, and boulders often arranged in fining-upward cycles.

The friable clay laminations at the bottom of sub-unit 1a are interpreted to be lacustrine sediment. Based on the core observations, there is little (if any) evidence of sedimentary transport in the thick diamictic layer at the top of sub-unit 1a. However, considering this layer as in situ altered bedrock would be problematic as it overlies stratified sedimentary rocks. This unusual stratigraphy could indicate reverse faulting or a large rock slide that moved a thick coherent slab of rock over stratified rocks. The latter interpretation is preferred due to the interstratification of this breccia-like material with other types of sedimentary rock layers at similar elevations in other nearby cores (cf. VTH2014-08). The sandy and coarsening-upward sequence of unit 3 is interpreted to be a glaciofluvial outwash deposit. The diamicton of sub-units 4c and 5b has clear evidence for a glacial origin (iron or bullet-shaped clasts with striations) and it is interpreted as a subglacial traction till. The localized stratification and grading (observed as clast gradation and textural layering) may be evidence for local reworking or resedimentation (Evans, 2017). The coarse-grained interlayers in the till (sub-units 5a and 5c) could indicate an increase in subglacial meltwater activity or a transition to an ice-marginal setting. Unit 6 is interpreted as glaciofluvial in origin.

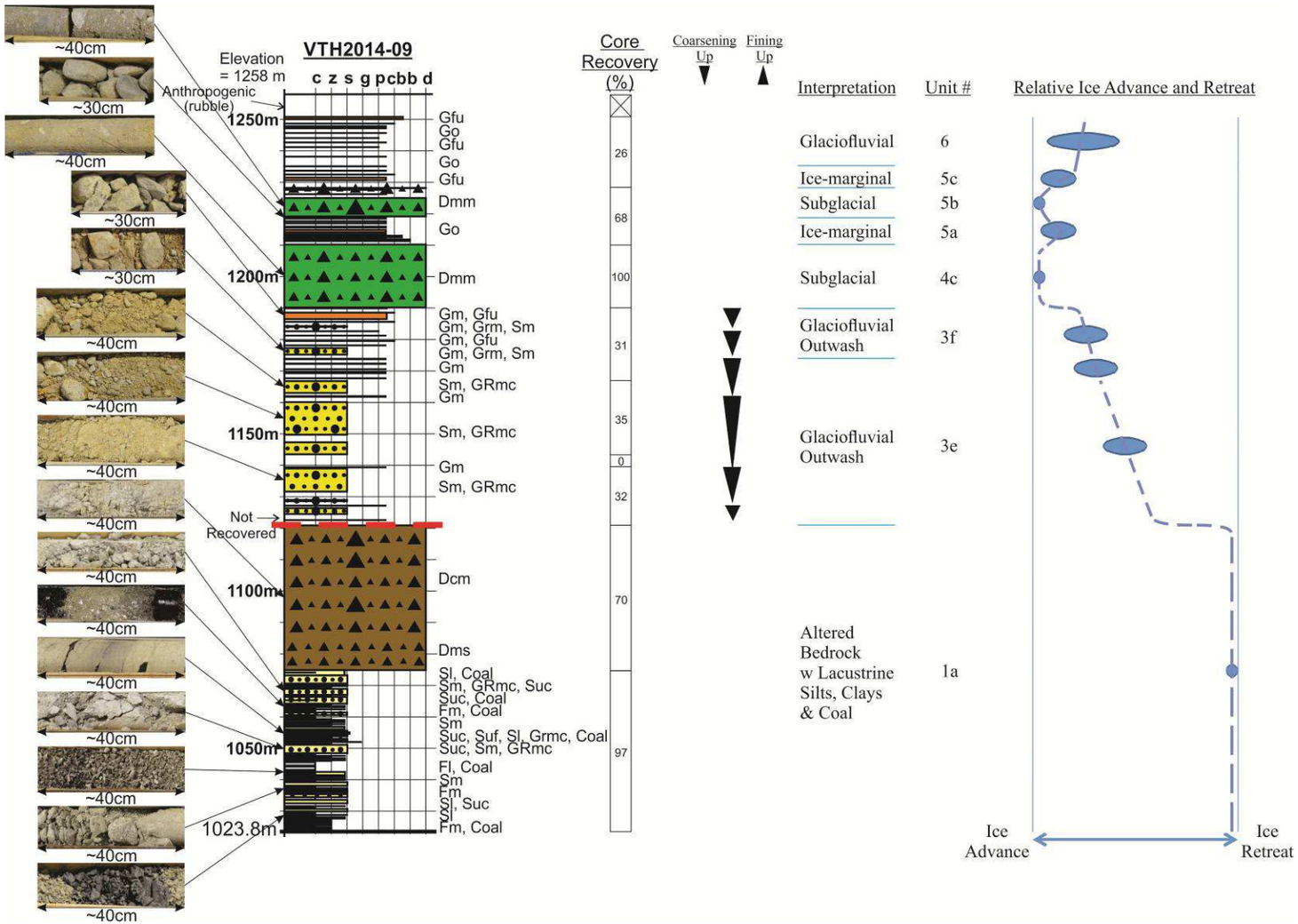

Figure 3.7 Stratigraphic log of core VTH-2014-09, located next to the Valley pit (see Figure 3.1 for location). The red dashed line corresponds to the base of the Quaternary sediments. See Table 3.1 for code descriptions. Stratigraphic unit numbers correspond to the stratigraphic framework (cf. Sect. 3.2.3). Relative ice advance/retreat history is shown to the right; blue circles represent relative uncertainty.

Figure 3.8 A bullet-shaped pebble found in the till of core VTH2014-09 at an elevation of approximately 1206.5m.

Figure 3.9 Core VTH2014-09 at an elevation of 1207.9 to 1207.4m, showing textural layering and clast gradation forming a distinct interbed within a diamicton sub-unit.

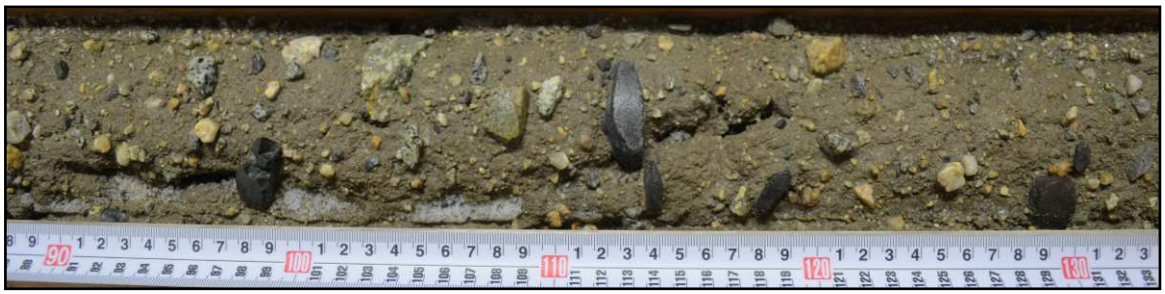

Figure 3.10 Core VTH2014-09 at an elevation of 1206.4 to 1206.0m, showing preferred horizontal orientation of clasts in the diamicton sub-unit.

3.1.6 Core VTH2014-10

Core VTH2014-10 is located between cores VTH2014-07 and VTH2014-09 (**Figure 3.1c**). The lowermost sub-unit (elevation range from 1041.9 to 1048.2 m asl) is composed of sand that is rich in granules (sub-unit 1a; **Figure 3.11**). This is overlain by a sub-unit (1b) consisting of fine to medium sand with granules, pebbles and occasional cobbles (elevation range from 1048.2 to 1078.5 m asl). The larger clasts are angular to rounded, irregularly shaped, and composed of varied lithologies. Some of them have been broken in-situ, and they are flat and elongated at the bottom. There are also localized thin coal beds and laminae and localized bands of oxidation or organic-rich material within the sub-unit. It is heterogeneous and interstratified with a few thin layers of matrix-supported massive diamicton at the middle. The diamicton is characterized by a silty matrix, granules and pebbles that are angular to rounded, irregularly shaped and composed of various lithologies. Overlying these beds is a diamicton bed (sub-unit 2a) with a silt matrix, granules, pebbles, cobbles and boulders (elevation range from 1079.4 to 1102.5 m asl). The larger clasts are angular to rounded, irregularly shaped, and some have disintegrated. Localized oxidation and stratification of the matrix with colour changes near the middle are present. The top portion of sub-unit 2a is interrupted by beds of sand with or without gravel, a thin layer of pebbles and cobbles fining upward to granules, other thin interbeds of pebbles and cobbles and a layer of silty clay. The larger clasts are irregularly shaped, sometimes faceted, angular to subrounded pebbles and cobbles. Overlying sub-unit 2a is a thin fine sand layer with a granule-rich bottom which fines upward to silt and then to more clayey sediment (elevation range from 1103.0 to 1115.1 m asl), which forms the bottom half of sub-unit 3d in this core. The clay-rich layer has a fissile structure. The top portion of this sub-unit (3d) consists of a layer of fissile fine sand with cm-scale beds of clay or granules, interbedded with the same type of diamicton found below, a very thin granule and pebble layer, and laminae and a bed of silt (elevation range from 1115.4 to 1128.2 m asl). It is overlain by clean sand and layers of poorly-sorted massive fine sand mixed with granules and larger clasts (elevation range from 1128.2 to 1153.7 m asl). The clasts are irregularly shaped, angular to subrounded pebbles and cobbles of varied but mostly felsic coarse-grained igneous lithology. Above sub-unit 3d are several thin layers of faceted, angular to subrounded pebbles and cobbles of mostly coarse-grained but also fine-grained igneous lithology (elevation range from 1155.4 to 1169.3 m asl). Some layers show

normal grading (fining-upward trend). These more heterogeneous layers form sub-unit 3e. The clast layers (sub-unit 4b) alternate with thin beds of a matrix-supported, massive diamicton (sub-unit 4a) for about 18m (elevation range from 1169.3 to 1179.6 m asl). The diamicton has a clayey to silty fine-sand matrix, granules, pebbles and cobbles. The clasts are faceted, irregularly shaped, angular to subangular and of variable lithology. Several pebbles are weathered and prone to disaggregation. The top part of the stratigraphy is dominated by matrix-supported, stratified diamictons with several interbeds. The diamictons (sub-units 4c, 5b and 5d) have a silty matrix, as well as granules and faceted, irregularly shaped, angular to subrounded pebbles and cobbles of varied lithologies. A thin bed of brittle, highly fractured silty clay (Fm) is found within sub-unit 4c (elevation range from 1186.9 to 1187.2 m asl). In between the diamicton sub-units, there are a few thin sandy beds with granules and pebbles and several thin layers of faceted, angular to subrounded pebbles and cobbles which sometimes coarsen upward (sub-units 5a and 5c). They are capped by a 7.5m-thick unit of the same type of pebbles and cobbles (unit 6).

Sub-unit 1a is interpreted to be disintegrated bedrock, due to the uniform lithology and angular nature of its clasts. The presence of thin diamictic layers in sub-unit 1b could indicate debris flows and proximity of ice (glaciofluvial?). The clasts of sub-unit 2a, like sub-unit 1b, are varied in lithology and have rounded edges; however, the grain size distribution of sub-unit 2a is more consistent than that of sub-unit 1b. Sub-unit 2a is thus interpreted to be subglacial till with outwash material. The contrasting layers of sub-unit 3d are interpreted to have been deposited in an ice-contact lake environment under the influence of an oscillating ice margin. The heterogeneous layers of sub-unit 3e are interpreted to be deposited in a glaciofluvial outwash environment. Sub-units 4a and 4b could represent an oscillating ice margin environment, although they could well be entirely subglacial with till and subglacial glaciofluvial layers interstratified. The diamictons of sub-units 4c, 5b and 5d are interpreted to be subglacial, and the clast layers with or without sand (sub-units 5a and 5c) ice-marginal. The thin bed of brittle, highly fractured silty clay (Fm) found within sub-unit 4c (elevation range from 1186.9 to 1187.2 m asl) is of uncertain origin. Unit 6 is interpreted to be glaciofluvial in origin.

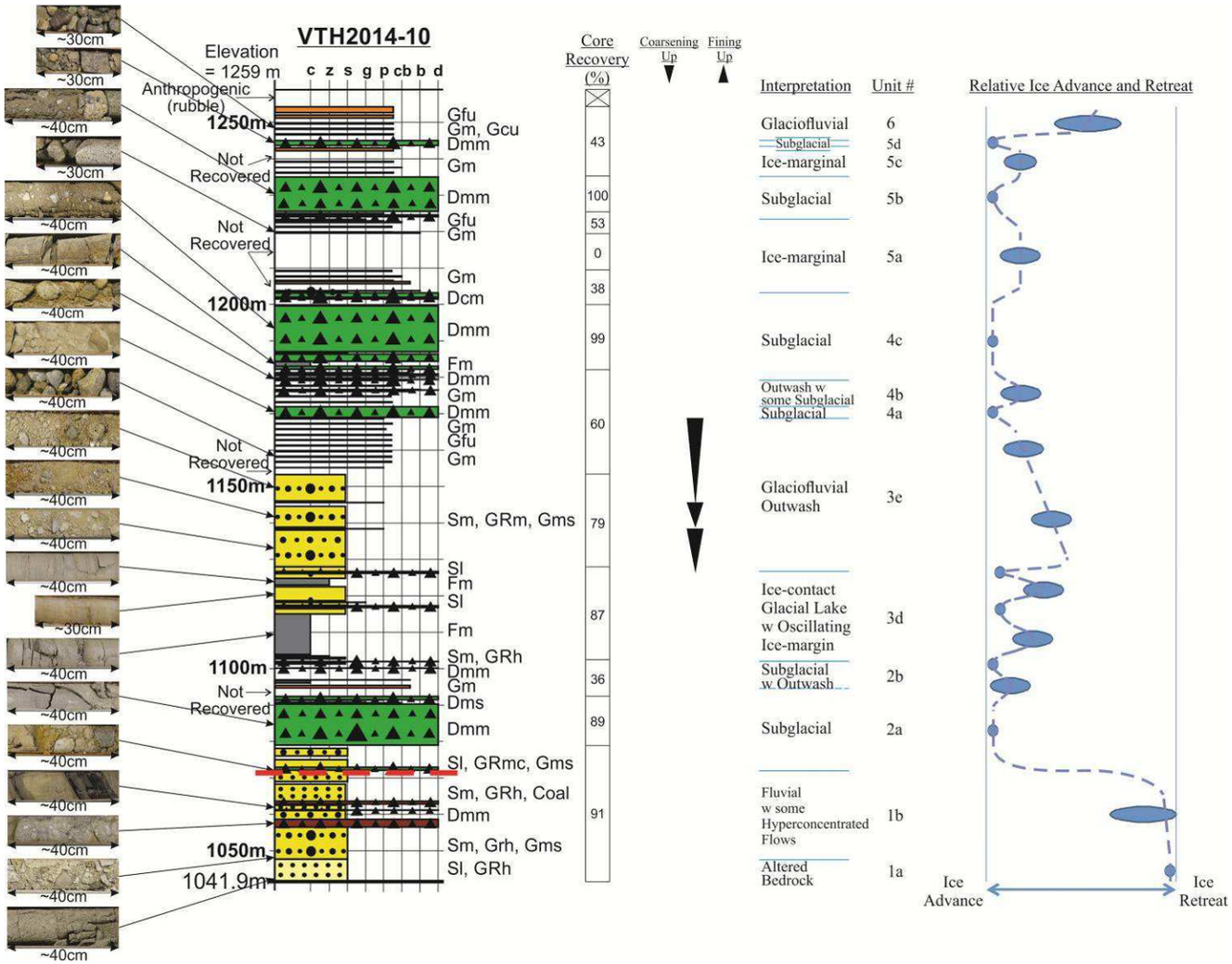

Figure 3.11 Stratigraphic log of core VTH-2014-10, located next to the Valley pit (see Figure 3.1 for location). The red dashed line corresponds to the base of the Quaternary sediments. See Table 3.1 for code descriptions. Stratigraphic unit numbers correspond to the stratigraphic framework (cf. Sect. 3.2.3). Relative ice advance/retreat history is shown to the right; blue circles represent relative uncertainty.

3.1.7 Core VTH2014-11

Core VTH2014-11 is from a borehole located about 100m southeast of core VTH2014-06 (**Figure 3.1c**). The stratigraphy (**Figure 3.12**) begins with a massive, hard and dense clay layer with a 1m-thick coal interbed (elevation range: 1043.9 to 1051.5 m asl). It is overlain by a diamicton interbedded with clay, silt, coal and other organic-rich layers (elevation range: 1051.5 to 1107.7 m asl). The diamicton is matrix-supported, except for a segment near the top that is clast-supported. The latter is mostly massive, except for the bottom part and one segment in the middle which is stratified. It is composed of white, greasy, argillaceous and disintegrating rock with a silt matrix, as well as granules and some irregularly-shaped, angular to subrounded, felsic coarse-grained igneous pebbles. Some clay interbeds are hard and dense, with few darker, smooth, shiny surfaces, whereas others are soft & crumbly. The silt interbeds are soft at the bottom of the sub-unit, and get stiffer towards the top. It is overlain by a ~58m-thick layer of diamicton (elevation range: 1107.7 to 1165.2 m asl) similar to the one below, although more massive. This upper diamicton is thus generally massive and dominantly matrix-supported, except at the bottom where it is clast-supported. There is also one layer of angular, irregularly shaped, felsic coarse-grained igneous pebbles and cobbles in the middle of this diamicton (elevation range: 1148.0 to 1145.9 m asl), which are highly disintegrated clasts of the same type as that found in the diamicton. This sequence (sub-unit 1a) is overlain by a thin matrix-supported massive diamicton (elevation range: 1165.2 to 1168.3 m asl). This diamicton (sub-unit 4a) has a silt matrix, granules and faceted, irregularly shaped, subangular to subrounded pebbles and cobbles. It is overlain by a ~31m-thick sub-unit of massive, gravely sand with a few faceted, irregularly shaped, angular to rounded pebbles and cobbles (sub-unit 4b; elevation range: 1168.3 to 1199.3 m asl). The clasts show a wide variety of lithologies and some are brittle and prone to disintegration. The stratification in the upper portion of the sub-unit is more clearly defined, and it has several thin layers of faceted, angular to subangular pebbles and cobbles which are mostly weathered and oxidized rock fragments. The lithology is varied but the dominant one is felsic coarse-grained igneous. Overlying sub-unit 4b is another matrix-supported, massive diamicton (sub-unit 4c; elevation range: 1204.8 to 1217.0 m asl). It has a silty clay matrix, granules, and faceted, irregularly shaped, angular to sub-rounded pebbles and cobbles of a varied lithology. The remaining

upper portion of the core consists of thin diamictic layers interstratified with massive sand, silt and clay, as well as layers rich in pebbles and cobbles (unit 5). The sand layers are massive and some contain granules and faceted, irregularly shaped, subangular, igneous pebbles. The pebble and cobble layers are characterized by faceted, irregularly shaped, angular to rounded clasts of mixed lithology. The top is capped by a ~8m-thick layer of pebbles and cobbles of the same type (unit 6).

The massive, hard and dense clay layer with the coal interbed at the bottom of the stratigraphy is interpreted to be lacustrine. Sub-unit 1a is interpreted as non-glacial disintegrated bedrock interlayered with sedimentary silts, clays and coal. The overall texture, the mixed lithologies of the clasts and their shapes together suggest a glacial origin for sub-unit 4a. The sand and gravel of sub-unit 4b is interpreted to be a sediment gravity flow deposit. The diamicton of sub-unit 4c is also interpreted to be glacial in origin. The diamictic layers of unit 5 appear to be washed-out till, while the others are ice-marginal sediments. Unit 6 is interpreted to be glaciofluvial in origin.

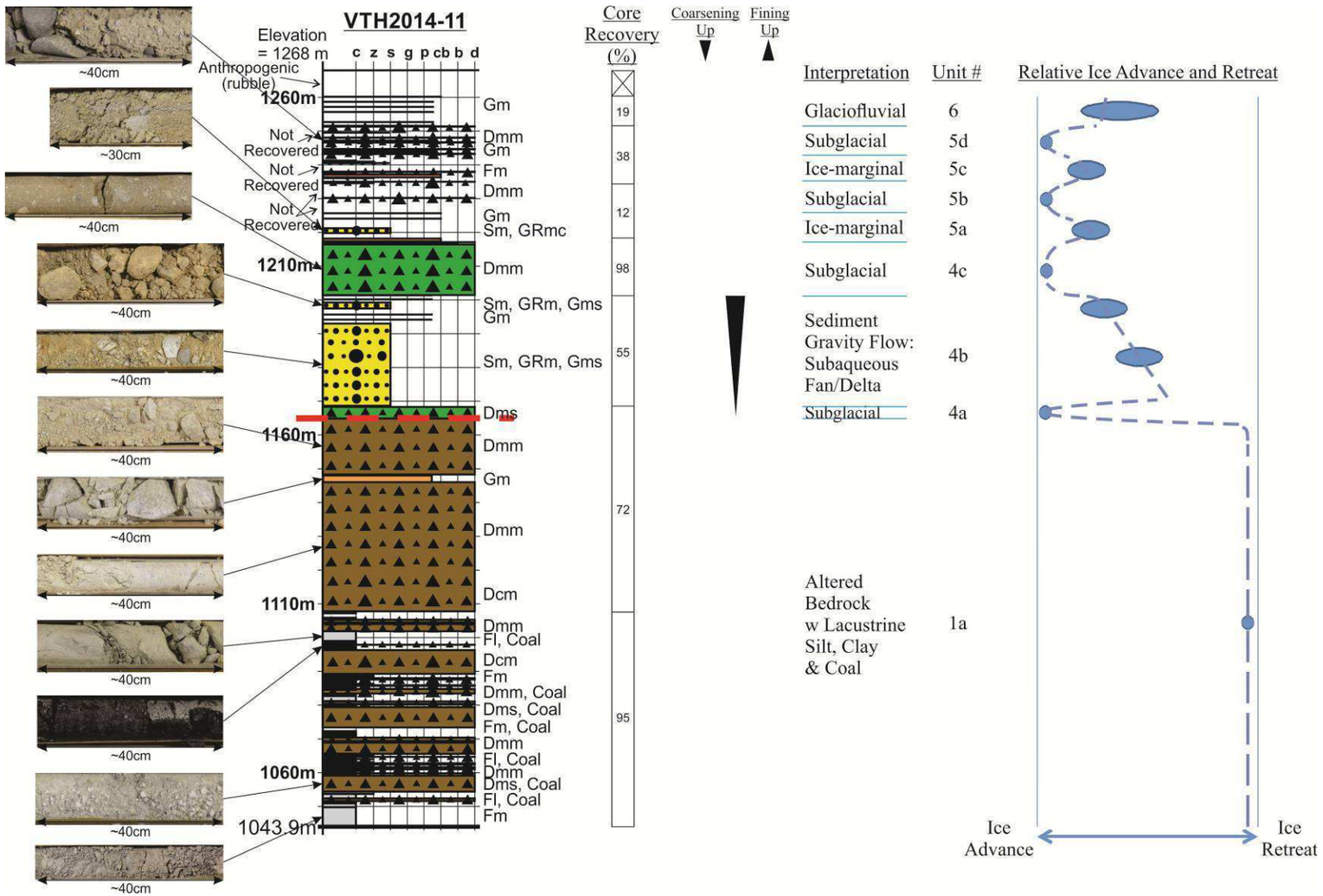

Figure 3.12 Stratigraphic log of core VTH-2014-11, located next to the Valley pit (see Figure 3.1 for location). The red dashed line corresponds to the base of the Quaternary sediments. See Table 3.1 for code descriptions. Stratigraphic unit numbers correspond to the stratigraphic framework (cf. Sect. 3.2.3). Relative ice advance/retreat history is shown to the right; blue circles represent relative uncertainty.

3.1.8 Core VTH2014-13A

Core VTH2014-13A is from a borehole located approximately halfway between cores VTH2014-03 and VTH2014-07 (**Figure 3.1c**). The lowermost sub-unit (3d: ranging from 1127.1 to 1133.9 m asl) consists of fissile laminated silty clay directly overlying weathered Guichon Creek Batholith bedrock that becomes massive clayey silt in its uppermost part (**Figure 3.13**). It is overlain by matrix-supported, massive diamictons (sub-unit 4a ranging from 1033.9 to 1153.8 m asl, sub-unit 4c ranging from 1168.5 to 1176.0 m asl, and sub-unit 5b ranging from 1183.5 to 1209.9 m asl). The diamictons have a silt matrix, granules and faceted, irregularly shaped, angular to rounded pebbles and cobbles. These clasts are often weathered and of mixed lithology. The fine-grained igneous clasts are generally more rounded than the coarse-grained igneous ones. Sub-unit 4b is a massive poorly-sorted gravelly sand with layers of pebbles with occasional cobbles (elevation range: 1153.8 m asl to 1168.5 m asl). Sub-unit 5a consists of pebbles and cobbles (elevation range: 1176.0 to 1183.5 m asl). Sub-unit 5c is composed of gravelly sand with pebbles and cobbles (elevation range: 1209.9 to 1213.6 m asl). The pebbles and cobbles of sub-units 4b, 5a and 5c are faceted, irregularly shaped, angular to rounded, often highly weathered and igneous. The stratigraphy is capped by a ~30m-thick unit (6) consisting of pebbles and cobbles layers like those below, with a very thin interbed of washed-out sand with faceted, subangular, igneous pebbles and cobbles.

Sub-unit 3d is interpreted to be glaciolacustrine. The diamictons of sub-units 4a, 4c and 5b are interpreted to be subglacial traction till. Sub-unit 4b is interpreted to be outwash, while sub-units 5a and 5c are interpreted to be ice-marginal deposits. Unit 6 is interpreted to be mostly glaciofluvial in origin, with some ice-marginal at the bottom.

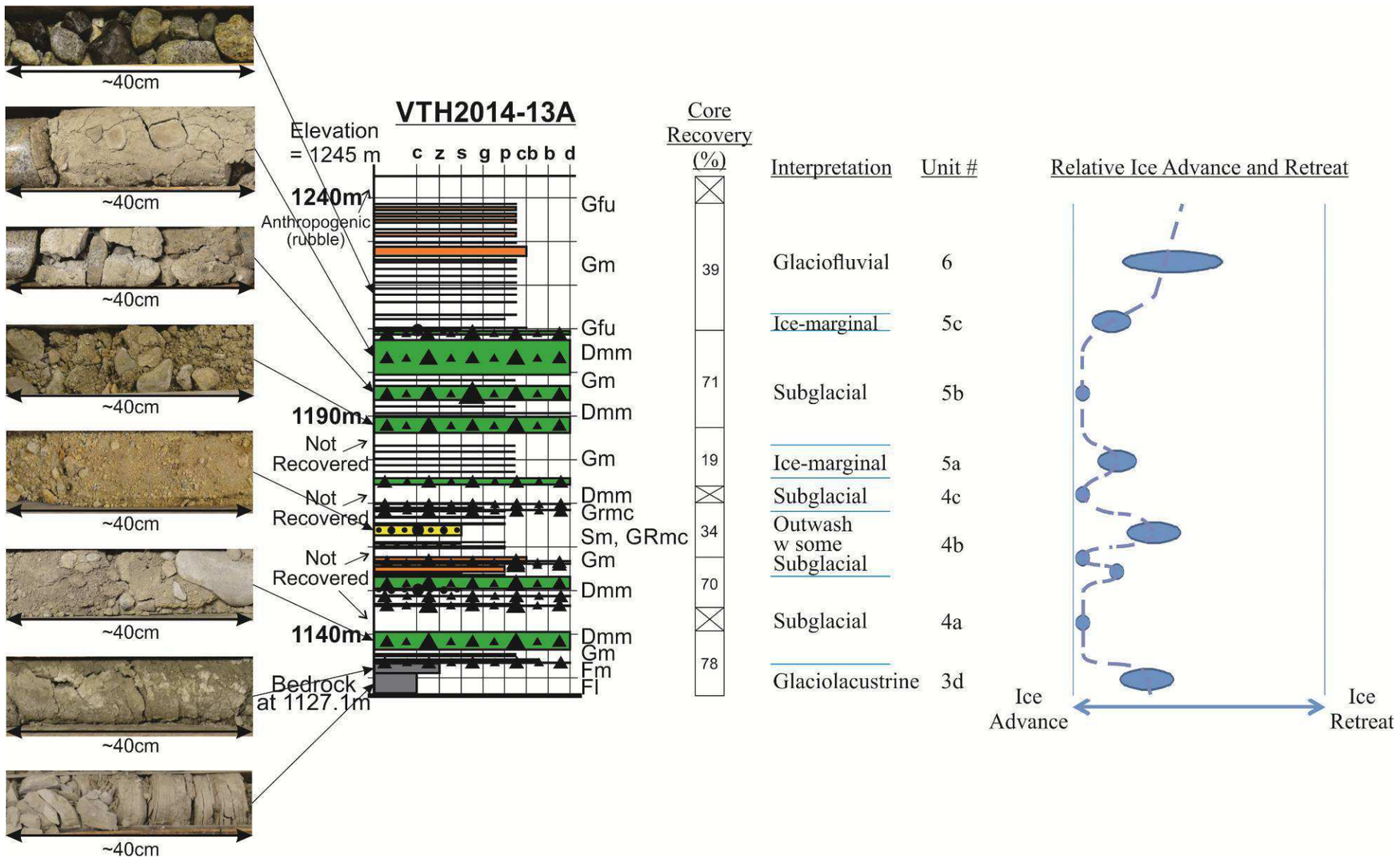

Figure 3.13 Stratigraphic log of core VTH-2014-13A, located next to the Valley pit (see Figure 3.1 for location). See Table 3.1 for code descriptions. Stratigraphic unit numbers correspond to the stratigraphic framework (cf. Sect. 3.2.3). Relative ice advance/retreat history is shown to the right; blue circles represent relative uncertainty.

3.1.9 Core JA16-001

Core JA16-001 is from a borehole drilled over the J.A. target (**Figure 3.1a**). The stratigraphy (**Figure 3.14**) begins with a unit (elevation range from 1021.2 to 1061.0 m asl) consisting of coarse material, mainly pebbles, cobbles and occasional boulders overlying Guichon Creek batholith bedrock. These clasts are elongate to irregularly shaped with angular to subangular edges. They are all grey in colour and coarse-grained igneous rocks. The clasts are not oxidized, suggesting a reduced environment during the subsequent burial and emplacement of these materials. This unit is interrupted by a few thin layers of massive silty clay, massive silt, and a matrix-supported, massive diamicton. This diamicton has a silty clay matrix, granules, pebbles and cobbles. The large clasts are also mostly grey coarse-grained igneous rocks, but a few are fine-grained igneous, and some display a greater degree of edge rounding. The diamicton becomes more dominant going up the succession (elevation range from 1061.7 to 1068.7 m asl). Minor coal laminae appear in an intervening silty clay bed. Another diamicton overlies this (elevation range from 1069.7 to 1075.7 m asl), with a wider range of lithologies and less angularity of its clasts. It is interrupted by a layer of pebbles and cobbles. Overlying this is a 16.6m-thick clay unit (elevation range from 1075.7 to 1092.3 m asl), which is laminated with silt in its lower portion. Above the laminated portion, the clay is mostly massive, with planar or gently dipping fractures, slickensides and offset horizons. Within the middle portion of the clay unit, angular to subangular, dark fine-grained igneous pebbles occur. The unit also contains near the top a lamina and irregular pockets of black sand. It is overlain by a thin (1.3m) diamicton, which is in turn overlain by an heterogeneous massive unit consisting of medium to coarse sand, granules, as well as pebbles and cobbles which are igneous, angular to rounded, faceted, and elongated or irregularly shaped (elevation range from 1093.6 to 1097.3 m asl). A ~33m-thick unit consisting of coarse particles, mainly pebbles and cobbles (elevation range from 1097.7 to 1131.1 m asl) overlies this thin unit. Most clasts are faceted, irregularly shaped, subangular to subrounded, and of varied lithology, although fine-grained igneous clasts appear to dominate. The unit appears to be crudely stratified as some small-scale, stacked coarsening-upward trends were observed, especially near the middle of the unit. It becomes sandier at the top. This sequence is overlain by a ~33m-thick unit consisting mostly of massive silt, with minor

clayey layers, as well as a dark sand layer near the top (elevation range from 1132.2 to 1164.8 m asl). The unit grades into a matrix-supported diamicton, which dominates the top of the stratigraphy at this location. The diamicton has a silt matrix with varying amounts of clay, granules, and faceted, irregularly shaped, angular to subrounded pebbles, cobbles and boulders of a mixed lithology. This diamicton is interbedded with thin layers of faceted, irregularly shaped, angular to subangular pebbles, cobbles or boulders of a mostly felsic coarse-grained igneous lithology. The top is capped by thin massive, fine to coarse layers of sand with very few granules.

The coarse unit at the bottom of the stratigraphy (elevation range from 1021.2 to 1061.0 m asl) is interpreted to be rockfall material. The interlayered diamicton and fine sediments are interpreted to be fluvial sediments deposited amongst the rockfall clasts. The diamicton sequence ranging in elevation from 1061.7 to 1068.7 m asl is interpreted as non-glacial in origin due to the presence of coal laminae. The overlying diamicton (elevation range from 1069.7 to 1075.7 m asl) is interpreted as glacial in origin due to its wider range of lithologies and less angularity of its clasts. The pebble and cobble layer within this till is interpreted as outwash. The presence of isolated clasts within the otherwise clay-rich unit ranging from 1075.7 to 1092.3 m asl points to a possible ice-contact environment (i.e. dropstones). If the clay unit with dropstones records a glacial lake, the capping diamicton could be glacial in origin. The overlying two units (elevation range from 1093.6 to 1131.1 m asl) are interpreted to be a sediment gravity flow. The massive silt unit with minor clayey layers and sand near the top (elevation range from 1132.2 to 1164.8 m asl) is interpreted to be lacustrine. The top diamicton unit has all the typical characteristic of a till and is thus glacial in origin. The capping sand is interpreted to be outwash material.

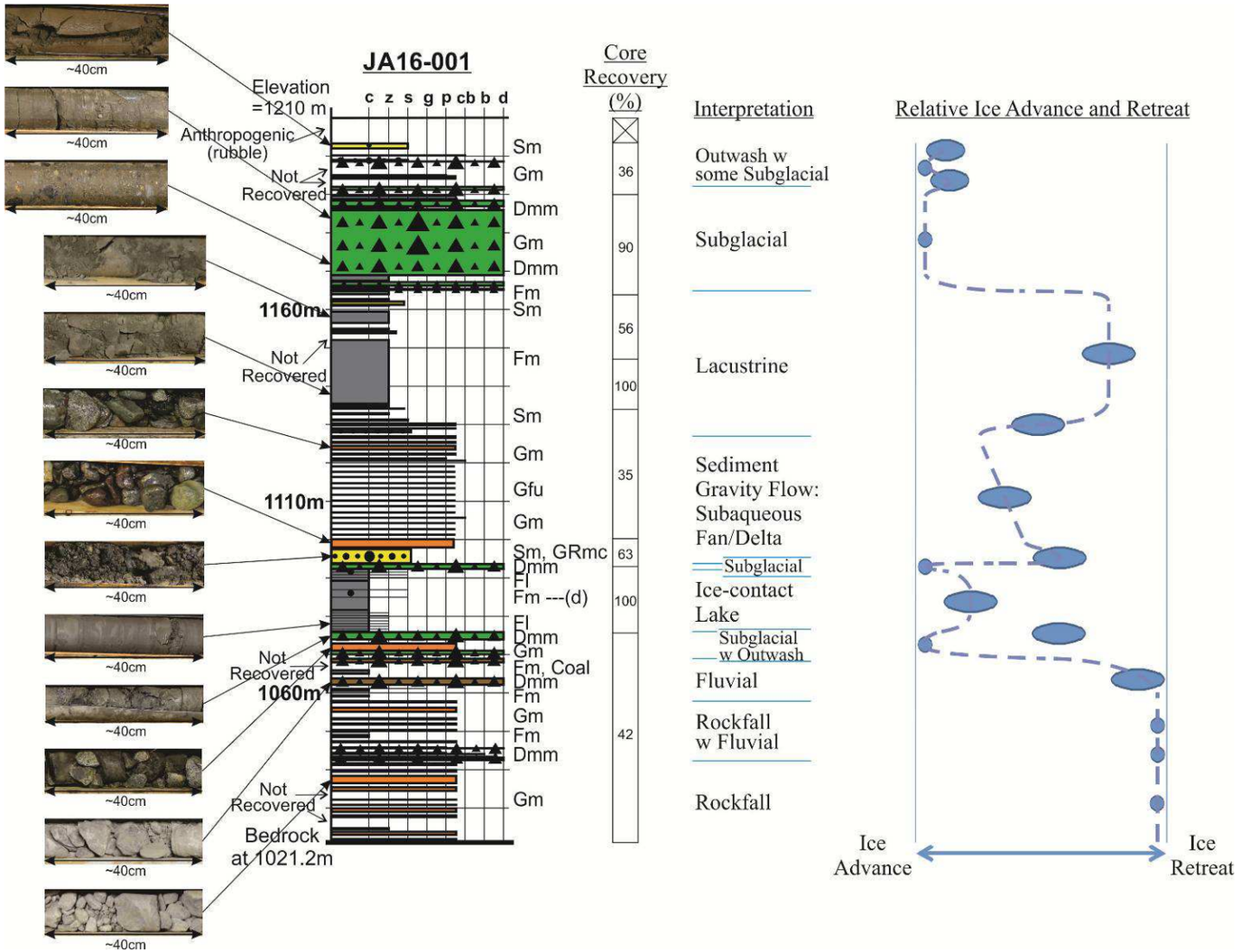

Figure 3.14 Stratigraphic log of core JA16-001, located at the J.A. target (see Figure 3.1 for location). See Table 3.1 for code descriptions. Stratigraphic unit numbers correspond to the stratigraphic framework (cf. Sect. 3.2.3). Relative ice advance/retreat history is shown to the right; blue circles represent relative uncertainty.

3.2 Geological Cross-Sections Linking Valley Pit Drillcores

Neighbouring borehole logs for the Valley pit cores were aligned vertically and horizontally and their units correlated to one another. Cross-sections were produced to show the stratigraphic architecture of the area of the boreholes just south of the Valley pit (**Figure 3.15**).

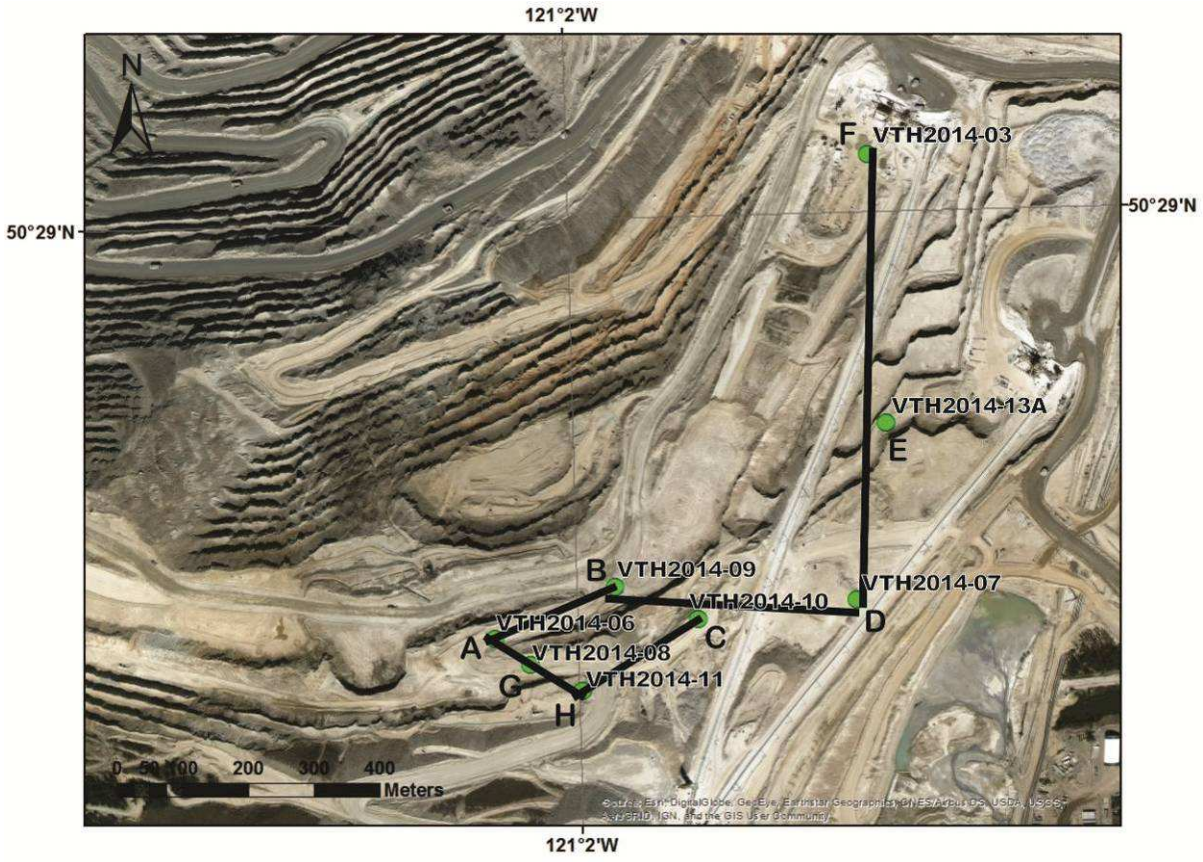

Figure 3.15 Position of cross-section lines.

3.2.1 Cross-Section A-B-C-D

This cross-section correlates boreholes VTH2014-08, VTH-2014-09, VTH-2014-10 and VTH2014-07 (**Figure 3.16**). It first shows thinning of Unit 1 towards the east and the concomitant rise of underlying igneous bedrock. The bedrock here is part of the altered bedrock footprint of the HVC system. It also shows that sub-unit 3e forms a tabular unit

extending over more than 500 meters from somewhere between boreholes 08 and 09, towards the east beyond borehole 07. Laterally extensive layers of crudely stratified poorly-sorted sand and gravel is a typical architectural element of braided river deposits that form by lateral and/or downstream accretion of gravel and sandy bars (Miall, 2010). The overlying stratigraphic succession (4a-c, 5a-d, and 6) appears consistent and relatively continuous between borehole 07 and 10, although with some clear lateral facies transitions which lead to some uncertainties about correlations. Nonetheless, it is more continuous than between boreholes 10, 09 and 08 because some diamicton layers are clearly missing in 09, such as sub-unit 4a. The top portion of unit 5, sub-units 5e and 5f, are only found at boreholes 07 and 08, respectively. That portion of unit 5 could have been more eroded at borehole 09 by fluvial processes related to unit 6, which is also thicker at that location. Glaciofluvial unit 6 is laterally continuous across all four boreholes.

Table 3.2 Legend of sediment types used in cross-sections.

Colour/Symbol	Sediment Type
	Altered rock diamicton of sub-unit 1a
	Silt and clay of sub-unit 1a
	Sand of sub-unit 1a
	Pebbles and cobbles of sub-unit 1a
	Other non-glacial diamicton
	Other pebbles and cobbles
	Other sand
	Other silt and clay
	Bedrock
● ▲	Clasts (circular for non-glacial, triangular for glacial sediment)
—	Laminations
~~	Deformation

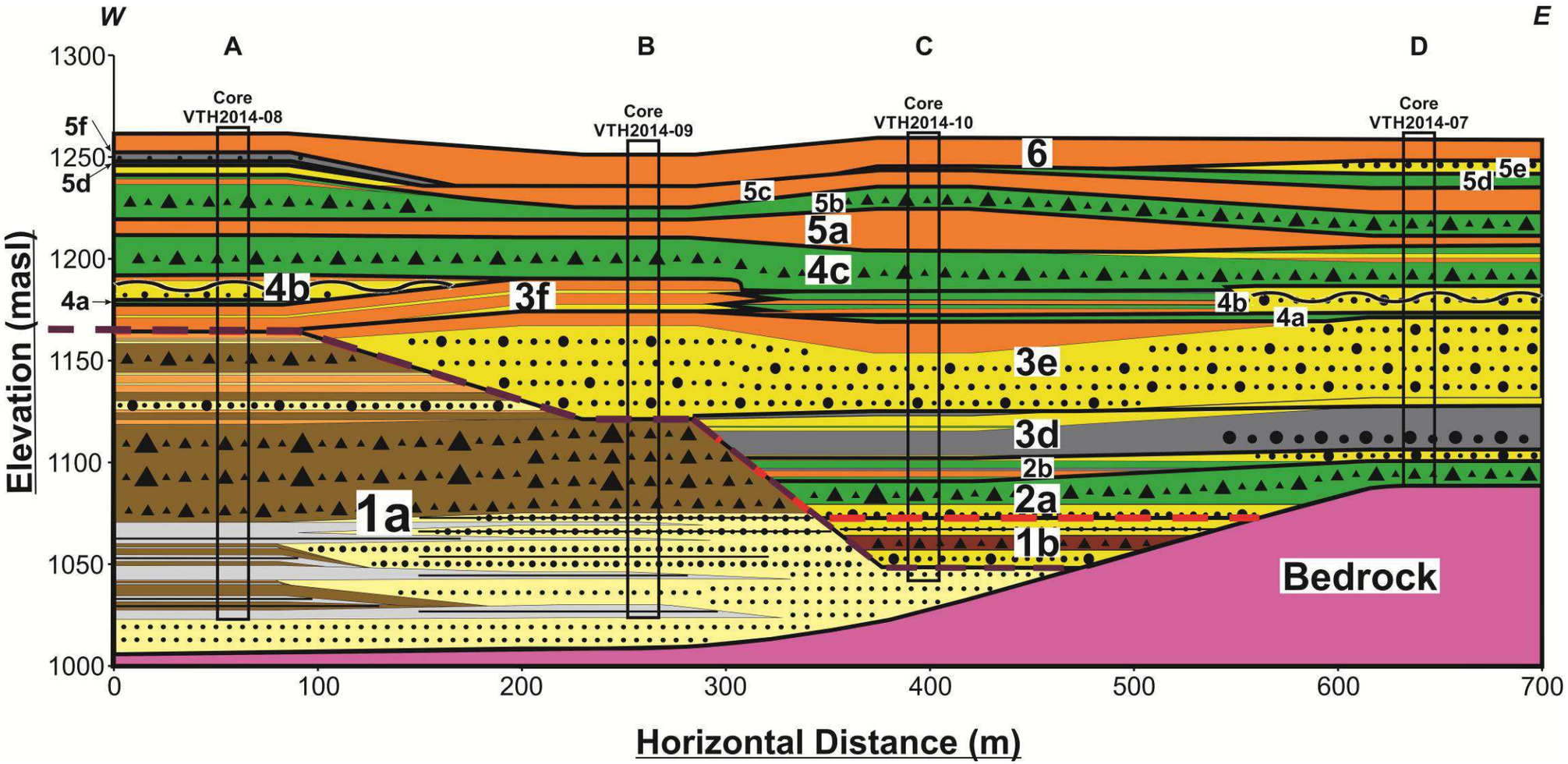

Figure 3.16 Interpreted cross-section through boreholes VTH2014-09, VTH2014-10 and VTH2014-07. See Table 3.2 for legend. The purple dashed line marks the unconformity between the altered bedrock sequence and the overlying unconsolidated sediments. The bedrock is granitic and part of the HVC alteration footprint. The red dashed line marks the unconformity between the pre-Quaternary material and the overlying Quaternary sediments. See Figure 3.15 for location.

3.2.2 Cross-Section F-E-D

This cross-section correlates boreholes VTH-2014-03, VTH-2014-13A and VTH2014-07 (**Figure 3.17**). These are the only three boreholes where unit 1 is missing. It indicates that unit 1 in all its complexity is spatially discontinuous and could be missing along most of the southeastern edge of the valley pit. It shows an irregular topography of the underlying igneous bedrock and its effect on the overlying stratigraphic architecture. Its northern end contains the lowest or deepest Quaternary rhythmites of all the studied cores; this layer corresponds to sub-unit 3a, which does not occur in the other cores. The unit overlying the rhythmites consists of poorly-sorted sand and gravel layers; this is sub-unit 3b. A succession of silt and clay and poorly-sorted sand and gravel sheets also occur at the base of borehole 07 at about 700 meters to the south, although at a much higher elevation. Specifically, the elevation difference between the rhythmites at the base of borehole 03 versus those at the base of borehole 07 is about 50 meters. This is a large elevation difference for lateral correlation of horizontally deposited laminated (lake) sediments. Therefore, and despite the similarities in the two sub-units (3a vs 3d), these are considered two distinct stratigraphic sub-units as shown in **Figure 3.17**. In addition to this, higher and thus younger layers of similar poorly-sorted sand/gravel continue to occur up the succession in borehole 03 at the same elevation as those of sub-unit 3e in borehole 07 and others.

The cross-section also shows more till deposition over the bedrock high, which points to more subglacial erosion of pre-existing layers (units 2 and 3) at that location and subsequent deposition of younger till. Finally, this cross-section indicates a northern limit to the extent of the uppermost glaciofluvial unit 6.

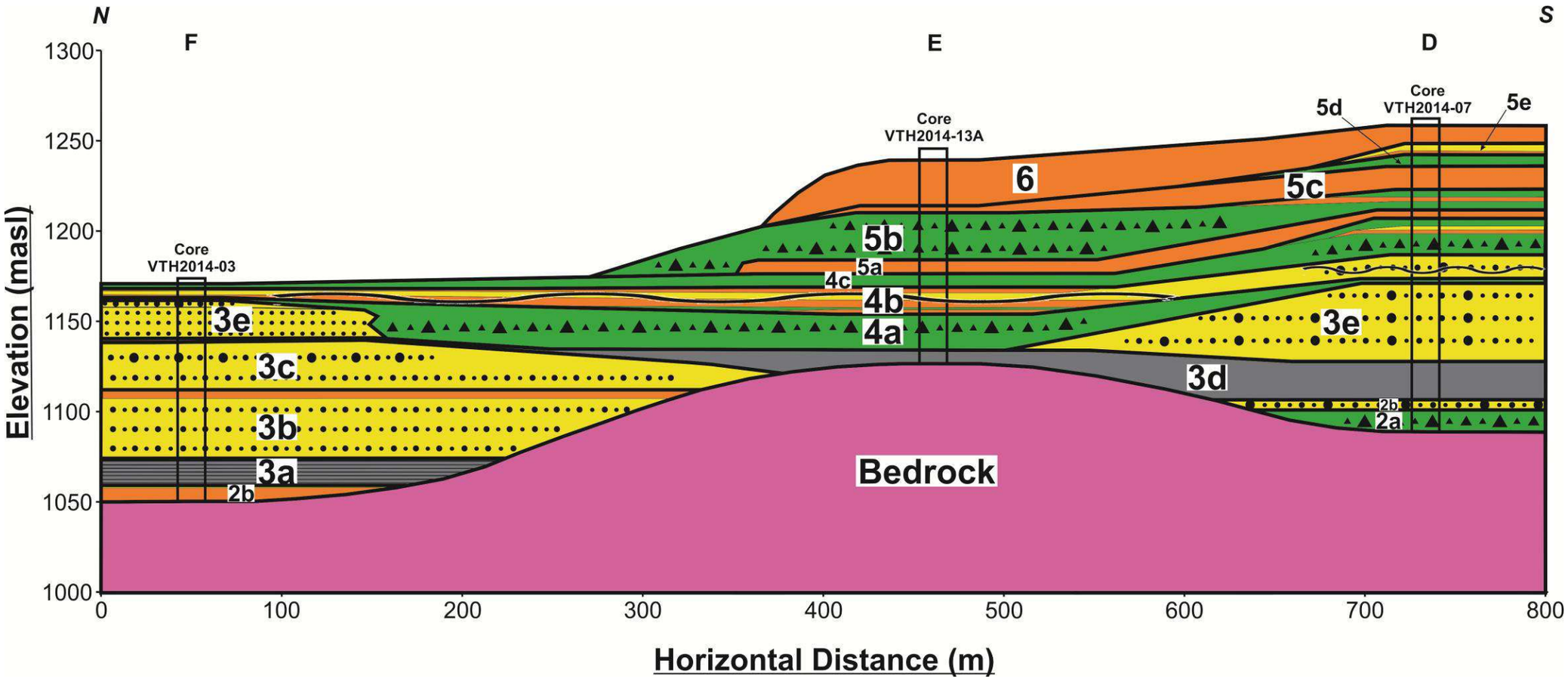

Figure 3.17 Interpreted cross-section through boreholes VTH2014-03, VTH2014-13A and VTH2014-07. See Table 3.2 for legend. The bedrock is granitic. See Figure 3.15 for location.

3.2.3 Cross-Section A-G-H

This cross-section correlates boreholes VTH-2014-08, VTH-2014-06 and VTH2014-11 (**Figure 3.18**). Overall, thirteen sub-units have been correlated across the three cores. At the base is unit 1a which has been identified at the base of all three boreholes. Assuming the elevation of all the boreholes are correct, the stratigraphic architecture shows some flexure of unit 1a along that cross-section. It appears to be the case based on the presence of part of unit 3 above sub-unit 1a at borehole VTH-2014-06, which is largely missing at the other two boreholes. The overlying glacial units show a consistent stratigraphy between borehole 08 and 11 and they were thus correlated.

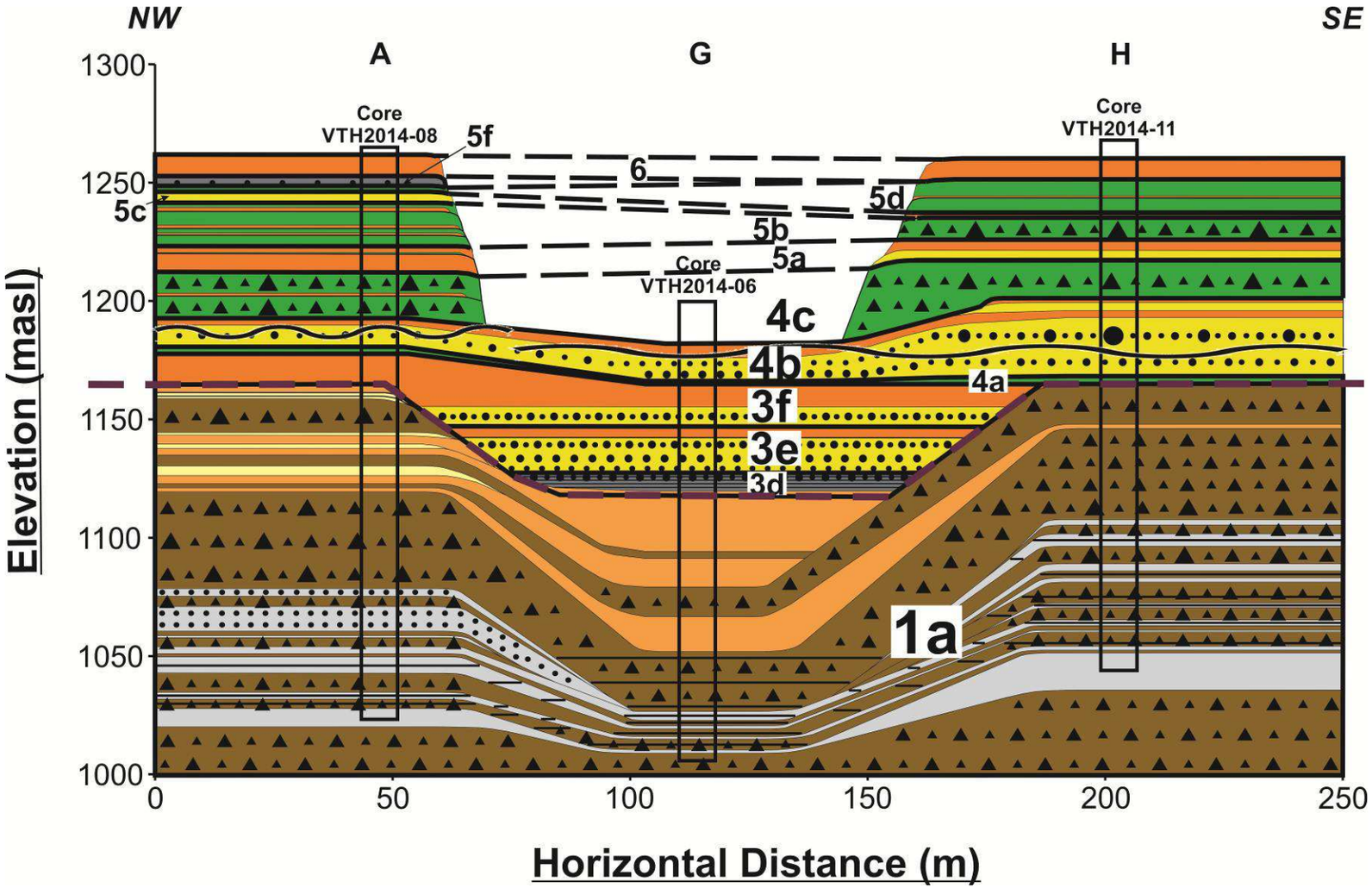

Figure 3.18 Interpreted cross-section through boreholes VTH2014-08, VTH2014-06 and VTH2014-11. See Table 3.2 for legend. The purple dashed line marks the unconformity between the pre-Quaternary altered bedrock sequence and the overlying Quaternary unconsolidated sediments. See Figure 3.15 for location.

3.2.4 Cross-Section H-C

This cross-section correlates boreholes VTH-2014-11 and VTH2014-10 (**Figure 3.19**). This section also shows the drop in elevation towards the east/northeast of the upper bounding surface of Unit 1 that is also observable from other cross-sections nearby. Here, it is drawn or interpreted as a sharp vertical step, but it could also be more gradual. Two similarly thick poorly-sorted stratified layers identified at both boreholes 11 and 10 are considered to belong to sub-unit 4b and 3e, respectively, rather than the same unit. This interpretative decision is due to the presence of the diamicton layer at about 1170 m asl which is considered to belong to sub-unit 4a, which also occurs at a similar elevation in borehole 07 (cf. Figure 3.24). It is also based on the evidence that these crudely stratified sediments appear to form tabular sheets that extend horizontally across other transects. The correlation of the rest of the succession (units 4c, 5, and 6) is more straightforward with most sub-units being laterally continuous with minor facies transitions.

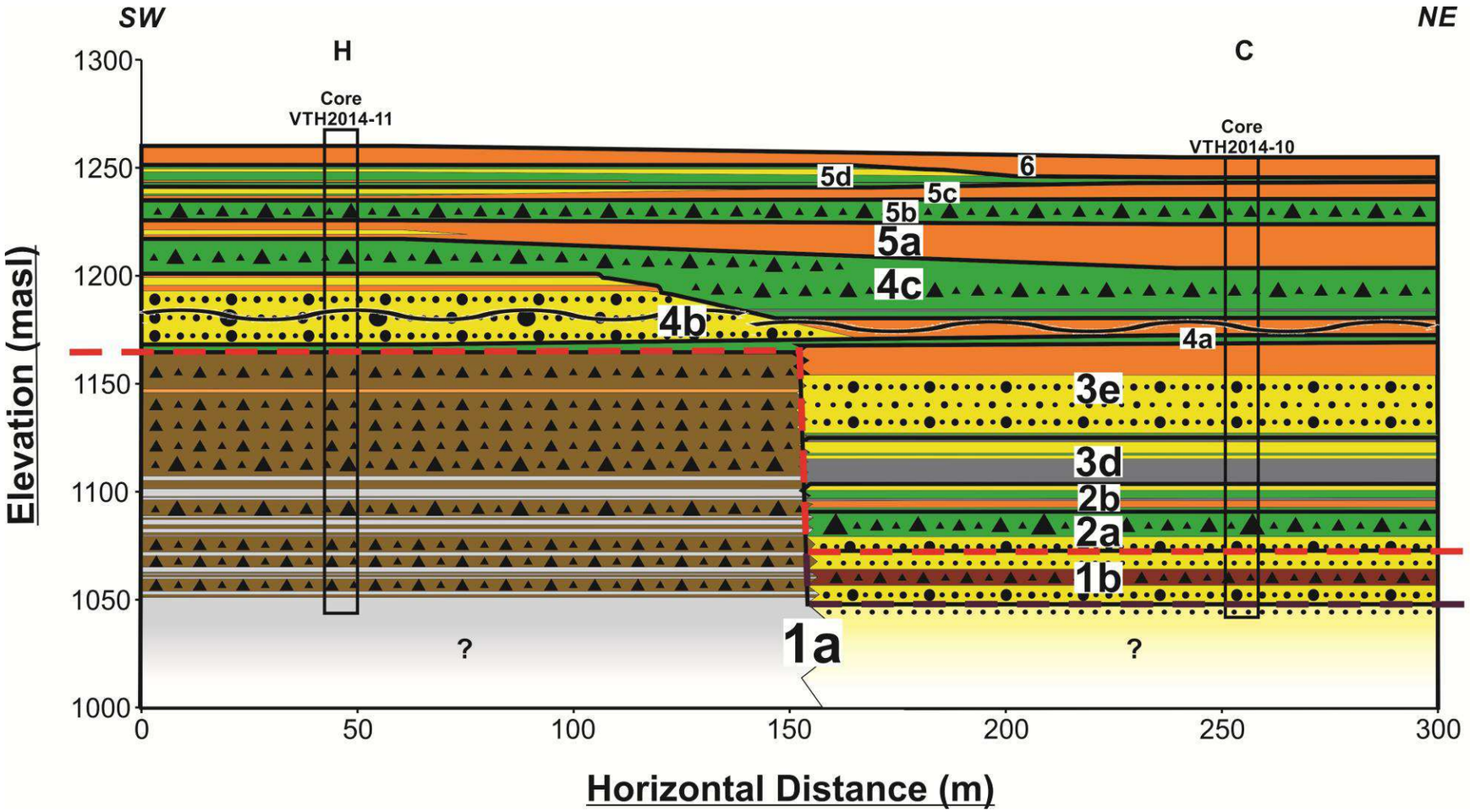

Figure 3.19 Interpreted cross-section through boreholes VTH2014-11 and VTH2014-10. See Table 3.2 for legend. The purple dashed line marks the unconformity between the altered bedrock sequence and the overlying unconsolidated sediments. The red dashed line marks the unconformity between the pre-Quaternary material and the overlying Quaternary sediments. The sharp vertical step of the top surface of sub-unit 1a between the two borehole could be more gradual. See Figure 3.15 for location.

3.3 Stratigraphic Analysis of J.A. Area

The seismic profile and core JA16-001 are shown in **Figure 3.20** and the 2-D stratigraphy is interpreted. The log of core JA16-001 (**Figure 3.14**) is overlain on the cross-section at the correct position along the transect and is shown to scale vertically. Solid coloured lines mark the tops of different horizontal units in the subsurface. Dashed coloured lines are extended out from these unit boundaries and connect to major unit boundaries of the core JA16-001 core stratigraphy. The coloured lines follow the main seismic reflectors, where seismic waves were reflected back to the receivers; typically these reflectors represent geological boundaries in the subsurface (Pugin et al, 2004). This occurs where there is a high-density contrast between two consecutive units. The topmost reflector (red line) traces to approximately where a lacustrine silt unit transitions into an underlying major sediment gravity flow pebble and cobble unit in JA16-001 core. The reflector at about 150 ms (yellow dashed line) seems to correspond to the boundary between ice-contact lake clay and an underlying major rockfall pebble and cobble unit in the JA16-001 core. The deepest reflector (green line) traces to approximately where a non-glacial diamicton interpreted as rockfall deposits with fluvial material transitions into a rockfall pebble and cobble unit in the JA16-001 core. There is also an intervening clay layer there, but it is likely too thin to have caused a reflector and appear on the seismic profile. These stratigraphic boundaries have been extended outwards from the JA16-001 borehole for up to 683m. The units seen in the seismic profile are relatively planar and level, indicating that the stratigraphy seen in the JA16-001 core is consistent laterally for at least about 700 metres in the southeast direction. This lends support to the proposed correlations between the valley cores nearby and presented above (Sect. 3.2) with the resulting tabular style of the stratigraphic architecture for several units in the study area.

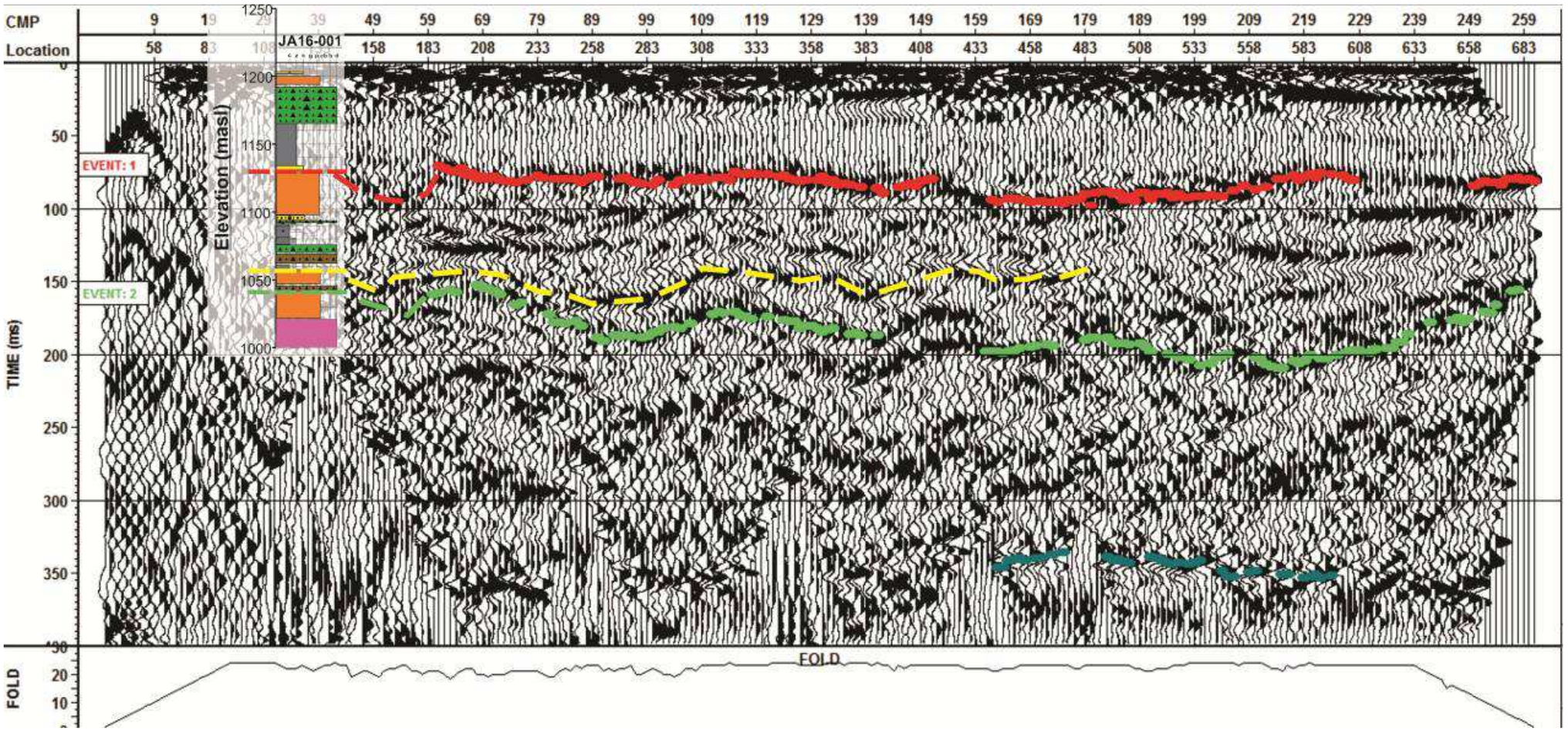

Figure 3.20 The seismic section of the survey done running across the JA16-001 borehole, with the JA16-001 log (see Figure 3.14) shown to scale vertically. Colored lines mark the tops of different horizontal boundaries in the subsurface; the ones within the unconsolidated sediments are correlated to contacts in the JA16-001 log.

3.4 Valley Pit Units

The sediment at site VP-1 in the Valley pit consists of a stiff, poorly-sorted diamicton with a sand or silt matrix, and subangular clasts up to boulder size of both local and distal lithologies (**Figure 3.21**). It is interpreted to be debris flow material. Its crude stratification differentiates it from till deposited directly by the ice. A thin outwash bed of laminated sand and/or silt is also present.

Figure 3.21 Section at location VP-1 on the northeast wall of the Valley Pit. Photo faces northeast. A stiff, poorly-sorted debris flow and thin outwash bed of laminated sand and/or silt are observed.

The stratigraphy at VP-2 contains dipping beds of stratified sand (**Figure 3.22**). This is overlain by unstructured material that is poorly-sorted and rich in coarse clasts, especially large cobbles and boulders. These beds are overlain by a massive, poorly-sorted material with a silt or sand matrix and subangular, boulder-size and smaller clasts of varying lithologies. The stratified, dipping sand is correlated to sub-unit 4b of the core units, and the top diamicton to one of the till sub-units 4c, 5b or 5d.

Figure 3.22 Section at location VP-2 on the northeast wall of the Valley Pit. Photo faces northeast. Dipping beds of stratified sand are overlain by poorly-sorted material. This section is correlated to sub-unit 4b.

The sediments at VP-3 consist mostly of anthropogenic material (part of the mine operation; **Figure 3.23**). This highly stiff, poorly-sorted and somewhat steeply-bedded material is interbedded with large angular clasts at one location. A thin layer of planar and gently dipping laminated fine-grained sediments is visible at the bottom, which is correlated to sub-unit 3d of the core units.

Figure 3.23 Section at location VP-3 on the east wall of the Valley Pit. Most of it consists of steeply-bedded avalanche material. Planar and gently dipping laminated fine sediments are visible underneath. Photo faces east. The bottom laminated sediments are correlated to sub-unit 3d.

At VP-4 there are units of bedded sand and laminated fine sediments (**Figure 3.24**). There is also a poorly-sorted massive diamicton with a silt or sand matrix with abundant subangular to subrounded clasts of all sizes and multiple lithologies. These units display glaciotectonic deformation, such as folds and steeply dipping beds. It is correlated to sub-unit 4b of the core units.

Figure 3.24 Section at location VP-4 on the northeast wall of the Valley Pit, exhibiting soft-sediment deformations. Photo faces northeast. This section is correlated to sub-unit 4b.

The stratigraphic sequence at VP-5 (**Figure 3.25**) is composed mostly of a thick layer of gently dipping beds of sandy sediment. Several beds and laminae are locally oxidized to varying degrees, however it was not observed further to the southeast. The coarser layers were likely a conduit for groundwater in a vadose zone setting, and therefore became oxidized, giving this unit an orange colour. These beds dip to the southeast at an angle of about 20°, which is within the normal range for a depositional interpretation. It is tentatively correlated to sub-units 3e and 3f of the core units (cf. Sect. 3.5.5 for details). This assumes lateral variation across the sub-units, and is uncertain.

Figure 3.25 Section at location VP-5 on the northeast wall of the Valley Pit, composed of dipping beds of sandy sediment. Photo faces northeast. This section is tentatively correlated to sub-units 3e and 3f.

The stratigraphy at VP-6 (**Figure 3.26**) consists of laminated clay, silt and fine sand. The beds are inclined by a few degrees. Organic matter (black colouring) and minor amounts of coal are present. It is correlated to sub-unit 3d of the core units, based on similar characteristics and thickness.

Figure 3.26 Section at location VP-6 on the north wall of the Valley Pit, where laminated, clay, silt and fine sand with organics are present. Photo faces northeast.

3.5 Composite Stratigraphic Framework

This section provides a summary of the stratigraphic units in the chronological order in which they were deposited and an interpretation of the depositional processes and environments which formed them. An understanding of the erosion, transport and deposition of the different sedimentary units and their place in the unconsolidated geological history of the area will be useful for explaining patterns in the concentrations of mineral and geochemical indicators of mineralization in these sediments.

Alain Plouffe of the Geological Survey of Canada identified and photographed some unconsolidated sediment units in the Valley pit, and correlated them to those of Bobrowsky et al.'s (1993) framework (Pers. comm); see "Valley Pit Observations by Alain Plouffe" in Appendix A.

3.5.1 Stratigraphic Framework

The stratigraphic units observed in the unconsolidated sediments around the Valley Pit are presented below as a stratigraphic framework for the area (**Figure 3.27**). A brief description, photos and interpretation are presented for each sub-unit in **Table 3.3**.

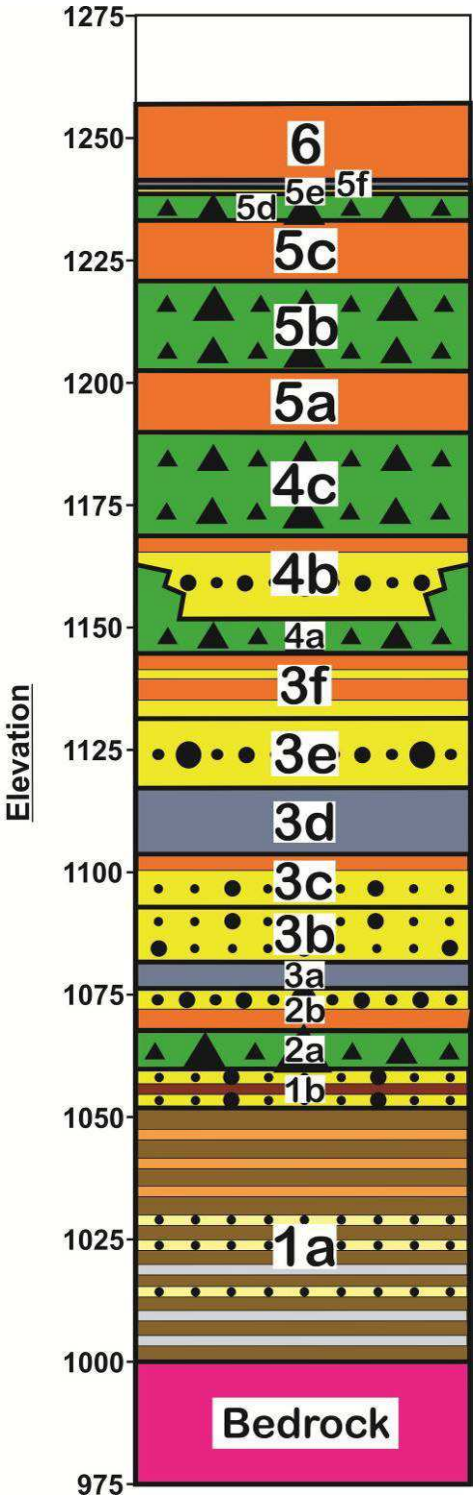

Figure 3.27 Composite stratigraphic framework for the unconsolidated sediments around the Valley pit. Elevations are average. See table 3.4 for legend. The stratigraphy consists of altered bedrock diamicton (1a) overlying bedrock, followed by other non-glacial diamicton, tills, pebbles and cobbles, sands, silts and clays.

Table 3.3 Description, photo and interpretation of each sub-unit of the unconsolidated sediment stratigraphy around the Valley pit.

Unit Number	Member	Description	Example Photo	Interpretation
1	a	• diamicton • white, crumbly, powdery & greasy • clasts angular and monolithic • interlayered with clays, silts, thin coals and organic-rich horizons in bottom half and breccias in top half • localized slickensides, granules, pebbles and organics present in clay and silt beds • matrix of bottom half becomes sandy at VTH2014-09	 ~40cm	• fault movement of Lornex and Highland Valley faults broke and crushed bedrock • further breakdown by clay alteration • disintegrated bedrock gradually fell/slid onto clay and silt sediments and coal as they were being deposited
	b	• sandy gravel with interbeds of sand • bottom locally-derived clasts subangular, elongate and flat • distal clasts blocky, more rounded • punctuated by a matrix-supported massive diamicton • some of pebbles rounded • coal and organics at top	 ~40cm	• outwash valley train punctuated by hyperconcentrated flow

2	a	• matrix-supported diamicton • intervening clast layers and silty clay bed in the Valley area	 ~40cm	• subglacial traction till • intervening clast pavements and a canal fill
	b	• heterogeneous • sand • gravel • clay • some diamicton	 ~40cm	• subglacial • outwash
3	a	• laminated clay	 ~30cm	• lacustrine
	b	• sand and gravel coarsening upward to pebbles and cobbles	 ~40cm	• sediment gravity flow • subaqueous delta or fan

	c	• fine sand and gravel coarsening upward to pebbles and cobbles	 ~40cm	• subaqueous delta or fan • fluvial at the top
	d	• laminated silt and clay • some localized dropstones	 ~40cm	• settled out of lake fed by glacial meltwater
	e	• sand and gravel coarsening upward to pebbles and cobbles	 ~40cm	• glaciofluvial outwash plain
	f	• pebbles and cobbles • some sand	 ~30cm	• proximal glaciofluvial outwash

4	a	• matrix-supported, massive diamicton	 ~40cm	• subglacial traction till
	b	• pebbles and cobbles • sand and gravel	 ~40cm	• outwash
	c	• matrix-supported, massive diamicton	 ~40cm	• subglacial traction till

5	a	• pebbles and cobbles • some sand	 ~30cm	• ice-marginal
	b	• matrix-supported, massive diamicton	 ~40cm	• deglacial till
	c	• pebbles and cobbles • some sand	 ~40cm	• ice-marginal
	d	• matrix-supported, massive diamicton	 ~40cm	• deglacial till

	e	• thin alternating laminae of fine sand and clay	 ~30cm	• outwash
	f	• silt with laminations and dropstones	 ~40cm	• ice-contact lake
6		• pebbles and cobbles • faceted • irregularly-shaped • angular to subangular • sometimes in fining upward cycles	 ~30cm	• glaciofluvial

3.5.2 Unit #1: Pre-Quaternary Sediments

Unit 1 consists of all pre-Quaternary unconsolidated sediments overlying bedrock. None of its constituent sediments display evidence of glacial transport.

Sub-unit 1a was encountered in boreholes VTH2014-06, VTH2014-08, VTH2014-09, VTH2014-10 and VTH2014-11 and is interpreted along cross-sections A-B-C-D, A-G-H and H-C (**Figures 3.16, 3.18 and 3.19**). It is a non-glacial diamicton interlayered with clays, silts, thin coals, organic-rich horizons, sand-size particles and pebble- to cobble-sized beds. The diamicton is characterized by angular and monolithic clasts and intervening less-disintegrated breccias with a shattered appearance, and slickensides are present in the clay and silt beds, suggesting that sub-unit 1a could have been formed by fault movement. The diamicton's crumbly, powdery, white, greasy nature indicates clay alteration. Bedrock fracturing branching off of the intersecting Lornex and Highland Valley faults (cf. Chap. 1 Sect. 1.3 for details) at the Valley deposit may have broken up the rock and served as conduits for hot fluids. The bedrock could have been hydrothermally altered, causing the mafic and some felsic minerals of the local Bethsaida granite facies to be replaced by clay minerals. Granules and pebbles are present in the clay and silt beds. The presence of slickensides denoting shearing and the similar appearance and grain size curves (Figure B.7d of Appendix B) of some of these clay and silt beds to the altered rock diamicton suggests that these interbedded silts and clays could also be the result of fault movement of the Lornex and Highland Valley faults. They have possibly been physically weathered and hydrothermally altered so heavily that not much remains except silt- and clay-sized particles. The top half of the diamicton is interlayered with highly angular pebbles and cobbles, which are probably broken bedrock fragments with no matrix or clast-rich sand where the altered bedrock is not broken down as much. Varying amounts of fault abrasion, compaction and clay alteration would have resulted in the sub-unit's characteristics differing somewhat over short distances. It is important to note that a stratified sedimentary layer is present below altered bedrock. This layer forms the very bottom clay layer, and is massive, hard, dense, friable and without any clasts. Organics and thin coal beds are also present in the silt and clay layers throughout the sub-unit. The presence of coal-rich beds throughout the broken-down bedrock material is not explained by the preceding interpretation, and so it is possible that this sub-unit could have

instead been formed by several rock falls or slides onto pre-Quaternary sedimentary material. The rock falls or slides would have occurred with enough time in between them to allow new sediments to accumulate on top of the rockfall before the next one. The bottom clay was possibly pre-Quaternary lake-bottom sediment. Faulting branching off of the Lornex and Highland Valley faults and resulting hydrothermal alteration may still have occurred after, but at a lesser degree than that suggested by the preceding interpretation. This would explain the degree of compaction and crumbling of the bottom clay, as well as the presence of the slickensides and clay alteration. This second interpretation explains all of the features of this sub-unit, and therefore seems more likely to be correct.

Sub-unit 1b overlies 1a in borehole VTH2014-10, and appears in cross-sections A-B-C-D and H-C (**Figures 3.16 and 3.19**). It is a sandy gravel with interbeds of sand, punctuated by a matrix-supported massive diamicton with a silt matrix and subangular to rounded granules to pebbles. The clasts at the bottom are subangular, elongate and flat, and the rest are a mix of these and blocky, more rounded ones. Coal and organics are found in the upper part of the sub-unit. The main depositional environment for sub-unit 1b is interpreted as fluvial. The shattered pebbles and cobbles at the bottom and the highly compacted, almost lithified nature of this sub-unit suggest that fault movement may have continued after deposition, resulting in compression and breakdown of some of the clasts. The intervening diamicton is interpreted as a sedimentary gravity flow.

3.5.3 Unit #2: Subglacial Till and Proximal Outwash

Unit 2 records the arrival of the first known glaciation in the area, as well as its retreat. It consists of glacially-transported diamicton overlain by outwash material deposited as the ice margin was receding.

Sub-unit 2a was encountered in boreholes VTH2014-07 and VTH2014-10 and is interpreted along cross-sections A-B-C-D, F-E-D, and H-C (**Figures 3.16, 3.17 and 3.19**). It overlies bedrock at VTH2014-07, and sub-unit 1b at VTH2014-10. It is a matrix-supported diamicton characterized by a silt matrix, clasts that are granule to boulder size, and some stratification. The larger clasts are angular to rounded, irregularly shaped. Several fragments

appear to be disintegrated clasts. This diamicton is interpreted as being subglacial till. The age of this till is uncertain but it is at least older than Late Wisconsin given the non-finite radiocarbon age of organic material in the overlying Unit 3 (see Figure 3.2). Shattered clasts are present in this till at the Valley boreholes, likely due to the ice riding over and including highly weathered bedrock up glacier flow. This is the deepest till observed in this study.

Sub-unit 2b overlies 2a in boreholes VTH2014-07 and VTH2014-10, and overlies bedrock in borehole VTH2014-03. It appears in cross-sections A-B-C-D, F-E-D, and H-C (**Figures 3.16, 3.17 and 3.19**). It is characterized by fine sand with granule to cobble size clasts that are angular to rounded and irregularly shaped at VTH2014-07. At VTH2014-10, it consists of a diamicton with clasts that have the same characteristics as that of 2a, as well as pebbles, cobble and boulder layers and a silty clay bed. A layer of faceted, rounded pebbles and cobbles followed by a thinner layer of the same type of clasts supported by a sand matrix make up sub-unit 2b at VTH2014-03. These are interpreted to have formed in a proglacial outwash or glaciofluvial setting, as the ice receded locally or the grounding line oscillated backwards and forwards.

3.5.4 Unit #3: Glacially-Influenced Lacustrine and Fluvial Deposits

Unit 3 consists of all the sediment deposited after the ice-proximal outwash (sub-unit 2b; see above) was left by the previous glacier tongue.

Sub-unit 3a was encountered in borehole VTH2014-03 overlying sub-unit 2b, and is interpreted along cross-section F-E-D (**Figure 3.17**). It consists of laminated clay, and is interpreted to be lacustrine. Sub-units 2b and 3a record the transition from a subglacial or ice proximal glaciofluvial environment to a more distal proglacial outwash and, finally, to a glaciolacustrine environment during an ice retreat phase (Figure 3.2).

Sub-unit 3b overlies 3a in borehole VTH2014-03, and appears in cross-section F-E-D (**Figure 3.17**). It consists of sand that is subhorizontally bedded with laminations & rounded pebbles at the bottom, followed by a gravelly sand characterized by faceted pebbles, poor sorting and lack of much bedding. It is capped by a few thin beds of faceted pebbles with

subangular to rounded edges. Sub-unit 3b is interpreted to be a sediment gravity flow due to its overall facies (poorly-sorted). The coarsening-upward succession suggests progradation of the system (closer proximity to source) and/or increasing energy of gravity flows. The facies association with underlying glacial lake sediments suggest progradation of a delta, or possibly a subaqueous fan setting. The top could also represent an outwash plain following drainage of the lake.

Sub-unit 3c overlies 3b in borehole VTH2014-03, and appears in cross-section F-E-D (**Figure 3.17**). It is similar in character to 3b, consisting of bedded, oxidized fine sand with granules and pebbles, as well as cobbles at the top. It is also interpreted to have been deposited in a subaqueous fan or delta setting, with an increasing fluvial influence at the top.

Sub-unit 3d was encountered in boreholes VTH2014-03, VTH2014-06, VTH2014-07, VTH2014-10 and VTH2014-13A and is interpreted along cross-sections A-B-C-D, F-E-D, A-G-H and H-C (**Figures 3.16 to 3.19**). It overlies sub-unit 3c at VTH2014-03, 1a at VTH2014-06, 2b at VTH2014-07 and VTH2014-10, and bedrock at VTH2014-13A. It is a silt and/or clay with localized laminations, organics and a few isolated, small groups of faceted, subangular clasts. It is interpreted to have formed in an ice-contact lake (glaciolacustrine) setting. The laminations are possibly varves demonstrating seasonal deposition and that the lake existed for at least a few years. The clasts were possibly ice-rafted from an ice-contact point on the lake that existed during part of the lake's existance. Radiocarbon dating of microfossils found in this sub-unit (**Figure 3.2**) yielded a non-finite age (i.e. greater than 50 ka BP). The silt and clay seen in the Valley pit at the bottom of VP-3 and at VP-6 (**Figures 3.23 and 3.26**) and observed by Alain Plouffe in the Valley pit at 11PMA047, 11PMA048 and 11PMA049 (**Figure 3.1b**) are likely sub-unit 3d as well. See Figure A.16 in Appendix A for Plouffe's observation.

Sub-unit 3e is found in boreholes VTH2014-03, VTH2014-06, VTH2014-07, VTH2014-09 and VTH2014-10 and is interpreted along cross-sections A-B-C-D, F-E-D, A-G-H and H-C (**Figures 3.16-3.19**). It overlies 3d at VTH2014-03, VTH2014-06, VTH2014-07 and VTH2014-10, and 1a at VTH2014-09. Sub-unit 3e is characterized by beds and laminae of moderately well-sorted sand which alternate between finer and coarser grain sizes ranging from clayey fine sand to coarse sand. They contain organics, granules, and a few

angular to rounded outsize clasts, some of which are iron-shaped and faceted. It is interbedded with or capped locally by sorted pebbles and cobbles. Due to its tabular architecture, sub-unit 3e is interpreted as a glaciofluvial outwash plain. The rounded clast edges and presence of some stratification and lamination indicate fluvial transport and influence during deposition.

Sub-unit 3f is found in boreholes VTH2014-06, VTH2014-08 and VTH2014-09 and is interpreted along cross-sections A-B-C-D and A-G-H (**Figures 3.16 and 3.18**). It overlies 3e at VTH2014-06 and VTH2014-09, and 1a at VTH2014-08. Sub-unit 3f is characterized by sandy gravel and pebble and cobble beds. The clasts are angular to rounded, and some are iron-shaped and faceted. Sub-unit 3f is interpreted as a sediment gravity flow in a proglacial glaciofluvial environment. Due to the coarsening-upward trend from 3e to 3f and the overlying subglacial till (sub-unit 4a), it is likely that 3f represents a more proximal outwash facies than 3e, which together with overlying unit 4a record an ice advance phase.

The foresets observed by Alain Plouffe at 11PMA046 in the Valley pit (**Figure 3.1b**), just to the west of VTH2014-03, dip towards the east and record a fan or delta at a similar elevation as sub-units 3e and 3f. See Figure A.17 in Appendix A for Plouffe's observation. The relationship between that delta and sub-units 3e and 3f is uncertain. A thick sequence of foreset beds of sand and gravel dipping to the southeast was also observed in the Valley pit at VP-5 (**Figure 3.25**), and a thinner part of the same sequence was observed by Alain Plouffe at 11PMA050 nearby (**Figure 3.1b**). See Figure A.18 in Appendix A for Plouffe's observation. The sequence seen at VP-5 and 11PMA050 were deposited by drainage into a lake from the northwest, and possibly are contemporaneous with the fan or delta deposit at 11PMA046. The underlying lacustrine silt and clay of sub-unit 3d, also seen at VP-6, are likely pro-fan/delta deposits, and coarsen upward into the fan or delta deposit, reflecting sand prograding into the lake. These foreset beds are at the eastern and southeastern edge of the Valley pit, and are perhaps the proximal glaciolacustrine facies of a lake once centered somewhere to the southeast of the Valley pit. The sand and gravel outwash and debris flow material observed by Plouffe at 11PMA051 (**Figure 3.1b**) is possibly also part of sub-units 3e and 3f. See Figure A.19 in Appendix A for Plouffe's observation.

3.5.5 Units #4 and #5: Glacial and Deglacial Cycles

Unit 4 consists of glacial sediment deposited during a second ice oscillation forwards. Unit 5 is composed of deglacial sediment deposited during overall retreat of this ice margin. The beginning of unit 5 is marked by the onset of thick ice-marginal pebble and cobble sub-units.

Sub-unit 4a was encountered in boreholes VTH2014-07, VTH2014-08, VTH2014-10, VTH2014-11 and VTH2014-13A and is interpreted along cross-sections A-B-C-D, F-E-D, A-G-H and H-C (**Figures 3.16 to 3.19**). It overlies 3e at VTH2014-07 and VTH2014-10, 3f at VTH2014-08, 1a at VTH2014-11 and 3d at VTH2014-13A. It is a massive, matrix-supported diamicton with a silt or clay matrix, granules and pebble- to cobble-sized clasts. It is interpreted as subglacial traction till. The till from previous advances was likely eroded or reworked by subsequent advances or outwash processes. This is the deepest widespread till seen in the stratigraphic section here, and is thin and likely partly eroded.

Sub-unit 4b is found overlying 4a in boreholes VTH2014-06, VTH2014-07, VTH2014-08, VTH2014-10, VTH2014-11 and VTH2014-13A and is interpreted along cross-sections A-B-C-D, F-E-D, A-G-H and H-C (**Figures 3.16 to 3.19**). It is characterized by gravelly sand and several thin pebble and cobble layers. The sand is sometimes bedded or laminated or contains organics. The clasts are faceted. This sub-unit coarsens upward at VTH2014-06, VTH2014-08 and VTH2014-11. It is interpreted as proglacial outwash, or sediment gravity flow from a subaqueous fan or delta setting. The sediments at VP-4 and VP-2 (**Figure 3.1b**) are right above Plouffe's 11PMA050 and 11PMA051 (which correspond to sub-units 3e and 3f). Therefore they likely correlate to sub-unit 4b. The sand and silt/clay at VP-4 are possibly the proglacial and subglacial outwash material; the diamicton is probably part of the subaqueous debris flow (**Figure 3.24**). The dipping beds of stratified sand at VP-2 (**Figure 3.22**) are possibly proglacial outwash.

Sub-unit 4c is found overlying 4b in boreholes VTH2014-07, VTH2014-08, VTH2014-10, VTH2014-11 and VTH2014-13A, and over 3f in VTH2014-09. Sub-unit 5b is found overlying 5a in boreholes VTH2014-07, VTH2014-08, VTH2014-09, VTH2014-10, VTH2014-11 and VTH2014-13A. Sub-unit 5d is found overlying 5c in boreholes VTH2014-

07, VTH2014-08, VTH2014-10 and VTH2014-11. They are all interpreted along cross-sections A-B-C-D, F-E-D, A-G-H and H-C (**Figures 3.16 to 3.19**). Sub-units 4c, 5b and 5d are massive diamictons which are silt or clay matrix-supported and include granules and pebble- to boulder-sized clasts. They include local, thin sand, gravel, silt or clay interlayers. These sub-units are all interpreted as subglacial traction till with clast pavements and meltwater canal fills. Many of the clasts are faceted or bullet-shaped and faintly striated, which is evidence of glacial transport. Some of them are brecciated, which could be the result of glacial mechanical crushing, although it could be due to the drilling process. The sand, silt and clay interbeds are interpreted as canal fill deposits following Piotrowski (2013). During periods of increased meltwater discharge, porewater pressures would have elevated the ice and decoupled it from the bed. Braided canal systems would have formed to drain away the highly variable supply of meltwater and sediment at the ice-bed interface (Evans and Benn, 2004). The thin sand, silt and clay interlayers in the till were probably laid down as meltwater deposits in these systems, which also washed out a few of the sand and till layers locally. These subglacial tills dominate the top of the stratigraphic section in the Valley pit area. Part of sub-unit 4c at VTH2014-09 shows a preferred horizontal orientation of its clasts. The clasts were rotated parallel to the ice-flow direction during transport (main direction of shear). Their low dip values could indicate deposition by basal meltout instead of lodgement (Evans and Benn, 2004). The overlying diamicton at VP-2 (**Figure 3.22**) is likely glacial till, and correlates to 4c, 5b or 5d.

Sub-unit 5a is found overlying 4c, and sub-unit 5c is found overlying 5b in boreholes VTH2014-07, VTH2014-08, VTH2014-09, VTH2014-10, VTH2014-11 and VTH2014-13A. They are interpreted along cross-sections A-B-C-D, F-E-D, A-G-H and H-C (**Figures 3.16 to 3.19**). Sub-units 5a and 5c are characterized mostly by pebbles and cobbles. They also include both gravelly and clean sands, and occasional thin silts and clays. Both sub-units are interpreted as ice-marginal deposits from an ice tongue that oscillated in the bedrock valley.

Sub-unit 5e is found overlying 5d in borehole VTH2014-07. It is interpreted along cross-sections A-B-C-D and F-E-D (**Figures 3.16 and 3.17**). It is characterized by thin laminae of alternating fine sand and clay. Sub-unit 5e is interpreted to be glacial outwash material.

Sub-unit 5f is found overlying 5d in borehole VTH2014-08. It is interpreted along cross-sections A-B-C-D and A-G-H (**Figures 3.16 and 3.18**). It is characterized by silt with laminations and dropstones. Sub-unit 5f is interpreted to have been deposited in an ice-contact lake setting.

3.5.6 Units #6: Glaciofluvial Deposits

Unit 6 was encountered in boreholes VTH2014-07, VTH2014-08, VTH2014-09, VTH2014-10, VTH2014-11 and VTH2014-13A and is interpreted along cross-sections A-B-C-D, F-E-D, A-G-H, and H-C (**Figures 3.16 to 3.19**). It overlies unit 5e at VTH2014-07, 5f at VTH2014-08, 5c at VTH2014-09 and VTH2014-13A, and 5d at VTH2014-10 and VTH2014-11. It is characterized by a particularly thick (up to ~20m) pebble and cobble layer. The clasts are faceted, irregularly-shaped, angular to subangular, and often in fining upward cycles. It is interpreted as a proglacial glaciofluvial deposit.

3.5 Comparison of Valley Pit Stratigraphy to that of Bobrowsky et al. (1993)

A previous study (Bobrowsky et al. 1993) identified and described different stratigraphic units in the unconsolidated sediment cover in the Valley pit (**Figure 3.28**). An interpretation of the depositional environment was made for each one, although some of the units combined multiple depositional environments. The units observed in the cores and Valley pit for this study are tentatively correlated to those of Bobrowsky (**Table 3.4**).

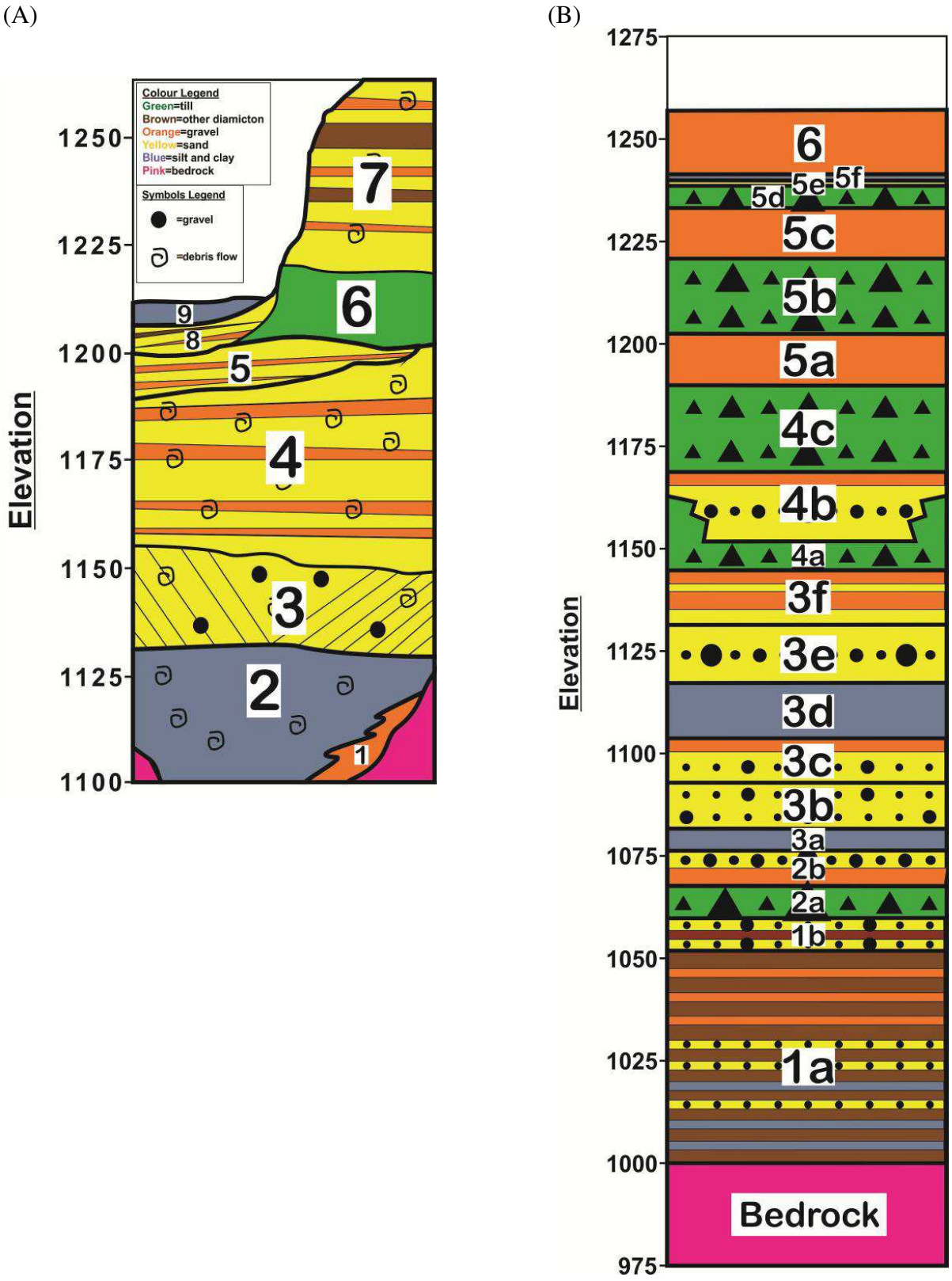

Figure 3.28 The stratigraphic framework of Quaternary sediments at the Valley Pit at Highland Valley, (A) according to Bobrowsky et al. (1993) and (B) based on this study.

Table 3.4 Correlations between the stratigraphic units observed in this study and by Bobrowsky et al. (1993).

Unit(s) from this study	**Bobrowsky et al.'s (1993) corresponding Valley pit unit(s)**
Not observed	#9 (sand, marl, peat and bryophytes)
Not observed	#8 (sand, gravel and diamicton interpreted as in situ ice decay)
5e, 6	#7 (sand, gravel and diamicton interpreted as supraglacial)
4c, 5a, 5b, 5c, 5d	#6 (diamicton with isolated sand and gravel)
4b	#5 (sand and gravel) Interpreted as subglacial outwash and possibly #4 (sand, gravel and diamicton) Interpreted as proglacial and subglacial outwash and resedimented subaqueous debris flows
4a	#4 (sand, gravel and diamicton) Interpreted as proglacial and subglacial outwash and resedimented subaqueous debris flows
3e and 3f VP-5 (delta)	#3 (sand & sandy gravel, steeply dipping) Interpreted as foreset beds created by prograding combining delta fronts) and #4 (sand, gravel and diamicton) Interpreted as proglacial and subglacial outwash and resedimented subaqueous debris flows
3d VP-6	#2 (clay and silt rhythmites): Interpreted as glaciolacustrine with intervening, massive, matrix and clast supported diamicton
1a and 1b	#1 (sandy gravel and silty sand, steeply dipping, strongly oxidized; interpreted as in-situ weathered bedrock, bedrock accumulated at bottom of steep slope, sand with organics & fluvial fan deposits; characteristic of steep slopes of deep valleys; 6-10m)

Bobrowsky et al. (1993) identified sub-unit 1a of this study as their unit #1 and interpreted it as in-situ weathered bedrock. Sub-unit 1b of this study could also be part of Bobrowsky et al.'s in-situ weathered bedrock unit, which included similar interbeds of sand with organics and fluvial fan deposits. Sub-units 1a and 1b of this study and Bobrowsky et al.'s corresponding unit #1 all have been described as being poorly-sorted and having local clasts. Bobrowsky et al.'s unit #1 lies on top of bedrock, like sub-unit 1a of this study. Bobrowsky et al.'s unit #1 consists of only sandy gravel and silty sand and most clasts are highly weathered, which is similar to this study's corresponding unit 1. Bobrowsky et al. described unit #1 as being strongly oxidized and its beds steeply dipping, which was not seen in this study's corresponding unit. However, the presence of beds of clay and silt were not noted, unlike for this study. It has been shown here that unit 1a of this study extends to about 100m in thickness in some areas, and can locally make up a much greater part of the unconsolidated sediment sequence than the corresponding 6-10m-thick unit #1 previously observed (Bobrowsky et al., 1993).

Sub-units 2a, 2b, 3a, 3b and 3c were not identified by Bobrowsky et al., likely due to lateral variation in the stratigraphy between the location of the cores and their observations in the Valley pit area. Bobrowsky et al.'s study did not go as deep into the sedimentary stratigraphy; bedrock was encountered in the pit at a higher elevation.

Sub-unit 3d likely corresponds to Bobrowsky et al.'s unit #2; both are described as silt and clay rhythmites overlying the weathered bedrock unit, and are found at similar elevations (1100 to 1130 m asl). This glaciolacustrine sub-unit overlies bedrock in some places, and glacial outwash in others. Bobrowsky et al. identified a matrix and clast supported diamicton with organics interlayered with the clay and silt rhythmites, which must be the weathered bedrock material (unit #1) and not till due to the presence of the organics. Sub-unit 3d of this study and Bobrowsky et al.'s corresponding unit #2 both consist of silt and/or clay with horizontal stratification, rhythmite laminae, and few dropstones. Bobrowsky et al.'s unit #2 was described as having rhythmites that coarsen and thicken with increasing elevation, which was not observed in this study. Organics were observed in the silt and clay in this study, which was not noted by Bobrowsky et al. (1993).

Sub-units 3e and 3f probably correspond to Bobrowsky et al.'s unit #3, which they also described as alternating sand and gravel and also positioned on top of their glaciolacustrine silt and clay unit (unit #2). Both sequences consist of alternating gravelly sand and sandy gravel that coarsen upward across the unit. However, 3f is coarser and more poorly-sorted. The glaciofluvial outwash (sub-units 3e and 3f) may have been deposited after the delta deposit (Bobrowsky et al.'s unit #3). The coarser outwash material may have cut into the finer, better-sorted delta sand and been deposited at the same elevation. Sub-units 3e and 3f are also similar to Bobrowsky et al.'s unit #4 because they both consist of poorly-sorted sand and gravel. Unlike unit #4 from Bobrowsky et al., 3e and 3f do not include any diamicton.

This study's unit 4a is a massive, matrix-supported diamicton with a silt or clay matrix, granules and pebble- to cobble-sized clasts. Unit #4 of Bobrowsky et al.'s framework consists of a diamicton that is both matrix and clast supported and poorly-stratified with beds of sand and gravel. Their unit #4 is particularly thick (up to 55m) and their interpretation includes a large range of possible depositional environments ranging from subglacial to proglacial outwash plain to possible subaqueous resedimented deposit. This suggest the possibility that they lumped together certain facies that were instead kept separated in different units in this study to avoid combining different depositional systems within the same stratigraphic unit.

Sub-unit 4b is correlated to Bobrowsky et al.'s unit #5, which they described as moderately-sorted sand and gravel beds and interpreted as ice-contact glaciofluvial. Both of these (sub)units consist of moderately-sorted sand and pebble and cobble beds. Bobrowsky et al. noted crossbeds with a regular dip, which were not observed in this study.

The till sub-units of 4c, 5b and possibly 5d, as well as the gravel and finer sediment sub-units of 5a and 5c likely correspond altogether to Bobrowsky et al.' as unit #6. This was interpreted as basal till, similar to this study, and all had an elevation around ~1200-1220 m asl. All of these (sub)units are composed of matrix-supported diamicton beds with sand and gravel lenses. Bobrowsky et al.'s unit #6 was also described as having crossbeds with a sandy matrix, which was not observed in this study. Units 5a and 5c of

this study are also correlated to Bobrowsky et al.'s unit #6. The main difference is unit 5 of this study appears to be more stratified than what is described by Bobrowsky et al. (1993) for their unit #6.

Units 5e and 6 of this study are correlated to part of Bobrowsky et al.'s unit #7. Both consist of sand or gravel beds at roughly the same elevation (~1220 to 1270 m asl) and are most likely laterally equivalent units. The main difference between the two is that Bobrowsky et al.'s unit #7 contains diamicton beds, and was interpreted to be different kinds of supraglacial sediments.

Unit 5f of this study was not identified by Bobrowsky et al. (1993) and their units #8 and #9 were not observed in this study. This is likely due to lateral variation in the stratigraphy in the Valley pit area.

This study has gone deeper into the unconsolidated sediment stratigraphy and identified a deeper till (sub-unit 2a) than the one described by Bobrowsky et al. (1993). Additionally, some of the non-glacial sequence that is present between the deepest till and the next till going up the stratigraphy has been newly identified in this study (sub-units 2b, 3a, 3b and 3c). The unit overlying bedrock that consists mostly of broken-down bedrock (unit 1) is shown here to make up a significantly greater part of the stratigraphy than previously described by Bobrowsky et al. Logging of continuous sonic drillcores also allowed for more detailed facies descriptions of all the units and a refinement of the interpretations of valley fill sediments and their overall sedimentary history.

3.6 Conclusions

This study has extended the known stratigraphic framework at Highland Valley. The units identified in this study were correlated to those of Bobrowsky et al.'s 1993 study, but several important differences have been noted. There is a deeper, older till as well as a deglacial sequence overlying it that were previously unpublished. This unit overlying bedrock is characterized by broken-down rock with sedimentary interlayers, and makes up a much larger portion of the stratigraphy than previously identified. It has

also been shown that the stratigraphy and facies may be variable across short distances laterally, although certain units extend laterally over several hundred metres.

The stratigraphy in the Highland Valley area is complex, recording local oscillations between many different glacial and non-glacial environments. The stratigraphic framework built for this study reduces the stratigraphy into six major units subdivided into sub-units according to facies associations and depositional environment interpretations. In addition, the borehole-to-borehole correlations and the interpreted seismic profile now provide four new cross-sections that bring new insights into the local stratigraphic architecture of the valley fill deposits in the vicinity of Highland Valley, as well as across the J.A. target.

The new stratigraphic framework will help organize compositional data into a meaningful stratigraphic context, and help the related provenance analysis (See Chap. 4). This will aid in refining the erosional, transport and depositional history of each unit.

Provenance and Footprint Indicators in the Unconsolidated Sediment Cover at Highland Valley

4.0 Introduction

An important objective of this research (cf. Chap. 1, Sect. 1.3) is to identify evidence of transported (detrital) particles from the Highland Valley mineralization bedrock footprint within the unconsolidated sediments and analyze it within the overall sediment provenance context. To this end, several samples from different drillcores and sedimentary units were collected and different fractions were analyzed for general provenance and footprint indicators analysis. This work is done by first assuming the stratigraphic analysis and correlations presented in Chapter 3 are correct; however, the internal compositional consistency within each stratigraphic unit, as well as the compositional differences between units are also examined and discussed herein.

Pebbles (>4 mm fraction) from a variety of different types of sediment samples from each core were recovered and classified by broad lithology groups (cf. Chap. 2, Sect. 2.2.3 for details). The size, shape and angularity/roundness of pebbles, as well as any signs of mineralization were noted. The first section below provides the plotted results of the pebble counts, which are used for provenance analysis of the stratigraphic units. A map of the surrounding bedrock geology (**Figure 4.1**) is used to determine the possible bedrock sources to which the clast lithologies are linked.

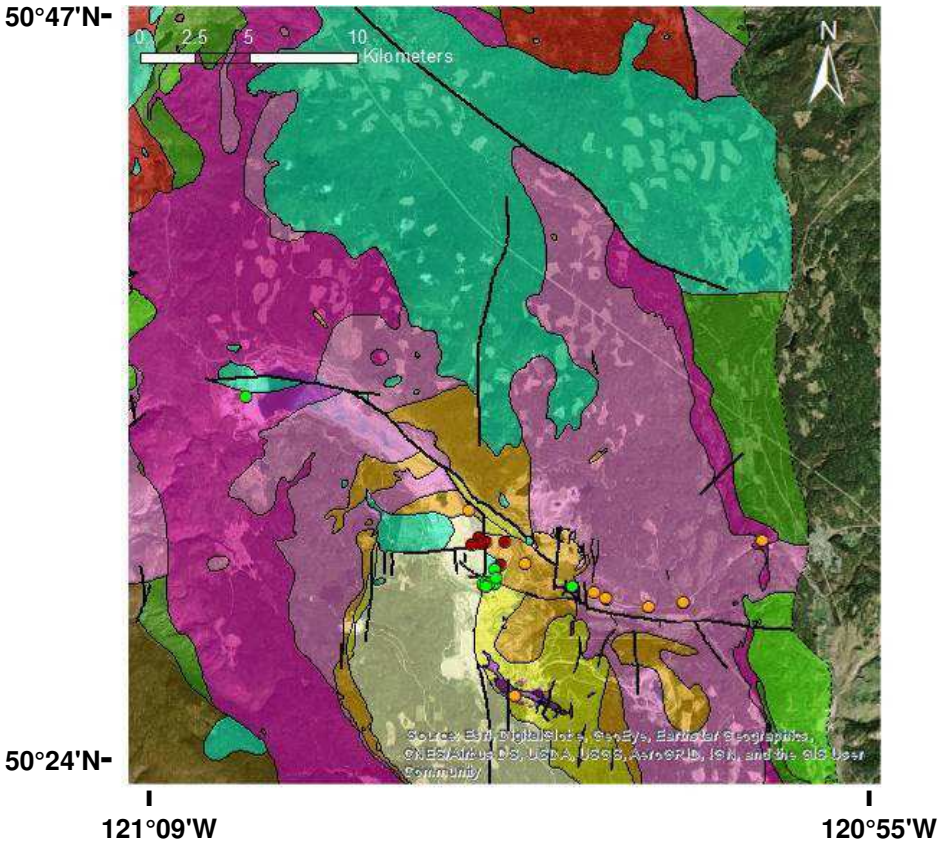

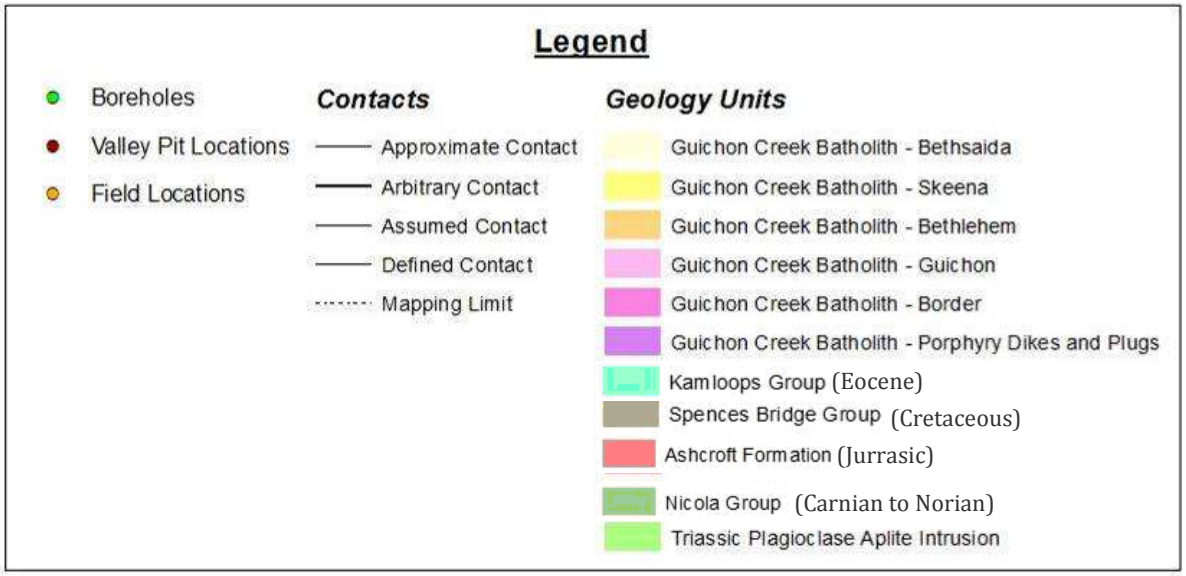

Figure 4.1 Simplified geologic map of the area around Highland Valley modified after Lee et al., 2018. The Guichon Creek Batholith is granitic; other units are multi-coloured volcanic and sedimentary. The locations of the boreholes and Valley Pit and field study sites are shown.

Heavy mineral analysis was done to determine whether minerals indicative of the porphyry copper system or hydrothermal alteration assemblage of the syn- to pre-mineral rocks are present in the unconsolidated sediment cover. Thirteen samples from select till and sand sub-units from different cores drilled over the major mineralized zones (Valley and J.A. cores) and one sample from the Highmont pit were analyzed (see Chap. 2; Fig. 2.1 for locations). Mineral grains were picked from different size fractions, all of them under 2mm. The analysis was done by Overburden Drilling Management Limited (cf. Chap. 2, Sect. 2.2.4 for the recovery process). The same process and the same indicator minerals of copper mineralization as those reported by Plouffe and Ferbey (2016) (see Chap. 2; Table 2.1) were used, making it possible to compare and integrate the results of the two studies.

Hyperspectral imaging was also applied to identify two minerals in the unconsolidated cover that are present in the alteration footprint (prehnite or kaolinite; Lesage et al., 2016; Byrne et al., 2017). This additional mineral analysis was conducted on the greater than 2mm (granules and pebbles) fraction of the same thirteen samples analyzed for heavy minerals. The spectral imaging was conducted at the University of Alberta Core Imaging Laboratory (cf. Chap. 2, Sect. 2.2.5 for the technique description).

Geochemical analysis for a wide range of elements was done in order to determine if chemical traces indicative of mineralization or alteration are present in the sedimentary cover. This analysis was performed on the same thirteen till and sand samples as those for which heavy mineral and hyperspectral analysis was done, as well as an additional twenty samples chosen from a variety of till and sand samples. One sample was also chosen from a till unit of the DH-15-GG core twelve kilometers northwest of the mine area in order to potentially obtain background values of element concentrations away from the major mineralized zone. The analysis was completed by ACME Analytical Laboratories (Bureau Veritas Company) in Vancouver, the same laboratory used by Plouffe and Ferbey (2016) to facilitate comparison of results between the two surveys (see Chap. 2, Sect 2.2.6 for details).

The focus of these analyses is on subglacial tills (61% of total samples analyzed for indicator composition). They represent a large proportion of the valley fill sediments,

especially near the surface, and are more likely to have more complete footprint signature due to the wide grain size range allowing all the above techniques to be applied. The results of these analyses are compared to the underlying altered and mineralized bedrock. Stratigraphic variation and potential effects related to changes in depositional environments are investigated.

4.1 Pebble Lithology Results and Related Provenance Analysis

The lithologies of clasts found in each unit were determined by observation during core logging or by observation under a microscope after disaggregation and sieving of 57 samples. The clasts were grouped based on lithological classes and counted. Existing literature such as d'Angelo et al. (2017) and Byrne et al. (2013), as well as consultation with experts on the geology of the area, was used to interpret the provenance of the clasts. Kevin Byrne and Guillaume Lesage both have extensive experience identifying Highland Valley bedrock lithologies while working on their PhDs as part of the NSERC-CMIC Footprints research project (Lesher et al., 2017). They assisted with identifying pebble samples.

4.1.1 Pebble Lithologies

Pebbles dominantly consist of coarse-grained igneous lithologies in most of the samples for which pebble counts were done (see Figure B.11 in Appendix B). A minor proportion of the pebbles in most samples was composed of fine-grained or aphanitic igneous, porphyritic, sedimentary, or metamorphic rock types. Pebbles were classed as fine-grained igneous if individual mineral grains could be observed without a lens, and as aphanitic igneous if individual grains could only be observed with the aid of a lens or microscope or were not visible at all, but there were signs that the pebble was igneous (interlocking grains, lack of mineral layering...). The fine-grained igneous and aphanitic types consist of a large variety of lithologies; a high number of colors make up the pebbles belonging to these classes. Ten recurring lithology types have been identified

from all of the pebbles and cobbles of the various till, diamicton, sand and pebble, and cobble samples taken from all the cores. They are summarized in Table B.4 of Appendix B. Photos of typical examples representing the two most common types, both belonging to the local Guichon Creek batholith, are shown below (**Figure 4.2**).

The coarse-grained igneous and porphyritic lithologies are inferred to be sourced from the local Guichon Creek Batholith, while the others were eroded distally outside the area of the batholith.

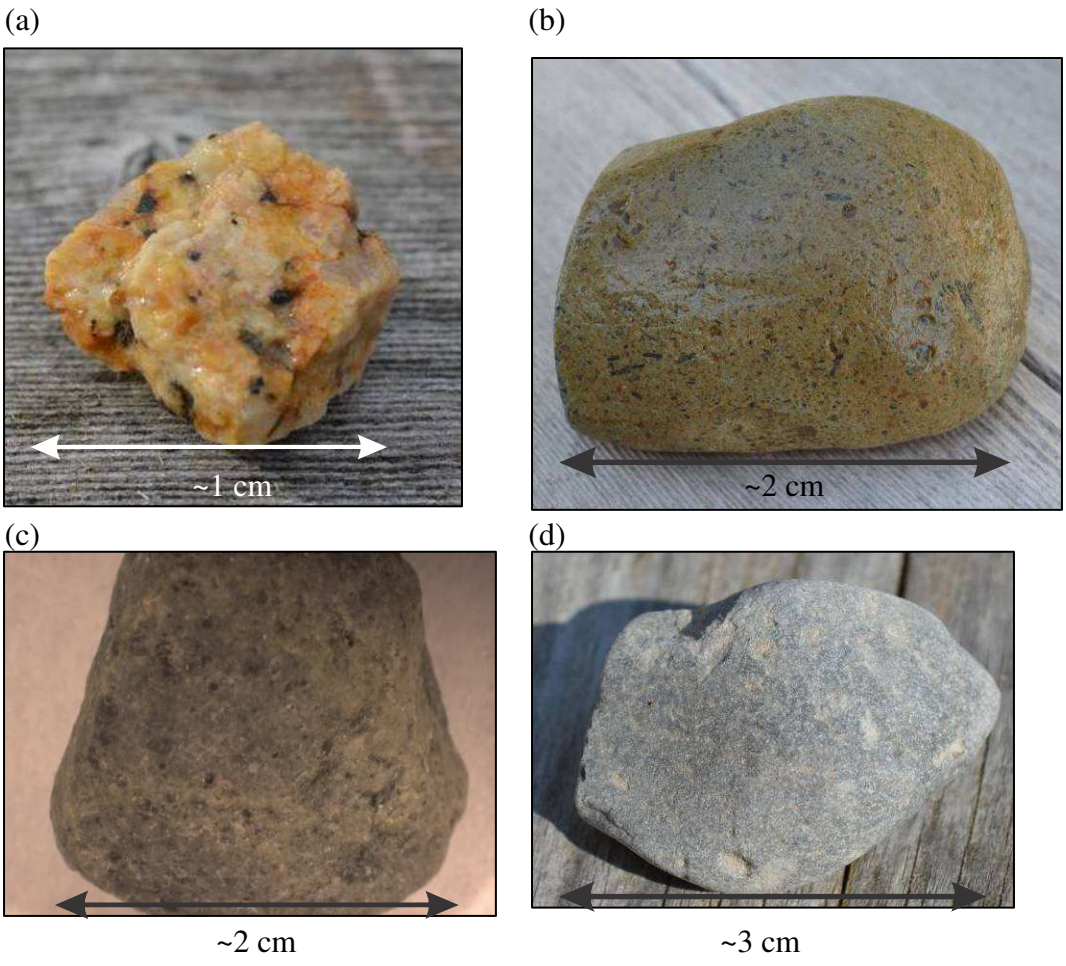

Figure 4.2 An oxidized felsic coarse-grained igneous pebble from the pebble and cobble sub-unit 5a of core VTH2014-08 (a), a porphyritic pebble from the poorly-sorted outwash sub-unit 4b of core VTH2014-13A (b), a fine-grained igneous pebble from the till sub-unit 5b of core VTH2014-09 (c), and an aphanitic igneous pebble from the till sub-unit 5b of core VTH2014-13A (d). These lithologies are typical of pebbles found in the unconsolidated sediments at Highland Valley.

Valley Pit Drillcore Units

Figure 4.3 shows the average relative proportions of the different lithology types for most of the units in the Valley pit drillcores (see Chap. 3, Sect. 3.5 for stratigraphic framework and unit numbers). The individual proportions for each sample were determined by doing pebble counts under a microscope. See Figure B.11 in Appendix B for individual sample pebble count data. The lithology types making up the pebbles in the other sub-units were determined visually by observation of the core.

The clasts in the non-glacial altered bedrock diamicton and the pebble and cobble layers of sub-unit 1a are dominated by a felsic, coarse-grained igneous lithology. Clasts in the sand and gravel as well as non-glacial diamicton of sub-unit 1b are lithologically more heterogeneous and include coarse and fine-grained igneous and multi-coloured volcanic rocks.

The till of sub-unit 2a contains the highest proportion of clasts that are not coarse-grained igneous (which dominates every other unit). The clasts consist of porphyritic lithologies (grey aphanitic or fine-grained groundmass with distinctly larger crystals, mostly black amphibole or pyroxenes, embedded in the groundmass), multi-coloured volcanics, as well as both coarse and fine-grained igneous rocks (equal grain sizes). The pebbles and cobbles of sub-unit 2b at VTH2014-03 are mostly both felsic and intermediate coarse-grained igneous. The lithologies of the sand and gravel layers of sub-unit 2b at VTH2014-07 show a variety of coarse and fine-grained igneous and multi-coloured volcanic rocks.

The coarse-grained igneous lithologies that dominate gravel of sub-units 3b and 3c at VTH2014-03 are almost all felsic (**Figure 4.3**). The dropstones found in the silt and clay of sub-unit 3d are varied in lithology; this includes coarse and fine-grained igneous and multi-coloured volcanics. However, the lithology of dropstones in 3d is locally dominated by felsic coarse-grained igneous at VTH2014-07 and VTH2014-10. The gravel in 3e consists mainly (94%) of coarse-grained igneous rocks. However, no coarse-grained igneous clasts are found at the base of sub-unit 3e at VTH2014-07 (Figure B.11

in Appendix B). The gravel in sub-unit 3f consists of varied coarse and fine-grained igneous and multi-coloured volcanic clasts.

The clasts in the till of sub-unit 4a consist of mixed lithologies, including coarse and fine-grained igneous and multi-coloured volcanics. They are dominated by felsic, coarse-grained igneous ones at VTH2014-03 and VTH2014-08 (Figure B.11 in Appendix B). The lithology of the gravel amongst the sand of sub-unit 4b is also varied, including coarse and fine-grained igneous and multi-coloured volcanics. The pebbles and cobbles at the top of 4b are dominantly felsic and intermediate coarse-grained or fine-grained igneous. The clasts of the till sub-unit 4c consist of various lithologies, including coarse and fine-grained igneous and multi-coloured volcanics.

The gravel of sub-units 5a and 5d and the clasts in the tills of sub-units 5b and 5d are of mixed lithologies, including coarse and fine-grained igneous and multi-coloured volcanics.

Unit 6 is composed of pebbles and cobbles of varied lithology. They are mostly felsic coarse-grained igneous, especially near the top of the unit, but also fine-grained igneous and multi-coloured (especially dark or red) volcanics. The unit is composed entirely of felsic coarse-grained igneous pebbles and cobbles at VTH2014-07.

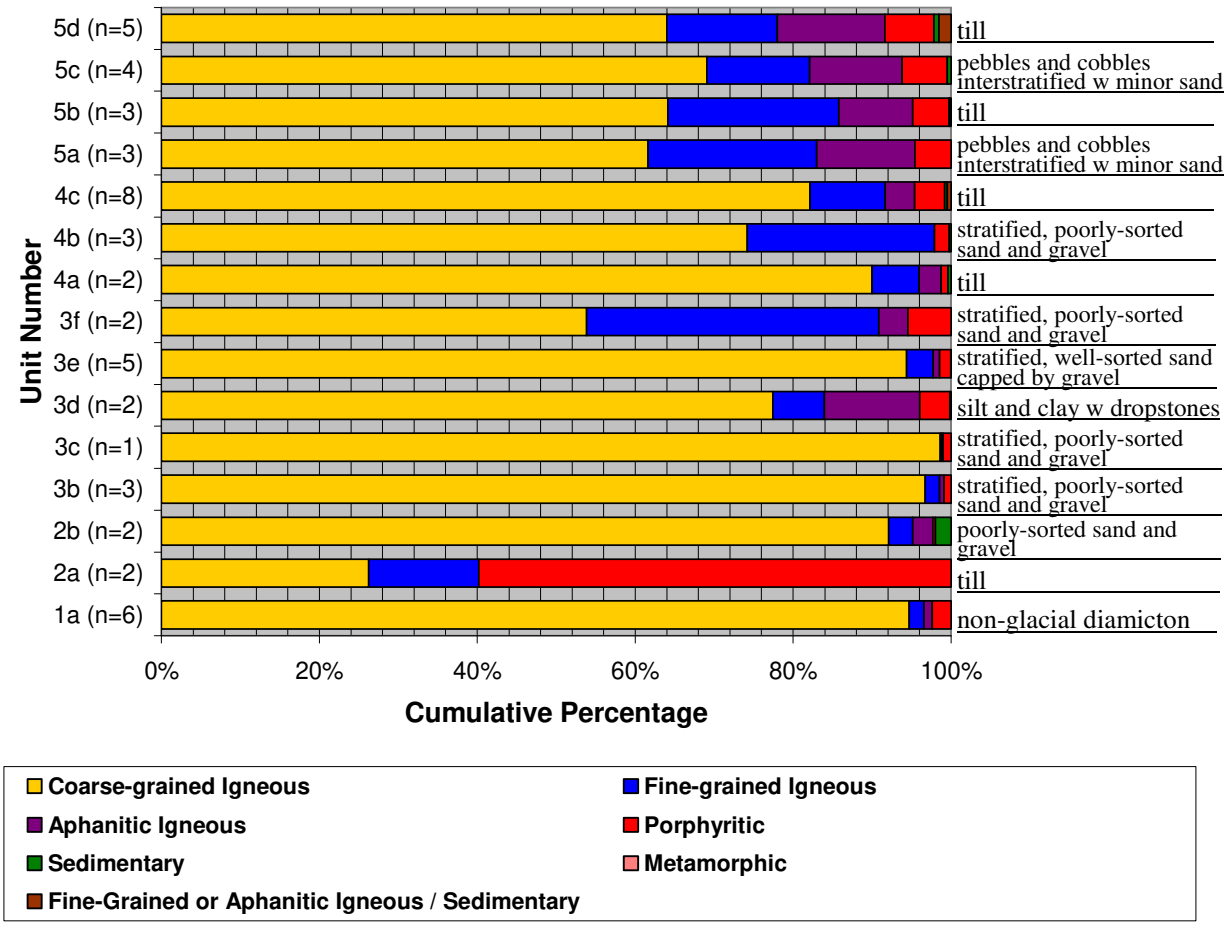

Figure 4.3 Pebble lithology types for different stratigraphic units in the unconsolidated sediment stratigraphy at the Valley pit area of Highland Valley. Percentages for each lithology type use data from one or multiple samples (averages) for each sub-unit. Number of samples are indicated on the left axis (n =). See Appendix B, Figure B.1 for details on sample location.

J.A. Units

Figure 4.4 shows the average relative proportions of the different lithology types for the units in the J.A. borehole for which pebble counts were done. The individual proportions for each sample were determined by doing pebble counts under a microscope. The lithology types making up the pebbles in the other sub-units were determined visually by observation of the core.

The pebble and cobble units and the clasts of the intervening non-glacial diamicton at the base of the J.A. core (elevation range from 1021.2 to 1068.7 meters) are all grey, coarse-grained igneous, with some fine-grained igneous towards the top. The overlying till includes a wider range of coarse and fine-grained igneous clasts. The bottom thick clay unit (elevation range from 1075.7 to 1092.3 meters) includes dark fine-grained dropstones. The lithology of the thick, poorly-sorted unit of sand, gravel, pebbles and cobbles (elevation range from 1097.3 to 1093.6 meters) consists mostly of fine-grained igneous rocks (especially green coloured, also maroons and grays), as well as a variety of coarse-grained igneous types. The thick pebble and cobble unit ranging from 1097.7 to 1130.2 meters consists mostly of fine-grained and aphanitic igneous rocks, with some coarse-grained igneous and porphyritic rocks as well (**Figure 4.4**). The top thick till includes clasts that are felsic to intermediate coarse-grained igneous and a wide variety of fine-grained igneous and porphyritic types (**Figure 4.4**).

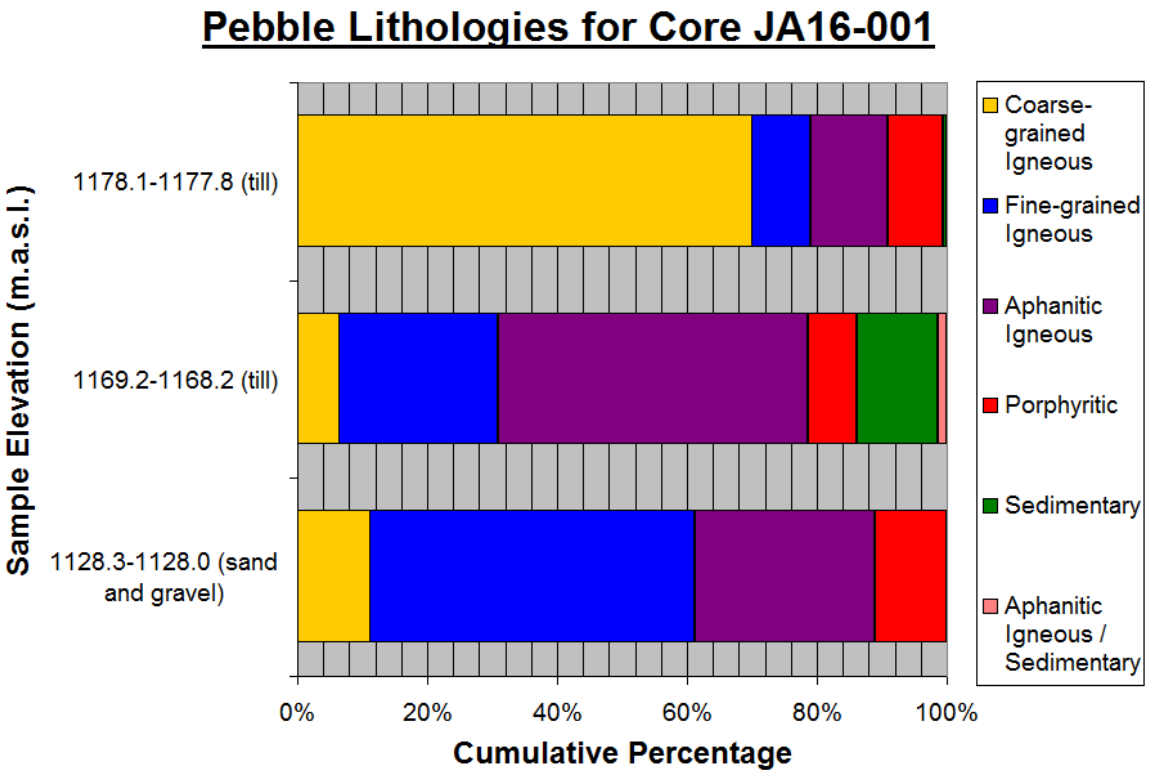

Figure 4.4 Pebble lithology types for select major stratigraphic units in the unconsolidated sediment stratigraphy at the J.A. area of Highland Valley.

DH-15-GG

The stratigraphy of core DH-15-GG is presented in appendix A. The clasts of the bottom conglomeratic unit (elevation range: 1081.7 to 1134.7 m asl) are volcanics of various types and colours and felsic coarse-grained igneous rocks. The lithology of the boulders at 1144.5 to 1146.3 m asl is felsic, coarse-grained igneous rock. The pebbles in the overlying mix of poorly-sorted sand and till (elevation range: 1146.3 to 1158.6 m asl) are composed of a mix of mainly dark volcanics and felsic, coarse-grained igneous lithologies. The pebble and cobble layers capping the stratigraphy are of fine-grained igneous, volcanic and sedimentary lithologies.

4.1.2 Provenance

The felsic coarse-grained igneous clasts are characteristic of the local granitic Guichon Creek batholith (**Figure 4.2**), which also hosts the mineralized zones. Therefore, these clasts are interpreted to be locally derived. The other lithologies identified in the clasts are most likely derived from the different bedrock lithologies surrounding the batholith (**Figure 4.1**). It is assumed that the majority are derived from northern locations based on the ice-flow record presented by Plouffe and Ferbey (2016). However, the deeper units in the valley could have been transported in directions not recorded in the uplands where most ice-flow indicators were measured; e.g. by thinner glacier lobes flowing along the valley. The following sub-sections present a more detailed interpretation for the different areas and stratigraphic units.

Valley Pit Drillcore Units

The felsic, coarse-grained igneous clasts in the diamicton and pebbles and cobbles of sub-unit 1a are likely fragments of the underlying Guichon Creek batholith bedrock. Their abundance (95%) and angularity suggest that they are likely derived from one proximal location, and supports the interpretation that this sub-unit is composed at least partly of local altered bedrock (cf. Chap. 3, Sect. 3.5.2).

The clasts at the bottom of sub-unit 1b are subangular, elongate, flat, and also consist mostly of felsic coarse-grained igneous rocks (~90%). However, more rounded clasts of various lithologies, including fine-grained igneous and multi-coloured volcanics, are found throughout the rest of it. Sub-unit 1b is interpreted as a debris flow deposit (see Chap. 3). The absence of clear evidence for a glaciation within the sedimentary record of unit 1 requires a different interpretation for the processes involved in bringing the more distal lithologies in that unit. A river running through the Valley and J.A. targets could explain the occurrence of more distal lithologies such as the volcanics. A debris flow dominated alluvial fan could have transported and deposited the local, weathered, Guichon Creek batholith clasts first. Guichon Creek batholith bedrock could have been locally frost-shattered or otherwise weathered (e.g. wall slope failure) from the valley walls, giving them their elongate, flat shapes. Higher up in the unit, the occurrence of more rounded pebbles and more varied lithologies suggest the environment evolved into a more extended fluvial system. The river could have brought clasts of Tertiary volcanics from outside of the Guichon Creek batholith and deposited them along with local clasts. Fluvial transport would have rounded the edges of the distal clasts to a higher degree than the locally derived ones.

The till of sub-unit 2a is composed of both local and distal material, but with a higher proportion (74%) of clasts not sourced from the local Guichon Creek batholith bedrock relative to the other units (**Figure 4.3**). This is the deepest and oldest identified till in the study area and its contrasting pebble composition relative to the younger tills suggest a different ice-flow configuration for this older till sheet.

The pebbles and cobbles and sand and gravel of sub-unit 2b are interpreted as grounding line wedge or outwash deposits of the retreating glacier margin. The pebbles and cobbles are mostly (92%) local Guichon Creek batholith (felsic, coarse-grained igneous), but also partly distal fine-grained igneous and volcanics (6%). The clasts found in the underlying till of sub-unit 2a were dominantly distally-derived, such as the porphyritic and fine-grained volcanic rocks, whereas the ice-marginal to pro-glacial sub-unit 2b contains more locally sourced Guichon Creek batholith clasts This suggest that material from sub-unit 2b is not just derived from the erosion and reworking of

underlying sub-unit 2a, but that new material was produced from direct erosion of local bedrock. Local bedrock erosion rates thus appear to have been higher during the ice retreat phase, which increased locally-sourced debris in sub-unit 2b. Several factors could explain this change in subglacial erosion and provenance (distal vs. proximal) during an ice retreat phase. For instance, studies have linked an increase of bedrock erosion through quarrying near the melting margins of ice sheets to large subglacial water pressure fluctuations in the ablation zone (e.g. Iverson, 1991; Sugden et al., 1992; Roberts and Long, 2005). This type of mechanisms could explain the observations of increased local lithologies in ice-marginal and proglacial deposits in the study area including those of sub-unit 2b. The pebbles and cobbles of sub-unit 2b at VTH2014-03 show evidence of glacial transportation (faceting), but also evidence of at least some fluvial transport (rounded edges).

The lithologies of the gravel and pebbles and cobbles of sub-units 3b and 3c almost all match that of the local Guichon Creek batholith (felsic, coarse-grained igneous). These sub-units form a local deposit that was identified in a single borehole (see Chap. 3, Figures 3.2 and 3.17) and interpreted as a debris flow dominated subaqueous fan. The local provenance of the deposit lends additional support to the interpretation that it forms a local unit related to local processes (i.e. sediment gravity flows).

The dropstones of sub-unit 3d are varied in lithology, and therefore came from both distal and local sources. The presence of dropstones indicate it was an ice-contact lake. A relatively high proportion of distal clasts in the dropstone population is not surprising given the likelihood of icebergs to contain far-travelled englacial debris.

The gravel, pebbles and cobbles of sub-unit 3e are of mostly local lithologies, while those of sub-unit 3f are of mixed local and distal lithologies. The outwash that formed 3f likely occurred with material that had a distal source and previously been eroded and deposited by ice or fluvial processes.

The clasts of the tills, ice-marginal or outwash deposits of sub-units 4a, 4b, 4c, 5a, 5b, 5c and 5d consist of mostly (62-90%) felsic, coarse-grained igneous rocks, as well as fine-grained igneous and volcanic types, and thus have both a local and distal provenance.

The ice sheet eroded material from the Tertiary volcanics bedrock up ice-flow direction to the north of the Guichon Creek batholith, as well as the local Guichon Creek batholith. The distal volcanic clasts are more rounded than the local Guichon Creek batholith ones, which is consistent with a longer transport distance.

The pebbles and cobbles of unit 6 are also varied in lithology. However, they are mostly felsic coarse-grained igneous, especially near the top of the unit, and entirely felsic coarse-grained igneous at VTH2014-07. The unit thus shows an upward increase in the local:distal ratio. This unit is interpreted to be fluvial in origin.

J.A. Units

The clasts of the lowermost unit (see Chap. 3, Fig. 3.14; 1021.2 to 1068.7 meters asl) are dominantly felsic coarse-grained (~95%). This composition together with the high angularity of the clasts of this and the intervening non-glacial diamicton suggest it consists of rockfall material from the local Guichon Creek batholith bedrock. However, some fine-grained igneous clasts appear towards the top of the unit, indicating an input of sediment sourced distally from outside the batholith. This distal material could have been transported by the ice that deposited the overlying till, and deposited as outwash amongst the rockfall material.

The overlying till (see Chap. 3, Fig. 3.14; 1069.7 to 1075.7 meters asl) includes a wider range of lithologies, and therefore has both a local and distal provenance. The clasts are still somewhat more angular than is usual for tills and contain a greater proportion of local Guichon Creek batholith clasts. One possible explanation for the abundance of local angular clasts in the till is that some of the rockfall debris was subglacially re-entrained and then deposited over a short distance by the advancing ice front. These local angular clasts could also have been produced by faulting in the area (see Chap. 1, Fig. 1.6), and subsequently transported and then deposited over a short distance by the advancing ice front.

The thick fine-grained unit (see Chap. 3, Fig. 3.14; 1075.7 to 1092.3 meters asl) which is interpreted as an ice-contact lake includes dark-coloured, fine-grained

dropstones. This suggests a distal source, which would be consistent with a higher proportion of far-travelled englacial debris in the icebergs relative to subglacial diamictons.

The thick gravelly sand and overlying pebbles with cobbles units (see Chap. 3, Fig. 3.14; 1093.6 to 1131.1 meters asl) interpreted as a sediment gravity flow consists of varied lithologies, but mostly (89%) distally-derived, fine-grained igneous ones. The distal provenance is somewhat surprising given the low textural maturity of the deposit. This distal signature and the similar appearance of the gravelly sand to the thin till unit directly underlying it at ~1093 meters asl (see Chap. 3, Fig. 3.14) could indicate that the sediment gravity flow re-entrained pre-existing material that was rich in distal debris.

The top thick subglacial till (see Chap. 3, Fig. 3.14) consists of mostly (94%) distal lithologies of a wide variety of types at the bottom of the unit. This proportion changes to become dominated (70%) by local lithologies (Guichon Creek batholith). This transition indicates a shift in provenance from outside the batholith to inside of it.

DH-15-GG

The clasts of the bottom conglomeratic unit (see Appendix A, Figure A.2; elevation range: 1081.7 to 1134.7 m asl) are volcanics of various types and colours and felsic coarse-grained igneous. The lithology of the boulders at 1144.5 to 1146.3 m asl is felsic, coarse-grained igneous rock. The pebbles in the overlying mix of poorly-sorted sand and till (elevation range: 1146.3 to 1158.6 m asl) are composed of a mix of mainly dark volcanics and felsic, coarse-grained igneous lithologies. The pebble and cobble layers capping the stratigraphy are of fine-grained igneous, volcanic and sedimentary lithologies.

4.1.3 Summary of Provenance and Implications

The main results and provenance interpretation presented above show that most units identified in drillcores in the study area have a dominant local signature with a high proportion of clast lithologies consistent with a Guichon Creek batholith source. This is especially the case for units interpreted to have been deposited by meltwater related

processes in ice-marginal or proglacial settings, such as sub-units 2b and 3b-e. Some tills have a higher proportion of distally-derived lithologies (e.g. sub-unit 2a). However, tills of sub-unit 4a and 4c have a higher proportion of locally-derived clasts relative to the other till units. Interestingly, these two till units directly overlie sorted units that are also rich in locally-derived clasts (e.g. sub-unit 3e). This could indicate re-entrainment of clasts from underlying units; a process referred to as lithological inheritance (Trommelen et al. 2013). **Table 4.1** present a summary of the findings regarding provenance of each unit. This general provenance analysis will be used as a guide to the interpretation and discussion of the other results presented in the sub-sections below. In the following sub-sections below, a summary of the results of mineral indicators and geochemical pathfinders are described and interpreted in terms of bedrock footprint signature (Lesher et al., 2017). Some of these assemblages may reflect proximal footprint while others may be more consistent with the distal footprint. This will be compared to the pebble lithology provenance analysis in order to identify any relationship (or lack thereof). However, it is important to note that there could be differences in provenance of clast fractions versus finer matrix fraction due to the different processes involved in the erosion and transport of particles of different sizes (Benn and Evans 2010). Finally, a comparison of results from subsurface tills with surface tills (Plouffe and Ferbey, 2016) is presented.

Table 4.1 Summary of provenance based on pebble lithology counts and depositional environment for the Valley Pit unconsolidated sediment units. See Chap. 3, Fig. 3.27 for details regarding the stratigraphic framework of the Valley Pit area.

Sub-unit	**Provenance (based on clast lithology)**	**Depositional Environment**
1a	Local dominant	Bedrock fall/slide onto previous lacustrine
1b	Hybrid mixed	Debris flow
2a	Distal dominant	Subglacial
2b	Local dominant	Subglacial
3a	Unknown	Glaciolacustrine
3b	Local dominant	Subaqueous delta/fan

3c	Local dominant	Subaqueous delta/fan
3d	Local dominant or hybrid mixed	Glacial-fed lake
3e	Local dominant	Glaciofluvial outwash plain
3f	Hybrid mixed	Proximal glaciofluvial
4a	Local dominant	Subglacial
4b	Local dominant	Proglacial
4c	Local dominant	Subglacial
5a	Hybrid mixed	Ice-marginal
5b	Local dominant	Subglacial
5c	Local dominant	Ice-marginal
5d	Local dominant	Subglacial
5e	Unknown	Ice-marginal/proximal
5f	Unknown	Ice-contact lake
6	Local dominant	Proglacial

4.2 Hyperspectral Results and Footprint Analysis

4.2.1 Hyperspectral Results

The pebble-sized fraction (>2mm) was analyzed for the alteration minerals prehnite and kaolinite for various poorly-sorted samples (till and others) from the Valley and J.A. cores and Highmont pit using hyperspectral techniques (see Chap. 2, Sect. 2.2.5 for details). These two minerals were detected in every unconsolidated cover sub-unit analyzed. The proportion of the top surface of the pebbles made up by prehnite and kaolinite for each sample is shown below (**Figures 4.5 and 4.6**).

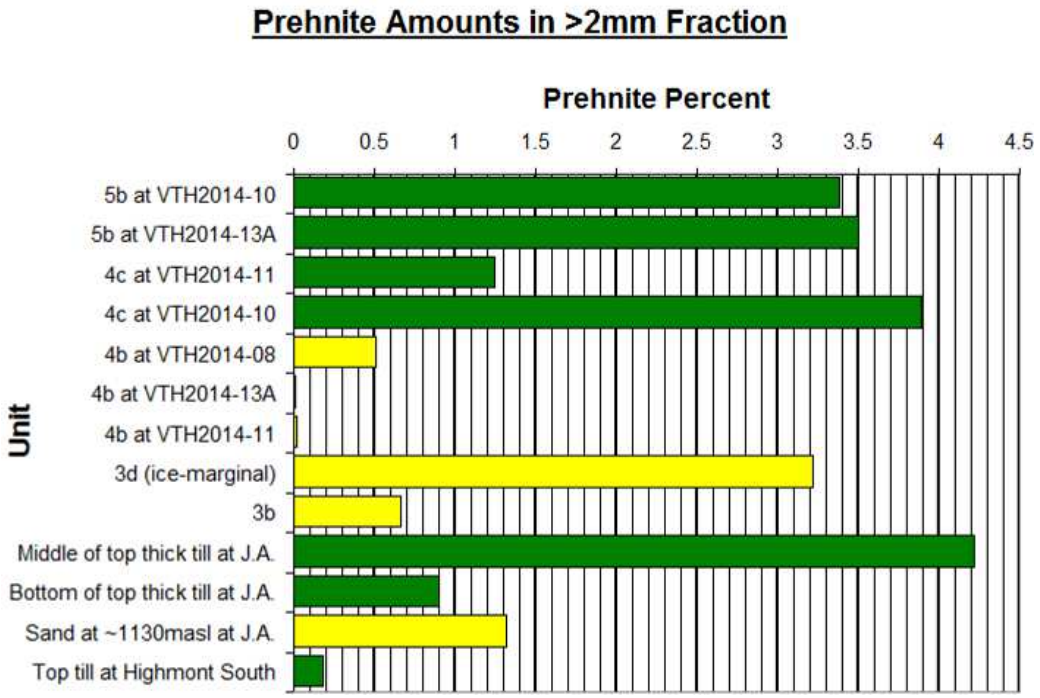

Figure 4.5 Prehnite percent in the >2 mm fraction of select stratigraphic sub-units. Green bars are for till samples while yellow bars are for sand and gravel samples.

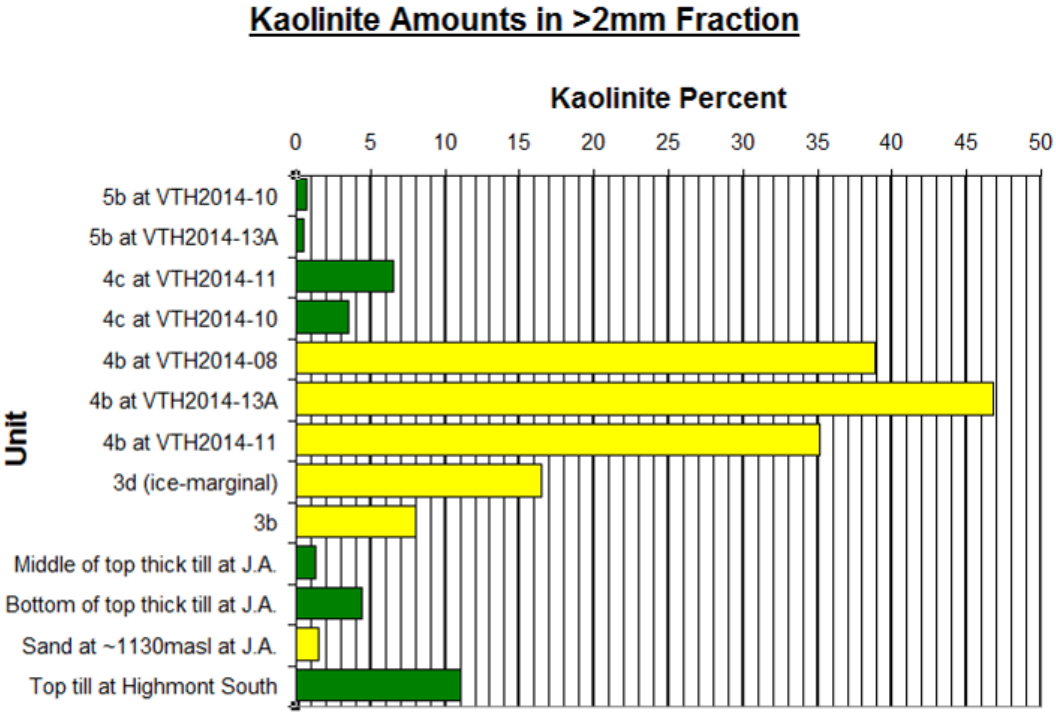

Figure 4.6 Kaolinite percent in the >2 mm fraction of select stratigraphic sub-units. Green bars are for till samples while yellow bars are for sand and gravel samples.

4.2.2 Hyperspectral Footprint Analysis

Prehnite

Prehnite is formed by propylitic alteration in the distal bedrock alteration zones of the Highland Valley system (D'Angelo et al., 2017; Byrne 2019; Byrne et al., in-review). It increases in abundance with distance from the mineralization, within about fifteen kilometers of the mineralized zones (Lesher et al., 2017). In the Valley pit area, fractures with prehnite fill or halos are present in the bedrock underneath and up to about a kilometer north of the Valley boreholes (Kevin Byrne, Pers. comm.). They are also present at the Bethlehem mineralization's distal alteration zone north (up ice-flow direction) of the J.A. borehole, and in the proximal and distal areas surrounding the Lornex mineralized zone north (up ice-flow direction) of the Highmont South pit.

There is an apparent negative correlation between prehnite amount and the proportion of Guichon Creek pebbles in the Valley Pit sub-units. Specifically, as the percent of locally-derived Guichon Creek pebbles increases, the prehnite concentration decreases (see Figure C.52 in Appendix C). In sub-unit 4c, there is considerably less prehnite at core VTH2014-11 than at VTH2014-10. However there is also a higher local signature at VTH2014-11 than at VTH2014-10 (82.6% and 73.5 % coarse-grained igneous, respectively).

This relationship is not apparent for the samples from the J.A. area. Two of the three samples contain a low prehnite concentration, and a high percent of locally-derived pebbles (see Figure C.52 in Appendix C).

Kaolinite

Kaolinite is a product of argillic alteration at the Valley and Lornex mineralized zones along and adjacent to major structures (Casselman et al., 1995; Byrne et al., 2013). It is found within 1.5 kilometers from mineralization, and part of the proximal alteration mineral assemblage (Lesher et al., 2017; Lesage et al., in-review). There are no known alteration zones containing kaolinite immediately north (up glacier flow direction) of the

Highland Valley system. The kaolinite in the unconsolidated cover at the Valley Pit and J.A. areas is thus undefined. It may be from an unknown local source around Highland Valley or from an unknown source north of and possibly outside the Highland Valley system. Alternatively, it may be from the J.A. and Lornex proximal alteration zones, having been transported north during an earlier glaciation or by ancient fluvial processes. The Lornex mineralized zone is within a few kilometers north (up ice-flow direction) of the Highmont South area, and may therefore be a source for the kaolinite at Highmont South.

There is a moderate positive correlation between kaolinite amount and Guichon Creek pebbles for the Valley Pit sub-units. Specifically, as the percentage of locally-derived (Guichon Creek batholith lithology) pebbles increases, the kaolinite concentration also generally increases (see Figure C.53 in Appendix C). Notably, the pebbles within sandy sub-unit 4b, interpreted as outwash deposit, have a much higher kaolinite content than pebbles from the till sub-units analyzed for hyperspectral (Figure 4.8). Interestingly, this sub-unit 4b overlies a till (4a) that has a dominantly local pebble provenance (Figure 4.3). This lends support to the idea that there could be an unknown local source of kaolinite alteration in the vicinity of Highland Valley. No correlation exists between kaolinite content and provenance for the J.A. units.

4.3 Indicator Mineral Results and Footprint Analysis

4.3.1 Indicator Mineral Results

Samples were selected in order to get the best lateral coverage over the mine zone where mineralization is significant, as well as to sample as many of the major till and sand units as possible over a variety of depths into the sediment cover. Focus was on the thick till units, because they comprise a significant portion of the unconsolidated sediment stratigraphy at Highland Valley, and can be compared to Plouffe and Ferbey's (2016) till results. Table C.1 (Appendix C) contains detailed information regarding location, depth and elevation intervals and unit descriptions for these thirteen samples.

The dry weight of the samples which were analyzed for heavy minerals ranged from 1.1 to 9.3 kilograms. The number of picked indicator mineral grains for each set of results was thus normalized to 5 kg. **Figure 4.7** shows these results for each unit. A set of photos of key mineral grains found in the samples are in Appendix C in the "Indicator Mineral Results" section.

(a)

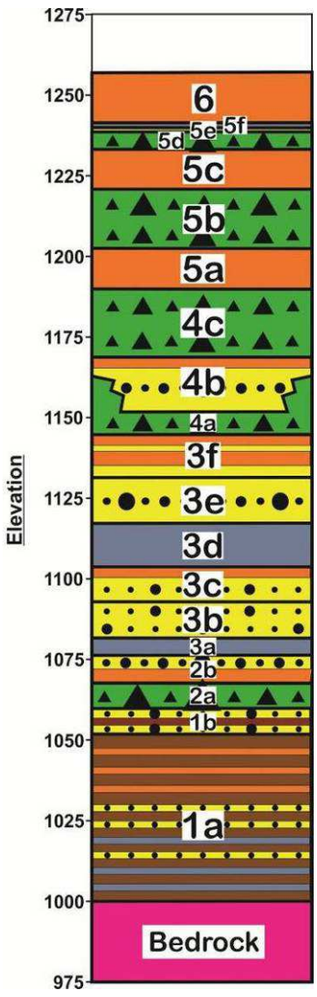

Sub-Unit	Indicator Mineral Results (counts normalized to 5 kg)
5b	Core VTH2014-10: **Number of Heavy Mineral Grains - High Counts** Py (PC) 0 100 200 300 400 500 **Number of Grains (Normalized to Total Sample Weight of 5kg)** **Number of Heavy Mineral Grains - Low Counts** Py (Nonfer) Cpy Adr Mn-Ep Cr 0 20 40 60 80 100 **Number of Grains (Normalized to Total Sample Weight of 5kg)** Core VTH2014-13A: Py (PC) Py (Nonfer) Cpy Adr Mn-Ep Cr 0 10 20 30 40 50
4c	Core VTH2014-10: Ma Py (PC) 0 500 1000 1500 2000 2500 VG Py (Nonfer) Cov Low-Cr Di Mn-Ep Cr Red Ru 0 20 40 60 80 100 120 Core VTH2014-11: Py (Nonfer) VG Cpy Cov Adr Low-Cr Di Mn-Ep Red Ru Cr Ja 0 50 100 150 200 250
4b	Core VTH2014-08: VG Py (PC) Py (Nonfer) Mn-Ep Cr Ja 0 50 100 150 200 250 Core VTH2014-11: Py (Nonfer) Py (PC) Mn-Ep Cr Ja 0 20 40 60 80 100 120 Core VTH2014-13A: Py (PC) 0 200 400 600 800 1000 Py (Nonfer) Cpy Mn-Ep Low-Cr Di Cr 0 5 10 15 20 25 30

(b)

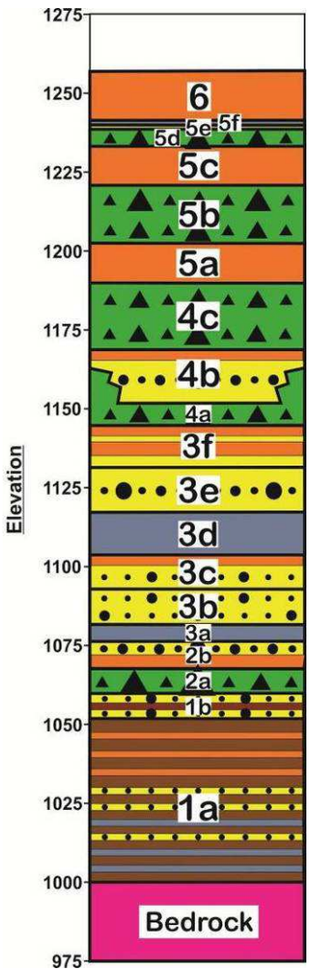

3d	Core VTH2014-10:
3b	Core VTH2014-03:
Sand at ~1130 m asl at J.A. (cf. Chap. 3, Sect. 3.1.9)	
Thick till dominating top of stratigraphy at J.A. (cf. Chap. 3, Sect. 3.1.9)	Sample from middle of unit:
	Sample from bottom of unit:
Top till at Highmont South	

(c)

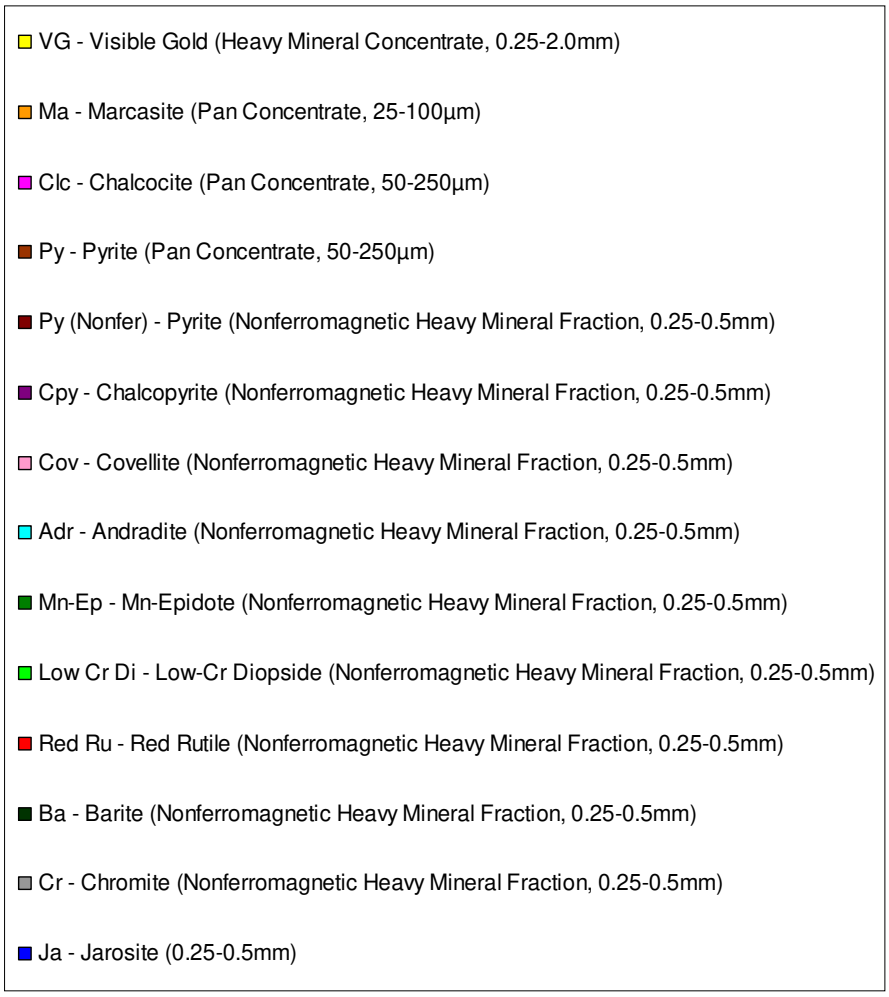

Figure 4.7 Indicator mineral results by stratigraphic unit.

4.3.2 Indicator Mineral Footprint Analysis

Sub-unit 5b, interpreted as subglacial till, contains pyrite, chalcopyrite, andradite, Mn-epidote, and chromite in both of its two samples analyzed.

Sub-unit 4c, a subglacial till, includes visible gold, pyrite, covellite, Mn-epidote, low-Cr diopside, red rutile, and chromite in both samples. In addition, abundant marcasite is found in one sample only, and chalcopyrite, andradite, and jarosite in the other.

Sub-unit 4b, a poorly-sorted outwash deposit, contains pyrite, Mn-epidote, and chromite in all three of its analyzed samples. Jarosite is found in two of the three samples analyzed, visible gold in one, and chalcopyrite and low-Cr diopside in another one of the three.

Sub-unit 3d, a glacial lake deposit, contains pyrite, abundant Mn-epidote, and chromite.

Sub-unit 3b, consisting of poorly-sorted sediment gravity flow material, contains pyrite, abundant Mn-epidote, low-Cr diopside, chromite, and jarosite.

The poorly-sorted sand and gravel unit at ~1130 m asl at J.A. is interpreted to be sediment gravity flow material. It contains pyrite, chalcopyrite, covellite, abundant low-Cr diopside, and abundant chromite.

In the till unit dominating the top of the J.A. stratigraphy, visible gold, covellite (including an anomalously high value), chromite, and jarosite are found throughout the unit. Abundant chalcocite, as well as chalcopyrite, andradite, and Mn-epidote are found only in the sample at the middle of the unit, while pyrite and barite are found only in the lower sample.

Chalcopyrite and pyrite are the most indicative of mineralization at Highland Valley. They are found within 15 kilometers and 6 kilometers, respectively, of mineralized zones. (Lesher et al., 2017). Chalcopyrite is mostly an ore indicator increasing in abundance towards the centres of mineralization (Lee et al. in Lesher et al., 2017; Lee et al., 2018). Pyrite is a proximal and medial alteration footprint indicator increasing in abundance towards the mineralizations (Lee et al. in Lesher et al., 2017; Lee et al., 2018). Chalcopyrite is most abundant in the shallowest till sub-unit sampled (sub-unit 5b). It is also found in lower abundance in the poorly-sorted sand and gravel unit at ~1130 m asl at J.A. Chalcopyrite is found inconsistently in sub-unit 4b (a poorly-sorted outwash deposit) and in the top till unit at J.A. Pyrite is most abundant in the poorly-sorted sand and gravel unit at ~1130 m asl at J.A. Significant counts of it were also obtained in the top till unit at J.A. (bottom sample only) as well as sub-unit 3b (poorly-sorted sediment gravity flow material). Every other sub-unit contains moderate amounts of pyrite, except for the top till at Highmont South.

No positive correlation exists between the proportion of clasts that are locally derived (Guichon Creek batholith) and the number of pyrite grains for the unconsolidated samples analyzed. The two samples with the highest normalized numbers of pan concentrate pyrite (25-500µm) grains, one from the bottom of the thick till unit dominating the top of the J.A. stratigraphy and the other from the sand unit at ~1130 m asl also at J.A., have the lowest proportions of locally derived pebbles (6.3 and 11.1%, respectively). The sample from the sand unit at ~1130 m asl at J.A. also has a nonferromagnetic fraction pyrite (0.25-0.5mm) count an order of magnitude higher than for all the other samples, despite having the second lowest (11.1%) proportion of locally derived pebbles. No apparent correlation exists between the proportion of clasts that are locally derived (Guichon Creek batholith) and the amount of chalcopyrite grains for the unconsolidated samples analyzed.

Chromite and diopside are porphyry copper indicator minerals (John et al., 2010), but they are rare to absent within the Highland Valley system. Pyrite, chromite, and diopside are resistate minerals that are not easily physically weathered (Kelley et al., 2011; Averill, 2013; Eppinger et al., 2013). The abundant pyrite, low-Cr diopside, and chromite in the sand and gravel unit at ~1130 from the J.A. core may therefore have been transported from another mineralized zone up the glacier flow direction. Diopside was observed in the sodic-calcic and locally in the potassic alteration assemblages at Highland Valley (Lesage et al., 2016). Diopside is also found as part of the hornfels and sodic alteration assemblages of alkalic porphyry copper-gold systems (Byrne and Tosdal, 2014; Lee et al., 2020, in-review). The Mount Polley prospect about 235 kilometers to the NNW from Highland Valley is an alkalic porphyry copper-gold system (Plouffe et al., 2016), whereas the Highland Valley porphyry system is calc-alkaline with different alteration types (Casselman et al., 1995; Lesage et al., 2016; Byrne, 2019). The low-Cr diopside found in the surficial cover at Highland Valley may have originated from the Highland Valley system, or from another alkalic porphyry copper-gold system up ice-flow direction from Highland Valley. The sand and gravel unit at ~1130 at J.A. is interpreted to have been formed in a subaqueous fan or delta environment. The provenance of the sand and gravel fan or delta unit is interpreted to be mostly north of the main mineralized zones of the Highland Valley system, but partly local as well (see section 4.1.2). The unit overlies subglacial deposits, so the distally-sourced fan or delta material may have come from the underlying glacial deposit. Glacial processes may have therefore eroded

the pyrite, low-Cr diopside, and chromite grains from outside of the Highland Valley system. It is not known whether the pyrite and chromite grains in this unit originate locally from the J.A. target, the Bethlehem system located within a few kilometers up the ice-flow direction, or outside of the Highland Valley system.

Chalcocite occurs in the Bethlehem phase (Byrne et al., 2013). Chalcocite grains were found in the top till at JA16-001. The Bethlehem phase is up ice-flow direction from JA16-001.

There is no known occurrence of visible gold grains in the mineralized bedrock at Highland Valley. At the Mount Polley prospect about 235 kilometers to the NNW from Highland Valley, surficial till samples contain gold grains (at least 15 grains per 10 kilograms) derived from the Cu-Au mineralization there (Plouffe et al., 2016). This anomalous gold grain count at Mount Polley exists as a surficial dispersal train about three to five kilometers long (Plouffe et al., 2016). Indicators of bedrock mineralization in sediment cover are increasingly attenuated towards the surface (Proudfoot et. al., 1995), but the signal may still be detectable in a deeper unit, and this may be the case for the Mount Polley visible gold dispersal train. Gold is able to survive physical transport (Averill, 2013). The gold grains in deeper till at the Valley pit area of Highland Valley may be part of a large-scale subsurface dispersal train extending from Mount Polley, the closest known mineral occurrence, or another unknown distant mineral occurrence. An equivalent of at least 7.5 grains per 5 kilograms of sample was found in the Mount Polley surficial samples that were part of the dispersal train, while 3-5 gold grains were found in an equal amount in some of the Highland Valley subsurface till or sand and gravel samples. Visible gold is only found in one of the sand and gravel sub-units analyzed, which is expected given the inferred distal source and the high density of gold compared to the other minerals found in the samples. The rock particles comprising these sub-units would likely have been selectively entrained by the fluvial processes forming these environments. The significantly denser gold grains would have been left behind, and not transported beyond the ice margin to the subaqueous fan, delta or outwash plain.

Epidote is present in alteration resulting from mineralization at Highland Valley (Lesage et al., 2016; D'Angelo et al., 2017; Byrne, 2019). However, albite-epidote-hornfels

facies metamorphism is widespread in the Nicola Group (Preto et al., 1979); it is therefore also present in un-mineralized bedrock up the glacier-flow direction from Highland Valley. Mn-epidote is found in some of the subsurface units in abundances an order of magnitude higher than those of the surficial till samples (Plouffe and Ferbey, 2016), but it is not known whether these grains originate from un-mineralized bedrock or from alteration resulting from mineralization. Mn-epidote counts are therefore not a useful footprint indicator of mineralization at Highland Valley. More information is needed about the characteristics of the Mn-epidote grains found in the sediment cover (i.e. mineral chemistry) in order to determine whether their provenance is from mineralized bedrock or not.

4.3.3 Hand Sample Observation

Minerals resulting from porphyry copper mineralization were also observed in local Guichon Creek batholith pebble and cobble hand samples for a few of the samples for which pebble counts were done.

In sub-unit 1a of the unconsolidated sediment succession, fine gold, bronze, and copper coloured grains, as well as azurite grains were found. Malachite and azurite are both copper minerals common in the Highland Valley system. The bronze coloured grains may be bornite, a major copper sulphide mineral in the Highland Valley porphyry system (Perkins, 2011). The yellow, gold, or copper coloured grains may be chalcopyrite, and the gold coloured grains may also be pyrite, both also major copper sulphide minerals at Highland Valley (Nesse, 2000). These indicators could be sourced from underlying mineralized bedrock, which would be consistent with the interpretation that this sedimentary sub-unit 1a consists of disintegrated local bedrock (cf. Chap.3, Sect. 3.5.2).

A minor proportion of the pebbles of a sample taken from the upper part of the ice-contact fan or delta deposit sub-unit 4b (cf. Chap. 3, Sect. 3.5.5) are porphyries likely belonging to the Guichon Creek Batholith that contain medium to large-grained, yellow to light gold coloured phenocrysts. These may be gold, pyrite, or chalcopyrite grains.

In sub-unit 5c, interpreted as ice-marginal (cf. Chap. 3, Sect. 3.5.5), a minor amount of fine gold, bronze, or copper coloured grains, malachite grains, and fine malachite, or azurite inclusions were observed in coarse, black mafic grains in one of the samples.

No pebble counts were done for the minor, localized sub-units of 1b, 5e, 5f, or for unit 6. Glacial lake sub-unit 3a did not include any pebbles or cobbles. No visible indicator minerals were found in the samples from some of the till sub-units (2a, 4a, 4c, 5b, or 5d) as well as coarser subaqueous and glaciofluvial sub-units (2b, 3b, 3c, 3e, 3f, and 5a) and glacial lake sub-unit 3d. However, the occurrence of visible copper mineralization in pebbles of sub-units 4b and 5c demonstrates the presence of a porphyry copper mineral footprint in the subsurface stratigraphic units. These sub-units are all dominantly locally-derived (see Sect 4.1.2 above).

4.4 Geochemical Results and Footprint Analysis

4.4.1 Geochemical Results

The same samples as those used for indicator mineral and hyperspectral analyses were also analyzed for matrix geochemistry, with some additional samples added in order to get a better lateral and vertical coverage. See Chap. 2, Sect. 2.2.6 for methodological details and Table C.2 of Appendix C for location, depth and elevation intervals, and unit description information for the 33 samples analyzed for geochemistry. **Figure 4.8** shows the results for each unit. The results shown here were obtained from the partial digestion method.

(a)

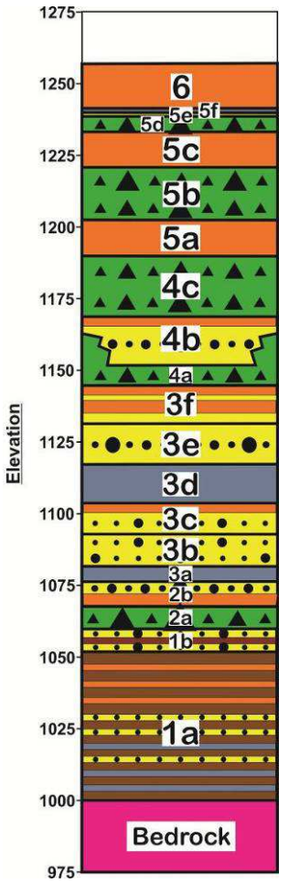

Sub-Unit	Geochemical Results
5d (n=4)	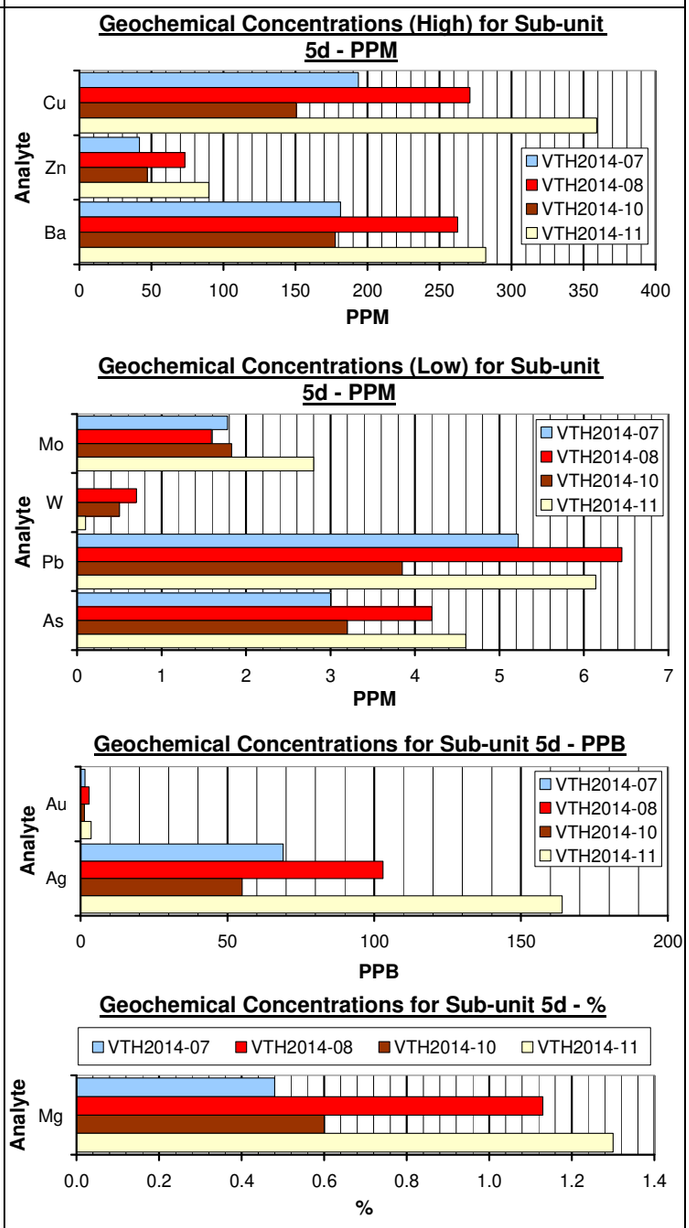
5c (n=1)	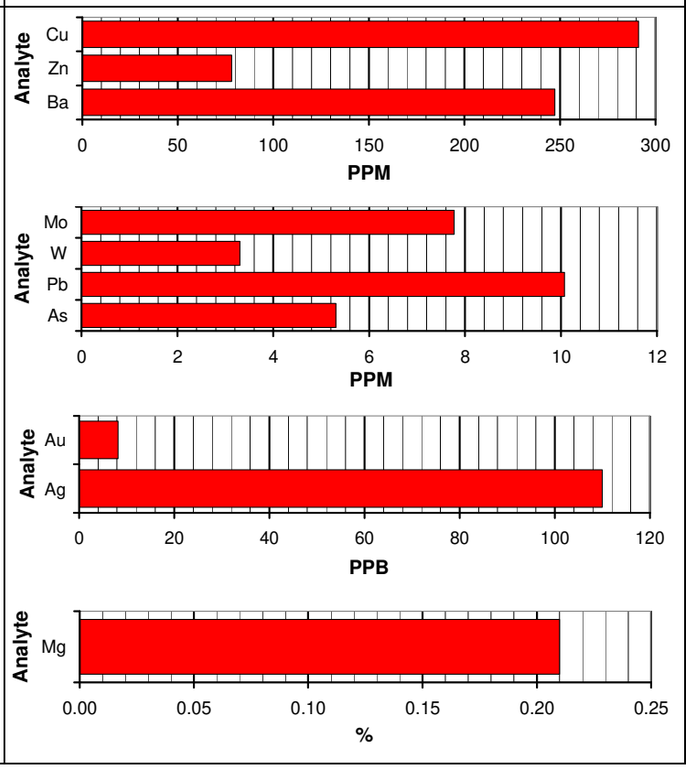

(b)

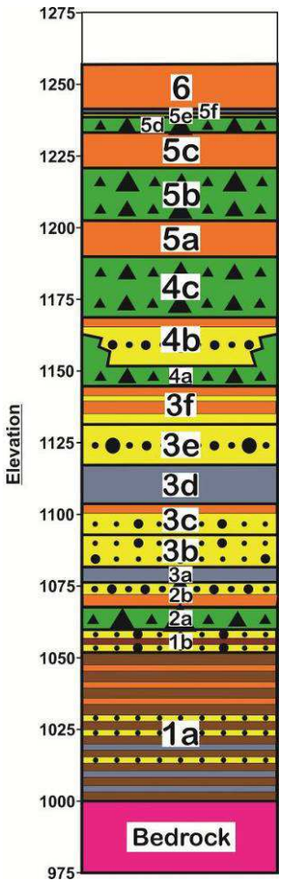
Elevation
1275
1250
1225
1200
1175
1150
1125
1100
1075
1050
1025
1000
975
6
5e
5f
5d
5c
5b
5a
4c
4b
4a
3f
3e
3d
3c
3b
3a
2b
2a
1b
1a
Bedrock

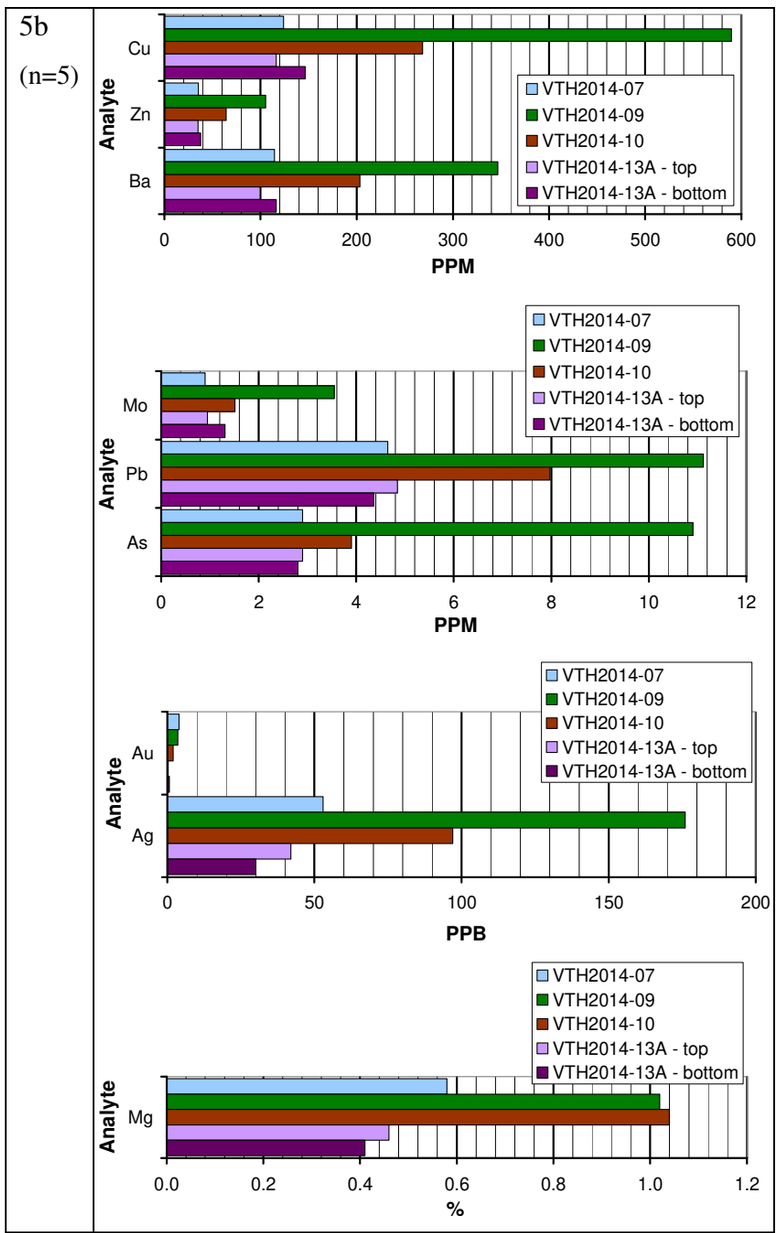
5b
(n=5)
Analyte
Cu
Zn
Ba
VTH2014-07
VTH2014-09
VTH2014-10
VTH2014-13A - top
VTH2014-13A - bottom
0
100
200
300
400
500
600
PPM
Mo
Pb
As
2
4
6
8
10
12
Au
Ag
50
150
PPB
Mg
0.0
0.2
0.4
0.6
0.8
1.0
1.2
%

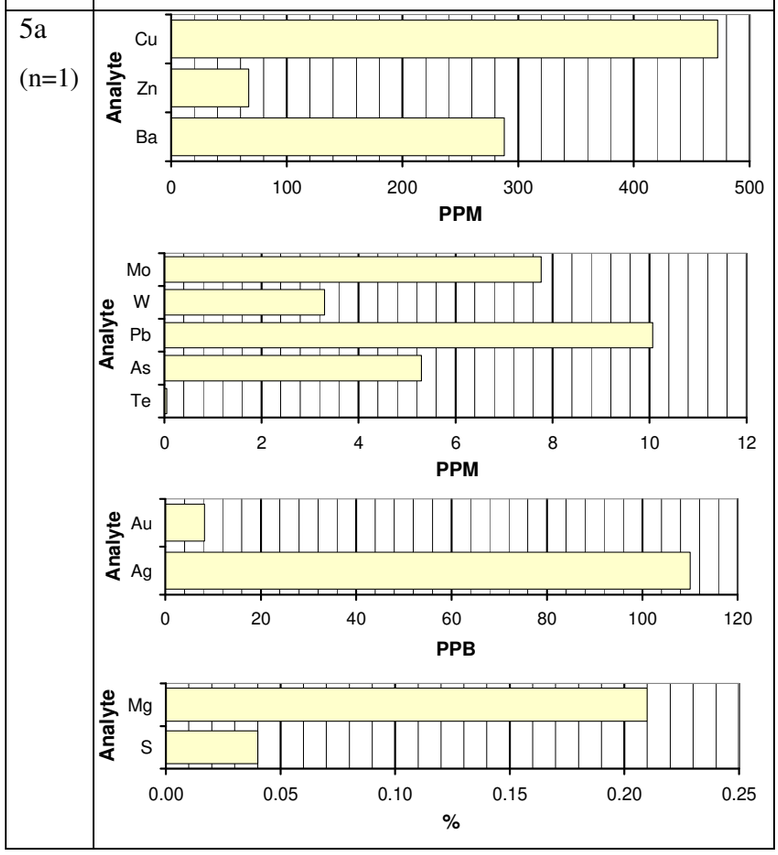
5a
(n=1)
Analyte
Cu
Zn
Ba
0
100
200
300
400
500
PPM
Mo
W
Pb
As
Te
2
4
6
8
10
12
Au
Ag
20
40
60
80
100
120
PPB
Mg
S
0.00
0.05
0.10
0.15
0.20
0.25
%

(c)

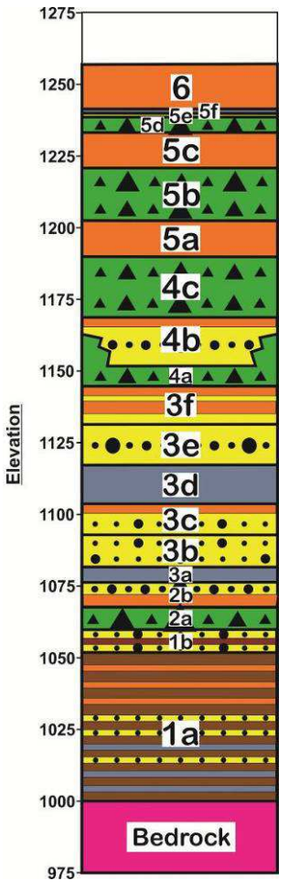
Elevation
1275
1250
1225
1200
1175
1150
1125
1100
1075
1050
1025
1000
975
6
5e
5f
5d
5c
5b
5a
4c
4b
4a
3f
3e
3d
3c
3b
3a
2b
2a
1b
1a
Bedrock

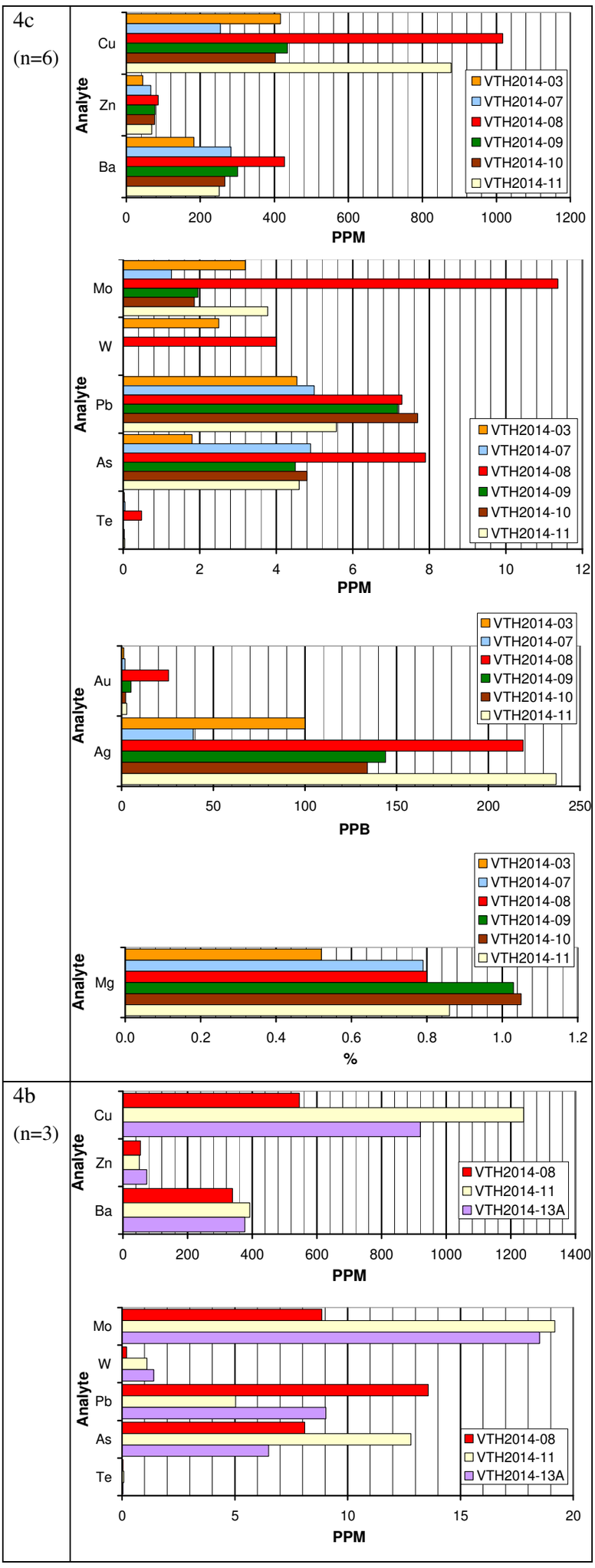
4c
(n=6)
Analyte
Cu
Zn
Ba
VTH2014-03
VTH2014-07
VTH2014-08
VTH2014-09
VTH2014-10
VTH2014-11
0
200
400
600
800
1000
1200
PPM
Mo
W
Pb
As
Te
0
2
4
6
8
10
12
PPM
Au
Ag
0
50
100
150
200
250
PPB
Mg
0.0
0.2
0.4
0.6
0.8
1.0
1.2
%
4b
(n=3)
VTH2014-08
VTH2014-11
VTH2014-13A
0
200
400
600
800
1000
1200
1400
PPM
0
5
10
15
20
PPM

(d)

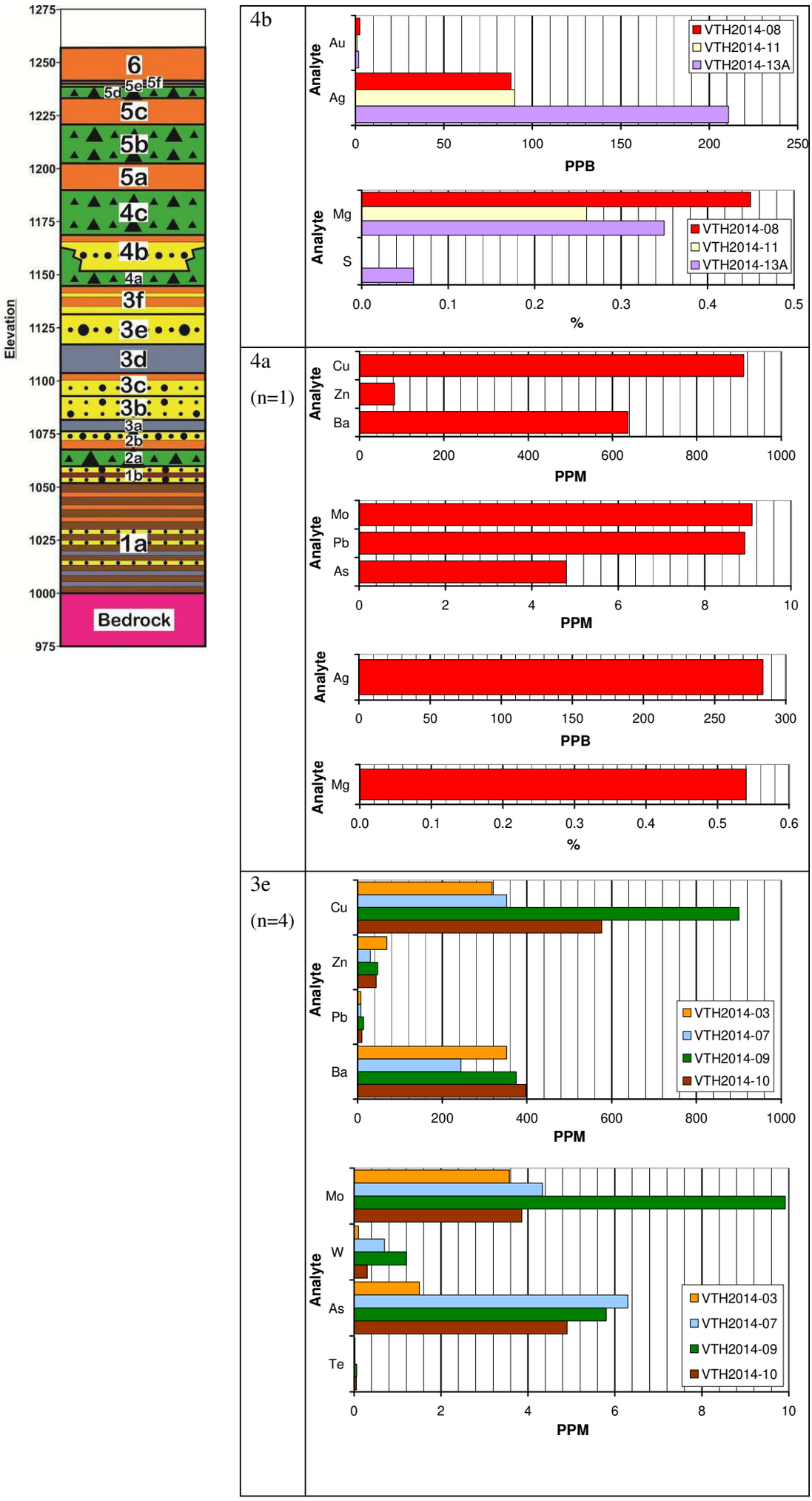
Elevation
1275
1250
1225
1200
1175
1150
1125
1100
1075
1050
1025
1000
975
6
5e
5f
5d
5c
5b
5a
4c
4b
4a
3f
3e
3d
3c
3b
3a
2b
2a
1b
1a
Bedrock
4b
Analyte
Au
Ag
VTH2014-08
VTH2014-11
VTH2014-13A
0
50
100
150
200
250
PPB
Analyte
Mg
S
VTH2014-08
VTH2014-11
VTH2014-13A
0.0
0.1
0.2
0.3
0.4
0.5
%
4a
(n=1)
Analyte
Cu
Zn
Ba
0
200
400
600
800
1000
PPM
Analyte
Mo
Pb
As
0
2
4
6
8
10
PPM
Analyte
Ag
0
50
100
150
200
250
300
PPB
Analyte
Mg
0.0
0.1
0.2
0.3
0.4
0.5
0.6
%
3e
(n=4)
Analyte
Cu
Zn
Pb
Ba
VTH2014-03
VTH2014-07
VTH2014-09
VTH2014-10
0
200
400
600
800
1000
PPM
Analyte
Mo
W
As
Te
VTH2014-03
VTH2014-07
VTH2014-09
VTH2014-10
0
2
4
6
8
10
PPM

(e)

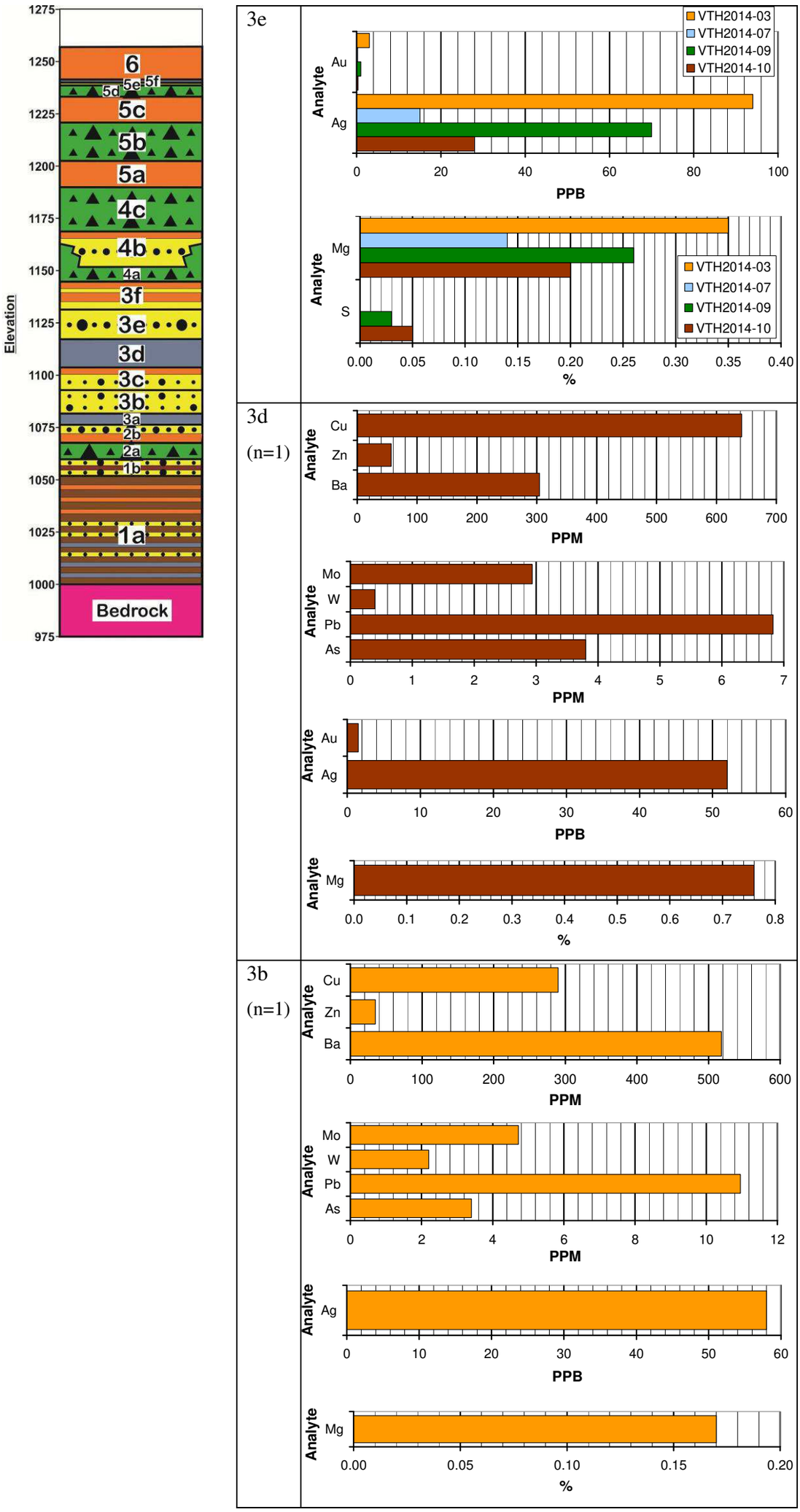
Elevation
1275
1250
1225
1200
1175
1150
1125
1100
1075
1050
1025
1000
975
6
5e
5f
5d
5c
5b
5a
4c
4b
4a
3f
3e
3d
3c
3b
3a
2b
2a
1b
1a
Bedrock
3e
VTH2014-03
VTH2014-07
VTH2014-09
VTH2014-10
Analyte
Au
Ag
PPB
Mg
S
%
3d
(n=1)
Cu
Zn
Ba
PPM
Mo
W
Pb
As
3b
(n=1)

(f)

J.A.

(n=4)

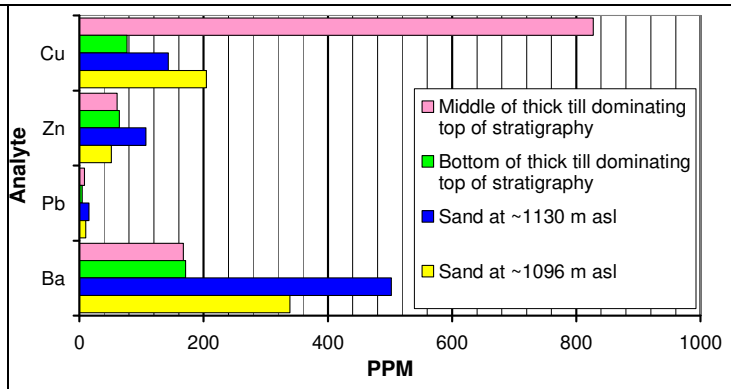
Cu
Zn
Pb
Ba
Analyte
0
200
400
600
800
1000
PPM
Middle of thick till dominating top of stratigraphy
Bottom of thick till dominating top of stratigraphy
Sand at ~1130 m asl
Sand at ~1096 m asl

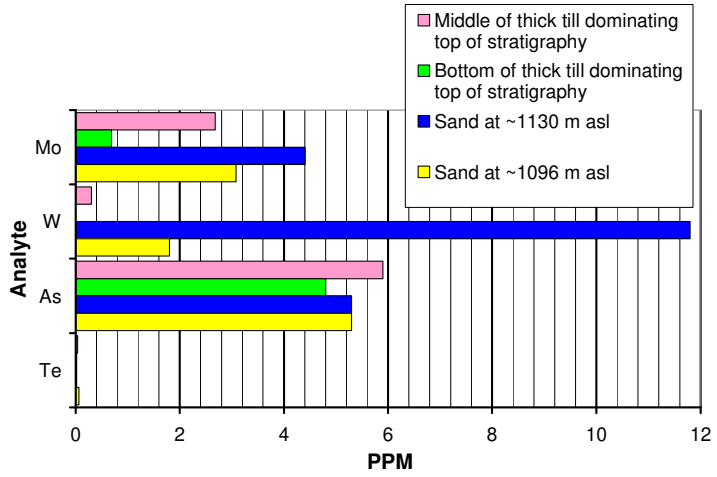
Mo
W
As
Te
Analyte
0
2
4
6
8
10
12
PPM
Middle of thick till dominating top of stratigraphy
Bottom of thick till dominating top of stratigraphy
Sand at ~1130 m asl
Sand at ~1096 m asl

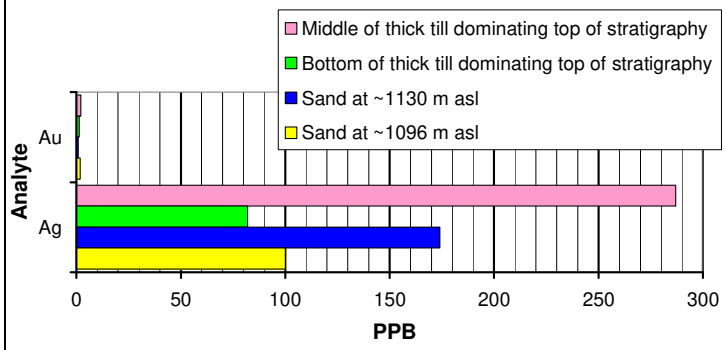
Au
Ag
Analyte
0
50
100
150
200
250
300
PPB
Middle of thick till dominating top of stratigraphy
Bottom of thick till dominating top of stratigraphy
Sand at ~1130 m asl
Sand at ~1096 m asl

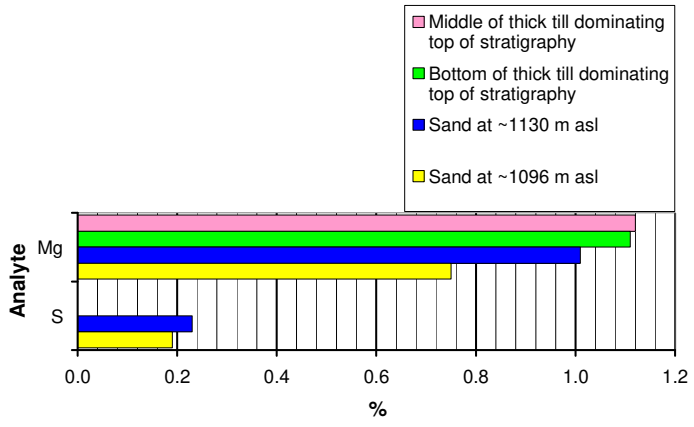
Mg
S
Analyte
0.0
0.2
0.4
0.6
0.8
1.0
1.2
%
Middle of thick till dominating top of stratigraphy
Bottom of thick till dominating top of stratigraphy
Sand at ~1130 m asl
Sand at ~1096 m asl

(g)

Top till at Highmont South (n=1)	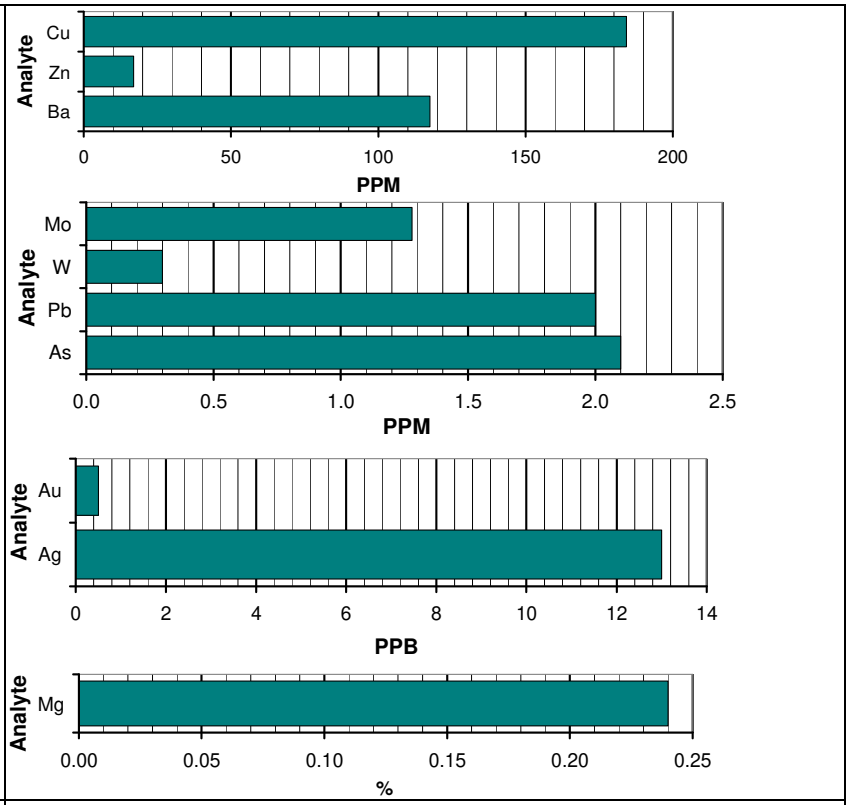
Till at DH-15-GG (n=1)	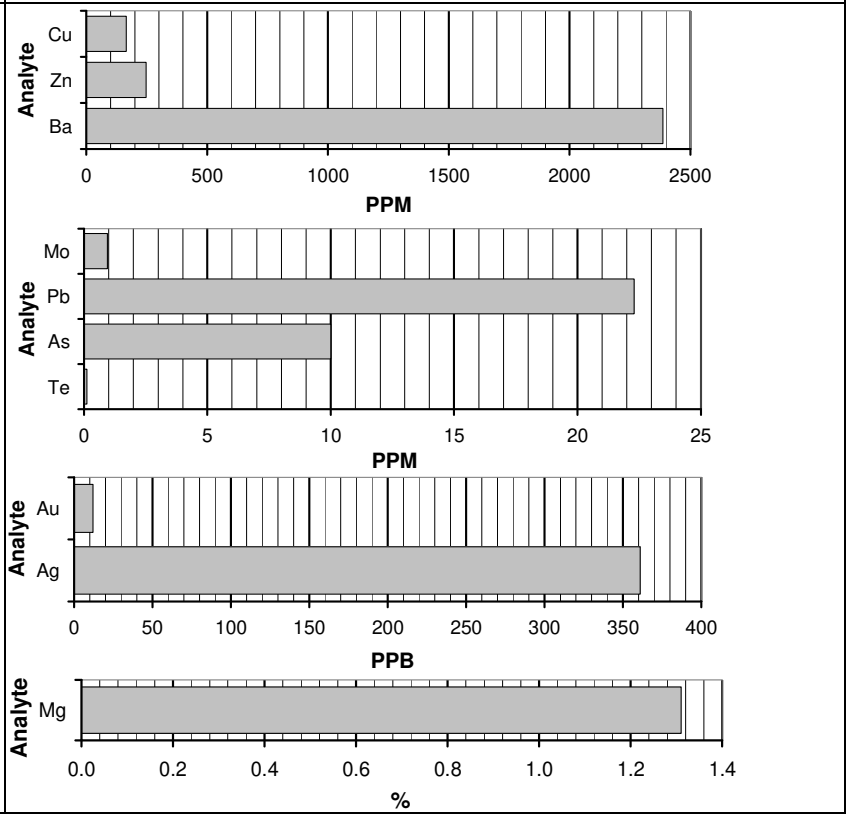

Figure 4.8 Geochemical results by stratigraphic unit. Values shown as a percentage are by weight percentage.

4.4.2 Geochemical Footprint Analysis

The elements copper, molybdenum, gold, and nickel are most indicative of mineralization at Highland Valley. These are components of the ore, proximal and medial bedrock footprint (within about six kilometers) of mineralization at Highland Valley; they increase in concentration towards the centres of mineralization (Lee et al. in Lesher et al., 2017; Lee et al., 2018). Tungsten atoms may chemically substitute for molybdenum atoms in porphyry copper systems due to their similar atomic properties, and it commonly occurs in porphyry systems (John et al., 2010; Sillitoe, 2010). Iron, magnesium, zinc, and lead are components of the ore, proximal, medial, and distal footprints (over fifteen kilometers) of mineralization; they increase in concentration with distance from the mineralized zones (Lesher et al., 2017). Tin, arsenic, antimony, barium, tellurium, bismuth, silver, and sulphur are generally found in anomalous concentrations at porphyry copper deposits (Berger et al., 2008). Sulphur may be derived from sulphide minerals (i.e. bornite, chalcopyrite, pyrite) are part of the proximal and medial bedrock footprint of mineralization at Highland Valley (Casselman et al., 1995; Byrne et al., 2013). There is a zone up to 500 meters wide surrounding the mineralized zones in which there are anomalous sulphur concentrations in the bedrock (Casselman et al., 1995). **Figures 4.9 and 4.10** show quantile-quantile plots for select elements for the till and sand samples, respectively. These were used to find anomalous values.

Till Units

One of the four samples (VTH2014-11; **Figure 4.8**) from sub-unit 5d, a subglacial till, has a relatively high concentration of magnesium (**Figure 4.9h**). This suggests a distal footprint contribution for this sub-unit, due to magnesium concentration in the bedrock footprint increasing with distance from the mineralized zones; however, this is based on a single sample out of four.

Two of the five samples (VTH2014-09 and VTH2014-10; **Figure 4.8**) from sub-unit 5b, a sub-glacial till, have relatively high magnesium concentrations (**Figure 4.9h**). One of these samples also has a relatively high concentration of arsenic (**Figure 4.9j**).

Sub-unit 5b has a distal footprint geochemical signature based on its magnesium concentrations, while the elevated arsenic level is indicative of mineralization.

Two of the six samples (VTH2014-08 and VTH2014-11; **Figure 4.8**) from sub-unit 4c, a subglacial till, contain relatively high copper and silver concentrations (**Figures 4.9a and 4.9k**). One of these samples also has relatively high concentrations of molybdenum, tungsten, and arsenic (**Figures 4.9b, 4.9c, and 4.9j**). Furthermore, this sample has elevated gold, tellurium, and bismuth concentrations all an order of magnitude higher than all the other samples from the Highland Valley cores (**Figures 4.9d, 4.9n, and 4.9o**). A third sample also has an anomalous concentration of tungsten (**Figure 4.9c**). Two others of the six samples have elevated magnesium levels (**Figure 4.9h**). The elevated copper, molybdenum, tungsten, gold, and arsenic concentrations are indicative of mineralization and indicate a source proximal to the mineralized zones, while the elevated magnesium, tellurium, and bismuth concentrations suggest a distal footprint contribution.

Sub-unit 4a, a subglacial till, has one of the highest concentrations of both copper and barium for this dataset (**Figures 4.9a and 4.9l**), as well as a relatively high molybdenum concentration (**Figure 4.9b**). However, this is based on a single sample (VTH2014-08).

The sample from the middle of the top thick till at J.A. has relatively high levels of both copper and arsenic (**Figures 4.9a and 4.9j**). Both samples from this top thick till have relatively high magnesium concentrations (**Figure 4.9h**). The elevated copper concentration is indicative of mineralization, while the elevated magnesium concentration suggests a distal footprint contribution.

The till sample from core DH-15-GG is located twelve kilometers to the northwest of the Highland Valley mineralized zones. It is located over the outer edge of the distal footprint (3-15 kilometers) of the Highland Valley system, and its pebbles consist of mostly distally-derived material from outside the Guichon Creek batholith. Its composition can serve as a comparison for that of the unconsolidated samples collected over or very close to the mineralized zones at Highland Valley, which have a mostly local, Guichon Creek batholith source. Most or all of the Highland Valley till samples have

greater values of copper, molybdenum, and tungsten than the till sampled at DH-15-GG (**Figures 4.9a, 4.9b, and 4.9c**). Zinc, lead, nickel, and barium concentrations are significantly higher (246, 22, 102, and 2387 ppm, respectively) at DH-15-GG than for the till samples from Highland Valley (17-105, 2-11, 8-39, and 100-636 ppm, respectively; **Figures 4.9e, 4.9f, 4,9g, and 4.9l**). The gold, magnesium, iron, arsenic, silver, antimony, tellurium, and bismuth values at DH-15-GG are the highest or one of the highest of their respective datasets, and are anomalous compared to samples from the cores at Highland Valley (**Figures 4.9d, 4.9h-k, and 4.9m-o**). The low concentrations of copper, molybdenum, and tungsten in the sample from DH-15-GG compared to the Highland Valley samples, and the high concentrations of zinc, lead, magnesium, and iron, tellurium, and bismuth at DH-15-GG compared to the Highland Valley samples indicate a distal footprint contribution for DH-15-GG. In contrast, the high concentrations of gold and nickel suggest a contribution from the Highland Valley mineralization.

(a)

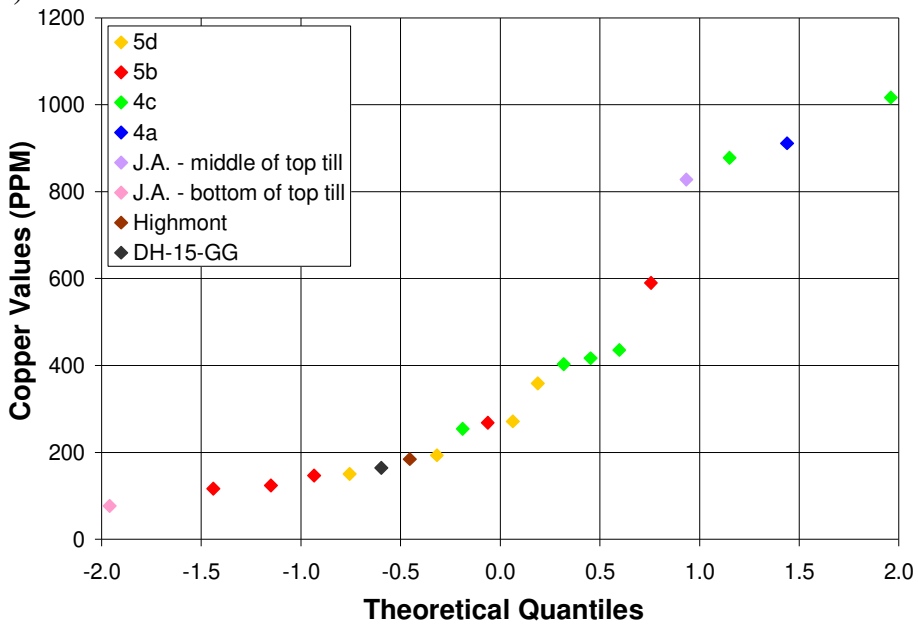

(b)

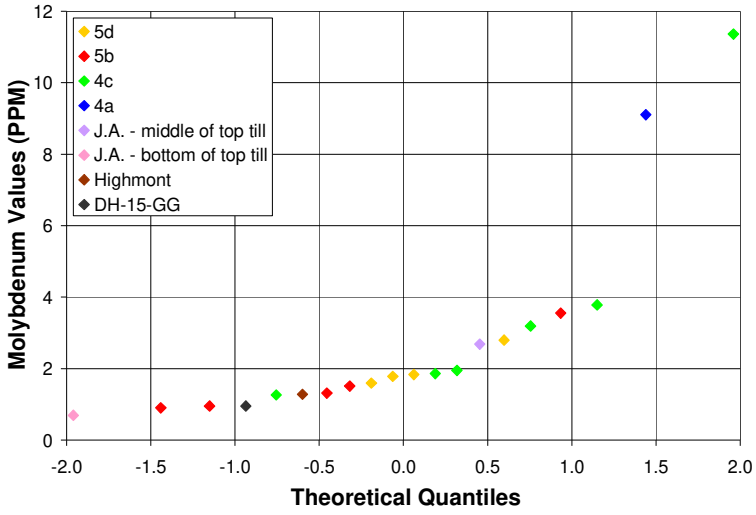
Molybdenum Values (PPM)
Theoretical Quantiles
5d
5b
4c
4a
J.A. - middle of top till
J.A. - bottom of top till
Highmont
DH-15-GG

(c)

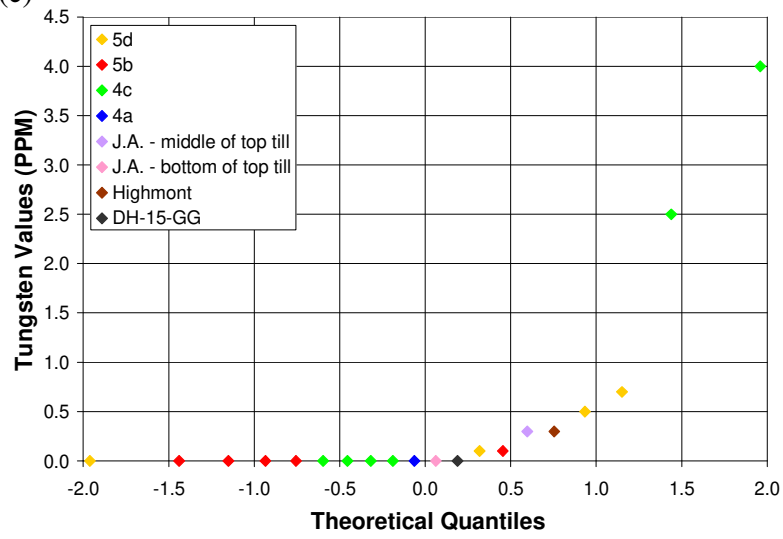
Tungsten Values (PPM)
Theoretical Quantiles
5d
5b
4c
4a
J.A. - middle of top till
J.A. - bottom of top till
Highmont
DH-15-GG

(d)

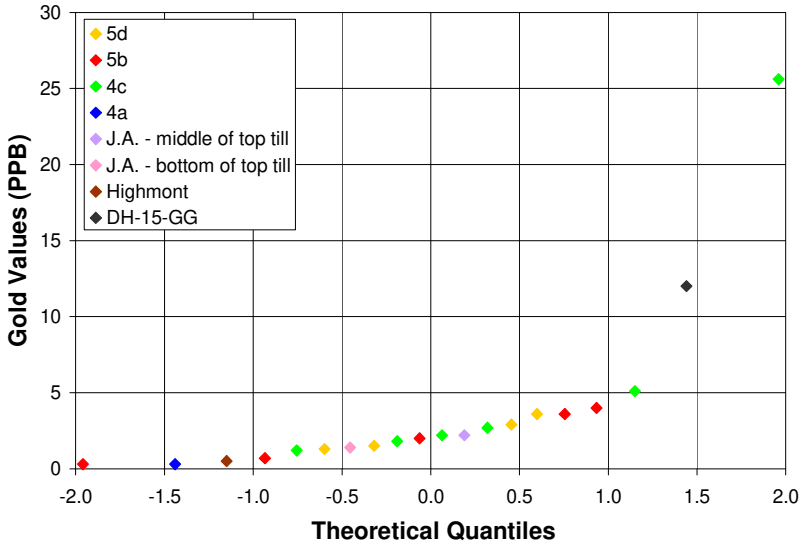
Gold Values (PPB)
Theoretical Quantiles
5d
5b
4c
4a
J.A. - middle of top till
J.A. - bottom of top till
Highmont
DH-15-GG

(e)

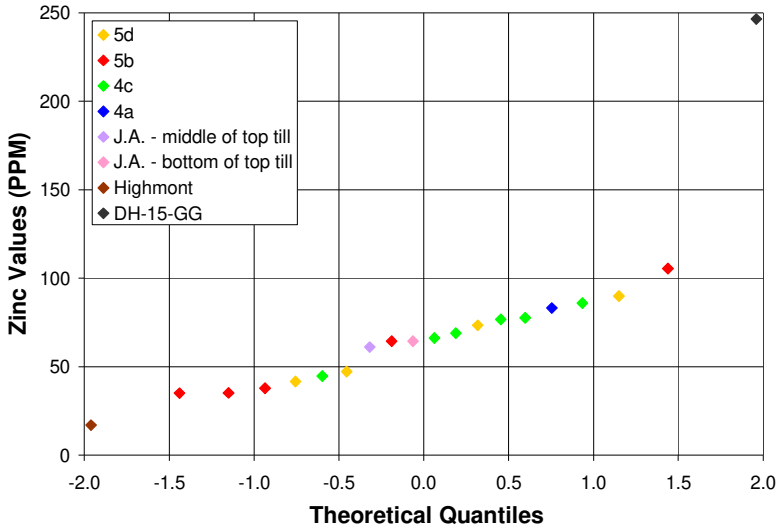
5d
5b
4c
4a
J.A. - middle of top till
J.A. - bottom of top till
Highmont
DH-15-GG
Zinc Values (PPM)
250
200
150
100
50
0
-2.0
-1.5
-1.0
-0.5
0.0
0.5
1.0
1.5
2.0
Theoretical Quantiles

(f)

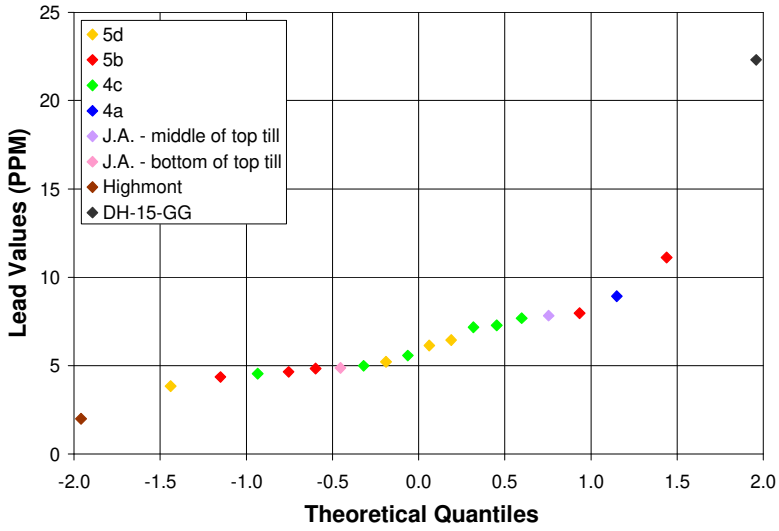
5d
5b
4c
4a
J.A. - middle of top till
J.A. - bottom of top till
Highmont
DH-15-GG
Lead Values (PPM)
25
20
15
10
5
0
-2.0
-1.5
-1.0
-0.5
0.0
0.5
1.0
1.5
2.0
Theoretical Quantiles

(g)

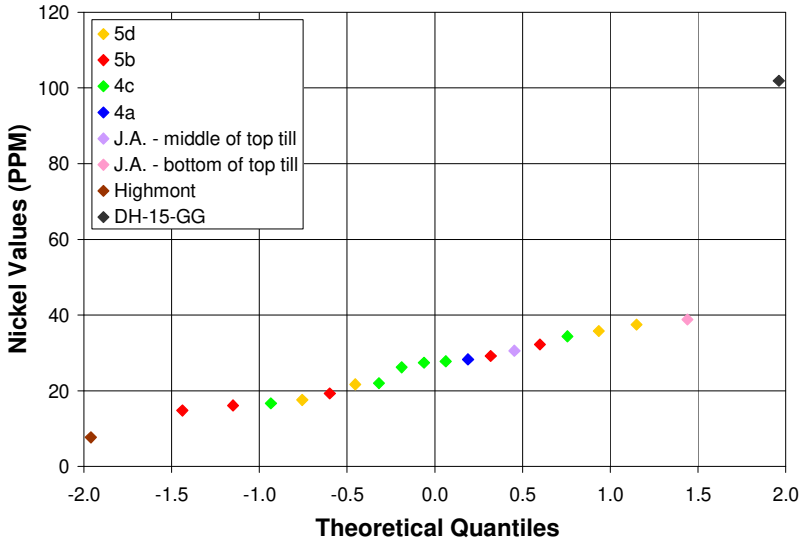
5d
5b
4c
4a
J.A. - middle of top till
J.A. - bottom of top till
Highmont
DH-15-GG
Nickel Values (PPM)
120
100
80
60
40
20
0
-2.0
-1.5
-1.0
-0.5
0.0
0.5
1.0
1.5
2.0
Theoretical Quantiles

(h)

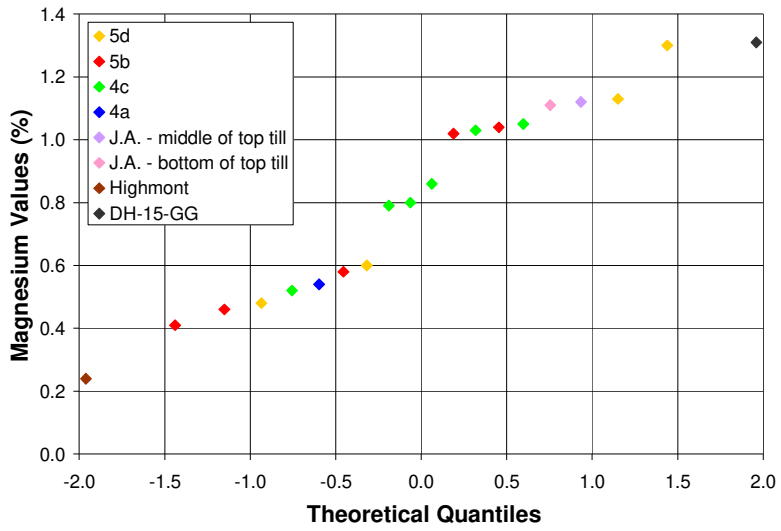
Magnesium Values (%)
Theoretical Quantiles
5d
5b
4c
4a
J.A. - middle of top till
J.A. - bottom of top till
Highmont
DH-15-GG

(i)

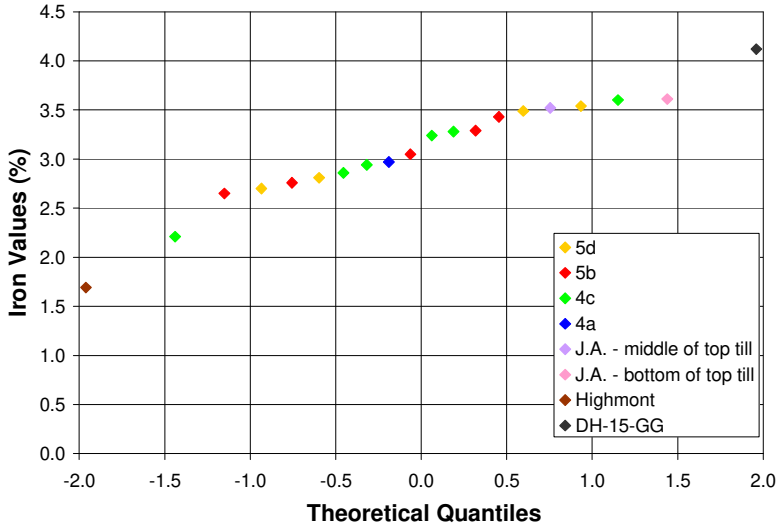
Iron Values (%)
Theoretical Quantiles
5d
5b
4c
4a
J.A. - middle of top till
J.A. - bottom of top till
Highmont
DH-15-GG

(j)

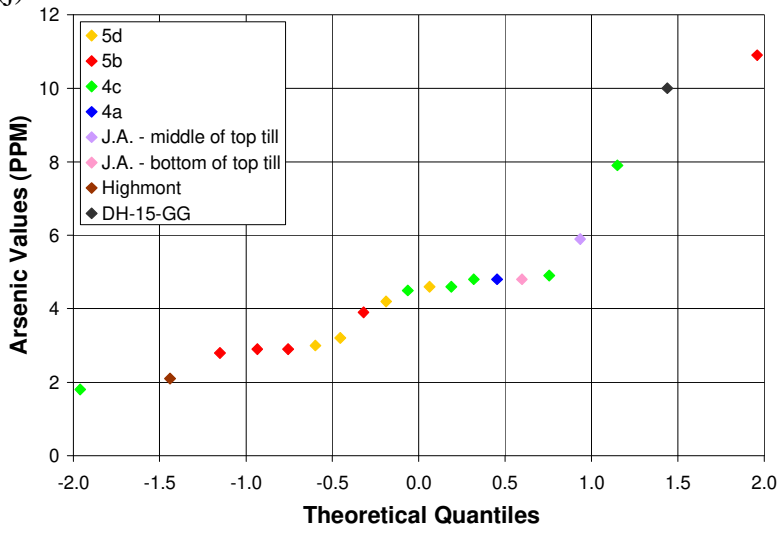
Arsenic Values (PPM)
Theoretical Quantiles
5d
5b
4c
4a
J.A. - middle of top till
J.A. - bottom of top till
Highmont
DH-15-GG

(k)

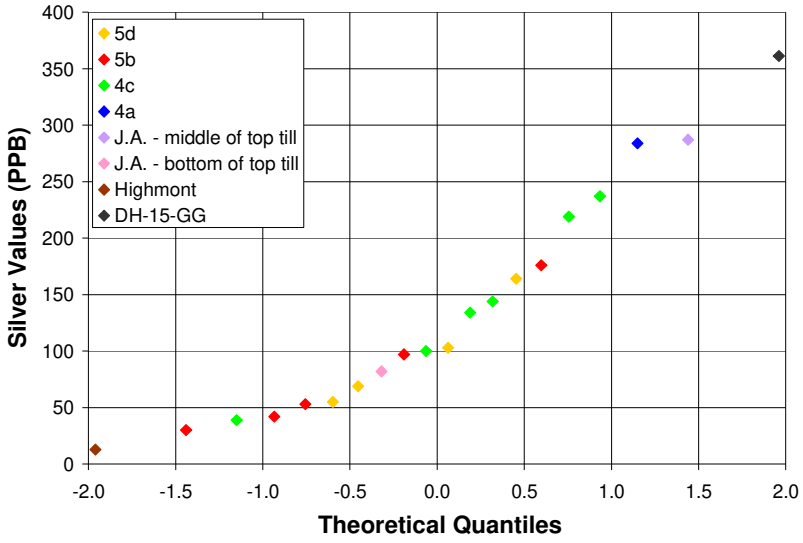
Silver Values (PPB)
Theoretical Quantiles
5d
5b
4c
4a
J.A. - middle of top till
J.A. - bottom of top till
Highmont
DH-15-GG

(l)

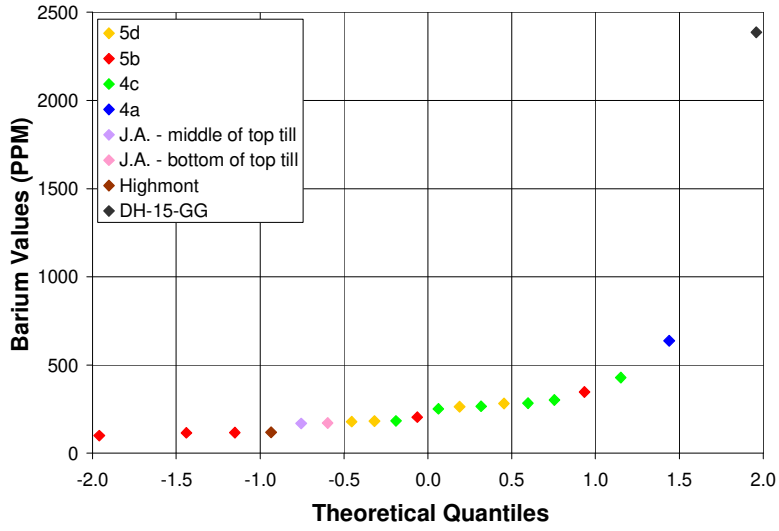
Barium Values (PPM)
Theoretical Quantiles
5d
5b
4c
4a
J.A. - middle of top till
J.A. - bottom of top till
Highmont
DH-15-GG

(m)

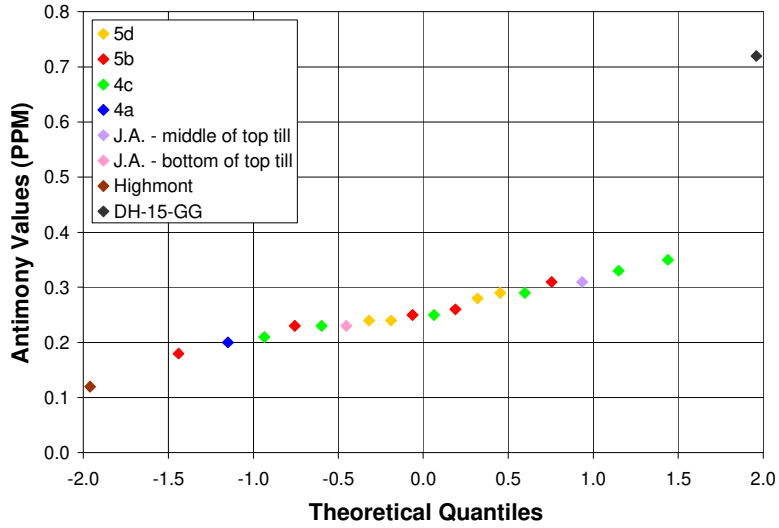
Antimony Values (PPM)
Theoretical Quantiles
5d
5b
4c
4a
J.A. - middle of top till
J.A. - bottom of top till
Highmont
DH-15-GG

(n)

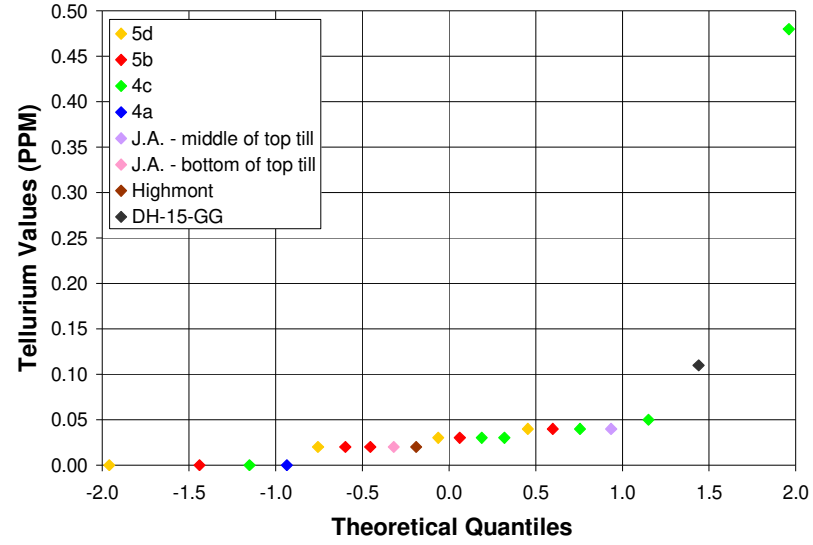

(o)

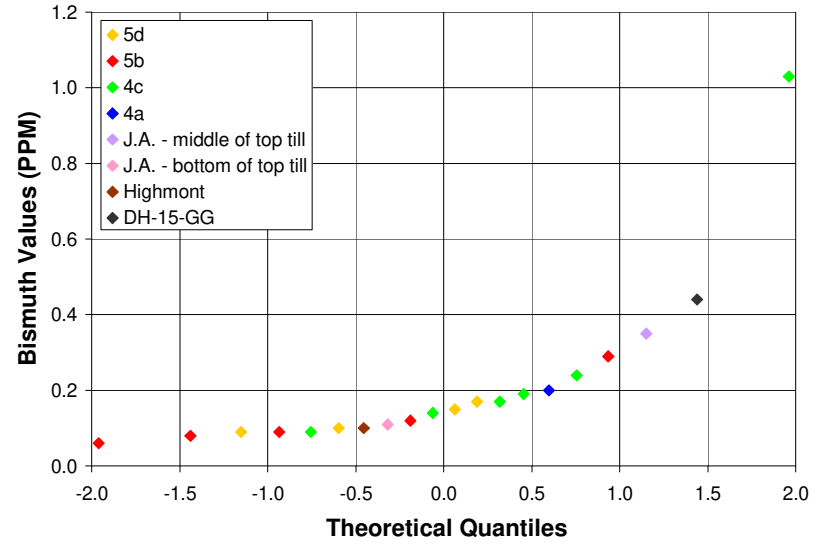

Figure 4.9 Select element concentrations for till samples. Values are colour-coded by stratigraphic unit.

Sand Units

Sub-unit 5c, an ice-marginal deposit of poorly-sorted sand, contains relatively high tungsten, gold, and magnesium concentrations (**Figures 4.10c, 4.10d, and 4.10g**). The elevated tungsten and gold concentrations are indicative of mineralization, while the elevated magnesium suggests a distal footprint contribution.

Sub-unit 5a, an ice-marginal deposit of poorly-sorted sand, contains relatively high molybdenum and tungsten concentrations (**Figures 4.10b and 4.10c**), both indicative of mineralization.

All of the three samples from sub-unit 4b, a poorly-sorted outwash deposit, contain relatively high molybdenum concentrations (**Figure 4.10b**). Two of these samples have relatively high copper concentrations (**Figure 4.10a**). One of these two samples also has a relatively high arsenic concentration (**Figure 4.10i**). The third sample has a relatively high lead concentration (**Figure 4.10f**). Sub-unit 4b shows a strong geochemical signal of mineralization; the highest copper and the two highest molybdenum values of the dataset are from this sub-unit. However, the elevated lead concentration indicates a distal footprint contribution.

One of the four samples from sub-unit 3e, consisting of poorly-sorted glaciofluvial outwash, contains relatively high copper, molybdenum, and lead concentrations (**Figures 4.10a, 4.10b, and 4.10f**). Another one of the four samples has a relatively high tin concentration (**Figure 4.10h**). The elevated copper, molybdenum, and tin concentrations are indicative of mineralization, while the elevated lead concentration suggests a distal footprint contribution.

Sub-unit 3d, a glacial lake deposit, contains an elevated concentration of magnesium (**Figure 4.10g**), which indicates a distal footprint contribution.

Sub-unit 3b, a subaqueous sediment gravity flow deposit, contains an anomalously high concentration of barium (**Figure 4.10j**).

The shallower sand sample (at ~1130 m asl) at J.A. has a tungsten concentration an order of magnitude higher than all the others for this dataset (**Figure 4.10c**), and relatively high concentrations of zinc, lead, and barium (**Figures 4.10e, 4.10f, and 4.10j**). Both sand samples have sulphur concentrations an order of magnitude higher than all other samples (**Figure 4.10k**), and anomalous magnesium concentrations (**Figure 4.10g**). The elevated concentrations of zinc lead, and magnesium indicate a distal footprint contribution for this unit, while the elevated tungsten may be an indicator of mineralization. These samples were taken from a unit interpreted to have been a

subaqueous fan or delta. This unit overlies subglacial till, which may have been the original source of the sulphur footprint of mineralization. This erosion of material containing sulphur in elevated concentrations may have been particularly effective at the Bethlehem mineralized zone north (up ice-flow direction) or at the J.A. mineralized zone, either of which are possible sources.

(a)

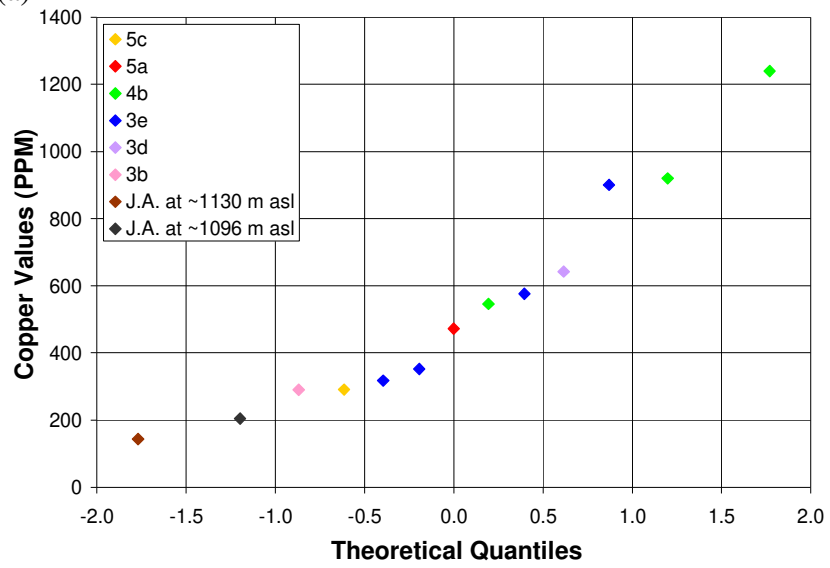

(b)

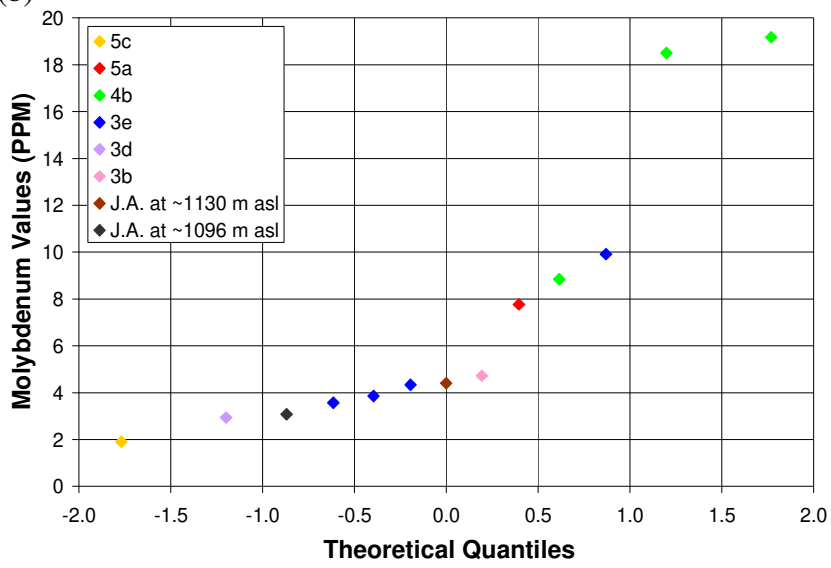

(c)

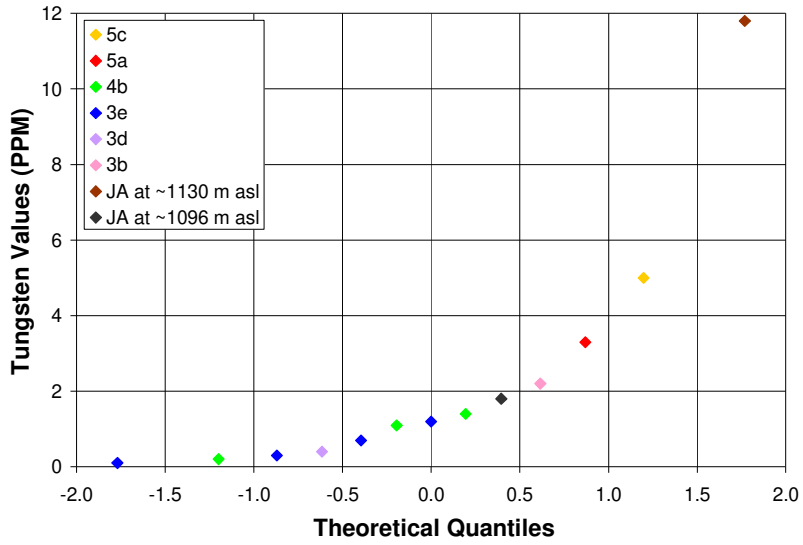
5c
5a
4b
3e
3d
3b
JA at ~1130 m asl
JA at ~1096 m asl
Tungsten Values (PPM)
Theoretical Quantiles

(d)

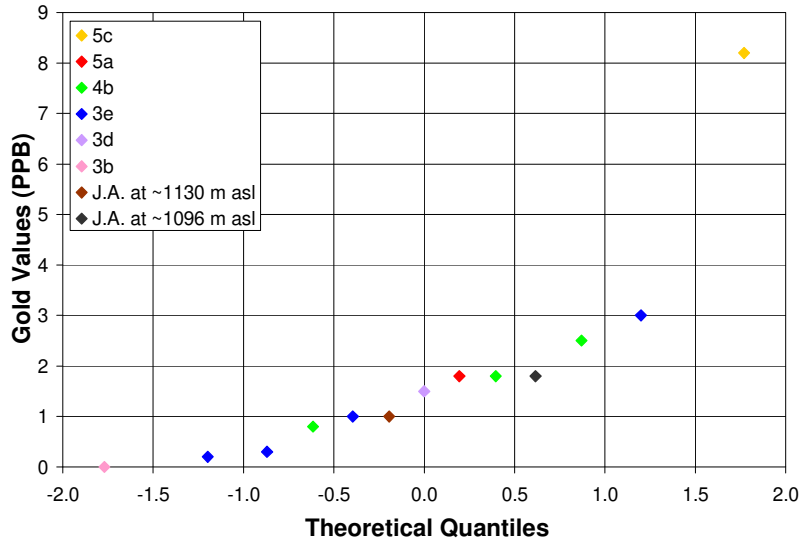
5c
5a
4b
3e
3d
3b
J.A. at ~1130 m asl
J.A. at ~1096 m asl
Gold Values (PPB)
Theoretical Quantiles

(e)

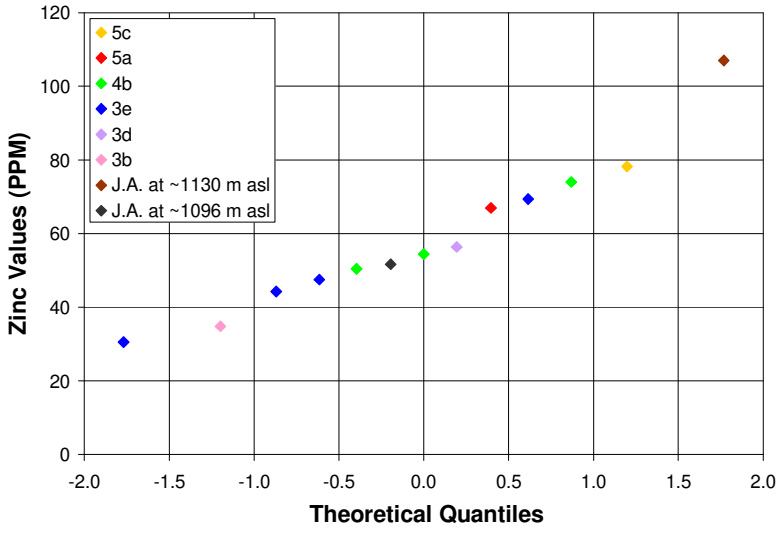
5c
5a
4b
3e
3d
3b
J.A. at ~1130 m asl
J.A. at ~1096 m asl
Zinc Values (PPM)
Theoretical Quantiles

(f)

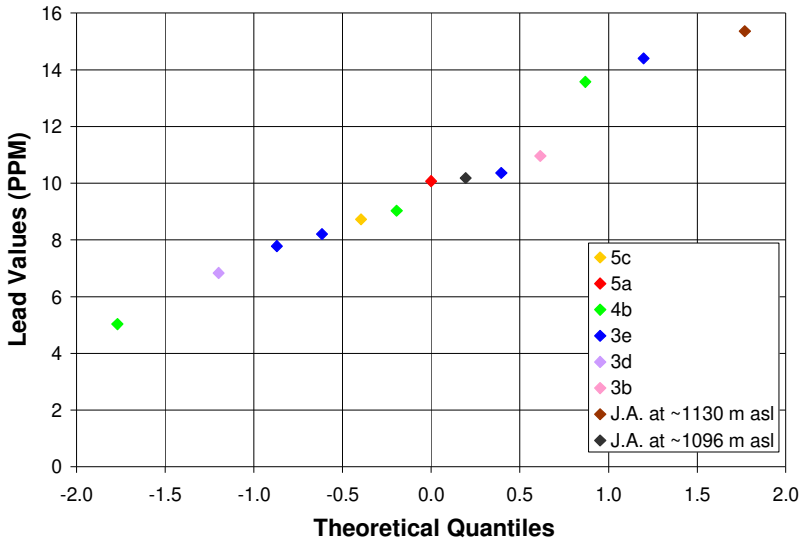
Lead Values (PPM)
Theoretical Quantiles
5c
5a
4b
3e
3d
3b
J.A. at ~1130 m asl
J.A. at ~1096 m asl

(g)

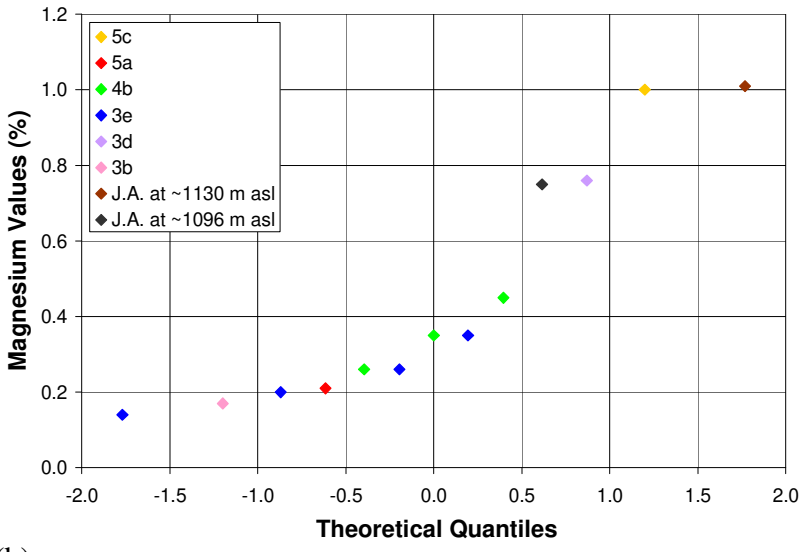
Magnesium Values (%)
Theoretical Quantiles
5c
5a
4b
3e
3d
3b
J.A. at ~1130 m asl
J.A. at ~1096 m asl

(h)

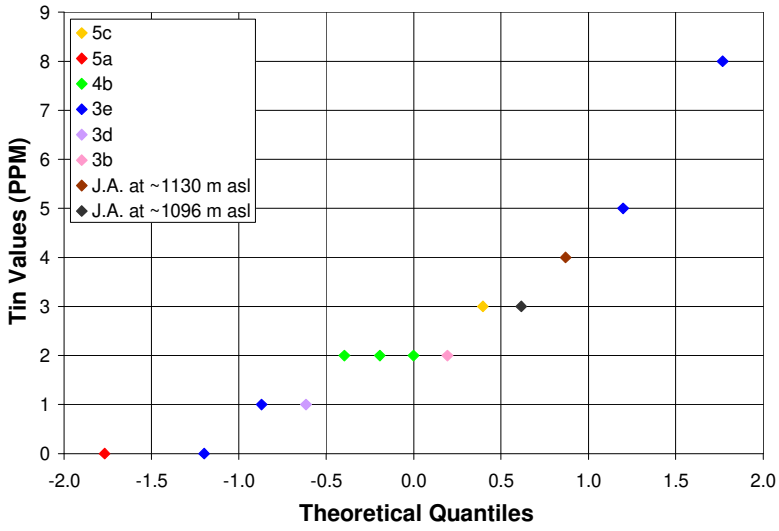
Tin Values (PPM)
Theoretical Quantiles
5c
5a
4b
3e
3d
3b
J.A. at ~1130 m asl
J.A. at ~1096 m asl

(i)

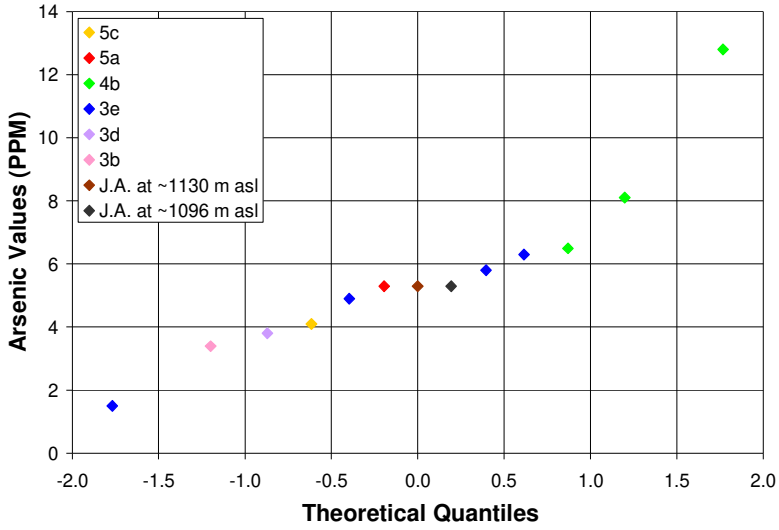

(j)

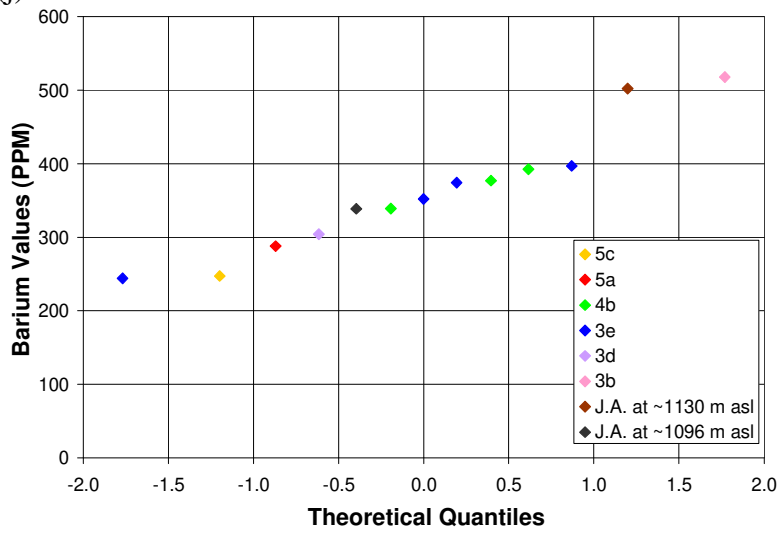

(k)

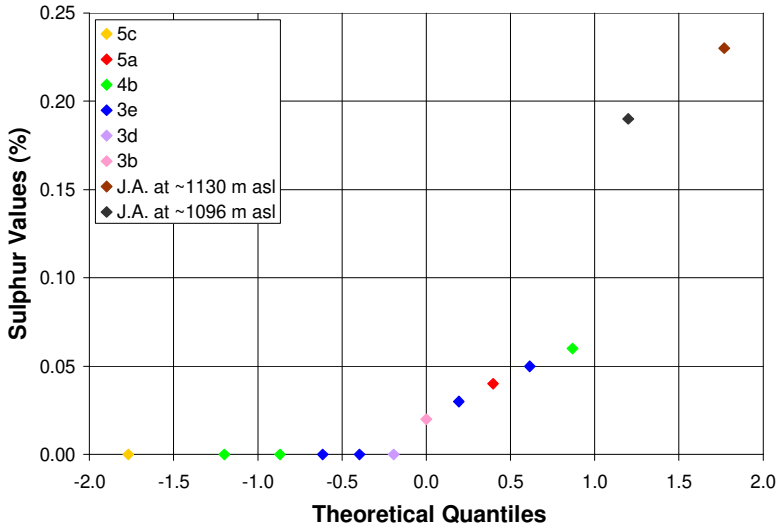

Figure 4.10 Select element concentrations for sand samples. Values are colour-coded by stratigraphic unit.

Sub-units 3e, 4a, 4b, and 4c show the strongest geochemical signal of mineralization. These sub-units have the highest elevated values of key indicator elements (copper, molybdenum), and/or elevated values of many different indicator elements. Sub-units 4a and 4c are the first widespread glacial tills in the area, and sub-units 3e and 4b are poorly-sorted outwash deposits.

There is a weak correlation between both copper and molybdenum concentrations and provenance for the Valley Pit sub-units. Copper and molybdenum concentrations increase with the percent of pebbles that are locally-derived (Guichon Creek batholith lithology) (see Figures C.88 and C.89 in Appendix C). There is a very weak negative correlation between nickel concentration and the proportion of pebbles that are locally-derived for the Valley Pit samples. There is no relationship between gold concentration and provenance for the Valley Pit samples. The proportion of pebbles that are locally-derived is consistent with copper concentration for the J.A. units sampled. No other obvious relationship between geochemistry and pebble provenance were identified for the J.A. samples.

There is a weak correlation between magnesium concentration and provenance for the Valley Pit sub-units. Magnesium concentrations decrease with the percent of pebbles that are locally-derived (Guichon Creek batholith lithology) (see Figures C.88 and C.89 in Appendix C). There is a very weak negative correlation between iron concentration and the proportion of pebbles that are locally-derived for the Valley Pit samples. No clear relationship was found between zinc and lead concentrations and provenance of pebbles for the Valley Pit samples.

4.5 Key Footprint Assemblages by Unit

Sub unit 5b (till), 4c (till), 4b (glaciofluvial), 3d (glaciolacustrine), and 3b (glaciofluvial), as well as the sand at ~1130 m asl at J.A., (cf. Chap. 3, Sect. 3.1.9), the thick till dominating top of stratigraphy at J.A. (cf. Chap. 3, Sect. 3.1.9), and the top till at Highmont South have been analyzed with all the techniques employed to determine if there are footprint indicators present (hyperspectral, indicator mineral, geochemical).

Sub-unit 5b, interpreted as subglacial till sourced dominantly from local Guichon Creek batholith material, contains pyrite, abundant chalcopyrite, andradite, Mn-epidote, and chromite. Two of five samples from this sub-unit have relatively high magnesium concentrations, and one of these also has a relatively high concentration of arsenic.

Sub-unit 4c, a subglacial till sourced dominantly locally, includes visible gold, pyrite, covellite, Mn-epidote, low-Cr diopside, red rutile, and chromite in both samples. In addition, abundant marcasite is found in one sample only, and chalcopyrite, andradite, and jarosite in the other. Two of the six samples contain relatively high copper concentrations. One of these samples also has elevated molybdenum, tungsten, arsenic, gold, tellurium, and bismuth concentrations. The latter three are all an order of magnitude higher than all the other Highland Valley samples. Two others of the six samples have elevated magnesium levels.

Sub-unit 4b, a poorly-sorted outwash deposit consisting of locally sourced material, contains abundant pyrite, Mn-epidote, and chromite in all three of its analyzed samples. Jarosite is found in two of the three samples analyzed, visible gold in one, and chalcopyrite and low-Cr diopside in another one of the three. All of these samples contain relatively high molybdenum concentrations. Two of them have relatively high copper concentrations. One of these two samples also has a relatively high arsenic concentration, while the third has a relatively high lead concentration. Sub-unit 4b shows a strong geochemical signal of mineralization; the highest copper and the two highest molybdenum values of the dataset are from this sub-unit.

Sub-unit 3d, a glacial lake deposit sourced dominantly locally, contains pyrite, abundant Mn-epidote, and chromite. It also contains an elevated magnesium concentration.

Sub-unit 3b, consisting of poorly-sorted sediment gravity flow material sourced dominantly from local Guichon Creek batholith, contains abundant pyrite, abundant Mn-epidote, low-Cr diopside, chromite, and abundant jarosite. It also contains an anomalously high barium concentration.

The poorly-sorted sand and gravel unit at ~1130 m asl at J.A. is interpreted to be sediment gravity flow material sourced mostly from outside the Guichon Creek batholith. It contains abundant pyrite, chalcopyrite, covellite, abundant low-Cr diopside, and abundant chromite. It has both a tungsten and a sulphur concentration an order of magnitude higher than all the others for this dataset, and relatively high concentrations of zinc, lead, magnesium, and barium.

The bottom of the thick till unit dominating the top of the J.A. stratigraphy is sourced mostly from outside the Guichon Creek batholith, while the middle is dominantly Guichon Creek batholith material. Visible gold, covellite (including an anomalously high count), chromite, and jarosite are found throughout the unit. Abundant chalcocite, as well as chalcopyrite, andradite, and Mn-epidote are found only in the sample at the middle of the unit, while abundant pyrite and barite are found only in the lower sample. The sample from the middle of the unit has relatively high levels of both copper and arsenic. Both samples from this top thick till have relatively high magnesium concentrations.

Prehnite and kaolinite are detectable in all the units analyzed. Their amounts reflect the proportion of local vs. distal provenance in the unit. Prehnite is the product of distal bedrock alteration at the Highland Valley system, and its concentration in the unconsolidated sediment likewise decreases as the degree of local provenance increases (Lesage et al., 2016; Byrne, 2019). Kaolinite is part of the proximal bedrock alteration mineral assemblage, and similarly its concentration in the sediment cover increases with the percentage of pebbles that are locally-derived.

Additional samples from sub-units 5d, 5c, 5a, 4a, and 3e, as well as an additional sand unit from J.A. (at ~1096 m asl), and a till unit from core DH-15-GG were analyzed for geochemical elements. One of the four samples from sub-unit 5d, a subglacial till sourced dominantly from local Guichon Creek batholith, has a relatively high concentration of magnesium. Sub-unit 5c, an ice-marginal deposit of poorly-sorted sand sourced mostly locally, contains relatively high gold, tungsten, and magnesium concentrations. Sub-unit 5a is an ice-marginal deposit of poorly-sorted sand that is a mix of both local and distal lithologies. It contains relatively high molybdenum and tungsten concentrations. Sub-unit 4a, a subglacial till sourced dominantly from local Guichon

Creek batholith, has one of the highest concentrations of both copper and barium for this dataset, and a relatively high molybdenum concentration. One of the four samples from sub-unit 3e, consisting of poorly-sorted glaciofluvial outwash sourced mostly locally, contains relatively high copper, molybdenum, and lead concentrations. Another one of the four samples has a relatively high tin concentration. The deeper J.A. sand sample (at ~1096 m asl) is sourced mostly from outside the Guichon Creek batholith. It has a relatively high magnesium concentration, and a sulphur concentration an order of magnitude higher than all other samples. The sample from a till at core DH-15-GG consists of mostly distally-derived material from outside the Guichon Creek batholith. Zinc, nickel, barium, lead concentrations are significantly higher (246, 102, 2387 ppm, respectively) at DH-15-GG than for the samples from the mineralized zones (17-107, 7-39, 100-636 ppm, respectively). The gold, arsenic, antimony, tellurium, bismuth, silver, magnesium, and iron values at DH-15-GG are the or one of the highest of their respective datasets, with most samples from the cores at the Highland Valley mineralized zones having lower values.

Sub-units 4c (subglacial till), 4b (poorly-sorted outwash), 4a (subglacial till), and 3e (poorly-sorted outwash) show the strongest footprint of mineralization. They contain a relatively high variety and/or abundance or concentration of minerals and elements derived from the ore zones of porphyry copper mineralization. All are sourced dominantly locally from the Guichon Creek batholith that hosts the mineralization. It is not clear whether the units contain more of a local or distal footprint, as most of them contain elements in concentrations that are expected for both locally and distally derived material. There is also considerable internal variability; certain boreholes seem to have a higher footprint indication than other boreholes for some of the units (cf. Sect. 4.3.2 and 4.4.2). The top till at Highmont South does not have any indicator mineral or element anomalies (see **Figure 4.9a-o**).

4.6 Comparison with Plouffe and Ferbey (2016)

The results for this study are compared with those of Plouffe and Ferbey (2016) who analyzed shallow hand-dug till samples from the Highland Valley area and the surrounding region. This is done in order to determine the effect of stratigraphy on the dispersion patterns in areas of thick or highly variable drift thickness. The surficial till sampled in Plouffe and Ferbey's study (2016; PF16) is assumed to correlate to tills in unit 5 of this study. The same laboratory and procedures were used for both studies.

4.6.1 Indicator Mineral Results Comparison

Q-Q plots were used to compare indicator mineral results for both this study and Plouffe and Ferbey's shallow till samples (2016; **Figure 4.11**). This method was used to determine whether results from drillcore till samples obtained in this study differ from surficial till (PF16). All results are normalized to 5kg (dry weight). The indicator mineral results for this study are presented by stratigraphic unit alongside averages and anomaly thresholds for PF16 data in Table C.3 of Appendix C.

(a)

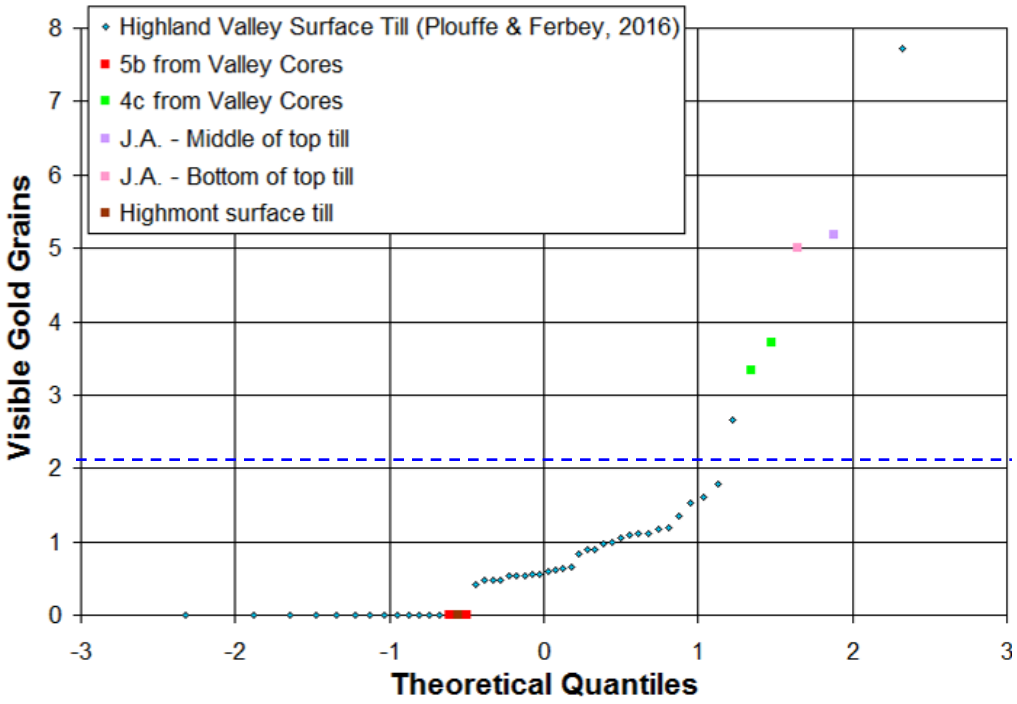

(b)

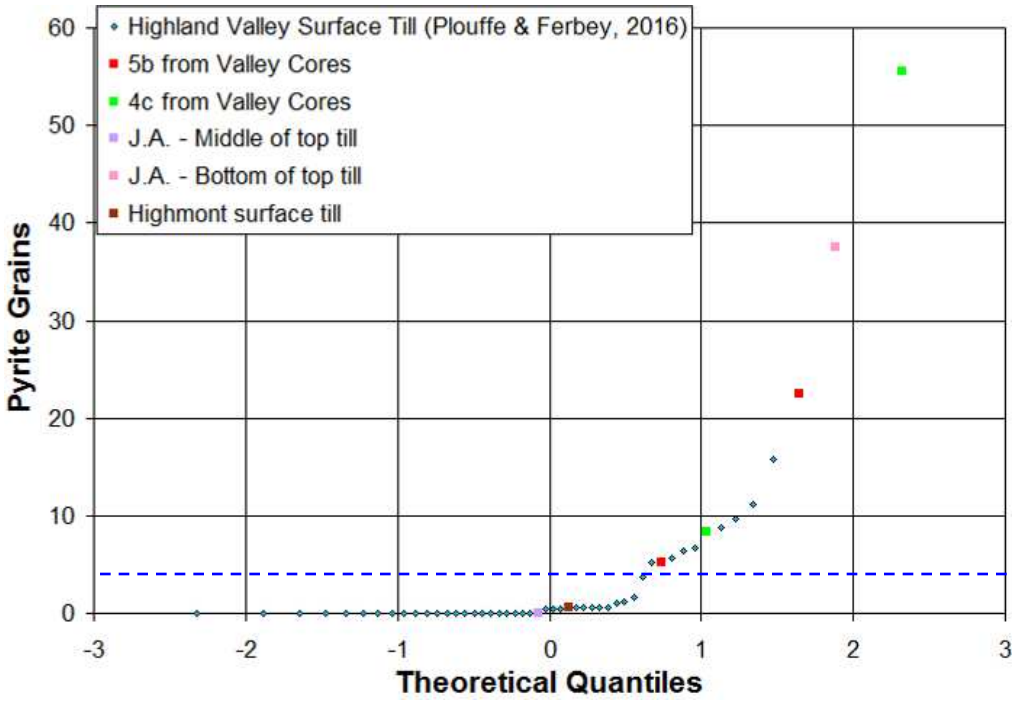
Highland Valley Surface Till (Plouffe & Ferbey, 2016)
5b from Valley Cores
4c from Valley Cores
J.A. - Middle of top till
J.A. - Bottom of top till
Highmont surface till
Pyrite Grains
Theoretical Quantiles
60
50
40
30
20
10
0
-3
-2
-1
0
1
2
3

(c)

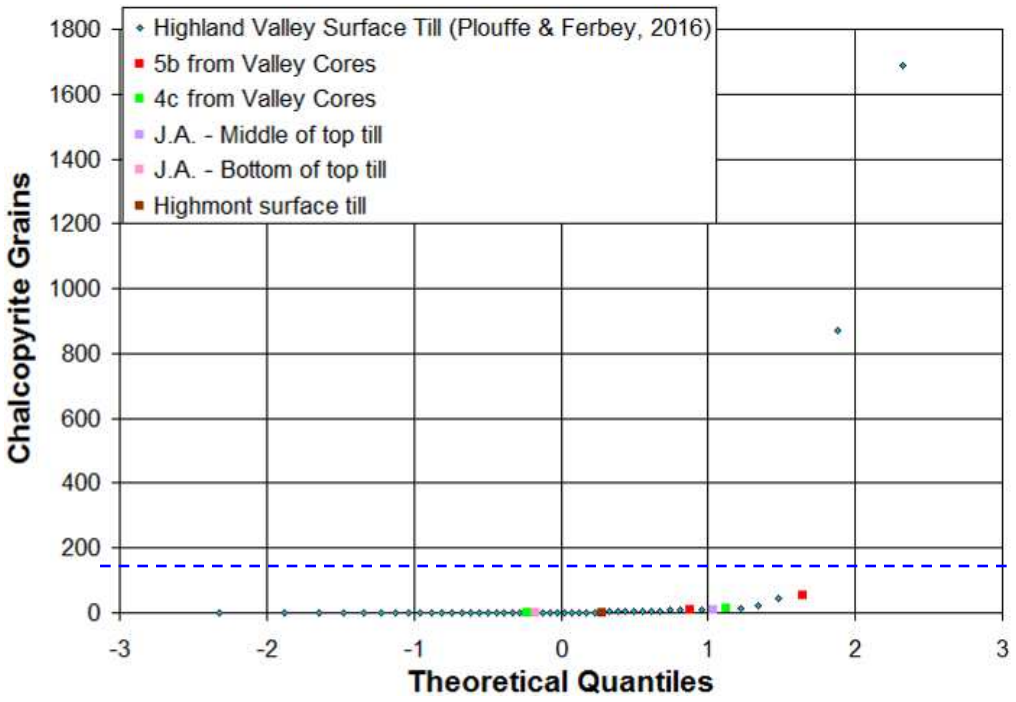
Highland Valley Surface Till (Plouffe & Ferbey, 2016)
5b from Valley Cores
4c from Valley Cores
J.A. - Middle of top till
J.A. - Bottom of top till
Highmont surface till
Chalcopyrite Grains
Theoretical Quantiles
1800
1600
1400
1200
1000
800
600
400
200
0
-3
-2
-1
0
1
2
3

(d)

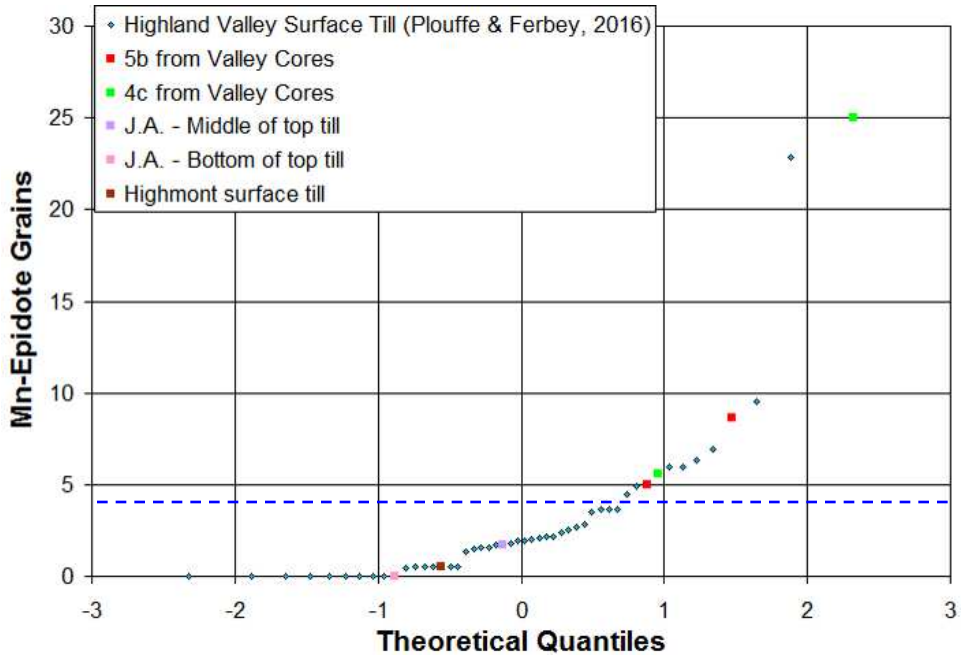

(e)

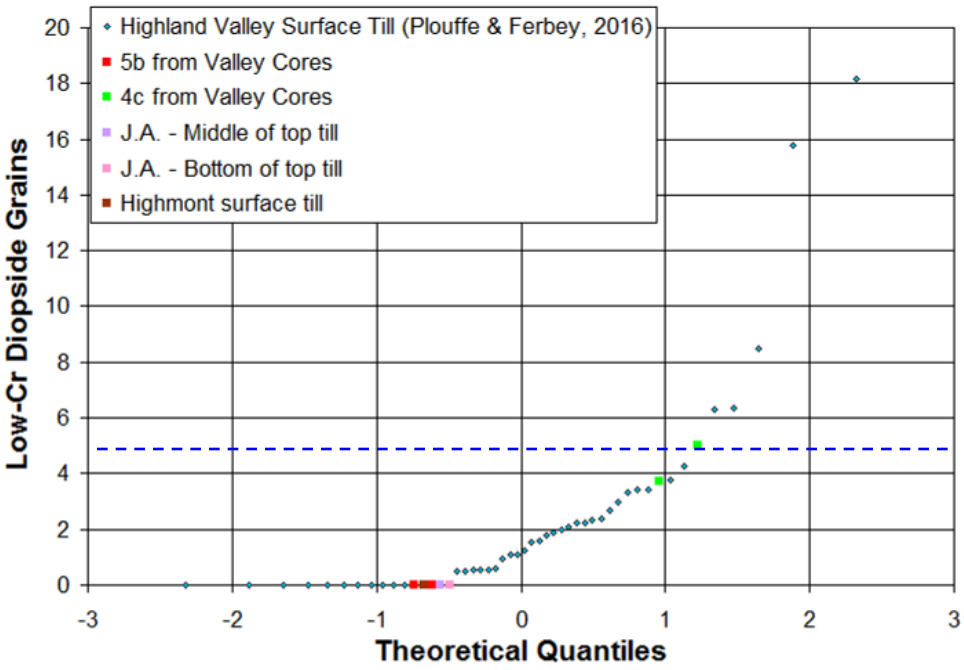

Figure 4.11 Indicator mineral results for tills from this study and for Plouffe and Ferbey's shallow till samples (2016). Both datasets are normalized to five kilograms. The dashed blue line indicates the anomaly threshold for shallow samples (PF16).

Both samples (elevations of 1196 and 1208 m asl) from the deepest till sub-unit (4c) analyzed at the Valley pit area contain a higher number of visible gold grains (four and three grains; see **Figure 4.11a**) than the anomaly threshold for shallow till samples collected from Highland Valley (PF16). Both samples (elevations of 1169 and 1178 m asl, over 30 m deep) from the single till unit at J.A. also contain an anomalous number of visible gold grains compared to surficial till (five grains each; see **Figure 4.11a**). The lack of gold grains in the shallower till sub-unit (5b) may be due to low counts overall. The deeper till samples from the Valley Pit area and the J.A. subsurface till samples for this study provided consistently higher visible gold grain counts than the average count for surficial or shallower samples, but the counts are still low.

Anomalous grain counts for pyrite (relative to the threshold for anomaly for the Highland Valley area determined from surficial samples) were found for every unit analyzed (sub-units 5b and 4c and top till at J.A.; see **Figure 4.11b**) except for the Highmont top till. Anomalous Mn-epidote counts (relative to the Highland Valley anomaly threshold) are also present for both of the Valley Pit area tills analyzed (sub-units 5b and 4c; see **Figure 4.11d**). Higher grain counts of pyrite, Mn-epidote and low-Cr diopside were found in the deeper till sub-unit 4c than in the shallower till sub-unit analyzed. This suggests that the surficial till in the area may be diluted relative to deeper tills. This could be due to greater incorporation of freshly eroded material in the youngest till that is not from the footprint area. This is to be expected in the study area because thick pre-existing sediments, as evidenced by the observed stratigraphy, partly covered the local bedrock, which shielded it from glacial erosion.

4.6.2 Geochemical Results Comparison

Q-Q plots were also used to compare geochemical results for both this study and Plouffe and Ferbey's shallow till samples (2016). This method was used to determine whether results from drillcore till samples obtained in this study differ from surficial till (PF16). PF16 shallow till sample from the Highland Valley area (**Figure 4.12)** and from a wider, regional area (**Figure 4.13**) are compared. The geochemical results for the tills of

this study are presented by stratigraphic unit alongside averages and anomaly thresholds for PF16 data in Table C.4 of Appendix C.

(a)

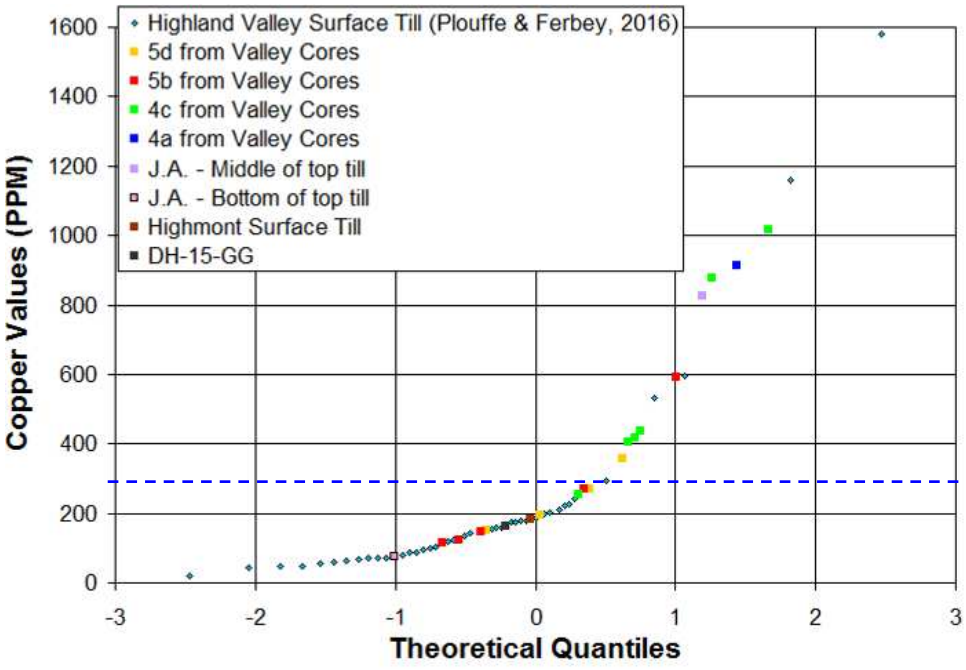

(b)

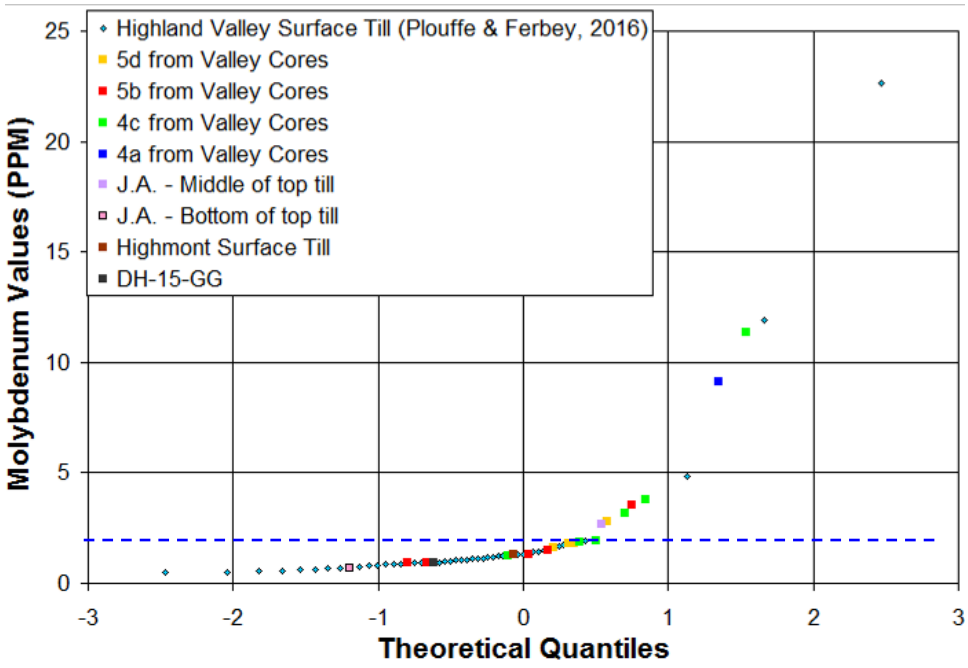

(c)

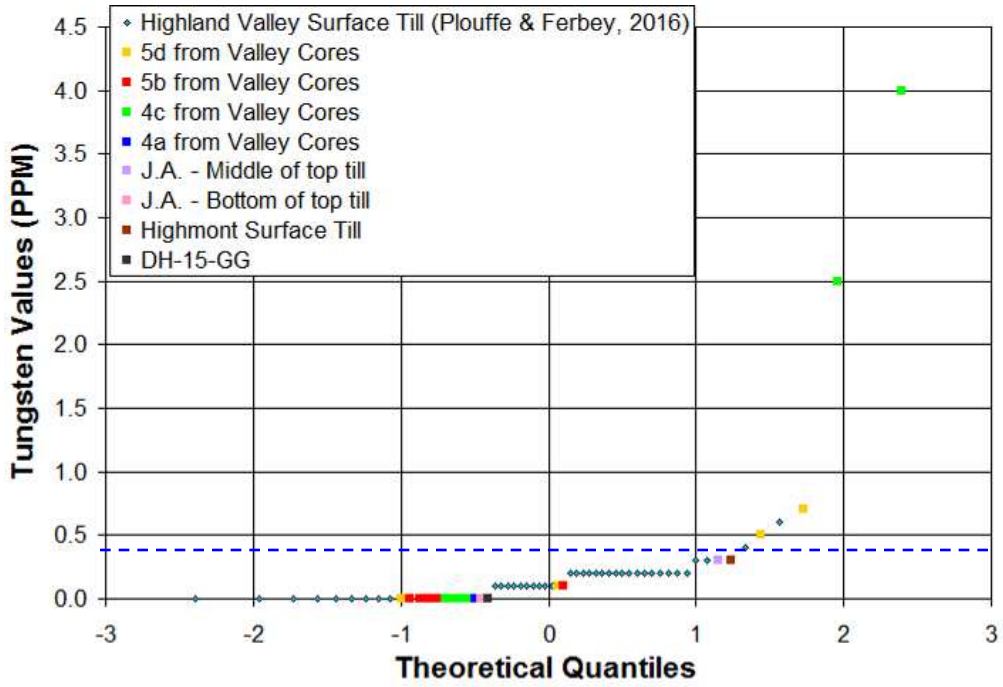
Highland Valley Surface Till (Plouffe & Ferbey, 2016)
5d from Valley Cores
5b from Valley Cores
4c from Valley Cores
4a from Valley Cores
J.A. - Middle of top till
J.A. - Bottom of top till
Highmont Surface Till
DH-15-GG
Tungsten Values (PPM)
4.5
4.0
3.5
3.0
2.5
2.0
1.5
1.0
0.5
0.0
-3
-2
-1
0
1
2
3
Theoretical Quantiles

(d)

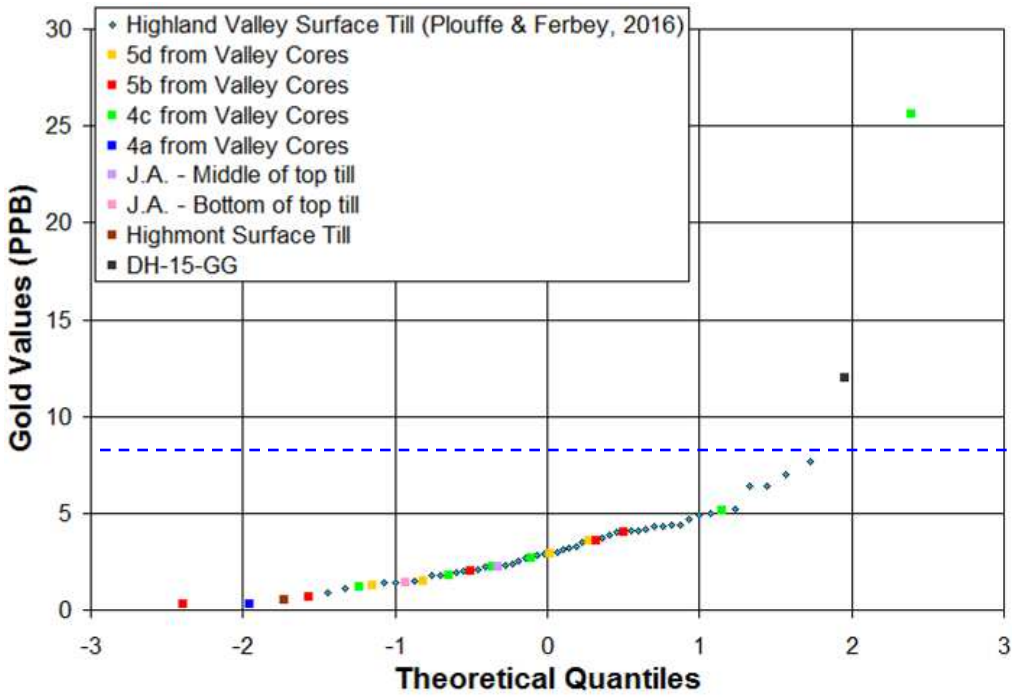
Highland Valley Surface Till (Plouffe & Ferbey, 2016)
5d from Valley Cores
5b from Valley Cores
4c from Valley Cores
4a from Valley Cores
J.A. - Middle of top till
J.A. - Bottom of top till
Highmont Surface Till
DH-15-GG
Gold Values (PPB)
30
25
20
15
10
5
0
-3
-2
-1
0
1
2
3
Theoretical Quantiles

(e)

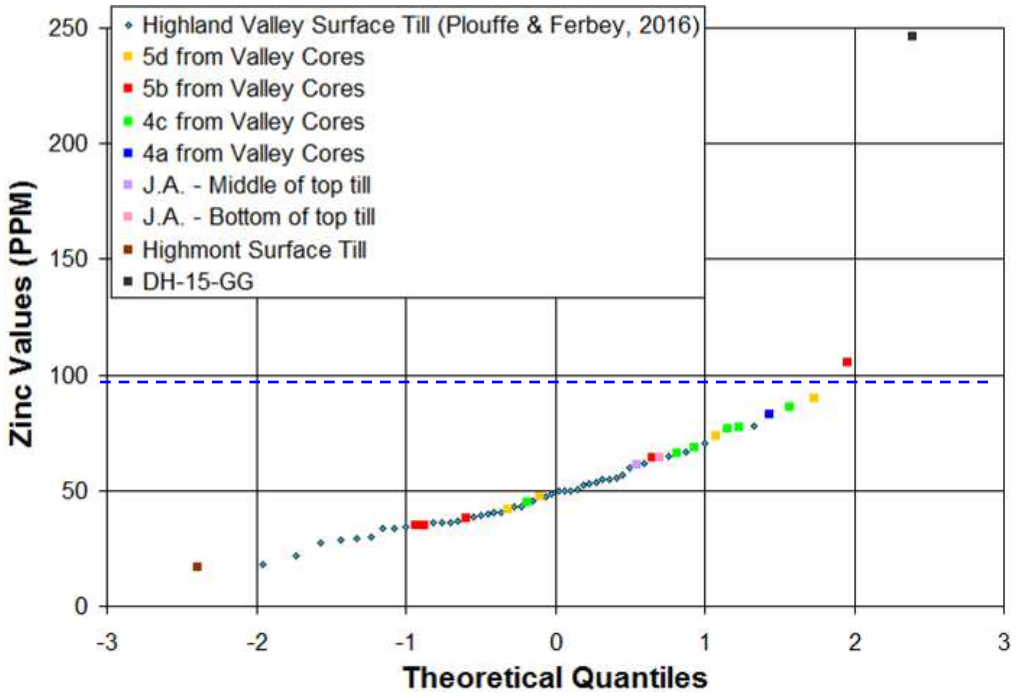
Highland Valley Surface Till (Plouffe & Ferbey, 2016)
5d from Valley Cores
5b from Valley Cores
4c from Valley Cores
4a from Valley Cores
J.A. - Middle of top till
J.A. - Bottom of top till
Highmont Surface Till
DH-15-GG
Zinc Values (PPM)
250
200
150
100
50
0
-3
-2
-1
0
1
2
3
Theoretical Quantiles

(f)

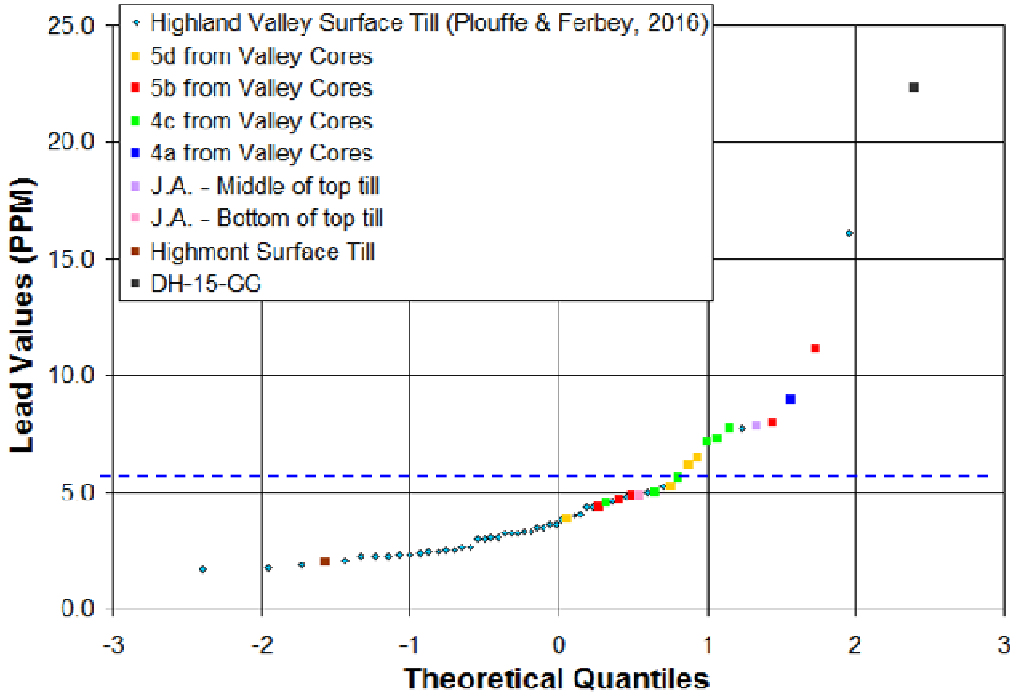
Highland Valley Surface Till (Plouffe & Ferbey, 2016)
5d from Valley Cores
5b from Valley Cores
4c from Valley Cores
4a from Valley Cores
J.A. - Middle of top till
J.A. - Bottom of top till
Highmont Surface Till
DH-15-CC
Lead Values (PPM)
25.0
20.0
15.0
10.0
5.0
0.0
-3
-2
-1
0
1
2
3
Theoretical Quantiles

(g)

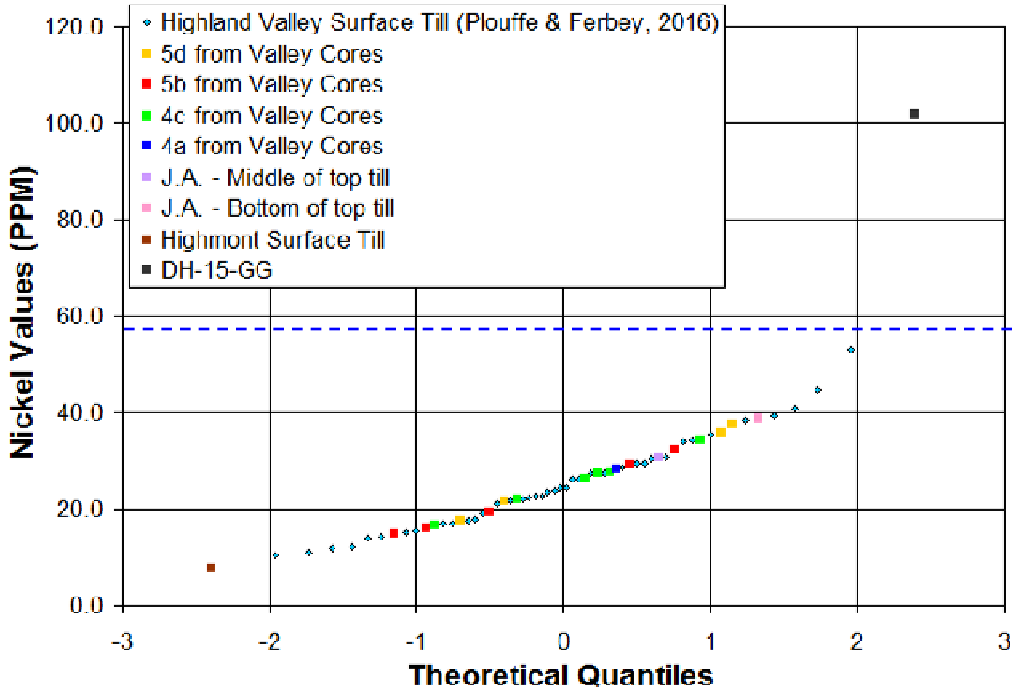
Highland Valley Surface Till (Plouffe & Ferbey, 2016)
5d from Valley Cores
5b from Valley Cores
4c from Valley Cores
4a from Valley Cores
J.A. - Middle of top till
J.A. - Bottom of top till
Highmont Surface Till
DH-15-GG
Nickel Values (PPM)
120.0
100.0
80.0
60.0
40.0
20.0
0.0
-3
-2
-1
0
1
2
3
Theoretical Quantiles

(h)

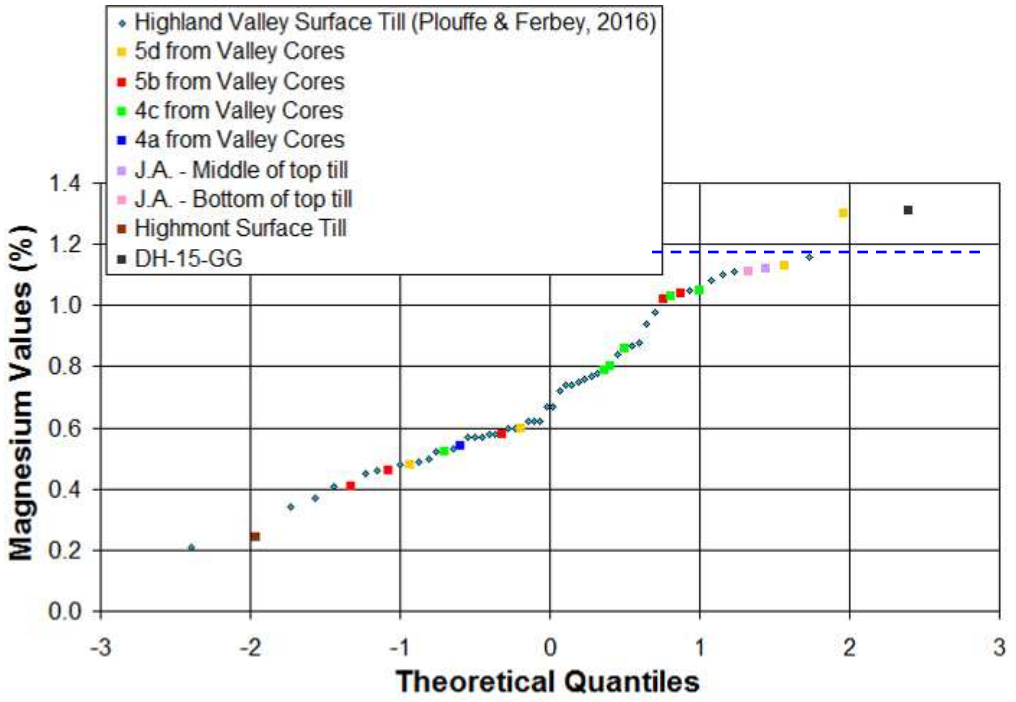
Highland Valley Surface Till (Plouffe & Ferbey, 2016)
5d from Valley Cores
5b from Valley Cores
4c from Valley Cores
4a from Valley Cores
J.A. - Middle of top till
J.A. - Bottom of top till
Highmont Surface Till
DH-15-GG
Magnesium Values (%)
1.4
1.2
1.0
0.8
0.6
0.4
0.2
0.0
-3
-2
-1
0
1
2
3
Theoretical Quantiles

(i)

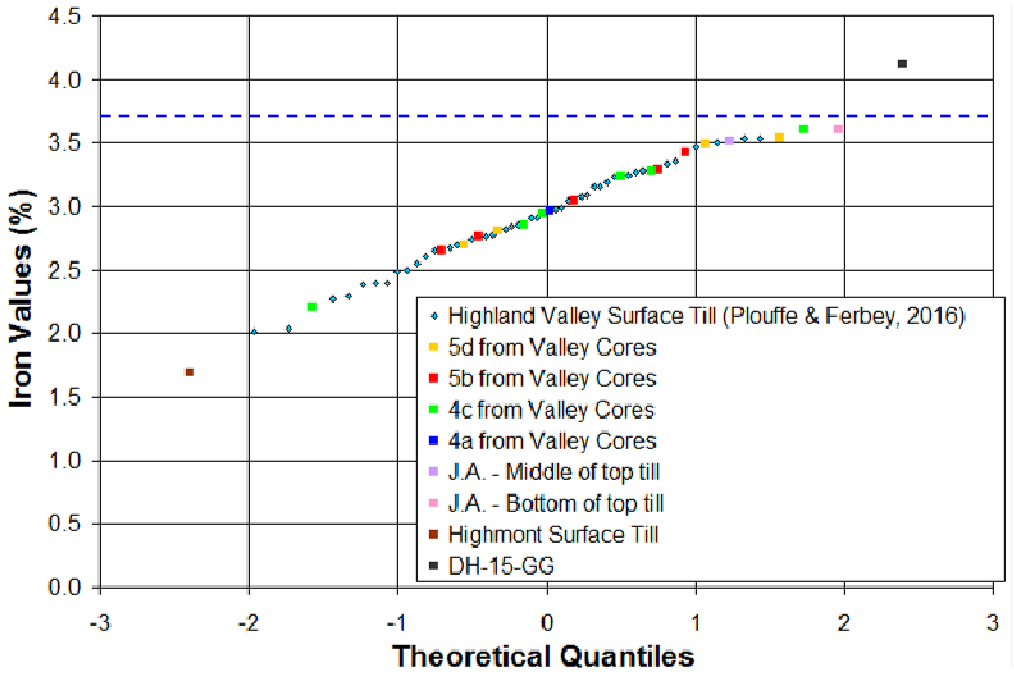
Iron Values (%)
4.5
4.0
3.5
3.0
2.5
2.0
1.5
1.0
0.5
0.0
-3
-2
-1
0
1
2
3
Theoretical Quantiles
Highland Valley Surface Till (Plouffe & Ferbey, 2016)
5d from Valley Cores
5b from Valley Cores
4c from Valley Cores
4a from Valley Cores
J.A. - Middle of top till
J.A. - Bottom of top till
Highmont Surface Till
DH-15-GG

(j)

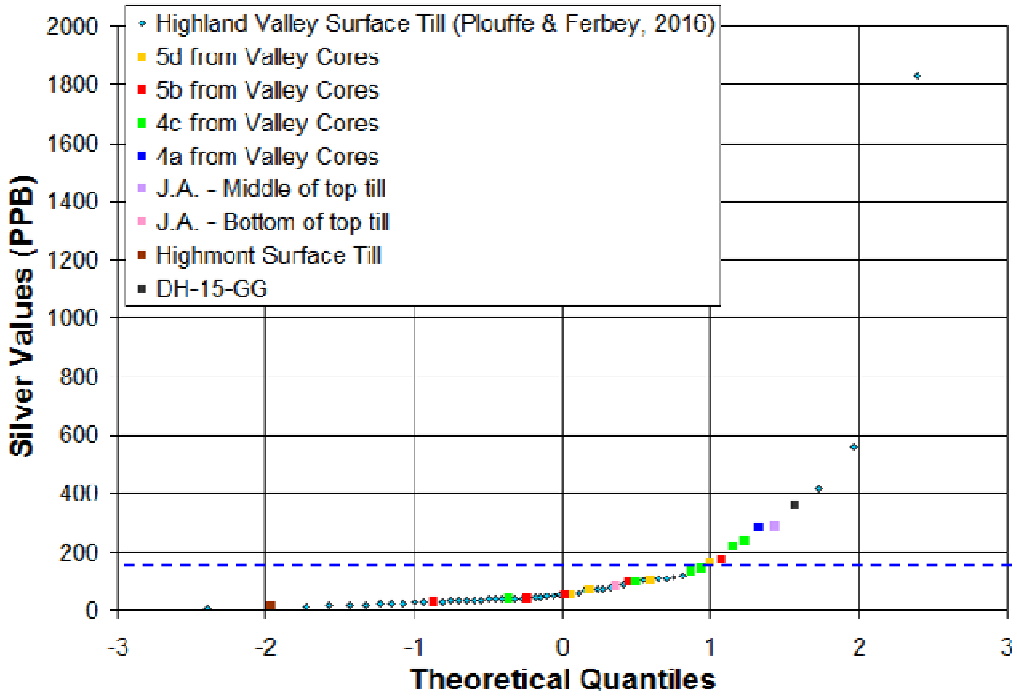
Silver Values (PPB)
2000
1800
1600
1400
1200
1000
800
600
400
200
0
-3
-2
-1
0
1
2
3
Theoretical Quantiles
Highland Valley Surface Till (Plouffe & Ferbey, 2016)
5d from Valley Cores
5b from Valley Cores
4c from Valley Cores
4a from Valley Cores
J.A. - Middle of top till
J.A. - Bottom of top till
Highmont Surface Till
DH-15-GG

(k)

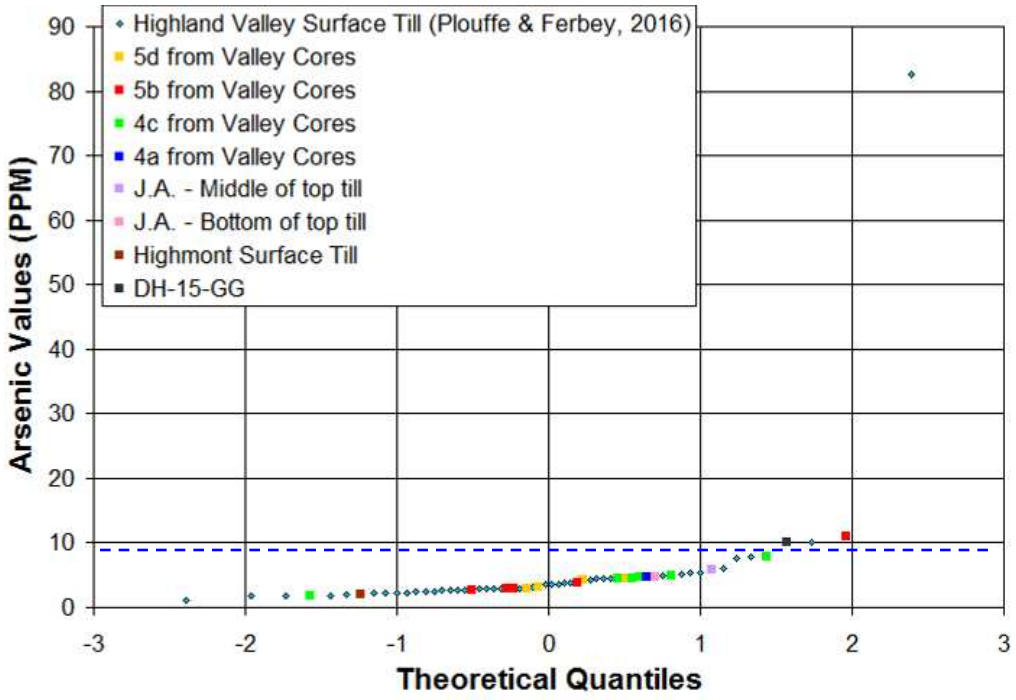
Highland Valley Surface Till (Plouffe & Ferbey, 2016)
5d from Valley Cores
5b from Valley Cores
4c from Valley Cores
4a from Valley Cores
J.A. - Middle of top till
J.A. - Bottom of top till
Highmont Surface Till
DH-15-GG
Arsenic Values (PPM)
Theoretical Quantiles
0
10
20
30
40
50
60
70
80
90
-3
-2
-1
0
1
2
3

(l)

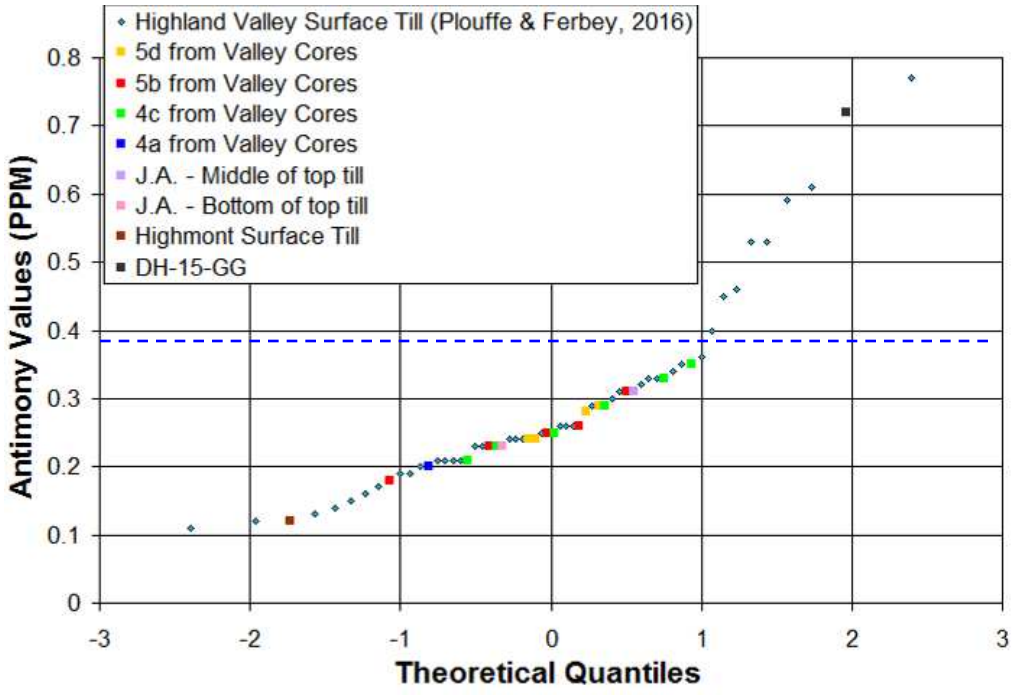
Highland Valley Surface Till (Plouffe & Ferbey, 2016)
5d from Valley Cores
5b from Valley Cores
4c from Valley Cores
4a from Valley Cores
J.A. - Middle of top till
J.A. - Bottom of top till
Highmont Surface Till
DH-15-GG
Antimony Values (PPM)
Theoretical Quantiles
0
0.1
0.2
0.3
0.4
0.5
0.6
0.7
0.8
-3
-2
-1
0
1
2
3

(m)

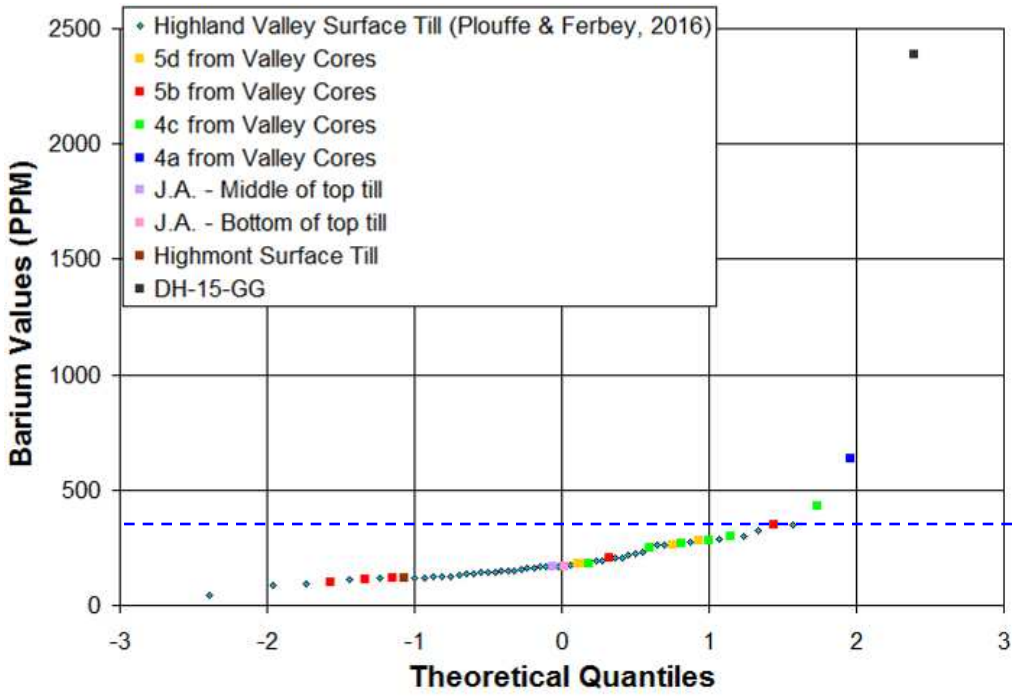
Highland Valley Surface Till (Plouffe & Ferbey, 2016)
5d from Valley Cores
5b from Valley Cores
4c from Valley Cores
4a from Valley Cores
J.A. - Middle of top till
J.A. - Bottom of top till
Highmont Surface Till
DH-15-GG
Barium Values (PPM)
2500
2000
1500
1000
500
0
-3
-2
-1
0
1
2
3
Theoretical Quantiles

(n)

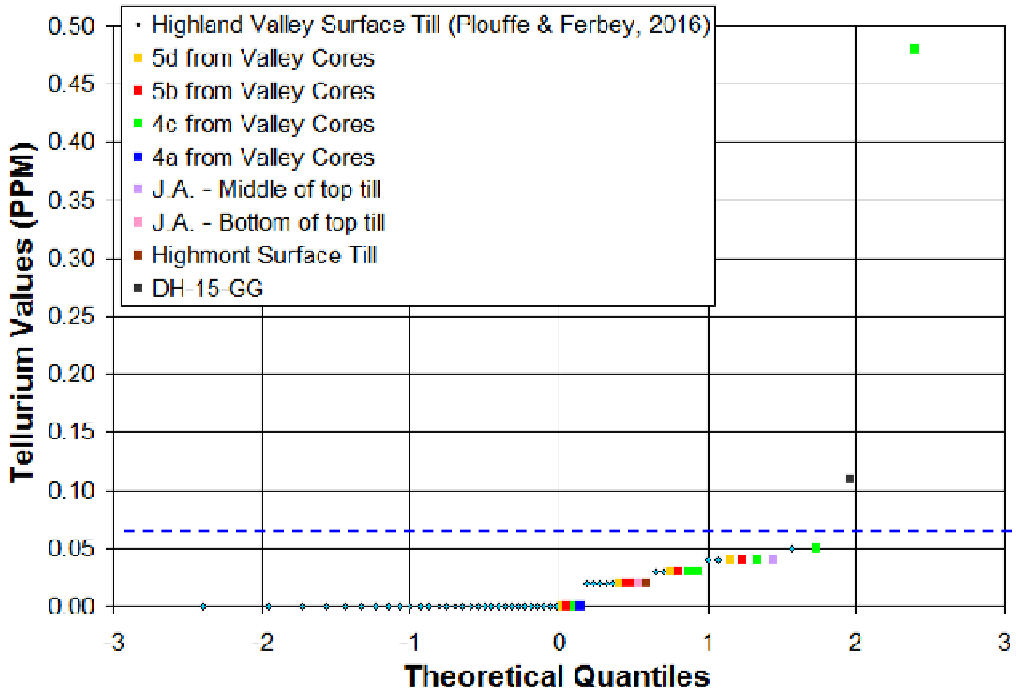
Highland Valley Surface Till (Plouffe & Ferbey, 2016)
5d from Valley Cores
5b from Valley Cores
4c from Valley Cores
4a from Valley Cores
J.A. - Middle of top till
J.A. - Bottom of top till
Highmont Surface Till
DH-15-GG
Tellurium Values (PPM)
0.50
0.45
0.40
0.35
0.30
0.25
0.20
0.15
0.10
0.05
0.00
3
2
1
0
1
2
3
Theoretical Quantiles

(o)

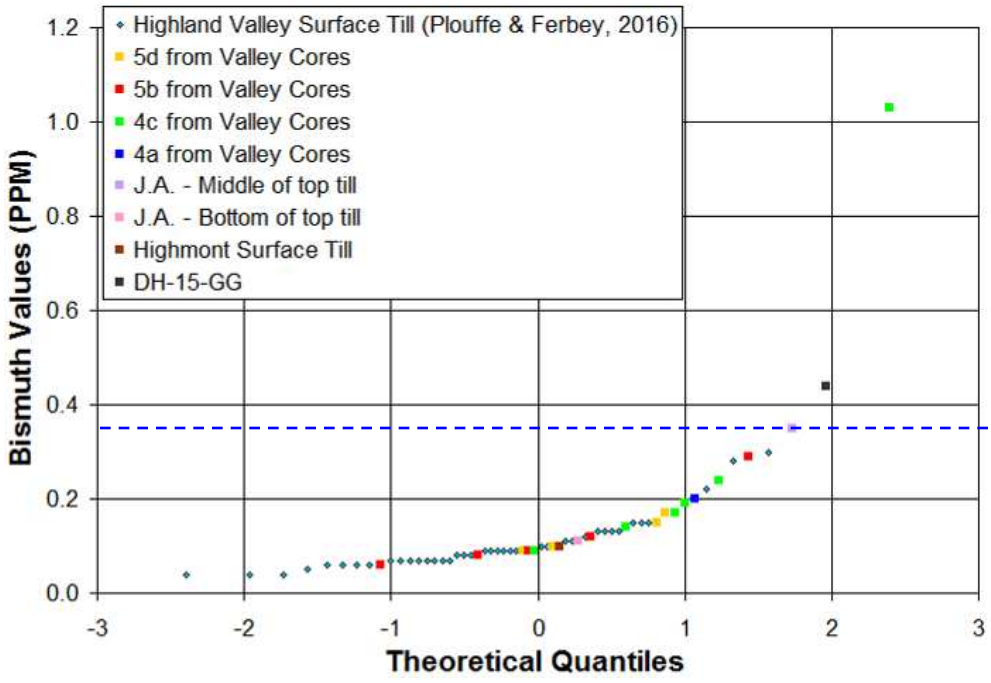

(p)

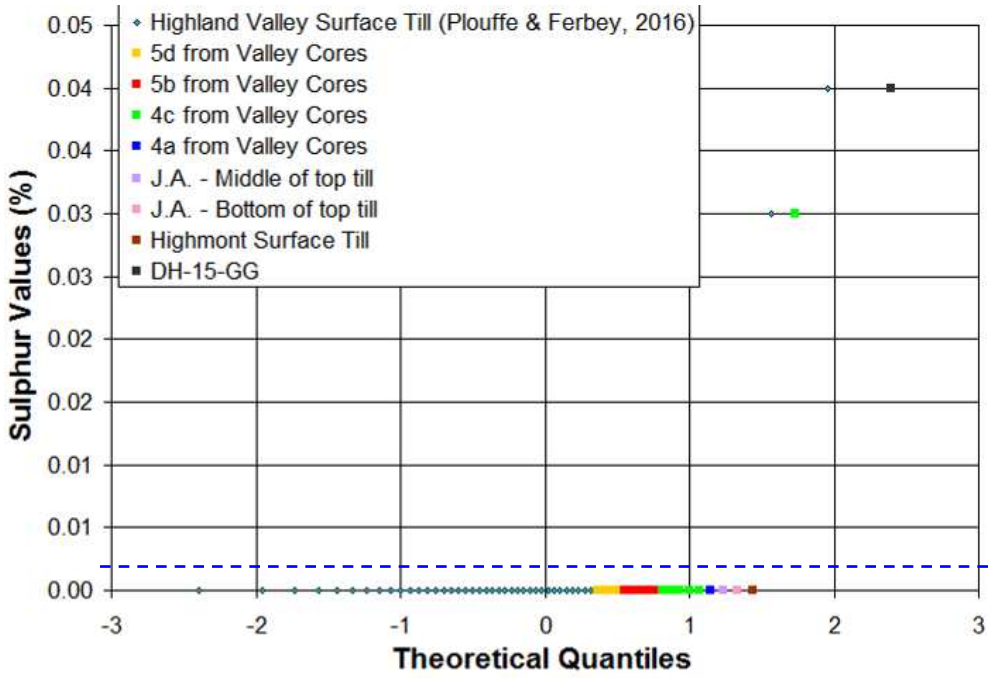

Figure 4.12 Geochemical results for tills from this study and for Plouffe and Ferbey's Highland Valley shallow till samples (2016). The dashed blue line indicates the anomaly threshold for shallow samples (PF16).

Every till sub-unit analyzed at the Valley pit area as well as the top till at J.A. contains a higher concentration of copper, molybdenum, lead, silver, and bismuth than the anomaly thresholds for shallow till samples collected from Highland Valley (PF16; **Figures 4.12a, 4.12b, 4.12f, 4.12j, and 4.12o**). The anomalies were usually more consistent for sub-unit 4c; every or almost every sample from that sub-unit contained copper, molybdenum, lead, silver, and bismuth anomalies compared to the PF16 dataset. There is at least one zinc anomaly for every sub-unit in the Valley Pit area, as well as for the till at DH-15-GG (**Figure 4.12e**).

Sub-unit 4c also contains anomalous amounts of many other elements: tungsten, gold, arsenic, barium, tellurium (see **Figures 4.12c, 4.12d, 4.12k, 4.12m, and 4.12n**). These anomalies always occur at one particular location (VTH2014-08). The number of elements that are found in concentrations above the anomaly threshold in this sub-unit as well as the relative consistency of these anomalies for all or almost all samples from this sub-unit indicate that sub-unit 4c shows the strongest geochemical footprint of mineralization. Sub-unit 4c is an approximately 20-m-thick subglacial traction till, which is the last sub-unit deposited during a second ice oscillation in this area (cf. Chap. 3, Sect. 3.2 and 3.5.5 for details). However, based on the correlations and cross-sections developed in this study, it appears to be the thickest and most widespread subsurface till in the area (cf. Chap. 3, Sect. 3.2.1, Fig. 3.16). Not all samples have a strong footprint signature, nonetheless, the glacial phase that produced that till was sufficiently effective at eroding mineralized bedrock and thus entraining more traces of mineralization. The copper and molybdenum anomaly thresholds for regional shallow till samples are about 240 ppm and about 2.5 ppm, respectively (**Figures 4.13a-b**; PF16). There is a greater number of sub-surface till samples (this study) than Highland Valley shallow till samples (PF16) with values higher than the regional anomaly for both copper and molybdenum (**Figures 4.12a-b**). The copper and molybdenum values of the till sub-units of this study are thus more consistently anomalous compared to regional surficial till values than those of the Highland Valley surficial till values, reflecting possible dilution of these two elements in surficial till relative to deeper tills.

The tungsten, gold, tellurium, and bismuth anomaly thresholds for regional shallow till samples are about 0.7 ppm, 17 ppb, 0.12 ppm, and 0.4 ppm, respectively (**Figures 4.13c-f**) (PF16). There are no Highland Valley shallow till samples (PF16) with values higher than the regional anomalies for these elements (**Figures 4.12c-d, and 4.12n-o**). However, there is at least one sub-surface sample (all from sub-unit 4c) with a value higher than the regional anomalies for these elements (**Figures 4.12c-d and 4.12n-o**). Tungsten, gold, tellurium, and bismuth anomalies may therefore be missed if analyzing only surficial and not sub-surface till units.

The till at DH-15-GG also has an anomalous concentrations of gold, lead, nickel, magnesium, iron, silver, arsenic, antimony, barium, tellurium, bismuth, and sulphur relative to PF16 Highland Valley samples (**Figures 4.12d and 4.12f-p**). DH-15-GG is outside of the major mineralized zones of the Highland Valley system; it is about twelve kilometers to the northwest, up the ice-flow direction. However, it is still within the Guichon Creek Batholith, and other intrusion-related porphyry mineralization may exist in that area which may explain the anomalies here.

(a)

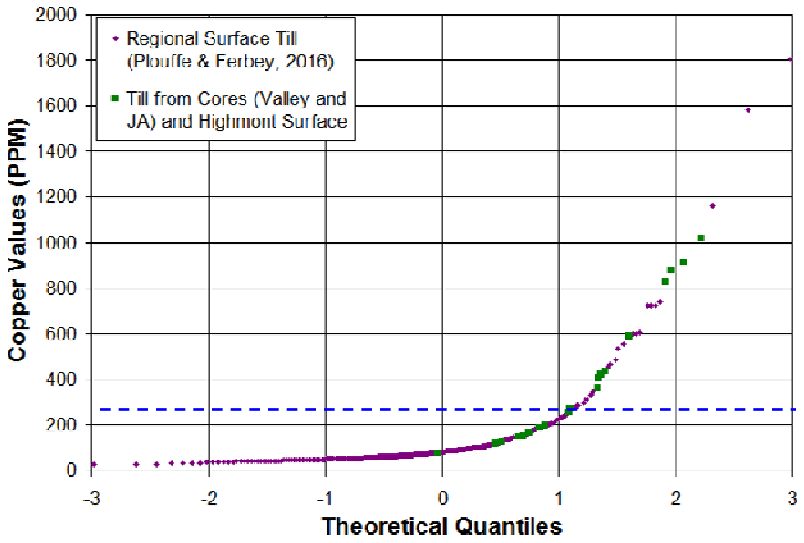

(b)

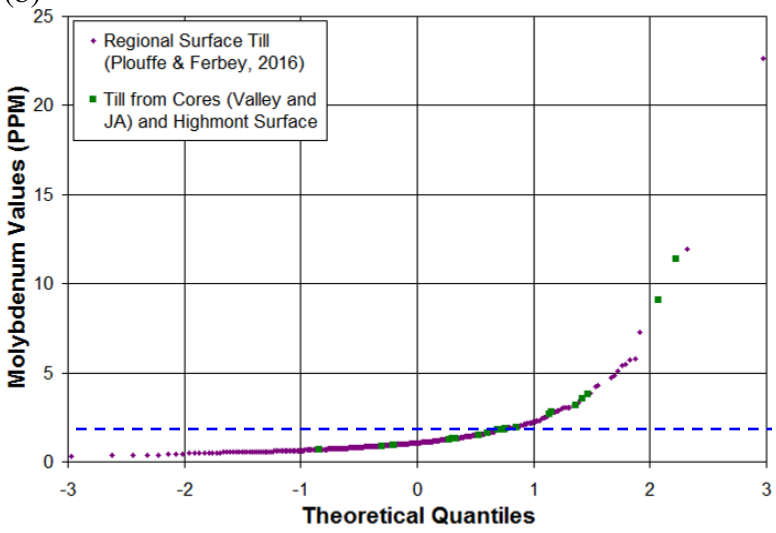
Regional Surface Till (Plouffe & Ferbey, 2016)
Till from Cores (Valley and JA) and Highmont Surface
Molybdenum Values (PPM)
Theoretical Quantiles

(c)

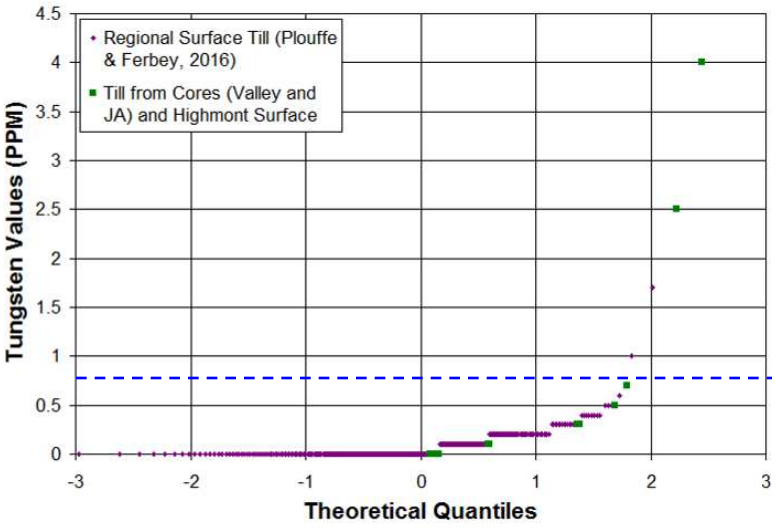
Regional Surface Till (Plouffe & Ferbey, 2016)
Till from Cores (Valley and JA) and Highmont Surface
Tungsten Values (PPM)
Theoretical Quantiles

(d)

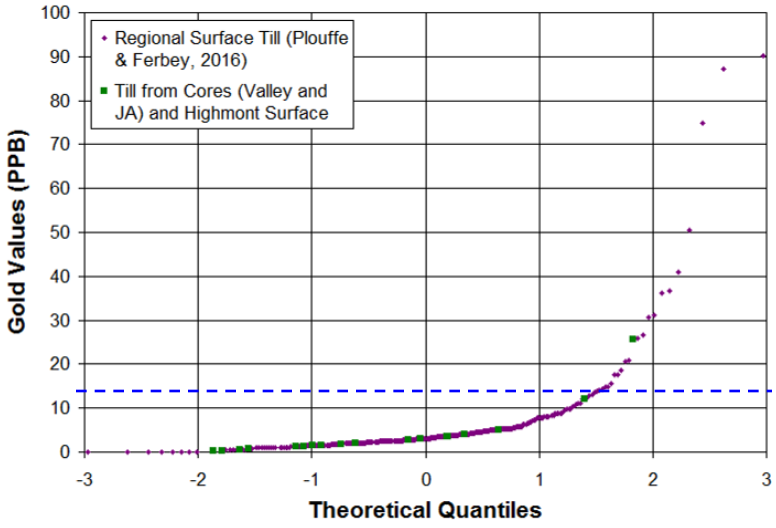
Regional Surface Till (Plouffe & Ferbey, 2016)
Till from Cores (Valley and JA) and Highmont Surface
Gold Values (PPB)
Theoretical Quantiles

(e)

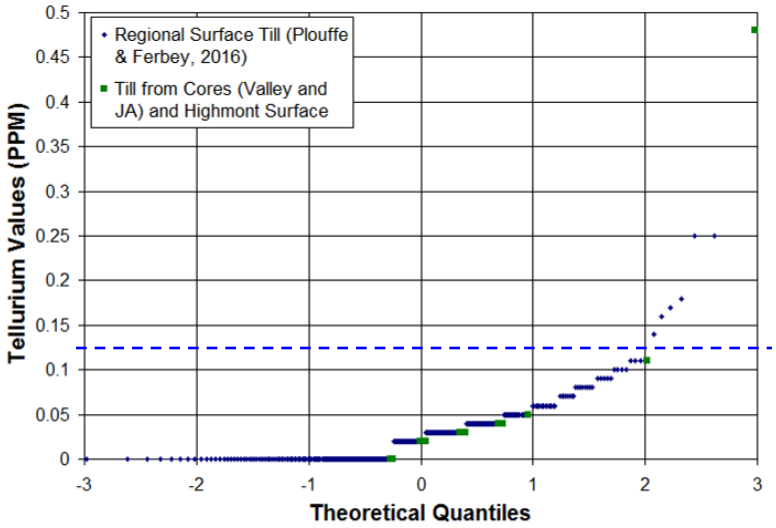

(f)

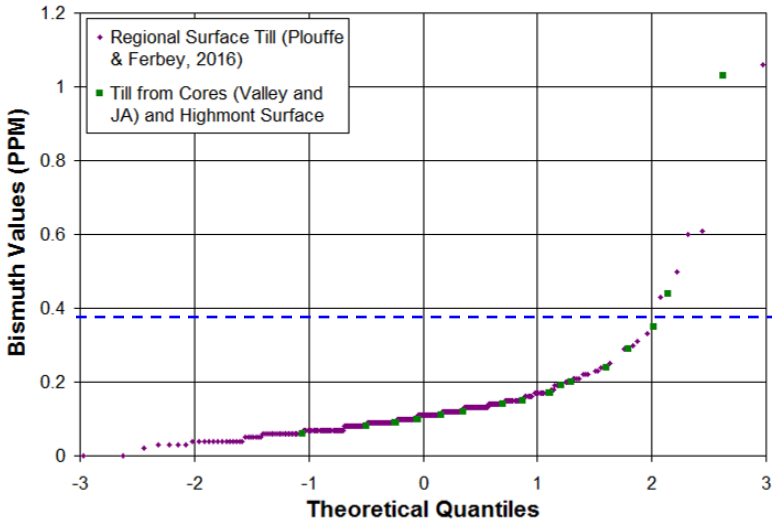

Figure 4.13 Geochemical results for tills from this study and for Plouffe and Ferbey's regional shallow till samples (2016). The dashed blue line indicates the anomaly threshold for shallow samples (PF16).

4.7 Comparison with Chouinard (2018)

The geochemical results for this study are compared with those of Chouinard's (2018) analysis of soil samples for samples in the Highmont South and J.A. areas (where sampling occurred for both studies). This is done in order to determine how the concentration of pathfinder elements changes between the subsurface and surficial soil.

Both sets of samples were analyzed with the same method at the same laboratory (aqua regia, ICP-MS at Bureau Veritas; cf. Chap. 2, Sect. 2.2.6).

At Highmont South, the concentrations for the subsurface till sample from this study are lower than for surficial soil samples for most elements. However, it is important to note that only one sample was analyzed from the Highmont South area in this study, and this sample may not be representative of the shallow till in the area. Median concentrations of select elements for samples from the upper B horizon soil layer (Chouinard, 2018) are shown alongside the concentrations for the Highmont South till sample from this study (**Table 4.2**). Copper, molybdenum, bismuth and silver were found in anomalous concentrations in these soil samples (according to probability plot distributions; Chouinard, 2018). Antimony, arsenic and tungsten are weakly anomalous (Chouinard, 2018). The area from which the Highmont South soil samples were taken overlies bedrock mineralization, and the surficial geology is composed mostly of till. The till sample from this study was taken from within Chouinard's Highmont South soil sampling area.

Table 4.2 Geochemical results for a till sample from this study compared to median values of Chouinard's (2018) upper B horizon soil samples. Both are from the same area at Highmont South overlying mineralization.

Element	**Highmont South Sample from this Study**	**Median Soil Sample Concentration (Chouinard, 2018)**
Cu (ppm)	184.26	212.45
Mo (ppm)	1.28	10.31
Ag (ppb)	13	82
Bi (ppm)	0.1	0.31
Sb (ppm)	0.12	0.1
As (ppm)	2.1	2.2
W (ppm)	0.3	0.4
Pb (ppm)	2	4.59
Zn (ppm)	16.9	22.8

The concentrations of porphyry copper pathfinder elements in the till and sand subsurface samples of this study in the J.A. area were generally either similar to or significantly higher than those of the soil samples in the same area. The copper concentration of one of this study's till samples is similar to those of the soil samples collected over till, while the other till sample has a copper concentration several times higher than the soil samples collected over till. The copper concentrations of the sand samples for this study is similar to those of the soil samples collected over sandy surficial material. The molybdenum concentrations of this study's till samples are similar to those of the soil samples collected over till; similarly those of this study's sand samples are similar to those of the soil samples collected over sandy surficial material. The silver concentration of one of this study's till samples is similar to those of the soil samples collected over till, while the other till sample has a silver concentration significantly higher than the soil samples collected over till.

Pathfinder element concentrations in tills are generally the lowest at Highmont South for this study (see Section 4.4.1 above); similarly, pathfinder element concentrations were generally much lower in the Highmont South soil samples than for the J.A. area soil samples, which was attributed to a lack of local glacial transport of mineralized material (Chouinard, 2018). Only vertical ion migration from the underlying mineralized bedrock occurred to bring traces of mineralization to the surface at Highmont South (Chouinard, 2018). In the J.A. area, element concentrations were higher in the subsurface (this study) as well as for soil samples (i.e. copper values up to 2,050 ppm vs 676 ppm at Highmont South, molybdenum values up to 149 ppm vs 35 ppm at Highmont South; Chouinard, 2018) concluded that physical transport of mineralized material to the area by glaciers was the cause.

4.8 Conclusions

Prehnite and kaolinite, which are characteristic of the distal and proximal alteration mineral assemblage, respectively, for the Highland Valley porphyry fluid system are both detectable in every unconsolidated cover sub-unit analyzed. The concentrations of both of these minerals in the sediment units are consistent with the degree of local provenance of

the units based on pebble lithology counts. Prehnite and kaolinite from pebbles recovered from Quaternary cover sediments may thus be used as footprint indicators and may also provide additional insights into the nature of the subcropping footprint assemblage (relative proximity to mineralization in the source area).

A number of different kinds of porphyry copper indicator minerals are found in each unconsolidated sediment unit. Chalcopyrite and pyrite are known to increase in concentration in the bedrock towards the centres of mineralization at Highland Valley; however, their concentrations in the unconsolidated cover are not consistent with the degree of local provenance (based on pebble counts) of each unit. Chalcopyrite is most abundant in the shallowest till sub-unit sampled (sub-unit 5b), and pyrite is most abundant in the poorly-sorted sand and gravel unit at ~1130 m asl at J.A. Pyrite anomalies higher than those of surficial samples are found in each Valley Pit area subsurface till unit analyzed as well as the J.A. top till. The visible gold and low-Cr diopside footprint found in the deeper till (4c) in the Valley pit area and the top thick till at J.A. may be part of a distal subsurface dispersal train extending from a mineral occurrence outside of Highland Valley, since these two indicators yielded low counts and are not specifically associated to the local footprints. Mn-epidote grains are more abundant in the Valley Pit subsurface units than the average for surficial till samples, but it is not known whether these grains originate from un-mineralized bedrock around Highland Valley or from alteration resulting from mineralization. More detailed mineral chemistry is needed in order for Mn-epidote to be a useful footprint indicator of mineralization at Highland Valley.

The strongest geochemical signal of mineralization is found in sub-units 3e (poorly-sorted outwash), 4a (subglacial till), 4b (poorly-sorted outwash), and 4c (subglacial till). These sub-units have the highest elevated values of key pathfinder elements (copper, molybdenum), and/or elevated values of several others.

Sub-units 3e, 4a, 4b, and 4c also show the strongest overall footprint of mineralization. Despite internal result variability (amongst different, neighbouring boreholes), they contain a relatively high variety and/or abundance or concentration of both minerals and elements indicative of porphyry copper mineralization, such as pyrite,

Mn-epidote, chromite, copper, and molybdenum. All are sourced dominantly locally from the Guichon Creek batholith that hosts the mineralization, but partly from the volcanic rocks and volcanogenic sediments outside of the batholith as well.

The sample from the bottom of the top thick till at J.A. and the surficial till sample at Highmont South show similar values to the surficial till data from Plouffe and Ferbey (2016) for all the geochemical elements and almost all the indicator minerals. However, all subsurface till units analyzed in the Valley pit area as well as the sample from the middle of the top till at J.A. show geochemical footprints of mineralization that are stronger than those of surficial samples. This is especially the case for copper, molybdenum, lead, silver, and bismuth. When compared to surficial till values, sub-unit 4c shows the highest number of anomalies and therefore appears to have the strongest geochemical footprint of mineralization. Sub-unit 4c is an approximately 20-m-thick subglacial traction till deposited during a second ice oscillation in this area (cf. Chap. 3, Sect. 3.2 and 3.5.5 for details). This is the thickest and most widespread subsurface till in the area. The results from this study suggest that more mineralized bedrock and surrounding footprint were available to glacial erosion during that glacial phase than during subsequent younger phase. This is because the preserved stratigraphy shielded more local bedrock in depressions during the younger glacial and related till production phases than earlier phases.

The difference in concentrations between deeper and shallower tills thus provide useful information into the dilution up the stratigraphy in areas of thick stratified drift. Additional, certain element (tungsten, gold, tellurium, and bismuth) anomalies relative to regional values are only present in sub-surface till units, and may be missed if analyzing only surficial till units. More subsurface samples are needed in the Highmont South and J.A. areas in order to more effectively compare geochemical results with those of soil sampling done in those areas.

Conclusions

5.1 Refining and Extending the Unconsolidated Sediment Stratigraphy at Highland Valley

Stratigraphic logging and analysis of ten drillcores and borehole-to-borehole correlations have produced a stratigraphic framework that organizes the stratigraphy above the Guichon Creek batholith into six major units. These six units have been subdivided into sub-units according to facies associations and depositional environment interpretations (cf. Chap. 3, Sect. 3.5.1, Fig. 3.27). Four new cross-sections (cf. Chap. 3, Sect. 3.2) and an interpreted seismic profile (cf. Chap. 3, Sect. 3.3, Fig. 3.20) improve our understanding of the stratigraphic architecture of the valley fill deposits at Highland Valley in the Valley Pit area and across the J.A. target.

The oldest unit (Unit 1) record pre-Quaternary events, and is characterized by interstratified fine-grained sediments and organics (coal), as well as thick non-glacial diamictons and breccias. It is overlain locally by subglacial and proglacial sediments (Unit 2 and Unit 3) which record an ice advance-retreat cycle over the study area, with changes in depositional environments from subglacial to glaciofluvial and glaciolacustrine. This lower part of the Quaternary glacial sequence is older than the limit of radiocarbon dating (>50 ka; Appendix B). The top of unit 3 (sub-units 3e-f) is a coarsening-upward succession that records a subsequent ice advance culminating by the deposition of the second subglacial traction till (Unit 4a) recognized in the study area; unit 4b records the start of the ice retreat phase that followed. Unit 5 is a complex unit of interstratified diamictons and various heterogeneous layers of sand and gravel and fine sediments. This unit is interpreted to record ice-marginal oscillations during the overall deglaciation, which eventually gave way to the proglacial glaciofluvial environment recorded by Unit 6, which is the youngest (top) unit intercepted by the boreholes.

The number and quality of the continuous drillcores have allowed for a detailed stratigraphic analysis that has led to several improvements and clarifications since Bobrowsky et al. (1993). Two new, previously unpublished units have been identified

and described; a deeper, older till, as well as an overlying deglacial sequence. These units are observed in depressions where they represent an important proportion of the buried sedimentary sequence. This study also reveals important lateral changes, both in the stratigraphy and internal facies characteristics, over relatively short distances. The new stratigraphic framework also groups units by facies associations and interpreted depositional environments. This is an important improvement over earlier published work, where limited observations of certain units led to the grouping of multiple depositional elements without clear descriptions of their internal vertical and lateral changes. As a result of this study, new insights have been made into the unconsolidated sediment stratigraphy at Highland Valley and the overall sequence of events as recorded by the buried sedimentary successions. Several uncertainties remain (some sub-unit correlations, precise depositional setting or process...) but a refined understanding of sedimentary cyclicity, dominated by at least two major ice advance and retreat cycles and additional minor oscillations of ice margins are now recognized in the Witches Brook creek valley sedimentary fill sequence.

5.2 Characterization of Physical Properties of Unconsolidated Sediment Units

Petrophysical (density, porosity, magnetic susceptibility, resistivity, and chargeability) and sedimentological (grain size) property measurements are available for the major cover units (Appendix B). In summary, the composition of the different units is highly variable. There are units consisting almost entirely of either gravel, sand, or silt and clay, as well as units consisting of nearly equal amounts of each. Average dry bulk density ranges from 1.5 to 3.7 g/cm^3, and average grain density ranges from 2.4 to 3.0 g/cm^3; many of the units are stiff and dense. Porosity is variable, ranging from 10.0 to 52.9 %. The magnetic susceptibilities, resistivities, and chargeabilities each vary by at least an order of magnitude. The magnetic susceptibility of the silt and/or clay sub-units decreases with depth. The till and non-glacial diamicton sub-units generally have a higher chargeability than the other units. These measurements define the characteristics of the

main unconsolidated sediment units. They may be useful for constraining future geophysical inversions and thus more accurate processing of future geophysical data.

5.3 Clast Provenance

A provenance interpretation is presented for every major unit in the unconsolidated sediment stratigraphy. The lithologies of clasts were first determined by observation during core logging or by using a microscope to group and count the pebbles (>4 mm fraction) for each unit. The clast lithologies were then linked to the known surrounding bedrock geology. Existing maps such as Lee et al. (2018) and McMillan et al. (2009) were consulted to determine the bedrock geology up the ice-flow direction. Literature such as d'Angelo et al. (2017) and Byrne et al. (2013) was used to determine the characteristics of the different bedrock lithologies in the area. Experts were consulted in order to better match pebble hand samples with the bedrock units. Kevin Byrne and Guillaume Lesage had both gained extensive experience identifying bedrock lithologies in the Highland Valley area while working on their PhDs as part of the NSERC-CMIC Footprints research project (Lesher et al., 2017). They assisted with identifying pebble samples. Most units have a high proportion of clast lithologies consistent with a Guichon Creek batholith source, which indicates a dominant local signature. Units interpreted to have been deposited in ice-marginal or proglacial settings by meltwater related processes generally have a more dominant local signature relative to other units. Tills have a higher proportion of distally-derived lithologies, especially Unit 2. Clast provenance analysis is relatively general, but it provides information that is useful for the more detailed analysis of footprint indicators related to the alteration and mineralized system at HVC. Lithological inheritance may have occurred during the process forming two of the till sub-units (4a and 4c), which have a higher proportion of locally-derived clasts relative to the other till units and directly overlie sorted units that are also rich in locally-derived clasts.

5.4 Patterns of Mineral Indicators and Geochemical Traces of Mineralization and their Provenance

This study identifies mineral indicators and geochemical pathfinders, with a focus on those associated with the HVC footprint (Bouzari et al., 2011; Kelley et al., 2011; Plouffe and Ferbey, 2016), and describes patterns in their distribution in the different stratigraphic units identified. It thus expands our knowledge of the spatial distribution of these footprint indicators away from buried mineralization and its related alteration, and it also provides new insights into the effect of stratigraphy on these patterns. One important question at the beginning was whether footprint indicators would be found in several units or just a few specific units. Another question was related to the possible effect of depositional environments and sediment properties on the distribution of footprint assemblages and characteristics from the mineralized centers.

Prehnite, a distal footprint alteration mineral at Highland Valley (Byrne, 2019), and kaolinite, a proximal footprint indicator (Lypackzewski et al., in-review), are both present in the pebbles of every unconsolidated Quaternary sub-unit analyzed (three out of six units). Several porphyry copper indicator minerals, such as pyrite, chalcopyrite, and jarosite, are also found in each of the Quaternary sediment cover sub-units that were analyzed. Two deep, poorly-sorted outwash (sub-units units 3e and 4b) and two deeper subglacial tills (sub-units 4a and 4c) have the highest anomalies of key pathfinder elements important at Highland Valley (e.g. Cu, Mo), as well as elevated values of several other porphyry copper pathfinder elements (e.g. Sn, As), and therefore show the strongest geochemical footprint of mineralization in the sedimentary sequence. The strongest overall footprint of mineralization is found in these same deeper sub-units. They contain a relatively high degree of variability or abundance of both minerals and elements that are indicative of porphyry copper mineralization (i.e. pyrite, Mn-epidote, chromite, copper, molybdenum). These sub-units are sourced mostly locally from the Guichon Creek batholith that hosts the mineralization, but also partially from the younger volcanic rocks and volcanogenic sediments that occur unconformably within the Guichon Creek batholith. This provides important insights into the overall dilution going up the stratigraphy and the related role these subsurface units may have played as a secondary

source of footprint material in younger (overlying) units due to sediment erosion and re-entrainment. The shallowest till sub-unit sampled contains a higher proportion of chalcopyrite grains relative to the deeper units, which may be due to a slight shift in ice flow direction forming this sub-unit that brought sediments from a different source that is more abundant in mineral indicators. A poorly-sorted sand and gravel unit at ~1130 m asl at J.A contains the most pyrite. A deeper till in the Valley pit area and the top thick till at J.A. both contain visible gold and low-Cr diopside. Due to their low counts and their absence from the local bedrock footprint (Lesher et al., 2017), these two mineral indicators may be a component of an unknown buried mineral occurrence. This could be part of a subsurface dispersal train extending from outside Highland Valley.

The type of footprint (proximal vs. distal) of the indicator assemblages has been compared to the provenance of the sub-unit based on pebble lithology analysis. The concentrations of prehnite and kaolinite are consistent with the degree of local provenance of the units (based on pebble counts; see Sect. 5.3). Consequently, the concentrations of prehnite and kaolinite from the pebbles of the Quaternary unconsolidated sediment cover may be used as footprint indicators and as estimates of the relative proximity to mineralization of the sub-unit's (or at least the pebbles') source area. However, the finer matrix fraction may have a different provenance due to different erosion and transport processes. For the other indicator minerals or geochemical elements, there is no obvious relationship between amount or concentration and extent of local provenance of each sub-unit.

5.5 Difference between Surface and Subsurface Unit Compositions

Results from subsurface tills (this study) were also compared with those from surface tills (Plouffe and Ferbey, 2016). Starting with indicator mineral grains, pyrite abundance is found to be greater in each subsurface till unit analyzed, except at Highmont, relative to surficial till. This could be due to the oxidizing conditions of the surficial till, which would have led to greater weathering of pyrite at the surface. Mn-epidote grains in the Valley Pit subsurface units also tend to be more abundant (mean =

12 grains) than in surficial till samples (mean = 3 grains). However, Mn-epidote is not a unique indicator of the HVC footprint; other sources could thus have contributed to this overall signal.

This study demonstrates that certain elements (tungsten, gold, tellurium, and bismuth) are found in concentrations that are anomalous relative to regional values only in sub-surface till units, and not in surficial ones. The geochemical HVC-type footprint of mineralization (Lesher et al., 2017) of all the subsurface till units analyzed proximal to HVC, as well as one of the top tills at J.A, is stronger than those of the surficial till. Copper, molybdenum, lead, silver, and bismuth values are particularly high in the subsurface samples compared to the surficial ones. The thickest and most widespread subsurface till in the area (sub-unit 4a), a subglacial traction till deposited by the second ice oscillation, appears to have the highest number of geochemical anomalies (compared to surficial averages). Some of these elements (e.g. Cu, Mo) tend to be sensitive to groundwater-mineral interactions; therefore, caution is needed in interpreting subsurface anomalies and their patterns.

Nonetheless, the relationship with other, more stable, indicators and pathfinders in the same sub-surface units suggest a relatively strong detrital origin. It can, therefore, be concluded that mineralized and altered bedrock was more accessible and available to glacial erosion during the older glacial phases. The preserved sedimentary cover in depressions most likely limited erosion of the local bedrock during the subsequent, younger till production phases. It is possible that a proportion of the footprint material in the younger units is derived from underlying units (e.g. 2 and 4) as opposed to underlying bedrock. This could explain the apparent dilution of the signal up the stratigraphy.

The differences in grain counts or element concentrations between deeper and shallower tills demonstrated by this study provide insights into the dilution up the stratigraphy where there is a thick transported cover. This study demonstrates that in areas of thick sedimentary cover, results from surficial surveys can be diluted. In this particular case, the degree of dilution was not sufficient to make it un-detectable or particularly elusive, but it is an important aspect to consider as other areas of thick glacial cover could exhibit a greater degree of dilution. In this case, important buried targets

could be missed by not investigating sub-surface units. Surficial indicator mineral or geochemical surveys successfully identify indicators of mineralization if bedrock is exposed in the area, but this may not be the case in other areas; hence, subsurface sediment sampling would be particularly useful. These conclusions may be valuable to consider when designing an exploration method or process in areas where there is a thick, stratified sediment cover.

5.6 Recommendations

Mineral chemistry analysis should be conducted on the detrital grains from this study in order to determine whether certain minerals in the sedimentary succession are useful footprint indicators of mineralization at Highland Valley. The mineral chemistry of the detrital grains could be compared with known bedrock mineral chemistry (Byrne, 2019; Ferbey et al., 2017; Lee et al., 2017; Lee et al., 2020; Lesage et al., in-review). It is not known whether the source of the Mn-epidote found in the unconsolidated cover at Highland Valley is the alteration resulting from mineralization at Highland Valley, or the un-mineralized bedrock (albite-epidote-hornfels facies metamorphism in the Nicola Group) up the glacier-flow direction. It is also unknown whether the low-Cr diopside and chromite in the sediment cover are a result of the Highland Valley mineralization, or another unknown mineral occurrence outside of it.

The spatial distribution of the footprint of mineralization in the unconsolidated cover and the differences and relationships of it to that of surficial samples has been described in this study. However, this study is based on a limited number of samples, especially for indicator mineral and hyperspectral analyses, and there are inconsistencies amongst the results in individual sub-units. Analysis of more samples would be useful in order to more rigorously define the characteristics and patterns of mineral indicators and element pathfinders throughout the sedimentary succession. More research could be done on why the shallowest till sub-unit sampled contains a higher proportion of chalcopyrite grains relative to the deeper units. More subsurface samples are needed in the Highmont South and J.A. areas for the purpose of comparing geochemical results of this study with

those of soil sampling done in those areas. Sampling of glaciofluvial sediment at the surface could be useful, as it would potentially contain a good footprint of mineralization.

References

Anderson, R.G., Plouffe, A., Ferbey, T., Dunn, C. E. 2012. The search for surficial expressions of buried Cordilleran porphyry deposits; background and progress in a new Targeted Geoscience Initiative 4 activity in the southern Canadian Cordillera, British Columbia. Geological Survey of Canada, Current Research 2012-7. 15 p.

Andrews, G.D.M., Plouffe, A., Ferbey, T., Russell, J.K., Brown, S.R., Anderson, R.G. 2011. The thickness of Neogene and Quaternary cover across the central Interior Plateau, British Columbia: analysis of water-well drill records and implications for mineral exploration potential. Canadian Journal of Earth Sciences. 48(6): 973-986.

Averill, S.A. 2013. Indicator mineral fingerprints in surficial sediments near Cu-Au deposits of the porphyry-epithermal-volcanogenic suite. In: McClenaghan, M.B., Plouffe, A. & Laython-Matthews, D. (editors.) Application of Indicator Mineral Methods to Mineral Exploration. Geological Survey of Canada, Open File 7553. 35-44.

Averill, S.A. 2011. Viable indicator minerals in surficial sediments for two major base metal deposit types: Ni-Cu-PGE and porphyry Cu. Geochemistry: Exploration, Environment, Analysis. 11: 279-292.

Baker, G., Society of Exploration Geophysicists. 1999. Processing near-surface seismic-reflection data: a primer. Society of Exploration Geophysics. Volume 9.

Bates, C., Phillips, D., Hild, J. 1992. Studies in P-Wave and 8-Wave Seismics.

Benn, D.I., Evans, D.J.A. 2010. Glaciers and Glaciation. Second Edition. London: Hodder Education.

Berger, B.R., Ayuso, R.A., Wynn, J.C., Seal, R.R. 2008. Preliminary Model of Porphyry Copper Deposits. U.S. U.S. Geological Survey Open File Report 2018-1321. 55p.

Bird, D.J., Coker, W.B. 1987. Quaternary Stratigraphy and Geochemistry at the Owl Creek Gold Mine, Timmins, Ontario, Canada. Journal of Geochemical Exploration. 28(1-3): 267-284.

Bobrowsky, P. T., Kerr, D. E., Sibbick, S. J., Newman, K. 1993. Drift Exploration Studies, Valley Copper Pit, Highland Valley Copper Mine, British Columbia. Stratigraphy and Sedimentology. British Columbia Geological Survey.

Bouzari, F., Hart, C. J. R., Barker, S., Bissig, T. 2011. Porphyry Indicator Minerals (PIMS): A New Exploration Tool for Concealed Deposits in South-Central British Columbia. Geoscience BC Report 2011-17.

Butt, C.R.M, Lintern, M., Anand, R.R. 2000. Evolution of regoliths and landscapes in deeply weathered terrain - implications for geochemical exploration. Ore Geology Reviews. 16(2-4): 167-183.

Byrne, K. 2019. Diagnostic Features of the Rocks and Minerals Peripheral to the Highland Valley Copper District, British Columbia, Canada: Implications for the genesis of porphyry Cu systems and their footprints [thesis]. [Alberta (ON]: University of Alberta.

Byrne, K., Lesage, G., Gleeson, S.A., Lee, R.G. 2017. Large-scale sodic calcic alteration around porphyry copper systems: Examples from the Highland Valley copper district, Guichon batholith, south-central British Columbia

Byrne, K., Stock, E., Ryan, J., Johnson, C., Nisenson, J., Jimenez, T.A., Lapointe, M., Stewart, H., Grubisa, G., Sykora, S. 2013. Porphyry Cu-(Mo) deposits in the

Highland Valley District, South Central British Columbia. Society of Economic Geologists, Inc., Guidebook Series. 44: 99–116.
Byrne, K., Tosdal, R.M. 2014. Genesis of the Late Triassic Southwest Zone Breccia-Hosted Alkalic Porphyry Cu-Au Deposit, Galore Creek, British Columbia, Canada. Economic Geology. 109(4): p. 915–938.
Casselman, M.J., McMillan, W.J., Newman, K.M. 1995. Highland Valley porphyry copper deposits near Kamloops, British Columbia: A review and update with emphasis on the Valley deposit. In: Porphyry Deposits of the Northwestern Cordillera of North America. The Canadian Institute of Mining and Metallurgy, Paper 8. p.161-191.
Chapman, J.B., Plouffe, A., Jackson, S.E., Ryan, J.J., Ferbey, T. 2015. Mineral markers of porphyry processes: regional and local signatures of porphyry prospectivity. In: Rogers, N., editor. TGI 4 - Intrusion Related Mineralisation Project: new vectors to buried porphyry-style mineralisation. Geological Survey of Canada, Open File 7843. 578 p.
Chouinard, R. L. M. 2018. Surficial Geochemical Tools for Cu-Mo Porphyry Exploration in Till-Covered Terrain [dissertation]. [Vancouver (B.C.)]: University of British Columbia.
Consolmagno, S.J., Britt, D.T. 2010. The density and porosity of meteorites from the Vatican collection. Meteoritics and Planetary Science, 33(6), 1231-1241.
D'Angelo, M., Alfaro, M., Hollings, P., Byrne, K., Piercey, S., Creaser, R.A. 2017. Petrogenesis and Magmatic Evolution of the Guichon Creek Batholith: Highland Valley Porphyry Cu ± (Mo) District, South-Central British Columbia. Economic Geology. 112: 1857-1888.
Doggett, M.D. 2000. Exploration in the new millennium: Will it be profitable? Paper presented at the Prospectors and Developers Association of Canada Annual Meeting, March 2000, 6 p.
Enkin, R.J., Cowan, D., Tigner, J., Severide, A., Gilmour, D., Tkachyk, A., Kilduff, M., Vidal, B., Baker, J. 2012. Physical Property Measurements at the GSC Paleomagnetism and Petrophysics Laboratory, including electric impedence spectrum methodology and analysis. Geological Survey of Canada, Open File 7227. 42p.
Enkin, R.J., Vidal, B.S., Baker, J., Struyk, N.M. 2008. Physical Properties and Paleomagnetic Database for South-Central British Columbia. Geological Fieldwork 2007, British Columbia Geological Survey. Paper 2008(1).
Evans, D.J.A. 2017. Conceptual ground models: British and Irish case studies. In: Griffiths, J.S., Martin, C.J. (editors). Engineering Geology and Geomorphology of Glaciated and Periglaciated Terrains. Geological Society, London, Engineering Geology Special Publication 28. p. 369-500.
Evans, D.J.A., Benn, D.I. (editors). 2004. A Practical Guide to the Study of Glacial Sediments. London: Edward Arnold. 266p.
Eyles, N., Miall, A.D. 2007. Canada Rocks: The Geologic Journey. 1st ed. Toronto, Canada: Fitzhenry & Whiteside. 512p.
Ferbey, T., Plouffe, A., Anderson, R.G. 2014. An integrated approach to search for buried porphyry-style mineralization in central British Columbia using geochemistry and mineralogy: a TGI-4 project. Geological Survey of Canada, Current Research 2014-2.

Ferbey, T., Plouffe, A., Bustard, A.L. 2016a. Geochemical, mineralogical, and textural data from tills in the Highland Valley Copper mine area, south-central British Columbia. British Columbia Geological Survey GeoFile 2016-11. Geological Survey of Canada, Open File 8119.

Ferbey, T., Plouffe, A., Bustard, A.L. 2016b. Porphyry Indicator Minerals in Tills of the Highland Valley Mine Area, South-Central British Columbia. Presentation for the Canadian Exploration Geophysical Society (KEGS), 2016.

Ferbey, T., Plouffe, A., Hickin, A.S. (editors). 2017. Indicator Minerals in Till and Stream Sediments of the Canadian Cordillera. Geological Association of Canada, Special Paper, Volume 50. Mineralogical Association of Canada, Topics in Mineral Sciences, Volume 47. 250 p.

Forsberg, R. 1984. A Study of Terrain Reductions, Density Anomalies and Geophysical Inversion Methods in Gravity Field Modelling. Ohio State University Colombus Department Of Geodetic Science and Surveying.

Fulton, R.J. 1965. Silt deposition in late-glacial lakes of southern British Columbia. American Journal of Science. 263(7): 553-570.

Fulton, R.J. 1967. Deglaciation studies in Kamloops region, an area of moderate relief, British Columbia. Geological Survey of Canada, Bulletin 154.

Fulton, R.J. 1969. Glacial lake history, southern Interior Plateau, British Columbia. Geological Survey of Canada, Paper 69-37.

Fulton, R.J., compiler. 1995. Surficial Materials of Canada. Geological Survey of Canada, Map 1880A, scale 1: 5,000,000.

Fulton, R.J., Irving. E., Wheadon, P.M. 1992. Stratigraphy and Paleomagnetism of Bruhnes and Matuyama (>790 ka) Quaternary Deposits at Merritt, British Columbia. Canadian Journal of Earth Sciences. 29: 76-92.

Gan, SW., Wang, SD., Chen, YK., Chen, J.L., Zhong, W., Zhang, C.L. 2016. Improved random noise attenuation using f–x empirical mode decomposition and local similarity. Appied Geophysics 13(1), 127-134.

Geological Survey of Canada, 2014. Surficial geology of Canada; Geological Survey of Canada, Canadian Geoscience Map 195 (preliminary, Surficial Data Model v. 2.0 conversion of Map1880A), scale 1:5,000,000.

Hashmi, S., Ward, B.C., Plouffe, A., Leybourne, M.I. Ferbey, T. 2015. Geochemical and mineralogical dispersal in till from the Mount Polley Cu-Au porphyry deposit, central British Columbia, Canada. Geochemistry: Exploration, Environment, Analysis. 15(2-3): 234-249.

Iverson, N.R. 1991. Potential Effects of Subglacial Water-Pressure Fluctuations on Quarrying. Journal of Glaciology. 37: 27-36.

Jago, C.P., Tosdal, R.M., Cooke, D.R., Harris, A.C. 2014. Vertical and Lateral Variation of Mineralogy and Chemistry in the Early Jurassic Mt. Milligan Alkalic Porphyry Au-Cu Deposit, British Columbia, Canada. Economic Geology. 109(4): p. 1005–1033.

John, D.A., Ayuso, R.A., Barton, M.D., Blakely, R.J., Bodnar, R.J., Dilles, J.H., Gray, Floyd, Graybeal, F.T., Mars, J.C., McPhee, D.K., Seal, R.R., Taylor, R.D., Vikre, P.G., 2010. Porphyry Copper Deposit Model. Chapter B of Mineral Deposit Models for Resource Assessment: U.S. Geological Survey Scientific Investigations Report 2010–5070–B. 169 p.

Kelley, K.D., Eppinger, R.G., Lang, J., Smith, S.M., Fey, D.L. 2011. Porphyry Cu indicator minerals in till as an exploration tool: example from the giant Pebble porphyry Cu-Au-Mo deposit, Alaska, USA. Geochemistry: Exploration, Environment, Analysis. 11: 321–334.

Kerr, D.E., Sibbick, S.J., Belik, G.D. 1993. Preliminary Results of Glacial Dispersion Studies on the Galaxy Property, Kamloops, B.C. In: Grant, B., Newell, J.M., editors. Geological Fieldwork 1992. British Columbia Ministry of Energy, Mines, and Petroleum Resources, Paper 1993-1. p. 439-443.

Kujansuu, R., Saarnisto, S.M. 1990. Glacier Indicator Tracing. Rotterdam: A.A. Balkema.

Lee, R.G., Byrne, K., Alfaro, M., D'Angelo, M., Hart, C.J.R., Hollings, P., Gleeson, S.A. 2017. Assessing the zircon compositional evolution from the Guichon Creek Batholith and Highland Valley Copper deposit, south-central B.C. Conference paper presented at: 14th SGA Biennial Meeting, August 2017, Quebec City. Volume: 3.

Lee, R.G., Byrne, K., Lesage, G. 2020. Distal Alteration Assemblages of Late Triassic to Early Jurassic Porphyry Copper Deposits, British Columbia, Canada: A Green Rock Perspective. Canadian Institute of Mining and Metallurgy, Special Volume.

Lesage, G., Byrne, K., Lypaczewski, P., Lee, R.G., Hart, C.J.R. 2016. Characterizing the District-scale Alteration Surrounding a Large Porphyry Cu System: the Footprint of Highland Valley Copper, British Columbia. Poster presented at: Geological Association of Canada - Mineralogical Association of Canada Joint Annual Meeting, 2016, Whitehorse, Yukon.

Lesher, M., Hannington, M., Galley, A., Ansdell, K., Astic, T., Banerjee, N., Beauchamp, S., Beaudoin, G., Bertelli, M., Bérubé, C. et al. 2017. Integrated Multi-Parameter Exploration Footprints of the Canadian Malartic Disseminated Au, McArthur River-Millennium Unconformity U, and Highland Valley Porphyry Cu Deposits: Preliminary Results from the NSERC-CMIC Mineral Exploration Footprints Research Network. In: Tschirhart, V., Thomas, M.D., editors. Proceedings of Exploration 17: Sixth Decennial International Conference on Mineral Exploration. p. 221–238.

Luck, P.M., Chouinard, R.L., Winterburn, P.A. 2019. Organic-compound pathfinders in soil for base- and precious-metal exploration in British Columbia. Geoscience BC Summary of Activities 2018: Minerals and Mining, Geoscience BC, Report 2019-1. p. 27–32.

McClenaghan, M.B., Parkhill, M.A., Pronk, A.G., Seaman, A.A., McCurdy, M.W., Poulin, R.S., McDonald, A.M., Kontak, D.J., Leybourne, M.I. 2015. Till, stream sediment, and stream water geochemical signatures of intrusion-hosted Sn-W deposits: examples from the Sisson W-Mo and Mount Pleasant Sn-W-Mo-Bi-In deposits, New Brunswick. In: Rogers, N., editor. TGI 4 – Intrusion Related Mineralisation Project: New Vectors to Buried Porphyry-Style Mineralisation. Geological Survey of Canada, Open File 7843. p. 39-58.

McClenaghan, M.B., Parkhill, M.A., Pronk, A.G., Sinclair, W.D. 2017. Indicator mineral and till geochemical signatures of the Mount Pleasant W-Mo-Bi and Sn-Zn-In deposits, New Brunswick, Canada. Journal of Geochemical Exploration. 172: 151-166.

McClenaghan, M.B., Ward, B.C., Kkjarsgaard, I.M., Kjarsgaard, B.A., Kerr, D.E., Dredge, L.A. 2000. Indicator mineral and till geochemical dispersal patterns

associated with the Ranch Lake kimberlite, Lac de Gras region, NWT, Canada. Geochemistry: Exploration, Environment, Analysis. 2: p. 299–30.
McConnell, J.W., Batterson, M.J. 1987. The Strange Lake Zr-Y-Nb-Be-REE deposit, Labrador: A geochemical profile in till, lake and stream sediment and water. Journal of Geochemical Exploration. 29: 105-127.
McMillan, W.J. 1976. Geology and genesis of the Highland Valley ore deposits and the Guichon Creek batholith. In: Porphyry Deposits of the Canadian Cordillera. The Canadian Institute of Mining and Metallurgy, Special Volume 15. p. 85-104.
McMillan, W. J. 1985. Geology and ore deposits of the Highland Valley Camp. Field guide and reference manual series, No. 1. Geological Association of Canada, Mineral Deposits Division.
McMillan, W.J., Anderson, R. G., Chan, R., Chow, W. 2009. Geology and mineral occurences (MINFILE), the Guichon Creek Batholith and Highland Valley porphyry copper district, British Columbia. Geological Survey of Canada, Open File 6079. 2 sheets.
Miall, A. 2010. The Geology of Stratigraphic Sequences. Second Edition. New York: Springer-Verlag Berlin Heidelberg. 522 p.
Mihalynuk, M.G. 2007. Neogene and Quaternary Chilcotin Group cover rocks in the Interior Plateau, south-central British Columbia: a preliminary 3-D thickness model. Geological Fieldwork 2006, BC Ministry of Energy, Mines and Petroleum Resources. Paper 2007(1).
Mitchinson, D.E., Enkin, R.J., Hart, C.J.R. 2013. Linking Porphyry Deposit Geology to Geophysics via Physical Properties: Adding Value to Geoscience BC Geophysical Data. Geoscience BC Report 2013-14.
Nesse, W.D. 2000. Introduction to Mineralogy. New York, Oxford: Oxford University Press. 442 p.
Norton, D.L. 1984. Theory of Hydrothermal Systems. Annual Review of Earth and Planetary Sciences. 12: 155-178.
Osatenko, M.J., Jones, M.B. 1976. Valley Copper. In: Sutherland Brown, A., editor. Porphyry Deposits of the Canadian Cordillera. Canadian Institute of Mining and Metallurgy, Special Volume 15. p. 130-143.
Paulen, R.C., McMartin, I., editors. 2009. Application of till and stream sediment heavy mineral and geochemical methods to mineral exploration in western and northern Canada. Geological Association of Canada, Short Course Notes 18.
Pears, G., Reid, J., Chalke, T. 2017. Advances in Geologically Constrained Modelling and Inversion Strategies to Drive Integrated Interpretation in Mineral Exploration. In: Tschirhart, V., Thomas, M.D., editors. Proceedings of Exploration 17: Sixth Decennial International Conference on Mineral Exploration. p. 221–238.
Perkins, D. 2011. Mineralogy. Third Edition. Upper Saddle River, New Jersey: Pearson Prentice Hall. 504 p.
Pisiak, L.K., Canil, D., Grondahl, C., Plouffe, A., Ferbey, T., Anderson, R.G. 2015. Magnetite as a porphyry Cu indicator mineral in till: a test using the Mount Polley porphyry Cu-Au deposit, British Columbia. Geoscience BC Summary of Activities 2014. Geoscience BC, Report 2015-1. p. 141-150.

Piotrowski, J.A., 2013. Channelized Subglacial Drainage Under Soft-Bedded Ice Sheets: Evidence from Small N-Channels in Central European Lowland. Geological Quarterly. 43: p. 153-162

Plouffe, A. 1998. Detrital transport of metals by glaciers, an example from the Pinchi Mine, central British Columbia. Environmental Geology. 33(2-3): 183-196.

Plouffe, A., Anderson, R.G., Gruenwald, W., Davis, W.J., Bednarski, J.M. Paulen, R.C. 2011. Integrating ice-flow history, geochronology, geology, and geophysics to trace mineralized glacial erratics to their bedrock source: An example from south-central British Columbia. Canadian Journal of Earth Sciences. 48(6): 1113-1129.

Plouffe, A., Bednarski, J.M., Huscroft, C.A., Anderson, R.G., McCuaig, S.J. 2010. Glacial sediments geochemistry of the Bonaparte Lake map area (NTS 92P), south central British Columbia. Geological Survey of Canada, Open File 6440.

Plouffe, A., Ferbey, T. 2016. Till geochemistry, mineralogy, and textural data near four Cu porphyry deposits in British Columbia. Geological Survey of Canada, Open File 8038. British Columbia Geological Survey, GeoFile 2016-10. 44 p.

Plouffe, A., Ferbey, T. 2017. Porphyry Cu indicator minerals in till: A method to discover buried mineralization. In: Ferbey, T., Plouffe, A., Hickin, A., editors. Indicator Minerals in Till and Stream Sediments of the Canadian Cordillera. Mineral Association of Canada, Topics in Mineral Sciences Volume 47, Geological Association of Canada, Special Paper 50. 129-159.

Plouffe, A., Ferbey, T., 2018. Surficial geology of the Highland Valley Copper mine area (parts of NTS 092I/06, 7, 10 and 11), British Columbia. Ministry of Energy, Mines and Petroleum Resources, British Columbia Geological Survey Geoscience Map 2018-01, scale 1:50,000.

Plouffe, A., Ferbey, T., Levson, V. M., Bond, J. D. 2012. Glacial history and drift prospecting in the Canadian Cordillera: recent developments. Geological Survey of Canada, Open File 7261. 51 p.

Potter, D. K. 2007. Magnetic Susceptibility as a Rapid, Nondestructive Technique for Improved Petrophysical Parameter Prediction. Petrophysics. 48(3): 191-201.

Preto, V.A. Osatenko, M.J., McMillan, W.J., Armstrong, R.L. 1979. Isotopic Dates and Strontium Isotopic Ratios for Plutonic and Volcanic Rocks in the Quesnel Trough and Nicola Belt, south-central British Columbia. Canadian Journal of Earth Sciences. 16: 1658-1672.

Proudfoot, D.N., Bobrowsky, P.T., Meldrum, D.G. 1995. Drift exploration potential maps derived from terrain geology maps. In: Bobrowsky, P.T., Sibbick, S.J., Newell, J.M., Matysek, P.F, editors. Drift Exploration in the Canadian Cordillera. British Columbia Ministry of Energy, Mines and Petroleum Resources, Paper 1995-2. p. 43-52.

Pugin, A.J.M., Larson, T.H., Sargent, S.L., McBride, J.H., Bexfield, C.E. 2004. Near-surface mapping using SH-wave and P-wave seismic land-streamer data acquisition in Illinois, U.S.. The Leading Edge, 23(7), 677-682.

Roberts, D. H., Long, A. J. 2005. Streamlined Bedrock Terrain and Fast Ice Flow, Jakobshavns Isbrae, West Greenland: Implications for Ice Stream and Ice Sheet Dynamics. Boreas. 34(1): 25–42.

Rogers, N., editor. 2015. TGI 4 - Intrusion Related Mineralisation Project: new vectors to buried porphyry-style mineralisation. Geological Survey of Canada, Open File 7843. 578 p.

Ryder, J.M., Fulton. R.J, Clague. J.J. 1991. The Cordilleran Ice Sheet and the Glacial Geomorphology of Southern and Central British Columbia. Géographie Physique et Quaternaire. 45(3): 365-377.

Shilts, W.W. 1996. Drift exploration. In: Menzies, J., editor. Glacial Environments, Sediment Forms and Techniques. Butterworth Heinemann, p. 411–439.

Sillitoe, R.H. 2010. Porphyry Copper Systems. Economic Geology. 105: 3-41.

Sinclair, W.D. 2007. Porphyry deposits. In: Goodfellow, W.D., editor. Mineral Deposits of Canada: A Synthesis of Major Deposit-Types, District Metallogeny, the Evolution of Geological Provinces, and Exploration Methods. Geological Association of Canada, Mineral Deposits Division, Special Publication No. 5. p. 223-243.

Snow, R.J., Coker, W.B. 1987. Overburden geochemistry related to W-Cu-Mo mineralization at Sisson Brook, New Brunswick, Canada: An example of short- and long-distance glacial dispersal. Journal of Geochemical Exploration. 28(1-3): 353-368.

Stea, R.R., Finck, P.W. 2001. An Evolutionary Model of Glacial Dispersal and Till Genesis in Maritime Canada. In: McClenaghan, M.B., Bobrowsky, P.T., Hall, G.E.M., Cook, S.J. (editors). Drift Exploration in Glaciated Terrain. Geological Society of London Special Publication 185: 237-265.

Sugden, D.E., Glasser, N., Clapperton, C.M. 1992. Evolution of Large Roches Moutonnées. Geografiska Annaler, Series A. 74: 253–264.

Tamari, S. 2004. Optimum design of the constant-volume gas pycnometer for determining the volume of solid particles. Measurement Science and Technology, 15(3).

Tappert, M.C., Rivard, B., Giles, D., Tappert, R., Mauger, A. 2013. The mineral chemistry, near-infrared, and mid-infrared reflectance spectroscopy of phengite from the Olympic Dam IOCG deposit, South Australia. Ore Geology Reviews 53: 26-38.

Teck Resources Limited, 2017. Horizons - 2017 Annual Report.

Trommelen, M. S., Ross, M., Campbell, J.E. 2013. Inherited Clast Dispersal Patterns: Implications for Palaeoglaciology of the SE Keewatin Sector of the Laurentide Ice Sheet. Boreas. 42(3): 693-713.

van der Meer, F.D., van der Werff, H.M.A., van Ruitenbeek, F.J.A., Hecker, C.A., Bakker, W.H., Noomen, M.F., van der Meijde, M., Carranza, E.J.M., de Smeth, J.B., Woldai, T. 2012. Multi- and Hyperspectral Geologic Remote Sensing: A Review. International Journal of Applied Earth Observation and Geoinformation. 14(1): 112-128.

Waldner, M.W., Smith, G.D., Willis, R.O. 1976. Lornex. In: Sutherland Brown, A., editor. Porphyry Deposits of the Canadian Cordillera. Canadian Institute of Mining and Metallurgy, Special Volume 15. p. 120-129.

Yilmaz, O. 2001. Seismic Data Analysis: Processing, Inversion, and Interpretation of Seismic Data (Volume 1). Society of Exploration Geophysics. Volume 1.

Zimmer, M.A. 2004. Seismic velocities in unconsolidated sands: Measurements of pressure, sorting, and compaction effects.

Appendix A - Stratigraphy

(a)

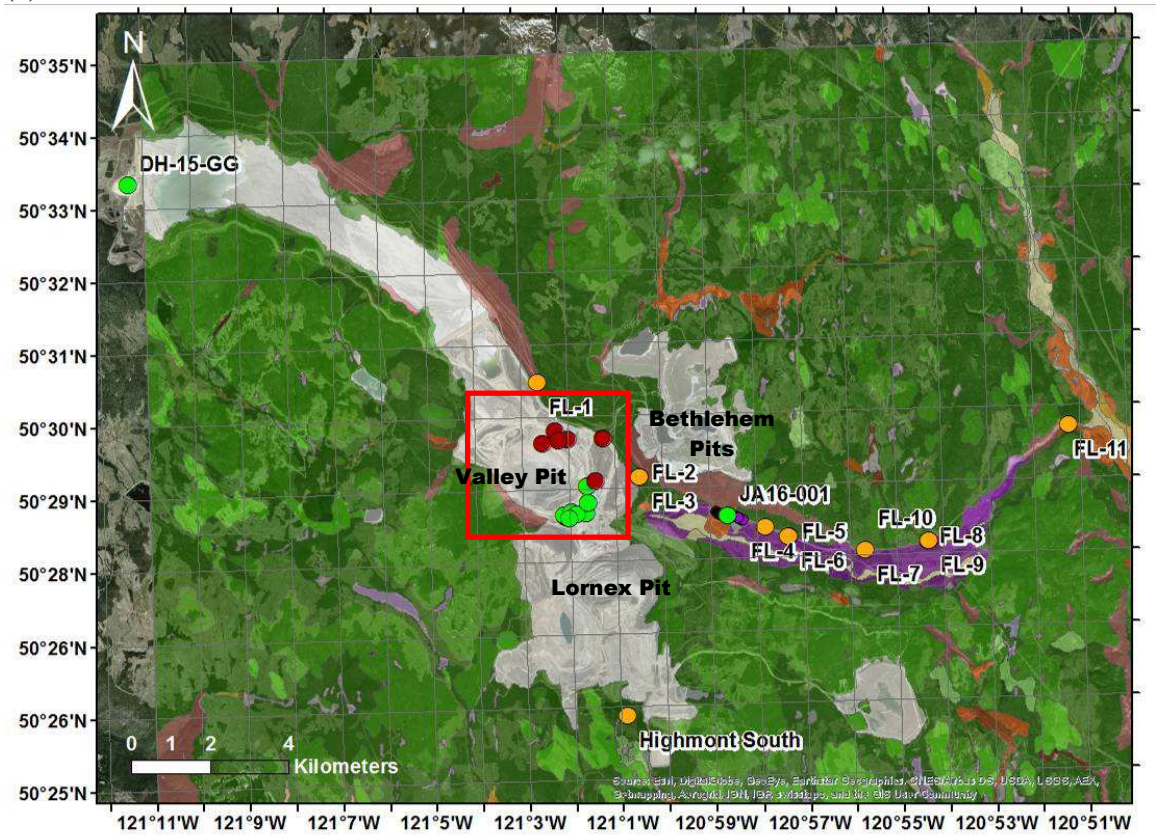

(cont'd next page)

(b)

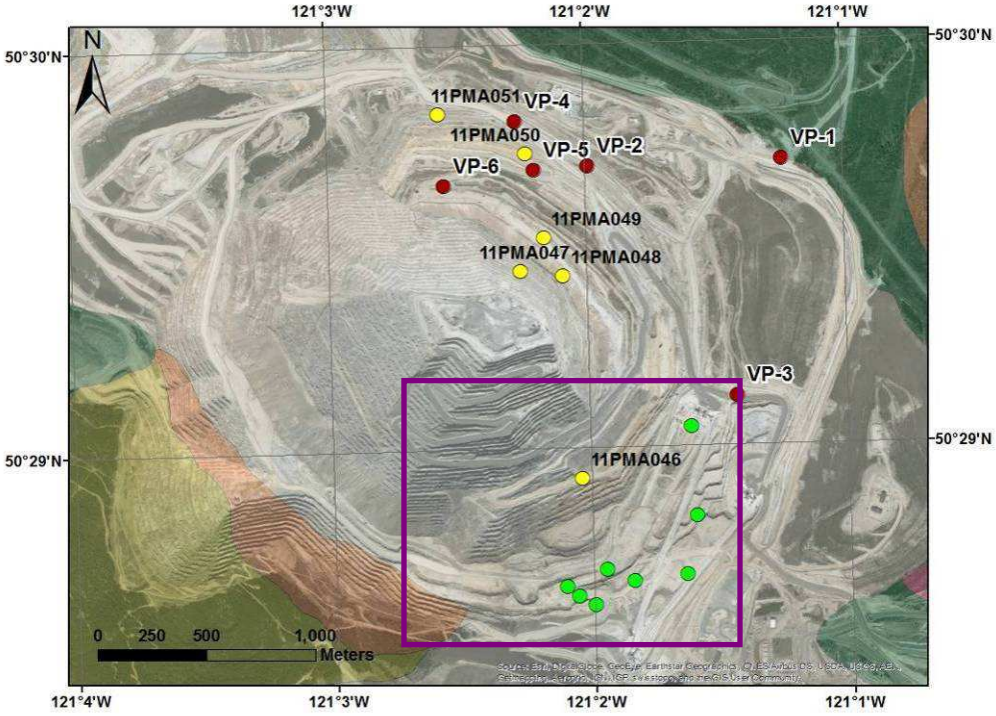
121°3'W
121°2'W
121°1'W
50°30'N
N
11PMA051
VP-4
11PMA050
VP-5
VP-2
VP-1
VP-6
11PMA049
11PMA047
11PMA048
VP-3
50°29'N
11PMA046
0 250 500 1,000
Meters
121°4'W
121°3'W
121°2'W
121°1'W

(c)

(cont'd next page)

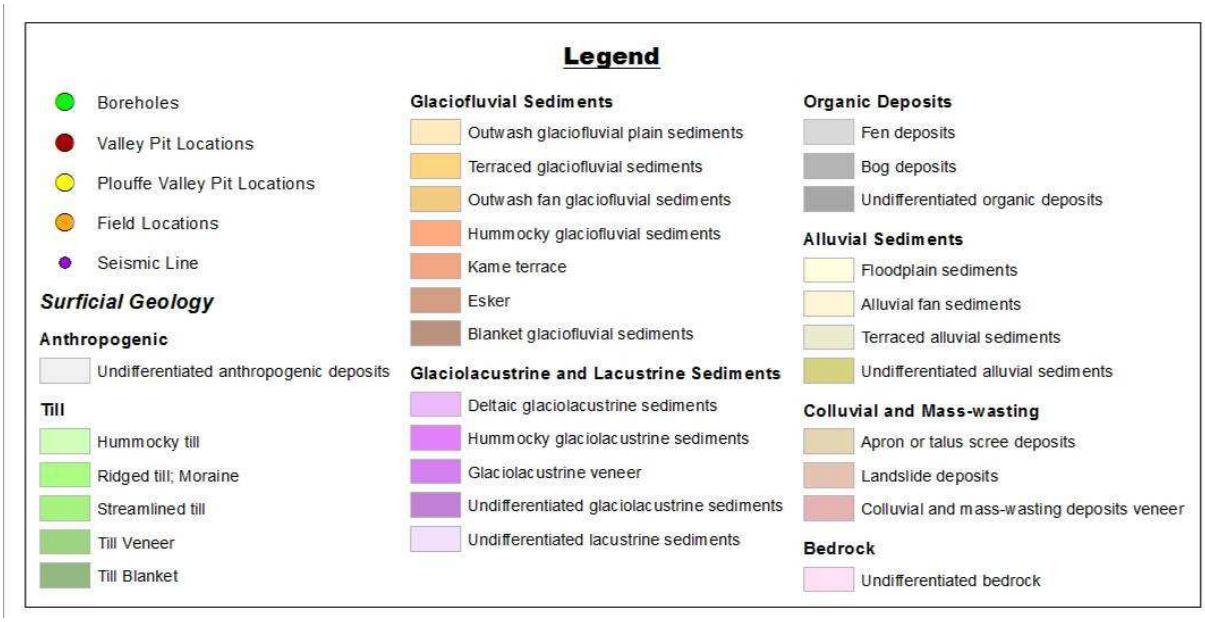

Figure A.1 The surficial geology of the study area (Plouffe et al., 2018) as well as the locations of boreholes and field sites (a). The inset map (b) shows the observation locations for this study (red-filled circles), for Alain Plouffe's study (yellow-filled circles) and of the boreholes (green-filled circles) in the Valley pit (red squared box). A

second inset map (c) shows the locations of the individual boreholes around the Valley pit (purple squared box).

Stratigraphy at Core DH-15-GG

Core DH-15-GG is from a borehole drilled several kilometers to the northwest of the major mineralized zones (**Figure A.1a**). The stratigraphy here (**Figure A.2**) is dominated by a lithified and stratified conglomeratic unit (elevation range: 1081.7 to 1134.7 m asl). The unit consists mostly of granule-sized particles and has pebbles, cobbles and boulders near its base and its top. The clasts are volcanics of various types and colours and felsic coarse-grained igneous. Lenses and irregularly-shaped fragments of coal occur throughout the conglomeritic unit, with the thickest (approx. 0.5m-thick) layer located near the base of it. The base of the conglomerate contains gently sloping planar contacts. The unit is overlain by a thin layer of clast-supported, massive diamicton with a silt matrix, granules and small pebbles (elevation range: 1134.7 to 1136.1 m asl). This layer is in turn overlain by stiff dense clay with silt and organic-rich laminations (elevation range: 1136.1 to 1142.6 m asl), followed by a few thin layers of clast-supported, massive diamicton with sand interbeds (elevation range: 1142.7 to 1144.5 m asl). The diamicton has a clayey matrix with angular to subangular pebbles and cobbles

and fragments of coal. The sand interbeds are poorly lithified and contains a few granules. The diamicton is overlain by angular, highly weathered, disintegrating, felsic, coarse-grained igneous boulders (elevation range: 1144.5 to 1146.3 m asl). Overlying the boulders is a 12m-thick unit of massive, lithified diamicton with granules and irregularly shaped, angular to subrounded pebbles and cobbles of various lithologies (elevation range: 1146.3 to 1158.6 m asl). The diamicton is interpreted to be glacial in origin. The stratigraphy is capped by pebble and cobble layers with granules in both coarsening and fining upward cycles. The pebbles and cobbles are irregularly shaped, angular to subangular and fine-grained igneous, volcanic or sedimentary rock clasts.

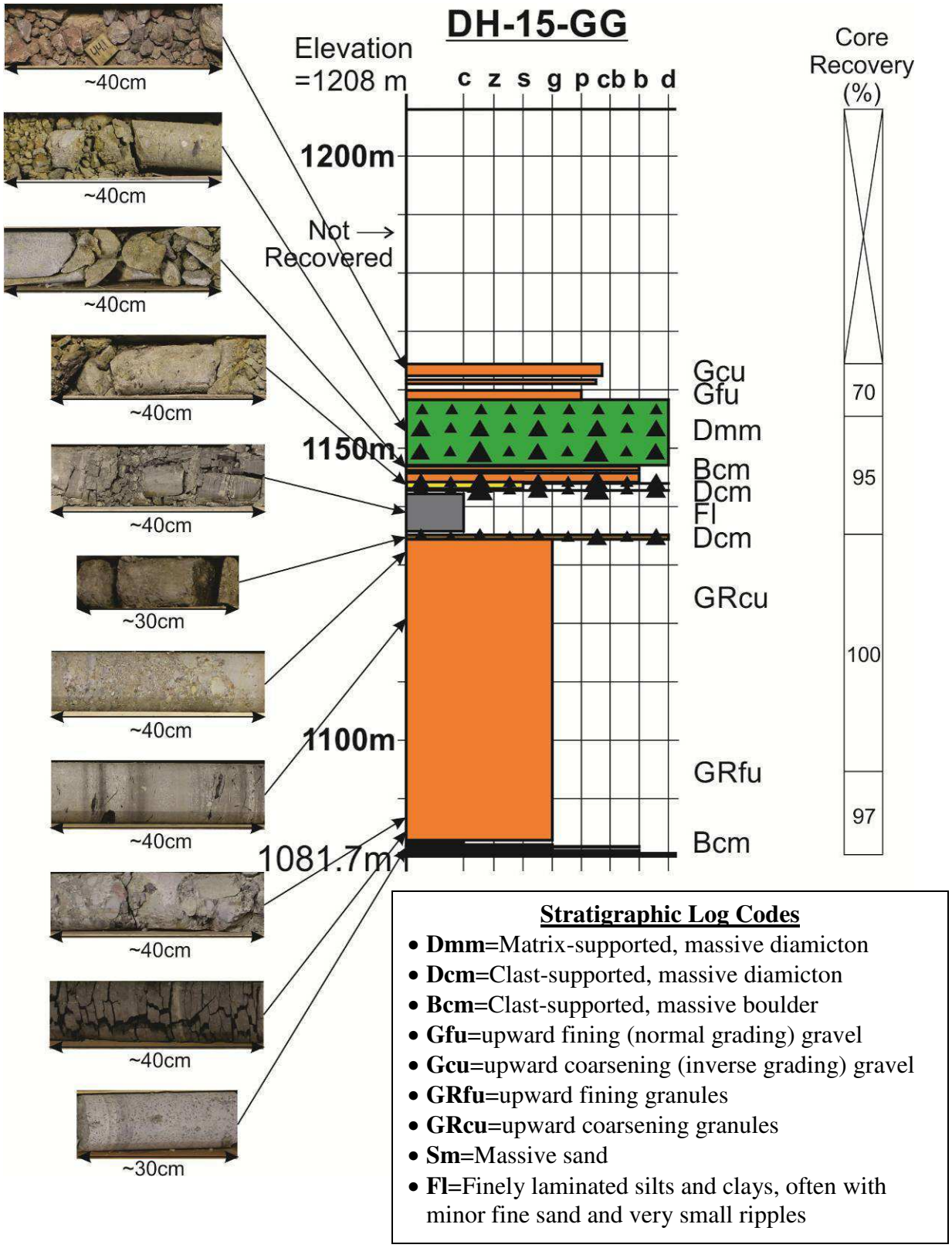

Figure A.2 Interpolated stratigraphic log for core DH-15-GG, located twelve kilometers to the northwest of the major mineralized zones (see Figure 6.1a for location).

Surficial Sediments

Road Cuts

The surficial sediments in the region were studied where they were exposed along the road running to and alongside the mine (**Figure A.1a**). Tills, sands and silts were observed.

The surfical sediments at FL-1, FL-3, FL-4 and FL-5 (**Figure A.3**) are very stiff tills. They are composed of a silty matrix, granules and generally subangular pebbles, cobbles and boulders of a mixed but mostly felsic coarse-grained igneous lithology. Many of the clasts are faceted and some are iron-shaped (**Figure A.4**).

Figure A.3 Stiff, clast-rich till with silt matrix at roadcut FL-5.

Figure A.4 Faceted clast found in till at roadcut FL-4.

The surface sediment at FL-2 is sand with granules and angular to subangular pebbles. Boulders are also present in the vicinity.

The surficial sediment at FL-6 is fine sand (**Figure A.5**). It fines downward to silt at about 3 metres below the ground surface, at which point granules, pebbles and cobbles also appear. The fine sand and silt are interlayered at the transition between the two. This sand and silt layer overlies the till unit at FL-5, and thins to almost nothing at that location (**Figure A.6**).

Figure A.5 Fine sand at roadcut FL-6 with interlayered silt and clasts at bottom.

Figure A.6 Fine sand unit overlying till at roadcut FL-6, with the contact between the two shown as a dashed line.

At FL-7 is interlayered, lenticular sand and silt (**Figure A.7**). The sand forms ripples, and the silt is draped on top of these ripples as laminations (**Figure A.8**). This unit fines upward and turns into planar laminated silt near the top (**Figure A.9**).

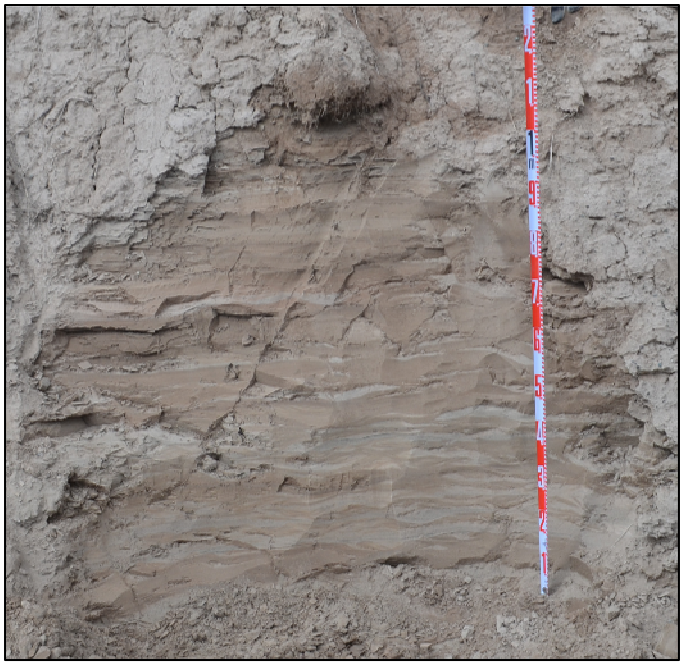

Figure A.7 Interlayered, lenticular sand and silt at roadcut FL-7.

Figure A.8 Bottom of figure 36; rippled sand with silt laminations draped overtop at roadcut FL-7.

Figure A.9 Top of figure 36; planar laminated silt at roadcut FL-7.

The surface sediment at FL-8 is a very stiff till with a clayey silt matrix (**Figure A.10**). It is rich in granules as well as subangular pebbles, cobbles and boulders whose lithology is highly varied but mostly felsic coarse-grained igneous. Most of the clasts are faceted and some are iron-shaped.

Figure A.10 Stiff, clast-rich till with clay matrix at roadcut FL-8.

The surficial sediments at FL-9 consist of the same till as at FL-8 overlain by a thin layer of laminated silt (**Figure A.11**). The silt layer is only visible for a few tens of metres; it pinches out going westward until the till becomes the topmost layer.

Figure A.11 Laminated silt overlying till at roadcut FL-9.

At FL-10 is the same till as at FL-8, and this is overlain by a thin layer of stiff clay with fine sand lenses (**Figure A.12**). The sand lenses are wavy, and some erosional scours into the clay are observed. This unit is overlain by a thin fine sand unit with clay lenses (**Figure A.13**).

Figure A.12 Stiff clay with fine sand lenses at roadcut FL-10.

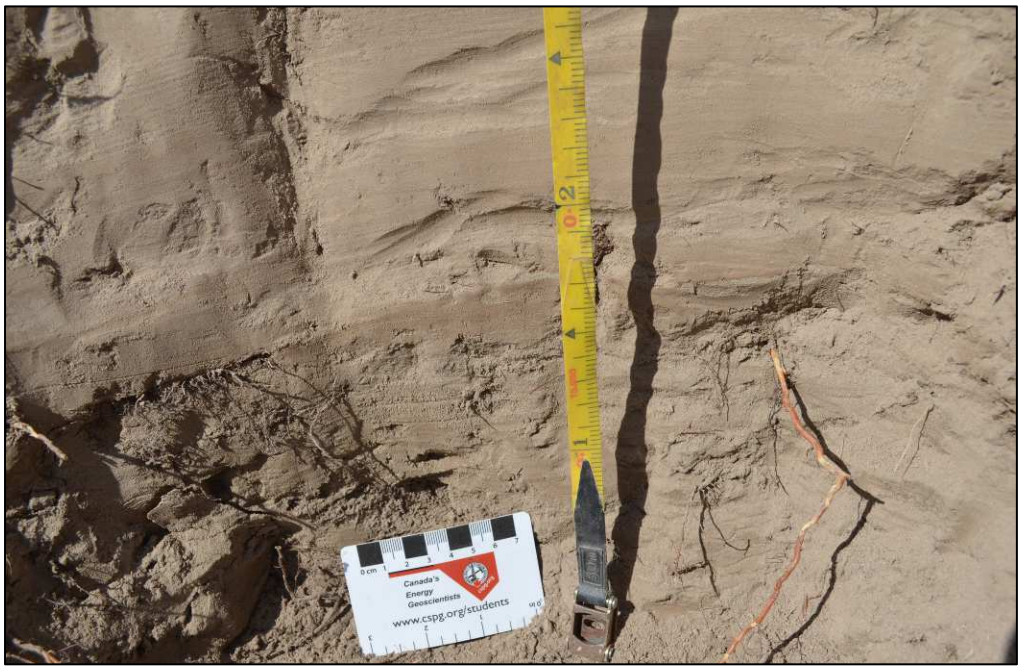

Figure A.13 Fine sand with clay lenses at roadcut FL-10.

The surface sediment at FL-11 is a highly consolidated till with a sandy silt matrix (**Figure A.14**). It is rich in granules and subangular pebbles, cobbles and boulders of a highly variable lithology. Most of the clasts are faceted and some are iron-shaped.

Figure A.14 Highly consolidated till with sandy silt matrix at roadcut FL-11.

Highmont Excavation

The surficial sediment at the excavation dug adjacent to the Highmont pit at Highmont South (**Figure A.1a**) consist of fine to medium sand with granules and subangular pebbles, cobbles and boulders (**Figure A.15**).

Figure A.15 Sand with granule- to boulder-sized clasts at the Highmont South excavation pit.

Valley Pit Observations by Alain Plouffe

Figure A.16 Silt and clay glaciolacustrine unit observed by Alain Plouffe in the Valley pit at stations 11PMA047, 11PMA048 and 11PMA049. See figure 6.1b for location.

Figure A.17 Deltaic foresets of delta unit dipping to the east observed by Alain Plouffe in the Valley pit at station 11PMA046. See figure 6.1b for location.

Figure A.18 Deltaic foresets of delta unit dipping to the southeast observed by Alain Plouffe in the Valley pit at station 11PMA050. See figure 6.1b for location.

Figure A.19 Sand and gravel of proglacial and subglacial outwash and resedimented subaqueous debris flow unit observed by Alain Plouffe in the Valley pit at station 11PMA051. See figure 6.1b for location.

Appendix B - Properties of Stratigraphic Units

Physical properties were measured in order to define the characteristics of the main units of the unconsolidated sediment stratigraphy. The following subsections present these properties. The petrophysical properties are useful for constraining geophysical inversions.

Petrophysical Properties

Dry bulk density values for samples from most of the different units from each core have been calculated (**Table B.1**). All of these measurements, which were made on short hand samples and long 3.0-4.5m sections of core (cf. Chap. 2, Sect. 2.2 for details), were compiled to come up with an average unconsolidated sediment cover density at each borehole location (cf. Chap. 2, Sect. 2.2.1 for details). First, a density was assigned to every single sub-unit of each core. A density calculated from measurements made of a sample from that same sub-unit of the same core was used if one existed. If not, a density determined from a sample of a nearby similar sub-unit in the same core with the same grain or clast size was assigned. If none existed, then the density of a similar unit with the same grain or clast size from a nearby core was used. Next, the vertical proportion of each sub-unit in the entire known core succession was calculated by dividing each sub-unit's length by the total length of known and deduced material in the whole core. This vertical proportion was multiplied by the assigned density to obtain a weighted density for each sub-unit. Finally, the weighted densities for each sub-unit were all added up to calculate the average density for each core. The result is a set of average values of the unconsolidated sediment dry bulk density at different locations (**Table B.2**). This helps to determine an overall unconsolidated sediment bulk density, which would be useful when doing geophysical inversions here or at other areas with a cover of unconsolidated sediment over bedrock.

Table B.1 Location, depth and elevation intervals, sedimentary unit and density for each interval of core that had dry bulk density measured.

Core Name	Depth Interval (m)	Elevation Interval (m)	Sedimentary Unit	Density (g/cm3)
VTH2014-03	85.7-92.6	1088.1-1081.2	coarse sand with pebbles & granules	1.775
VTH2014-03	99.1	1074.7	fine sand with laminations	1.804
VTH2014-03	100.3-103.5	1073.5-1070.3	silty clay	1.395
VTH2014-03	105.45-110.0	1068.3-1063.8	silty clay	1.554
VTH2014-03	106.15-106.25	1067.6-1067.5	silty clay	1.541
VTH2014-06	23.6-26.0	1179.4-1174.5	sand with granules	1.727
VTH2014-06	26.3-29.0	1174.2-1171.5	fine-medium sand with pebbles & granules	1.773
VTH2014-06	29.3-36.5	1171.2-1164.0	fine-medium sand with pebbles & granules & cobbles	1.857
VTH2014-06	43.8-46.7	1156.7-1153.8	pebbles & cobbles	1.966
VTH2014-06	66.5-69.5	1134.0-1131.0	poorly sorted sand with pebbles & granules	1.716
VTH2014-06	72.5-75.5	1128.0-1125.0	silt & clay	1.790
VTH2014-06	75.5-78.5	1125-1122.0	silt & clay	1.404
VTH2014-06	162.0-165.5	1038.5-1035.0	diamicton with clay, silt & coal interbeds	2.093
VTH2014-06	165.5-170.0	1035.0-1030.5	diamicton with clay, silt & coal interbeds	2.014
VTH2014-06	169.4-169.55	1031.1-1030.9	diamicton with clay, silt & coal interbeds	2.114
VTH2014-06	170.0-174.5	1030.5-1026.0	diamicton with clay, silt & coal interbeds	2.125
VTH2014-06	176.3-176.5	1024.2-1024.0	diamicton with clay, silt & coal interbeds	2.303

VTH2014-06	179.0-183.5	1021.5-1017.0	diamicton with clay, silt & coal interbeds	2.232
VTH2014-06	179.6-179.7	1020.9-1020.8	diamicton with clay, silt & coal interbeds	2.168
VTH2014-06	183.5-188.0	1017.0-1012.5	diamicton with clay, silt & coal interbeds	1.897
VTH2014-06	192.5-194.0	1008.0-1006.5	diamicton with clay, silt & coal interbeds	1.876
VTH2014-07	20.8-24.5	1241.3-1237.6	till	2.277
VTH2014-07	24.25-24.44	1237.8-1237.6	boulder	2.154
VTH2014-07	38.9-39.1	1223.2-1223.0	boulder	2.655
VTH2014-07	39.8-42.8	1179.4-1174.5	till	1.988
VTH2014-07	42.8-50.0	1215.1-1212.1	till & cobbles	2.411
VTH2014-07	43.7-43.8	1218.4-1218.3	boulder	2.772
VTH2014-07	63.5-68.0	1198.6-1194.1	till	2.501
VTH2014-07	68.0-72.5	1194.1-1189.6	till	2.615
VTH2014-07	72.5-77.0	1189.6-1185.1	till	2.803
VTH2014-07	92.0-96.5	1170.1-1165.6	diamicton	2.474
VTH2014-07	101.0-105.5	1161.1-1156.6	sand rich in granule, pebbles & cobbles interspersed with thin diamicton beds	2.181
VTH2014-07	103.55-103.6	1158.5	sand rich in granule, pebbles & cobbles interspersed with thin diamicton beds	1.803
VTH2014-07	103.7-103.8	1158.4-1158.3	sand rich in granule, pebbles & cobbles interspersed with thin diamicton beds	1.910

VTH2014-07	105.5-110.0	1156.6-1152.1	sand rich in granule, pebbles & cobbles interspersed with thin diamicton beds	2.229
VTH2014-07	114.5-119.0	1147.6-1143.1	sand rich in granule, pebbles & cobbles interspersed with thin diamicton beds	2.257
VTH2014-07	119.0-123.5	1143,1-1138.6	sand rich in granule, pebbles & cobbles interspersed with thin diamicton beds	2.182
VTH2014-07	123.5-128.0	1138.6-1134.1	sand rich in granule, pebbles & cobbles interspersed with thin diamicton beds	2.153
VTH2014-07	128.0-132.5	1134.1-1129.6	sand rich in granule, pebbles & cobbles interspersed with thin diamicton beds & fine sand	1.923
VTH2014-07	130.4-130.5	1131.7-1131.6	fine sand	1.689
VTH2014-07	132.5-137.0	1129.6-1125.1	fine sand & silt	1.956
VTH2014-07	135.05-135.1	1127	silt	1.883
VTH2014-07	136	1126.1	silt	1.727
VTH2014-07	136.1	1126	silt	1.752
VTH2014-07	137.0-141.5	1125.1-1120.6	silt & clay	1.900
VTH2014-07	141.3	1120.8	clay	1.854
VTH2014-07	141.5-146.0	1120.6-1116.1	clay	1.624
VTH2014-07	143.6	1118.5	clay	1.852
VTH2014-07	150.2-155.0	1111.9-1107.1	clay	1.588

VTH2014-07	155.0-159.5	1107.1-1102.6	clay & diamicton	2.266
VTH2014-07	159.5-164.0	1102.6-1098.1	diamicton	1.995
VTH2014-07	164.0-168.5	1198.1-1093.6	diamicton	1.995
VTH2014-07	177.5-182.0	1084.6-1080.1	diamicton	2.377
VTH2014-08	13.3-15.5	1251.3-1249.1	silt	1.902
VTH2014-08	15.5-18.5	1249.1-1246.1	till	2.339
VTH2014-08	18.5-22.3	1246.1-1242.3	sand with pebbles & granules	2.194
VTH2014-08	78.5-83.0	1186.1-1181.6	fine sand	1.924
VTH2014-08	121.3-125.7	1143.3-1138.9	cobbles & boulders interlayered with pebbly sand	1.805
VTH2014-08	186.5-191.0	1078.1-1073.6	clay	2.108
VTH2014-08	188.45-188.65	1076.1-1075.9	clay	2.222
VTH2014-08	191.0-195.5	1073.6-1069.1	clay & silt with coal	2.135
VTH2014-08	193.6-193.7	1071.0-1070.9	silt	2.133
VTH2014-08	195.5-200.0	1069.1-1064.6	silt with coal	1.723
VTH2014-08	197.2-197.3	1067.4-1067.3	coal	2.254
VTH2014-08	198.6-198.9	1066.0-1065.7	silt	2.137
VTH2014-08	200.0-201.5	1064.6-1063.1	silt with coal	1.617
VTH2014-08	204.5-209.0	1060.1-1055.6	altered rock & clay	2.275
VTH2014-08	206.5-206.7	1058.1-1057.9	clay	2.375
VTH2014-08	207.0-207.1	1057.6-1057.5	clay	2.282
VTH2014-08	207.8-207.9	1056.8-1056.7	altered rock	2.304
VTH2014-08	209.0-213.5	1055.6-1051.1	altered rock, clay & silt	2.075

VTH2014-08	210.25-210.3	1054.3	silt	2.080
VTH2014-08	212.9	1051.7	clay	2.504
VTH2014-08	213.5-218.0	1051.1-1046.6	interbedded silt, clay & coal	1.973
VTH2014-08	214.2-214.3	1050.4-1050.3	clay & silt	2.422
VTH2014-08	214.3-214.5	1050.3-1050.1	silt & altered rock	2.161
VTH2014-08	215.9-216.0	1048.7-1048.6	clay	2.078
VTH2014-08	216.3-216.4	1048.3-1048.2	clay	2.269
VTH2014-08	217.4-217.6	1047.2-1047.0	clay	2.322
VTH2014-08	222.5-222.9	1042.1-1041.7	solid rock	2.524
VTH2014-08	222.5-226.5	1042.1-1038.1	solid rock, highly altered rock, clay & silt	2.230
VTH2014-08	222.9-223.05	1041.7-1041.5	solid rock	2.368
VTH2014-08	223.0-223.1	1041.6-1041.5	highly altered rock	2.637
VTH2014-08	226.5-230.7	1038.1-1033.9	diamicton & clay	1.730
VTH2014-08	229.1-229.2	1035.5-1035.4	diamicton	2.056
VTH2014-08	229.4-229.5	1035.2-1035.1	diamicton	2.229
VTH2014-08	230.7-230.8	1033.9-1033.8	clay	2.188
VTH2014-08	230.7-234.8	1033.9-1029.8	clay, silt & diamicton	1.799
VTH2014-08	232.5	1032.1	silt	2.184
VTH2014-08	233.5-233.6	1031.1-1031.0	diamicton	2.196
VTH2014-08	235.1-235.2	1029.5-1029.4	clay	1.939
VTH2014-08	235.7-235.8	1028.9-1028.8	diamicton	2.003
VTH2014-08	238.9-241.5	1025.7-1023.1	clay	1.504

VTH2014-09	33.9-36.5	1224.4-1221.8	till & pebbles & cobbles	2.166
VTH2014-09	45.9-49.4	1212.4-1208.9	till & pebbles, cobbles & boulders	2.565
VTH2014-09	49.4-52.4	1208.9-1205.9	till & pebbles & cobbles	2.395
VTH2014-09	52.4-55.25	1205.9-1203.1	till & pebbles & cobbles	2.598
VTH2014-09	55.2-57.5	1203.1-1200.8	till & pebbles & cobbles	2.446
VTH2014-09	57.5-60.1	1200.8-1198.1	till & pebbles & cobbles	2.284
VTH2014-09	60.1-62.6	1198.2-1195.7	till & pebbles & cobbles	2.299
VTH2014-09	62.6-65.3	1195.1-1193.0	till & pebbles & cobbles	2.046
VTH2014-09	65.3-70.0	1193.0-1188.3	till & pebbles & cobbles	3.412
VTH2014-09	97.8-108.2	1160.5-1150.1	sand with cobbles, pebbles & granules	1.414
VTH2014-09	108.2-114.5	1150.1-1143.8	sand with cobbles, pebbles & granules	1.371
VTH2014-09	185.0-189.5	1073.3-1068.8	disintegrated sand-, granule- & pebble-sized rock with interlayers of silt & clay	2.451
VTH2014-09	191.3-191.5	1067.0-1066.8	silt	2.110
VTH2014-09	207.0-207.2	1051.3-1051.1	fine sand	1.991
VTH2014-09	212.0-216.5	1046.3-1041.8	coal, clay, & minor fine sand	1.853
VTH2014-10	24.3-27.3	1235.1-1232.1	till	2.500
VTH2014-10	27.3-29.9	1232.1-1229.5	till	1.920
VTH2014-10	29.9-32.9	1229.5-1226.5	till	2.304
VTH2014-10	55.0-55.3	1204.4-1204.1	boulder	3.666
VTH2014-10	59.9-62.9	1199.5-1196.5	till	2.128
VTH2014-10	62.9-65.6	1196.5-1193.8	till	2.321

VTH2014-10	63.8-64.0	1195.6-1195.4	till	2.811
VTH2014-10	65.8-68.8	1193.6-1190.6	till	2.659
VTH2014-10	68.8-71.8	1190.6-1187.6	till	2.546
VTH2014-10	69.0-69.5	1190.4-1189.9	till	2.090
VTH2014-10	71.4-74.2	1188.0-1185.2	till & sand with granules	2.522
VTH2014-10	71.4-74.2	1188.0-1185.2	till & sand with granules	2.758
VTH2014-10	74.8-77.8	1184.6-1181.6	till, clay & cobbles & boulders	2.033
VTH2014-10	75.1-75.2	1184.3-1184.2	clay	1.796
VTH2014-10	77.8-84.3	1181.6-1175.1	diamicton & pebbles, cobbles & boulders	2.397
VTH2014-10	82.7-82.86	1176.7-1176.54	boulder	1.080
VTH2014-10	84.3-90.1	1175.1-1169.3	diamicton & pebbles & cobbles	2.464
VTH2014-10	89.8-89.95	1169.6-1169.45	diamicton	1.718
VTH2014-10	114.6-118.3	1144.8-1141.1	diamicton	3.731
VTH2014-10	118.3-122.3	1141.1-1137.1	diamicton & pebbles & cobbles	3.955
VTH2014-10	130.5-135.0	1128.9-1124.4	diamicton & fine sand & silt	2.172
VTH2014-10	135.0-139.5	1124.4-1119.9	fine sand & silt	2.183
VTH2014-10	143.2	1116.2	fine sand	2.122
VTH2014-10	145.1	1114.3	clay	1.794
VTH2014-10	147.3	1112.1	clay	1.561
VTH2014-10	148.5-153.0	1110.9-1106.4	clay	1.901
VTH2014-10	149.25	1110.15	clay	2.007
VTH2014-10	150.3	1109.1	clay	1.841

VTH2014-10	151.9	1107.5	clay	1.967
VTH2014-10	152.6	1106.8	clay	1.683
VTH2014-10	154.1	1105.3	clay	1.702
VTH2014-10	154.9	1104.5	clay	1.843
VTH2014-10	155.45	1103.95	fine sand	1.835
VTH2014-10	156.2	1103.2	fine sand	1.774
VTH2014-10	156.4-156.5	1103.0-1102.9	fine sand	2.130
VTH2014-10	157.6	1101.8	fine sand	1.747
VTH2014-10	162.4-162.55	1097.0-1096.85	clay	2.112
VTH2014-10	171.0-175.5	1088.4-1083.9	diamicton	2.439
VTH2014-10	172.2-172.3	1087.2-1087.1	diamicton	1.971
VTH2014-10	175.5-180.0	1083.9-1079.4	diamicton	2.508
VTH2014-10	180.0-184.5	1079.4-1074.9	sand with cobbles, pebbles & granules	2.457
VTH2014-10	186.9-187.2	1072.5-1072.2	boulder	3.505
VTH2014-10	187.25-187.4	1072.15-1072.0	sand with cobbles, pebbles & granules	2.678
VTH2014-10	191.75-191.9	1067.65-1067.5	fine sand with granules	2.347
VTH2014-10	192.9-193.1	1066.5-1066.3	fine sand with granules	2.571
VTH2014-10	193.5-198.0	1065.9-1061.4	sand with cobbles, pebbles & granules & diamicton	2.377
VTH2014-10	193.7-193.9	1065.7-1065.5	fine sand with granules	1.988
VTH2014-10	195.8-195.9	1063.6-1063.5	diamicton	2.082
VTH2014-10	197.1-197.4	1062.3-1062.0	fine sand with granules	2.053

VTH2014-10	197.75-197.9	1061.65-1061.5	diamicton	2.108
VTH2014-10	198.0-202.5	1061.4-1056.9	fine sand with pebbles & granules & diamicton	2.242
VTH2014-10	198.7-198.8	1060.7-1060.6	fine sand with pebbles & granules	1.948
VTH2014-10	202.5-207.0	1056.9-1052.4	sand with granules & diamicton	2.391
VTH2014-10	207.0-211.4	1052.4-1048.0	sand with cobbles, pebbles & granules	2.476
VTH2014-10	211.4-211.6	1048.0-1047.8	sand with granules	2.109
VTH2014-10	211.4-211.6	1048.0-1047.8	sand with granules	2.257
VTH2014-10	211.4-211.7	1048.0-1047.8	sand with granules	2.109
VTH2014-10	211.4-215.8	1048.0-1043.6	sand with granules	2.320
VTH2014-10	211.75-211.9	1047.65-1047.5	sand with granules	2.229
VTH2014-10	213.2-213.35	1046.2-1046.05	sand with granules	2.467
VTH2014-10	214.05-214.2	1045.35-1045.2	sand with granules	2.203
VTH2014-10	214.1-214.25	1045.3-1045.15	sand with granules	2.289
VTH2014-10	214.6-214.8	1044.8-1044.6	sand with granules	2.237
VTH2014-10	214.7-214.9	1044.7-1044.5	sand with granules	2.251
VTH2014-11	51.1-51.5	1216.8-1216.4	boulder	2.637
VTH2014-11	51.5-54.3	1216.4-1213.6	till	1.981
VTH2014-11	52.5-52.6	1215.4-1215.3	till	2.331
VTH2014-11	53.7-53.9	1214.2-1214.0	till	2.105
VTH2014-11	54.3-56.9	1213.6-1211.0	till	1.935
VTH2014-11	56.9-59.8	1211.0-1208.1	till	1.999

VTH2014-11	57.5-57.7	1210.4-1210.2	till	1.369
VTH2014-11	59.3-59.5	1208.6-1208.4	till	1.416
VTH2014-11	59.8-62.5	1208.1-1205.4	till	1.967
VTH2014-11	60.4-60.7	1207.5-1207.2	till	1.995
VTH2014-11	60.7-60.8	1207.2-1207.1	till	2.165
VTH2014-11	61.6-61.9	1206.3-1206.0	till	1.350
VTH2014-11	61.9-62.3	1206.0-1205.6	till	2.056
VTH2014-11	62.5-65.7	1205.4-1202.2	till	2.063
VTH2014-11	63.3-63.5	1204.6-1204.4	till	1.842
VTH2014-11	80.0-84.5	1187.9-1183.4	sand with cobbles, pebbles & granules	2.377
VTH2014-11	84.2-84.5	1183.7-1183.4	boulder	1.873
VTH2014-11	84.5-89.0	1183.4-1178.9	sand with cobbles, pebbles & granules	2.111
VTH2014-11	89.0-95.0	1178.9-1172.9	sand with cobbles, pebbles & granules	2.060
VTH2014-11	113.0-117.5	1154.9-1150.4	diamicton	1.588
VTH2014-11	143.0-147.5	1124.9-1120.4	diamicton	2.081
VTH2014-11	147.5-151.7	1120.4-1116.2	diamicton	2.358
VTH2014-11	151.7-156.5	1116.2-1111.4	diamicton	2.525
VTH2014-11	156.5-161.0	1111.4-1106.9	diamicton & clay	2.377
VTH2014-11	160.0-160.2	1107.9-1107.7	diamicton	2.290
VTH2014-11	160.3-160.4	1107.6-1107.5	clay	2.058
VTH2014-11	160.4-160.5	1107.5-1107.4	clay	1.977
VTH2014-11	163.5-163.6	1104.4-1104.3	clay & diamicton	1.962

VTH2014-11	165.0-165.1	1102.9-1102.8	diamicton	2.298
VTH2014-11	165.5-170.0	1102.4-1097.9	diamicton, clay & coal	1.979
VTH2014-11	166.7-166.8	1101.2-1101.1	clay	2.199
VTH2014-11	167.9-168.0	1100.0-1099.9	clay	2.509
VTH2014-11	168.1-168.2	1099.8-1099.7	clay	2.303
VTH2014-11	170.0-174.5	1097.9-1093.4	clay, diamicton & coal	2.085
VTH2014-11	170.2-170.4	1097.7-1097.5	clay	1.906
VTH2014-11	170.4-170.6	1097.5-1097.3	clay	2.045
VTH2014-11	171.0-171.1	1096.9-1096.8	coal	1.420
VTH2014-11	173.2-173.4	1094.7-1094.5	diamicton	2.207
VTH2014-11	174.5-179.0	1093.4-1088.9	clay & diamicton	2.542
VTH2014-11	179.0-183.5	1088.9-1084.4	clay, diamicton, silt & coal	2.178
VTH2014-11	179.2	1088.7	clay & silt	2.047
VTH2014-11	180.6-180.7	1087.3-1087.2	clay	1.875
VTH2014-11	181.2-181.3	1086.7-1086.6	clay	2.068
VTH2014-11	181.9-182.0	1086.0-1085.9	coal	2.296
VTH2014-11	183.5-188.0	1084.4-1079.9	diamicton, clay & coal	2.020
VTH2014-11	186.7-186.8	1081.2-1081.1	clay	2.387
VTH2014-11	186.8-186.9	1081.1-1081.0	diamicton	2.226
VTH2014-11	188.0-192.5	1079.9-1075.4	clay & diamicton	2.199
VTH2014-11	188.5	1079.4	clay	2.128
VTH2014-11	191.5-191.6	1076.4-1076.3	diamicton	2.182

VTH2014-11	192.2-192.4	1075.7-1075.5	diamicton	2.138
VTH2014-11	192.5-197.0	1075.4-1070.9	clay & diamicton	1.989
VTH2014-11	193.7-193.8	1074.2-1074.1	diamicton	1.905
VTH2014-11	197.0-201.5	1070.9-1066.4	clay, diamicton, silt & coal	2.302
VTH2014-11	201.5-205.25	1066.4-1062.7	interlayered diamicton, clay & silt	1.864
VTH2014-11	203.8-203.9	1064.1-1064.0	silt	2.322
VTH2014-11	204.4-204.5	1063.5-1063.4	clay	2.025
VTH2014-11	205.5-209.0	1062.4-1058.9	interlayered diamicton, clay & silt	1.789
VTH2014-11	209.0-213.5	1058.9-1054.4	diamicton	2.179
VTH2014-11	213.5-218.0	1054.4-1049.9	interlayered, silt, clay, diamictite & coal	1.464
VTH2014-11	215.7-215.9	1052.2-1052.0	diamicton	1.895
VTH2014-11	218.0-222.5	1049.9-1045.4	clay	1.846
VTH2014-11	222.5-224.0	1045.4-1043.9	clay	1.311
VTH2014-13A	36.4-36.5	1209.0-1208.9	till	2.472
VTH2014-13A	37.5-37.7	1207.9-1207.7	till	1.900
VTH2014-13A	38.9-39.0	1206.5-1206.4	till	2.495
VTH2014-13A	41.5-44.0	1203.9-1201.4	till	2.129
VTH2014-13A	44.0-48.9	1201.4-1196.5	till, cobbles & pebbles	2.201
VTH2014-13A	46.8-47.0	1198.6-1198.4	cobble	2.179
VTH2014-13A	48.9-54.0	1196.5-1191.4	till, cobbles & pebbles	2.128
VTH2014-13A	75.5-81.8	1169.9-1163.6	diamicton, granules to cobbles and sand with cobbles, pebbles	2.069

			& granules	
VTH2014-13A	91.6-94.6	1153.8-1150.8	diamicton	2.364
VTH2014-13A	99.4-99.5	1146.0-1145.9	cobble	2.724
VTH2014-13A	104.4-104.5	1141.0-1140.9	diamicton	2.707
VTH2014-13A	104.6-108.5	1140.8-1136.9	diamicton	2.290
VTH2014-13A	110.8-111.0	1134.6-1134.4	boulder	2.788
VTH2014-13A	115.2	1130.2	clay	2.034
VTH2014-13A	116.7-116.8	1128.7-1128.6	clay	1.923
JA16-001	5.5-8.5	1204.2-1201.2	sand with granules	1.561
JA16-001	19.0-23.6	1168.2-1165.7	till, pebbles & cobbles	2.129
JA16-001	25.4-25.7	1184.3-1184.0	till	1.564
JA16-001	27.7-30.2	1182.0-1179.5	till and pebbles and cobbles	2.096
JA16-001	29.4-29.6	1180.3-1180.1	till	1.388
JA16-001	30.2-33.2	1179.5-1176.5	till and pebbles and cobbles	1.935
JA16-001	30.6	1179.1	till	2.115
JA16-001	31.6-31.9	1178.1-1177.8	till	1.861
JA16-001	33.2-36.4	1176.5-1173.3	till and pebbles, cobbles and boulder	2.237
JA16-001	35.0-35.3	1174.7-1174.4	boulder	2.304
JA16-001	36.4-39.4	1173.3-1170.3	till	2.109
JA16-001	37.9-38.4	1171.8-1171.3	till	1.873
JA16-001	39.4-43.3	1170.3-1166.4	till & silt	2.155
JA16-001	40.5-40.8	1169.2-1168.9	till	1.354

JA16-001	43.3-47.4	1166.4-1162.3	interlayered silt & till	1.761
JA16-001	47.4-51.6	1162.3-1158.1	silt & fine sand	1.577
JA16-001	51.6-56.3	1158.1-1153.4	silt & fine sand	1.646
JA16-001	64.0-66.9	1145.7-1142.8	silt	1.684
JA16-001	64.5-64.6	1145.2-1145.1	silt	1.564
JA16-001	69.5-72.3	1140.2-1137.4	silt	1.754
JA16-001	70.1-70.3	1139.6-1139.4	silt	1.731
JA16-001	72.3-74.5	1137.4-1135.2	silt	1.878
JA16-001	112.9-118.9	1096.8-1090.8	sand with cobbles, pebbles & granules & diamicton & clay	2.207
JA16-001	118.0-118.1	1091.7-1091.6	clay	2.057
JA16-001	118.9-122.5	1090.8-1087.2	clay	1.909
JA16-001	119.6-119.7	1090.1-1090.0	clay	2.310
JA16-001	121.7-122.0	1088.0-1087.7	clay	1.746
JA16-001	122.5-127	1087.2-1082.7	clay	1.828
JA16-001	124.3-124.5	1085.4-1085.2	clay	1.774
JA16-001	126.5	1083.2	clay	1.835
JA16-001	127-131.5	1082.7-1078.2	clay	1.705
JA16-001	128.8	1080.9	clay	1.649
JA16-001	134.5-134.6	1075.2-1075.1	diamicton	1.945
JA16-001	141.4-141.5	1068.3-1068.2	diamicton	2.137
JA16-001	160.1-160.2	1049.6-1049.5	clay	1.768
DH-15-GG	54.0-54.2	1154.3-1154.1	sand w granules to cobbles	1.368

DH-15-GG	54.6-57.6	1153.7-1150.7	sand w granules to cobbles	2.445
DH-15-GG	57.1-57.3	1151.2-1151.0	sand w granules to cobbles	1.320
DH-15-GG	57.6-60.6	1150.7-1147.7	sand w granules to cobbles	2.372
DH-15-GG	57.95	1150.3	sand w granules to cobbles	1.888
DH-15-GG	57.95-58.1	1150.3-1150.2	sand w granules to cobbles	1.506
DH-15-GG	60.4-60.5	1147.9-1147.8	sand w granules to cobbles	2.249
DH-15-GG	60.6-63.6	1147.7-1144.7	boulder & sand w granule to cobbles	2.149
DH-15-GG	63.6-66.6	1144.7-1141.7	diamicton & boulder & sand w granules & clay	1.197
DH-15-GG	66.6-69.6	1141.7-1138.7	clay	1.569
DH-15-GG	69.6-72.6	1138.7-1135.7	clay	1.594
DH-15-GG	72.6-75.6	1135.7-1132.7	diamicton & conglomerate	1.777
DH-15-GG	74.7-75.6	1133.6-1132.7	conglomerate	1.873
DH-15-GG	75.6-78.6	1132.7-1129.7	conglomerate	2.048
DH-15-GG	79.1-79.2	1129.2-1129.1	conglomerate	2.063
DH-15-GG	79.2-79.7	1129.1-1128.6	conglomerate	1.899
DH-15-GG	82.1-82.5	1126.2-1125.8	conglomerate	1.879
DH-15-GG	82.5-82.7	1125.8-1125.6	conglomerate	1.909
DH-15-GG	83.8-83.9	1124.5-1124.4	conglomerate	2.094
DH-15-GG	85.2-85.3	1123.1-1123.0	conglomerate	1.800
DH-15-GG	85.6-86.1	1122.7-1122.2	conglomerate	1.714
DH-15-GG	86.7-87.3	1121.6-1121.0	conglomerate	1.585
DH-15-GG	89.6-90.6	1118.7-1117.7	conglomerate	1.691

DH-15-GG	93.5-93.6	1114.8-1114.7	conglomerate	1.907
DH-15-GG	95.5-95.9	1112.8-1112.4	conglomerate	1.868
DH-15-GG	98.1-99.2	1110.2-1109.1	conglomerate	2.037
DH-15-GG	99.6-102.6	1108.7-1105.7	conglomerate	1.926
DH-15-GG	102.6-103.1	1105.7-1105.2	conglomerate	1.842
DH-15-GG	107.1-108	1101.2-1100.3	conglomerate	1.860
DH-15-GG	108.5-108.6	1099.8-1099.7	conglomerate	1.913
DH-15-GG	109.1-109.2	1099.2-1099.1	conglomerate	1.820
DH-15-GG	111.7-111.8	1096.6-1096.5	conglomerate	1.951
DH-15-GG	115.8-115.9	1092.5-1092.4	conglomerate	2.249
DH-15-GG	117.6-118.1	1090.7-1090.2	conglomerate	2.302
DH-15-GG	120.5-120.8	1087.8-1087.5	conglomerate	1.562
DH-15-GG	125.6-125.8	1082.7-1082.5	conglomerate & coal	1.464
DH-15-GG	126.45-126.5	1081.8	diamicton	2.566
DH-15-GG	126.5-126.7	1081.8-1081.6	boulder	1.988

Table B.2 Location, average unconsolidated sediment cover density and depth of cover for each core.

Core	**UTM X**	**UTM Y**	**Average Unconsolidated Sediment Cover Density (g/cm^3)**	**Range of Densities in Sediment Cover (g/cm^3)**	**Thickness of Cover (m)**
VTH2014-03	639977	5594320	1.785	1.395-2.179	124.2
VTH2014-06	639464	5593540	2.491	1.404-3.666	194.0
VTH2014-07	639961	5593640	2.164	1.588-2.803	172.9

VTH2014-08	639410	5593580	2.132	1.504-3.666	241.5
VTH2014-09	639592	5593660	2.321	1.371-3.666	234.5
VTH2014-10	639720	5593610	2.601	1.080-3.955	217.5
VTH2014-11	639543	5593500	2.064	1.311-2.637	224.0
VTH2014-13A	640005	5593910	2.217	1.775-2.788	118.3
JA16-001	643566	5593575	1.929	1.354-2.310	188.5
DH-15-GG	628325	5601980	1.794	1.197-2.566	126.6

Petrophysical properties were measured for samples from a variety of different units from all of the cores drilled over the major mineralized zones (**Figure B.1**). Grain density values have been determined for thirty of these samples. The grain density of the silt and/or clay sub-units decreases with depth (**Figure B.2**).

Twenty five samples had their porosity determined. The porosity is calculated by determining the difference between the weights of the dry and wet saturated sample (which is the weight of all the water that could be held in the pores of each sample), dividing this by the density of water, and then dividing the result by the bulk volume was taken as the final porosity for each sample where this method was successfully used. The porosity of the silt and/or clay sub-units generally decreases with depth (**Figure B.3**).

Magnetic susceptibility, resistivity and chargeability values have been determined for 32 intact core samples belonging to different sedimentary units from all the cores drilled over the major mineralized zones. The magnetic susceptibility of the silt and/or clay sub-units decreases with depth (**Figure B.4**). The resistivity of one of the non-glacial diamicton sub-units was much higher than for all the other samples from all the different sub-units, by at least an order of magnitude (**Figure B.5**). The till and non-glacial diamicton sub-units generally have a higher chargeability than the other units (**Figure B.6**).

(a)

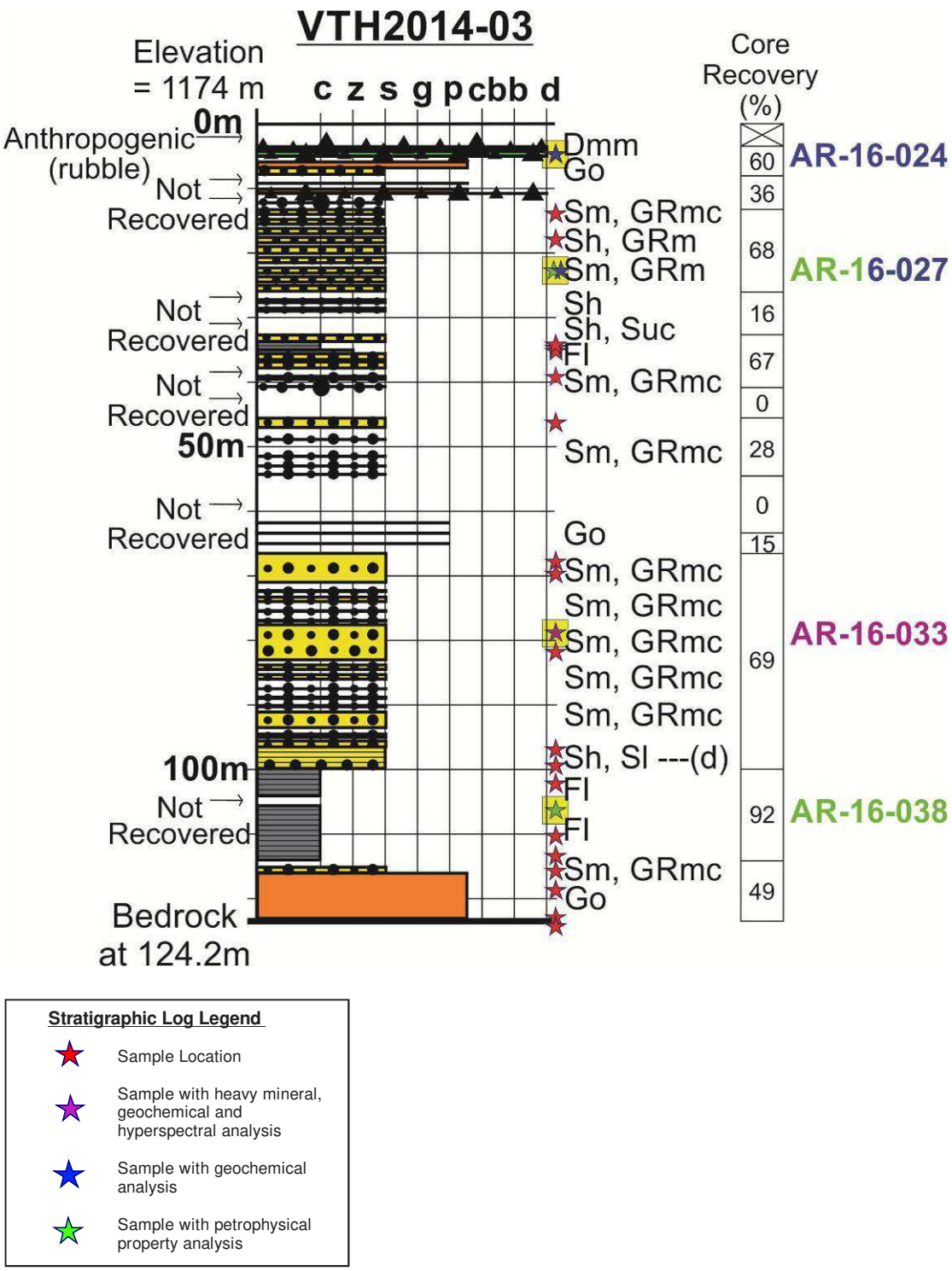

Stratigraphic Log Legend

- Sample Location
- Sample with heavy mineral, geochemical and hyperspectral analysis
- Sample with geochemical analysis
- Sample with petrophysical property analysis

(b)

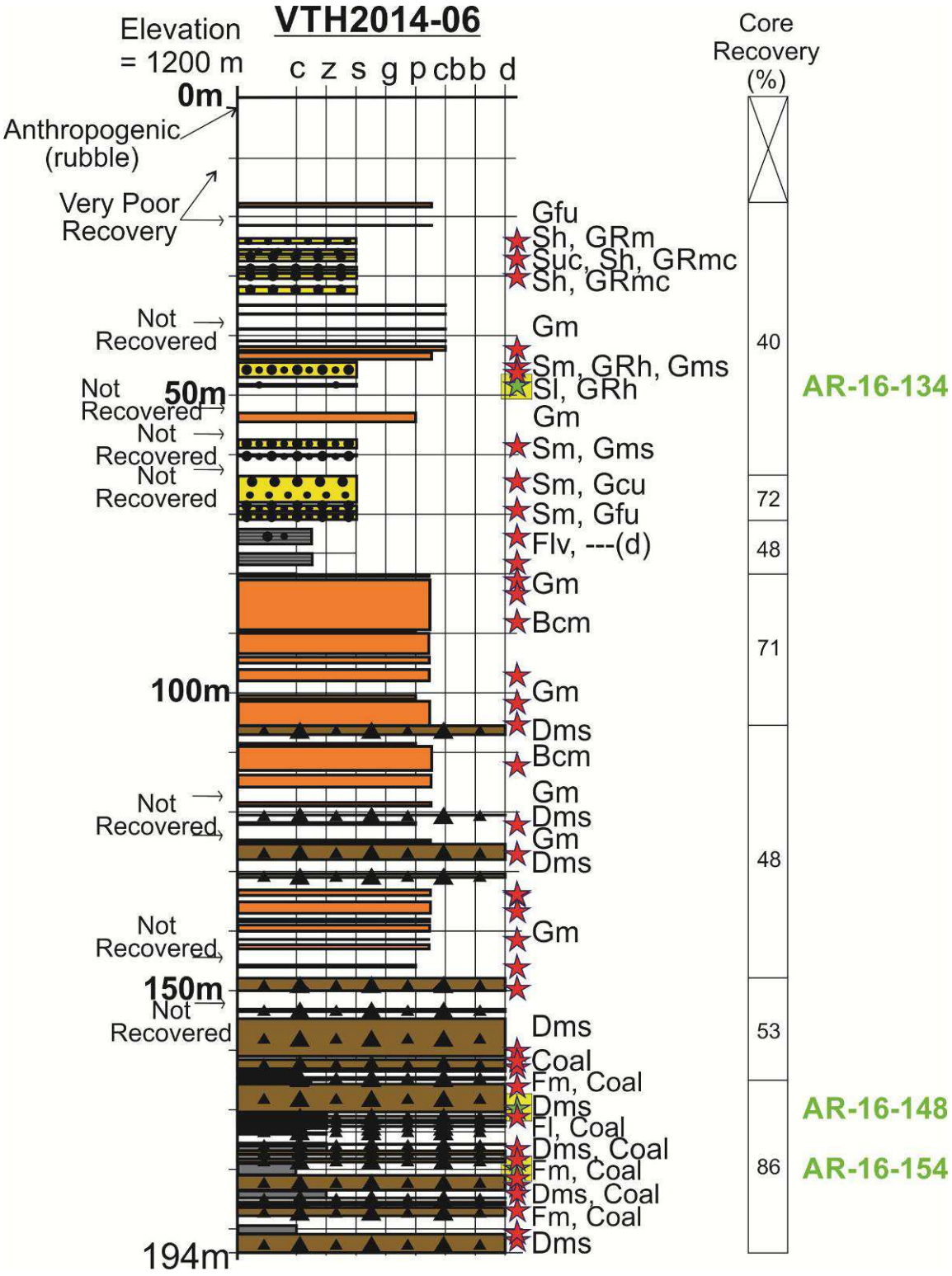
VTH2014-06
Elevation
= 1200 m
c z s g p cb b d
Core
Recovery
(%)
0m
Anthropogenic
(rubble)
Very Poor
Recovery
Not
Recovered
50m
100m
150m
194m
Gfu
Sh, GRm
Suc, Sh, GRmc
Sh, GRmc
Gm
Sm, GRh, Gms
Sl, GRh
Gm
Sm, Gms
Sm, Gcu
Sm, Gfu
Flv, ---(d)
Gm
Bcm
Gm
Dms
Bcm
Gm
Dms
Gm
Dms
Gm
Dms
Coal
Fm, Coal
Dms
Fl, Coal
Dms, Coal
Fm, Coal
Dms, Coal
Fm, Coal
Dms
40
72
48
71
48
53
86
AR-16-134
AR-16-148
AR-16-154

(c)

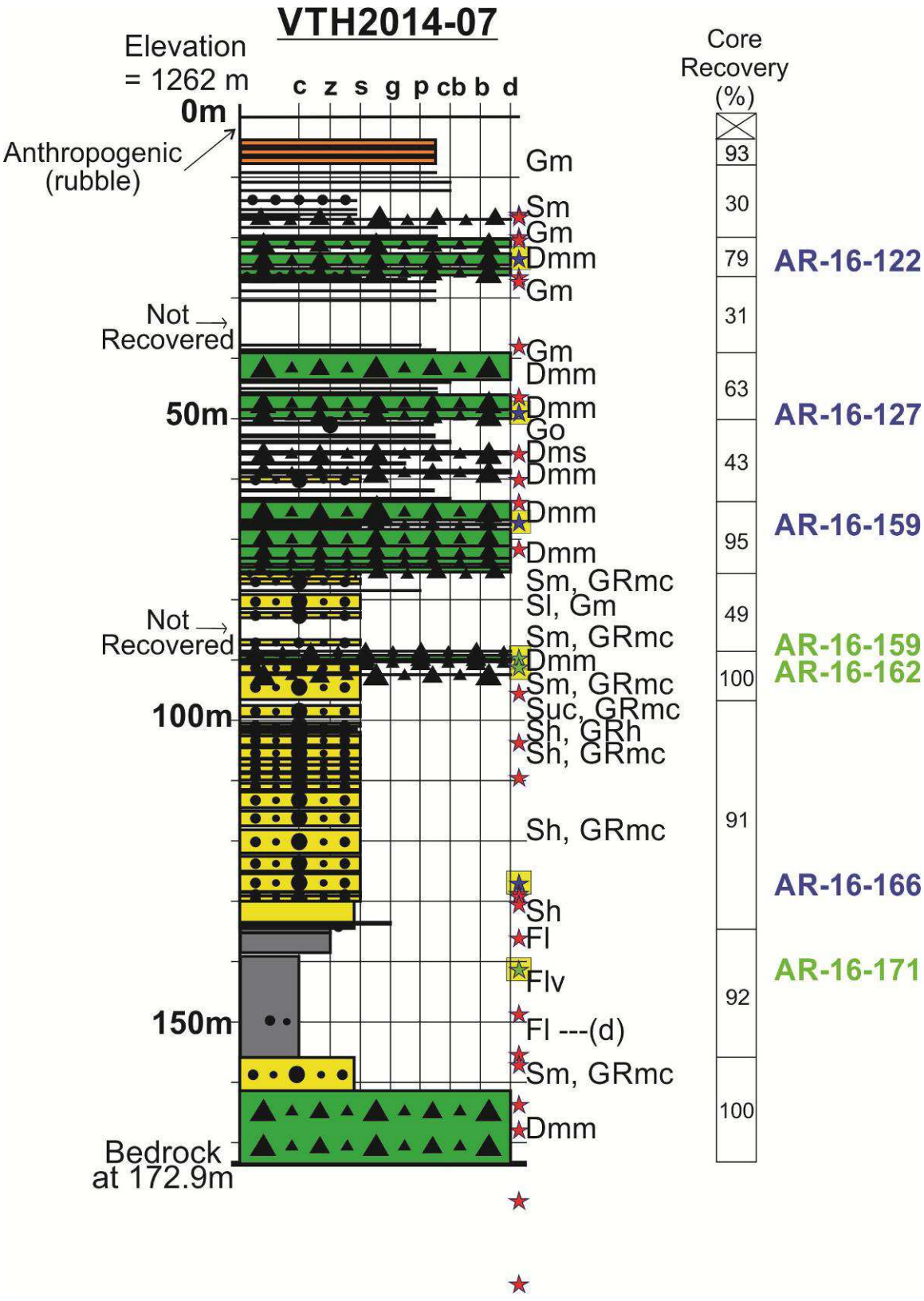
VTH2014-07
Elevation
= 1262 m
c z s g p cb b d
Core
Recovery
(%)
0m
Anthropogenic
(rubble)
Not
Recovered
50m
Not
Recovered
100m
150m
Bedrock
at 172.9m
Gm
Sm
Gm
Dmm
Gm
Gm
Dmm
Dmm
Go
Dms
Dmm
Dmm
Dmm
Sm, GRmc
Sl, Gm
Sm, GRmc
Dmm
Sm, GRmc
Suc, GRmc
Sh, GRh
Sh, GRmc
Sh, GRmc
Sh
Fl
Flv
Fl ---(d)
Sm, GRmc
Dmm
93
30
79
31
63
43
95
49
100
91
92
100
AR-16-122
AR-16-127
AR-16-159
AR-16-159
AR-16-162
AR-16-166
AR-16-171

(d)

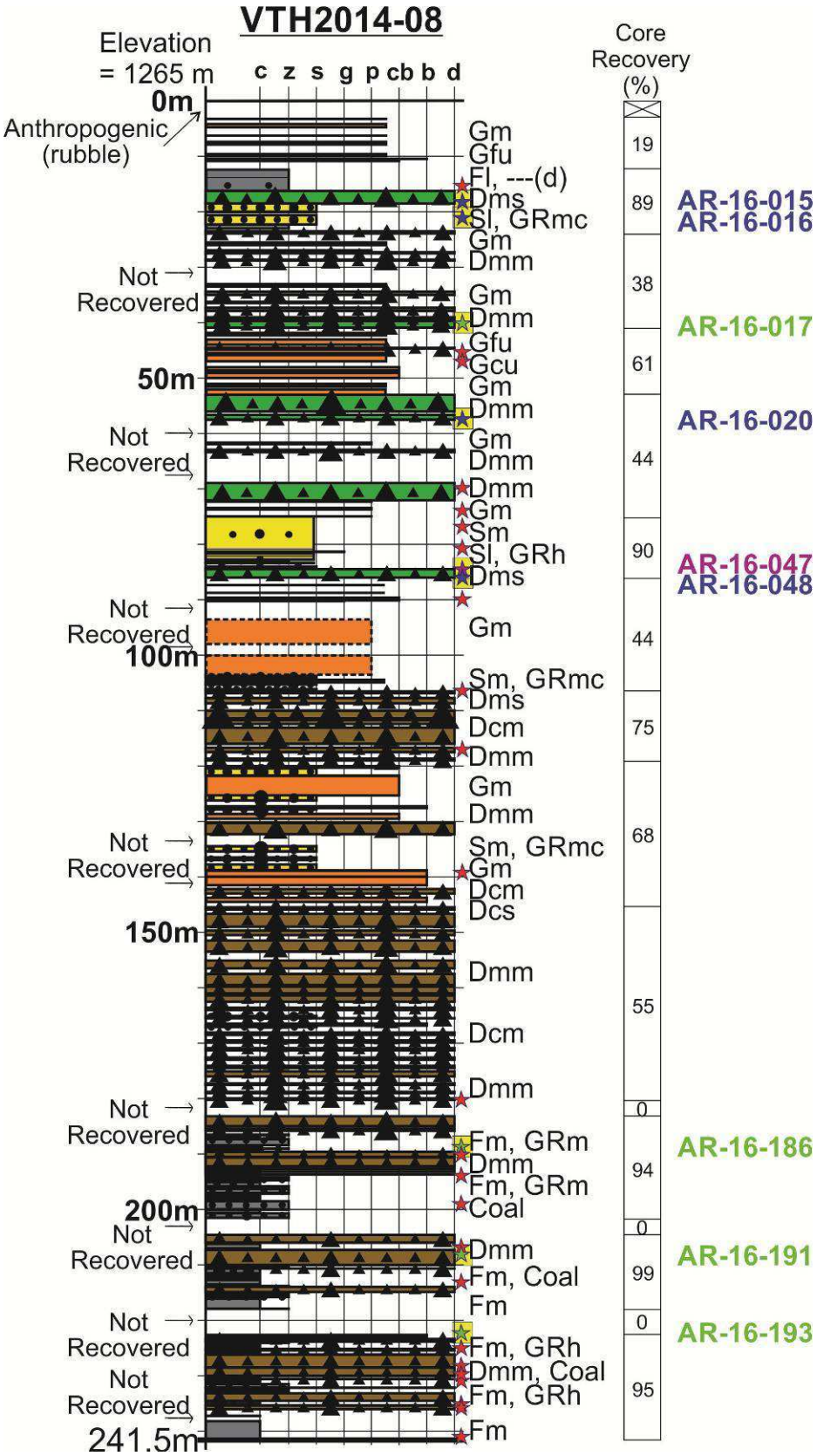
VTH2014-08
Elevation
= 1265 m
c z s g p cb b d
Core
Recovery
(%)
0m
Anthropogenic
(rubble)
Gm
Gfu
Fl, ---(d)
Dms
Sl, GRmc
Gm
Dmm
Not
Recovered
Gm
Dmm
Gfu
Gcu
50m
Gm
Dmm
Not
Recovered
Gm
Dmm
Dmm
Gm
Sm
Sl, GRh
Dms
Not
Recovered
Gm
100m
Sm, GRmc
Dms
Dcm
Dmm
Gm
Dmm
Not
Recovered
Sm, GRmc
Gm
Dcm
Dcs
150m
Dmm
Dcm
Dmm
Not
Recovered
Fm, GRm
Dmm
Fm, GRm
Coal
200m
Not
Recovered
Dmm
Fm, Coal
Fm
Not
Recovered
Fm, GRh
Dmm, Coal
Not
Recovered
Fm, GRh
Fm
241.5m
19
89
38
61
44
90
44
75
68
55
0
94
0
99
0
95
AR-16-015
AR-16-016
AR-16-017
AR-16-020
AR-16-047
AR-16-048
AR-16-186
AR-16-191
AR-16-193

(e)

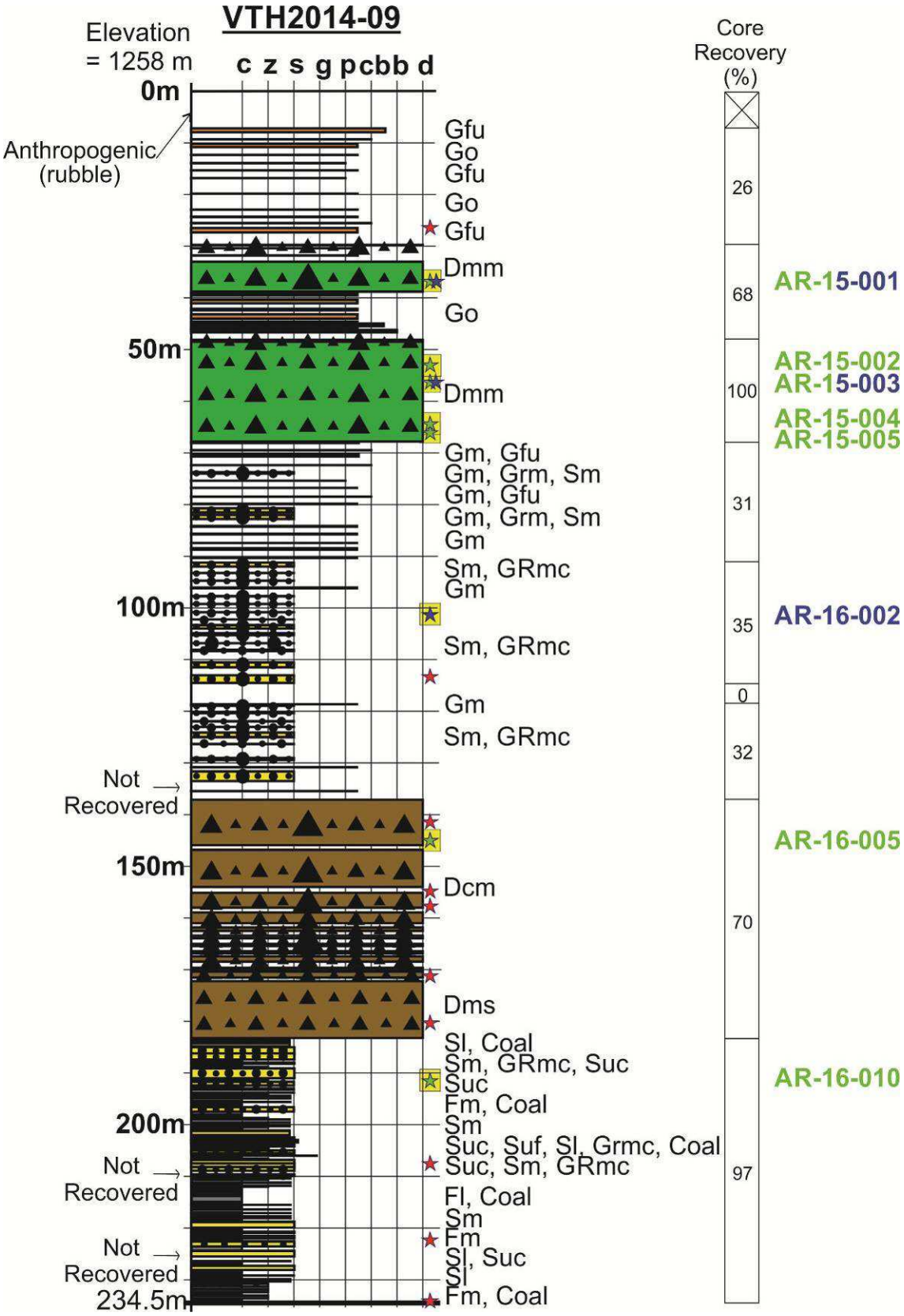
VTH2014-09
Elevation
= 1258 m
c z s g p cbb d
Core
Recovery
(%)
0m
Anthropogenic
(rubble)
Gfu
Go
Gfu
Go
Gfu
Dmm
Go
50m
Dmm
Gm, Gfu
Gm, Grm, Sm
Gm, Gfu
Gm, Grm, Sm
Gm
Sm, GRmc
Gm
100m
Sm, GRmc
Gm
Sm, GRmc
Not
Recovered
150m
Dcm
Dms
Sl, Coal
Sm, GRmc, Suc
Suc
Fm, Coal
Sm
200m
Suc, Suf, Sl, Grmc, Coal
Not
Recovered
Suc, Sm, GRmc
Fl, Coal
Sm
Fm
Not
Recovered
Sl, Suc
Sl
234.5m
Fm, Coal
26
68
100
31
35
0
32
70
97
AR-15-001
AR-15-002
AR-15-003
AR-15-004
AR-15-005
AR-16-002
AR-16-005
AR-16-010

(f)

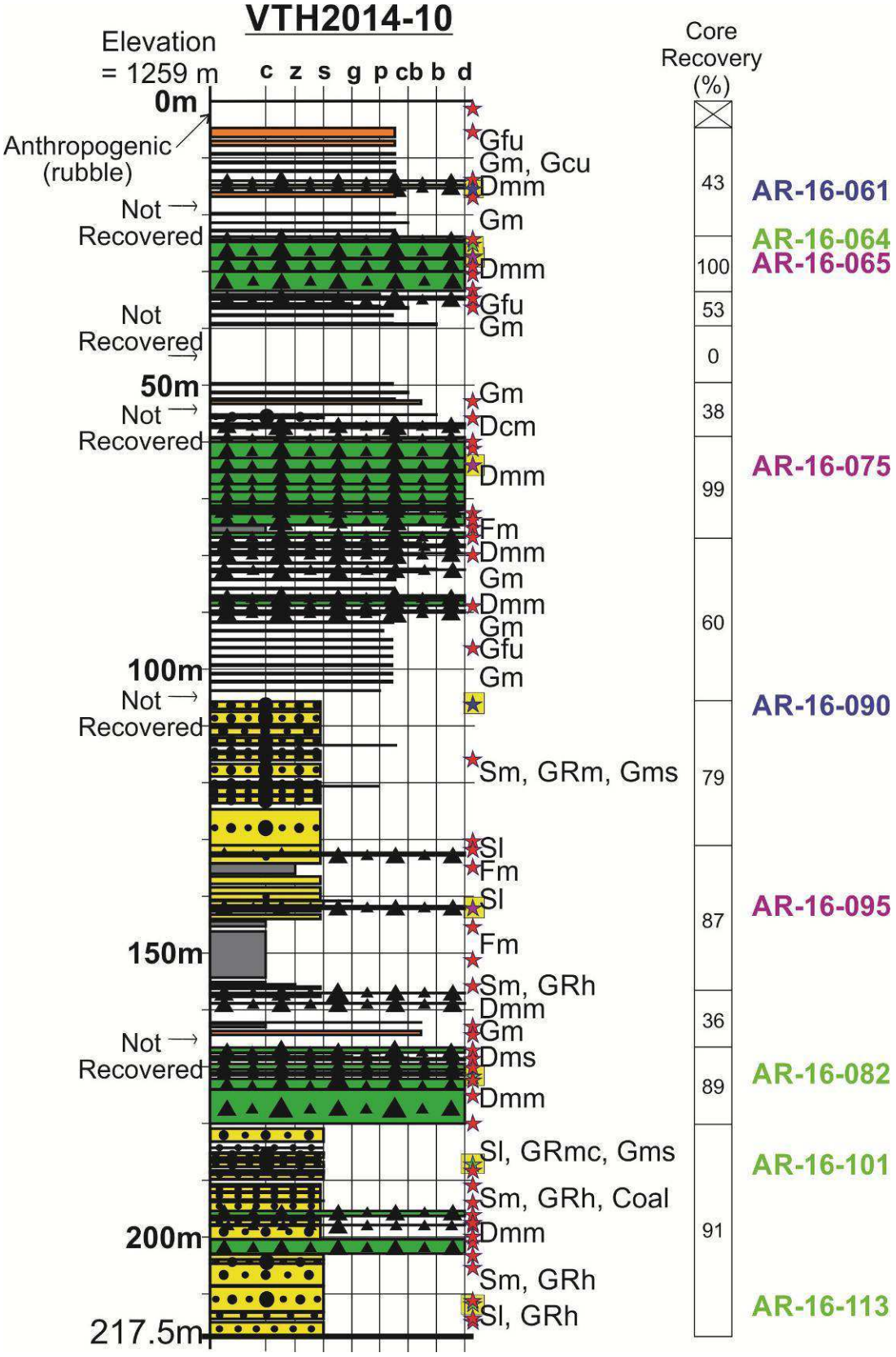
VTH2014-10
Elevation
= 1259 m
c z s g p cb b d
Core
Recovery
(%)
0m
Anthropogenic
(rubble)
Not
Recovered
Gfu
Gm, Gcu
Dmm
Gm
Dmm
Gfu
Gm
50m
Gm
Dcm
Dmm
Fm
Dmm
Gm
Dmm
Gm
Gfu
Gm
100m
Sm, GRm, Gms
Sl
Fm
Sl
Fm
150m
Sm, GRh
Dmm
Gm
Dms
Dmm
Sl, GRmc, Gms
Sm, GRh, Coal
200m
Dmm
Sm, GRh
Sl, GRh
217.5m
43
100
53
0
38
99
60
79
87
36
89
91
AR-16-061
AR-16-064
AR-16-065
AR-16-075
AR-16-090
AR-16-095
AR-16-082
AR-16-101
AR-16-113

(g)

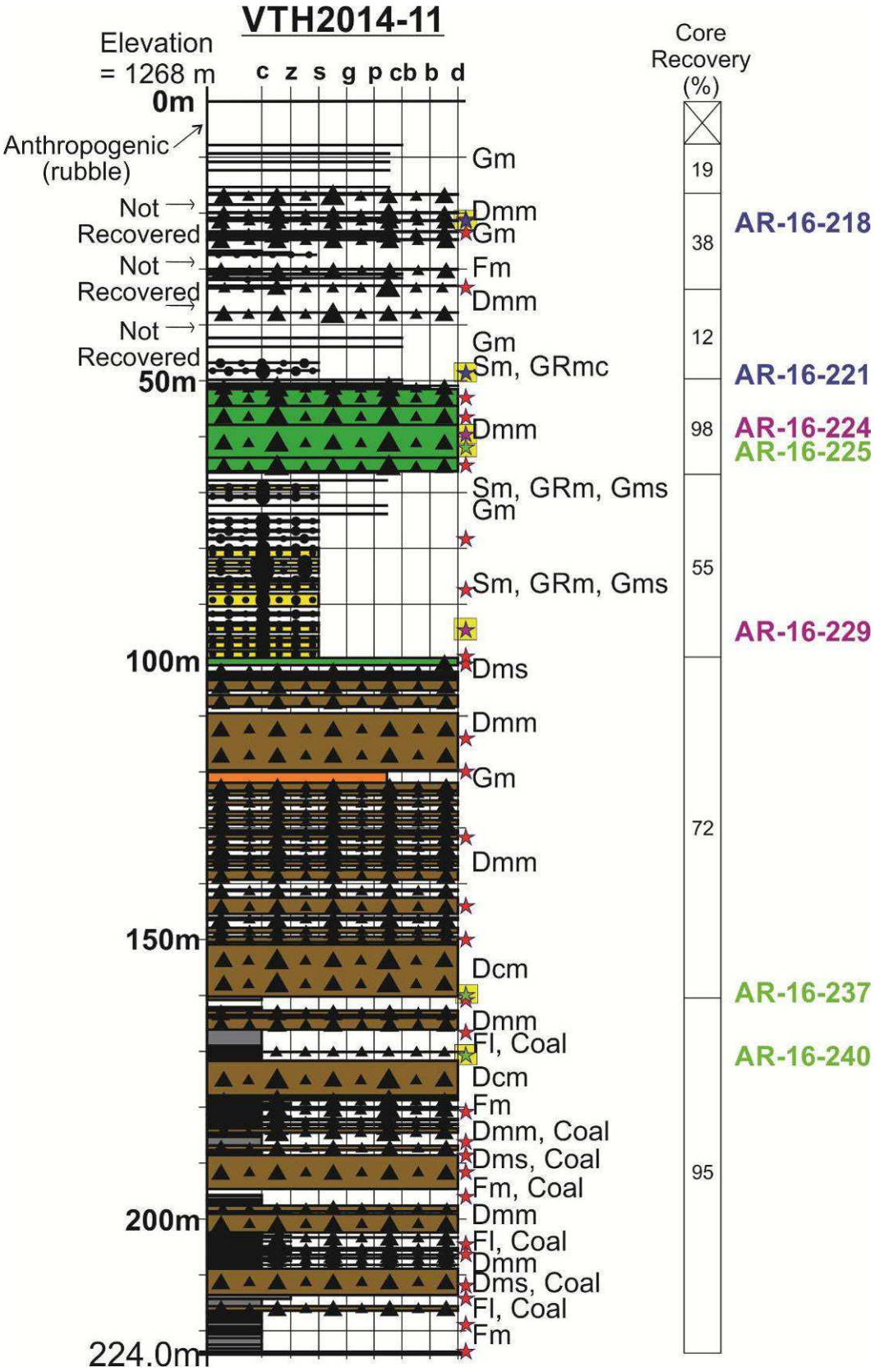
VTH2014-11
Elevation
= 1268 m
c z s g p cb b d
Core
Recovery
(%)
0m
Anthropogenic
(rubble)
Not
Recovered
Not
Recovered
Not
Recovered
50m
100m
150m
200m
224.0m
Gm
Dmm
Gm
Fm
Dmm
Gm
Sm, GRmc
Dmm
Sm, GRm, Gms
Gm
Sm, GRm, Gms
Dms
Dmm
Gm
Dmm
Dcm
Dmm
Fl, Coal
Dcm
Fm
Dmm, Coal
Dms, Coal
Fm, Coal
Dmm
Fl, Coal
Dmm
Dms, Coal
Fl, Coal
Fm
19
38
12
98
55
72
95
AR-16-218
AR-16-221
AR-16-224
AR-16-225
AR-16-229
AR-16-237
AR-16-240

(h)

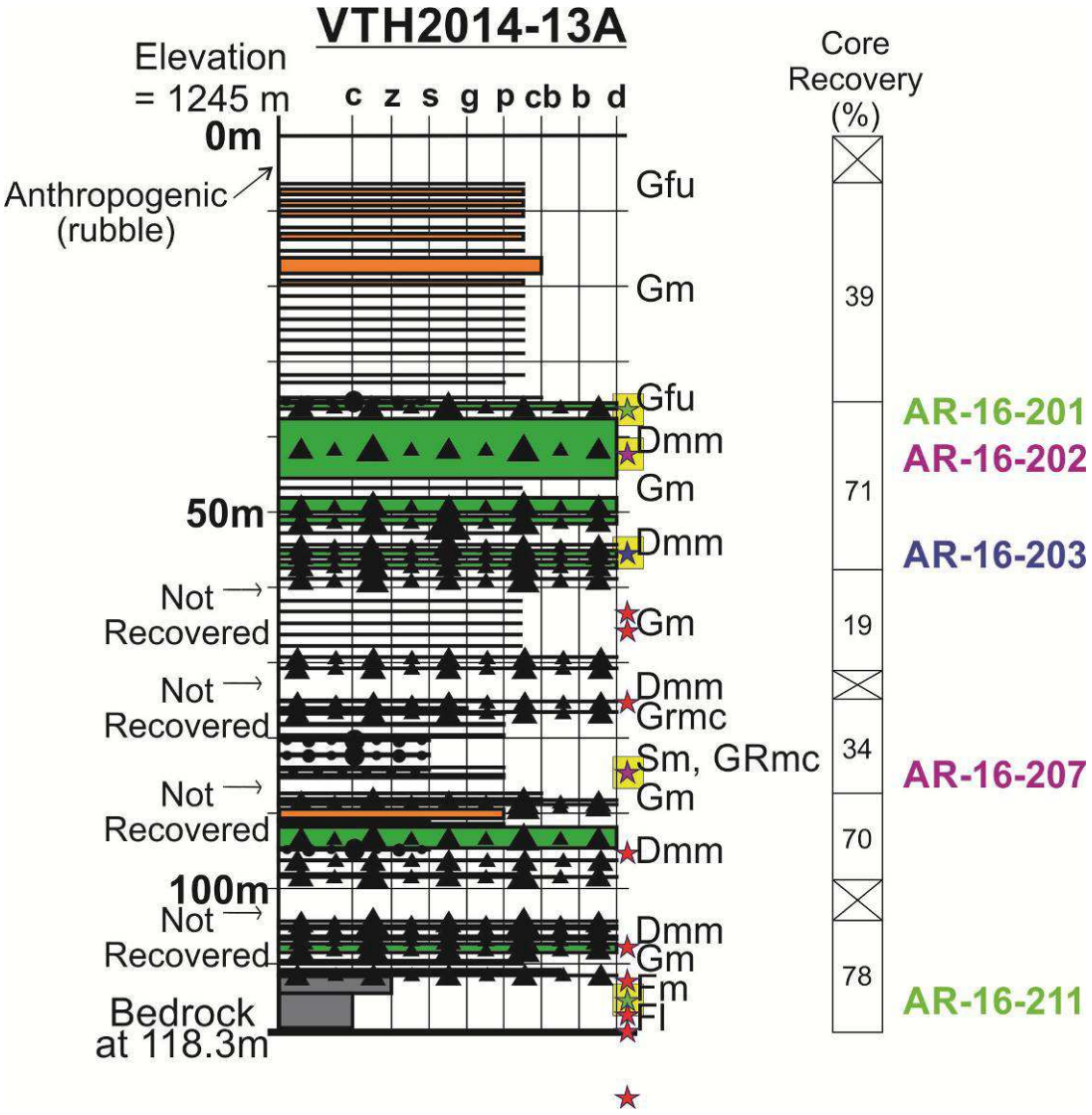
VTH2014-13A
Elevation
= 1245 m
c z s g p cb b d
0m
Anthropogenic
(rubble)
Gfu
Gm
Gfu
Dmm
Gm
50m
Dmm
Not
Recovered
Gm
Not
Recovered
Dmm
Grmc
Sm, GRmc
Not
Recovered
Gm
Dmm
100m
Not
Recovered
Dmm
Gm
Fm
Fl
Bedrock
at 118.3m
Core
Recovery
(%)
39
71
19
34
70
78
AR-16-201
AR-16-202
AR-16-203
AR-16-207
AR-16-211

(i)

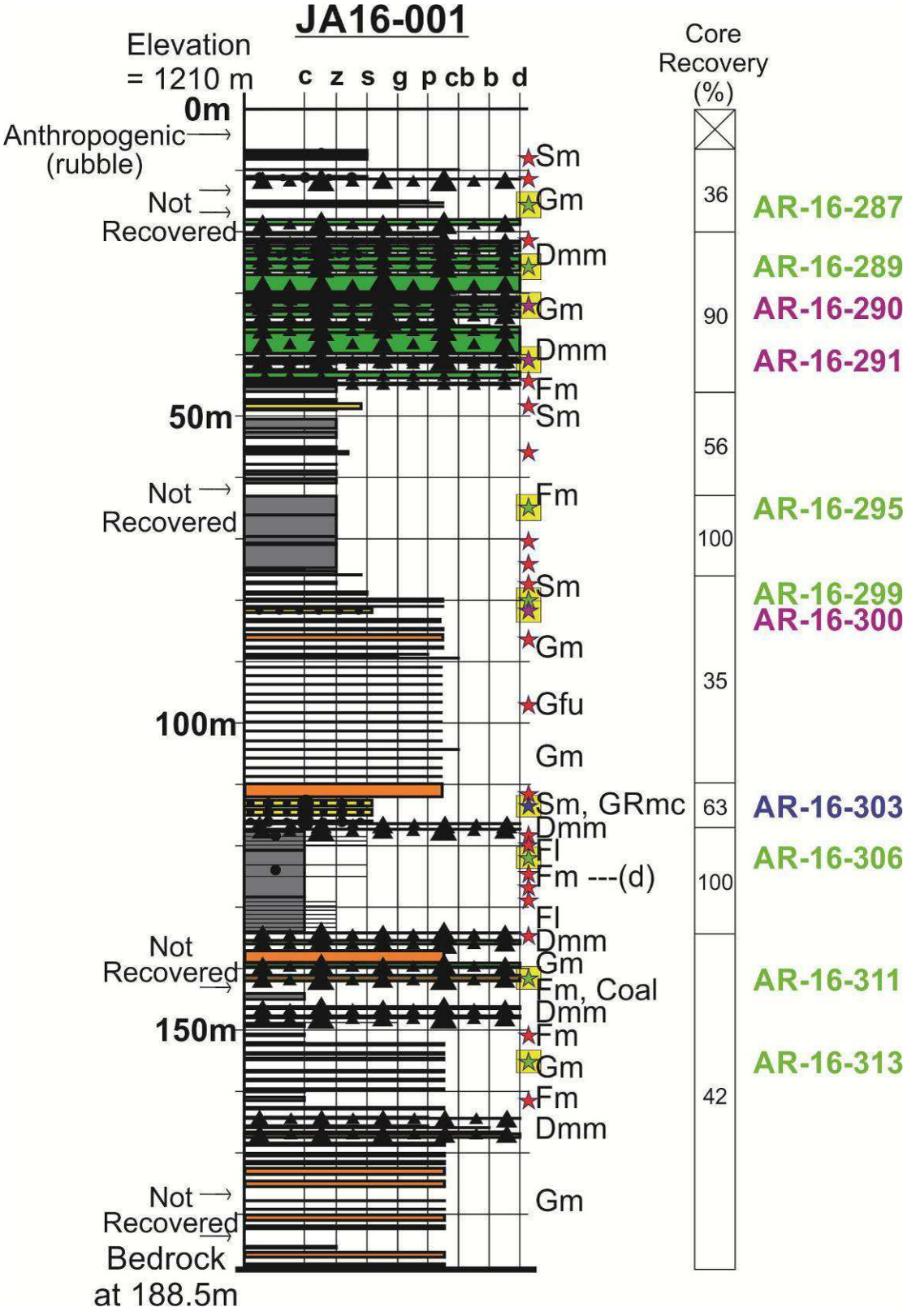
JA16-001
Elevation
= 1210 m
c z s g p cb b d
Core
Recovery
(%)
0m
Anthropogenic
(rubble)
Not
Recovered
50m
Not
Recovered
100m
Not
Recovered
150m
Not
Recovered
Bedrock
at 188.5m
Sm
Gm
Dmm
Gm
Dmm
Fm
Sm
Fm
Sm
Gm
Gfu
Gm
Sm, GRmc
Dmm
Fl
Fm ---(d)
Fl
Dmm
Gm
Fm, Coal
Dmm
Fm
Gm
Fm
Dmm
Gm
36
90
56
100
35
63
100
42
AR-16-287
AR-16-289
AR-16-290
AR-16-291
AR-16-295
AR-16-299
AR-16-300
AR-16-303
AR-16-306
AR-16-311
AR-16-313

(j)

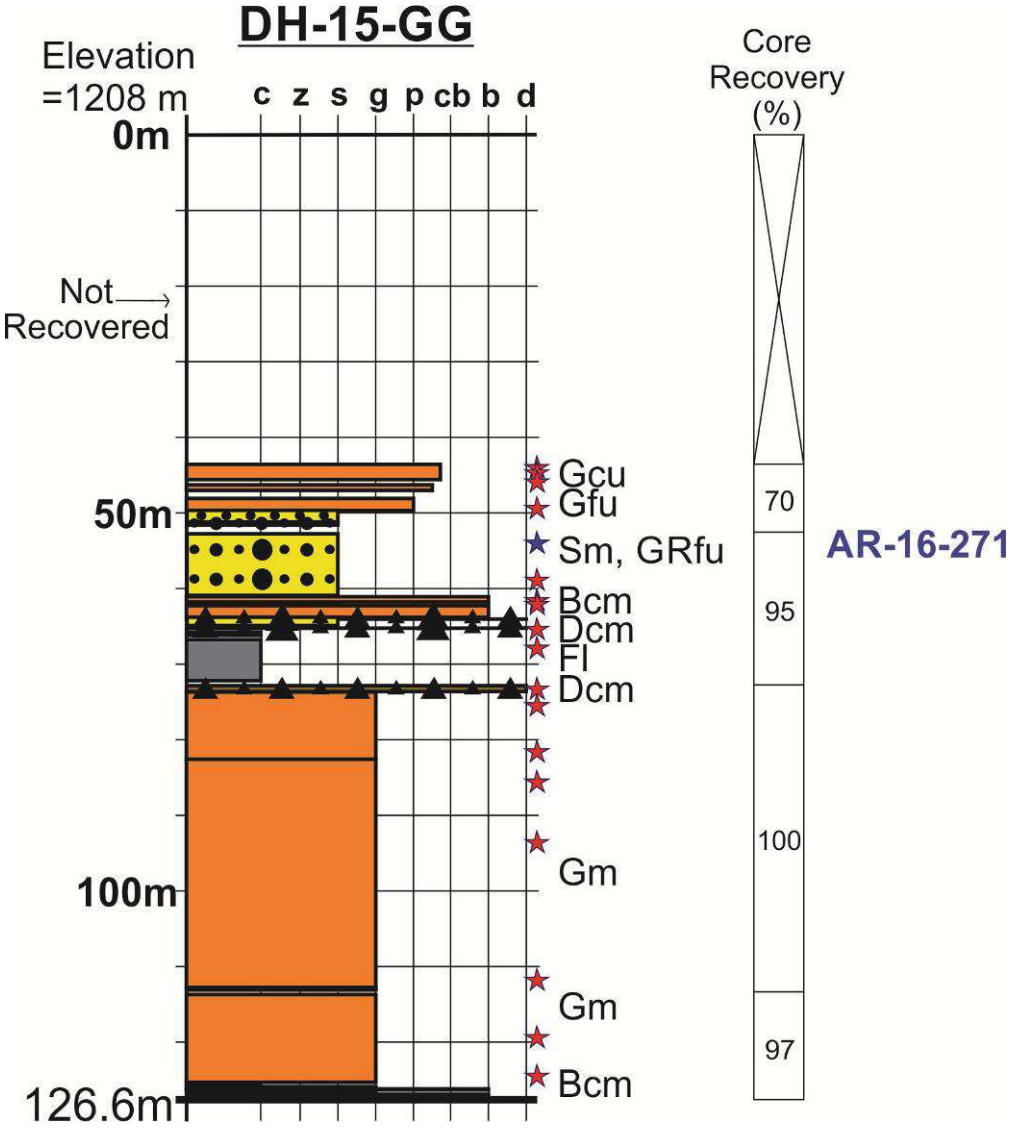

Figure B.1 Stratigraphic log of cores (a) VTH2014-03, (b) VTH2014-06, (c) VTH2014-07, (d) VTH2014-08, (e) VTH2014-09, (f) VTH2014-10, (g) VTH2014-11, (h) VTH2014-13A, (i) JA16-001 and (j) DH15-GG with sample locations, including samples used for heavy mineral, geochemical, hyperspectral or petrophysical analysis.

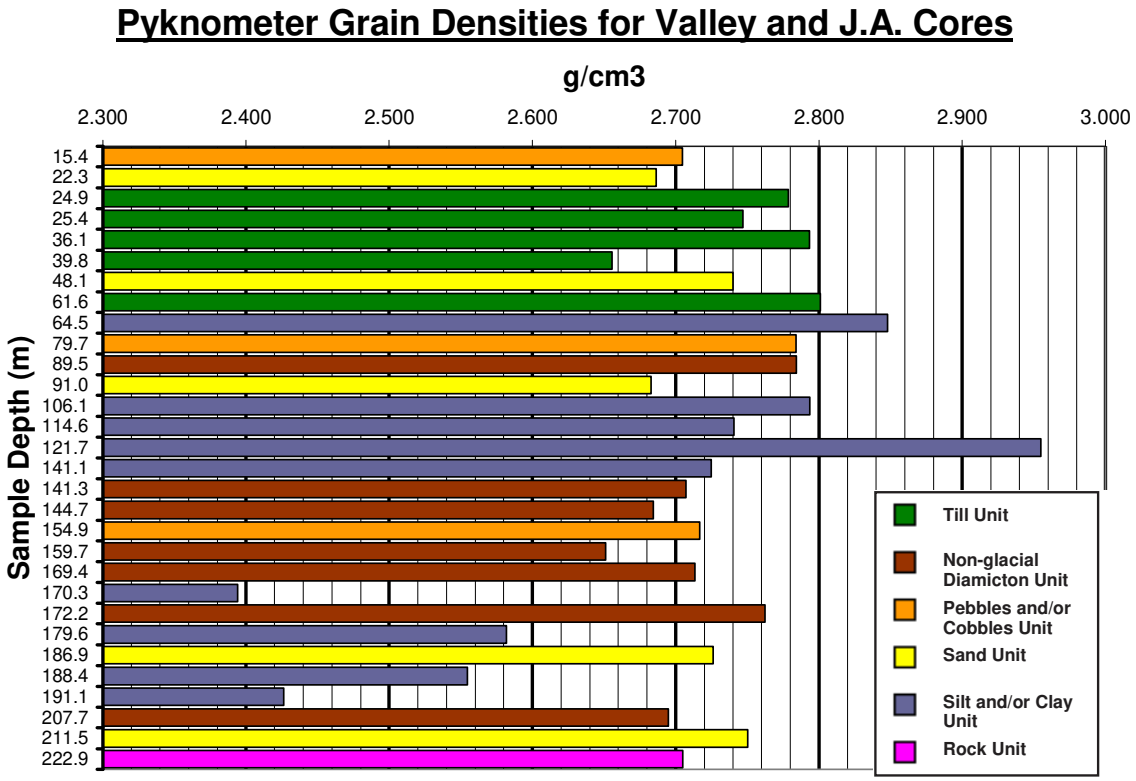

Figure B.2 Pyknometer grain density vs. sample depth.

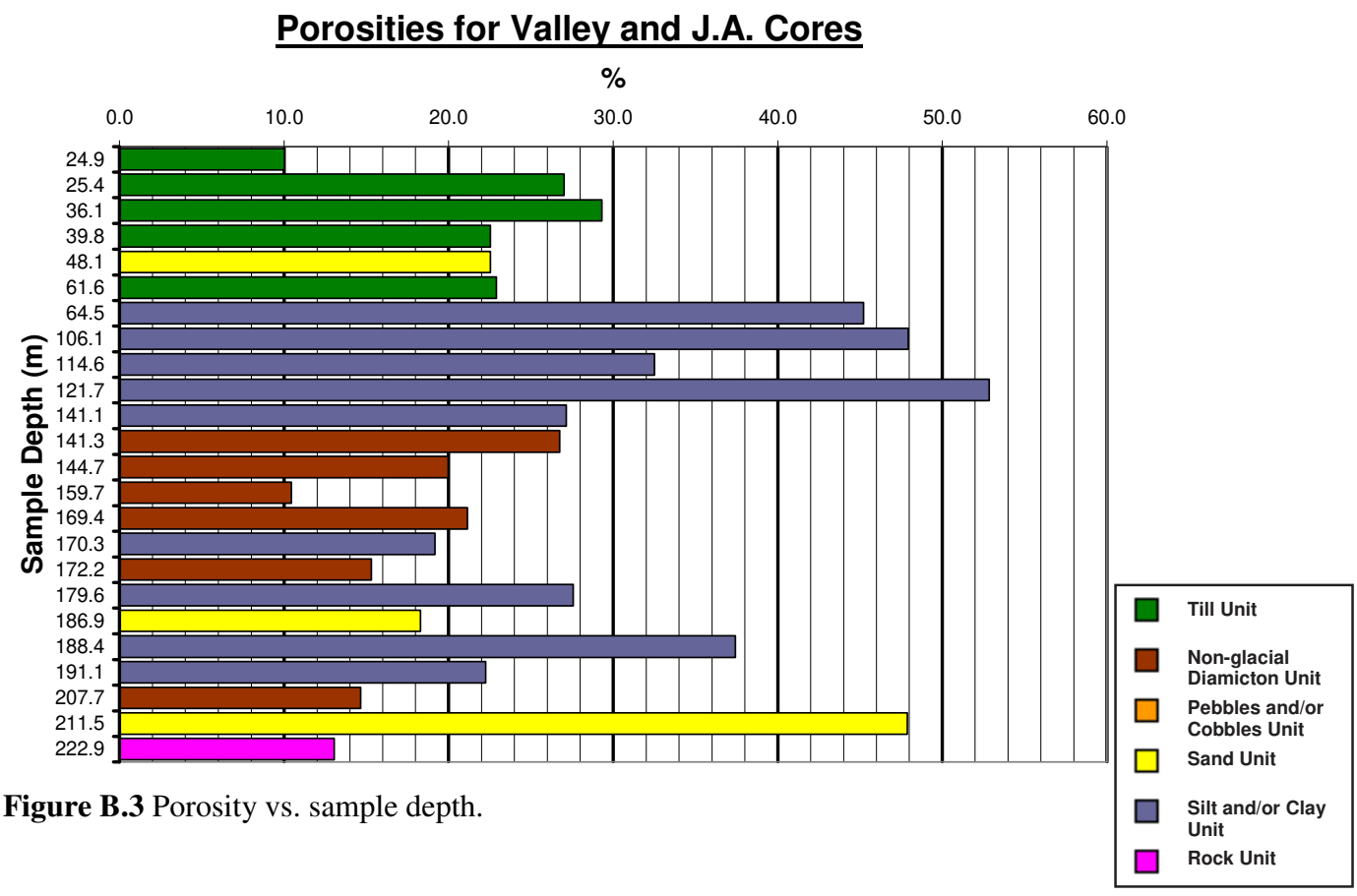

Figure B.3 Porosity vs. sample depth.

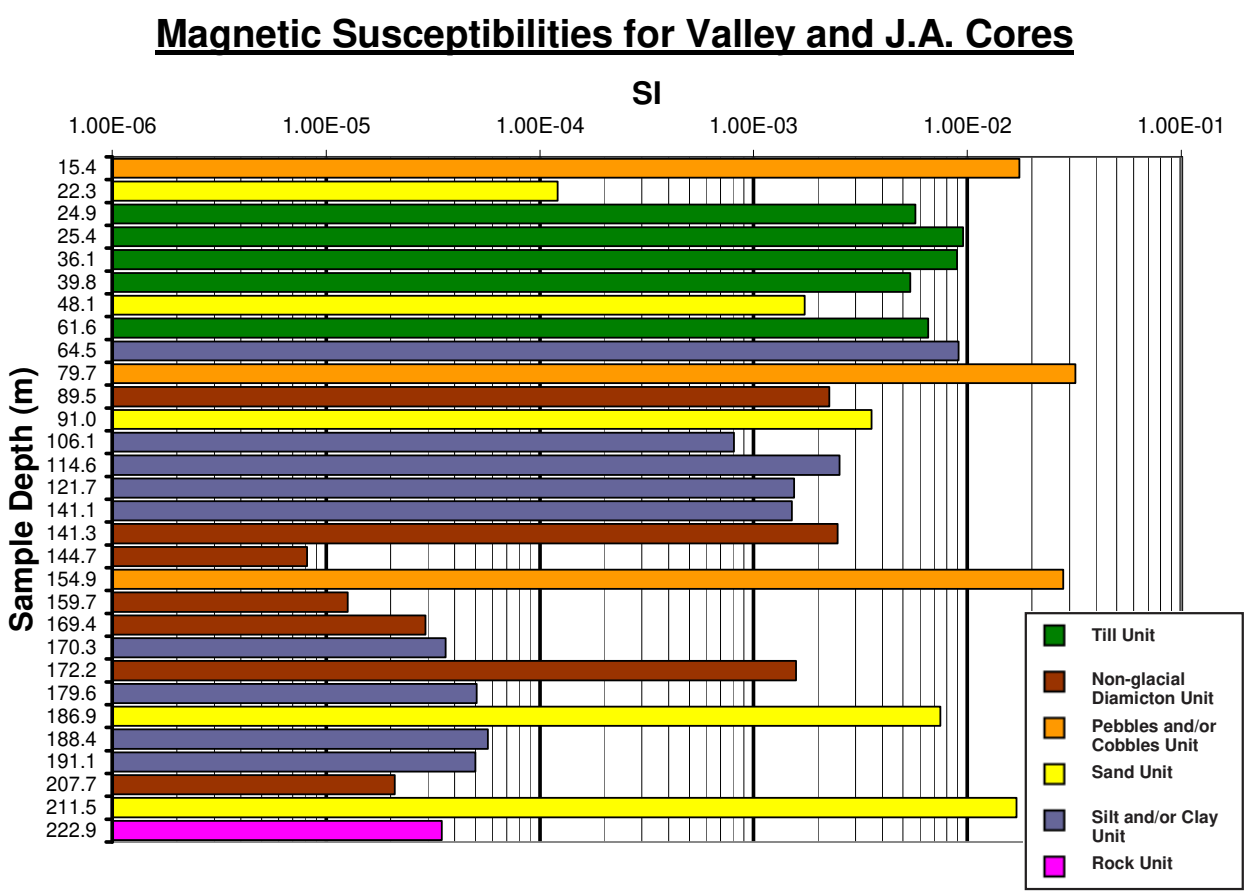

Figure B.4 Magnetic susceptibility vs. sample depth.

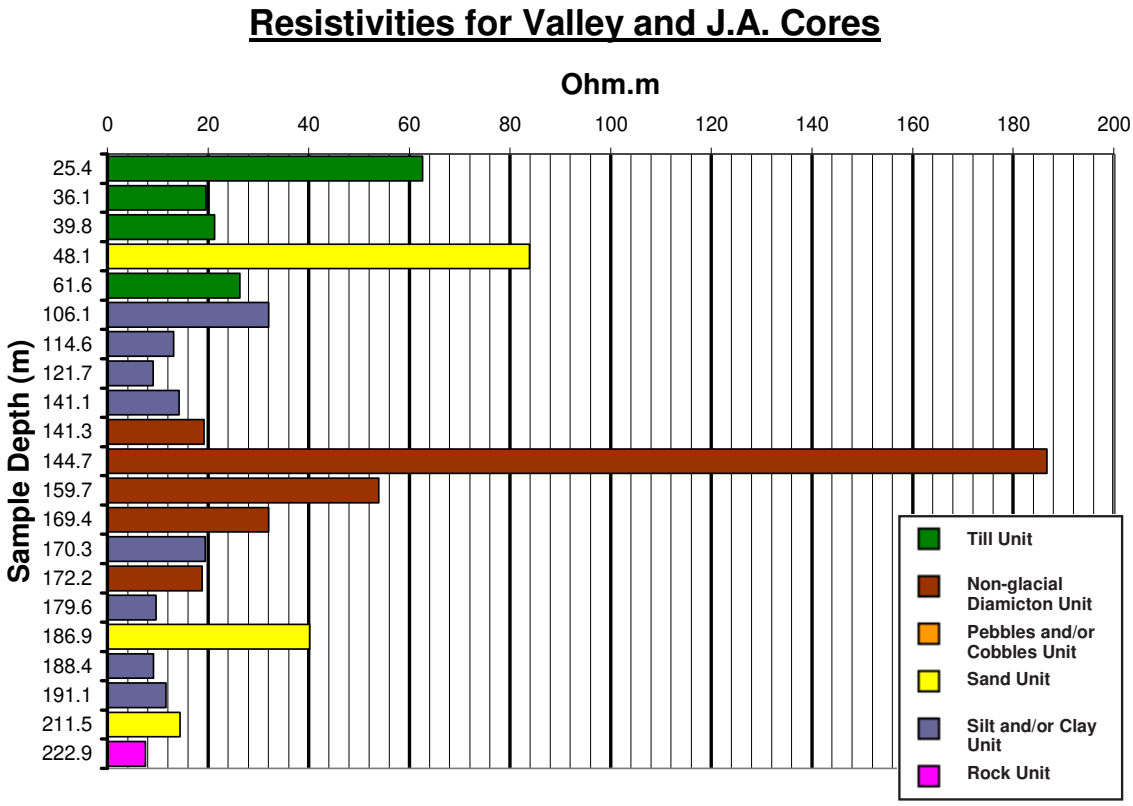

Figure B.5 Resistivity vs. sample depth.

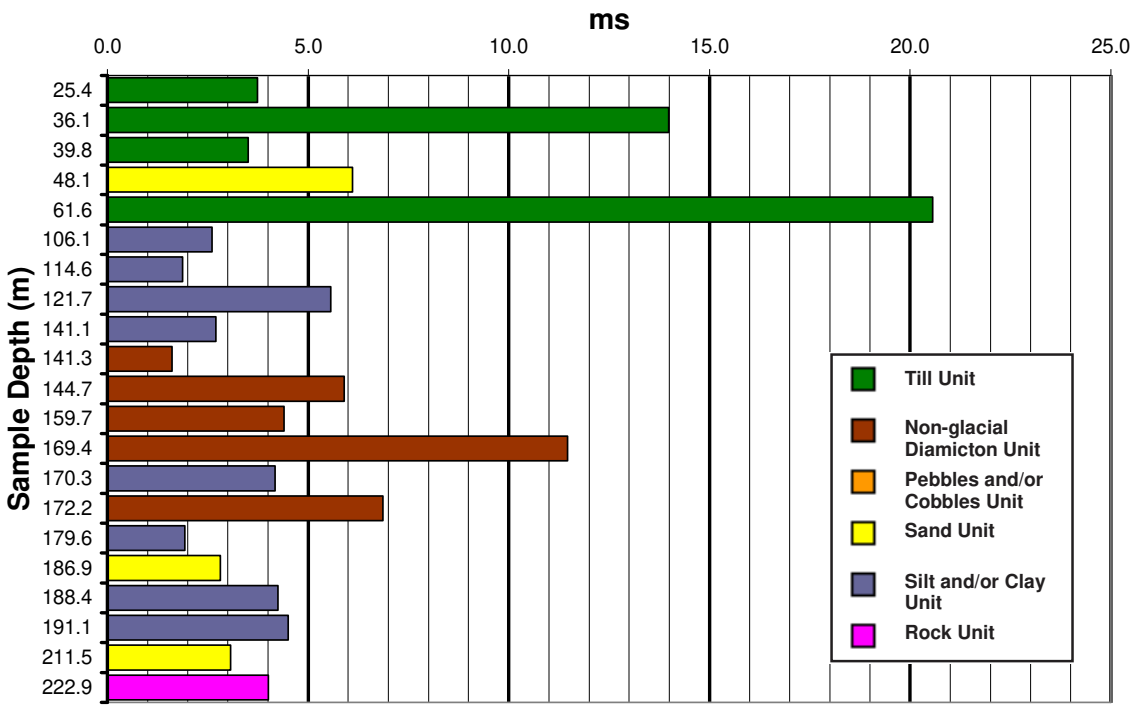

Figure B.6 Chargeability vs. sample depth.

Sedimentological Properties

Cumulative grain size curves have been plotted for select samples from each core and from the Highmont pit (**Figure B.7**). Each of these samples has been plotted on ternary diagrams showing the relative proportions of gravel, sand and silt or clay (**Figure B.8**).

(a)

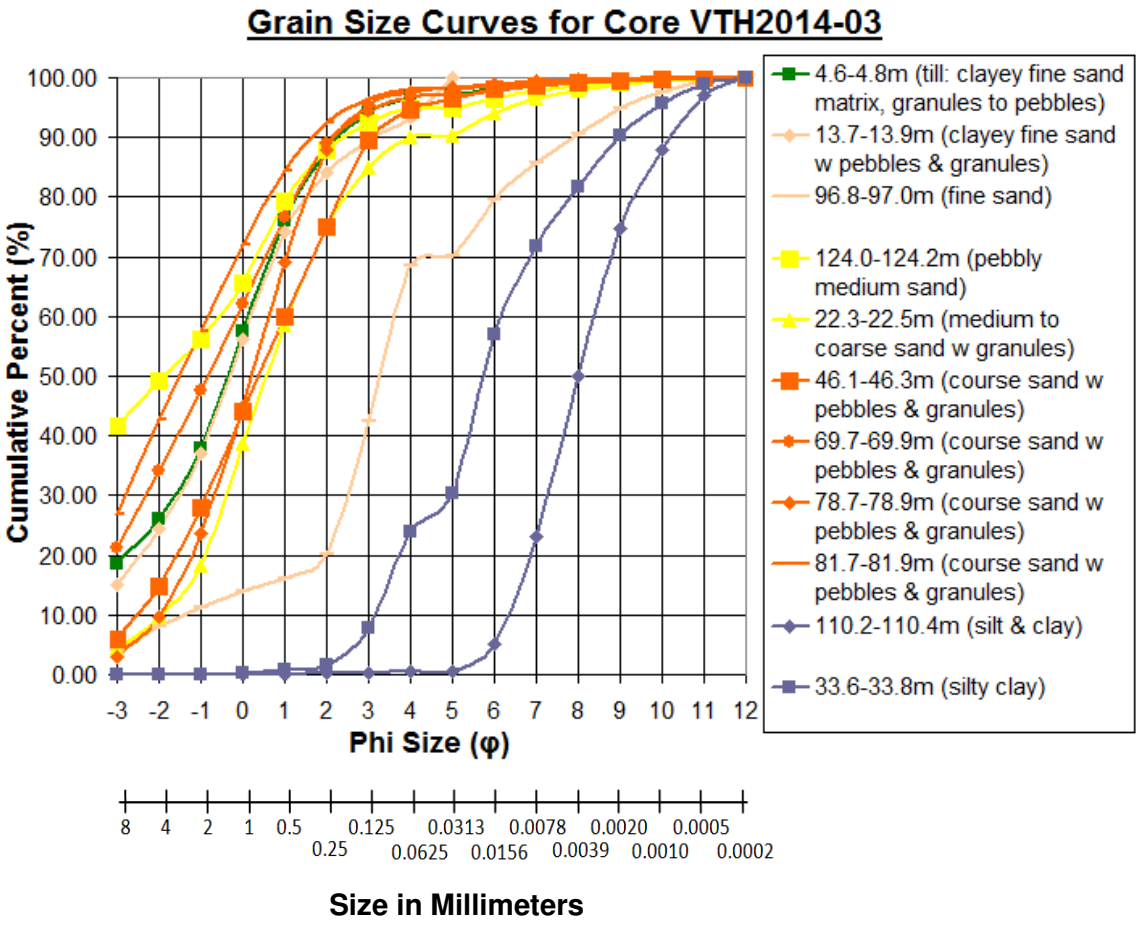
Grain Size Curves for Core VTH2014-03
Cumulative Percent (%)
100.00
90.00
80.00
70.00
60.00
50.00
40.00
30.00
20.00
10.00
0.00
-3 -2 -1 0 1 2 3 4 5 6 7 8 9 10 11 12
Phi Size (φ)
8 4 2 1 0.5 0.25 0.125 0.0625 0.0313 0.0156 0.0078 0.0039 0.0020 0.0010 0.0005 0.0002
Size in Millimeters
4.6-4.8m (till: clayey fine sand matrix, granules to pebbles)
13.7-13.9m (clayey fine sand w pebbles & granules)
96.8-97.0m (fine sand)
124.0-124.2m (pebbly medium sand)
22.3-22.5m (medium to coarse sand w granules)
46.1-46.3m (course sand w pebbles & granules)
69.7-69.9m (course sand w pebbles & granules)
78.7-78.9m (course sand w pebbles & granules)
81.7-81.9m (course sand w pebbles & granules)
110.2-110.4m (silt & clay)
33.6-33.8m (silty clay)

(b)

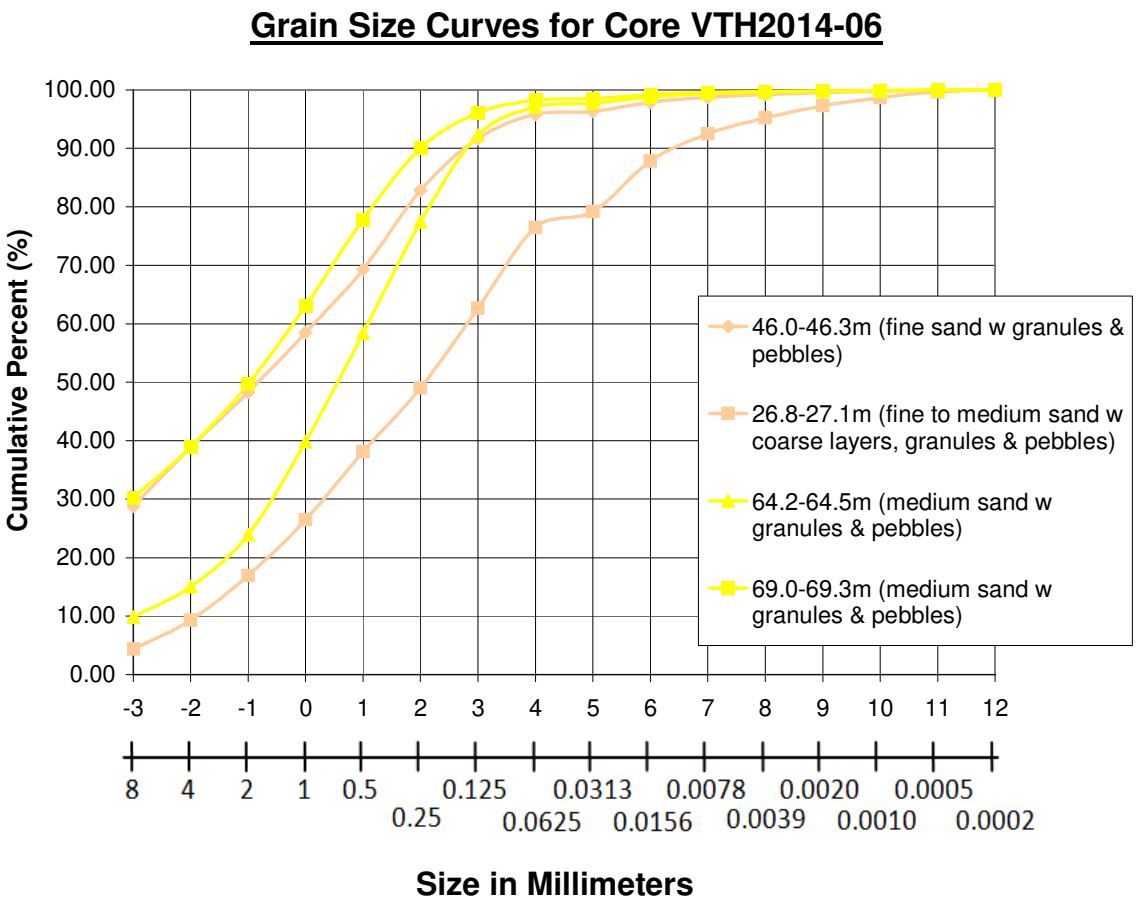
Grain Size Curves for Core VTH2014-06
Cumulative Percent (%)
100.00
90.00
80.00
70.00
60.00
50.00
40.00
30.00
20.00
10.00
0.00
-3 -2 -1 0 1 2 3 4 5 6 7 8 9 10 11 12
8 4 2 1 0.5 0.25 0.125 0.0625 0.0313 0.0156 0.0078 0.0039 0.0020 0.0010 0.0005 0.0002
Size in Millimeters
46.0-46.3m (fine sand w granules & pebbles)
26.8-27.1m (fine to medium sand w coarse layers, granules & pebbles)
64.2-64.5m (medium sand w granules & pebbles)
69.0-69.3m (medium sand w granules & pebbles)

(c)

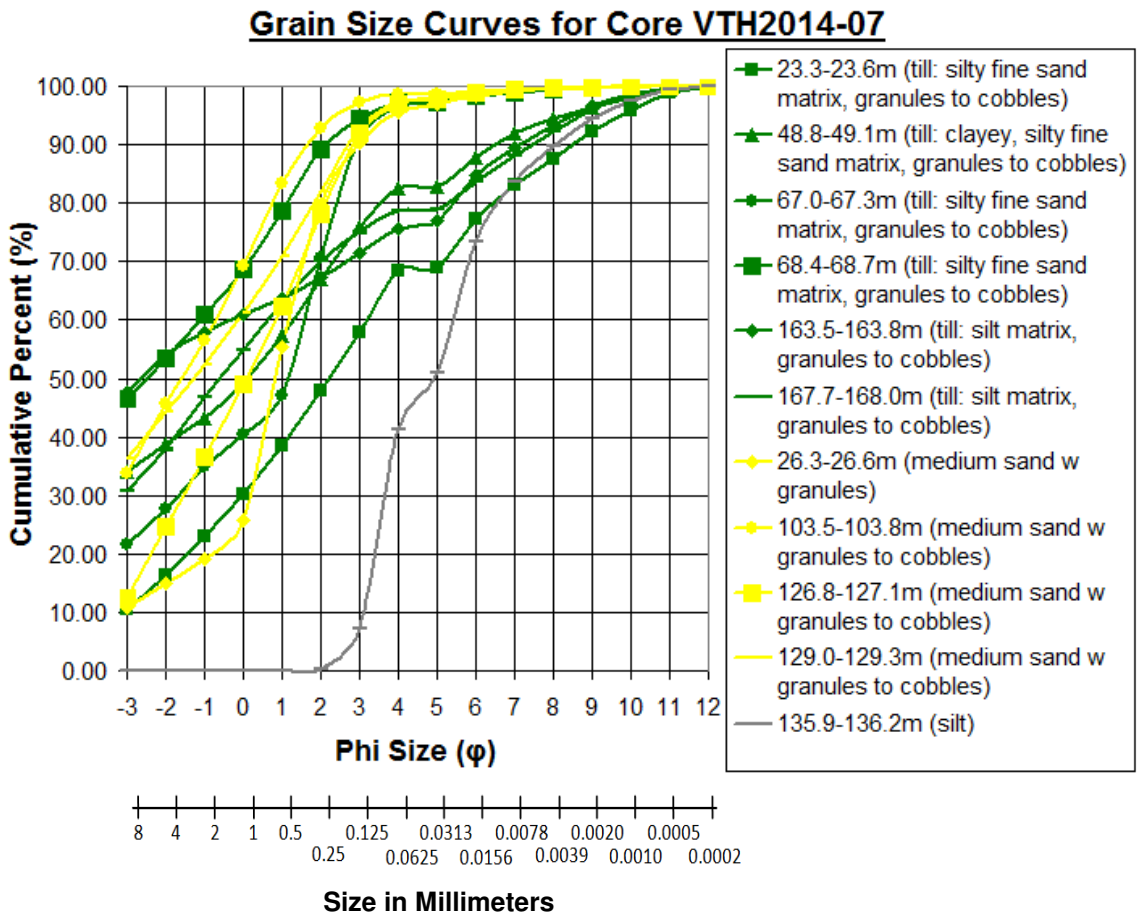
Grain Size Curves for Core VTH2014-07
Cumulative Percent (%)
100.00
90.00
80.00
70.00
60.00
50.00
40.00
30.00
20.00
10.00
0.00
-3 -2 -1 0 1 2 3 4 5 6 7 8 9 10 11 12
Phi Size (φ)
8 4 2 1 0.5 0.25 0.125 0.0625 0.0313 0.0156 0.0078 0.0039 0.0020 0.0010 0.0005 0.0002
Size in Millimeters
23.3-23.6m (till: silty fine sand matrix, granules to cobbles)
48.8-49.1m (till: clayey, silty fine sand matrix, granules to cobbles)
67.0-67.3m (till: silty fine sand matrix, granules to cobbles)
68.4-68.7m (till: silty fine sand matrix, granules to cobbles)
163.5-163.8m (till: silt matrix, granules to cobbles)
167.7-168.0m (till: silt matrix, granules to cobbles)
26.3-26.6m (medium sand w granules)
103.5-103.8m (medium sand w granules to cobbles)
126.8-127.1m (medium sand w granules to cobbles)
129.0-129.3m (medium sand w granules to cobbles)
135.9-136.2m (silt)

(d)

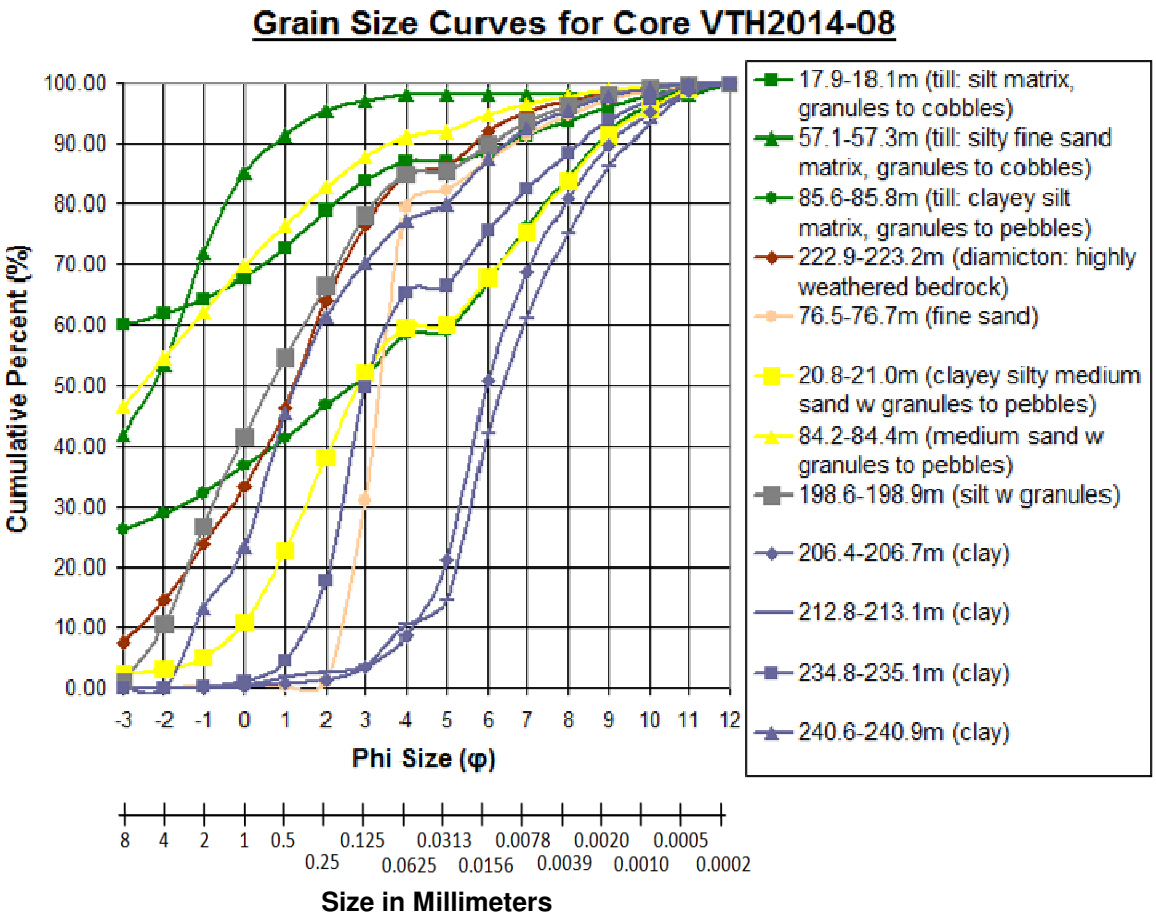
Grain Size Curves for Core VTH2014-08
Cumulative Percent (%)
100.00
90.00
80.00
70.00
60.00
50.00
40.00
30.00
20.00
10.00
0.00
-3 -2 -1 0 1 2 3 4 5 6 7 8 9 10 11 12
Phi Size (φ)
8 4 2 1 0.5 0.25 0.125 0.0625 0.0313 0.0156 0.0078 0.0039 0.0020 0.0010 0.0005 0.0002
Size in Millimeters
17.9-18.1m (till: silt matrix, granules to cobbles)
57.1-57.3m (till: silty fine sand matrix, granules to cobbles)
85.6-85.8m (till: clayey silt matrix, granules to pebbles)
222.9-223.2m (diamicton: highly weathered bedrock)
76.5-76.7m (fine sand)
20.8-21.0m (clayey silty medium sand w granules to pebbles)
84.2-84.4m (medium sand w granules to pebbles)
198.6-198.9m (silt w granules)
206.4-206.7m (clay)
212.8-213.1m (clay)
234.8-235.1m (clay)
240.6-240.9m (clay)

(e)

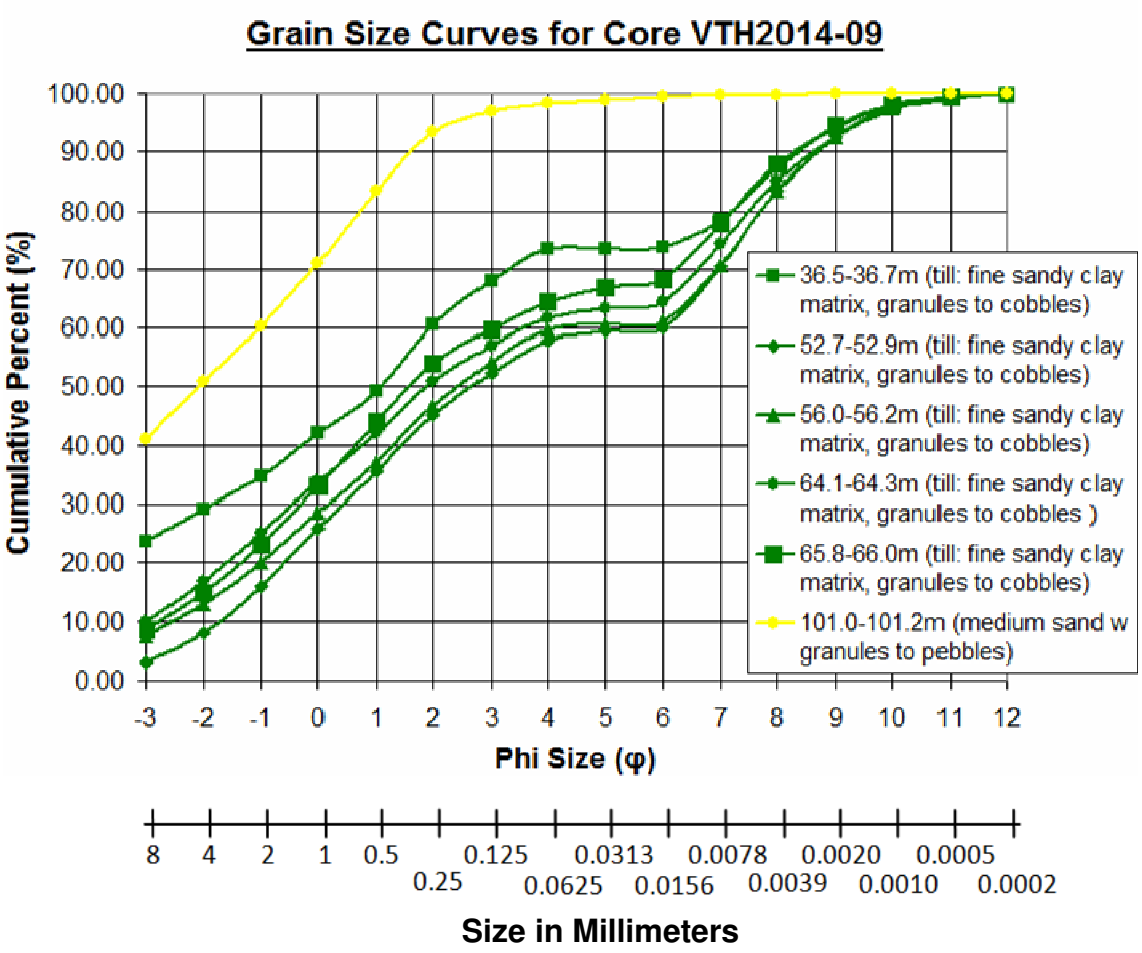
Grain Size Curves for Core VTH2014-09
Cumulative Percent (%)
100.00
90.00
80.00
70.00
60.00
50.00
40.00
30.00
20.00
10.00
0.00
-3 -2 -1 0 1 2 3 4 5 6 7 8 9 10 11 12
Phi Size (φ)
8 4 2 1 0.5 0.25 0.125 0.0625 0.0313 0.0156 0.0078 0.0039 0.0020 0.0010 0.0005 0.0002
Size in Millimeters
36.5-36.7m (till: fine sandy clay matrix, granules to cobbles)
52.7-52.9m (till: fine sandy clay matrix, granules to cobbles)
56.0-56.2m (till: fine sandy clay matrix, granules to cobbles)
64.1-64.3m (till: fine sandy clay matrix, granules to cobbles)
65.8-66.0m (till: fine sandy clay matrix, granules to cobbles)
101.0-101.2m (medium sand w granules to pebbles)

(f)

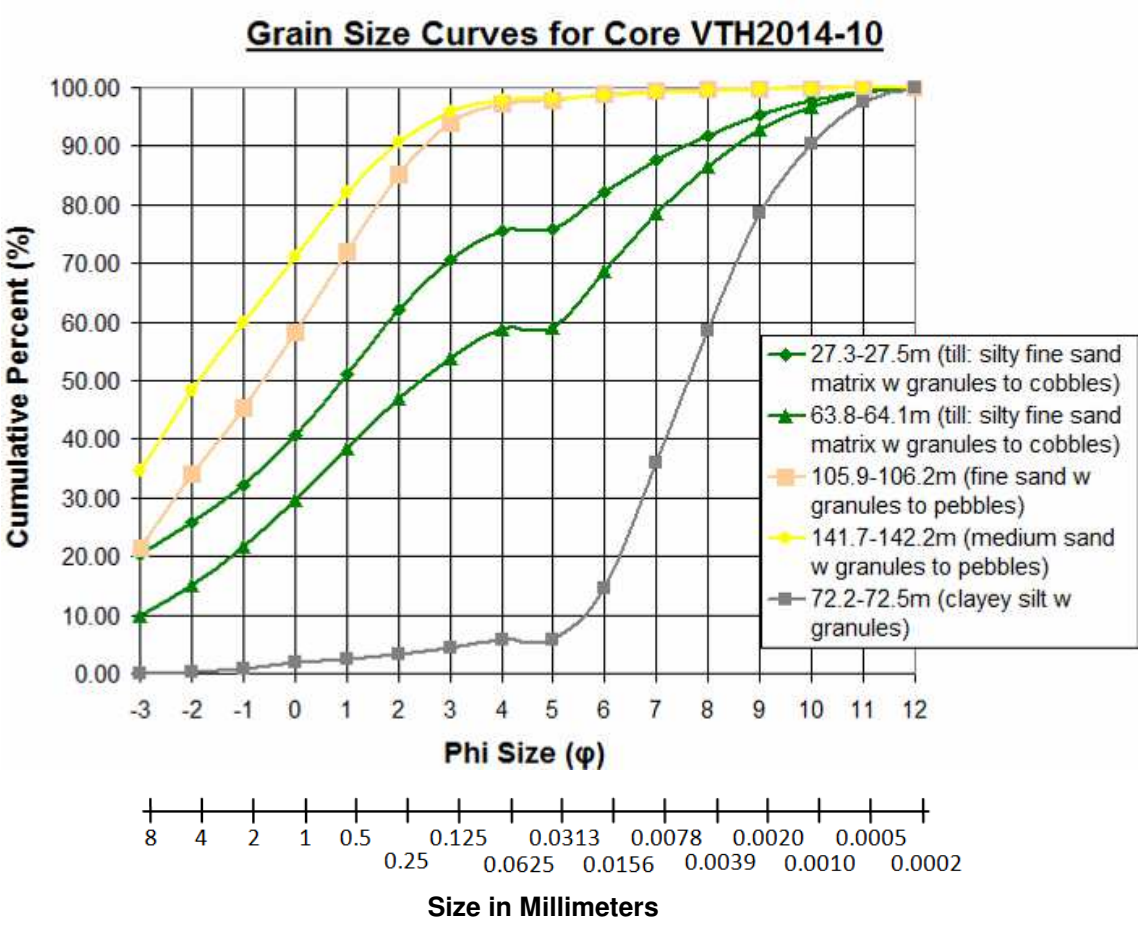
Grain Size Curves for Core VTH2014-10
Cumulative Percent (%)
100.00
90.00
80.00
70.00
60.00
50.00
40.00
30.00
20.00
10.00
0.00
-3 -2 -1 0 1 2 3 4 5 6 7 8 9 10 11 12
Phi Size (φ)
27.3-27.5m (till: silty fine sand matrix w granules to cobbles)
63.8-64.1m (till: silty fine sand matrix w granules to cobbles)
105.9-106.2m (fine sand w granules to pebbles)
141.7-142.2m (medium sand w granules to pebbles)
72.2-72.5m (clayey silt w granules)
8 4 2 1 0.5 0.25 0.125 0.0625 0.0313 0.0156 0.0078 0.0039 0.0020 0.0010 0.0005 0.0002
Size in Millimeters

(g)

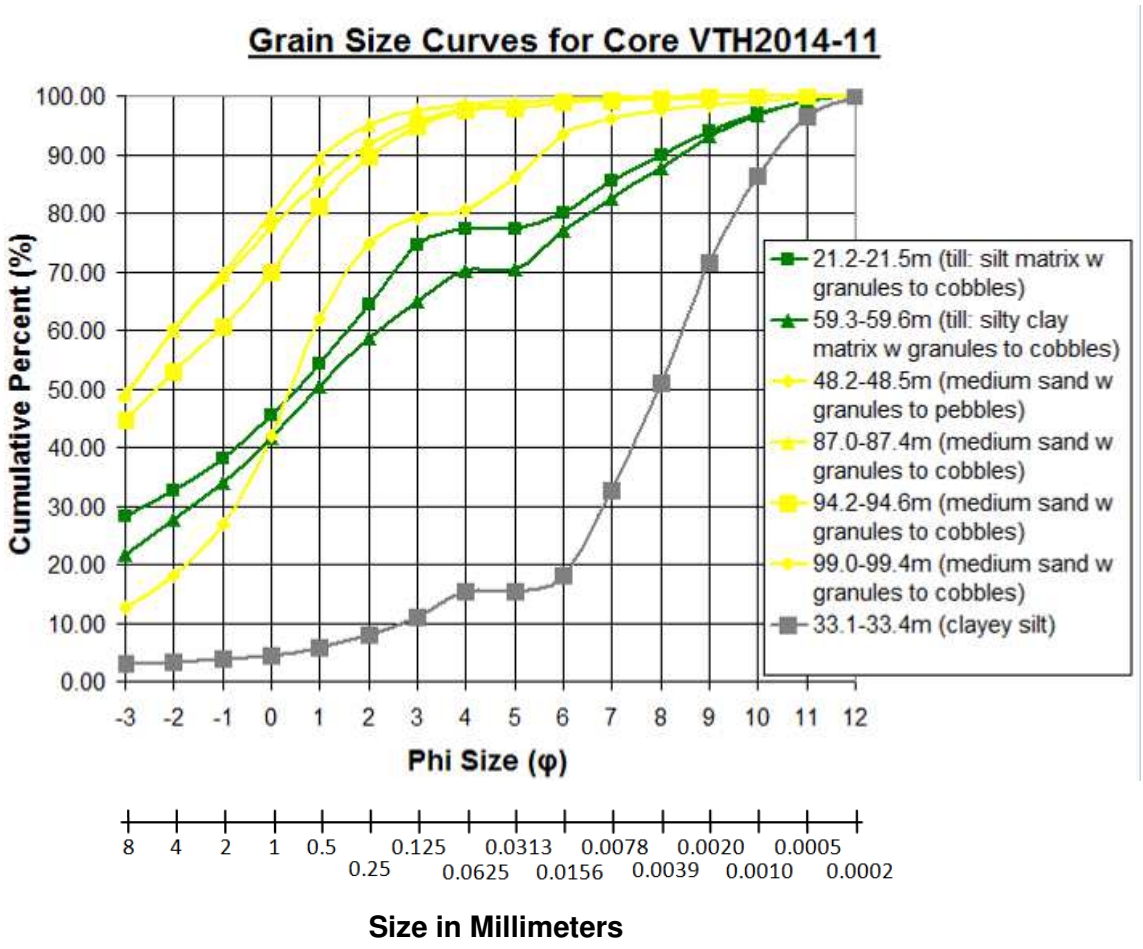
Grain Size Curves for Core VTH2014-11
Cumulative Percent (%)
100.00
90.00
80.00
70.00
60.00
50.00
40.00
30.00
20.00
10.00
0.00
-3 -2 -1 0 1 2 3 4 5 6 7 8 9 10 11 12
Phi Size (φ)
8 4 2 1 0.5 0.25 0.125 0.0625 0.0313 0.0156 0.0078 0.0039 0.0020 0.0010 0.0005 0.0002
Size in Millimeters
21.2-21.5m (till: silt matrix w granules to cobbles)
59.3-59.6m (till: silty clay matrix w granules to cobbles)
48.2-48.5m (medium sand w granules to pebbles)
87.0-87.4m (medium sand w granules to cobbles)
94.2-94.6m (medium sand w granules to cobbles)
99.0-99.4m (medium sand w granules to cobbles)
33.1-33.4m (clayey silt)

(h)

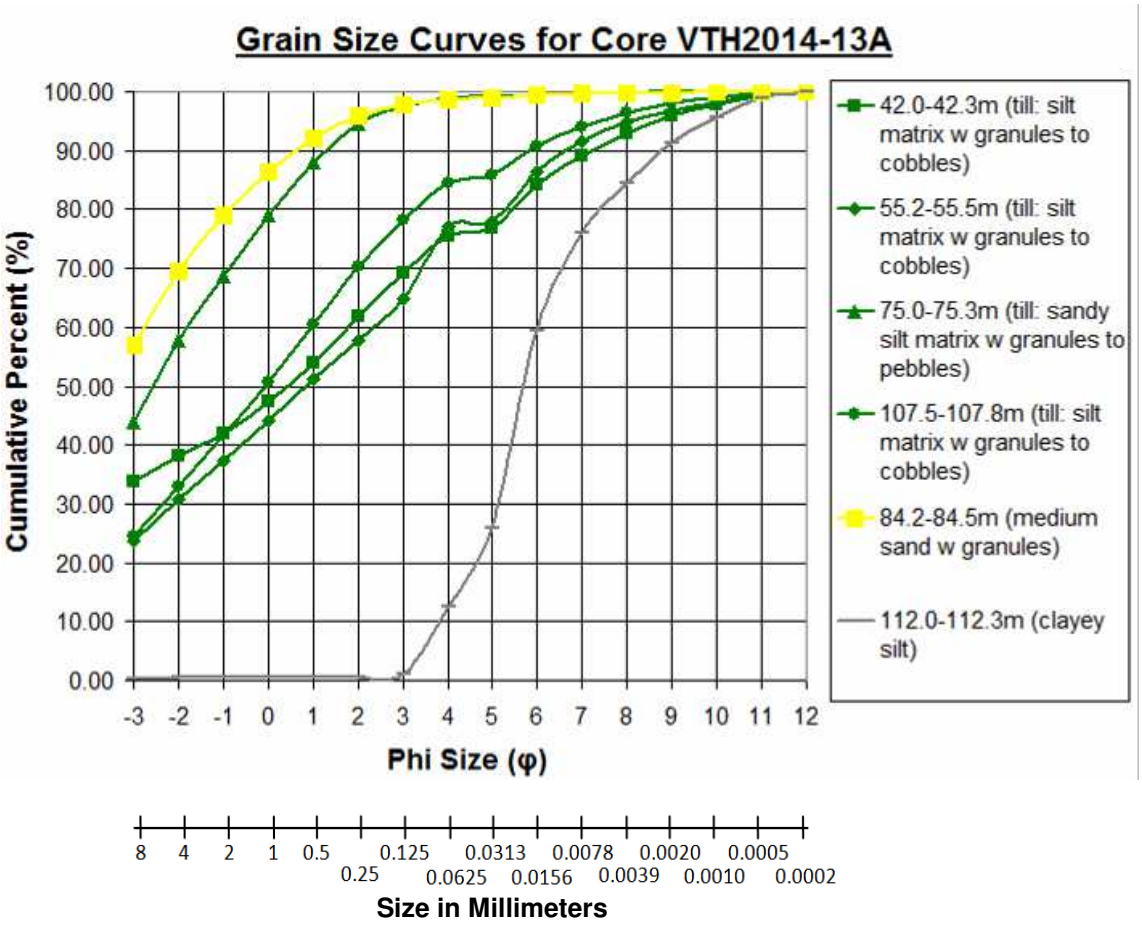
Grain Size Curves for Core VTH2014-13A
Cumulative Percent (%)
100.00
90.00
80.00
70.00
60.00
50.00
40.00
30.00
20.00
10.00
0.00
-3 -2 -1 0 1 2 3 4 5 6 7 8 9 10 11 12
Phi Size (φ)
42.0-42.3m (till: silt matrix w granules to cobbles)
55.2-55.5m (till: silt matrix w granules to cobbles)
75.0-75.3m (till: sandy silt matrix w granules to pebbles)
107.5-107.8m (till: silt matrix w granules to cobbles)
84.2-84.5m (medium sand w granules)
112.0-112.3m (clayey silt)
8 4 2 1 0.5 0.25 0.125 0.0625 0.0313 0.0156 0.0078 0.0039 0.0020 0.0010 0.0005 0.0002
Size in Millimeters

(i)

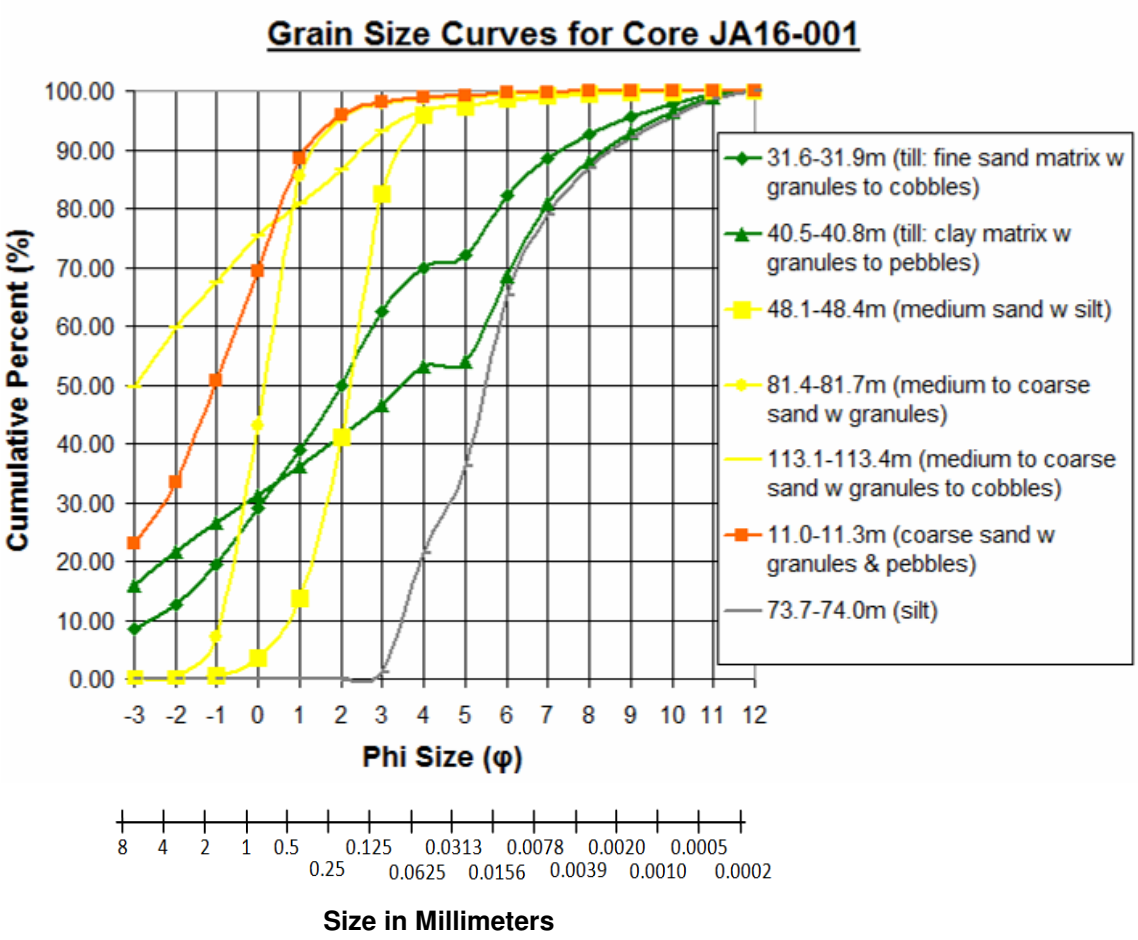
Grain Size Curves for Core JA16-001
Cumulative Percent (%)
100.00
90.00
80.00
70.00
60.00
50.00
40.00
30.00
20.00
10.00
0.00
-3 -2 -1 0 1 2 3 4 5 6 7 8 9 10 11 12
Phi Size (φ)
31.6-31.9m (till: fine sand matrix w granules to cobbles)
40.5-40.8m (till: clay matrix w granules to pebbles)
48.1-48.4m (medium sand w silt)
81.4-81.7m (medium to coarse sand w granules)
113.1-113.4m (medium to coarse sand w granules to cobbles)
11.0-11.3m (coarse sand w granules & pebbles)
73.7-74.0m (silt)
8 4 2 1 0.5 0.25 0.125 0.0625 0.0313 0.0156 0.0078 0.0039 0.0020 0.0010 0.0005 0.0002
Size in Millimeters

(j)

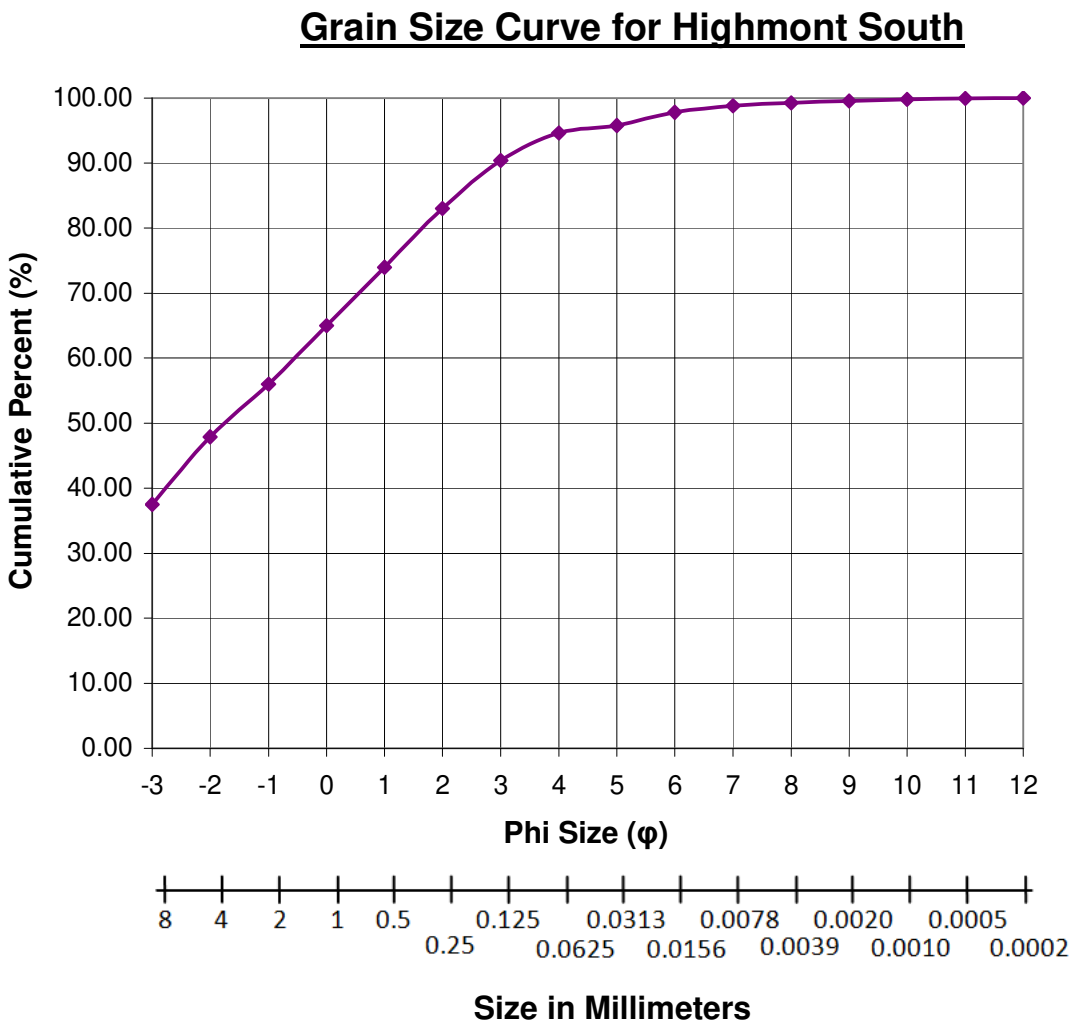

Figure B.7 Plot of cumulative grain size for samples from (a) VTH2014-03, (b) VTH2014-06, (c) VTH2014-07, (d) VTH2014-08, (e) VTH2014-09, (f) VTH2014-10, (g) VTH2014-11, (h) VTH2014-13A, (i) JA16-001 and (j) Highmont South.

(a)

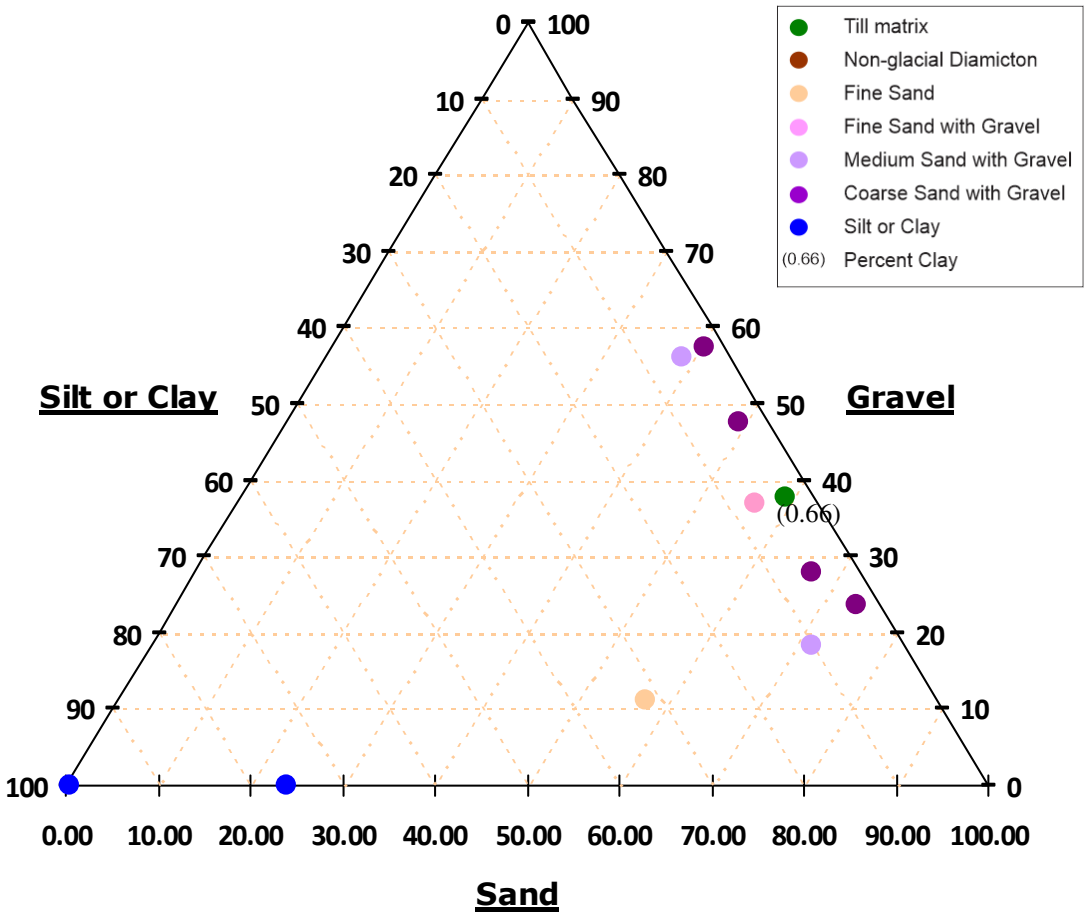
Grain Size Distribution for Samples from Core VTH2014-03
Till matrix
Non-glacial Diamicton
Fine Sand
Fine Sand with Gravel
Medium Sand with Gravel
Coarse Sand with Gravel
Silt or Clay
(0.66) Percent Clay
Silt or Clay
Gravel
Sand
(0.66)
0 100
10 90
20 80
30 70
40 60
50 50
60 40
70 30
80 20
90 10
100 0
0.00 10.00 20.00 30.00 40.00 50.00 60.00 70.00 80.00 90.00 100.00

(b)

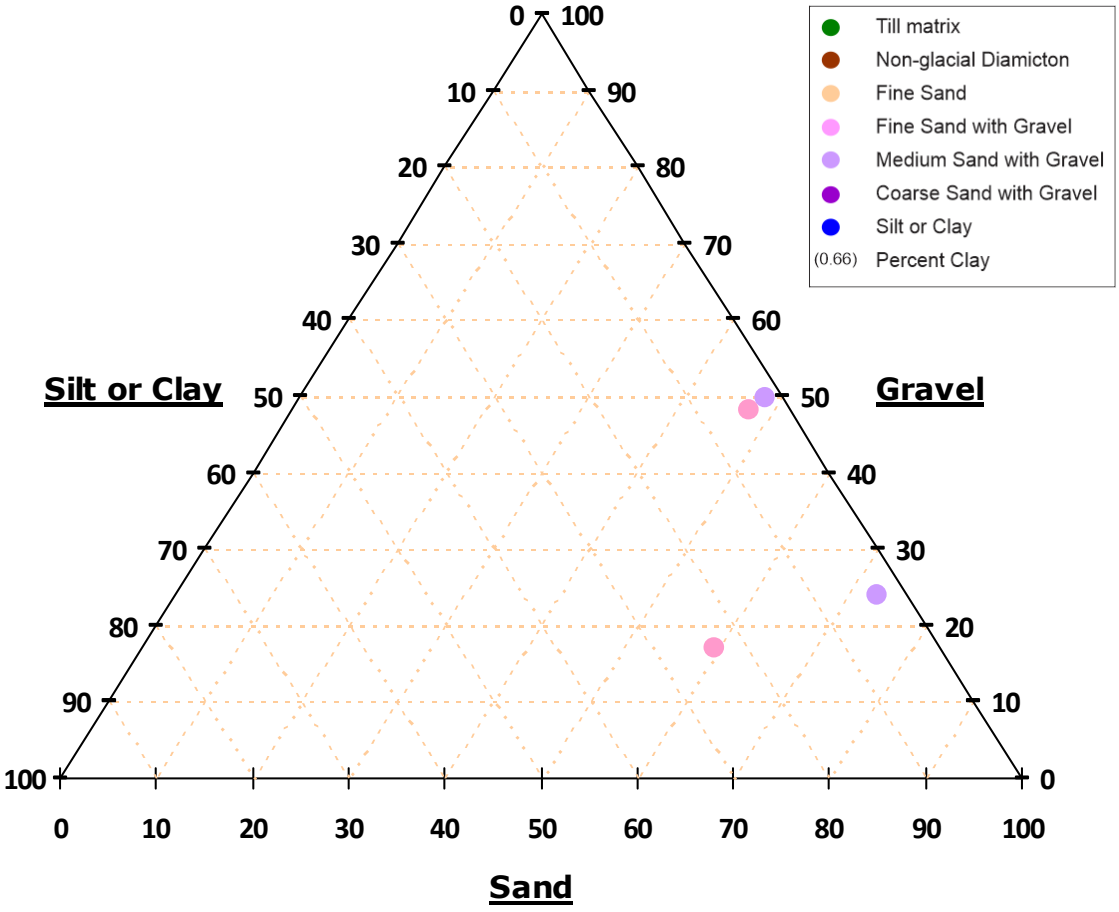
Grain Size Distribution for Samples from Core VTH2014-06
Till matrix
Non-glacial Diamicton
Fine Sand
Fine Sand with Gravel
Medium Sand with Gravel
Coarse Sand with Gravel
Silt or Clay
(0.66) Percent Clay
Silt or Clay
Gravel
Sand
0
10
20
30
40
50
60
70
80
90
100

(c)

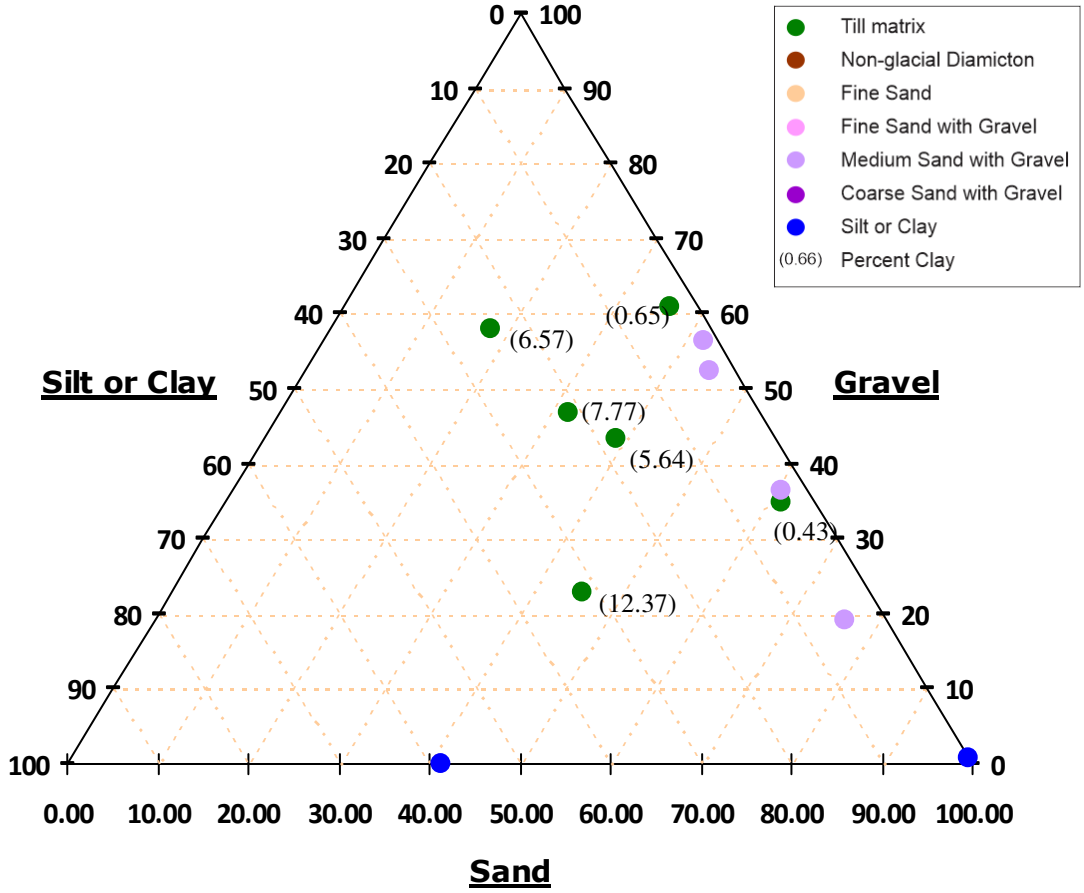
Grain Size Distribution for Samples from Core VTH2014-07
Till matrix
Non-glacial Diamicton
Fine Sand
Fine Sand with Gravel
Medium Sand with Gravel
Coarse Sand with Gravel
Silt or Clay
(0.66) Percent Clay
(6.57)
(0.65)
(7.77)
(5.64)
(0.43)
(12.37)
Silt or Clay
Gravel
Sand
0 100
10 90
20 80
30 70
40 60
50 50
60 40
70 30
80 20
90 10
100 0
0.00 10.00 20.00 30.00 40.00 50.00 60.00 70.00 80.00 90.00 100.00

(d)

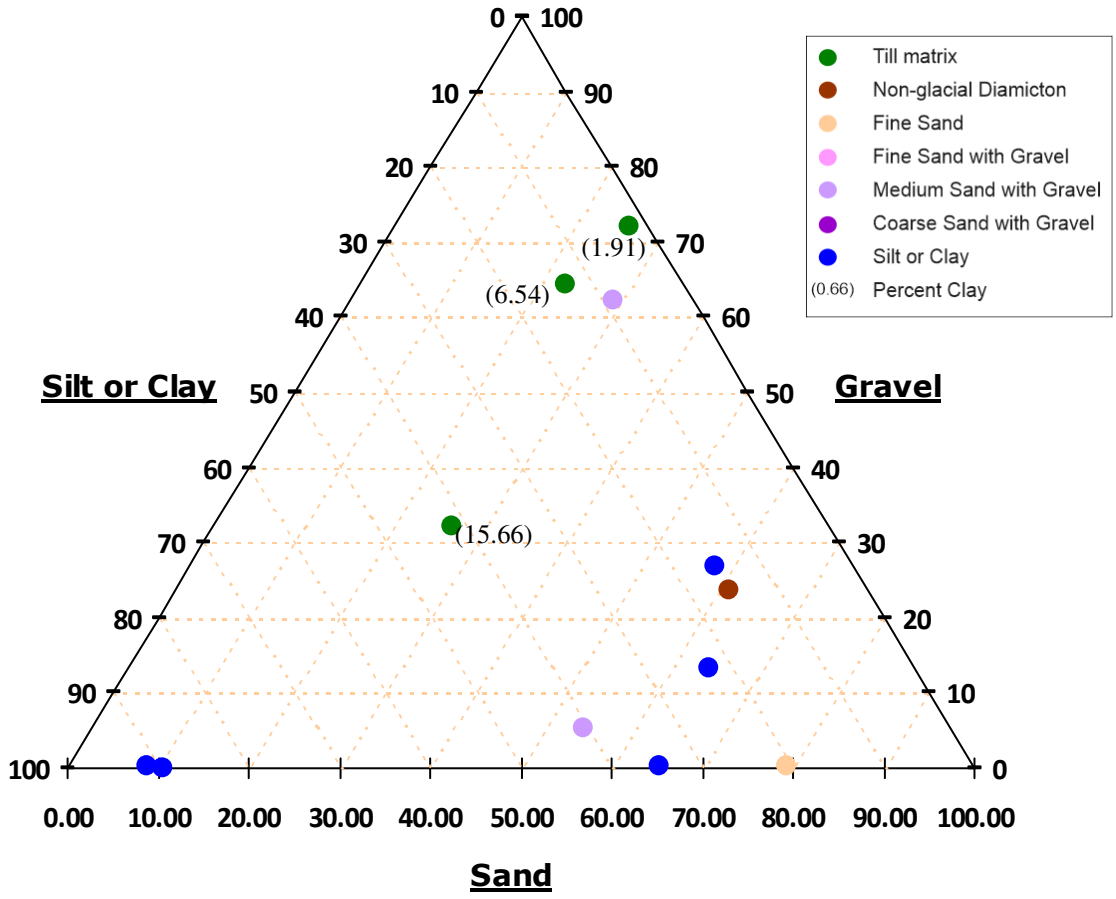
Grain Size Distribution for Samples from Core VTH2014-08
Till matrix
Non-glacial Diamicton
Fine Sand
Fine Sand with Gravel
Medium Sand with Gravel
Coarse Sand with Gravel
Silt or Clay
(0.66) Percent Clay
(1.91)
(6.54)
(15.66)
Silt or Clay
Gravel
Sand
0 100
10 90
20 80
30 70
40 60
50 50
60 40
70 30
80 20
90 10
100 0
0.00 10.00 20.00 30.00 40.00 50.00 60.00 70.00 80.00 90.00 100.00

(e)

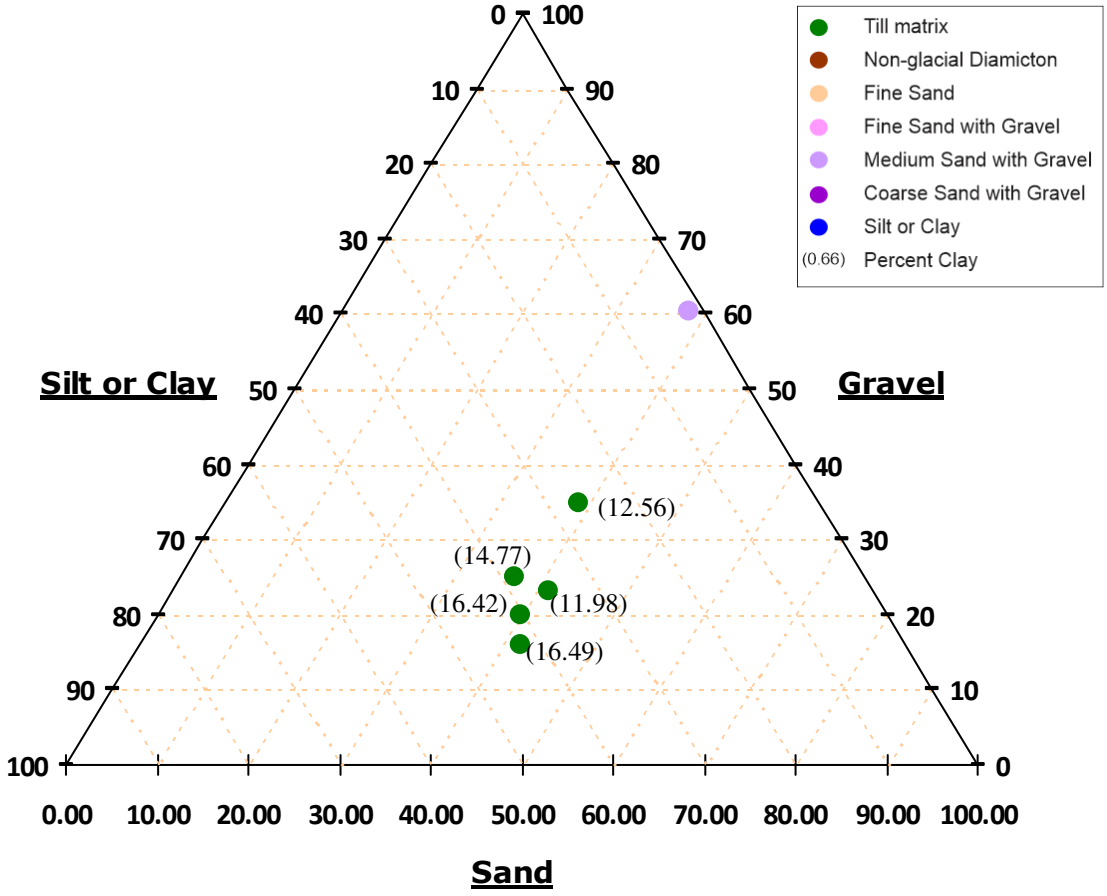
Grain Size Distribution for Samples from Core VTH2014-09
Till matrix
Non-glacial Diamicton
Fine Sand
Fine Sand with Gravel
Medium Sand with Gravel
Coarse Sand with Gravel
Silt or Clay
(0.66) Percent Clay
Silt or Clay
Gravel
Sand
(12.56)
(14.77)
(16.42)
(11.98)
(16.49)
0 100
10 90
20 80
30 70
40 60
50 50
60 40
70 30
80 20
90 10
100 0
0.00 10.00 20.00 30.00 40.00 50.00 60.00 70.00 80.00 90.00 100.00

(f)

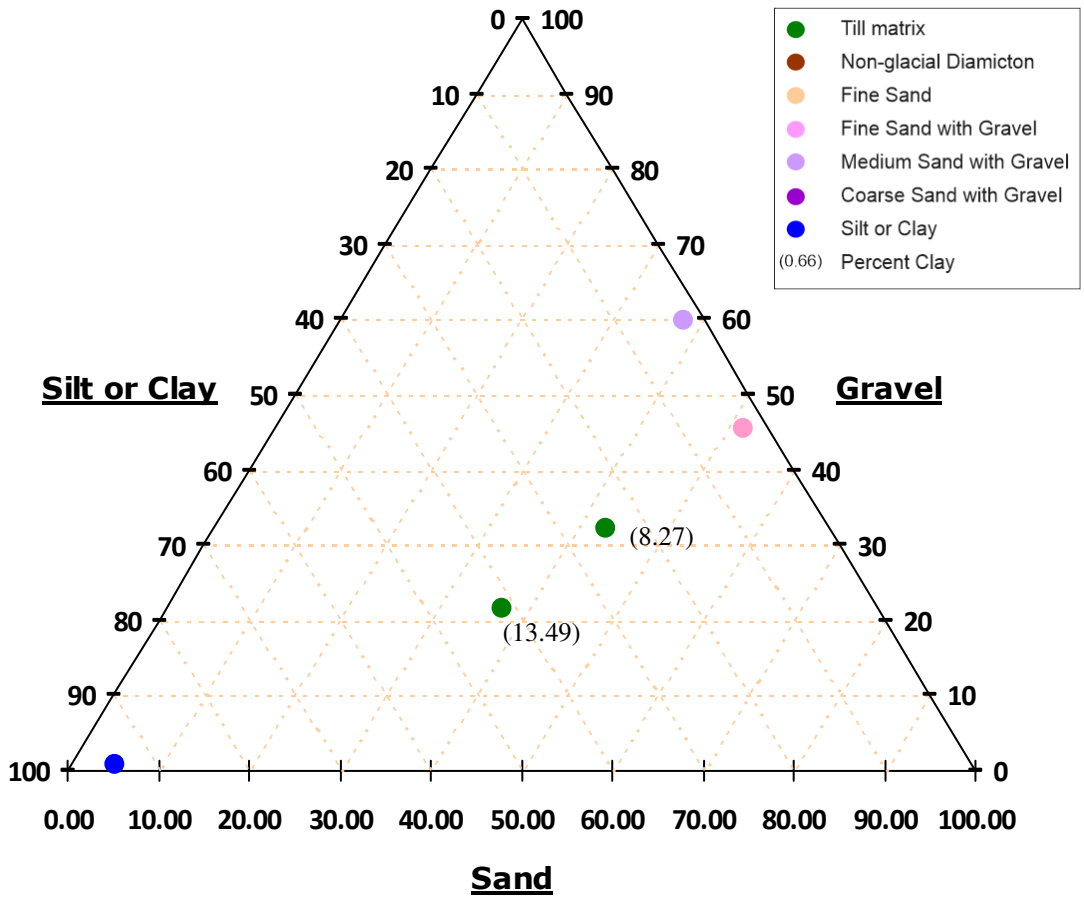
Grain Size Distribution for Samples from Core VTH2014-10
Till matrix
Non-glacial Diamicton
Fine Sand
Fine Sand with Gravel
Medium Sand with Gravel
Coarse Sand with Gravel
Silt or Clay
(0.66) Percent Clay
Silt or Clay
Gravel
Sand
(8.27)
(13.49)
0 100
10 90
20 80
30 70
40 60
50 50
60 40
70 30
80 20
90 10
100 0
0.00 10.00 20.00 30.00 40.00 50.00 60.00 70.00 80.00 90.00 100.00

(g)

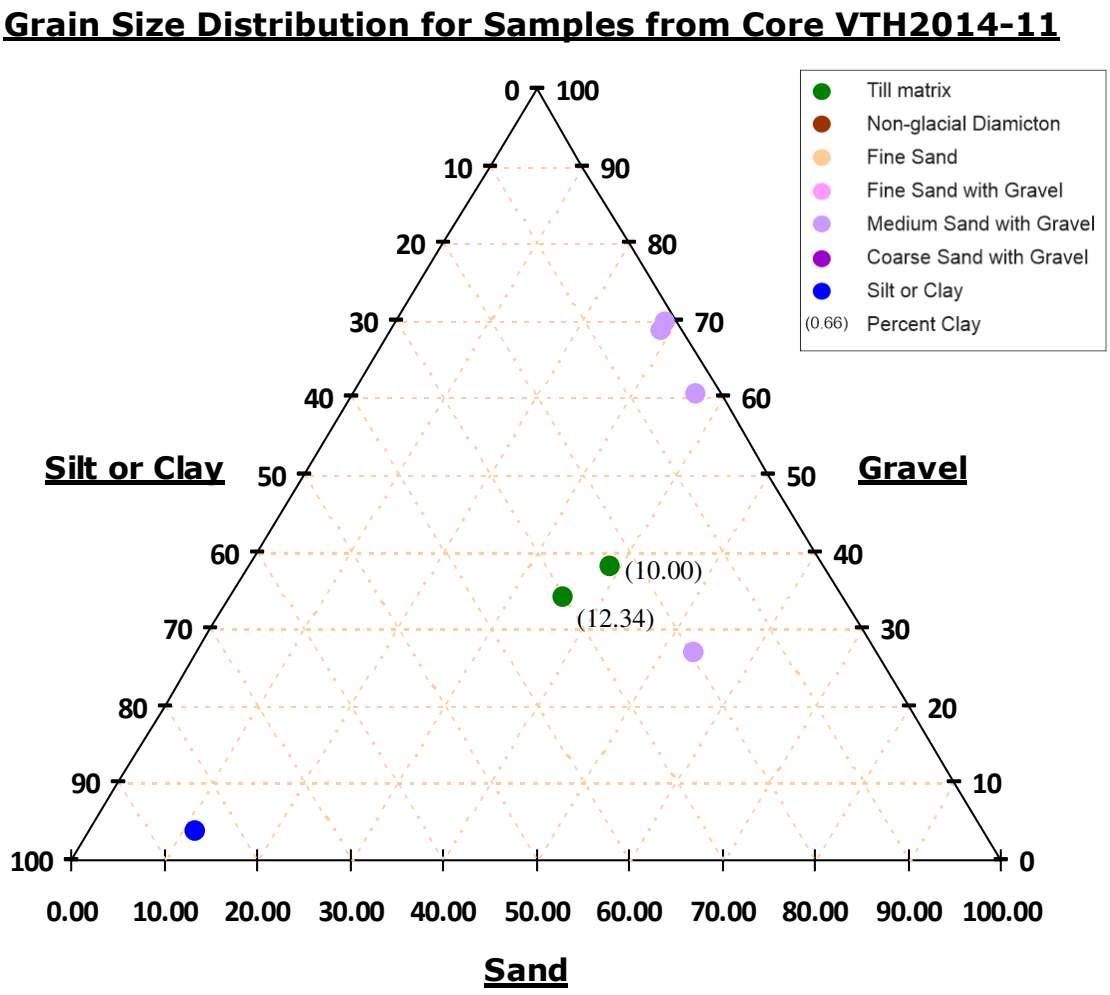
Grain Size Distribution for Samples from Core VTH2014-11
Till matrix
Non-glacial Diamicton
Fine Sand
Fine Sand with Gravel
Medium Sand with Gravel
Coarse Sand with Gravel
Silt or Clay
(0.66) Percent Clay
Silt or Clay
Gravel
Sand
(10.00)
(12.34)
0 100
10 90
20 80
30 70
40 60
50 50
60 40
70 30
80 20
90 10
100 0
0.00 10.00 20.00 30.00 40.00 50.00 60.00 70.00 80.00 90.00 100.00

(h)

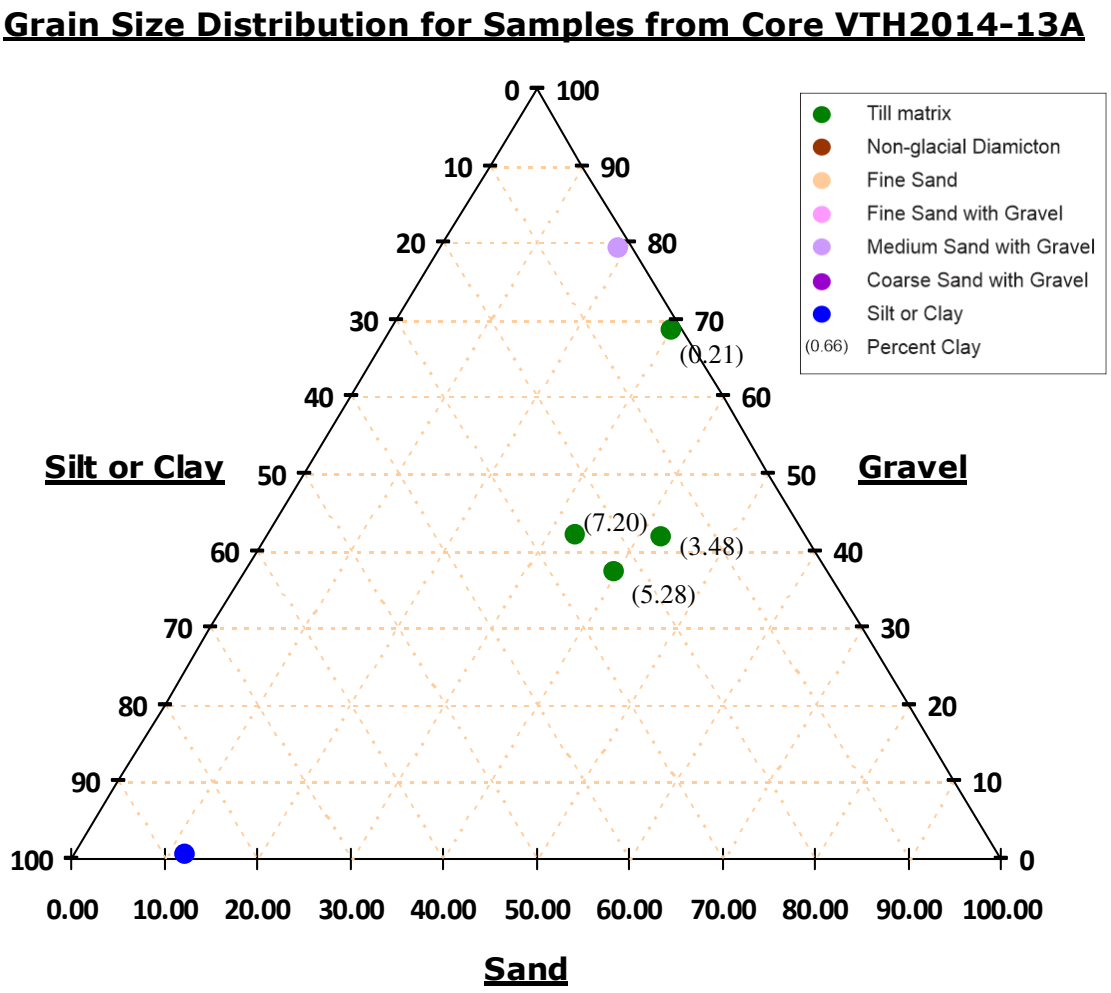
Grain Size Distribution for Samples from Core VTH2014-13A
Till matrix
Non-glacial Diamicton
Fine Sand
Fine Sand with Gravel
Medium Sand with Gravel
Coarse Sand with Gravel
Silt or Clay
(0.66) Percent Clay
(0.21)
(7.20)
(3.48)
(5.28)
Silt or Clay
Gravel
Sand
0 100
10 90
20 80
30 70
40 60
50 50
60 40
70 30
80 20
90 10
100 0
0.00 10.00 20.00 30.00 40.00 50.00 60.00 70.00 80.00 90.00 100.00

(i)

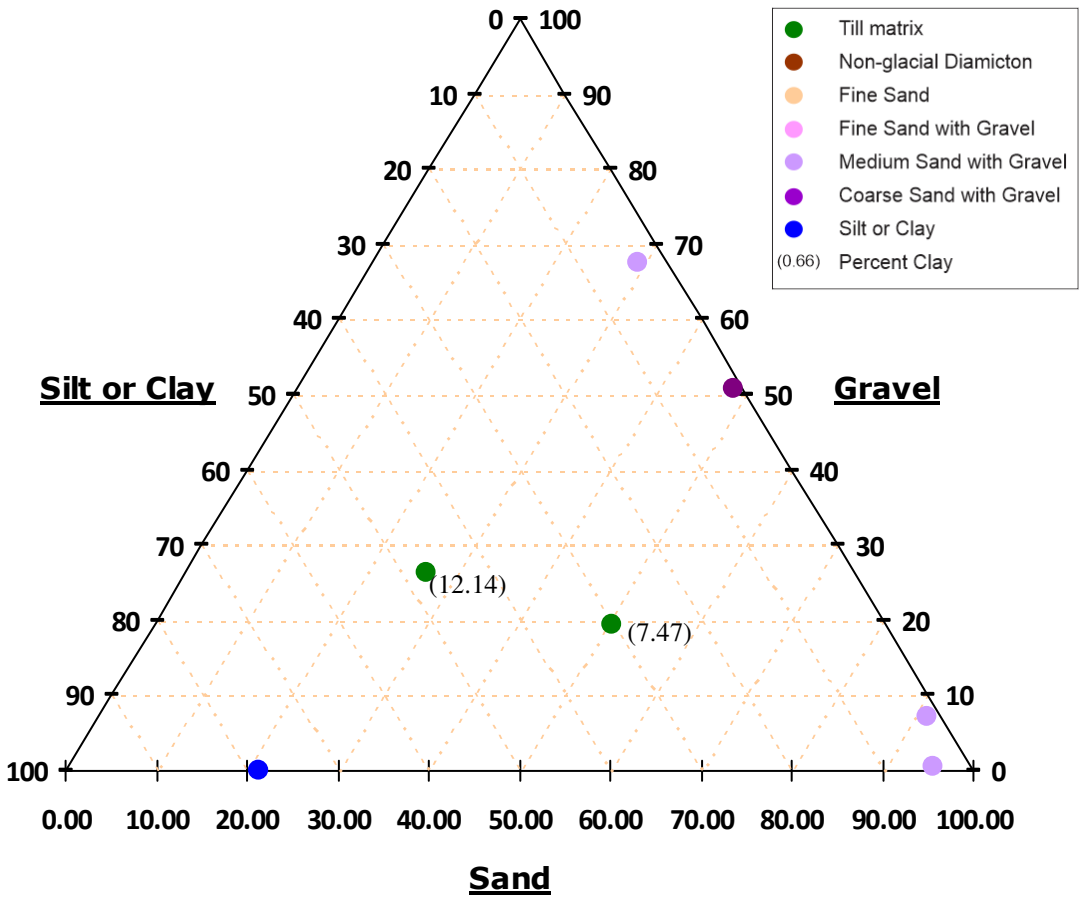
Grain Size Distribution for Samples from Core JA16-001
Till matrix
Non-glacial Diamicton
Fine Sand
Fine Sand with Gravel
Medium Sand with Gravel
Coarse Sand with Gravel
Silt or Clay
(0.66) Percent Clay
Silt or Clay
Gravel
Sand
(12.14)
(7.47)
0 100
10 90
20 80
30 70
40 60
50 50
60 40
70 30
80 20
90 10
100 0
0.00 10.00 20.00 30.00 40.00 50.00 60.00 70.00 80.00 90.00 100.00

(j)

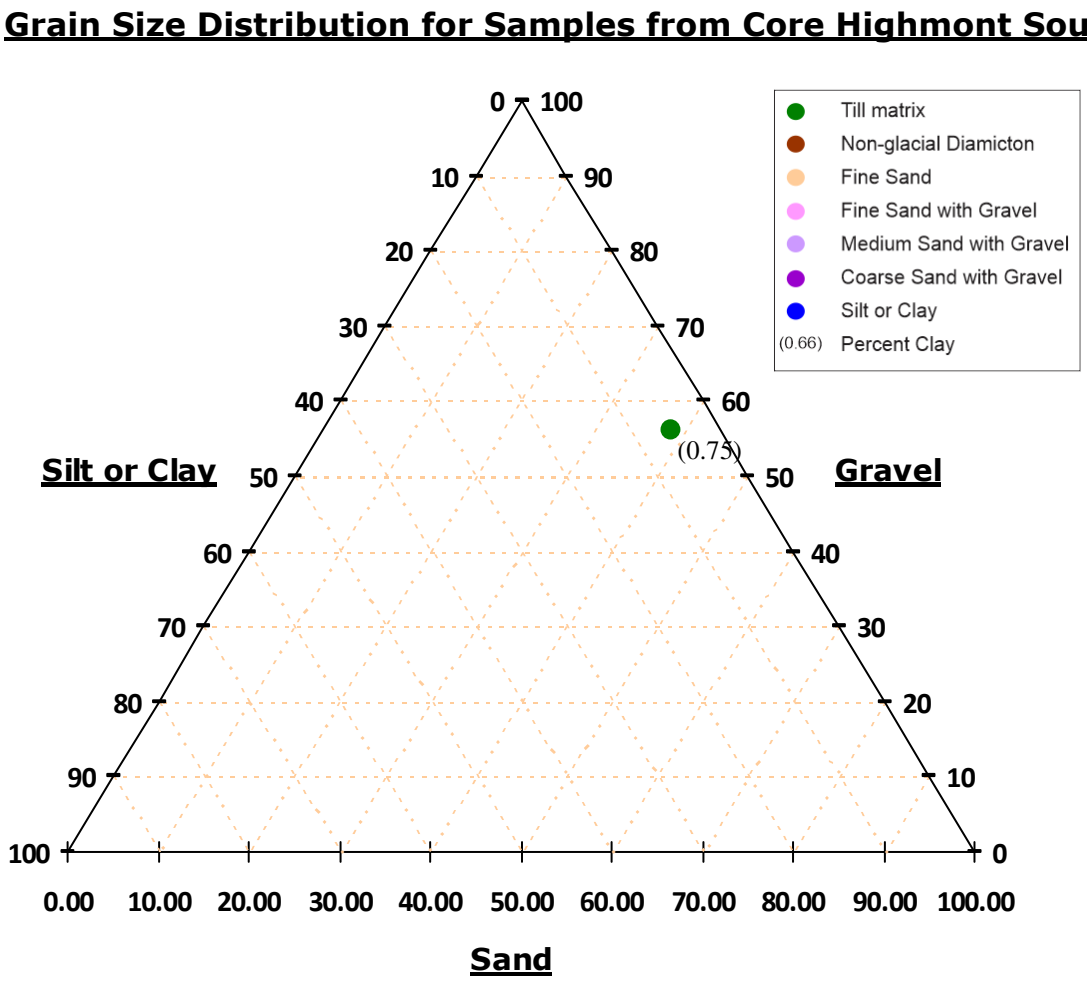

Figure B.8 Ternary diagrams for samples from (a) VTH2014-03, (b) VTH2014-06, (c) VTH2014-07, (d) VTH2014-08, (e) VTH2014-09, (f) VTH2014-10, (g) VTH2014-11, (h) VTH2014-13A, (i) JA16-001 and (j) Highmont South.

A summary of the petrophysical property values and the average composition for the main stratigraphic sub-units at Highland Valley is shown in **Table B.3**.

Table B.3 Petrophysical property values and grain size data for the major units of the unconsolidated sediment stratigraphy at Highland Valley.

Unit / Sub-Unit	Mean Dry Bulk Density (g/cm^3)	Mean Grain Density Values (g/cm^3)	Porosity Values (%)	Mean Magnetic Susceptibility Values (SI)	Resistivity Values (Ohm·m)	Chargeability Values (ms)	Mean % Gravel	Mean % Sand	Mean % Silt and Clay
Non-glacial diamicton in 1a	2.2	2.684 2.651 2.714 2.695 2.705	20.0 10.5 21.2 14.6 13.0	8.15E-06 1.26E-05 2.91E-05 2.10E-05 3.49E-05	187 54 32 8	5.9 4.4 11.5 4.0	23.7	61.0	15.3
Silts and clays in 1a	2.2	2.394 2.582 2.555 2.426	19.2 27.6 37.4 22.3	3.61E-05 5.07E-05 5.73E-05 5.01E-05	19 10 9 12	4.2 1.9 4.2 4.5	8.1	41.3	50.6
Coal in 1a	2.0	–	–	–	–	–	–	–	–
Pebbles and cobbles in 1a	2.4	–	13.0	–	–	–	–	–	–
Sand and gravel in 1a	2.1	2.750	47.9	1.69E-02	14	3.1	–	–	–
1b	2.2	2.726	18.3	7.47E-03	40	2.8	–	–	–
2a	2.5	2.762	15.3	1.58E-03	19	6.9	52.3	24.9	22.8
2b	1.9	–	–	–	–	–	56.1	38.7	5.2
3a	1.5	2.794	47.9	8.10E-04	32	2.6	0.02	0.5	99.5

3b	1.8	–	–	–	–	–	35.1	55.2	9.8
3c	–	–	–	–	–	–	27.9	66.8	5.3
3d	1.8	2.741 2.725	32.5 27.1	2.52E-03 1.51E-03	13 14	1.9 2.7	12.2	42.9	44.9
3e	2.2	2.683	–	1.21E-04 3.56E-03	–	–	42.2	54.2	3.6
3f	2.0	2.740	22.5	1.74E-03	84	6.1	48.3	47.5	4.2
4a	2.4	2.784	–	2.26E-03	–	–	36.9	34.5	28.6
4b	1.9	–	–	–	–	–	51.0	40.4	8.6
4c	2.2	2.801	22.9	6.55E-03	26	20.6	34.6	37.6	27.8
5a	3.7	–	–	–	–	–	26.9	53.7	19.5
5b	2.3	2.779 2.794 2.656	10.0 29.3 22.5	5.71E-03 8.95E-03 5.40E-03	20 21	14.0 3.5	32.2	34.3	33.4
5c	2.4	–	–	–	–	–	12.2	65.3	22.5
5d	2.2	–	–	–	–	–	41.8	35.7	22.5
5f	1.9	–	–	–	–	–	–	–	–
6	2.2	–	–	–	–	–	–	–	–
Rockfall pebbles and cobbles at bottom of core JA16-001 (**Figure 3.14**)	–	2.720	–	1.11E-02	–	–	–	–	–
Bottom clay interlayering with	1.768	–	–	–	–	–	–	–	–

rockfall pebbles & cobbles at bottom of core JA16-001 (**Figure 3.14**)									
Non-glacial diamicton at bottom of core JA16-001 (**Figure 3.14**)	2.137	2.707	44.8 26.7	2.47E-03	11 19	2.7 6.2	–	–	–
Lower subglacial till at core JA16-001 (**Figure 3.14**)	1.945	–	–	–	–	–	–	–	–
Bottom thick ice-contact lake clay and silt at core JA16-001 (**Figure 3.14**)	1.868	2.955	52.9	1.54E-03	9	5.6	–	–	–
Sediment gravity flow sand and gravel at core JA16-001 (**Figure 3.14**)	–	–	–	–	–	–	37.3	60.4	2.3
Sediment gravity flow pebbles and cobbles at core JA16-001 (**Figure 3.14**)	–	2.780	–	1.32E-02	–	–	–	–	–
Top thick lacustrine silt at core JA16-001 (**Figure 3.14**)	1.690581	2.848	45.2	9.08E-03	–	–	0.0	21.4	78.6
Top thick subglacial till at core JA16-001 (**Figure 3.14**)	1.894	2.747	27.0	9.53E-03	63	3.7	22.9	38.6	38.5
Top outwash pebbles and cobbles at core JA16-001 (**Figure 3.14**)	–	2.710	–	2.03E-02	–	–	–	–	–

Top outwash sand at core JA16-001 (**Figure 3.14**)	1.561	–	–	–	–	–	50.7	48.3	1.0

Macrofossil Analysis

Macrofossil analysis was done at Université Laval on two samples. These are both from a bed of silty clay interpreted to be glaciolacustrine within the sediment gravity flow unit (elevation range: 1138.75 to 1140.25 metres) of core VTH2014-03. The organic matter in both is made up entirely of moderately decomposed brown moss (**Figure B.9**). The top sample contained fragments of shells as well as unidentified, crumbly, cylindrical structures (**Figure B.10A**). The bottom sample contained small pieces of charcoal (**Figure B.10B**). The organic matter for one of the samples was dated and found to have a ^{14}C age of >52,800 years before present.

Figure B.9 Moderately decomposed brown moss making up the organic matter in the glaciolacustrine silty clay samples from core VTH2014-03.

(A) (B)

Figure B.10 Fragments of shells as well as unidentified, crumbly, cylindrical structures in the top sample (A), and charcoal in the bottom sample (B) of glaciolacustrine silty clay from core VTH2014-03.

Pebble Lithology

(a)

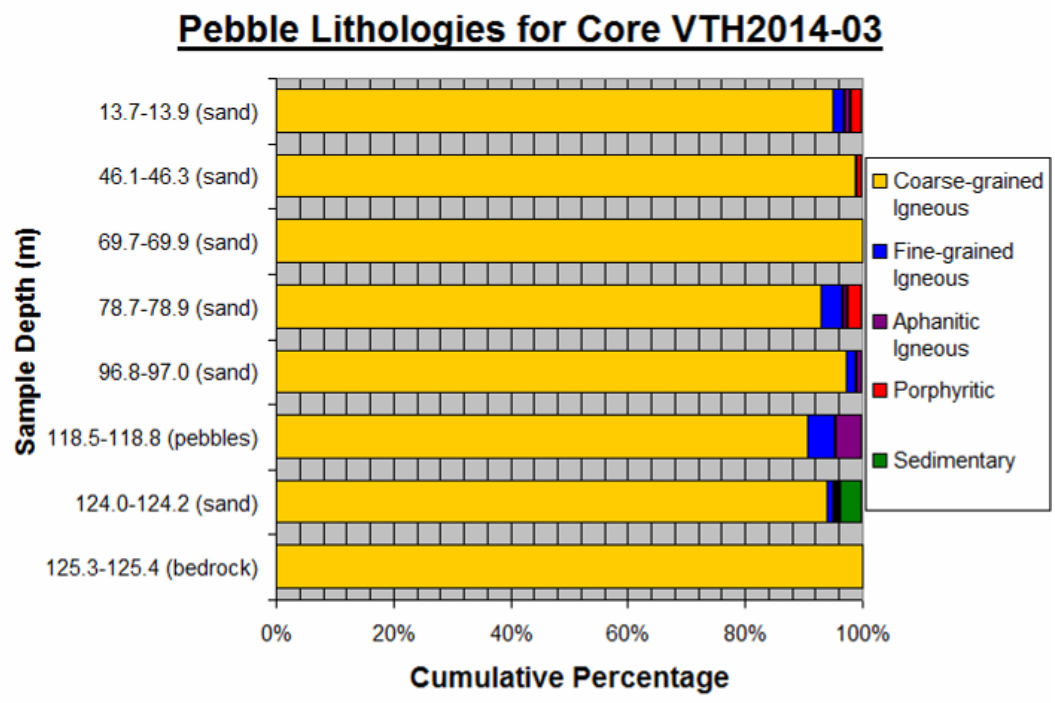

(b)

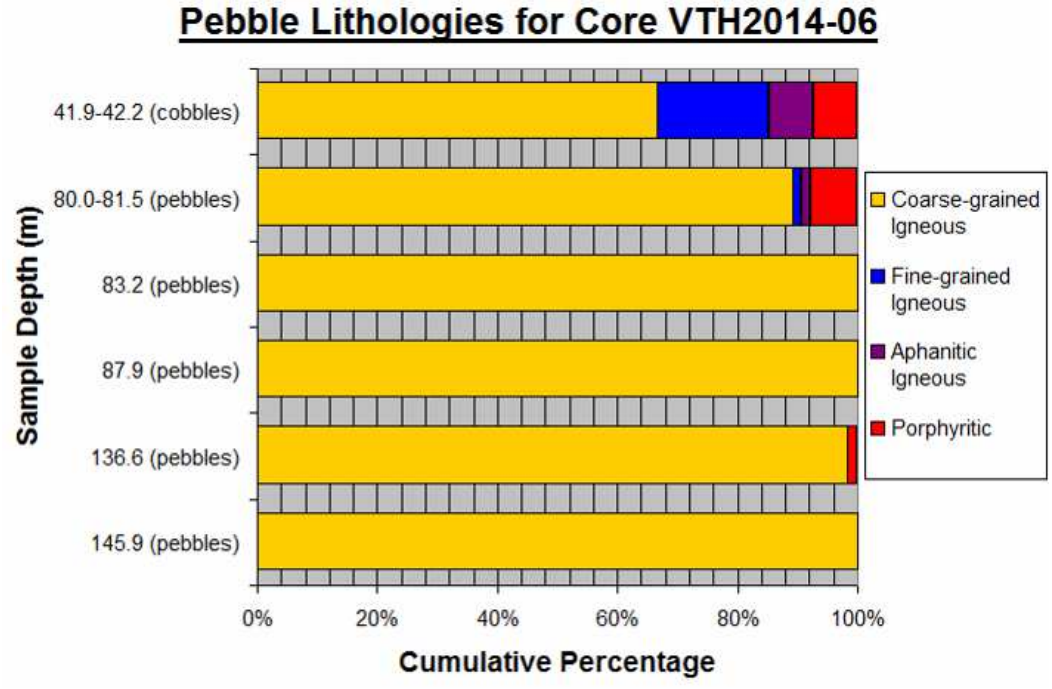

(c)

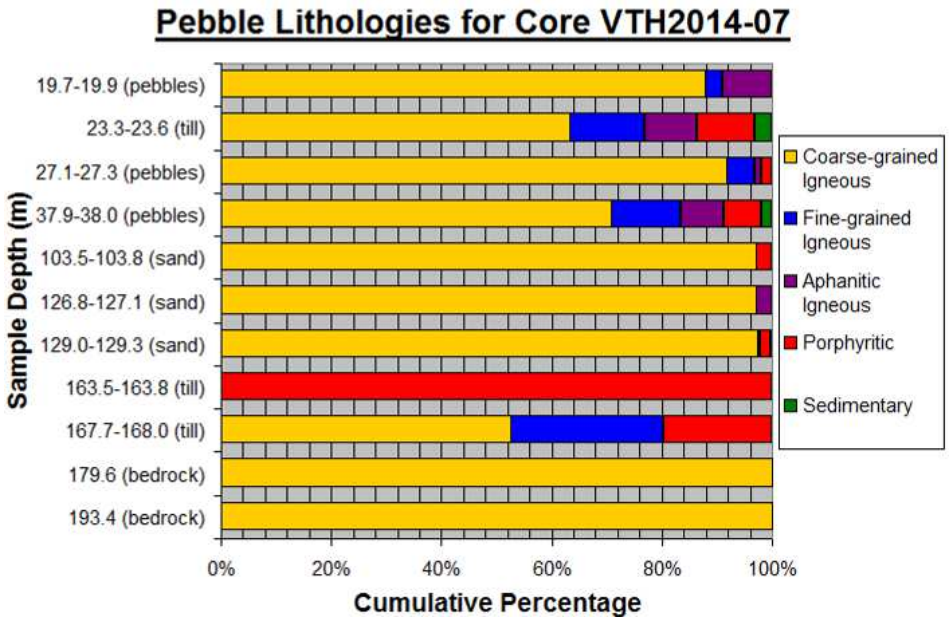
Pebble Lithologies for Core VTH2014-07
19.7-19.9 (pebbles)
23.3-23.6 (till)
27.1-27.3 (pebbles)
37.9-38.0 (pebbles)
103.5-103.8 (sand)
126.8-127.1 (sand)
129.0-129.3 (sand)
163.5-163.8 (till)
167.7-168.0 (till)
179.6 (bedrock)
193.4 (bedrock)
Sample Depth (m)
0%
20%
40%
60%
80%
100%
Cumulative Percentage
Coarse-grained Igneous
Fine-grained Igneous
Aphanitic Igneous
Porphyritic
Sedimentary

(d)

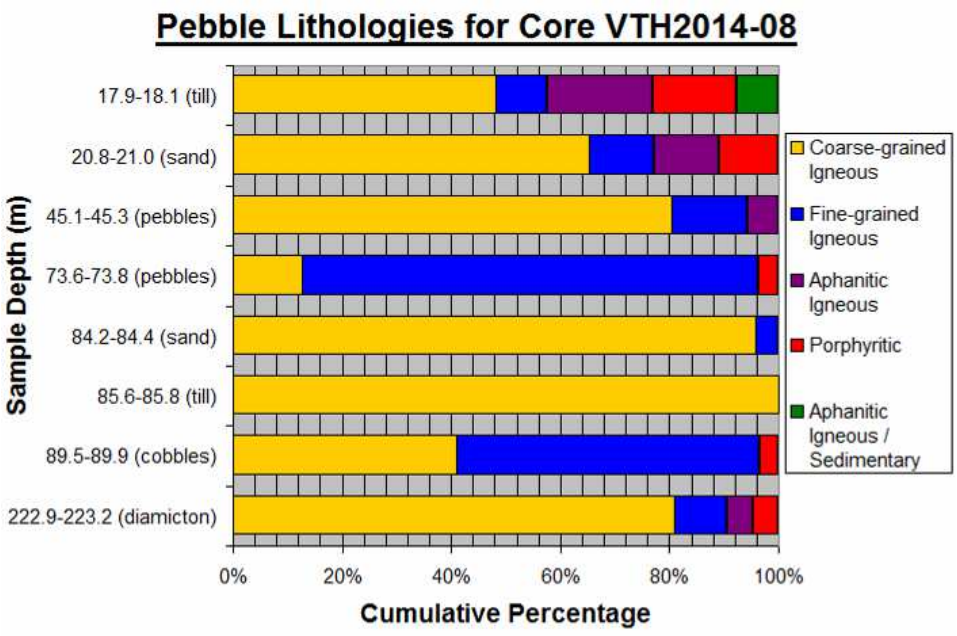
Pebble Lithologies for Core VTH2014-08
17.9-18.1 (till)
20.8-21.0 (sand)
45.1-45.3 (pebbles)
73.6-73.8 (pebbles)
84.2-84.4 (sand)
85.6-85.8 (till)
89.5-89.9 (cobbles)
222.9-223.2 (diamicton)
Sample Depth (m)
0%
20%
40%
60%
80%
100%
Cumulative Percentage
Coarse-grained Igneous
Fine-grained Igneous
Aphanitic Igneous
Porphyritic
Aphanitic Igneous / Sedimentary

(e)

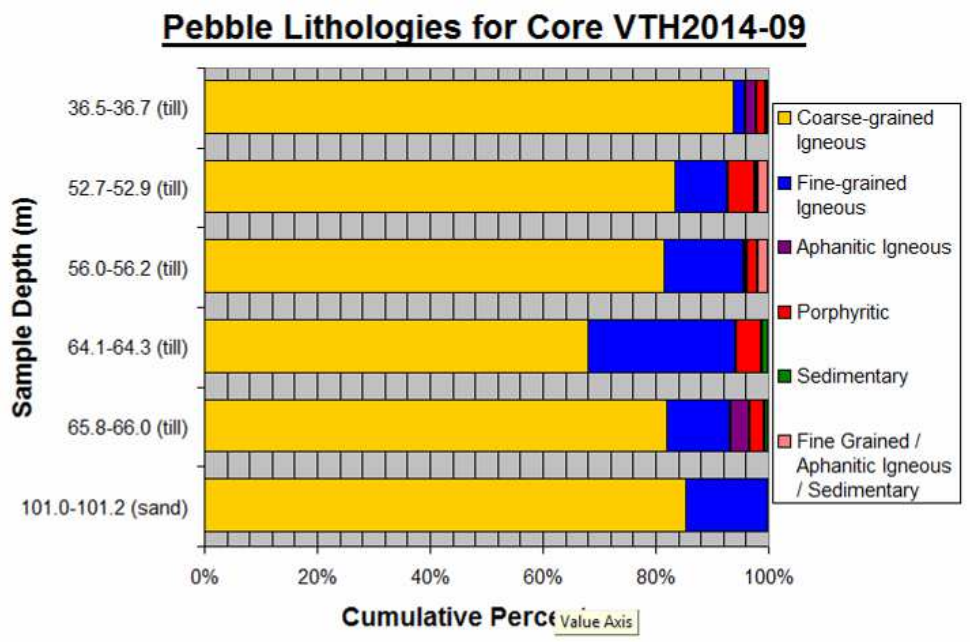
Pebble Lithologies for Core VTH2014-09
Sample Depth (m)
36.5-36.7 (till)
52.7-52.9 (till)
56.0-56.2 (till)
64.1-64.3 (till)
65.8-66.0 (till)
101.0-101.2 (sand)
0%
20%
40%
60%
80%
100%
Cumulative Perce
Value Axis
Coarse-grained Igneous
Fine-grained Igneous
Aphanitic Igneous
Porphyritic
Sedimentary
Fine Grained / Aphanitic Igneous / Sedimentary

(f)

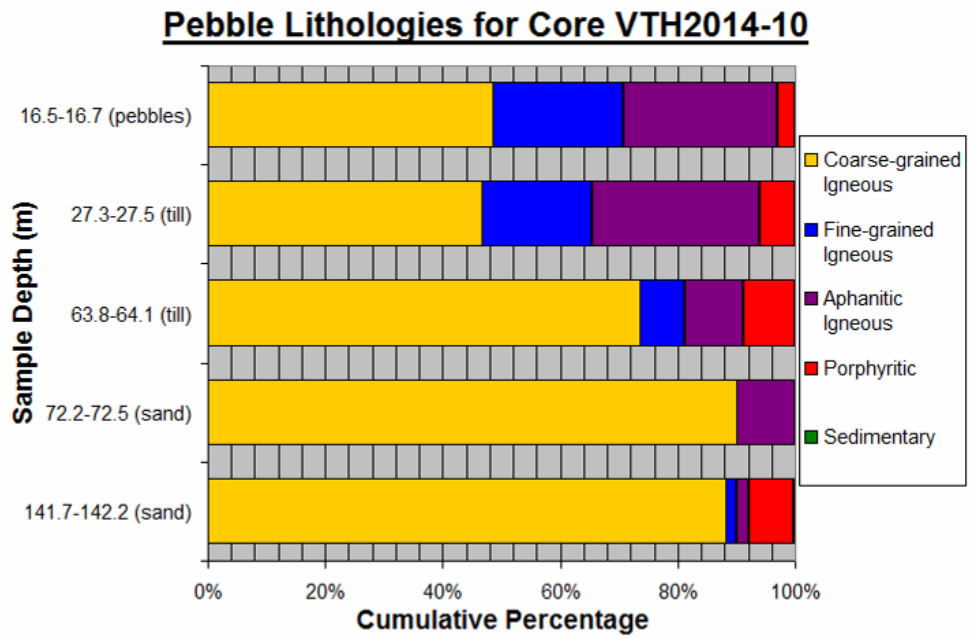
Pebble Lithologies for Core VTH2014-10
Sample Depth (m)
16.5-16.7 (pebbles)
27.3-27.5 (till)
63.8-64.1 (till)
72.2-72.5 (sand)
141.7-142.2 (sand)
0%
20%
40%
60%
80%
100%
Cumulative Percentage
Coarse-grained Igneous
Fine-grained Igneous
Aphanitic Igneous
Porphyritic
Sedimentary

(g)

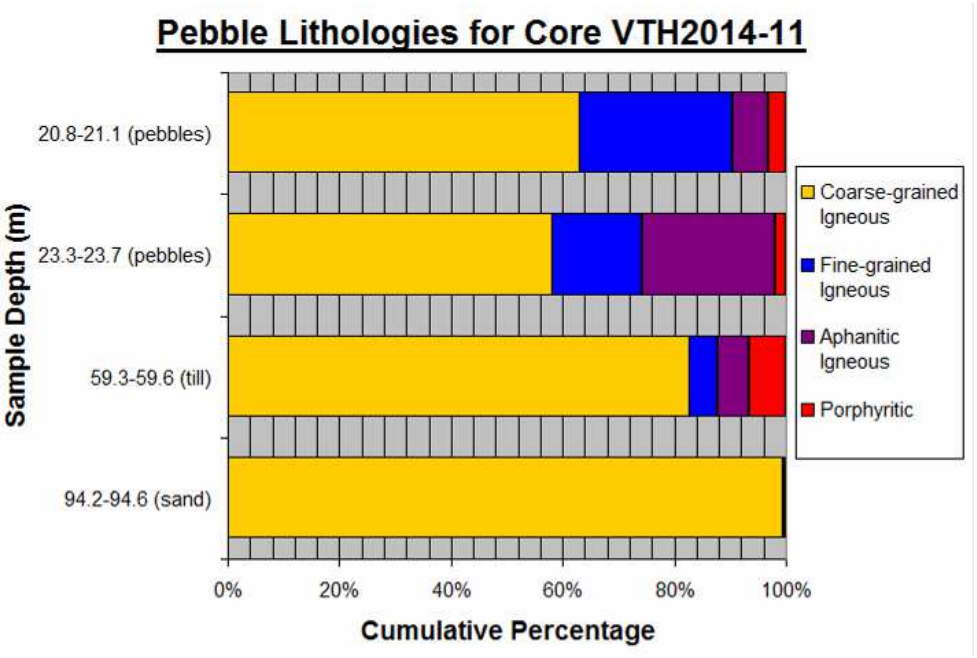

(h)

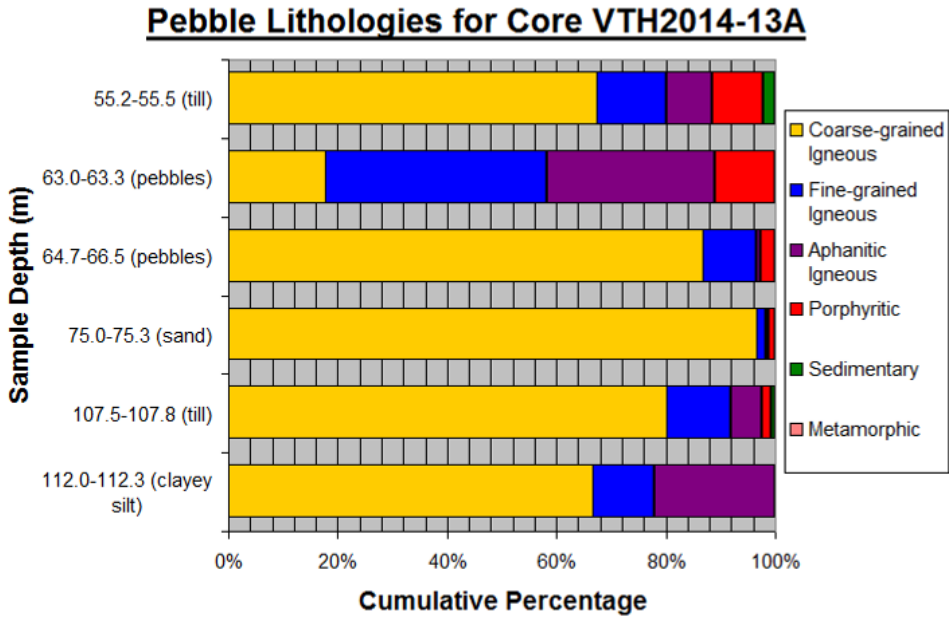

B.11 Relative proportions of the different lithology types making up the samples from core (a) VTH2014-03, (b) VTH2014-06, (c) VTH2014-07, (d) VTH2014-08, (e) VTH2014-09, (f) VTH2014-10, (g) VTH2014-11 and (h) VTH2014-13A.

Table B.4 Description of the ten recurring lithology types found in the core samples.

Lithology Type	**Description**
Oxidized felsic coarse-grained igneous	• orange-tinted, white or yellow felsic-coloured • mostly irregularly-shaped, subhedral, coarse quartz & feldspar • minor amount of irregularly-shaped, subhedral, fine-to-medium black minerals (biotite, amphiboles and/or pyroxenes)
Non-oxidized felsic coarse-grained igneous	• white or yellow felsic-coloured • mostly irregularly-shaped, subhedral, coarse quartz & feldspar • minor amount of irregularly-shaped, subhedral, fine-to-medium black minerals (biotite, amphiboles and/or pyroxenes)
Oxidized light intermediate coarse-grained igneous	• orange-tinted, white or pink light intermediate-coloured • mostly irregularly-shaped, subhedral, coarse quartz & feldspar • significant amount of irregularly-shaped, subhedral, fine-to-medium black minerals (biotite, amphiboles and/or pyroxenes)
Non-oxidized light intermediate coarse-grained igneous	• white or pink intermediate-coloured • mostly irregularly-shaped, subhedral, coarse quartz & feldspar • significant amount of irregularly-shaped, subhedral, fine-to-medium black minerals (biotite, amphiboles and/or pyroxenes)
Oxidized dark intermediate coarse-grained igneous	• orange-tinted, white or pink and black dark intermediate-coloured • about half irregularly-shaped, subhedral, coarse quartz & feldspar • about half irregularly-shaped, subhedral, fine-to-medium black minerals (biotite, amphiboles and/or pyroxenes)
Non-oxidized dark intermediate coarse-grained igneous	• white or pink and black dark intermediate-coloured • about half irregularly-shaped, subhedral, coarse quartz & feldspar • about half irregularly-shaped, subhedral, fine-to-medium black minerals (biotite, amphiboles and/or pyroxenes)
Non-oxidized felsic coarse-grained igneous with varied felsic minerals, slightly amorphous-looking	• coloured many shades of felsic (white, yellows, pinks...) • mostly irregularly-shaped or rounded, anhedral, fine to coarse quartz, feldspar and possibly other felsic minerals • minor amount of irregularly-shaped, subhedral, fine-to-medium black minerals (biotite, amphiboles and/or pyroxenes) • slightly amorphous-looking
Non-oxidized intermediate coarse-grained igneous with	• coloured many shades of felsic (white, yellows, pinks...), intermediate-coloured • mostly irregularly-shaped or rounded, anhedral, fine to coarse

varied felsic minerals, slightly amorphous-looking	quartz, feldspar and possibly other felsic minerals • significant amount of irregularly-shaped, subhedral, fine-to-medium black minerals (biotite, amphiboles and/or pyroxenes) • slightly amorphous-looking
Amorphous igneous	• white with grey flecks and tiny streaks; felsic-coloured; slightly orange-mottled • mostly amorphous quartz & feldspar • minor amount of irregularly-shaped, subhedral, aphanitic-to-medium grained black minerals (biotite, amphiboles and/or pyroxenes) • minor amount of fine-grained epidote grains and pistachio-coloured staining
Porphyritic with black tabular phenocrysts and grey groundmass	• elongated or tabular, euhedral, fine-to-medium black phenocrysts • very fine-grained grey groundmass

Appendix C - Indicator Mineral, Hyperspectral and Geochemical Analyses

Table C.1 Location & depth & elevation intervals & description of unit for each sample with indicator mineral & hyperspectral analyses done.

Sample ID	Source	Depth Interval (m)	Elevation of Sample (masl)	Unit
AR-16-033	Core VTH2014-03	78.7-78.9	1095.1-1094.9	course sand with pebbles & granules
AR-16-047	Core VTH2014-08	84.2-84.4	1180.4-1180.2	medium sand with pebbles & granules
AR-16-065	Core VTH2014-10	27.3-27.5	1232.1-1231.9	till; silty fine sand matrix with granules to cobbles
AR-16-075	Core VTH2014-10	63.8-64.1	1195.6-1195.4	till; silty fine sand matrix with granules to cobbles
AR-16-095	Core VTH2014-10	141.7-142.2	1117.7-1117.2	sand with granules
AR-16-224	Core VTH2014-11	59.3-59.6	1208.6-1208.3	diamicton; silty clay matrix with granules to cobbles
AR-16-229	Core VTH2014-11	94.2-94.6	1173.7-1173.3	sand with granules to cobbles
AR-16-202	Core VTH2014-13A	42.0-42.3	1203.4-1203.1	diamicton; silt matrix with granules to cobbles
AR-16-207	Core VTH2014-13A	84.2-84.5	1161.2-1160.9	sand with granules
AR-16-290	Core JA16-001	31.6-31.9	1178.1-1177.8	diamicton; silt matrix with granules to cobbles

AR-16-291	Core JA16-001	40.5-40.8	1169.2-1168.9	diamicton; clay matrix with granules to pebbles
AR-16-300	Core JA16-001	81.4-81.7	1128.3-1128.0	medium to coarse sand with granules
AR-16-116	Highmont South excavation	~45-70m from surface	1586-1561	till; silty fine sand matrix with granules to boulders

Table C.2 Location & depth & elevation intervals & description of unit for each sample with geochemical analysis done.

Sample ID	Source	Depth Interval (m)	Elevation of Sample (masl)	Unit
AR-16-024	Core VTH2014-03	4.6-4.8	1169.2-1169.0	till; clayey fine sand matrix with granules to pebbles
AR-16-027	Core VTH2014-03	22.3-22.5	1151.5-1151.3	medium to coarse sand with granules
AR-16-033	Core VTH2014-03	78.7-78.9	1095.1-1094.9	course sand with pebbles & granules
AR-16-122	Core VTH2014-07	23.3-23.6	1238.8-1238.5	till; silty fine sand matrix with granules to cobbles
AR-16-127	Core VTH2014-07	48.8-49.1	1213.3-1213.0	till; clayey, silty fine sand matrix with granules to cobbles
AR-16-159	Core VTH2014-07	68.4-68.7	1193.7-1193.4	till; silty fine sand matrix with granules to cobbles
AR-16-166	Core VTH2014-07	126.8-127.1	1135.3-1135.0	sand with granules to cobbles
AR-16-015	Core VTH2014-08	17.9-18.1	1246.7-1246.5	till; silt matrix with granules to

				cobbles
AR-16-016	Core VTH2014-08	20.8-21.0	1243.8-1243.6	clayey silty medium sand with granules to pebbles
AR-16-020	Core VTH2014-08	57.1-57.3	1207.5-1207.3	till; silty fine sand matrix with granules to cobbles
AR-16-047	Core VTH2014-08	84.2-84.4	1180.4-1180.2	medium sand with pebbles & granules
AR-16-048	Core VTH2014-08	85.6-85.8	1179.0-1178.8	till; clayey silt matrix with granules to pebbles
AR-15-001	Core VTH2014-09	36.5-36.7	1221.8-1221.6	till; fine sandy clay matrix with granules to cobbles
AR-15-003	Core VTH2014-09	56.0-56.2	1202.3-1202.1	till; fine sandy clay matrix with granules to cobbles
AR-16-002	Core VTH2014-09	101.0-101.2	1157.3-1157.1	sand with granules to pebbles
AR-16-061	Core VTH2014-10	15.3-15.5	1244.1-1243.9	till; silty fine sand matrix with granules to cobbles
AR-16-065	Core VTH2014-10	27.3-27.5	1232.1-1231.9	till; silty fine sand matrix with granules to cobbles
AR-16-075	Core VTH2014-10	63.8-64.1	1195.6-1195.4	till; silty fine sand matrix with granules to cobbles
AR-16-090	Core VTH2014-10	105.9-106.2	1153.5-1153.2	fine sand with granules to cobbles
AR-16-095	Core VTH2014-10	141.7-142.2	1117.7-1117.2	sand with granules
AR-16-218	Core VTH2014-11	21.2-21.5	1246.7-1246.4	till; silt matrix with granules to

				cobbles
AR-16-221	Core VTH2014-11	48.2-48.5	1219.7-1219.4	sand with granules to pebbles
AR-16-224	Core VTH2014-11	59.3-59.6	1208.6-1208.3	diamicton; silty clay matrix with granules to cobbles
AR-16-229	Core VTH2014-11	94.2-94.6	1173.7-1173.3	sand with granules to cobbles
AR-16-202	Core VTH2014-13A	42.0-42.3	1203.4-1203.1	diamicton; silt matrix with granules to cobbles
AR-16-203	Core VTH2014-13A	55.2-55.5	1190.2-1189.9	till; silt matrix with granules to cobbles
AR-16-207	Core VTH2014-13A	84.2-84.5	1161.2-1160.9	sand with granules
AR-16-290	Core JA16-001	31.6-31.9	1177.8-1178.1	diamicton; silt matrix with granules to cobbles
AR-16-291	Core JA16-001	40.5-40.8	1168.9-1169.2	diamicton; clay matrix with granules to pebbles
AR-16-300	Core JA16-001	81.4-81.7	1128.0-1129.3	medium to coarse sand with granules
AR-16-303	Core JA16-001	113.1-113.4	1096.6-1096.3	medium & sand with granules to cobbles
AR-16-116	Highmont South excavation	~45-70m from surface	1561-1586	till; silty fine sand matrix with granules to boulders
AR-16-271	Core DH-15-GG	53.7-54.0	1154.6-1154.3	lithified till; granules to cobbles

Indicator Mineral Results

Table C.3 Lab report of indicator mineral analysis from Overburden Drilling Management Limited.

(a)

Gold Grain Summary

Client: University of Waterloo
File Name: 20177410 - University of Waterloo - Reman - AR16 - PCIM - February 2017
Total Number of Samples in this Report: 13
ODM Batch Number(s): 7410

Sample Number	Number of Visible Gold Grains				Nonmag HMC Weight (g)*	Calculated PPB Visible Gold in HMC			
	Total	Reshaped	Modified	Pristine		Total	Reshaped	Modified	Pristine
AR-16-033	0	0	0	0	3.6	0	0	0	0
AR-16-047	1	1	0	0	3.2	310	310	0	0
AR-16-065	0	0	0	0	5.6	0	0	0	0
AR-16-075	2	2	0	0	8.4	51	51	0	0
AR-16-095	0	0	0	0	2.0	0	0	0	0
AR-16-116	0	0	0	0	15.2	0	0	0	0
AR-16-202	0	0	0	0	8.4	0	0	0	0
AR-16-207	0	0	0	0	3.2	0	0	0	0
AR-16-224	2	2	0	0	8.8	43	43	0	0
AR-16-229	0	0	0	0	4.0	0	0	0	0
AR-16-290	3	3	0	0	9.2	49	49	0	0
AR-16-291	2	2	0	0	6.4	12	12	0	0
AR-16-300	0	0	0	0	6.0	0	0	0	0

(b)

Detailed Gold Grain Data

Client: University of Waterloo
File Name: 20177410 - University of Waterloo - Reman - AR16 - PCIM - February 2017
Total Number of Samples in this Report: 13
ODM Batch Number(s): 7410

Sample Number	Dimensions (µm)			Number of Visible Gold Grains				Nonmag HMC Weight* (g)	Calculated V.G. Assay in HMC (ppb)	Metallic Minerals in Pan Concentrate
	Thickness	Width	Length	Reshaped	Modified	Pristine	Total			
AR-16-033	No Visible Gold									~300 grains pyrite (25-250µm).
AR-16-047	18 C	75	100	1			1		310	~50 grains pyrite (25-150µm).
							1	3.2	310	
AR-16-065	No Visible Gold									~200 grains pyrite (25-250µm).
AR-16-075	8 C	25	50	1			1		9	~200 grains pyrite (25-250µm).
	15 C	25	125	1			1		42	~1000 grains marcasite (25-100µm).
							2	8.4	51	
AR-16-095	No Visible Gold									~100 grains pyrite (25-200µm).
AR-16-116	No Visible Gold									~20 grains pyrite (25-100µm).
AR-16-202	No Visible Gold									1 grain pyrite (100µm).
AR-16-207	No Visible Gold									~500 grains pyrite (25-250µm).

AR-16-224	5	C	25	25	1	1		3	~5000 grains metallic grease
	13	C	50	75	1	1		41	(contamination; 25-75µm).
						2	8.8	43	SEM check: Copper + molybdenum + tungsten carbide grease (drill contamination).
AR-16-229	No Visible Gold								~10 grains pyrite (25-150µm).
AR-16-290	5	C	25	25	1	1		3	SEM checks: 3 of ~500 chalcocite
	8	C	25	50	1	1		8	versus Fe-oxide candidates = 3
	13	C	50	75	1	1		39	chalcocite (50-250µm). Note: Chalcocite
						3	9.2	49	may variably include covallite and/or bornite.
									~200 grains metallic grease (drill contamination; 25-50µm).
AR-16-291	3	C	15	15	1	1		1	~500 grains pyrite (25-250µm).
	8	C	25	50	1	1		11	~20 grains metallic grease (drill
						2	6.4	12	contamination; 25-50µm).
AR-16-300	No Visible Gold								~1000 grains pyrite (25-500µm). ~20 grains brass (75-200µm; drill contamination).

(c)

PLATINUM GROUP MINERALS SUMMARY

Client: University of Waterloo
File Name: 20177410 - University of Waterloo - Reman - AR16 - PCIM - February 2017
Total Number of Samples in this Report: 13
ODM Batch Number(s): 7410

	Observed PGMs*		
Sample Number	Mineral	Number of Grains	Total Grains
AR-16-033	None Observed	0	0
AR-16-047	None Observed	0	0
AR-16-065	None Observed	0	0
AR-16-075	None Observed	0	0
AR-16-095	None Observed	0	0
AR-16-116	None Observed	0	0
AR-16-202	None Observed	0	0
AR-16-207	None Observed	0	0
AR-16-224	None Observed	0	0
AR-16-229	None Observed	0	0
AR-16-290	None Observed	0	0
AR-16-291	None Observed	0	0
AR-16-300	None Observed	0	0

*All samples are oxidized; therefore only native PGE minerals and the most resistant PGE arsenide and antimonide grains (no PGE sulphides or tellurides) are likely to be preserved.

(d)

S.G. >3.2 Porphyry Cu Indicator Mineral Log For Unglaciated Terrains

Client: University of Waterloo
File Name: 20177410 - University of Waterloo - Reman - AR16 - PCIM - February 2017
Total Number of Samples in this Report: 13
ODM Batch Number(s): 7410

	0.25 to 0.5 mm Nonferromagnetic Heavy Mineral Fraction																			
	Sulphie/Arsenide + Related Minerals					Mg/Mn/Al/Cr Minerals										Phosphates				
	>1.0 amp			<1.0 amp		>1.0 amp								<1.0 amp			>1.0 amp				
Sample Number	% Cpy	Misc. Prime PCIMs	% Py	% Gth	% Adr*	Misc. Prime PCIMs	% Mn-oxide	% Red Rutile	% Blond Ttn	% Ase	% Ky / Sil	% Tm	% St	% Ol	% Opx	% Cr	% Ap	% Mz	% Rose Zir	Remarks	Picked Grains
AR-16-033	0	0	Tr (5 gr)	Tr	0	Tr Mn-epidote (11 gr) Tr low-Cr diopside (2 gr)	0	0	0	0	0	0	0	0	0	Tr (5 gr)	0	0	0	Hematite/epidote-titanite assemblage. SEM checks from 0.25-0.5 mm fraction: 10 andradite versus titanite candidates = 10 titanite; 5 chromite candidates = 2 chromite and 3 hercynite (counted as chromite).	0.5-1.0 mm fraction: 2 Mn-epidote 0.25-0.5 mm fraction: 10 titanite resembling andradite 11 Mn-epidote 2 low-Cr diopside 2 chromtie 3 hercynite resembling chromite

AR-16-047	0	0	Tr (1 gr)	Tr	0	Tr Mn-epidote (3 gr)	0	0	0	0	0	0	0	0	0	Tr (2 gr)	0	0	0	Hematite/epidote-titanite assemblage. SEM check from 0.5-1.0 mm fraction: 1 chromite candidate = 1 hercynite.	0.5-1.0 mm fraction: 2 Mn-epidote 1 hercynite resembling chromite 0.25-0.5 mm fraction: 3 Mn-epidote 2 chromite**
AR-16-065	0.3 (~22 gr)	0	0.1 (9 gr)	Tr	Tr (2 gr)	Tr Mn-epidote (2 gr)	0	0	Tr	0	Tr	0	0	Tr (Fo)	0	Tr (2 gr)	Tr	0	0	Hematite-augite/epidote assemblage. SEM checks from 0.5-1.0 mm fraction: 1 chromite candidate = 1 hercynite; and 1 anorthopormorphic contamination candidate = 1 slag (Ca,Fe,Si,Al). SEM checks from 0.25-0.5 mm fraction: 3 andradite versus almandine candidates = 1 andradite, 1 spessartine and 1 titanite; 1 topaz versus kyanite candidate = 1 zircon; 2 chromite candidates = 1 chromite and 1 hercynite (counted as	0.5-1.0 mm fraction: 2 chalcopyrite 1 hercynite resembling chromite 1 slag (contamination) 0.25-0.5 mm fraction: 22 chalcopyrite 1 andradite 1 spessartine 1 titanite resembling andradite 2 Mn-epidote 1 zircon resembling topaz 1 chromite 1 hercynite resembling chromite 2 slag (contamination)

																			chromite); and 2 anorthopormorphic contamination candidates = 2 slag.	
AR-16-075	0	0.1% covellite (10 gr)	0.3 (~30 gr)	3	0	Tr Mn-epidote (3 gr) Tr low-Cr diopside (2 gr)	0	Tr (1 gr)	Tr	0	Tr	0	Tr	Tr (Fo)	0	Tr (6 gr)	0	0	0	Hematite/epidote assemblage. SEM checks from 0.25-0.5 mm fraction: 4 chalcopyrite versus pyrite candidates = 4 pyrite; 1 blue covellite versus bornite candidate = 1 covellite; and 2 chromite candidates = 1 chromite and 1 hercynite (counted as chromite). Note: Covellite may variably include	0.25-0.5 mm fraction: 4 pyrite resembling chalcopyrite 10 covellite 3 Mn-epidote 2 low-Cr diopside 1 red rutile 1 chromite 4 chromite** 1 hercynite resembling chromite

																		bornite.		
AR-16-095	0	0	0	Tr	0	0.8% Mn-epidote (9 gr)	0	0	Tr	0	0	0	0	0	0	Tr (3 gr)	Tr	0	0	Hematite/epidote-titanite assemblage.	0.5-1.0 mm fraction: 2 Mn-epidote 0.25-0.5 mm fraction: 9 Mn-epidote 3 chromite**

AR-16-116	Tr (4 gr)	0	Tr (1 gr)	Tr	Tr (2 gr)	Tr Mn-epidote (1 gr)	0	Tr (1 gr)	Tr	0	Tr	Tr	0	Tr (Fo)	0	Tr (2 gr)	Tr	0	0	Hematite/epidote-titanite assemblage. SEM checks from 0.25-0.5 mm fraction: 1 scheelite versus apatite candidate = 1 sillimanite; 1 barite versus sillimanite candidate = 1 sillimanite; 4 andradite versus titanite candidates = 2 andradite and 2 titianite; and 1 chromite candidate = 1 hercynite (counted as chromite).	0.5-1.0 mm fraction: 3 chalcopyrite 3 Mn-epidote 1 chromite** 0.25-0.5 mm fraction: 4 chalcopyrite 1 sillimanite resembling scheelite 1 sillimanite resembling barite 2 andradite 2 titanite resembling andradite 1 Mn-epidote 1 red rutile 2 chromite** 1 hercynite resembling chromite
AR-16-202	Tr (5 gr)	0	Tr (3 gr)	Tr	Tr (3 gr)	Tr Mn-epidote (5 gr)	0	0	Tr	0	Tr	0	0	Tr (Fo)	0	Tr (9 gr)	0	0	0	Hematite-augite/epidote assemblage. SEM checks from 0.25-0.5 mm fraction: 1 scheelite versus diopside candidate = 1 diopside; 1 barite versus sillimanite candidate = 1 sillimanite; and 3 andradite candidates = 2 andradite and 1	0.5-1.0 mm fraction: 2 chalcopyrite 1 chromite** 0.25-0.5 mm fraction: 5 chalcopyrite 1 diopside resembling scheelite 1 sillimanite resembling barite 2 andradite 1 grossular 5 Mn-epidote

																					grossular.	9 chromite**
AR-16-207	Tr (1 gr)	0	Tr (1 gr)	Tr	0	Tr Mn-epidote (6 gr) Tr corundum (1 gr)	0	0	Tr	0	Tr	0	0	0	0	Tr (6 gr)	0	0	0	Hematite/epidote-titanite assemblage. SEM check from 0.25-0.5 mm fraction: 1 topaz versus corundum candidate = 1 corundum.	0.25-0.5 mm fraction: 1 chalcopyrite 6 Mn-epidote 1 corundum 6 chromite**

AR-16-224	0.1 (8 gr)	1% covellite (~80 gr)	Tr (5 gr)	Tr	Tr (1 gr)	Tr Mn-epidote (15 gr) Tr low-Cr diopside (3 gr)	0	Tr (1 gr)	Tr	0	Tr	0	0	Tr (Fo)	0	Tr (7 gr)	Tr	0	0	Hematite/epidote assemblage. SEM checks from 0.25-0.5 mm fraction: 2 chalcopyrite versus pyrite candidates = 2 pyrite; 14 grey, blue-grey covellite candidates = 14 covellite; and 1 andradite candidate = 1 andradite. Note: Covellite may variably include bornite.	1.0-2.0 mm fraction: 1 Mn-epidote 0.5-1.0 mm fraction: 1 covellite 11 Mn-epidote 4 chromite** 0.25-0.5 mm fraction: 8 chalcopyrite ± malachite 2 pyrite resembling chalcopyrite 54 representative covellite 1 andradite 15 Mn-epidote 3 low-Cr diopside 1 red rutile 7 chromite**
AR-16-229	0	0	Tr (1 gr)	Tr	0	Tr Mn-epidote (2 gr)	0	0	Tr	0	Tr	0	0	Tr (Fo)	0	Tr (3 gr)	0	0	0	Hematite/epidote-titanite assemblage.	0.25-0.5 mm fraction: 2 Mn-epidote 3 chromite**

AR-16-290	Tr (6 gr)	5% covellite (~400 gr)	0	Tr	Tr (1 gr)	Tr Mn-epidote (1 gr)	0	0	Tr	0	Tr	0	0	0.5 (Fo)	Tr	Tr (1 gr)	0	0	0	Hematite-augite/epidote assemblage. SEM check from 0.25-0.5 mm fraction: 1 andradite candidate = 1 andradite. 0.5-1.0 mm fraction contains 3% (~40 grains) covellite. Note: Covellite may variably include bornite and/or chalcocite.	1.0-2.0 mm fraction: 5 covellite 0.5-1.0 mm fraction: 1 chalcopyrite 20 representative covellite 0.25-0.5 mm fraction: 6 chalcopyrite 20 representative covellite 1 andradite 1 Mn-epidote 1 chromite**
AR-16-291	0	Tr covellite (1 gr) Tr barite (1 gr)	0.3 (~15 gr)	Tr	0	0	0	0	Tr	0	Tr	0	0	Tr (Fo)	0	Tr (2 gr)	Tr	0	0	Hematite-augite/epidote assemblage. SEM check from 0.25-0.5 mm fraction: 1 barite versus sillimanite candidate = 1 barite.	0.5-1.0 mm fraction: 2 chromite** 0.25-0.5 mm fraction: 1 covellite 1 barite 2 chromite**
AR-16-300	Tr (3 gr)	Tr covellite (5 gr)	4 (~800 gr)	Tr	0	Tr low-Cr diopside (6 gr)	0	0	Tr	0	Tr	0	0	2 (Fo)	0	Tr (16 gr)	0	0	0	Augite-hematite/epidote assemblage. Covellite may variably include bornite.	0.5-1.0 mm fraction: 2 low-Cr diopside 8 chromite** 0.25-0.5 mm fraction: 3 chalcopyrite 5 covellite 6 low-Cr diopside 16 chromite**

(e)

S.G. 2.8-3.2 Porphyry Cu Indicator Mineral Data

Client: University of Waterloo
File Name: 20177410 - University of Waterloo - Reman - AR16 - PCIM - February 2017
Total Number of Samples in this Report: 13
ODM Batch Number(s): 7410

Sample Numbr	0.25-0.5 mm					Remarks	Picked Grains
			Major Sulphates				
	% Cu Minerals	Misc. Prime porphyry Cu Indicators	% Jarosite	% Alunite	% Tourmaline		
AR-16-033	0	0	Tr (~20 gr)	0	0	SEM checks: 10 jarosite versus leucoxene candidates = 7 jarosite and 3 leucoxene.	0.25-0.5 mm fraction: 7 representative jarosite 3 leucoxene resembling jarosite
AR-16-047	0	0	Tr (~10 gr)	0	0	SEM checks: 5 jarosite versus leucoxene candidates = 3 jarosite and 2 leucoxene.	0.25-0.5 mm fraction: 3 representative jarosite 2 leucoxene resembling jarosite
AR-16-065	0	0	0	0	0		
AR-16-075	0	0	0	0	0		
AR-16-095	0	0	0	0	0	SEM checks: 3 jarosite versus leucoxene candidates = 3 leucoxene.	0.25-0.5 mm fraction: 3 leucoxene resembling jarosite

AR-16-116	0	0	0	0	0	SEM checks: 2 jarosite versus leucoxene candidates = 2 leucoxene; and 5 tourmaline candidates = 5 hornblende.	0.25-0.5 mm fraction: 2 leucoxene resembling jarosite 5 hornblende resembling tourmaline
AR-16-202	0	0	0	0	0		
AR-16-207	0	0	0	0	0		
AR-16-224	0	0	Tr (~20 gr)	0	0	SEM checks: 10 jarosite versus leucoxene candidates = 9 jarosite and 1 siderite.	0.25-0.5 mm fraction: 9 representative jarosite 1 siderite resembling jarosite
AR-16-229	0	0	Tr (~20 gr)	0	0	SEM checks: 10 jarosite versus leucoxene candidates = 9 jarosite and 1 leucoxene.	0.25-0.5 mm fraction: 9 representative jarosite 1 leucoxene resembling jarosite
AR-16-290	0	0	Tr (5 gr)	0	0	SEM checks: 5 jarosite versus leucoxene candidates = 5 jarosite.	0.25-0.5 mm fraction: 5 jarosite
AR-16-291	0	0	Tr (1 gr)	0	0	SEM checks: 2 jarosite versus leucoxene candidates = 1 jarosite and 1 ankerite.	0.25-0.5 mm fraction: 1 jarosite 1 ankerite resembling jarosite
AR-16-300	0	0	0	0	0		

(f)

Paramagnetic/Non-Paramagnetic Fraction Weights

Client: University of Waterloo
File Name: 20177410 - University of Waterloo - Reman - AR16 - PCIM - February 2017
Total Number of Samples in this Report: 13
ODM Batch Number(s): 7410

	Weight of 0.25-0.5 mm S.G >3.32 Nonferromagnetic Heavy Mineral Fractions (g)				
		Paramagnetic			Nonparamagnetic
Sample Number	Total	Strongly (<0.6 amp)	Moderately (0.6-0.8 amp)	Weakly (0.8-1.0 amp)	>1.0 amp
AR-16-033	1.06	0.17	0.04	0.16	0.69
AR-16-047	0.31	0.12	0.01	0.04	0.14
AR-16-065	1.49	0.28	0.13	0.40	0.68
AR-16-075	1.40	0.27	0.11	0.24	0.78
AR-16-095	0.21	0.05	0.01	0.05	0.10
AR-16-116	1.96	0.41	0.15	0.32	1.08
AR-16-202	1.99	0.50	0.12	0.45	0.92
AR-16-207	0.78	0.39	0.07	0.07	0.25
AR-16-224	1.78	0.49	0.11	0.26	0.92
AR-16-229	0.42	0.21	0.02	0.06	0.13
AR-16-290	1.81	0.41	0.15	0.45	0.80
AR-16-291	0.98	0.21	0.13	0.28	0.36
AR-16-300	3.83	0.87	0.38	0.96	1.62

(g)

Paramagnetic/Non-Paramagnetic Fraction Weights

Client: University of Waterloo

File Name: 20177410 - University of Waterloo - Reman - AR16 - PCIM - February 2017

Total Number of Samples in this Report: 13

ODM Batch Number(s): 7410

Green Epidote Estimates

Sample Number	Est: % Green Epidote in 0.25-0.5 mm 0.8-1.0 Amp Fraction
AR-16-033	80
AR-16-047	80
AR-16-065	60
AR-16-075	50
AR-16-095	70
AR-16-116	50
AR-16-202	40
AR-16-207	60
AR-16-224	50
AR-16-229	50
AR-16-290	40
AR-16-291	40
AR-16-300	30

(h)

Overburden Drilling Management Limited - Abbreviations Table

Raw Sample Weights and Descriptions Log

Largest Clast Size Present:

G:	Granules
P:	Pebbles
C:	Cobbles

Clast Composition:

V/S:	Volcanics and/or sediments
GR:	Granitics
LS:	Limestone, carbonates
OT:	Other lithologies (refer to footnotes)
TR:	Only trace present
NA:	Not applicable
OX:	Very oxidized, undifferentiated

Matrix Grain Size Distribution:

S/U:	Sorted or unsorted
SD:	Sand (F: Fine; M: Medium; C: Coarse)
ST:	Silt
CY:	Clay
Y:	Fraction present
+:	Fraction more abundant than normal
-:	Fraction less abundant than normal
N:	Fraction not present

Matrix Organics:

ORG: Y: Organics present in matrix
N: Organics absent or negligible in matrix
+: Matrix is mainly organic

Matrix Colour:

Primary:

BE:	Beige	GG:	Grey-green
BR:	Brick Red	PP:	Purple
GY:	Grey	PK:	Pink
GB:	Grey-beige	PB:	Pink-beige
GN:	Green	MN:	Maroon

Secondary (soil):

OC:	Ochre
BN:	Brown
BK:	Black

Secondary Colour Modifier:

L:	Light
M:	Medium
D:	Dark

Detailed Gold Grain Log

VG: Visible gold grains

Thickness:

M: Actual measured thickness of grain (µm)
C: Thickness of grain (µm) calculated from measured width and length

Kimberlite Indicator Mineral (KIM) Log

GP: Purple to red peridotitic garnet (G9/10 Cr-pyrope)
GO: Orange mantle garnet; includes both eclogitic pyrope-almandine (G3) and Cr-poor megacrystic pyrope (G1/G2) varieties; may include unchecked (by SEM) grains of common crustal garnet (G5) lacking diagnostic inclusions or crystal faces
DC: Cr-diopside; distinctly emerald green (paler emerald green low-Cr diopside picked separately)
IM: Mg-ilmenite; may include unchecked (by SEM) grains of common crustal ilmenite lacking diagnostic inclusions or crystal faces
CR: Chromite
FO: Forsterite

Metamorphosed/Magmatic Massive Sulphide Indicator Mineral (MMSIM) and Porphyry Cu Indicator Mineral (PCIM) Logs

Adr: Andradite
Ap: Apatite
Ase: Anatase
Aspy: Arsenopyrite
Ax: Axinite
Cpx: Clinopyroxene
Cpy: Chalcopyrite
Cr: Chromite
Fay: Fayalite
Gh: Gahnite
Gr: Grossular
Gth: Goethite
Ilm: Ilmenite
Ky: Kyanite
Mz: Monazite
Ol: Olivine
Opx: Orthopyroxene
PGM: Platinum group-bearing mineral
Py: Pyrite
REM: Rare earth-bearing mineral
Sil: Sillimanite
Spi: Spinel
Sps: Spessartine
St: Staurolite
Tm: Tourmaline
Ttn: Titanite
Zir: Zircon

Other

HMC: Heavy mineral concentrate
UV: Ultra-violet
EPD: Electric-pulse disaggregation
PGE: Platinum group element

Core VTH2014-03

Indicator mineral analysis was done on a sand sample with an elevation of 1095.1-1094.9 m asl from core VTH2014-03. The results are shown below (**Figure C.1**). This sample has a high Mn-epidote count (42 grains) compared to all the samples from the cores and Highmont pit (12 grains) (**Figure C.2**). It also has a higher number of Mn-epidote grains than the average for the Highland Valley shallow till samples collected by Plouffe and Ferbey (3 grains) (**Figure C.2**). A photo of these grains from the 0.25-0.5mm fraction from this sample is shown below (**Figure C.3**).

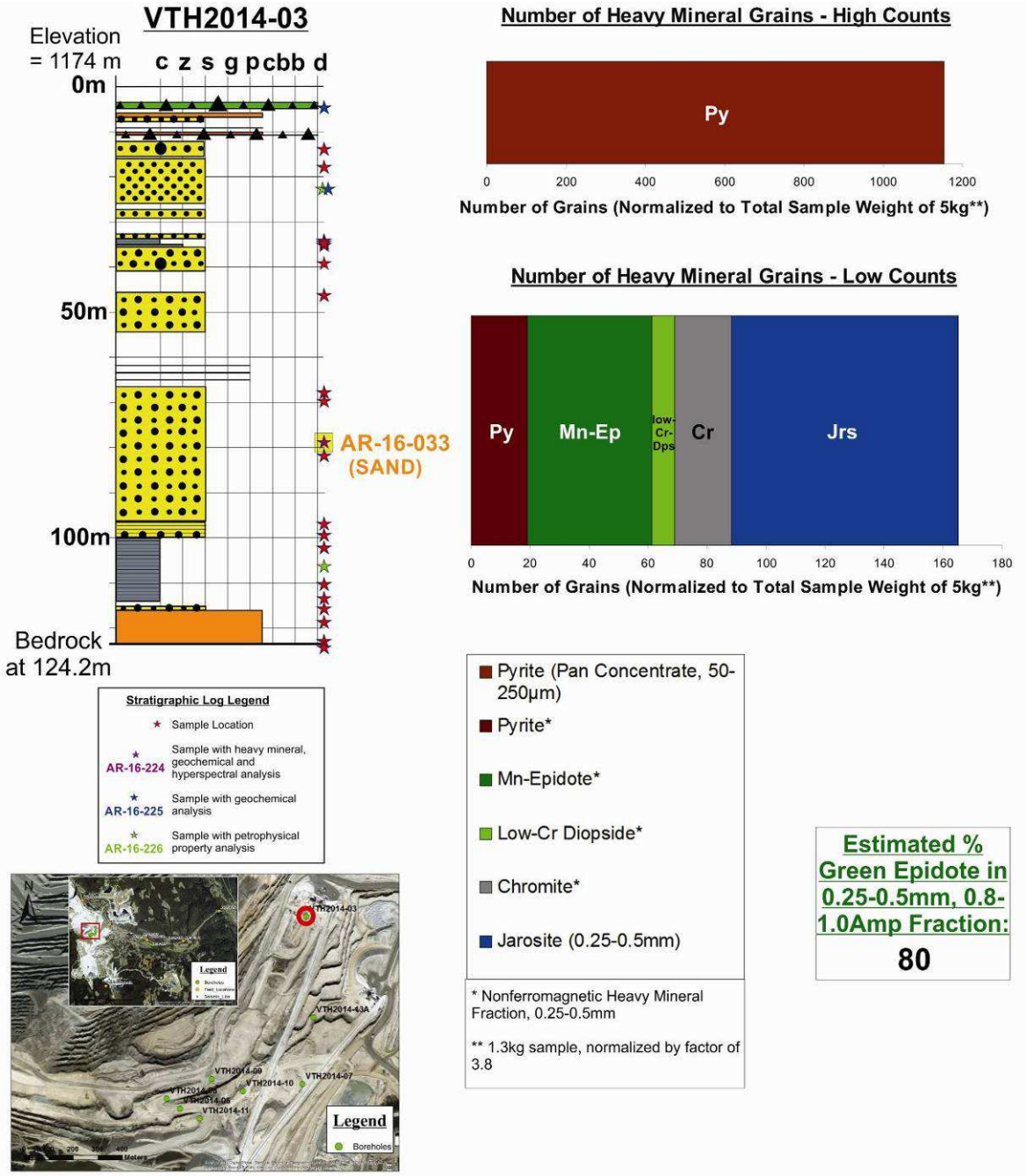

Figure C.1 Stratigraphic log, location map and indicator mineral results of core VTH2014-03. The location of collected samples is shown on the stratigraphic log and the sample for which indicator mineral analysis was done is highlighted.

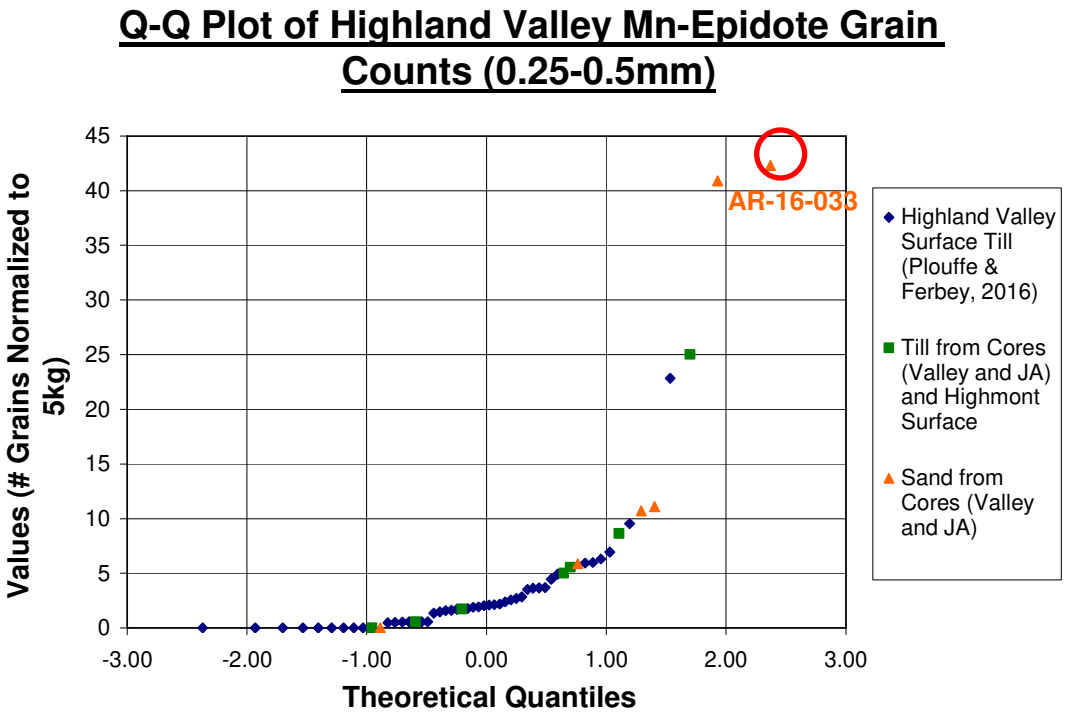

Figure C.2 Quantile-quantile plot of normalized Mn-epidote grain counts for this study and Plouffe and Ferbey's study (2016), with the sand sample from core VTH2014-03 highlighted.

Figure C.3 Mn-epidote grains from the 0.25-0.5mm fraction from sample AR-16-033 belonging to core VTH2014-03.

Core VTH2014-08

Indicator mineral analysis was done on a sand sample at an elevation of 1180.4-1180.2 m asl from core VTH2014-08. The results are shown below (**Figure C.4**). This sample has a higher number of visible gold grains (4 grains) than the average for the Highland Valley shallow till samples collected by Plouffe and Ferbey (1 grain) (**Figure C.5**). There is a higher concentration of calculated visible gold in the indicator mineral concentrate (0.25-2.0mm) of this sand sample (310ppb) than the average of the Highland Valley shallow till samples collected by Plouffe and Ferbey (7.9ppb) (**Figure C.6**). A photo of the Mn-epidote grains from the 0.25-0.5mm fraction from this sample is shown below (**Figure C.7**).

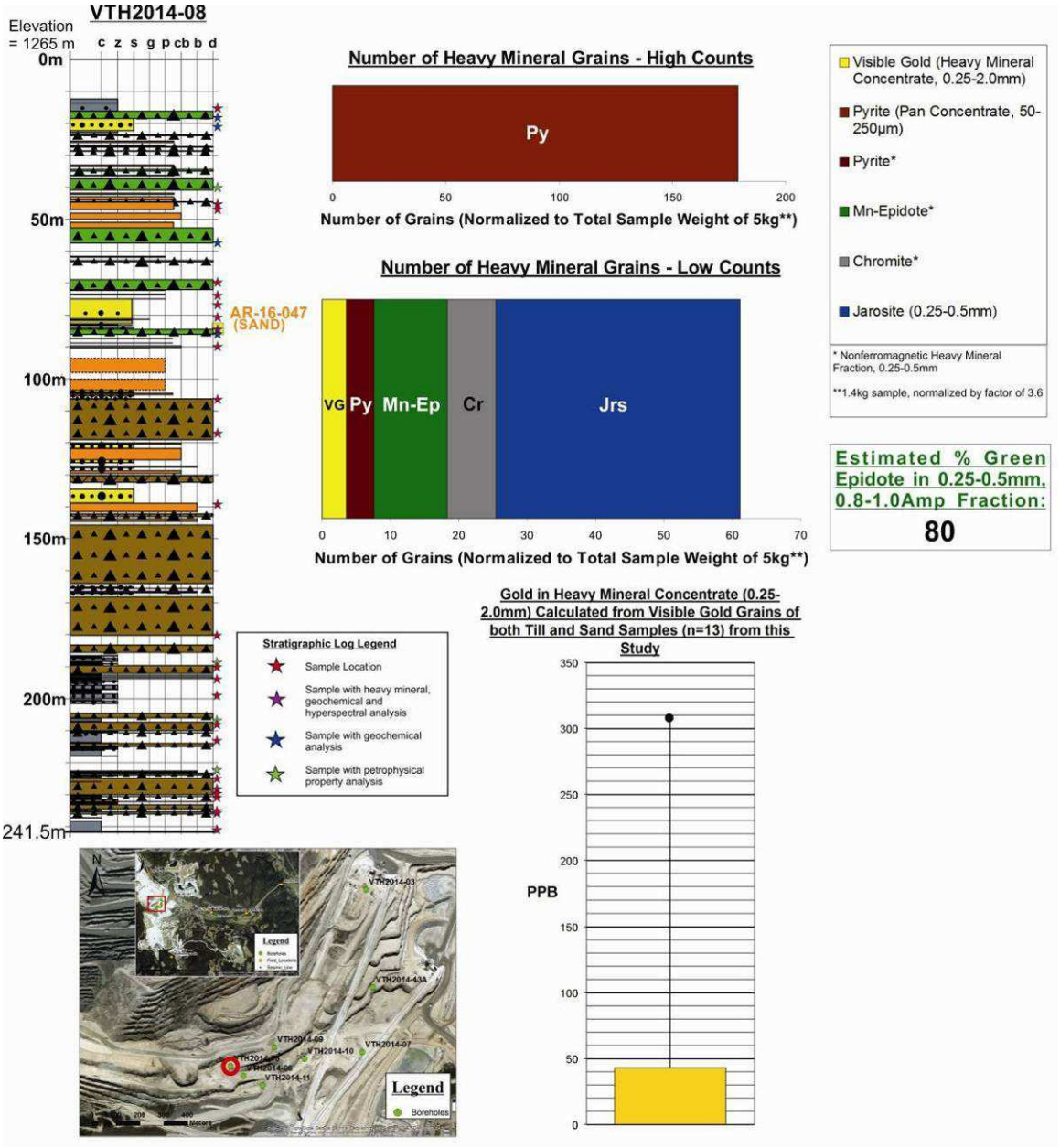

Figure C.4 Stratigraphic log, location map and indicator mineral results of core VTH2014-08. The location of collected samples is shown on the stratigraphic log and the sample for which indicator mineral analysis was done is highlighted.

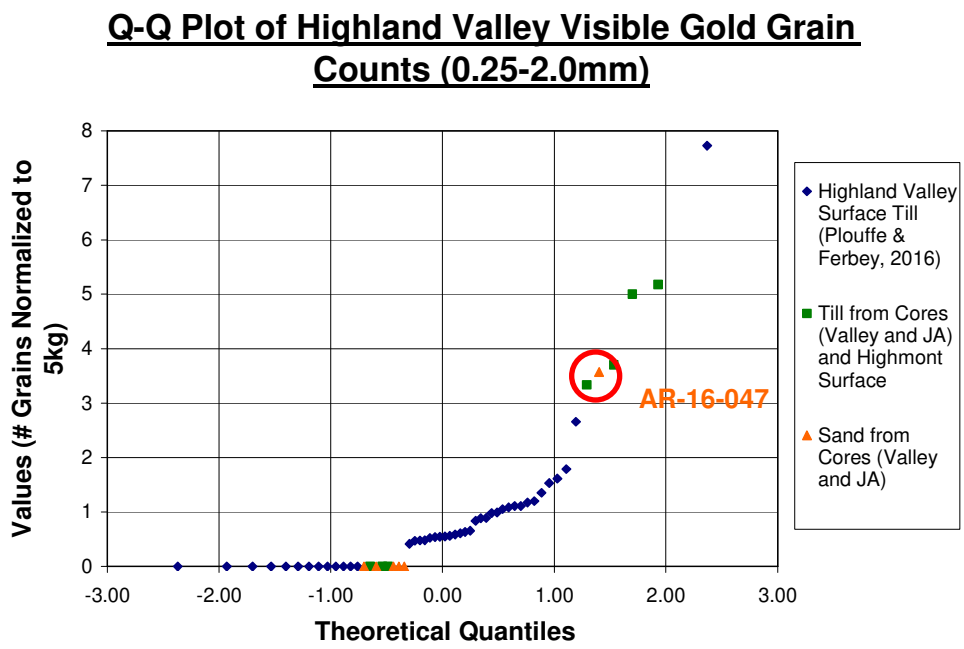

Figure C.5 Quantile-quantile plot of normalized visible gold grain counts for this study and Plouffe and Ferbey's study (2016), with the sand sample from core VTH2014-08 highlighted.

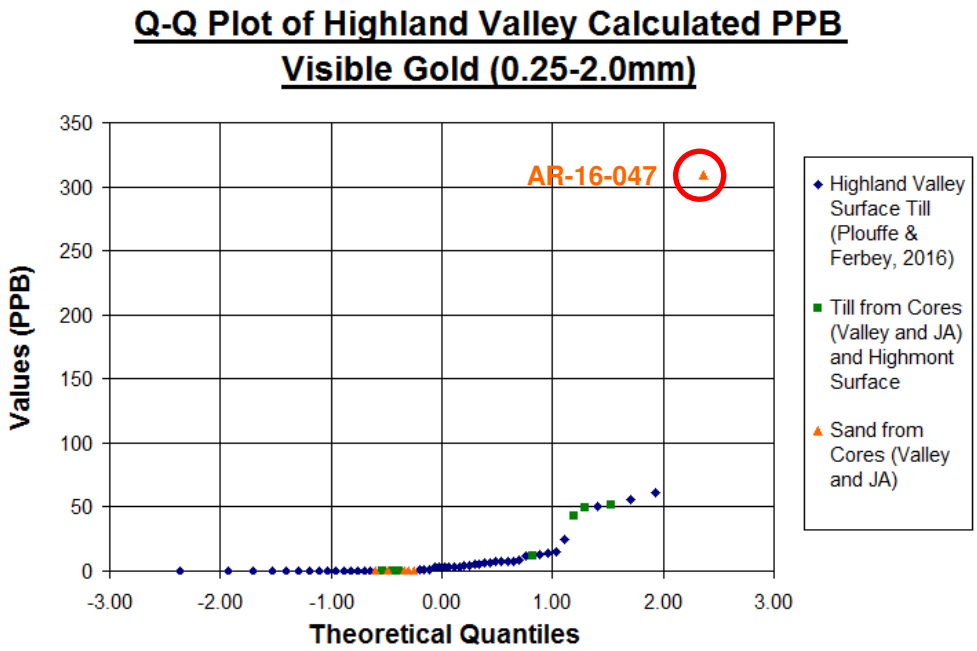

Figure C.6 Quantile-quantile plot of calculated visible gold in the indicator mineral concentrate for this study and Plouffe and Ferbey's study (2016), with the sand sample from core VTH2014-08 highlighted.

Figure C.7 Mn-epidote grains from the 0.25-0.5mm fraction from sample AR-16-047 belonging to core VTH2014-08.

Core VTH2014-10

Indicator mineral analysis was done on two till samples at elevations of 1232.1-1231.9 m asl and 1195.6-1195.4 m asl and one sand sample at an elevation of 1117.7-1117.2 m asl from core VTH2014-10. The results are shown below (**Figure C.8**).

The shallower till sample has a high chalcopyrite count (55 grains) compared to others in this study (8 grains). A photo of these grains from the 0.25-0.5mm fraction from this sample is shown below (**Figure C.9**). It also has a higher number of andradite grains (5 grains) than the average for all the samples from the cores and Highmont pit (1 grain).

The deeper till sample has a high marcasite count (1852 grains) compared to others in this study (142 grains). A photo of these grains from the 0.25-0.5mm fraction from this sample is shown below (**Figure C.10**). It also has a higher number of visible gold grains (4 grains) than the average for the Highland Valley shallow till samples collected by Plouffe and Ferbey (1 grain) (**Figure C.11**).

The sand sample has a high Mn-epidote count (41 grains) compared to all the samples from the cores and Highmont pit (12 grains) (**Figure C.12**). It also has a higher number of Mn-epidote grains than the average for the Highland Valley shallow till samples collected by Plouffe and Ferbey (3 grains) (**Figure C.12**). A photo of these grains from the 0.25-0.5mm fraction from this sample is shown below (**Figure C.13**).

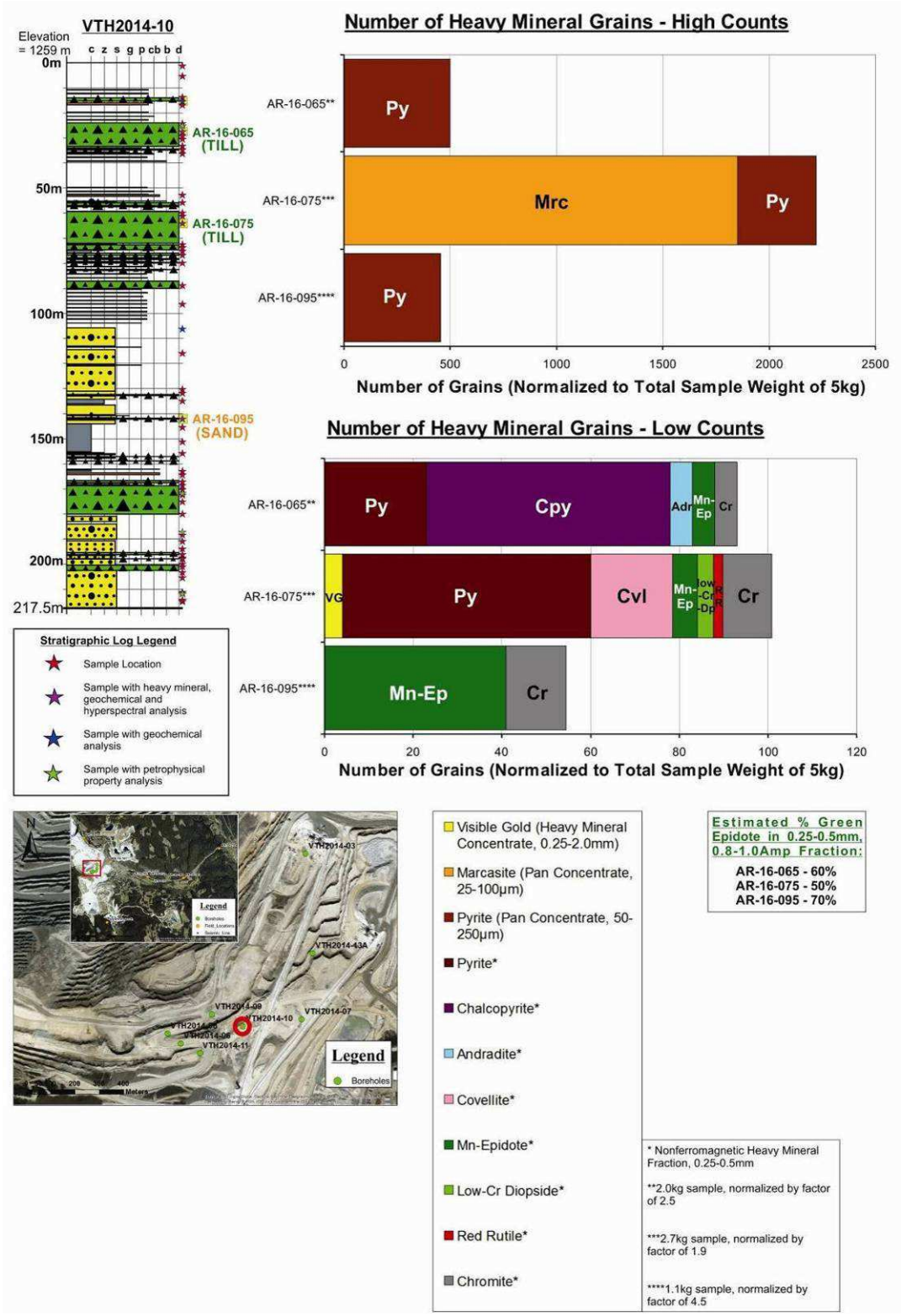

Figure C.8 Stratigraphic log, location map and indicator mineral results of core VTH2014-10. The location of collected samples is shown on the stratigraphic log and the samples for which indicator mineral analysis was done are highlighted.

Figure C.9 Chalcopyrite grains from the 0.25-0.5mm fraction from sample AR-16-065 belonging to core VTH2014-10.

Figure C.10 Marcasite grains from the 0.25-0.5mm fraction from sample AR-16-075 belonging to core VTH2014-10.

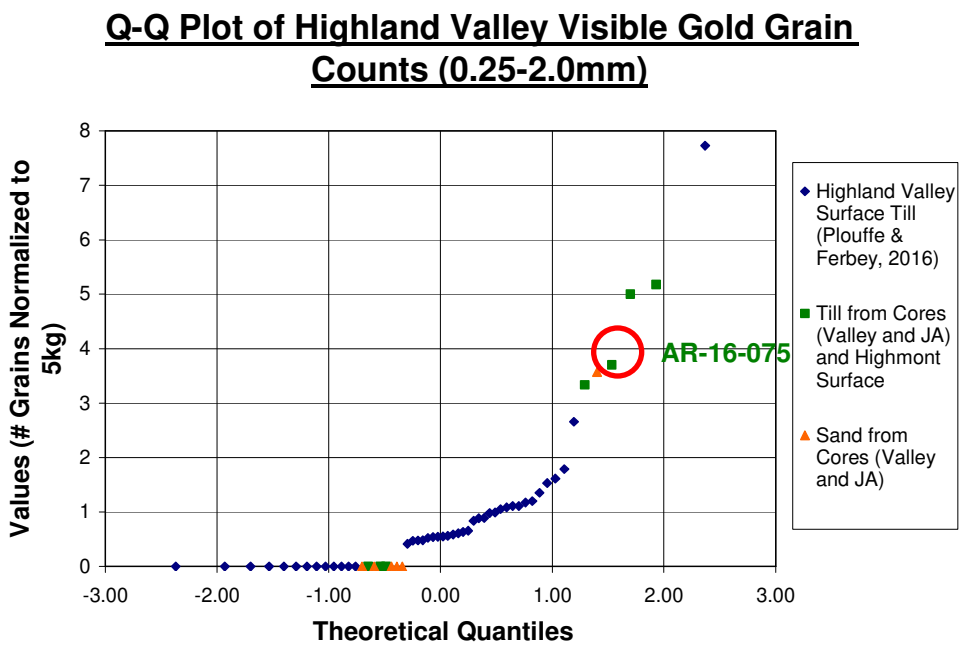

Figure C.11 Quantile-quantile plot of normalized visible gold grain counts for this study and Plouffe and Ferbey's study (2016), with the deeper till sample from core VTH2014-10 highlighted.

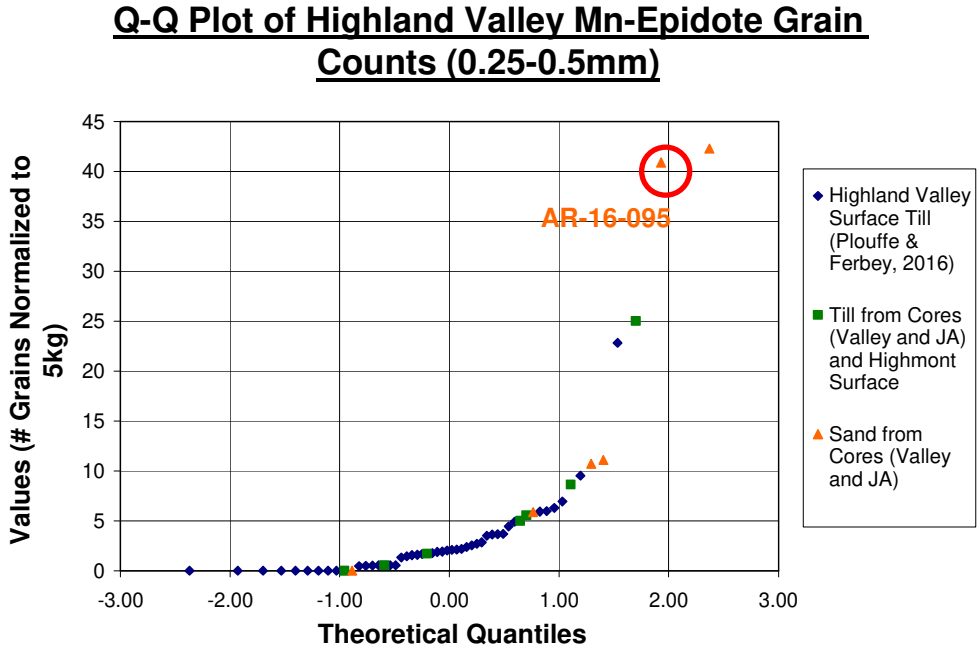

Figure C.12 Quantile-quantile plot of normalized Mn-epidote grain counts for this study and Plouffe and Ferbey's study (2016), with the sand sample from core VTH2014-10 highlighted.

Figure C.13 Mn-epidote grains from the 0.25-0.5mm fraction from sample AR-16-095 belonging to core VTH2014-10.

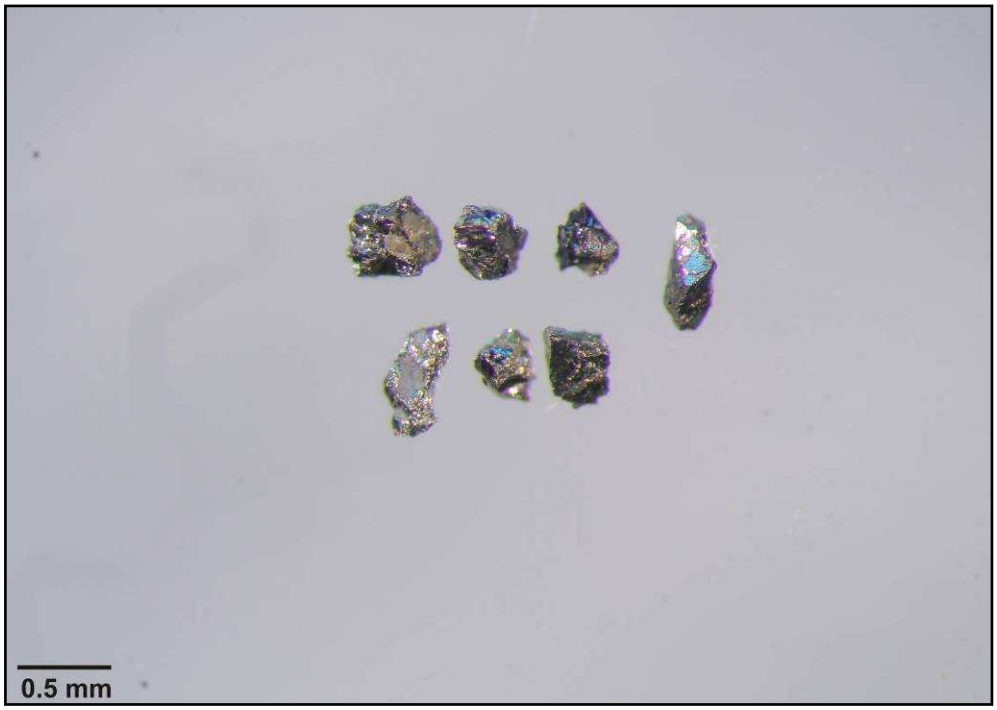

Figure C.14 Pyrite grains from the 0.25-0.5mm fraction from sample AR-16-065 belonging to core VTH2014-10.

Figure C.15 Mn-epidote grains from the 0.25-0.5mm fraction from sample AR-16-065 belonging to core VTH2014-10.

Figure C.16 Covellite grains from the 0.25-0.5mm fraction from sample AR-16-075 belonging to core VTH2014-10.

Figure C.17 Mn-epidote grains from the 0.25-0.5mm fraction from sample AR-16-075 belonging to core VTH2014-10.

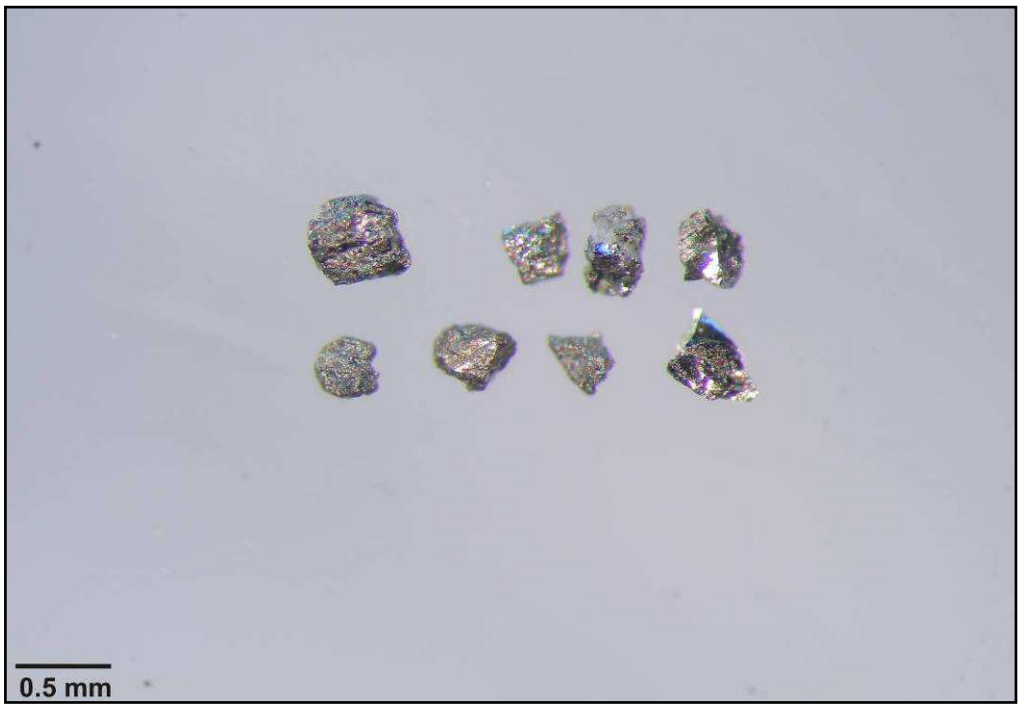

Figure C.18 Pyrite grains from the 0.25-0.5mm fraction from sample AR-16-075 belonging to core VTH2014-10.

Figure C.19 Rutile grain from the 0.25-0.5mm fraction from sample AR-16-075 belonging to core VTH2014-10.

Core VTH2014-11

Indicator mineral analysis was done on a till sample at an elevation of 1208.6-1208.3 m asl and a sand sample at an elevation of 1173.7-1173.3 m asl from core VTH2014-11. The results are shown below (**Figure C.20**). The till sample has a higher number of visible gold grains (3 grains) than the average for the Highland Valley shallow till samples collected by Plouffe and Ferbey (1 grain) (**Figure C.21**). It also has a higher number of Mn-epidote grains (25 grains) than the average for the Plouffe and Ferbey Highland Valley shallow till dataset (3 grains) (**Figure C.22**). A photo of these grains from the 0.25-0.5mm fraction from this sample is shown below (**Figure C.23**).

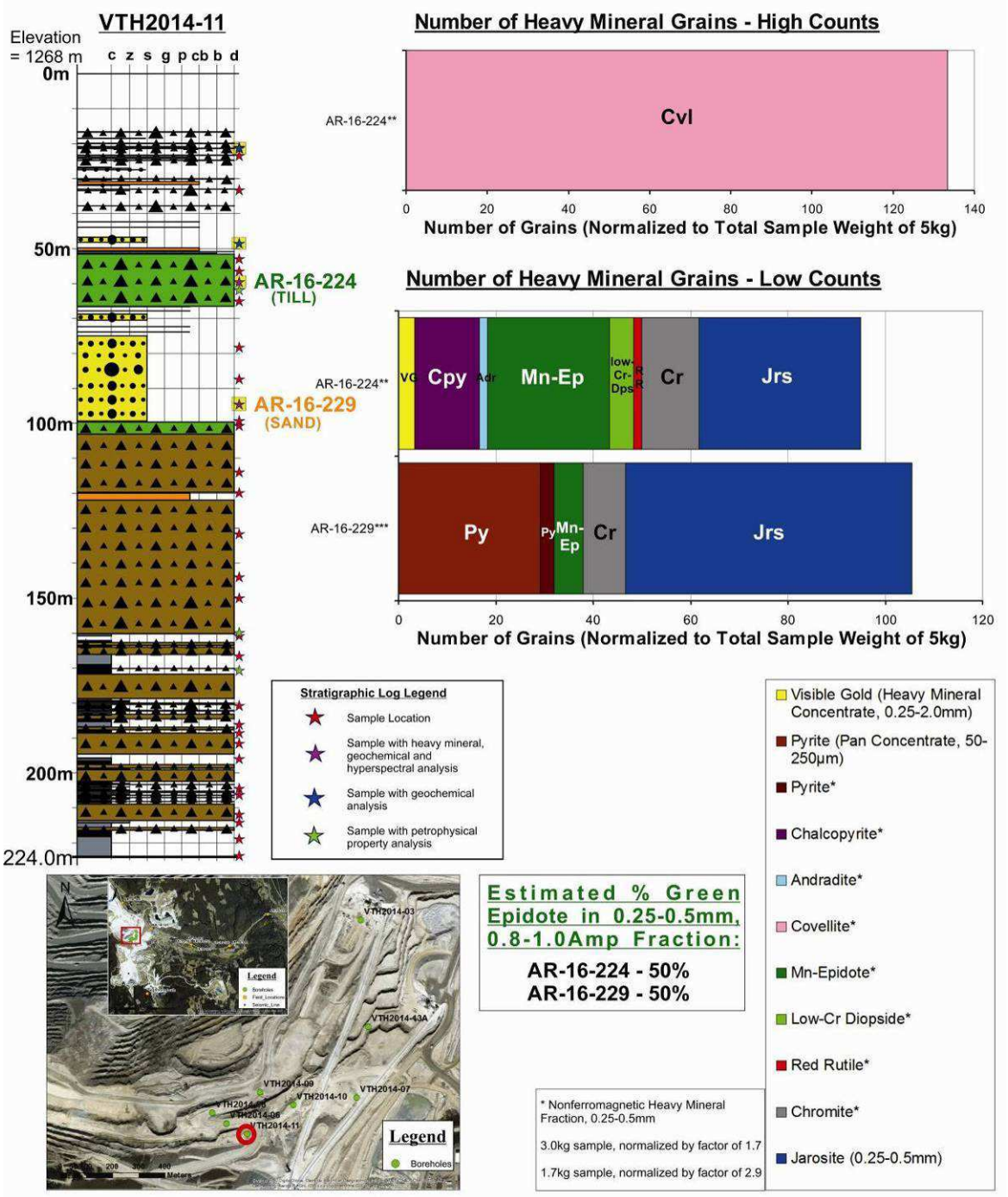

Figure C.20 Stratigraphic log, location map and indicator mineral results of core VTH2014-11. The location of collected samples is shown on the stratigraphic log and the samples for which indicator mineral analysis was done are highlighted.

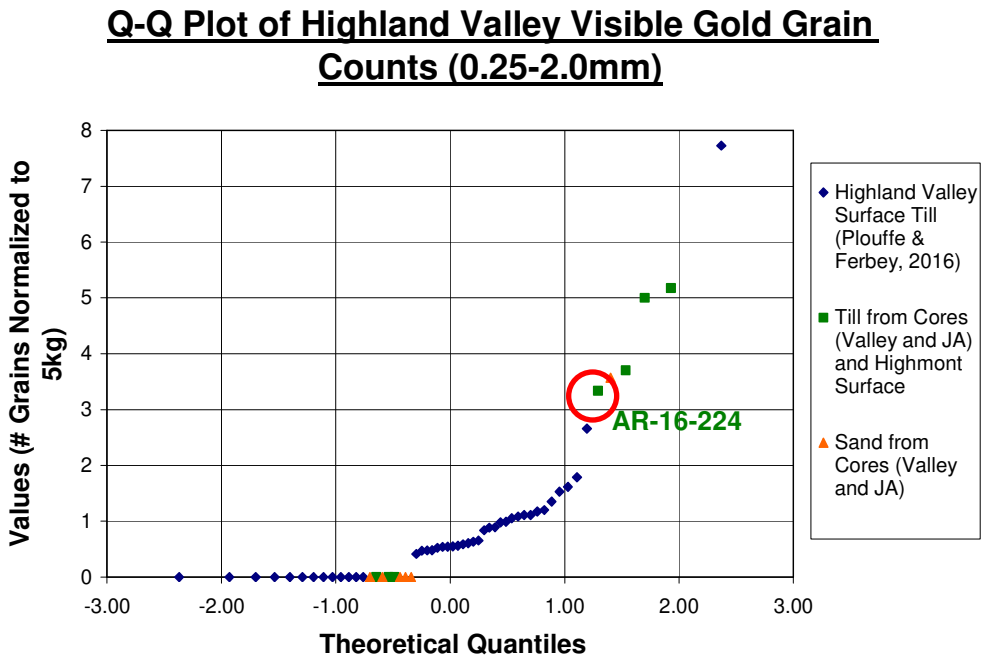

Figure C.21 Quantile-quantile plot of normalized visible gold grain counts for this study and Plouffe and Ferbey's study (2016), with the till sample from core VTH2014-11 highlighted.

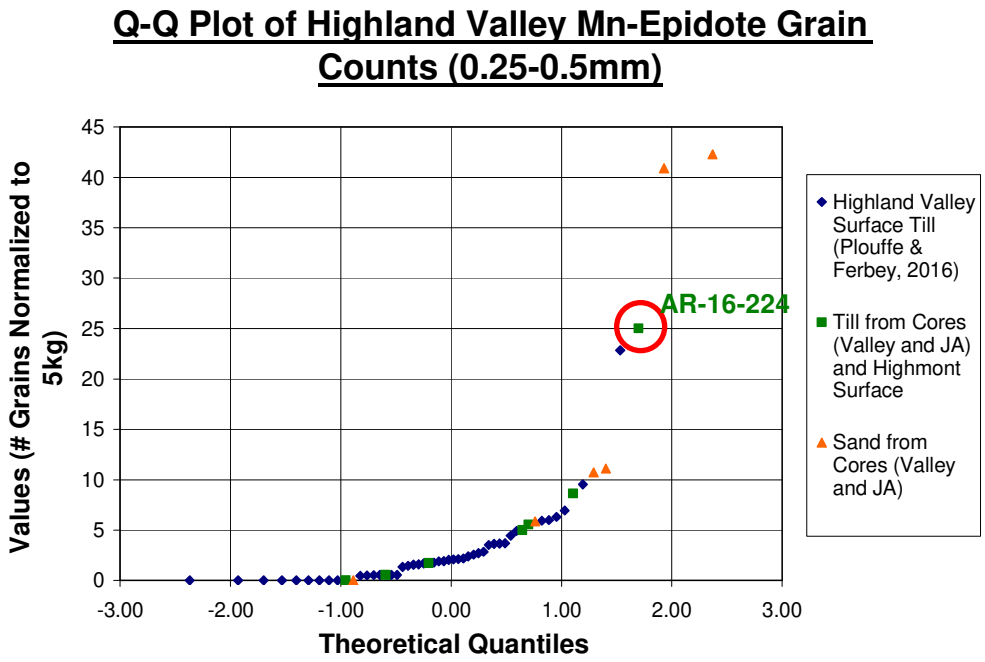

Figure C.22 Quantile-quantile plot of normalized Mn-epidote grain counts for this study and Plouffe and Ferbey's study (2016), with the till sample from core VTH2014-11 highlighted.

Figure C.23 Mn-epidote grains from the 0.25-0.5mm fraction from sample AR-16-224 belonging to core VTH2014-11.

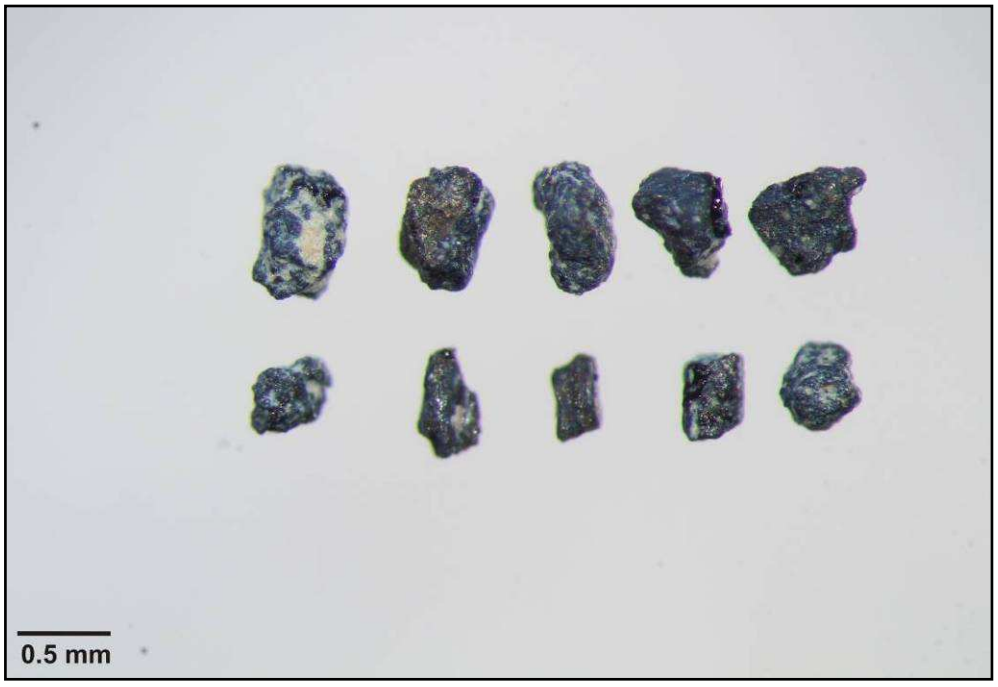

Figure C.24 Covellite grains from the 0.25-0.5mm fraction from sample AR-16-224 belonging to core VTH2014-11.

Figure C.25 Chalcopyrite grains from the 0.25-0.5mm fraction from sample AR-16-224 belonging to core VTH2014-11.

Figure C.26 Rutile grain from the 0.25-0.5mm fraction from sample AR-16-224 belonging to core VTH2014-11.

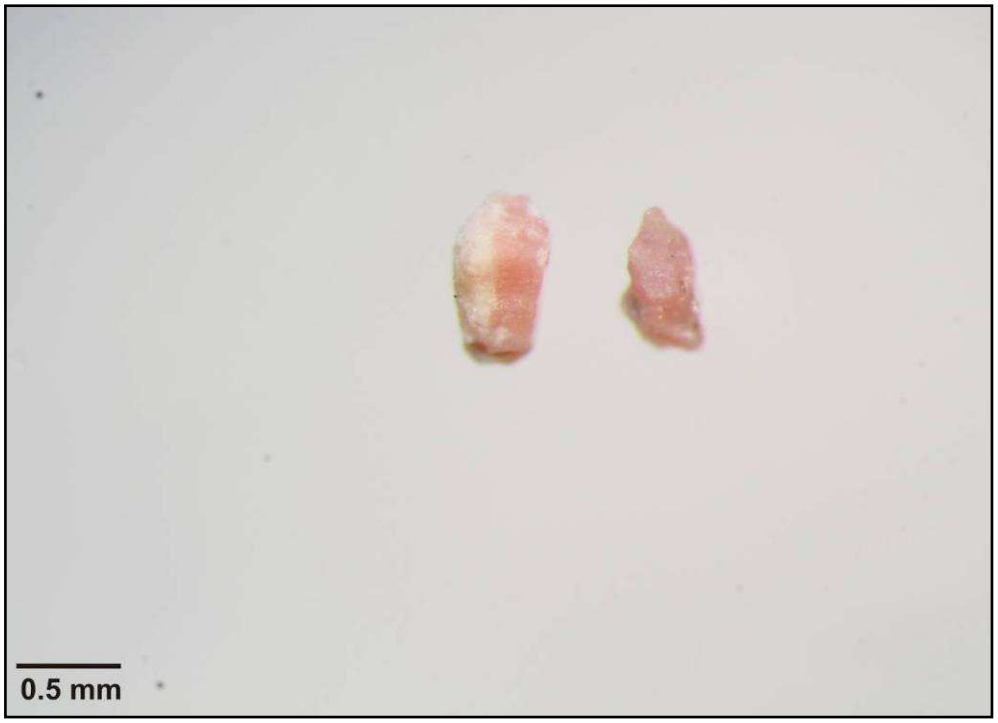

Figure C.27 Mn-epidote grains from the 0.25-0.5mm fraction from sample AR-16-229 belonging to core VTH2014-11.

Core VTH2014-13A

Indicator mineral analysis was done on a till sample at an elevation of 1203.4-1203.1 m asl and a sand sample at an elevation of 1161.2-1160.9 m asl from core VTH2014-13A. The results are shown below (**Figure C.28**). The till sample has a high andradite count (5 grains) compared to others in this study (1 grain).

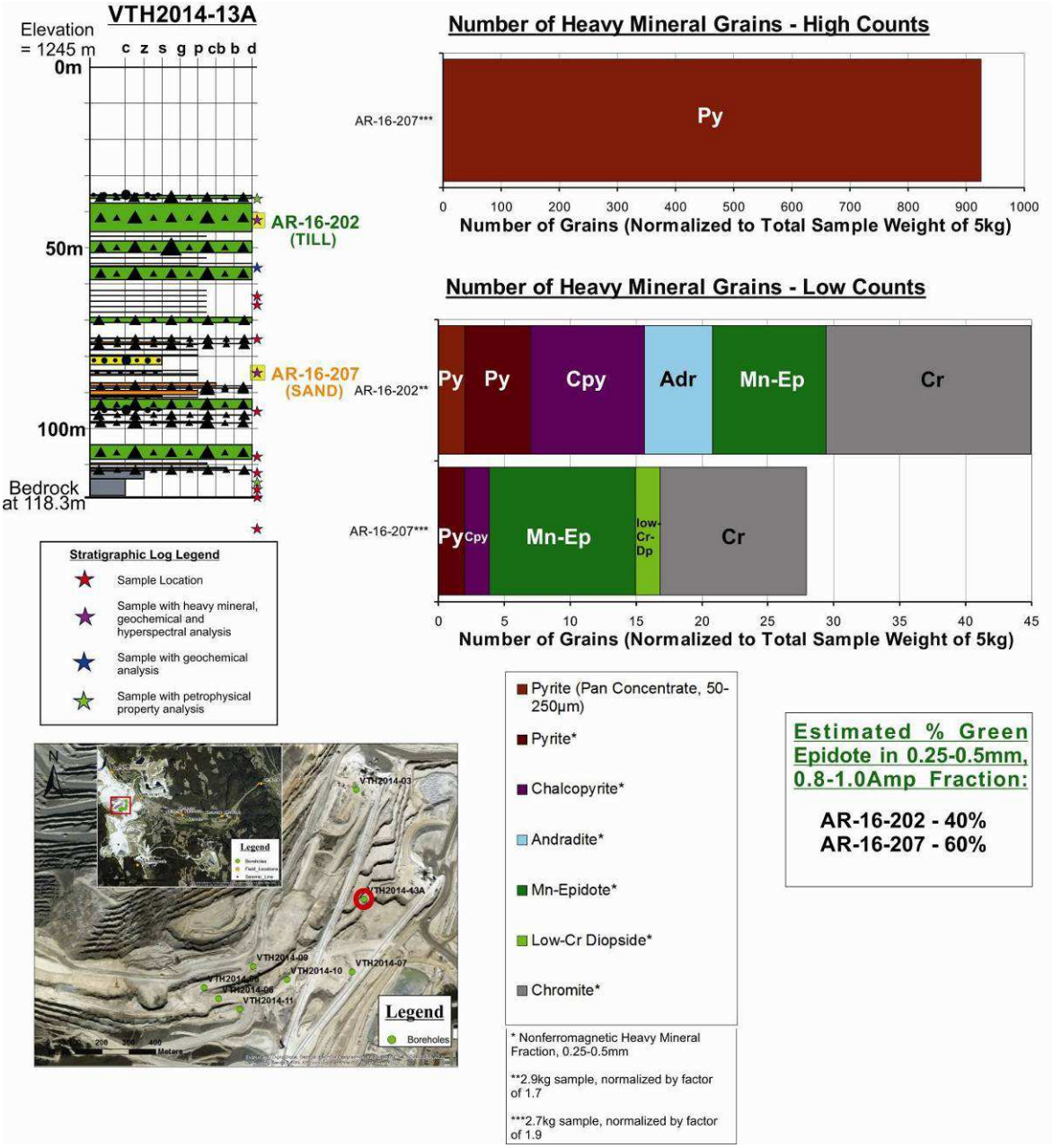

Figure C.28 Stratigraphic log, location map and indicator mineral results of core VTH2014-13A. The location of collected samples is shown on the stratigraphic log and the samples for which indicator mineral analysis was done are highlighted.

Figure C.29 Chalcopyrite grains from the 0.25-0.5mm fraction from sample AR-16-202 belonging to core VTH2014-13A.

Figure C.30 Mn-epidote grains from the 0.25-0.5mm fraction from sample AR-16-202 belonging to core VTH2014-13A.

Figure C.31 Chalcopyrite grain from the 0.25-0.5mm fraction from sample AR-16-207 belonging to core VTH2014-13A.

Figure C.32 Mn-epidote grains from the 0.25-0.5mm fraction from sample AR-16-207 belonging to core VTH2014-13A.

Core JA16-001

Indicator mineral analysis was done on two till samples at elevations of 1178.1-1177.8 m asl and 1169.2-1168.9 m asl and one sand sample at an elevation of 1128.3-1128.0 m asl from core JA16-001. The results are shown below (**Figure C.33**).

Both till samples have a higher number of visible gold grains (5 grains each) than the average for the Highland Valley shallow till samples collected by Plouffe and Ferbey (1 grain) (**Figure C.34**). The shallower till sample has a high covellite count (690 grains) compared to others in this study (66 grains). A photo of these grains from the 0.25-0.5mm fraction from this sample is shown below (**Figure C.35**).

The sand sample has a high pyrite count (2942 grains in the 0.025-0.5mm fraction, 2353 grains in the 0.25-0.5mm fraction) compared to others in this study (601 grains for the 0.025-0.5mm fraction, 193 grains for the 0.25-0.5mm fraction). It has a higher number of pyrite grains in the 0.25-0.5mm fraction than the average for the Highland Valley shallow till samples collected by Plouffe and Ferbey (2 grains) (**Figure C.36**). A photo of these grains from the 0.25-0.5mm fraction from this sample is shown below (**Figure C.37**). The sand sample has a high low-Cr diopside count (18 grains) compared to all the samples from the cores and Highmont pit (7 grains), and this count is higher than the average for the Highland Valley shallow till samples collected by Plouffe and Ferbey (3 grains) (**Figure C.38**). This sample also has a high chromite count (47 grains) compared to all the samples from the cores and Highmont pit (12 grains), and this count is higher than the average for the Highland Valley shallow till samples collected by Plouffe and Ferbey (5 grains) (**Figure C.39**).

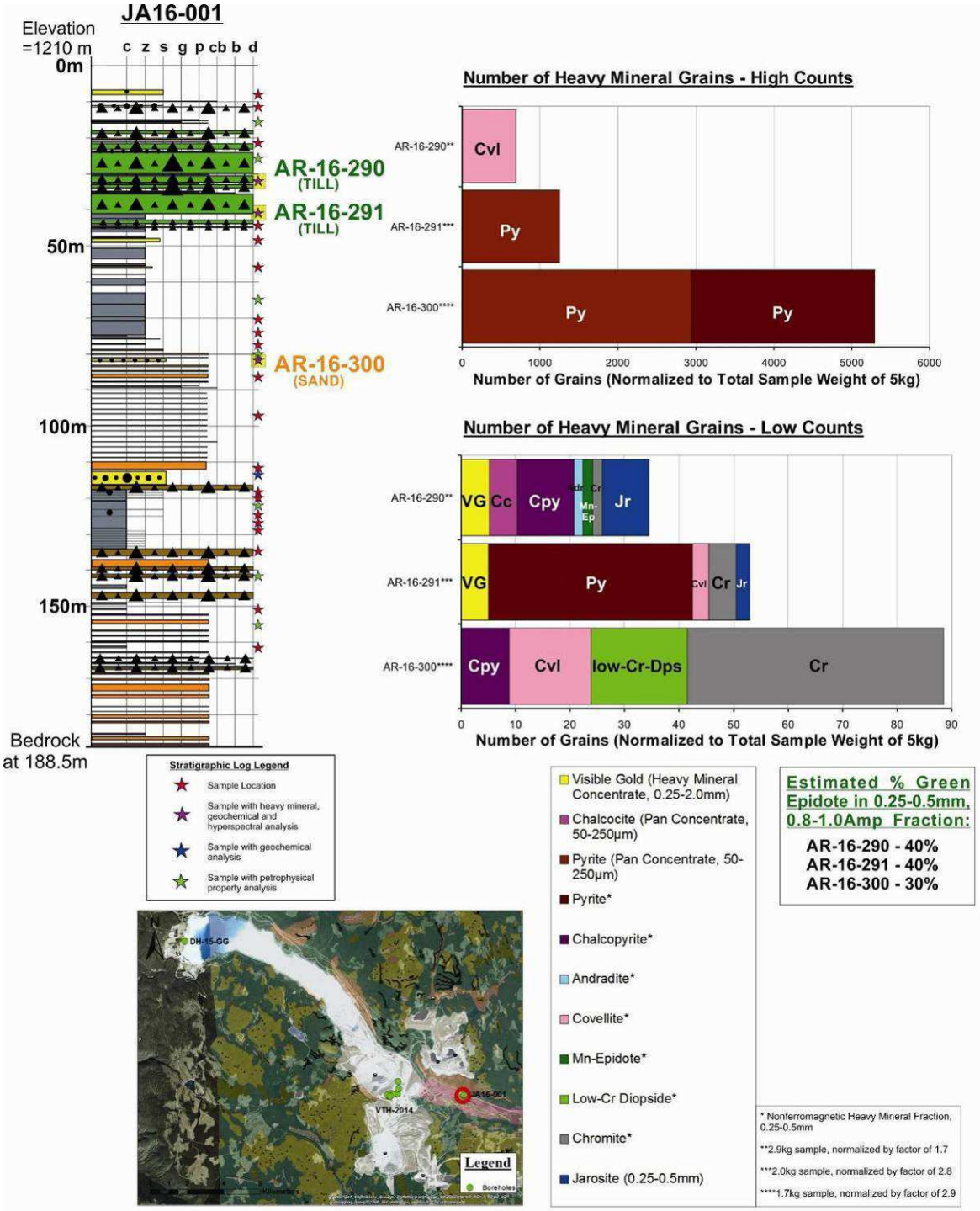

Figure C.33 Stratigraphic log, location map and indicator mineral results of core JA16-001. The location of collected samples is shown on the stratigraphic log and the samples for which indicator mineral analysis was done are highlighted.

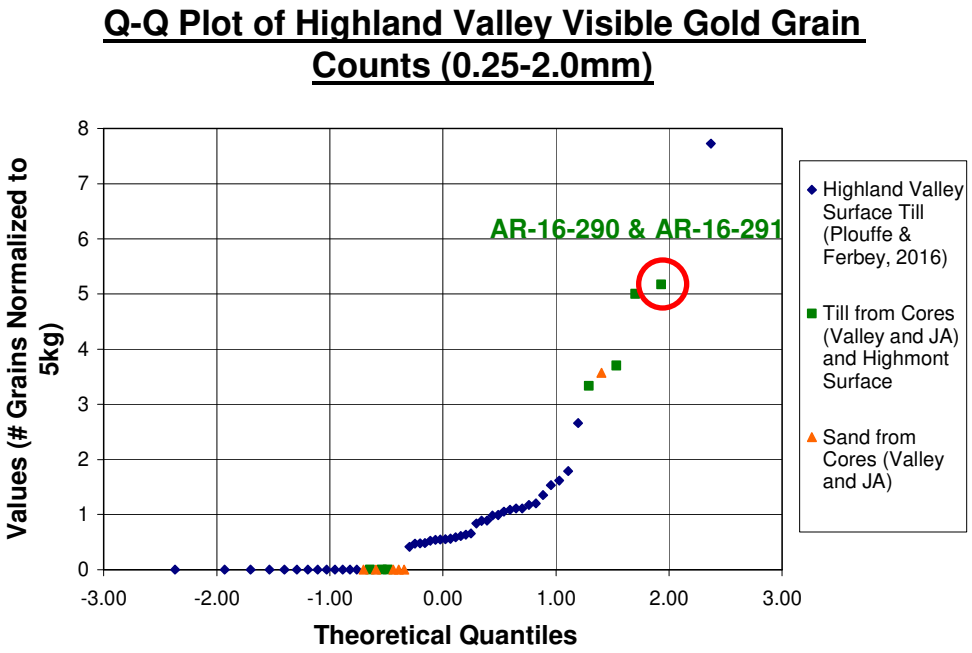

Figure C.34 Quantile-quantile plot of normalized visible gold grain counts for this study and Plouffe and Ferbey's study (2016), with the till samples from core JA16-001 highlighted.

Figure C.35 Covellite grains from the 0.25-0.5mm fraction from sample AR-16-290 belonging to core JA16-001.

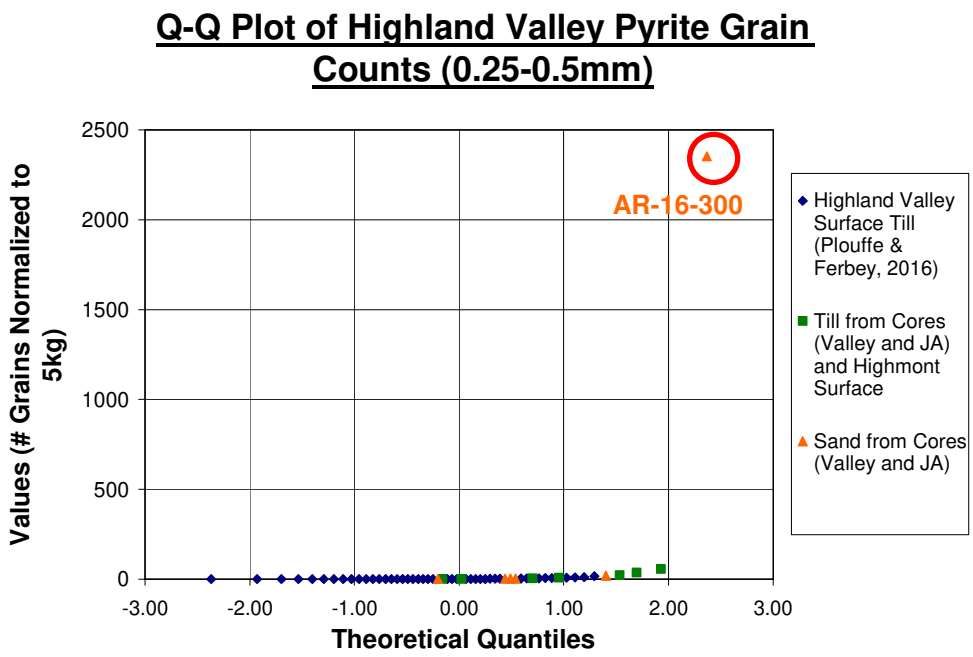

Figure C.36 Quantile-quantile plot of normalized pyrite grain counts for this study and Plouffe and Ferbey's study (2016), with the sand sample from core JA16-001 highlighted.

Figure C.37 Pyrite grains from the 0.25-0.5mm fraction from sample AR-16-300 belonging to core JA16-001.

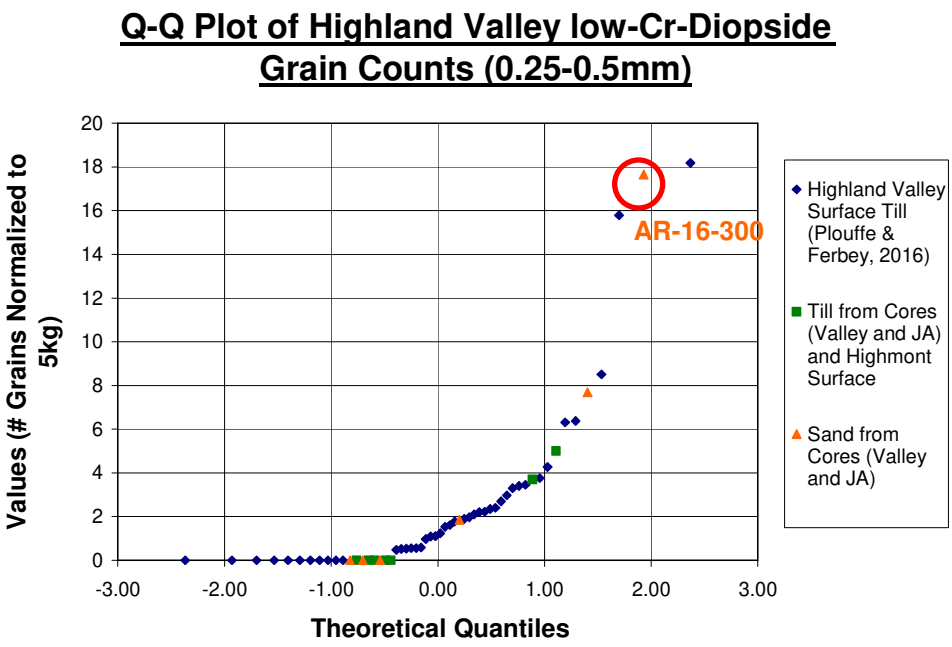

Figure C.38 Quantile-quantile plot of normalized low-Cr diopside grain counts for this study and Plouffe and Ferbey's study (2016), with the sand sample from core JA16-001 highlighted.

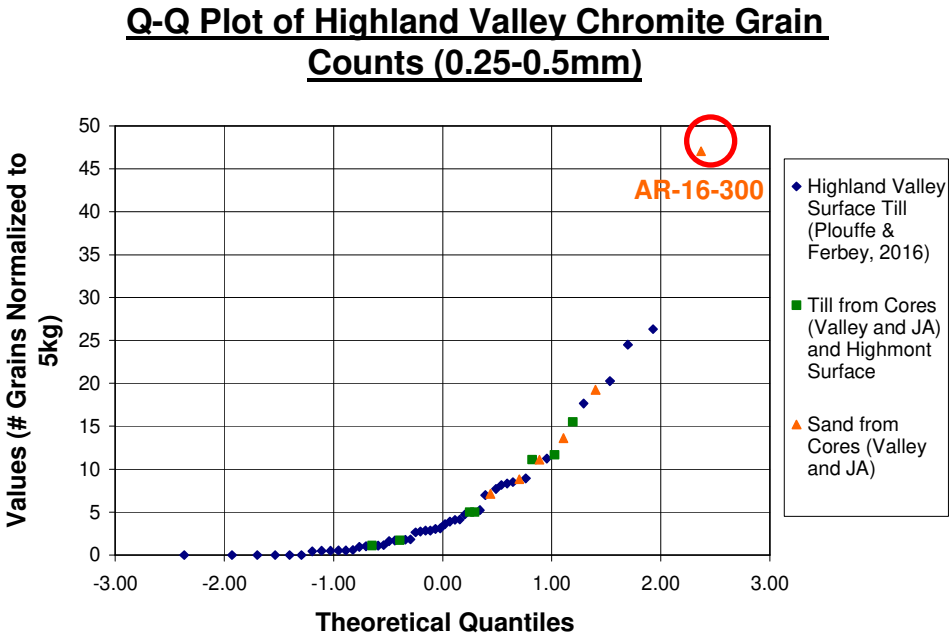

Figure C.39 Quantile-quantile plot of normalized chromite grain counts for this study and Plouffe and Ferbey's study (2016), with the sand sample from core JA16-001 highlighted.

Figure C.40 Chalcopyrite grains from the 0.25-0.5mm fraction from sample AR-16-290 belonging to core JA16-001.

Figure C.41 Mn-epidote grain from the 0.25-0.5mm fraction from sample AR-16-290 belonging to core JA16-001.

Figure C.42 Covellite grain from the 0.25-0.5mm fraction from sample AR-16-291 belonging to core JA16-001.

Figure C.43 Marcasite grains from the 0.25-0.5mm fraction from sample AR-16-291 belonging to core JA16-001.

Figure C.44 Pyrite grains from the 0.25-0.5mm fraction from sample AR-16-291 belonging to core JA16-001.

Figure C.45 Covellite grains from the 0.25-0.5mm fraction from sample AR-16-300 belonging to core JA16-001.

Figure C.46 Chalcopyrite grains from the 0.25-0.5mm fraction from sample AR-16-300 belonging to core JA16-001.

Figure C.47 Marcasite grains from the 0.25-0.5mm fraction from sample AR-16-300 belonging to core JA16-001.

Highmont South Pit

Indicator mineral analysis was done on a till sample 45-70m deep from the Highmont South shallow excavation. The results are shown below (**Figure C.48**). This sample has no significantly high mineral grain counts.

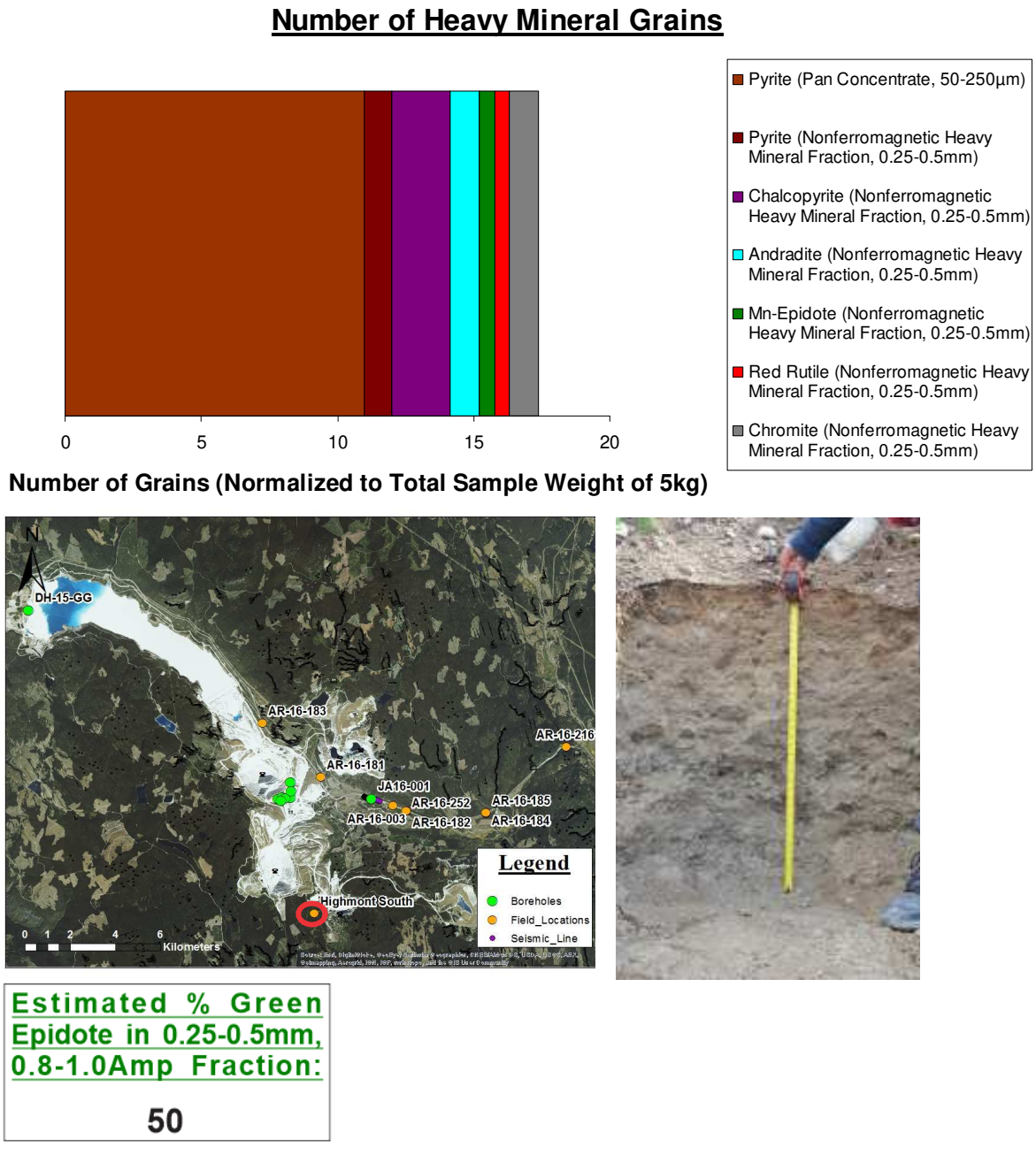

Figure C.48 Location map, photo and indicator mineral results of the Highmont South pit.

Figure C.49 Chalcopyrite grains from the 0.25-0.5mm fraction from sample AR-16-116 from the Highmont pit.

Figure C.50 Mn-epidote grain from the 0.25-0.5mm fraction from sample AR-16-116 from the Highmont pit.

Figure C.51 Rutile grain from the 0.25-0.5mm fraction from sample AR-16-116 from the Highmont pit.

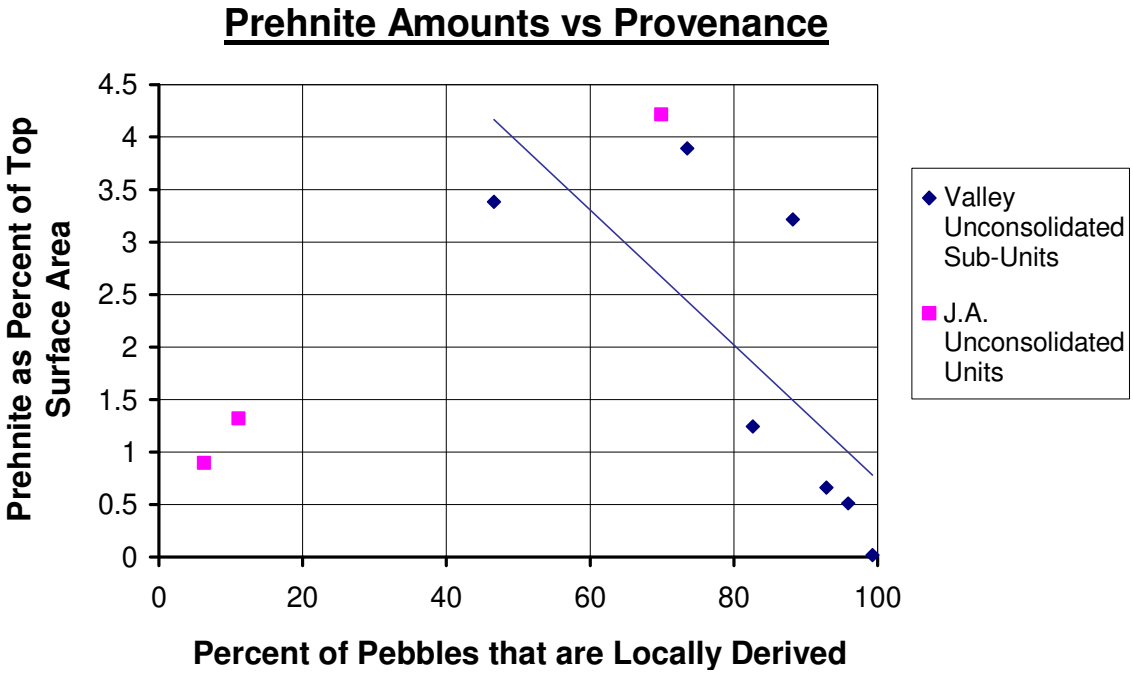

Figure C.52 Prehnite concentration vs proportion of sample that is locally (Guichon Creek batholith) derived.

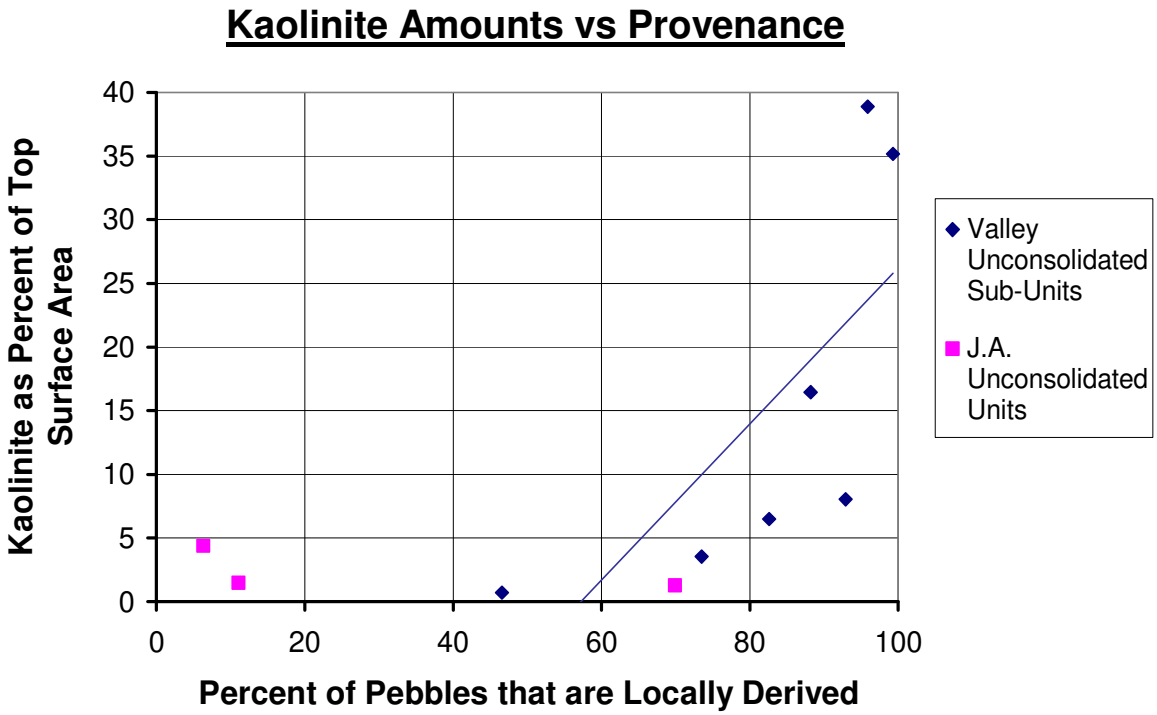

Figure C.53 Kaolinite concentration vs proportion of sample that is locally (Guichon Creek batholith) derived.

Geochemical Results

Table C.4 Lab report of geochemical analysis from Bureau Veritas Commodities Canada Limited.

(a)

Bureau Veritas Commodities Canada Ltd. Final Report

Client: Lakehead University
File Created: 30-Aug-17
Job Number: VAN17001625
Number of Samples: 15
Project: Highland Valley
Shipment ID:
P.O. Number:
Received: 02-Aug-17

	Method	LF200	LF200	LF200	LF200	LF200	LF200	LF200	LF200	LF200	LF200	LF200	LF200	LF200	LF200	LF200
	Analyte	SiO2	Al2O3	Fe2O3	MgO	CaO	Na2O	K2O	TiO2	P2O5	MnO	Cr2O3	Ba	Ni	Sc	LOI
	Unit	%	%	%	%	%	%	%	%	%	%	%	PPM	PPM	PPM	%
	MDL	0.01	0.01	0.04	0.01	0.01	0.01	0.01	0.01	0.01	0.01	0.002	1	20	1	-5.1
Sample	Type															
AR-16-030	Sediment Pulp	60.79	13.69	6.88	2.18	2.71	2.76	2.11	0.96	0.21	0.19	0.009	701	29	13	7.2
AR-16-033	Sediment Pulp	62.89	19.38	3.1	0.75	2.44	4.78	1.75	0.34	0.13	0.18	0.004	1143	<20	5	4
AR-16-047	Sediment Pulp	59.32	18.79	5.57	1.28	2.21	2.8	1.98	0.77	0.15	0.07	0.01	939	29	12	6.7
AR-16-065	Sediment	56.57	15.82	6.84	3.1	5.46	3.35	1.89	0.84	0.25	0.13	0.013	814	42	16	5.4
AR-16-075	Sediment	55.37	16.85	6.8	2.82	4.22	2.9	1.93	0.83	0.22	0.14	0.01	858	40	16	7.6
AR-16-095	Sediment Pulp	60.49	16	5.2	1.9	3.75	3.37	1.76	0.64	0.22	0.11	0.01	939	41	11	6.2
AR-16-224	Sediment	56.84	17.72	6.1	2.26	3.51	3.15	2.02	0.75	0.2	0.12	0.009	838	36	14	6.9
AR-16-229	Sediment Pulp	60.43	20.04	4.3	0.81	1.61	3.2	2.04	0.53	0.17	0.08	0.005	998	<20	7	6.4
AR-16-202	Sediment	61.84	14.85	6.17	2.15	5.44	3.95	1.71	0.81	0.25	0.09	0.014	770	29	14	2.4

	Sediment															
AR-16-207	Pulp	60.19	18.56	4.52	1.08	2.76	3.45	1.78	0.58	0.2	0.1	0.007	1004	22	9	6.4
AR-16-290	Sediment	55.45	15.38	7.5	3.31	5.6	2.95	1.8	0.92	0.25	0.13	0.014	742	46	18	6.3
AR-16-291	Sediment	52.36	15.06	7.77	3.11	6.62	2.73	1.45	0.99	0.24	0.14	0.018	681	52	20	9.2
	Sediment															
AR-16-300	Pulp	55.17	15.34	6.79	3.05	6.41	3.21	1.76	0.72	0.25	0.13	0.011	1155	37	16	6.8
	Sediment															
AR-16-116	Pulp	67.29	15.79	3.78	1.03	2.67	4.66	1.33	0.55	0.14	0.04	0.008	613	<20	8	2.5
	Sediment															
AR-16-120	Pulp	60.6	13.75	6.89	2.18	2.73	2.77	2.15	0.97	0.21	0.19	0.008	734	25	13	7.3
Pulp Duplicates																
	Sediment															
AR-16-120	Pulp	60.6	13.75	6.89	2.18	2.73	2.77	2.15	0.97	0.21	0.19	0.008	734	25	13	7.3
AR-16-120	REP															
	Sediment															
AR-16-033	Pulp	62.89	19.38	3.1	0.75	2.44	4.78	1.75	0.34	0.13	0.18	0.004	1143	<20	5	4
AR-16-033	REP	63.14	19.26	3.08	0.74	2.41	4.72	1.72	0.34	0.14	0.17	0.005	1156	<20	5	4
	Sediment															
AR-16-120	Pulp	60.6	13.75	6.89	2.18	2.73	2.77	2.15	0.97	0.21	0.19	0.008	734	25	13	7.3
AR-16-120	REP															
Reference Materials																
STD GS311-1	STD															
STD GS910-4	STD															
STD SO-19	STD	61.05	13.74	7.33	2.85	5.86	4.02	1.26	0.7	0.31	0.13	0.481	491	456	26	1.9
STD SO-19	STD	60.68	13.93	7.35	2.89	5.88	4.08	1.28	0.7	0.31	0.13	0.487	507	461	26	1.9
STD																
OREAS45EA	STD															
STD DS11	STD															
BLK	BLK															
BLK	BLK	<0.01	<0.01	<0.04	<0.01	<0.01	<0.01	<0.01	<0.01	<0.01	<0.01	<0.002	4	<20	<1	0
BLK	BLK															
Prep Wash																
ROCK-VAN	Prep Blank	70.44	14.36	3.25	1.03	2.2	4.47	2.03	0.36	0.1	0.09	<0.002	812	<20	7	1.5

(b)

Method	LF200	LF200	LF200	LF200	LF200	LF200	LF200	LF200	LF200	LF200	LF200	LF200	LF200	LF200	LF200
Analyte	Sum	Be	Co	Cs	Ga	Hf	Nb	Rb	Sn	Sr	Ta	Th	U	V	W

	Unit	%	PPM	PPM	PPM	PPM	PPM	PPM	PPM	PPM	PPM	PPM	PPM	PPM	PPM	PPM
	MDL	0.01	1	0.2	0.1	0.5	0.1	0.1	0.1	1	0.5	0.1	0.2	0.1	8	0.5
Sample	Type															
AR-16-030	Sediment Pulp	99.8	2	17.8	0.9	17.3	12.7	11.1	45.1	2	329.1	0.7	6.6	2	102	<0.5
AR-16-033	Sediment Pulp	99.83	<1	12.1	1	20.2	4.6	4.7	35.8	2	646.2	0.4	4	2.1	65	7
AR-16-047	Sediment Pulp	99.77	2	9.8	3.1	20.8	6.8	8.9	54.2	2	437	0.6	6.3	2.2	105	3.8
AR-16-065	Sediment	99.76	3	21.9	2	17.1	4.7	5.7	49.5	3	633.8	0.4	5.5	2	162	1.4
AR-16-075	Sediment	99.76	1	21	3.8	19.1	4.3	5.9	54.7	2	529.8	0.3	5.8	2.5	149	2.5
AR-16-095	Sediment Pulp	99.75	<1	15.3	2.3	16.6	5.2	6.4	40	1	578.6	0.4	4.2	1.8	114	5
AR-16-224	Sediment	99.71	2	18	2.8	21	4.3	6.3	52.7	<1	529.6	0.6	5.2	2.2	139	2.8
AR-16-229	Sediment Pulp	99.7	<1	6.8	3.2	22.4	6.5	5.7	41.3	2	427.1	0.3	3.8	2.5	85	9
AR-16-202	Sediment	99.8	1	14.8	1.1	13.8	5.9	4.8	38.6	2	692.6	0.3	4.4	1.8	165	1.1
AR-16-207	Sediment Pulp	99.72	3	8.3	3.4	22.2	8.1	6.6	40.2	2	451.1	0.5	5	2.5	94	13.5
AR-16-290	Sediment	99.69	<1	24.1	2.9	17.3	5	5.8	52.8	2	553.4	0.4	5.8	2.3	181	4.2
AR-16-291	Sediment	99.81	2	24.4	2.1	16.2	3.6	7.5	39	1	513.7	0.5	4.2	1.7	189	1.6
AR-16-300	Sediment Pulp	99.78	<1	17.4	2.5	16	4.7	7.5	43.2	4	559.1	0.6	8.1	3.2	156	29.3
AR-16-116	Sediment Pulp	99.82	2	5.1	1.2	14.9	7.8	3.6	27.3	<1	615.3	0.3	2.8	2	116	3.1
AR-16-120	Sediment Pulp	99.8	<1	18.1	0.9	16.2	13.1	10.1	45.1	2	328.3	0.7	6.3	2.4	104	0.8
Pulp Duplicates																
AR-16-120	Sediment Pulp	99.8	<1	18.1	0.9	16.2	13.1	10.1	45.1	2	328.3	0.7	6.3	2.4	104	0.8
AR-16-120	REP															
AR-16-033	Sediment Pulp	99.83	<1	12.1	1	20.2	4.6	4.7	35.8	2	646.2	0.4	4	2.1	65	7
AR-16-033	REP	99.82	<1	11.5	1.1	20.2	5.2	4.5	35.5	2	631.6	0.5	4.4	1.9	64	7.9
AR-16-120	Sediment Pulp	99.8	<1	18.1	0.9	16.2	13.1	10.1	45.1	2	328.3	0.7	6.3	2.4	104	0.8
AR-16-120	REP															
Reference Materials																
STD GS311-1	STD															
STD GS910-4	STD															
STD SO-19	STD	99.78	22	25.3	4.3	16.8	3.4	70.6	20.5	19	342.5	4.9	14.2	20.7	158	11.1
STD SO-19	STD	99.78	24	24.6	4.6	16.6	3.3	72.1	20.9	19	347.9	4.9	14	22.6	160	10.2
STD OREAS45EA	STD															
STD DS11	STD															
BLK	BLK															
BLK	BLK	<0.01	<1	<0.2	<0.1	<0.5	<0.1	<0.1	<0.1	<1	1.2	<0.1	<0.2	<0.1	<8	<0.5
BLK	BLK															
Prep Wash																

ROCK-VAN	Prep Blank	99.92	<1	4.3	0.4	14.8	3.6	7.2	40.5	<1	223.6	0.5	3.3	1.6	37	0.6

(c)

	Method	LF200	LF200	LF200	LF200	LF200	LF200	LF200	LF200	LF200	LF200	LF200	LF200	LF200	LF200	LF200
	Analyte	Zr	Y	La	Ce	Pr	Nd	Sm	Eu	Gd	Tb	Dy	Ho	Er	Tm	Yb
	Unit	PPM	PPM	PPM	PPM	PPM	PPM	PPM	PPM	PPM	PPM	PPM	PPM	PPM	PPM	PPM
	MDL	0.1	0.1	0.1	0.1	0.02	0.3	0.05	0.02	0.05	0.01	0.05	0.02	0.03	0.01	0.05
Sample	Type															
AR-16-030	Sediment Pulp	510.3	35.8	29.1	74.5	7.62	31	6.26	1.59	6.62	1.02	6.27	1.37	4.09	0.6	4.07
AR-16-033	Sediment Pulp	166.2	10.5	15.8	34.6	3.61	13.6	2.64	0.76	2.41	0.35	1.94	0.42	1.28	0.19	1.18
AR-16-047	Sediment Pulp	255.2	18.6	27.3	58.1	6.44	25.5	4.54	1.1	4.24	0.63	3.6	0.7	2.03	0.31	2.06
AR-16-065	Sediment	183.4	17.8	20.4	42.2	5.42	23	4.39	1.18	4.2	0.58	3.37	0.74	1.99	0.28	1.82
AR-16-075	Sediment	156.7	18.2	22.2	46.2	5.68	23.2	4.59	1.11	4.03	0.62	3.53	0.72	2.03	0.28	1.93
AR-16-095	Sediment Pulp	185.4	16.8	19.1	43.7	4.74	19.4	3.9	1.04	3.73	0.54	3.1	0.67	1.98	0.28	1.94
AR-16-224	Sediment	155.2	17.7	20.6	44	5.28	21.9	4.36	1.15	3.91	0.55	3.3	0.67	1.98	0.29	2
AR-16-229	Sediment Pulp	225.2	14	19.6	39.3	4.43	17	3.19	0.91	2.96	0.43	2.59	0.51	1.6	0.24	1.69
AR-16-202	Sediment	206.8	17.3	19.4	39.6	5.04	20.5	4.27	1.14	4.1	0.59	3.44	0.68	1.98	0.29	1.92
AR-16-207	Sediment Pulp	286.6	17.8	23.1	48.7	5.39	21.2	4	0.99	3.85	0.54	3.14	0.7	2.08	0.32	2.21
AR-16-290	Sediment	182.6	19.1	21.3	45.8	5.74	23.7	5.11	1.2	4.66	0.67	3.93	0.76	2.24	0.31	2.08
AR-16-291	Sediment	127	20.5	19	39.6	4.92	20.5	4.24	1.26	4.4	0.67	3.89	0.76	2.14	0.32	2.03
AR-16-300	Sediment Pulp	158.5	20.2	21	39.8	5.18	21.8	4.54	1.11	4.44	0.64	3.81	0.76	2.21	0.33	2.12
AR-16-116	Sediment Pulp	290.9	11.4	16	27.3	4.05	15.9	2.96	0.8	2.57	0.37	1.96	0.43	1.35	0.2	1.53
AR-16-120	Sediment Pulp	521.4	34.4	29.3	74.1	7.76	30.7	6.61	1.62	6.41	1.02	6.2	1.34	4.1	0.61	4.07
Pulp Duplicates																
AR-16-120	Sediment Pulp	521.4	34.4	29.3	74.1	7.76	30.7	6.61	1.62	6.41	1.02	6.2	1.34	4.1	0.61	4.07
AR-16-120	REP															
AR-16-033	Sediment Pulp	166.2	10.5	15.8	34.6	3.61	13.6	2.64	0.76	2.41	0.35	1.94	0.42	1.28	0.19	1.18
AR-16-033	REP	187.7	11.5	16.5	36	3.74	14.9	2.71	0.74	2.43	0.33	2.19	0.39	1.14	0.18	1.18
AR-16-120	Sediment Pulp	521.4	34.4	29.3	74.1	7.76	30.7	6.61	1.62	6.41	1.02	6.2	1.34	4.1	0.61	4.07
AR-16-120	REP															
Reference Materials																
STD GS311-1	STD															
STD GS910-4	STD															
STD SO-19	STD	117.9	35.8	73.9	163.3	20	80.1	14.05	3.85	11.18	1.47	7.64	1.48	4.11	0.59	3.83
STD SO-19	STD	118.4	36.2	71.7	165.3	20.39	79	14.1	3.99	11.18	1.46	7.89	1.45	4.15	0.58	3.76

STD OREAS45EA	STD														
STD DS11	STD														
BLK	BLK														
BLK	BLK	0.2	<0.1	<0.1	<0.1	<0.02	<0.3	<0.05	<0.02	<0.05	<0.01	<0.05	<0.02	<0.03	<0.01	<0.05
BLK	BLK															
Prep Wash																
ROCK-VAN	Prep Blank	154.9	20.2	15.4	28.5	3.38	13.5	2.87	0.76	2.89	0.49	3.31	0.74	2.21	0.37	2.46

(d)

	Method	LF200	TC000	TC000	AQ250	AQ250	AQ250	AQ250	AQ250	AQ250	AQ250	AQ250	AQ250	AQ250	AQ250	AQ250
	Analyte	Lu	TOT/C	TOT/S	Mo	Cu	Pb	Zn	Ag	Ni	Co	Mn	Fe	As	U	Au
	Unit	PPM	%	%	PPM	PPM	PPM	PPM	PPB	PPM	PPM	PPM	%	PPM	PPM	PPB
	MDL	0.01	0.02	0.02	0.01	0.01	0.01	0.1	2	0.1	0.1	1	0.01	0.1	0.1	0.2
Sample	Type															
AR-16-030	Sediment Pulp	0.65	2.02	0.02	0.66	46.25	14.39	62.7	226	16.4	12.9	1023	2.98	16.5	0.9	7.9
AR-16-033	Sediment Pulp	0.2	0.12	0.02	4.72	289.85	10.96	34.8	58	7.9	9.6	1193	1.27	3.4	1	<0.2
AR-16-047	Sediment Pulp	0.37	0.06	<0.02	8.85	546	13.57	54.4	88	18.4	7.7	345	2.69	8.1	0.9	2.5
AR-16-065	Sediment	0.29	0.39	<0.02	1.51	268.51	7.97	64.4	97	29.2	15.9	687	3.29	3.9	0.8	2
AR-16-075	Sediment	0.31	0.39	<0.02	1.86	403.06	7.69	76.6	134	27.8	18.3	839	3.28	4.8	1	2.2
AR-16-095	Sediment Pulp	0.3	0.28	<0.02	2.94	642.09	6.83	56.4	52	30.4	13.1	639	2.52	3.8	0.7	1.5
AR-16-224	Sediment	0.28	0.26	<0.02	3.78	877.64	5.57	68.8	237	22	14.8	675	2.94	4.6	1.2	2.7
AR-16-229	Sediment Pulp	0.29	0.09	0.02	19.18	1239.13	5.03	50.4	90	12	5.5	533	2.06	12.8	1.2	0.8
AR-16-202	Sediment	0.31	0.22	<0.02	0.95	116.45	4.84	35	42	14.8	9	328	2.76	2.9	0.6	0.3
AR-16-207	Sediment Pulp	0.38	0.48	0.06	18.5	919.92	9.03	74	211	14.8	7	566	2.11	6.5	1	1.8
AR-16-290	Sediment	0.35	0.51	<0.02	2.68	827.46	7.84	61	287	30.6	17.5	673	3.52	5.9	0.9	2.2
AR-16-291	Sediment	0.31	0.78	<0.02	0.69	76.8	4.88	64.4	82	38.8	19.3	804	3.61	4.8	0.6	1.4
AR-16-300	Sediment Pulp	0.33	0.99	0.23	4.41	143.43	15.36	107	174	27.2	14.1	642	3.06	5.3	1.6	1
AR-16-116	Sediment Pulp	0.24	0.1	<0.02	1.28	184.26	2	16.9	13	7.7	3.1	146	1.69	2.1	0.5	0.5
AR-16-120	Sediment Pulp	0.61	1.99	0.02	0.62	46.11	13.41	57.7	217	15.9	13.2	1043	3.03	15.4	0.8	14.8
Pulp Duplicates																
AR-16-120	Sediment Pulp	0.61	1.99	0.02	0.62	46.11	13.41	57.7	217	15.9	13.2	1043	3.03	15.4	0.8	14.8
AR-16-120	REP		2.02	0.02												
AR-16-033	Sediment Pulp	0.2	0.12	0.02	4.72	289.85	10.96	34.8	58	7.9	9.6	1193	1.27	3.4	1	<0.2
AR-16-033	REP	0.21														
AR-16-120	Sediment Pulp	0.61	1.99	0.02	0.62	46.11	13.41	57.7	217	15.9	13.2	1043	3.03	15.4	0.8	14.8
AR-16-120	REP				0.66	44.54	13	60.6	222	15.9	12	1031	2.94	15.2	0.7	3.5

Reference Materials																
STD GS311-1	STD		1.04	2.39												
STD GS910-4	STD		2.75	8.06												
STD SO-19	STD	0.54														
STD SO-19	STD	0.56														
STD OREAS45EA	STD				1.35	675.82	13.15	29.9	241	351.8	51.5	377	20.94	10.1	1.7	54.4
STD DS11	STD				12.62	147.84	133.05	331.7	1658	73.9	13.6	964	2.86	43.6	2.5	51.7
BLK	BLK		<0.02	<0.02												
BLK	BLK	<0.01														
BLK	BLK				<0.01	<0.01	<0.01	<0.1	<2	<0.1	<0.1	<1	<0.01	<0.1	<0.1	<0.2
Prep Wash																
ROCK-VAN	Prep Blank	0.42	0.05	<0.02	0.36	5.23	0.8	35.8	3	0.9	3.7	523	1.82	0.6	0.4	0.6

(e)

	Method	AQ250	AQ250	AQ250	AQ250	AQ250	AQ250	AQ250	AQ250	AQ250	AQ250	AQ250	AQ250	AQ250	AQ250	AQ250
	Analyte	Th	Sr	Cd	Sb	Bi	V	Ca	P	La	Cr	Mg	Ba	Ti	B	Al
	Unit	PPM	PPM	PPM	PPM	PPM	PPM	%	%	PPM	PPM	%	PPM	%	PPM	%
	MDL	0.1	0.5	0.01	0.02	0.02	2	0.01	0.001	0.5	0.5	0.01	0.5	0.001	20	0.01
Sample	Type															
AR-16-030	Sediment Pulp	2.4	10.5	0.24	4.68	2.04	51	0.28	0.091	19.5	28	0.53	85.1	0.085	<20	1.58
AR-16-033	Sediment Pulp	3.2	43.8	0.11	0.26	0.13	33	0.42	0.064	10	9.3	0.17	518	0.024	<20	0.68
AR-16-047	Sediment Pulp	3	75.8	0.12	0.23	0.21	56	0.53	0.062	13.1	24	0.45	338.9	0.093	<20	1.69
AR-16-065	Sediment	3.4	84.3	0.12	0.26	0.12	100	1.73	0.109	12	31.7	1.04	203.5	0.148	<20	1.8
AR-16-075	Sediment	4	97.1	0.11	0.23	0.19	87	1.43	0.099	13.1	32.4	1.05	266.2	0.128	<20	2.15
AR-16-095	Sediment Pulp	2.7	133.3	0.1	0.28	0.19	62	1.34	0.098	12.1	40.5	0.76	304.2	0.073	<20	1.33
AR-16-224	Sediment	3.9	84.2	0.17	0.29	0.17	81	1.08	0.087	12.7	27.9	0.86	251.4	0.106	<20	1.94
AR-16-229	Sediment Pulp	2.4	63.4	0.12	0.63	0.31	43	0.43	0.068	12.1	19.9	0.26	392.6	0.045	<20	1.25
AR-16-202	Sediment	2.6	50.4	0.08	0.25	0.06	103	1.32	0.115	10	29.3	0.46	99.5	0.113	<20	0.89
AR-16-207	Sediment Pulp	3.4	47.5	0.2	0.28	0.22	47	0.94	0.081	12.7	24.2	0.35	377	0.04	<20	1.35
AR-16-290	Sediment	4.2	84.4	0.13	0.31	0.35	109	1.9	0.108	11.9	34	1.12	167.3	0.136	<20	1.91
AR-16-291	Sediment	2.5	85.6	0.18	0.23	0.11	104	2.57	0.098	11	44.7	1.11	170.8	0.122	<20	1.87
AR-16-300	Sediment Pulp	5.8	116	0.17	0.42	0.14	89	2.44	0.106	13.9	37.2	1.01	502.4	0.119	<20	1.52
AR-16-116	Sediment Pulp	1.2	29	<0.01	0.12	0.1	62	0.35	0.061	8.2	17.5	0.24	117.6	0.033	<20	0.73
AR-16-120	Sediment Pulp	1.9	9.3	0.22	4.28	2.02	52	0.28	0.078	17.5	26	0.53	79.2	0.077	<20	1.59
Pulp Duplicates																
AR-16-120	Sediment Pulp	1.9	9.3	0.22	4.28	2.02	52	0.28	0.078	17.5	26	0.53	79.2	0.077	<20	1.59

AR-16-120	REP														
AR-16-033	Sediment Pulp	3.2	43.8	0.11	0.26	0.13	33	0.42	0.064	10	9.3	0.17	518	0.024	<20	0.68
AR-16-033	REP															
AR-16-120	Sediment Pulp	1.9	9.3	0.22	4.28	2.02	52	0.28	0.078	17.5	26	0.53	79.2	0.077	<20	1.59
AR-16-120	REP	2	9.5	0.19	4.19	1.97	51	0.27	0.083	16.9	24.5	0.52	77.6	0.074	<20	1.57
Reference Materials																
STD GS311-1	STD															
STD GS910-4	STD															
STD SO-19	STD															
STD SO-19	STD															
STD OREAS45EA	STD	9.7	3.4	0.02	0.24	0.23	292	0.03	0.028	6.6	828.1	0.08	135	0.094	<20	3.09
STD DS11	STD	7.2	61.1	2.34	6.76	11.17	47	0.95	0.078	16.7	56.1	0.82	407.6	0.087	<20	1.04
BLK	BLK															
BLK	BLK															
BLK	BLK	<0.1	<0.5	<0.01	<0.02	<0.02	<2	<0.01	<0.001	<0.5	<0.5	<0.01	<0.5	<0.001	<20	<0.01
Prep Wash																
ROCK-VAN	Prep Blank	2.1	15	<0.01	0.04	<0.02	20	0.5	0.044	4.9	2	0.5	42.5	0.063	<20	0.82

(f)

	Method	AQ250	AQ250	AQ250	AQ250	AQ250	AQ250	AQ250	AQ250	AQ250	AQ250
	Analyte	Na	K	W	Sc	Tl	S	Hg	Se	Te	Ga
	Unit	%	%	PPM	PPM	PPM	%	PPB	PPM	PPM	PPM
	MDL	0.001	0.01	0.1	0.1	0.02	0.02	5	0.1	0.02	0.1
Sample	Type										
AR-16-030	Sediment Pulp	0.024	0.05	0.1	4.6	0.12	<0.02	95	0.4	0.02	5.8
AR-16-033	Sediment Pulp	0.062	0.07	2.2	1.6	0.03	0.02	6	<0.1	0.03	2.4
AR-16-047	Sediment Pulp	0.009	0.12	0.2	6	0.09	<0.02	34	<0.1	0.04	5
AR-16-065	Sediment	0.066	0.21	<0.1	5.7	0.09	<0.02	32	<0.1	0.02	6
AR-16-075	Sediment	0.024	0.21	<0.1	7	0.08	<0.02	32	<0.1	0.03	7.1
AR-16-095	Sediment Pulp	0.03	0.11	0.4	5.5	0.07	<0.02	44	<0.1	0.03	4.1
AR-16-224	Sediment	0.026	0.18	<0.1	6.2	0.07	<0.02	34	<0.1	0.04	6.2
AR-16-229	Sediment Pulp	0.033	0.1	1.1	3.5	0.06	<0.02	15	<0.1	0.08	3.3

AR-16-202	Sediment	0.049	0.08	<0.1	3.4	0.03	<0.02	14	<0.1	0.02	3.6
AR-16-207	Sediment Pulp	0.029	0.11	1.4	4.3	0.04	0.06	30	<0.1	0.04	4
AR-16-290	Sediment	0.051	0.19	0.3	5.9	0.08	<0.02	58	<0.1	0.04	6.2
AR-16-291	Sediment	0.046	0.16	<0.1	9.2	0.08	<0.02	90	0.2	0.02	5.7
AR-16-300	Sediment Pulp	0.214	0.13	11.8	6.1	0.06	0.23	61	<0.1	0.02	5
AR-16-116	Sediment Pulp	0.007	0.03	0.3	2.4	<0.02	<0.02	<5	<0.1	0.02	2.7
AR-16-120	Sediment Pulp	0.024	0.05	0.1	4	0.11	<0.02	92	0.3	0.03	5.5
Pulp Duplicates											
AR-16-120	Sediment Pulp	0.024	0.05	0.1	4	0.11	<0.02	92	0.3	0.03	5.5
AR-16-120	REP										
AR-16-033	Sediment Pulp	0.062	0.07	2.2	1.6	0.03	0.02	6	<0.1	0.03	2.4
AR-16-033	REP										
AR-16-120	Sediment Pulp	0.024	0.05	0.1	4	0.11	<0.02	92	0.3	0.03	5.5
AR-16-120	REP	0.023	0.05	<0.1	4.1	0.11	<0.02	93	0.2	0.03	5.7
Reference Materials											
STD GS311-1	STD										
STD GS910-4	STD										
STD SO-19	STD										
STD SO-19	STD										
STD OREAS45EA	STD	0.018	0.05	<0.1	70.9	0.06	0.04	7	0.6	0.09	11.5
STD DS11	STD	0.064	0.37	2.9	2.9	4.79	0.27	275	2.1	4.56	4.8
BLK	BLK										
BLK	BLK										
BLK	BLK	<0.001	<0.01	<0.1	0.1	<0.02	<0.02	<5	<0.1	<0.02	<0.1
Prep Wash											
ROCK-VAN	Prep Blank	0.044	0.07	<0.1	2.4	<0.02	<0.02	<5	<0.1	<0.02	3.5

(g)

File Created: 22-Feb-18
Job Number: VAN18000272
Number of Samples: 20
Project: Highland Valley
Shipment ID:
P.O. Number:
Received: 06-Feb-18

	Method	LF200	LF200	LF200	LF200	LF200	LF200	LF200	LF200	LF200	LF200	LF200	LF200	LF200	LF200	LF200
	Analyte	SiO2	Al2O3	Fe2O3	MgO	CaO	Na2O	K2O	TiO2	P2O5	MnO	Cr2O3	Ba	Ni	Sc	LOI
	Unit	%	%	%	%	%	%	%	%	%	%	%	PPM	PPM	PPM	%
	MDL	0.01	0.01	0.04	0.01	0.01	0.01	0.01	0.01	0.01	0.01	0.002	1	20	1	-5.1
Sample	Type															
AR-15-001	Sediment Pulp	54.67	18.3	6.61	2.51	3.28	2.72	2.42	0.78	0.18	0.14	0.007	896	33	14	8
AR-15-003	Sediment Pulp	55.88	16.96	6.63	2.7	4.14	3.02	1.99	0.84	0.22	0.14	0.009	799	32	15	7.1
AR-16-002	Sediment Pulp	58.66	21.35	4.11	0.8	2.01	3.99	2	0.43	0.14	0.09	0.004	924	<20	7	6
AR-16-015	Sediment Pulp	55.26	16.29	7.18	3.22	5.42	3.26	1.96	0.91	0.26	0.14	0.013	842	44	16	5.8
AR-16-020	Sediment Pulp	58.72	16.91	5.71	2.25	3.51	3.48	1.94	0.74	0.25	0.16	0.01	969	26	15	5.9
AR-16-024	Sediment Pulp	62.47	16.35	4.95	1.65	3.51	3.77	1.73	0.75	0.19	0.08	0.01	745	<20	12	4.2
AR-16-027	Sediment Pulp	60.62	19.61	3.49	0.98	2.02	2.91	2.11	0.72	0.07	0.06	0.009	940	29	10	7.1
AR-16-048	Sediment Pulp	57.3	18.78	5.92	1.39	2.56	2.63	1.57	0.92	0.07	0.05	0.013	1082	40	13	8.4
AR-16-061	Sediment Pulp	59.18	15.53	6.51	2.57	5.85	3.98	1.79	0.94	0.28	0.11	0.017	841	36	15	2.9
AR-16-090	Sediment Pulp	61.37	19.25	4.2	0.69	2.33	4.2	1.53	0.49	0.18	0.09	0.004	855	<20	7	5.3
AR-16-016	Sediment Pulp	56.53	16.16	6.63	2.96	5.32	3.39	1.94	0.84	0.25	0.13	0.012	837	47	15	5.5
AR-16-122	Sediment Pulp	61.64	14.96	6.04	2.09	5.11	3.88	1.77	0.81	0.25	0.1	0.015	788	30	13	3
AR-16-127	Sediment Pulp	60.42	14.5	6.64	2.4	5.81	3.66	1.83	0.83	0.24	0.1	0.014	704	34	15	3.3
AR-16-159	Sediment Pulp	58.91	15.4	7.19	2.52	4.44	3.41	1.77	0.91	0.27	0.13	0.013	881	38	17	4.7
AR-16-166	Sediment Pulp	64.32	18.29	3.65	0.52	1.9	4.6	1.44	0.42	0.15	0.14	0.003	679	<20	6	4.3
AR-16-203	Sediment Pulp	61.91	15.12	6.04	2.02	5.18	4.1	1.76	0.82	0.27	0.09	0.013	794	27	13	2.4
AR-16-218	Sediment Pulp	54.27	16.79	6.81	3.29	5.17	3.15	2.16	0.86	0.26	0.14	0.01	920	46	15	6.7
AR-16-221	Sediment Pulp	68.22	15.94	2.84	0.64	2.37	4.41	1.63	0.31	0.15	0.08	<0.002	792	<20	4	3.1
AR-16-271	Sediment Pulp	53.32	16.4	7.65	2.93	2.12	1.15	1.45	0.94	0.06	0.12	0.01	2690	107	22	13.3
AR-16-303	Sediment Pulp	56.41	14.08	7.96	2.91	7.22	3.11	1.63	0.99	0.26	0.13	0.024	899	38	20	4.9
Pulp Duplicates																
AR-16-027	Sediment Pulp	60.62	19.61	3.49	0.98	2.02	2.91	2.11	0.72	0.07	0.06	0.009	940	29	10	7.1
AR-16-027	REP															

AR-16-159	Sediment Pulp	58.91	15.4	7.19	2.52	4.44	3.41	1.77	0.91	0.27	0.13	0.013	881	38	17	4.7
AR-16-159	REP	59.27	15.23	7.14	2.48	4.39	3.39	1.74	0.92	0.27	0.13	0.013	885	46	17	4.7
AR-16-218	Sediment Pulp	54.27	16.79	6.81	3.29	5.17	3.15	2.16	0.86	0.26	0.14	0.01	920	46	15	6.7
AR-16-218	REP															
Reference Materials																
STD GS311-1	STD															
STD GS910-4	STD															
STD SO-19	STD	60.01	14.16	7.5	2.97	6.04	4.08	1.32	0.7	0.32	0.13	0.498	462	474	26	1.9
STD SO-19	STD	60.35	14.08	7.43	2.93	6	4	1.29	0.69	0.31	0.13	0.493	480	460	26	1.9
STD OREAS45EA	STD															
STD DS11	STD															
BLK	BLK															
BLK	BLK	0.03	<0.01	<0.04	<0.01	<0.01	<0.01	<0.01	<0.01	<0.01	<0.01	<0.002	<1	<20	<1	0
BLK	BLK															
Prep Wash																
ROCK-VAN	Prep Blank	70.34	14.2	3.3	1.05	2.09	4.73	2.02	0.35	0.09	0.09	<0.002	821	<20	7	1.6

(h)

	Method	LF200	LF200	LF200	LF200	LF200	LF200	LF200	LF200	LF200	LF200	LF200	LF200	LF200	LF200	LF200
	Analyte	Sum	Be	Co	Cs	Ga	Hf	Nb	Rb	Sn	Sr	Ta	Th	U	V	W
	Unit	%	PPM	PPM	PPM	PPM	PPM	PPM	PPM	PPM	PPM	PPM	PPM	PPM	PPM	PPM
	MDL	0.01	1	0.2	0.1	0.5	0.1	0.1	0.1	1	0.5	0.1	0.2	0.1	8	0.5
Sample	Type															
AR-15-001	Sediment Pulp	99.75	1	21.2	3.9	21.1	3.2	6.3	61.4	1	466.9	0.4	5.3	2.4	132	2.8
AR-15-003	Sediment Pulp	99.76	2	20	3.6	19.3	3.9	5.9	50.5	1	521.7	0.5	5.8	2.6	154	2.5
AR-16-002	Sediment Pulp	99.74	1	7.2	1.6	22	5	4.7	37.8	5	490.3	0.2	3.7	2.3	80	8.7
AR-16-015	Sediment Pulp	99.76	1	22.1	3.2	17.8	3.8	6	47.3	1	625.5	0.4	5.4	2	159	5.9
AR-16-020	Sediment Pulp	99.7	<1	16.3	3.2	17.5	4	5.4	41.7	<1	501.1	0.3	4.6	2.8	136	14.7
AR-16-024	Sediment Pulp	99.78	1	12.8	1.6	16.8	6.6	7.3	39.6	<1	558.4	0.6	5.3	2.1	118	11.3
AR-16-027	Sediment Pulp	99.83	<1	8.5	3.5	22.6	4.7	7.1	57.4	1	404.5	0.5	5.5	2.2	78	5.1
AR-16-048	Sediment Pulp	99.71	<1	10.5	4.4	20.8	5.4	9.3	65.5	1	459.8	0.8	4.5	2	90	2.8
AR-16-061	Sediment Pulp	99.77	<1	16.8	1.3	17	4.9	5.8	36	1	738.7	0.4	4.1	1.9	161	2.9
AR-16-090	Sediment Pulp	99.76	3	6.5	2	19.1	7.6	4.5	28.1	8	556.2	0.3	3.4	2.1	87	4.5
AR-16-016	Sediment Pulp	99.76	<1	19.8	2.7	17.2	3.8	5.7	46.6	3	633.4	0.3	4.6	1.9	148	23
AR-16-122	Sediment Pulp	99.79	<1	14	1.3	14.5	5.7	5.3	37.4	2	651.4	0.3	4.3	2.1	158	1.6
AR-16-127	Sediment Pulp	99.79	<1	15.8	1.6	14.3	6.2	5	41	1	625.6	0.3	4.8	1.8	183	0.9

AR-16-159	Sediment Pulp	99.77	2	19.6	2.6	16.9	6.2	5.5	43.4	1	588.6	0.4	5.3	2.2	163	1.6
AR-16-166	Sediment Pulp	99.83	2	5.9	1.9	19.3	7.2	4.5	25.7	<1	507.6	0.3	4.3	1.7	74	6.2
AR-16-203	Sediment Pulp	99.79	4	14.5	1.2	15.2	5.9	4.8	35.4	<1	716.6	0.3	3.8	1.9	150	1.4
AR-16-218	Sediment Pulp	99.76	<1	23.7	3.8	18.8	3.4	5.6	53.3	<1	619.3	0.4	5.2	1.9	145	2
AR-16-221	Sediment Pulp	99.81	<1	4.4	1.1	15.2	5.2	4.4	29.7	<1	539.7	0.3	4.3	1.9	58	7.5
AR-16-271	Sediment Pulp	99.76	<1	104.6	5.3	22.5	3.8	7.6	92.8	2	357.5	0.4	9.9	5.1	244	2.3
AR-16-303	Sediment Pulp	99.75	<1	18.7	1.5	15.3	7.6	7.3	36.5	3	598.5	0.5	5	2.7	216	9.6
Pulp Duplicates																
AR-16-027	Sediment Pulp	99.83	<1	8.5	3.5	22.6	4.7	7.1	57.4	1	404.5	0.5	5.5	2.2	78	5.1
AR-16-027	REP															
AR-16-159	Sediment Pulp	99.77	2	19.6	2.6	16.9	6.2	5.5	43.4	1	588.6	0.4	5.3	2.2	163	1.6
AR-16-159	REP	99.77	2	19.1	2.4	16.6	6	5.3	43.4	1	584.3	0.3	5.5	2	165	1.5
AR-16-218	Sediment Pulp	99.76	<1	23.7	3.8	18.8	3.4	5.6	53.3	<1	619.3	0.4	5.2	1.9	145	2
AR-16-218	REP															
Reference Materials																
STD GS311-1	STD															
STD GS910-4	STD															
STD SO-19	STD	99.78	15	24	4.2	16.4	2.9	67.1	19.5	18	341.6	4.7	12.9	20.1	161	10.8
STD SO-19	STD	99.78	17	25.3	4.6	16.7	3.2	69.4	19.7	19	337.3	4.8	13.3	21.7	160	9.2
STD OREAS45EA	STD															
STD DS11	STD															
BLK	BLK															
BLK	BLK	0.03	<1	<0.2	<0.1	<0.5	<0.1	<0.1	<0.1	<1	<0.5	<0.1	<0.2	<0.1	<8	<0.5
BLK	BLK															
Prep Wash																
ROCK-VAN	Prep Blank	99.93	1	4.5	0.4	13.8	3.4	5.1	34.4	<1	210.2	0.4	3.2	1.5	38	0.6

(i)

	Method	LF200	LF200	LF200	LF200	LF200	LF200	LF200	LF200	LF200	LF200	LF200	LF200	LF200	LF200	LF200
	Analyte	Zr	Y	La	Ce	Pr	Nd	Sm	Eu	Gd	Tb	Dy	Ho	Er	Tm	Yb
	Unit	PPM	PPM	PPM	PPM	PPM	PPM	PPM	PPM	PPM	PPM	PPM	PPM	PPM	PPM	PPM
	MDL	0.1	0.1	0.1	0.1	0.02	0.3	0.05	0.02	0.05	0.01	0.05	0.02	0.03	0.01	0.05
Sample	Type															
AR-15-001	Sediment Pulp	106.9	17.9	22.7	50.7	5.47	23.1	4.28	1.06	4.07	0.56	2.95	0.62	1.84	0.25	1.74
AR-15-003	Sediment Pulp	141.2	18	22.7	47.3	5.56	22.3	4.53	1.09	3.96	0.57	3.3	0.65	1.8	0.26	1.74
AR-16-002	Sediment Pulp	181.4	11.5	16.7	40.6	3.74	14.4	2.78	0.77	2.55	0.38	2.09	0.46	1.2	0.19	1.41
AR-16-015	Sediment Pulp	142.7	17.2	22.2	48	5.57	22.1	4.28	1.19	3.88	0.54	3.15	0.65	1.88	0.25	1.64

AR-16-020	Sediment Pulp	148.3	18.9	24.4	49.6	5.85	23.3	4.89	1.35	4.23	0.63	3.76	0.71	2.06	0.29	2.03
AR-16-024	Sediment Pulp	238.8	18.6	24.9	49	5.75	23.4	4.46	1.06	4.02	0.6	3.65	0.67	2.03	0.29	1.95
AR-16-027	Sediment Pulp	165.7	16.2	27.7	51	5.98	22.4	4.39	1.15	3.62	0.52	3.03	0.56	1.67	0.24	1.57
AR-16-048	Sediment Pulp	197.3	21.5	22.6	35	5.22	21.1	4.25	1.14	3.95	0.57	3.36	0.71	2.02	0.3	2.18
AR-16-061	Sediment Pulp	172.5	17	22.1	45.5	5.47	22.2	4.41	1.16	3.89	0.55	3.03	0.65	1.79	0.24	1.75
AR-16-090	Sediment Pulp	276.1	13.7	21.1	50.2	4.68	18.9	3.26	0.8	2.96	0.42	2.64	0.51	1.5	0.22	1.64
AR-16-016	Sediment Pulp	141.2	16.2	21.9	45.3	5.37	21.7	4.36	1.16	3.78	0.55	3.11	0.64	1.68	0.28	1.62
AR-16-122	Sediment Pulp	216.5	17.6	20.2	42.5	5.2	21.1	4.4	1.08	3.65	0.55	3.17	0.58	1.56	0.26	1.72
AR-16-127	Sediment Pulp	226.3	16.7	20.1	41.2	5.16	21.5	4.28	1.07	3.77	0.55	3.26	0.64	1.83	0.27	1.82
AR-16-159	Sediment Pulp	233.5	23	22.8	49.8	6.12	24.8	5.26	1.2	4.8	0.69	3.73	0.84	2.47	0.35	2.37
AR-16-166	Sediment Pulp	260.7	15.5	18.5	54.4	4.02	15.6	2.97	0.69	2.86	0.41	2.49	0.54	1.83	0.26	1.99
AR-16-203	Sediment Pulp	202.7	17.8	21	42.6	5.31	21.4	4.23	1.09	3.85	0.55	3.12	0.67	1.91	0.26	1.72
AR-16-218	Sediment Pulp	116.1	16.9	22.6	46	5.54	22.9	4.28	1.13	3.88	0.54	2.94	0.64	1.69	0.25	1.62
AR-16-221	Sediment Pulp	184.2	11.7	17	38.5	3.82	14.2	3.04	0.82	2.37	0.34	2.02	0.39	1.27	0.18	1.29
AR-16-271	Sediment Pulp	124.3	16.1	20.3	66.1	4.3	16.5	3.45	0.71	3.22	0.51	2.93	0.65	1.88	0.27	1.75
AR-16-303	Sediment Pulp	275.3	22	23.6	47.6	5.52	22.9	4.68	1.27	4.52	0.68	4.02	0.81	2.49	0.36	2.35
Pulp Duplicates																
AR-16-027	Sediment Pulp	165.7	16.2	27.7	51	5.98	22.4	4.39	1.15	3.62	0.52	3.03	0.56	1.67	0.24	1.57
AR-16-027	REP															
AR-16-159	Sediment Pulp	233.5	23	22.8	49.8	6.12	24.8	5.26	1.2	4.8	0.69	3.73	0.84	2.47	0.35	2.37
AR-16-159	REP	229.2	22.8	25	49.3	6.11	26.1	5.43	1.26	4.89	0.71	4.01	0.8	2.44	0.34	2.27
AR-16-218	Sediment Pulp	116.1	16.9	22.6	46	5.54	22.9	4.28	1.13	3.88	0.54	2.94	0.64	1.69	0.25	1.62
AR-16-218	REP															
Reference Materials																
STD GS311-1	STD															
STD GS910-4	STD															
STD SO-19	STD	112.5	36	74.1	167.7	19.14	74.4	13.03	3.62	10.4	1.35	7.27	1.36	3.83	0.51	3.61
STD SO-19	STD	111.7	36.8	76.1	168.2	19.65	74.7	13.28	3.75	10.28	1.41	7.1	1.43	3.99	0.56	3.44
STD OREAS45EA	STD															
STD DS11	STD															
BLK	BLK															
BLK	BLK	<0.1	<0.1	<0.1	<0.1	<0.02	<0.3	<0.05	<0.02	<0.05	<0.01	<0.05	<0.02	<0.03	<0.01	<0.05
BLK	BLK															
Prep Wash																
ROCK-VAN	Prep Blank	136.2	18.3	16.2	29.1	3.36	13.5	2.93	0.79	2.84	0.46	3.02	0.61	2.02	0.3	2.15

(j)

	Method	LF200	TC000	TC000	AQ250	AQ250	AQ250	AQ250	AQ250	AQ250	AQ250	AQ250	AQ250	AQ250	AQ250	AQ250
	Analyte	Lu	TOT/C	TOT/S	Mo	Cu	Pb	Zn	Ag	Ni	Co	Mn	Fe	As	U	Au
	Unit	PPM	%	%	PPM	PPM	PPM	PPM	PPB	PPM	PPM	PPM	%	PPM	PPM	PPB
	MDL	0.01	0.02	0.02	0.01	0.01	0.01	0.1	2	0.1	0.1	1	0.01	0.1	0.1	0.2
Sample	Type															
AR-15-001	Sediment Pulp	0.27	0.27	<0.02	3.55	589.78	11.12	105.4	176	32.2	19.5	848	3.43	10.9	1.4	3.6
AR-15-003	Sediment Pulp	0.29	0.34	0.02	1.95	435.75	7.17	77.5	144	27.4	17.6	803	3.24	4.5	1.5	5.1
AR-16-002	Sediment Pulp	0.23	0.13	0.02	9.92	900.25	14.4	47.5	70	15.9	6.6	611	1.93	5.8	1.4	1
AR-16-015	Sediment Pulp	0.25	0.46	<0.02	1.59	271.16	6.45	73.3	103	35.8	19.5	776	3.49	4.2	1.1	2.9
AR-16-020	Sediment Pulp	0.3	0.7	0.03	11.36	1016.85	7.28	85.9	219	26.2	13.4	1028	2.86	7.9	1.9	25.6
AR-16-024	Sediment Pulp	0.32	0.11	<0.02	3.19	416.84	4.54	44.6	100	16.7	10.8	366	2.21	1.8	0.7	1.2
AR-16-027	Sediment Pulp	0.25	0.19	<0.02	3.57	317.68	7.78	69.4	94	22.5	7.7	327	1.55	1.5	1.3	3
AR-16-048	Sediment Pulp	0.34	0.63	<0.02	9.1	911.32	8.93	83.1	284	28.3	8.7	260	2.97	4.8	1	0.3
AR-16-061	Sediment Pulp	0.24	0.25	<0.02	1.83	150.48	3.85	47.2	55	21.7	11.2	473	2.81	3.2	0.8	1.3
AR-16-090	Sediment Pulp	0.28	0.11	0.05	3.86	576.52	10.36	44.3	28	8.1	5.5	550	1.96	4.9	0.9	0.3
AR-16-016	Sediment Pulp	0.26	0.4	<0.02	1.9	291.12	8.73	78.2	110	37	16.7	693	3.2	4.1	1	8.2
AR-16-122	Sediment Pulp	0.28	0.2	0.02	1.78	193.74	5.22	41.6	69	17.6	9.4	430	2.7	3	0.7	1.5
AR-16-127	Sediment Pulp	0.28	0.29	<0.02	0.9	123.88	4.65	35.1	53	19.3	10	382	3.05	2.9	0.8	4
AR-16-159	Sediment Pulp	0.35	0.05	<0.02	1.26	254.14	4.99	66.2	39	34.4	15.3	739	3.6	4.9	0.8	1.8
AR-16-166	Sediment Pulp	0.34	0.06	<0.02	4.33	352.49	8.2	30.5	15	6.9	4.9	1026	1.85	6.3	0.5	0.2
AR-16-203	Sediment Pulp	0.29	0.22	<0.02	1.31	146.32	4.36	37.8	30	16.1	8.1	347	2.65	2.8	0.7	0.7
AR-16-218	Sediment Pulp	0.25	0.57	<0.02	2.8	359.04	6.14	89.8	164	37.5	20.5	900	3.54	4.6	1	3.6
AR-16-221	Sediment Pulp	0.23	0.23	0.04	7.77	472.34	10.07	67	125	6.8	3.8	544	1.46	5.3	0.9	1.8
AR-16-271	Sediment Pulp	0.27	0.87	0.04	0.95	164.42	22.3	246.4	361	101.9	103.9	855	4.12	10	3.2	12
AR-16-303	Sediment Pulp	0.38	0.84	0.18	3.08	204.42	10.18	51.7	100	25.9	12.9	538	3.39	5.3	1.1	1.8
Pulp Duplicates																
AR-16-027	Sediment Pulp	0.25	0.19	<0.02	3.57	317.68	7.78	69.4	94	22.5	7.7	327	1.55	1.5	1.3	3
AR-16-027	REP		0.18	<0.02												
AR-16-159	Sediment Pulp	0.35	0.05	<0.02	1.26	254.14	4.99	66.2	39	34.4	15.3	739	3.6	4.9	0.8	1.8
AR-16-159	REP	0.37														
AR-16-218	Sediment Pulp	0.25	0.57	<0.02	2.8	359.04	6.14	89.8	164	37.5	20.5	900	3.54	4.6	1	3.6
AR-16-218	REP				2.71	353.07	6.1	88.4	152	36.6	20.1	904	3.52	4.7	1	2.1
Reference Materials																
STD GS311-1	STD		1.03	2.31												
STD GS910-4	STD		2.72	8.4												

STD SO-19	STD	0.5														
STD SO-19	STD	0.53														
STD OREAS45EA	STD				1.54	707.67	14.76	31.4	245	385.6	55.6	395	21.85	10.9	1.9	52.9
STD DS11	STD				14.35	159.3	139.81	346	1783	84.3	14.4	1048	3.12	41.4	2.7	63.9
BLK	BLK		<0.02	<0.02												
BLK	BLK	<0.01														
BLK	BLK				<0.01	<0.01	<0.01	<0.1	<2	<0.1	<0.1	<1	<0.01	0.2	<0.1	<0.2
Prep Wash																
ROCK-VAN	Prep Blank	0.34	0.09	<0.02	0.98	3.18	1.2	42.2	5	2.1	4.5	558	1.94	1.1	0.4	0.7

(k)

	Method	AQ250	AQ250	AQ250	AQ250	AQ250	AQ250	AQ250	AQ250	AQ250	AQ250	AQ250	AQ250	AQ250	AQ250	AQ250
	Analyte	Th	Sr	Cd	Sb	Bi	V	Ca	P	La	Cr	Mg	Ba	Ti	B	Al
	Unit	PPM	PPM	PPM	PPM	PPM	PPM	%	%	PPM	PPM	%	PPM	%	PPM	%
	MDL	0.1	0.5	0.01	0.02	0.02	2	0.01	0.001	0.5	0.5	0.01	0.5	0.001	20	0.01
Sample	Type															
AR-15-001	Sediment Pulp	4.9	106.5	0.12	0.18	0.29	77	1.26	0.069	17.8	31.5	1.02	346.8	0.15	<20	2.7
AR-15-003	Sediment Pulp	4.7	105.3	0.16	0.21	0.24	90	1.45	0.086	15.2	29.6	1.03	300.9	0.145	<20	2.4
AR-16-002	Sediment Pulp	3.2	48.5	0.09	0.37	0.26	42	0.52	0.061	12.4	24.2	0.26	374.3	0.039	<20	1.29
AR-16-015	Sediment Pulp	4.1	107	0.11	0.29	0.15	97	1.76	0.102	15.4	34.3	1.13	262.7	0.178	<20	2.08
AR-16-020	Sediment Pulp	4	75.9	0.17	0.33	1.03	78	1	0.108	18.7	39.2	0.8	427.6	0.139	<20	1.88
AR-16-024	Sediment Pulp	3.3	51.5	0.09	0.25	0.14	60	0.7	0.078	12.1	21.9	0.52	182.6	0.091	<20	1.37
AR-16-027	Sediment Pulp	3.5	58.9	0.1	0.15	0.22	28	0.63	0.034	18.9	34.2	0.35	352.1	0.07	<20	1.84
AR-16-048	Sediment Pulp	3.2	112.7	0.2	0.2	0.2	48	0.69	0.031	15.3	42.1	0.54	636.3	0.179	<20	3.03
AR-16-061	Sediment Pulp	2.9	74.2	0.09	0.24	0.09	93	1.55	0.104	13.4	30.6	0.6	177.8	0.159	<20	1.16
AR-16-090	Sediment Pulp	2.5	78.7	0.09	0.42	0.16	47	0.52	0.077	12.3	12.3	0.2	397.1	0.033	<20	1.08
AR-16-016	Sediment Pulp	3.8	100.9	0.15	0.23	0.15	89	1.77	0.1	15	32	1	247.3	0.164	<20	1.91
AR-16-122	Sediment Pulp	2.7	52.5	0.1	0.24	0.1	93	1.2	0.101	11.3	28.5	0.48	181.2	0.12	<20	0.98
AR-16-127	Sediment Pulp	3.2	54.7	0.08	0.31	0.09	114	1.77	0.104	11	33.6	0.58	114.6	0.132	<20	1.1
AR-16-159	Sediment Pulp	3.9	64.8	0.18	0.35	0.09	100	1.14	0.114	15.5	37.7	0.79	282.7	0.165	<20	1.78
AR-16-166	Sediment Pulp	2.4	55.8	0.11	0.52	0.27	40	0.43	0.062	11.4	7.4	0.14	244.1	0.02	<20	0.65
AR-16-203	Sediment Pulp	2.7	51	0.06	0.23	0.08	88	1.2	0.111	12.2	25.9	0.41	116.2	0.12	<20	0.84
AR-16-218	Sediment Pulp	4.1	120.1	0.17	0.28	0.17	92	1.99	0.11	16.7	31.1	1.3	282.1	0.183	<20	2.35
AR-16-221	Sediment Pulp	3.7	54.8	0.12	0.25	0.28	36	0.57	0.063	12.9	7.9	0.21	287.9	0.023	<20	0.74
AR-16-271	Sediment Pulp	9.1	155.8	1.75	0.72	0.44	121	1.04	0.02	15.1	41.6	1.31	2386.9	0.137	<20	3.21
AR-16-303	Sediment Pulp	2.7	96	0.24	0.52	0.11	112	2.44	0.107	9.9	47.9	0.75	338.8	0.137	<20	1.22

Pulp Duplicates															
AR-16-027	Sediment Pulp	3.5	58.9	0.1	0.15	0.22	28	0.63	0.034	18.9	34.2	0.35	352.1	0.07	<20	1.84
AR-16-027	REP															
AR-16-159	Sediment Pulp	3.9	64.8	0.18	0.35	0.09	100	1.14	0.114	15.5	37.7	0.79	282.7	0.165	<20	1.78
AR-16-159	REP															
AR-16-218	Sediment Pulp	4.1	120.1	0.17	0.28	0.17	92	1.99	0.11	16.7	31.1	1.3	282.1	0.183	<20	2.35
AR-16-218	REP	4	118.3	0.17	0.24	0.17	91	2.1	0.107	16.3	31	1.29	272.4	0.181	<20	2.34
Reference Materials																
STD GS311-1	STD															
STD GS910-4	STD															
STD SO-19	STD															
STD SO-19	STD															
STD OREAS45EA	STD	10.7	3.8	<0.01	0.24	0.26	313	0.03	0.027	7.8	857.5	0.09	144.5	0.108	<20	3.48
STD DS11	STD	7.6	64.1	2.47	6.66	11.92	49	1.13	0.064	19.3	60.7	0.85	418.4	0.102	<20	1.17
BLK	BLK															
BLK	BLK															
BLK	BLK	<0.1	<0.5	<0.01	<0.02	<0.02	<2	<0.01	<0.001	<0.5	<0.5	<0.01	<0.5	<0.001	<20	<0.01
Prep Wash																
ROCK-VAN	Prep Blank	2.2	18.8	0.02	0.03	0.02	23	0.63	0.042	6.9	5.1	0.56	54.7	0.082	<20	0.91

(l)

	Method	AQ250	AQ250	AQ250	AQ250	AQ250	AQ250	AQ250	AQ250	AQ250	AQ250
	Analyte	Na	K	W	Sc	Tl	S	Hg	Se	Te	Ga
	Unit	%	%	PPM	PPM	PPM	%	PPB	PPM	PPM	PPM
	MDL	0.001	0.01	0.1	0.1	0.02	0.02	5	0.1	0.02	0.1
Sample	Type										
AR-15-001	Sediment Pulp	0.049	0.33	<0.1	7.7	0.13	<0.02	23	<0.1	0.04	8.1
AR-15-003	Sediment Pulp	0.04	0.25	<0.1	6.5	0.1	<0.02	33	<0.1	<0.02	7.4
AR-16-002	Sediment Pulp	0.081	0.1	1.2	2.8	0.05	0.03	34	<0.1	0.06	3.3
AR-16-015	Sediment Pulp	0.078	0.25	0.7	6.3	0.11	<0.02	24	<0.1	<0.02	6.5
AR-16-020	Sediment Pulp	0.057	0.16	4	6.7	0.09	0.03	36	<0.1	0.48	5.4
AR-16-024	Sediment	0.023	0.11	2.5	3.9	0.05	<0.02	26	<0.1	0.03	4.3

	Pulp Sediment										
AR-16-027	Pulp Sediment	0.013	0.13	0.1	4.7	0.07	<0.02	19	<0.1	0.02	5.4
AR-16-048	Pulp Sediment	0.019	0.2	<0.1	7	0.09	<0.02	17	<0.1	<0.02	7.9
AR-16-061	Pulp Sediment	0.081	0.12	0.5	3.5	0.05	<0.02	16	<0.1	0.03	4.3
AR-16-090	Pulp Sediment	0.067	0.08	0.3	2.8	0.03	0.05	17	<0.1	0.05	3
AR-16-016	Pulp Sediment	0.092	0.22	5	6	0.1	<0.02	37	<0.1	0.03	6.3
AR-16-122	Pulp Sediment	0.044	0.09	<0.1	3.2	0.04	<0.02	30	<0.1	0.02	3.7
AR-16-127	Pulp Sediment	0.056	0.11	0.1	3.6	0.03	<0.02	12	0.2	<0.02	4.2
AR-16-159	Pulp Sediment	0.04	0.16	<0.1	6.9	0.09	<0.02	36	<0.1	0.05	6.2
AR-16-166	Pulp Sediment	0.037	0.07	0.7	2.8	0.04	<0.02	14	0.1	0.02	2.1
AR-16-203	Pulp Sediment	0.044	0.09	<0.1	2.8	0.04	<0.02	16	<0.1	0.03	3.3
AR-16-218	Pulp Sediment	0.098	0.27	0.1	6.9	0.12	<0.02	47	0.1	0.04	7.5
AR-16-221	Pulp Sediment	0.083	0.08	3.3	1.9	0.04	0.04	12	0.2	0.05	2.2
AR-16-271	Pulp Sediment	0.026	0.36	<0.1	14.4	1.02	0.04	232	0.5	0.11	10.8
AR-16-303	Pulp Sediment	0.058	0.09	1.8	5.1	0.06	0.19	42	0.3	0.06	4.1
Pulp Duplicates											
AR-16-027	Pulp Sediment	0.013	0.13	0.1	4.7	0.07	<0.02	19	<0.1	0.02	5.4
AR-16-027	REP										
AR-16-159	Pulp Sediment	0.04	0.16	<0.1	6.9	0.09	<0.02	36	<0.1	0.05	6.2
AR-16-159	REP										
AR-16-218	Pulp Sediment	0.098	0.27	0.1	6.9	0.12	<0.02	47	0.1	0.04	7.5
AR-16-218	REP	0.097	0.27	0.1	7	0.11	<0.02	37	0.3	0.03	7.4
Reference Materials											

STD GS311-1	STD										
STD GS910-4	STD										
STD SO-19	STD										
STD SO-19	STD										
STD OREAS45EA	STD	0.021	0.06	<0.1	73	0.07	0.04	13	1.2	0.11	12.3
STD DS11	STD	0.074	0.41	2.2	3	4.91	0.31	272	2.4	4.41	4.9
BLK	BLK										
BLK	BLK										
BLK	BLK	<0.001	<0.01	<0.1	<0.1	<0.02	<0.02	<5	<0.1	<0.02	<0.1
Prep Wash ROCK-VAN	Prep Blank	0.07	0.09	<0.1	2.6	<0.02	<0.02	<5	<0.1	<0.02	3.9

Table C.5 Results for two standards analyzed with the other samples at Bureau Veritas with the total digest method. Both standards are Reference Sample Till-1 from Canadian Certified Reference Materials Project, Canada Centre for Mineral and Energy Technology.

Element	Standard True Value	Standard AR-16-030	Standard AR-16-120
SiO2 (%)	60.9	60.79	60.6
Al2O3 (%)	13.7	13.69	13.75
Fe2O3 (%)	6.82	6.88	6.89
MgO (%)	2.15	2.18	2.18
CaO (%)	2.72	2.71	2.73
Na2O (%)	2.71	2.76	2.77
K2O (%)	2.22	2.11	2.15
TiO2 (%)	0.98	0.96	0.97
P2O5 (%)	0.22	0.21	0.21
MnO (%)	0.18	0.19	0.19
LOI	7.3	7.2	7.3
Ba (ppm)	702	701	734
Ni (ppm)	24	29	25
Sc (ppm)	13	13	13
Be (ppm)	2.4	2	<1
Co (ppm)	18	17.8	18.1
Cs (ppm)	1	0.9	0.9
Hf (ppm)	13	12.7	13.1
Nb (ppm)	10	11.1	10.1
Rb (ppm)	44	45.1	45.1
Sr (ppm)	291	329.1	328.3
Ta (ppm)	0.7	0.7	0.7
Th (ppm)	5.6	6.6	6.3
U (ppm)	2.2	2	2.4
V (ppm)	99	102	104
W (ppm)	<1	<0.5	0.8
Zr (ppm)	502	510.3	521.4
Y (ppm)	38	35.8	34.4
La (ppm)	28	29.1	29.3
Ce (ppm)	71	74.5	74.1
Nd (ppm)	26	31	30.7
Sm (ppm)	5.9	6.26	6.61
Eu (ppm)	1.3	1.59	1.62
Tb (ppm)	1.1	1.02	1.02
Er (ppm)	3.6	4.09	4.1
Yb (ppm)	3.9	4.07	4.07

Table C.6 Results for two standards analyzed with the other samples at Bureau Veritas with the partial digest method with the acids HNO_3 and HCl. Both standards are Reference Sample Till-1 from Canadian Certified Reference Materials Project, Canada Centre for Mineral and Energy Technology.

Element	Standard True Value	Standard AR-16-030	Standard AR-16-120
Cu (ppm)	49	46.25	46.11
Mo (ppm)	1	0.66	0.62
Pb (ppm)	14	14.39	13.41
Zn (ppm)	71	62.7	57.7
Ag (ppb)	<200	226	217
Ni (ppm)	17	16.4	15.9
Co (ppm)	12	12.9	13.2
Mn (ppm)	1020	1023	1043
Fe (%)	3.4	2.98	3.03

Core VTH-2014-03

Geochemical analysis was done on a till sample 4.6-4.8m deep and two sand samples 22.3-22.5m and 78.7-78.9m deep from core VTH2014-03. The results that are of a significantly high concentration are shown below (**Figure C.54**). The till and lower sand samples have a higher concentration of tungsten (2.5ppm and 2.2ppm respectively) than the average of the Highland Valley shallow till samples collected by Plouffe and Ferbey (0.2ppm) (**Figure C.55**).

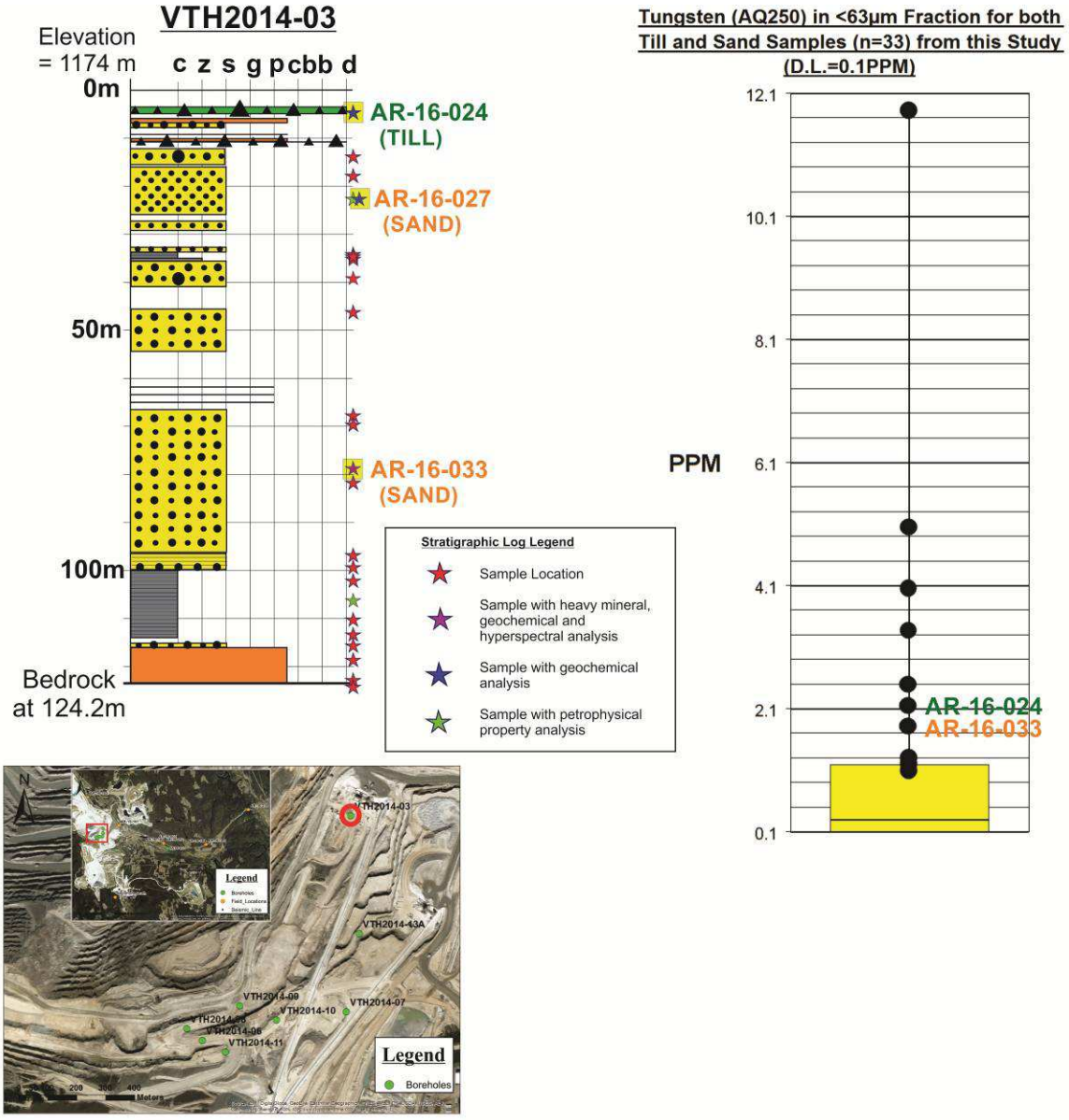

Figure C.54 Stratigraphic log, location map and significantly high geochemical results of core VTH2014-03. The location of collected samples is shown on the stratigraphic log and the samples for which geochemical analysis was done are highlighted.

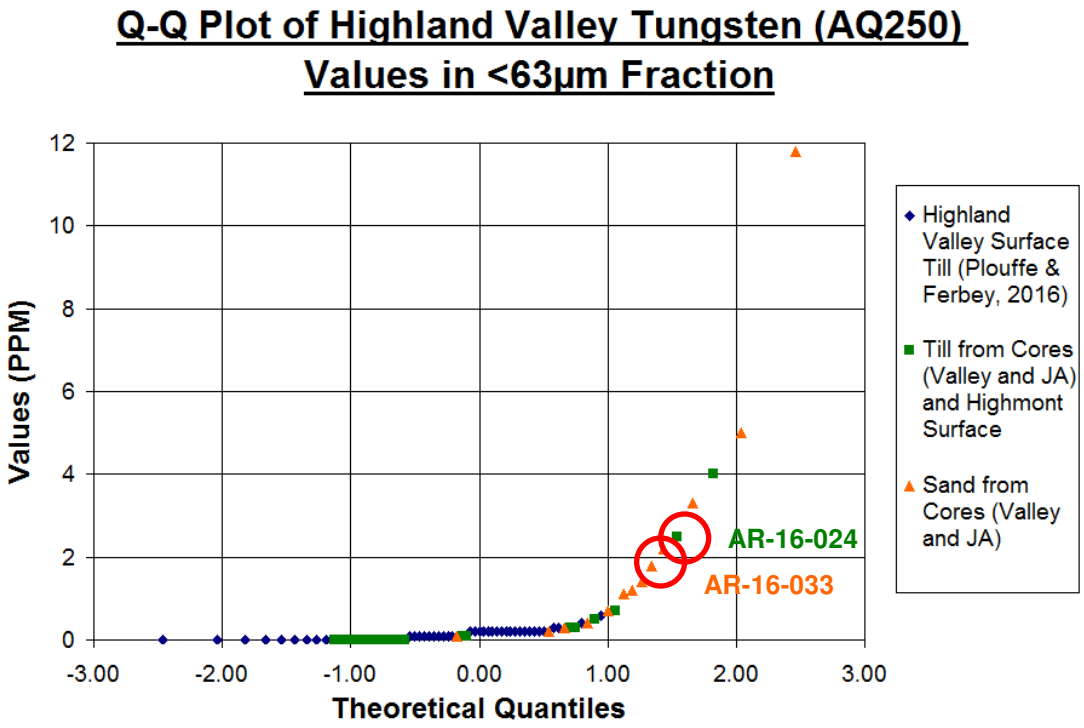

Figure C.55 Quantile-quantile plot of tungsten concentrations for this study and Plouffe and Ferbey's study (2016), with the till and lower sand samples from core VTH2014-03 highlighted.

Core VTH-2014-07

Geochemical analysis was done on three till samples 23.3-23.6m, 48.8-49.1m and 68.4-68.7m deep and one sand sample 126.8-127.1m deep from core VTH2014-07 (**Figure C.56**). None of the samples contained an element of interest at a significantly high concentration.

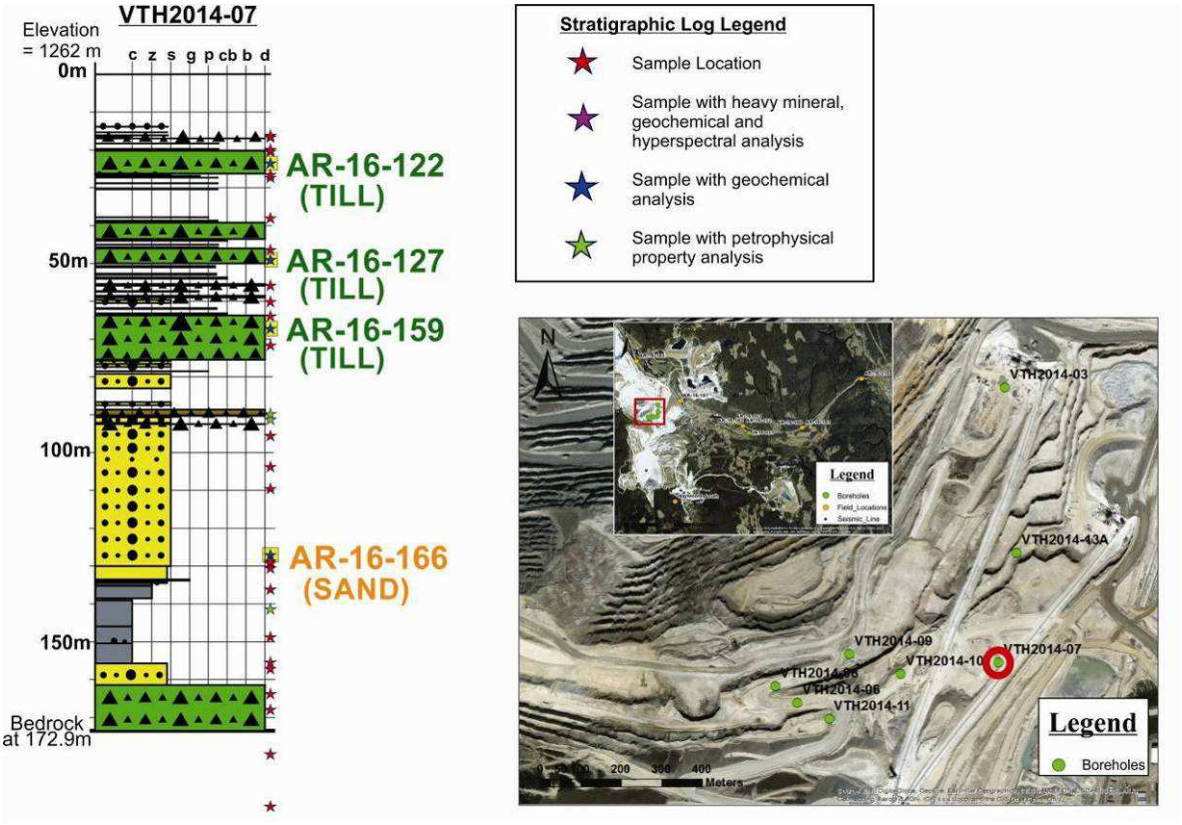

Figure C.56 Stratigraphic log and location map of core VTH2014-07. The location of collected samples is shown on the stratigraphic log and the samples for which geochemical analysis was done are highlighted.

Core VTH-2014-08

Geochemical analysis was done on three till samples 17.9-18.1m, 57.1-57.3m and 85.6-85.8m deep and two sand samples 20.8-21.0m and 84.2-84.4m deep from core VTH2014-08. The results that are of a significantly high concentration are shown below (**Figure C.57**). The lower two till samples and lower sand sample have a higher concentration of molybdenum (11.36ppm and 9.10ppm, and 8.85ppm respectively) than the average of the Highland Valley shallow till samples collected by Plouffe and Ferbey (1.9ppm) (**Figure C.58**). There is a higher concentration of gold, tellurium and bismuth for the middle till sample (25.6ppb, 0.48ppm, and 1.03ppm respectively) than the average of the Highland Valley shallow till samples collected by Plouffe and Ferbey (3.5ppb, 0.01ppm and 0.1ppm respectively)

(**Figures C.59, C.60 and C.61**). The middle till and upper sand samples have a higher concentration of tungsten (4.0ppm and 5.0ppm respectively) than the average of the Highland Valley shallow till samples collected by Plouffe and Ferbey (0.2ppm) (**Figure C.62**).

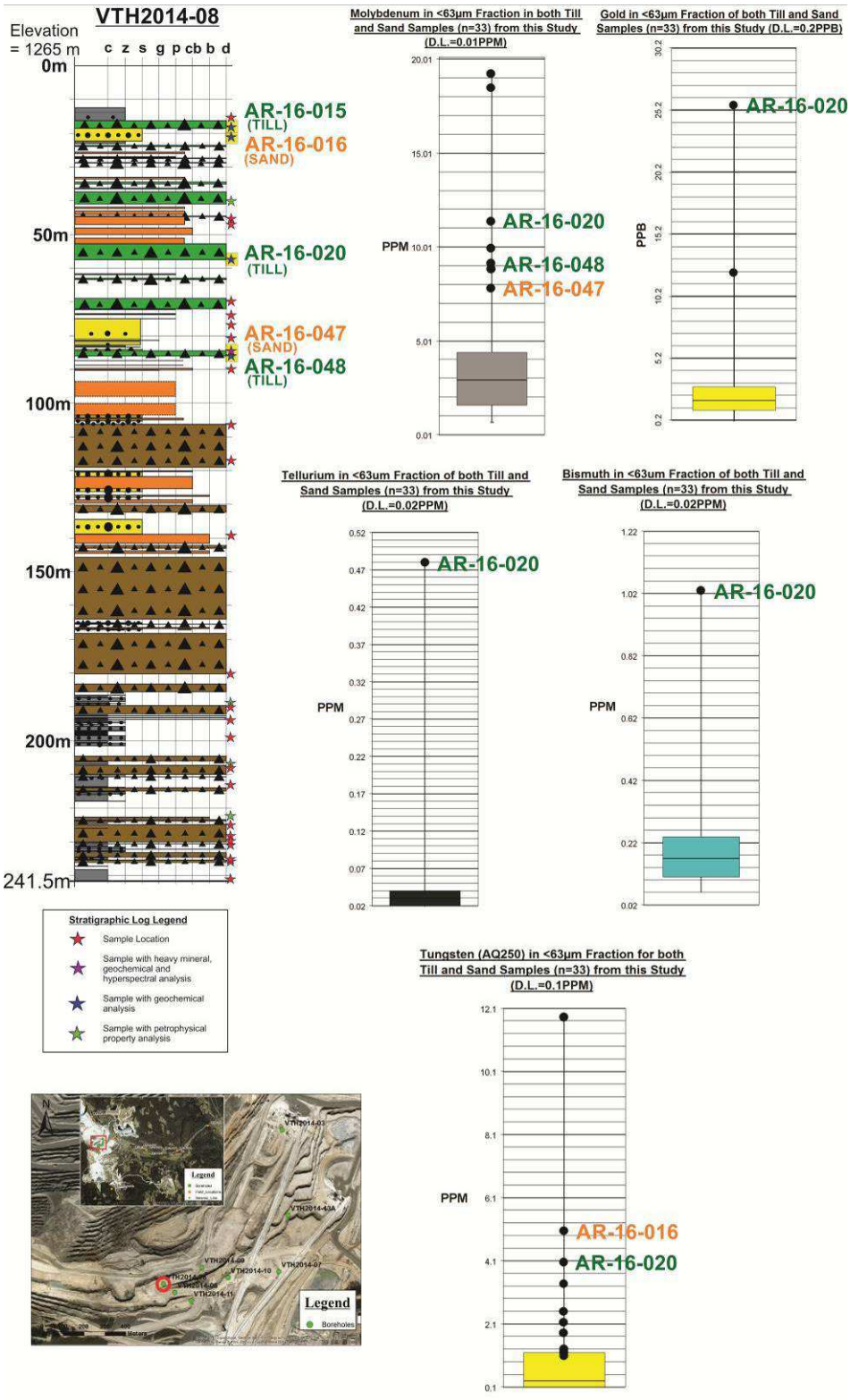

Figure C.57 Stratigraphic log, location map and significantly high geochemical results of core VTH2014-08. The location of collected samples is shown on the stratigraphic log and the samples for which geochemical analysis was done are highlighted.

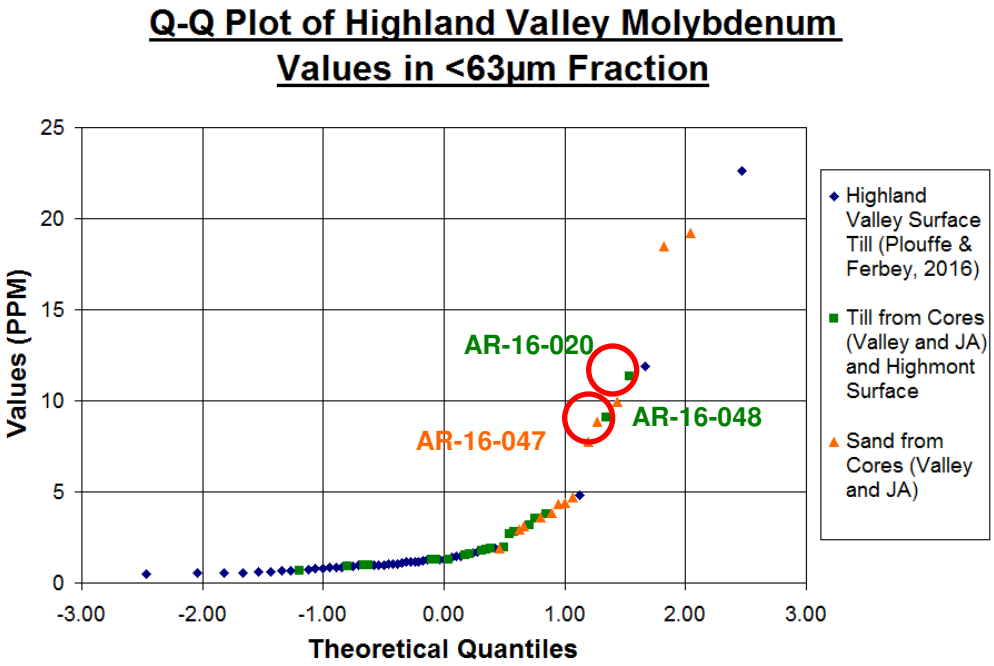

Figure C.58 Quantile-quantile plot of molybdenum concentrations for this study and Plouffe and Ferbey's study (2016), with the two lower till and lower sand samples from core VTH2014-08 highlighted.

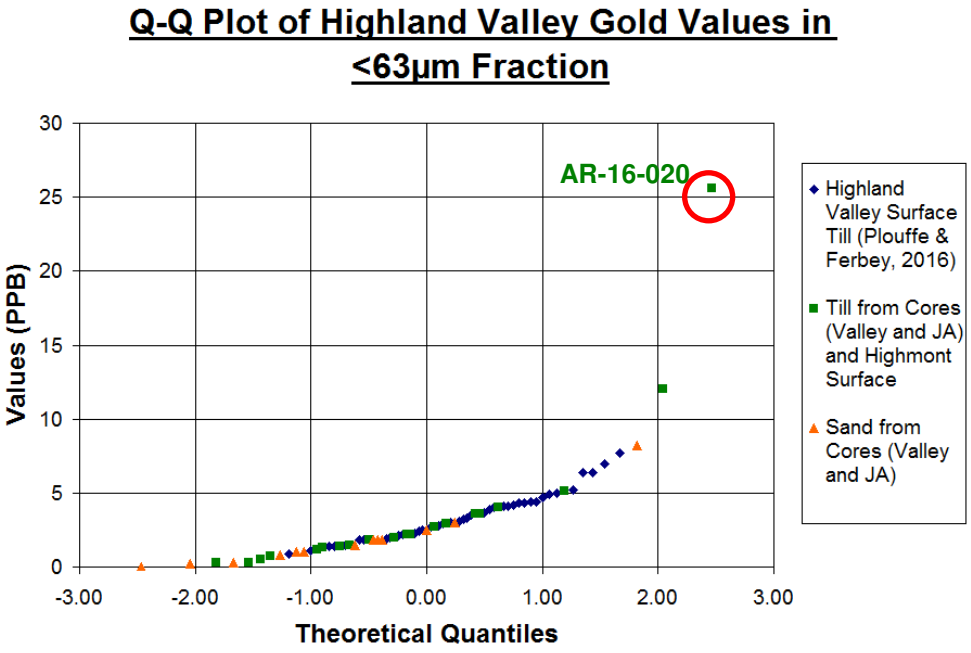

Figure C.59 Quantile-quantile plot of gold concentrations for this study and Plouffe and Ferbey's study (2016), with the middle till sample from core VTH2014-08 highlighted.

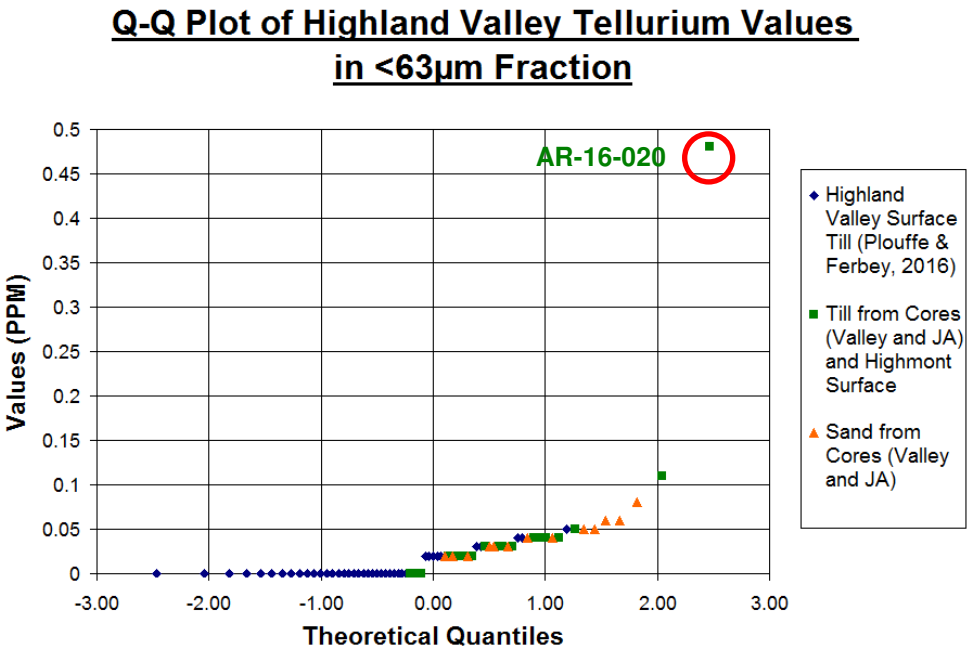

Figure C.60 Quantile-quantile plot of tellurium concentrations for this study and Plouffe and Ferbey's study (2016), with the middle till sample from core VTH2014-08 highlighted.

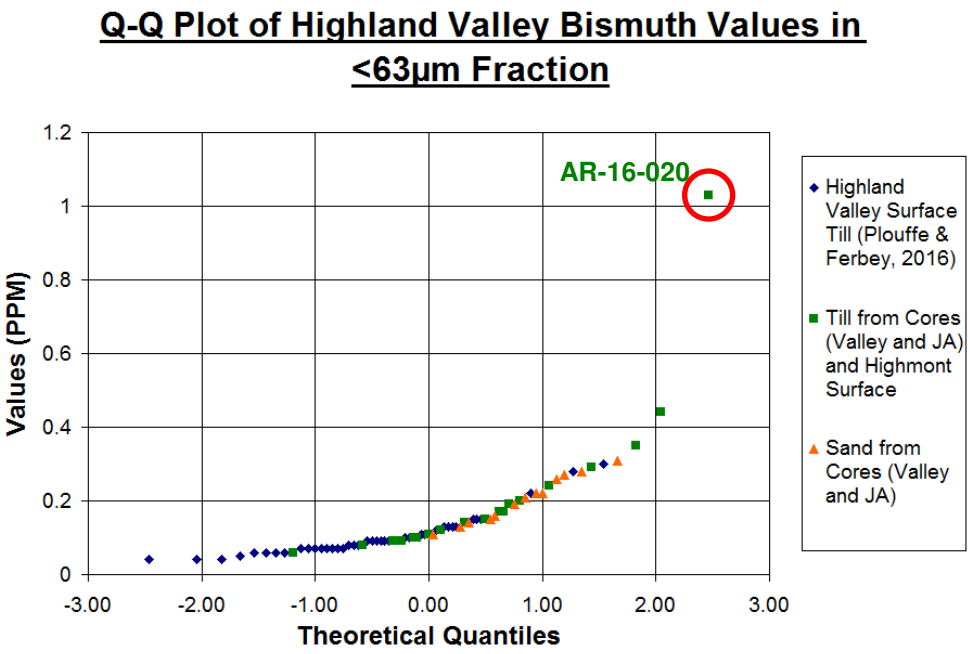

Figure C.61 Quantile-quantile plot of bismuth concentrations for this study and Plouffe and Ferbey's study (2016), with the middle till sample from core VTH2014-08 highlighted.

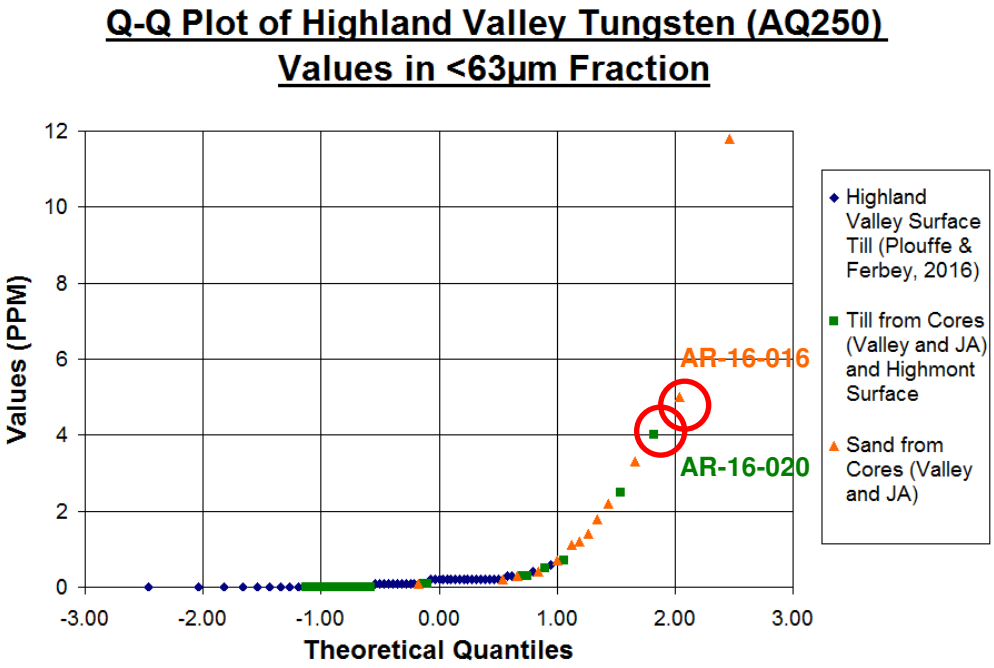

Figure C.62 Quantile-quantile plot of tungsten concentrations for this study and Plouffe and Ferbey's study (2016), with the middle till and upper sand samples from core VTH2014-08 highlighted.

Core VTH-2014-09

Geochemical analysis was done on two till samples 36.5-36.7m and 56.0-56.2m deep and a sand sample 101.0-101.2m deep from core VTH2014-09. The results that are of a significantly high concentration are shown below (**Figure C.63**). The sand sample has a higher concentration of molybdenum, tin and tungsten (9.92ppm, 5ppm and 1.2ppm respectively) than the average of the Highland Valley shallow till samples collected by Plouffe and Ferbey (1.9ppm, 0.4ppm and 0.2ppm respectively) (**Figures C.64, C.65 and C.66**).

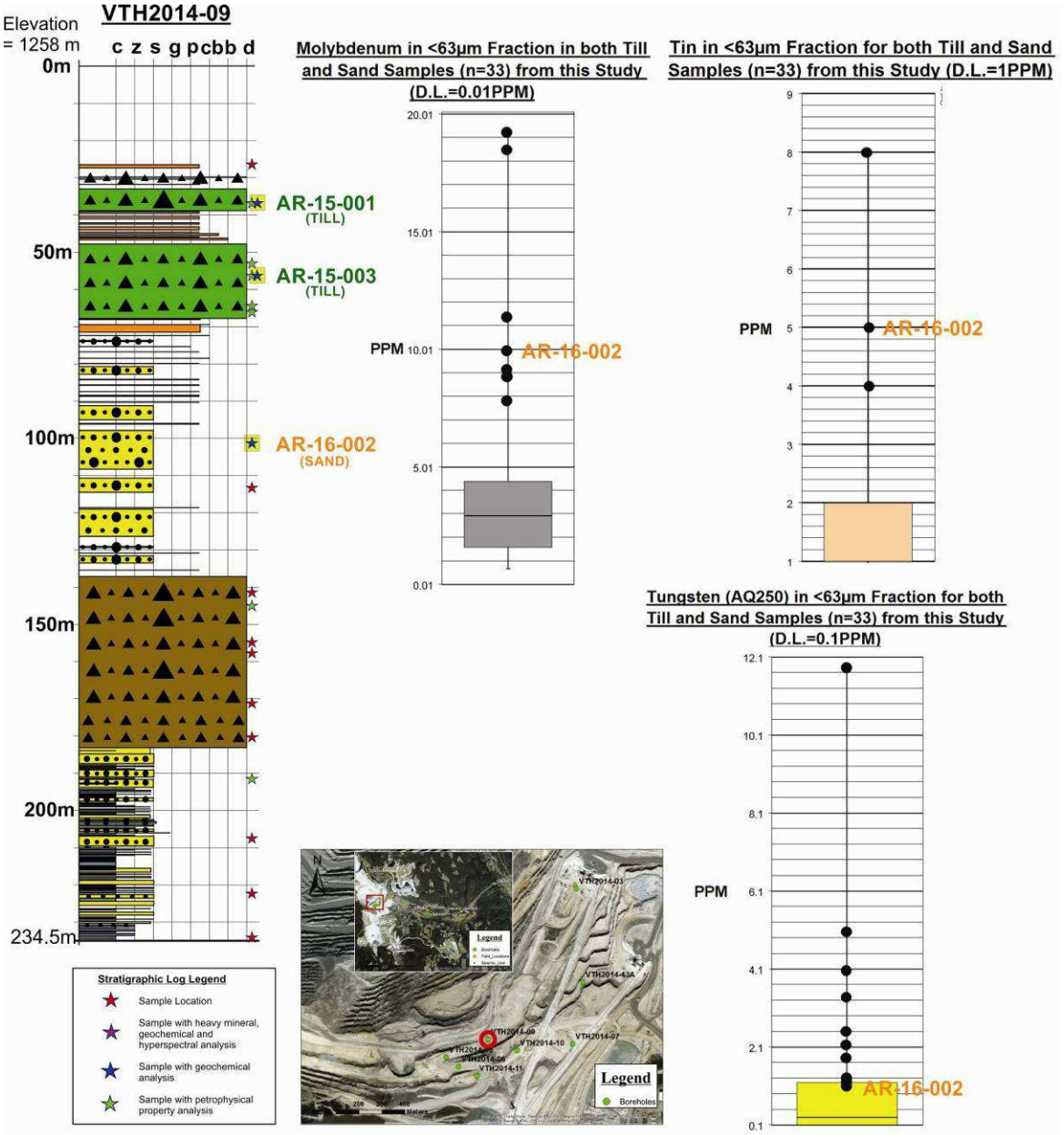

Figure C.63 Stratigraphic log, location map and significantly high geochemical results of core VTH2014-09. The location of collected samples is shown on the stratigraphic log and the samples for which geochemical analysis was done are highlighted.

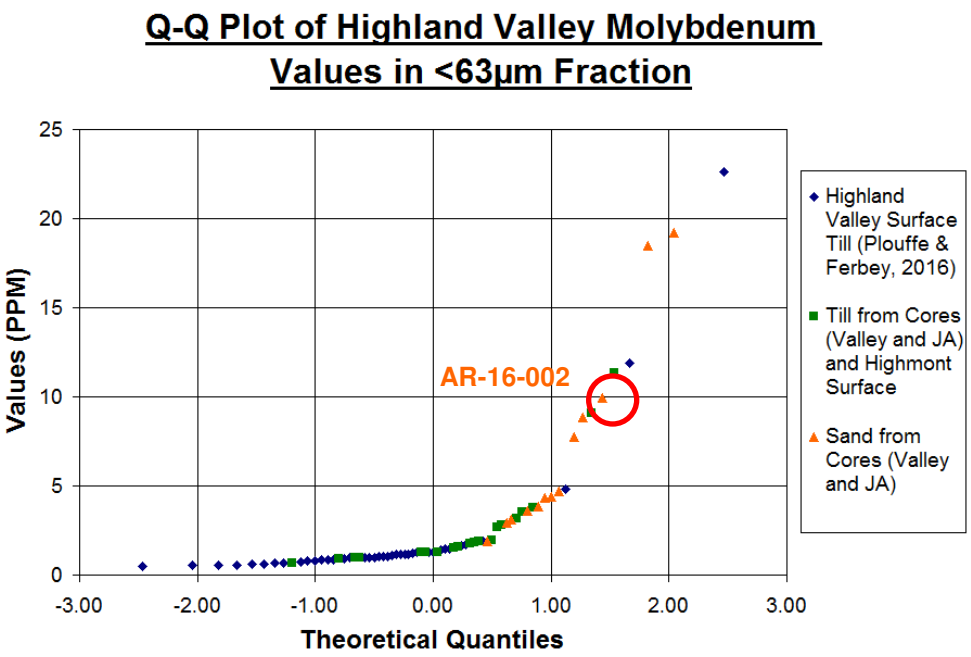

Figure C.64 Quantile-quantile plot of molybdenum concentrations for this study and Plouffe and Ferbey's study (2016), with the sand sample from core VTH2014-09 highlighted.

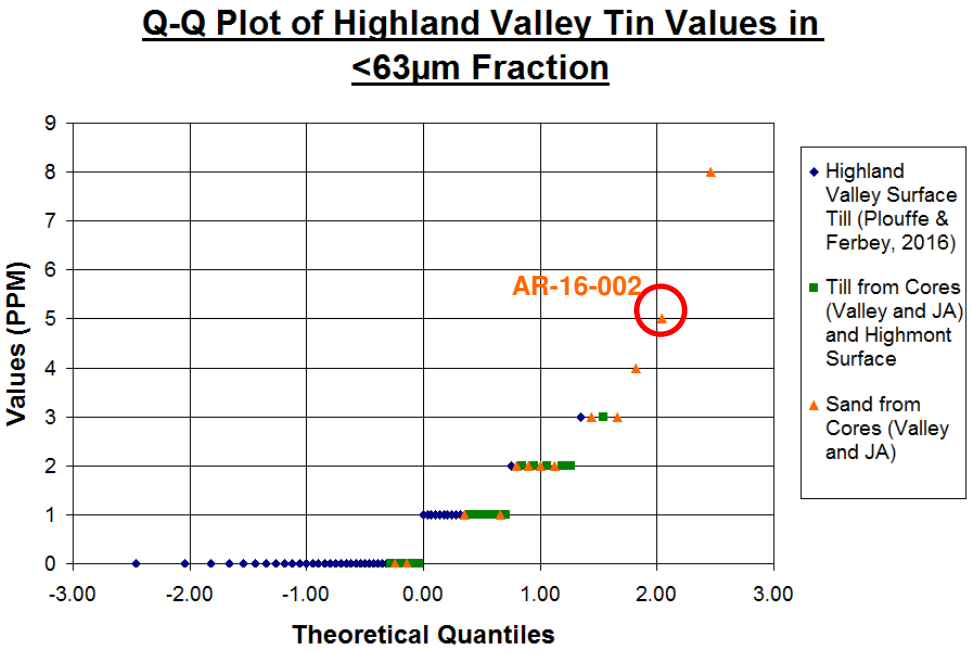

Figure C.65 Quantile-quantile plot of tin concentrations for this study and Plouffe and Ferbey's study (2016), with the sand sample from core VTH2014-09 highlighted.

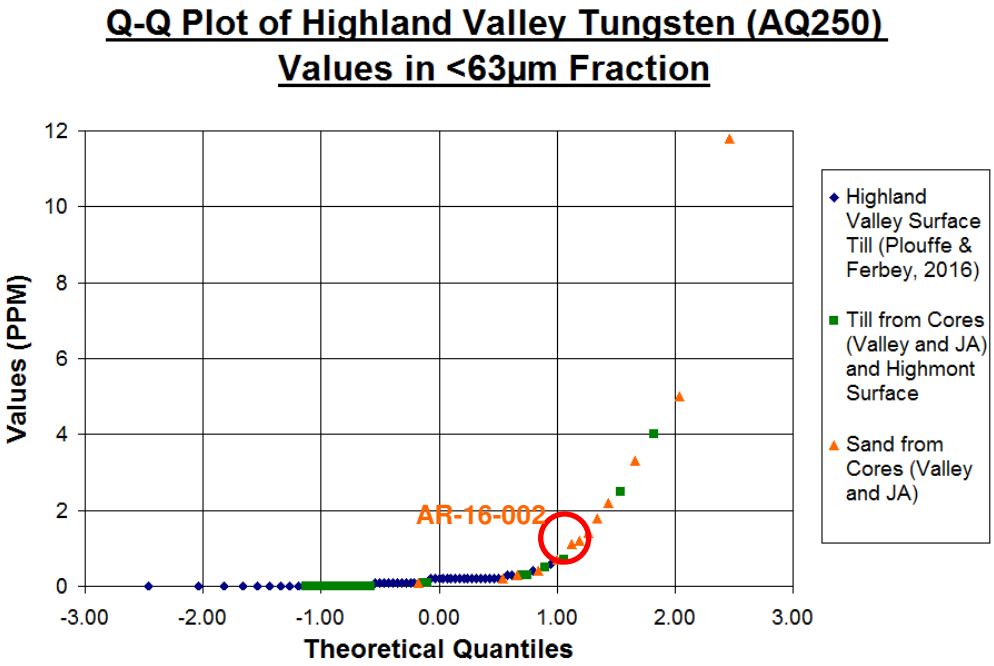

Figure C.66 Quantile-quantile plot of tungsten concentrations for this study and Plouffe and Ferbey's study (2016), with the sand sample from core VTH2014-09 highlighted.

Core VTH-2014-10

Geochemical analysis was done on three till samples 15.3-15.5m, 27.3-27.5m and 63.8-64.1m deep and two sand samples 105.9-106.2m and 141.7-142.2m deep from core VTH2014-10. The result that is of a significantly high concentration is shown below (**Figure C.67**). The upper sand sample has a higher concentration of tin (8ppm) than the average of the Highland Valley shallow till samples collected by Plouffe and Ferbey (0.4ppm) (**Figure C.68**).

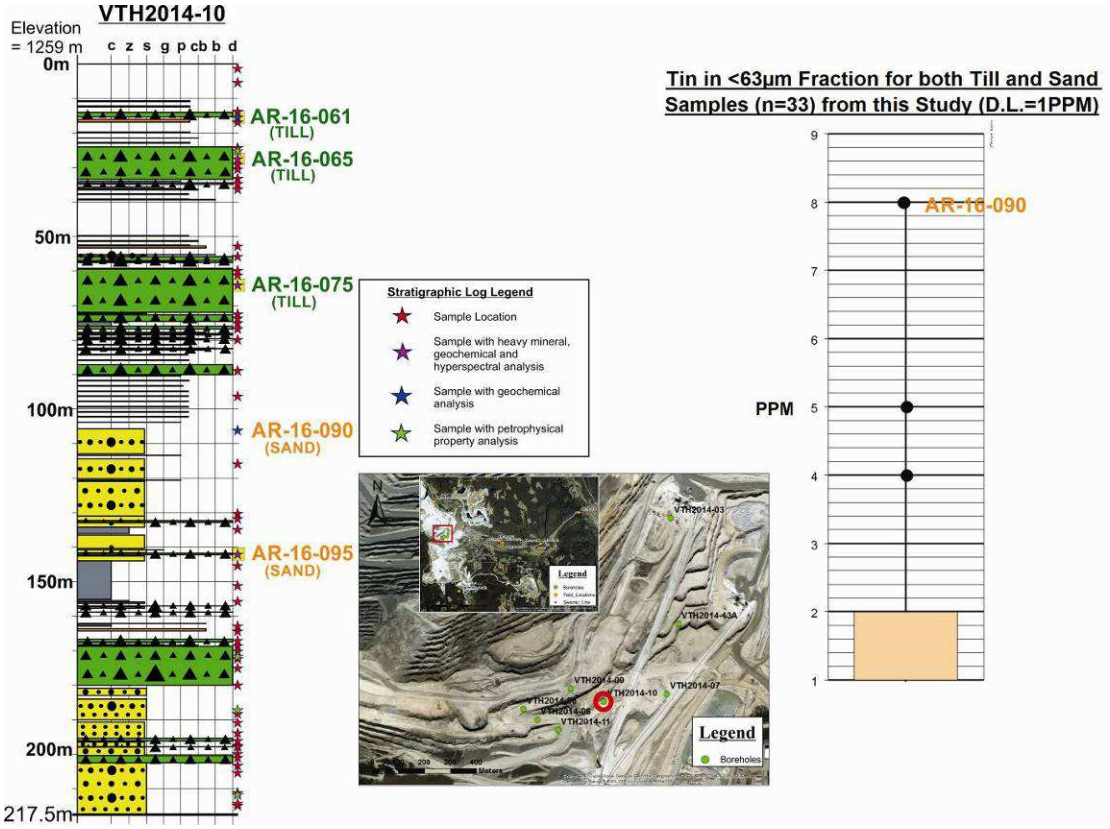

Figure C.67 Stratigraphic log, location map and significantly high geochemical results of core VTH2014-10. The location of collected samples is shown on the stratigraphic log and the samples for which geochemical analysis was done are highlighted.

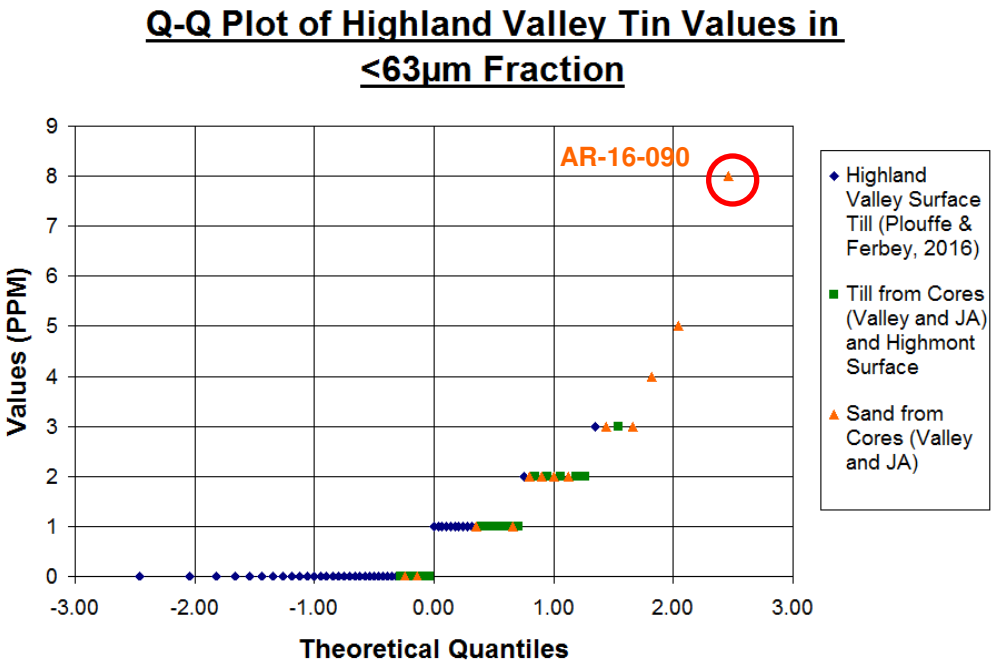

Figure C.68 Quantile-quantile plot of tin concentrations for this study and Plouffe and Ferbey's study (2016), with the upper sand sample from core VTH2014-10 highlighted.

Core VTH-2014-11

Geochemical analysis was done on two till samples 21.2-21.5m and 59.3-59.6m deep and two sand samples 48.2-48.5m and 94.2-94.6m deep from core VTH2014-11. The results that are of a significantly high concentration are shown below (**Figure C.69**). Both sand samples have a higher concentration of molybdenum (7.77ppm top one and 19.18ppm bottom one) as well as tungsten (3.3ppm top one and 1.1ppm bottom one) than the average of the Highland Valley shallow till samples collected by Plouffe and Ferbey (1.4ppm and 0.09ppm respectively) (**Figures C.70 and C.71**).

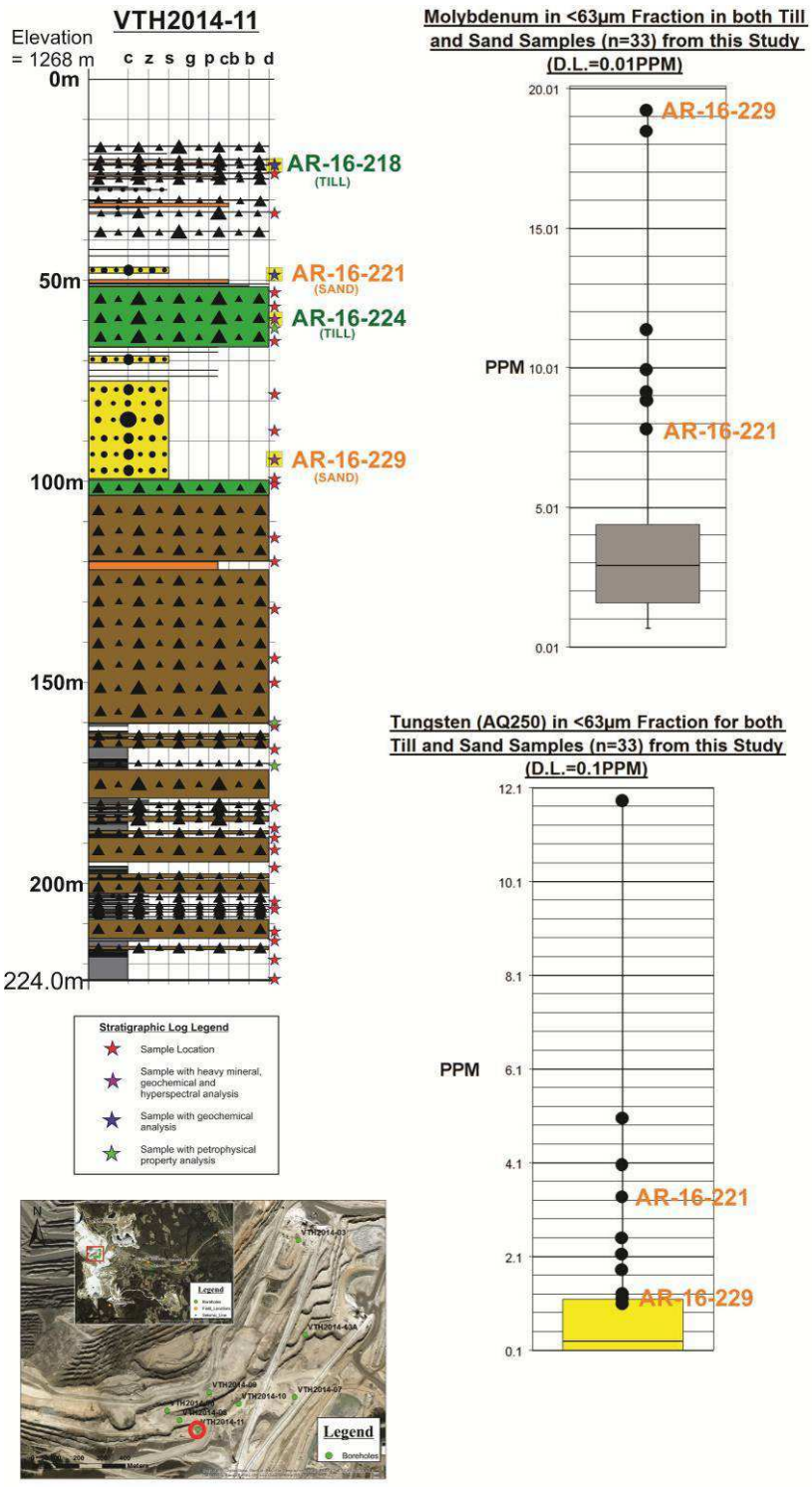

Figure C.69 Stratigraphic log, location map and significantly high geochemical results of core VTH2014-11. The location of collected samples is shown on the stratigraphic log and the samples for which geochemical analysis was done are highlighted.

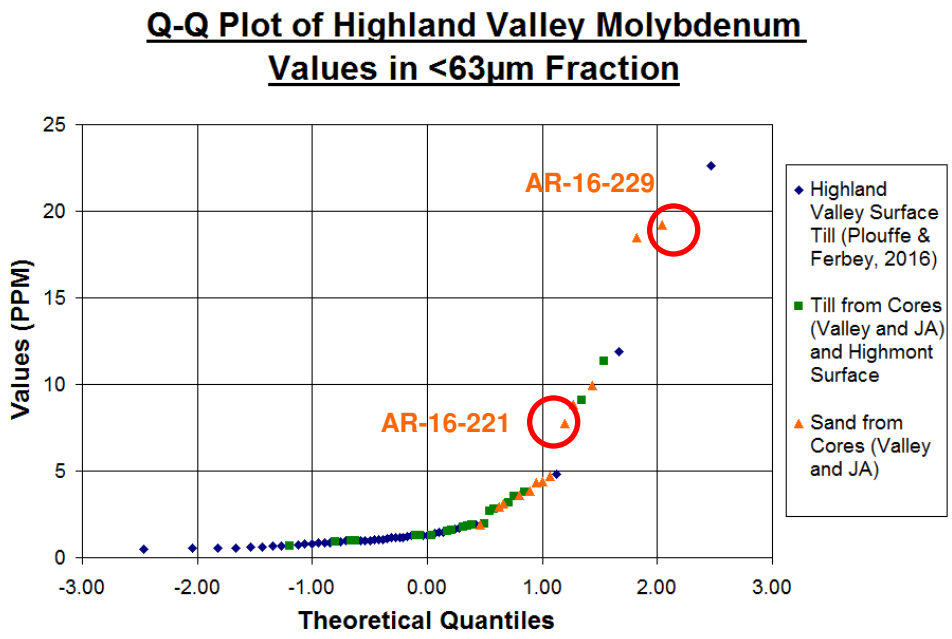

Figure C.70 Quantile-quantile plot of molybdenum concentrations for this study and Plouffe and Ferbey's study (2016), with the sand samples from core VTH2014-11 highlighted.

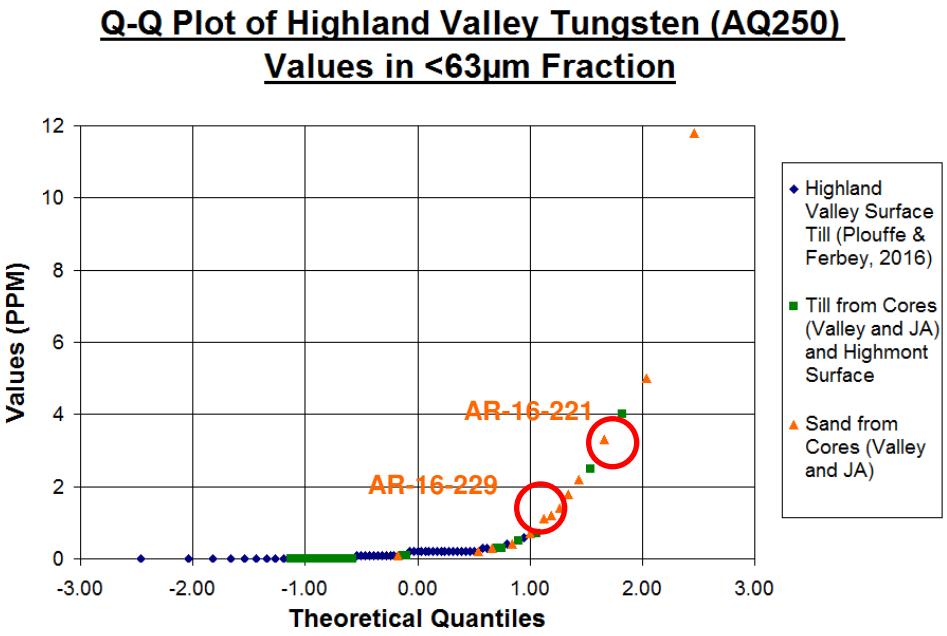

Figure C.71 Quantile-quantile plot of tungsten concentrations for this study and Plouffe and Ferbey's study (2016), with the sand samples from core VTH2014-11 highlighted.

Core VTH-2014-13A

Geochemical analysis was done on two till samples 42.0-42.3m and 55.2-55.5m deep and a sand sample 84.2-84.5m deep from core VTH2014-13A. The results that are of a significantly high concentration are shown below (**Figure C.72**). The sand sample has a higher concentration of molybdenum and tungsten (18.5ppm and 1.4ppm respectively) than the average of the Highland Valley shallow till samples collected by Plouffe and Ferbey (1.4ppm and 0.09ppm respectively) (**Figures C.73 and C.74**).

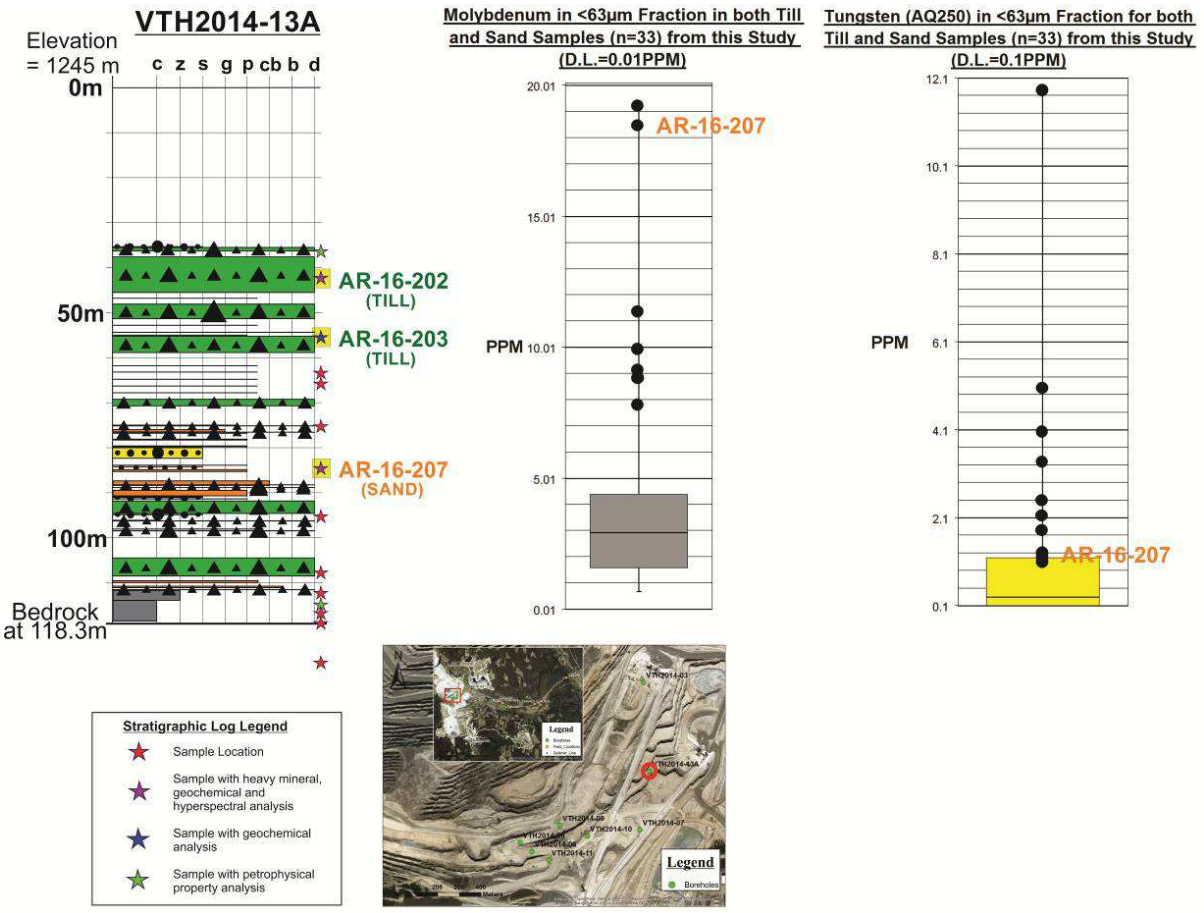

Figure C.72 Stratigraphic log, location map and significantly high geochemical results of core VTH2014-13A. The location of collected samples is shown on the stratigraphic log and the samples for which geochemical analysis was done are highlighted.

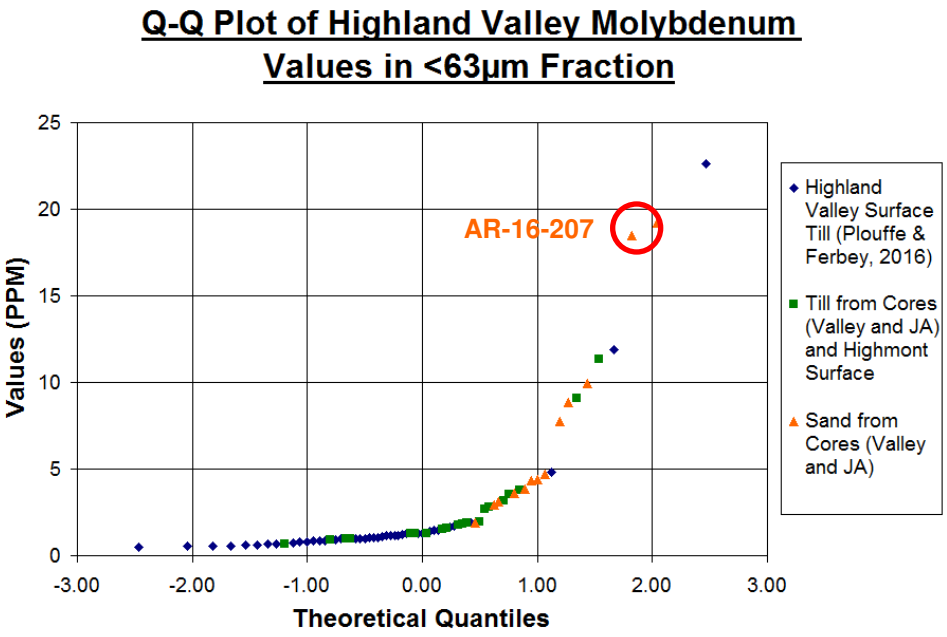

Figure C.73 Quantile-quantile plot of molybdenum concentrations for this study and Plouffe and Ferbey's study (2016), with the sand sample from core VTH2014-13A highlighted.

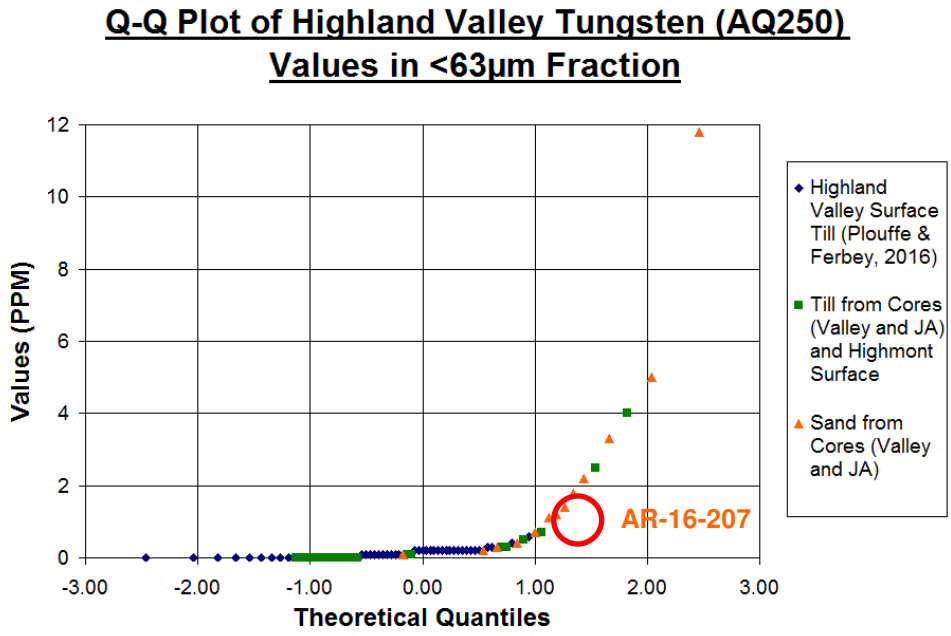

Figure C.74 Quantile-quantile plot of tungsten concentrations for this study and Plouffe and Ferbey's study (2016), with the sand sample from core VTH2014-13A highlighted.

Core JA16-001

Geochemical analysis was done on two till samples 31.6-31.9m and 40.5-40.8m deep and two sand samples 81.4-81.7m and 113.1-113.4m deep from core JA16-001. The results that are of a significantly high concentration are shown below (**Figure C.75**). The upper sand sample has a higher concentration of both tin and sodium (4ppm and 0.214% respectively) than the average of the Highland Valley shallow till samples collected by Plouffe and Ferbey (0.4ppm and 0.04% respectively) (**Figures C.76 and C.77**). Both sand samples have a higher concentration of tungsten (11.8ppm top one and 1.8ppm bottom one) as well as sulphur (0.23% top one and 0.19% bottom one) than the average of the Highland Valley shallow till samples collected by Plouffe and Ferbey (0.2ppm and 0.0008% respectively) (**Figures C.78 and C.79**).

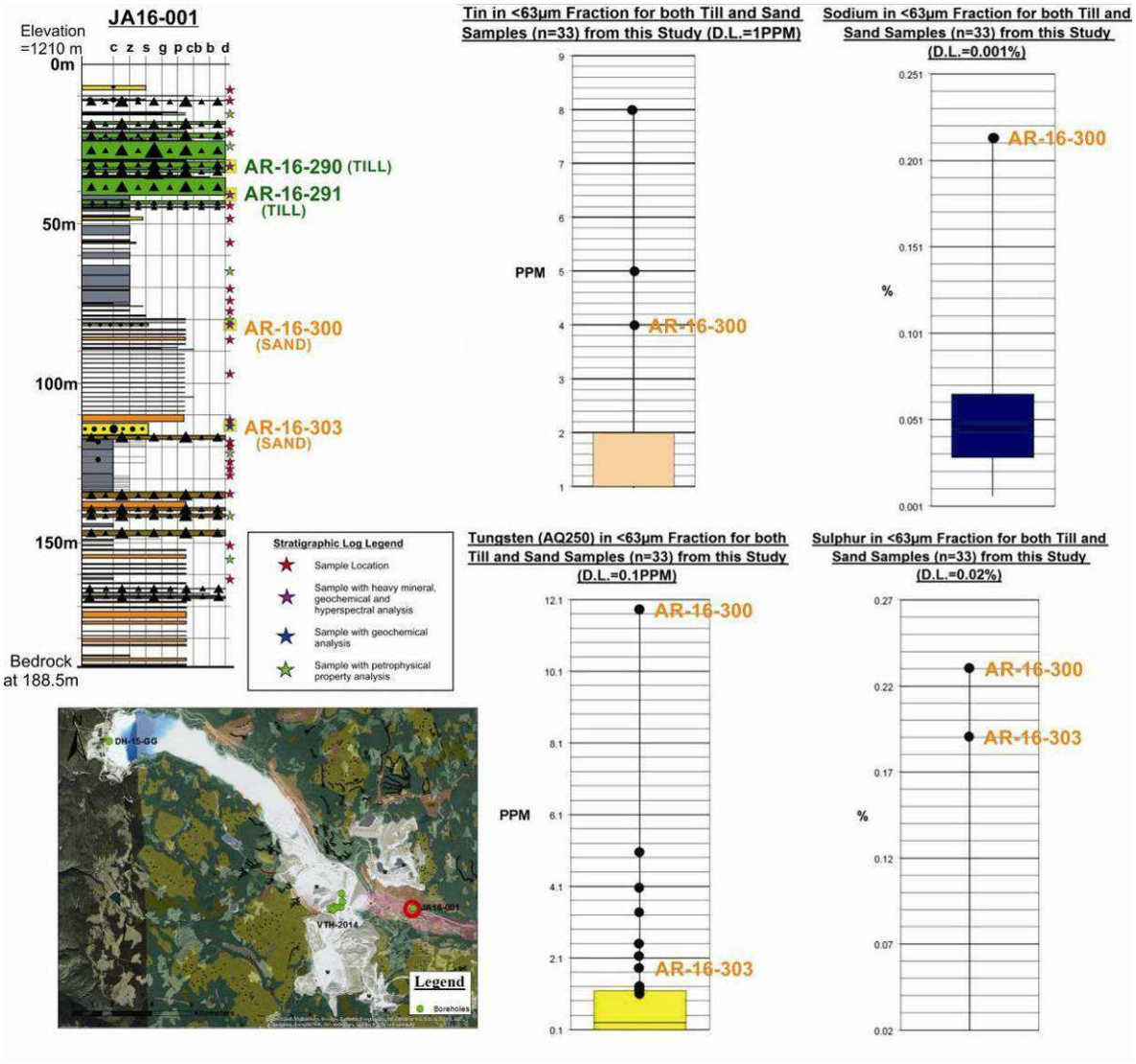

Figure C.75 Stratigraphic log, location map and significantly high geochemical results of core JA16-001. The location of collected samples is shown on the stratigraphic log and the samples for which geochemical analysis was done are highlighted.

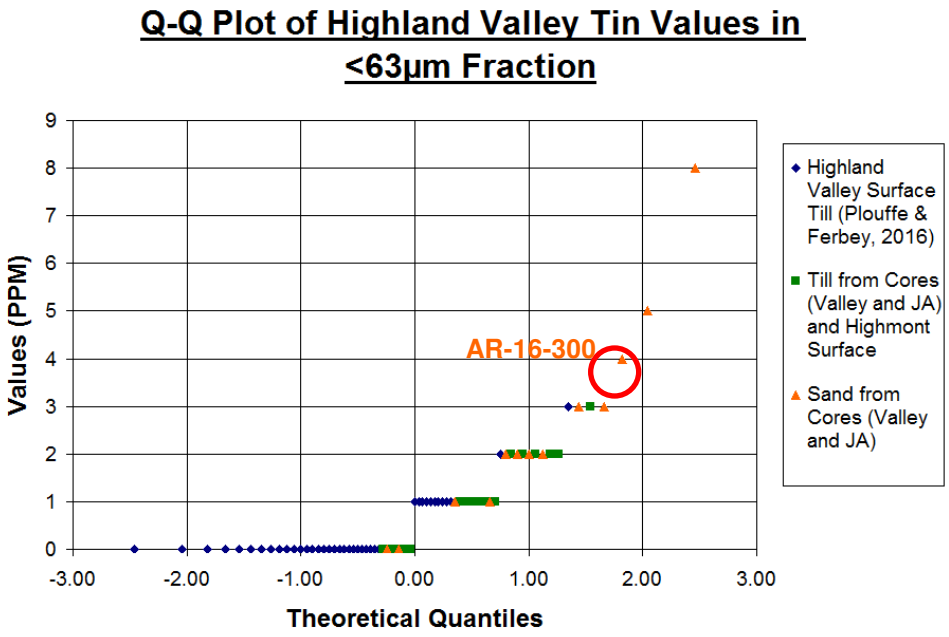

Figure C.76 Quantile-quantile plot of tin concentrations for this study and Plouffe and Ferbey's study (2016), with the upper sand sample from core JA16-001 highlighted.

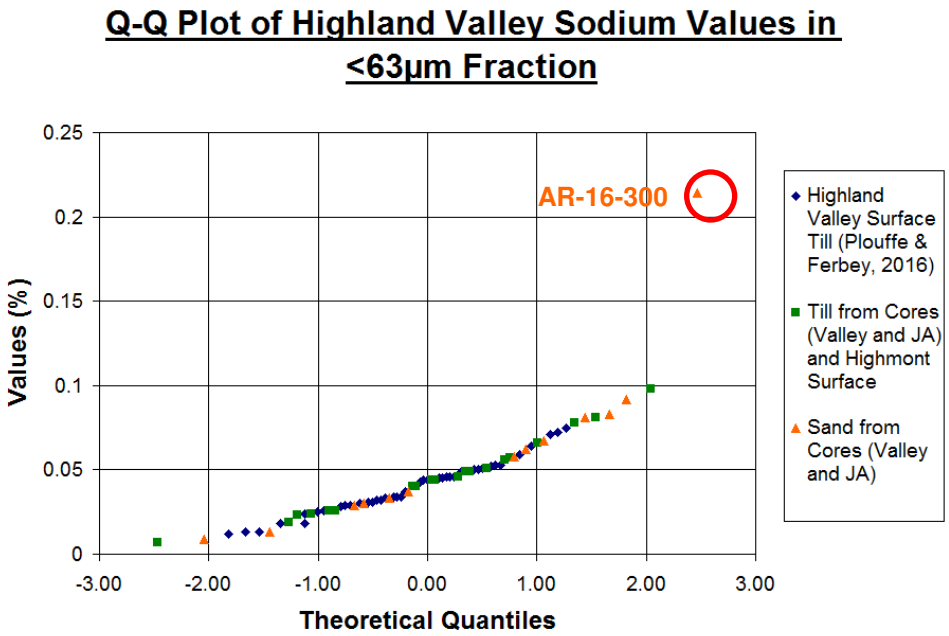

Figure C.77 Quantile-quantile plot of sodium concentrations for this study and Plouffe and Ferbey's study (2016), with the upper sand sample from core JA16-001 highlighted.

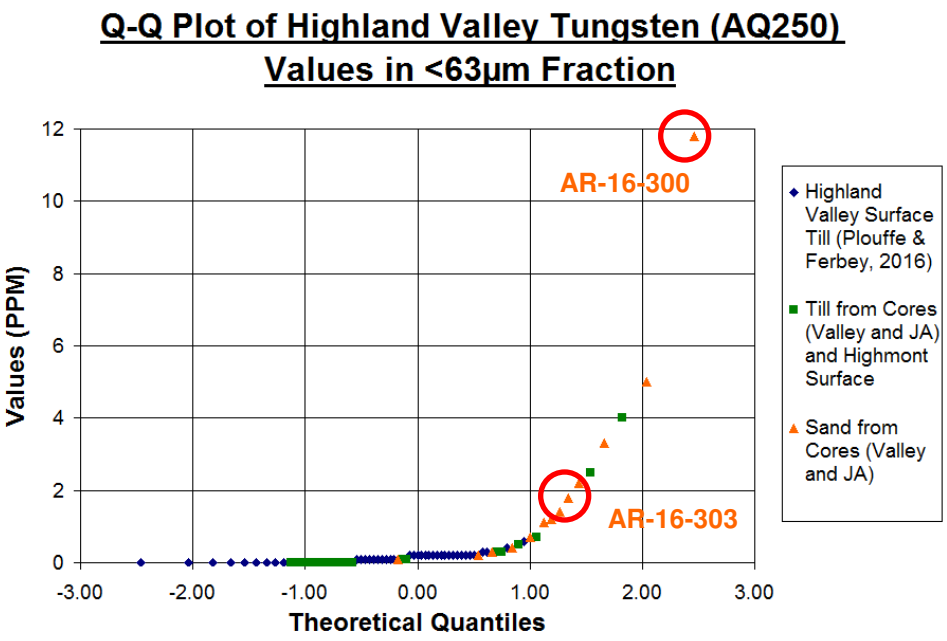

Figure C.78 Quantile-quantile plot of tungsten concentrations for this study and Plouffe and Ferbey's study (2016), with both sand samples from core JA16-001 highlighted.

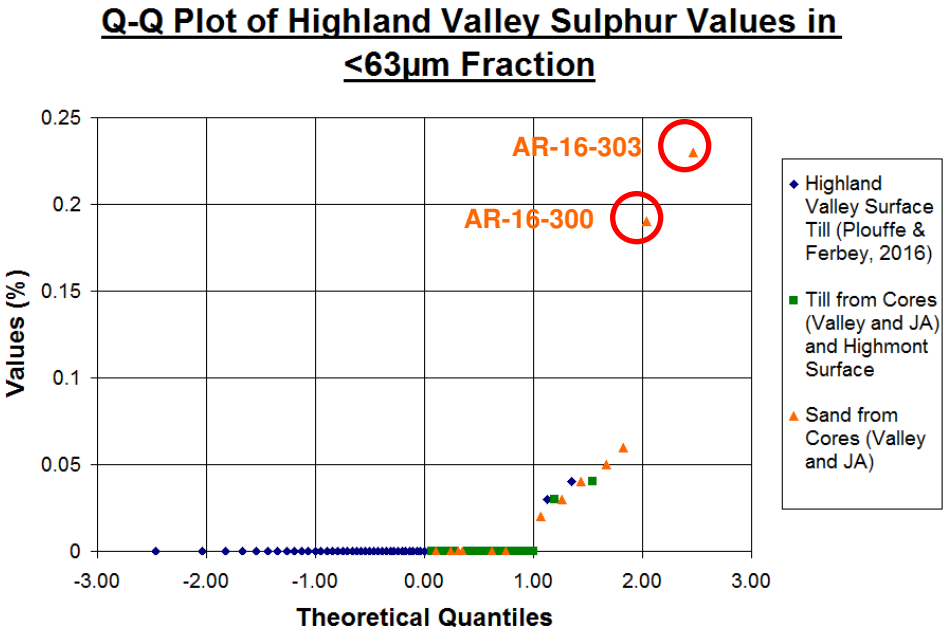

Figure C.79 Quantile-quantile plot of sulphur concentrations for this study and Plouffe and Ferbey's study (2016), with both sand samples from core JA16-001 highlighted.

Core DH-15-GG

Geochemical analysis was done on a sand and gravel sample 53.7-54.0m deep from core DH-15-GG. The results that are of a significantly high concentration are shown below (**Figure C.80**). This till sample has a higher concentration of gold, barium, zinc, nickel, cobalt, uranium and thallium (12.0ppb, 2386.9ppm, 246.4ppm, 101.9ppm, 103.9ppm, 3.2ppm and 1.02ppm respectively) than the average of the Highland Valley shallow till samples collected by Plouffe and Ferbey (3.5ppb, 175.8ppm, 45.3ppm, 25.0ppm, 11.8ppm, 0.7ppm and 0.05ppm respectively) (**Figures C.81, C.82, C.83, C.84, C.85, C.86 and C.87**).

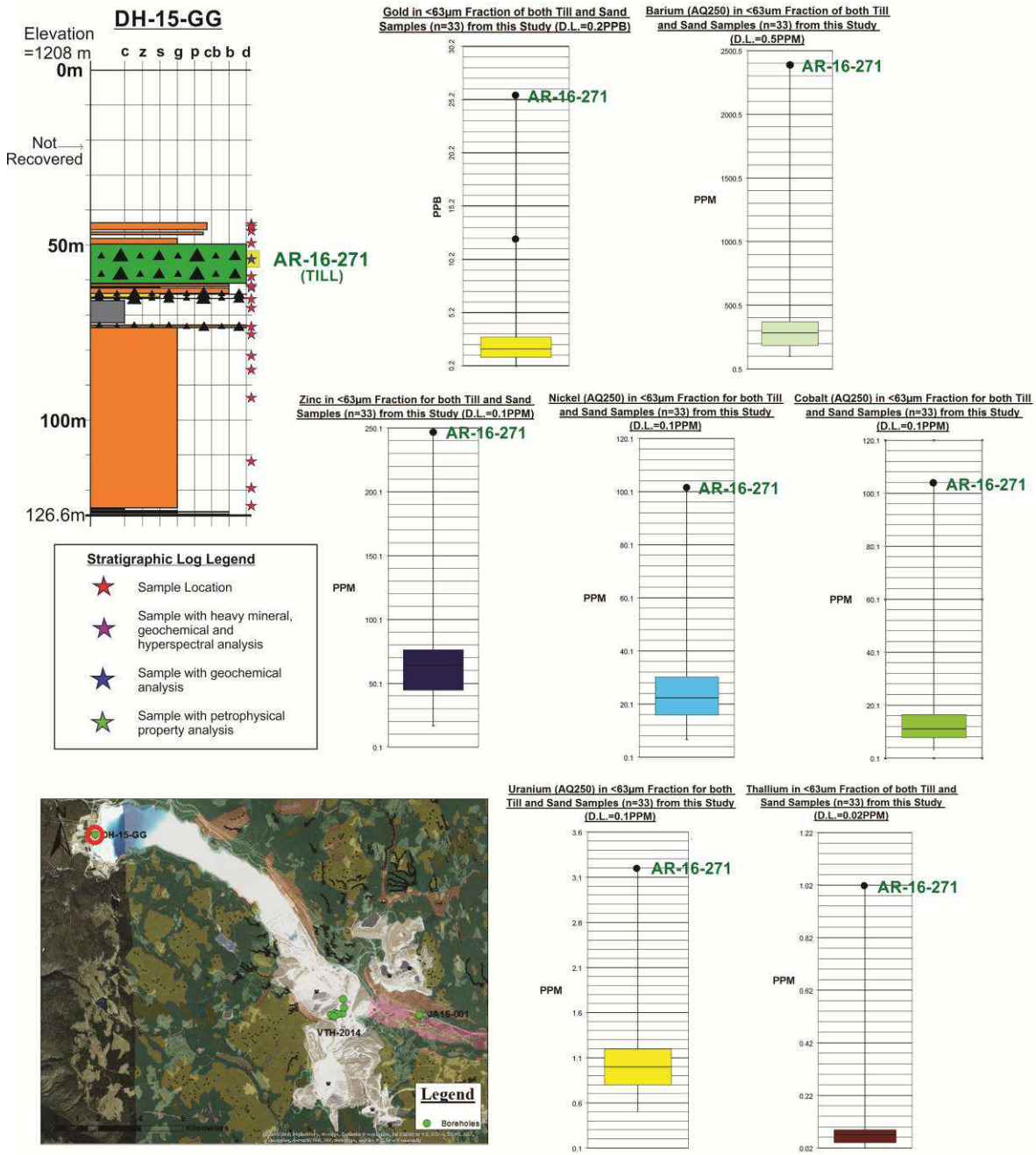

Figure C.80 Stratigraphic log, location map and significantly high geochemical results of core DH-15-GG. The location of collected samples is shown on the stratigraphic log and the samples for which geochemical analysis was done are highlighted.

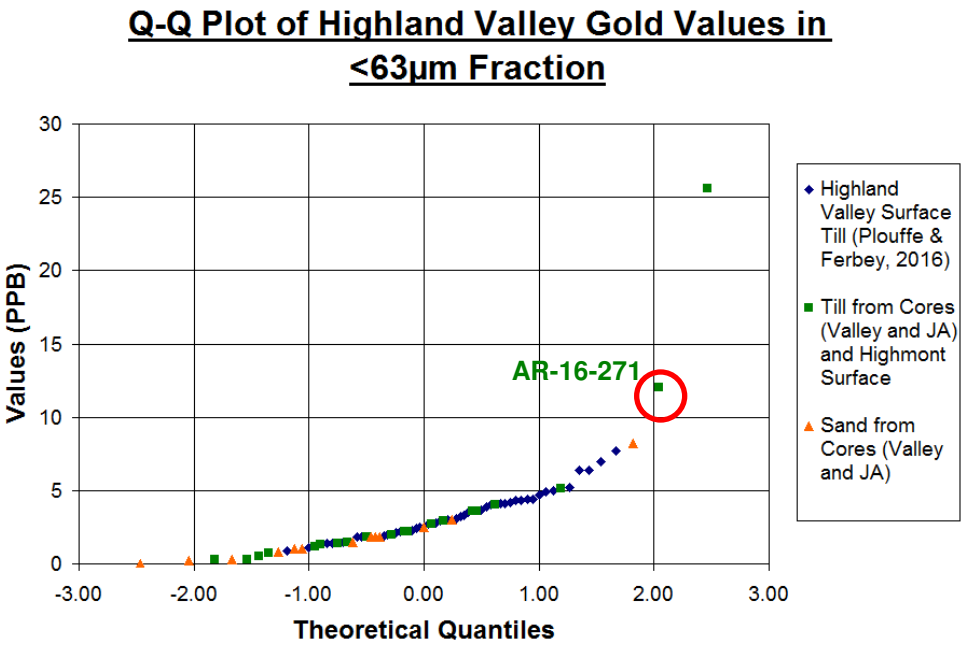

Figure C.81 Quantile-quantile plot of gold concentrations for this study and Plouffe and Ferbey's study (2016), with the till sample from core DH-15-GG highlighted.

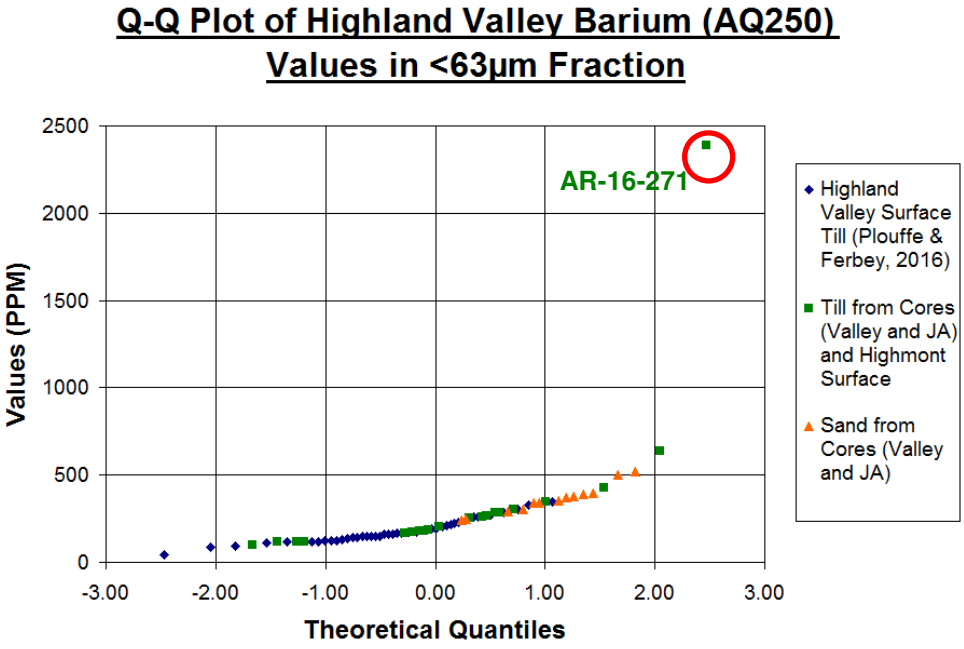

Figure C.82 Quantile-quantile plot of barium concentrations for this study and Plouffe and Ferbey's study (2016), with the till sample from core DH-15-GG highlighted.

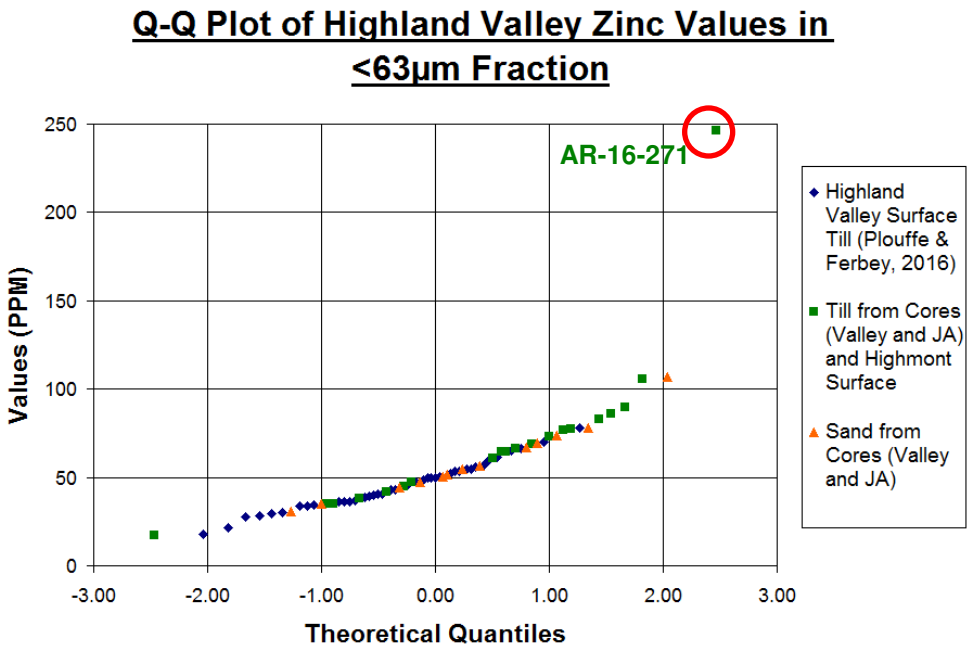

Figure C.83 Quantile-quantile plot of zinc concentrations for this study and Plouffe and Ferbey's study (2016), with the till sample from core DH-15-GG highlighted.

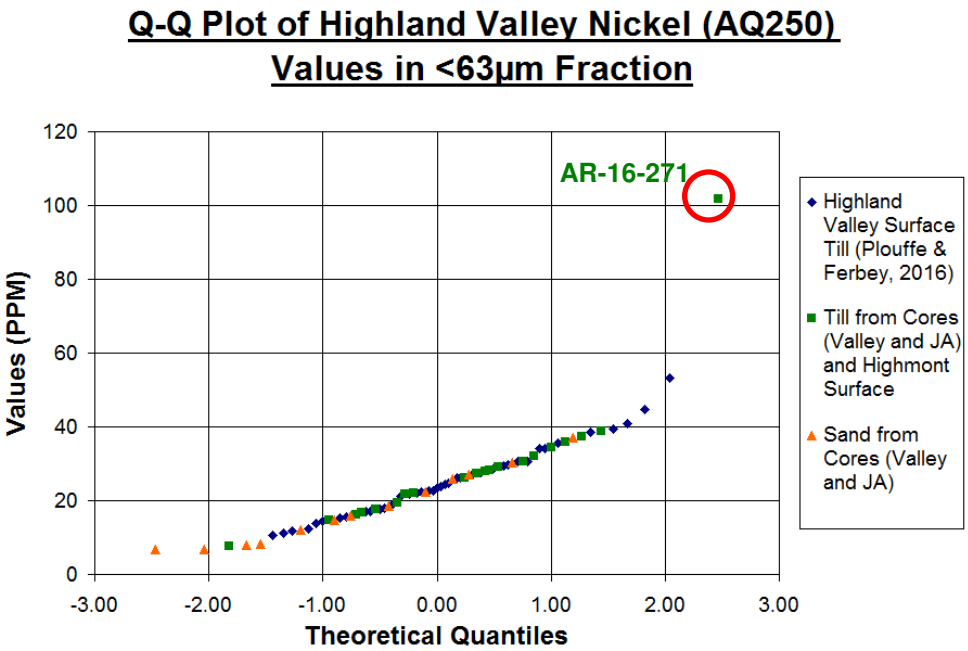

Figure C.84 Quantile-quantile plot of nickel concentrations for this study and Plouffe and Ferbey's study (2016), with the till sample from core DH-15-GG highlighted.

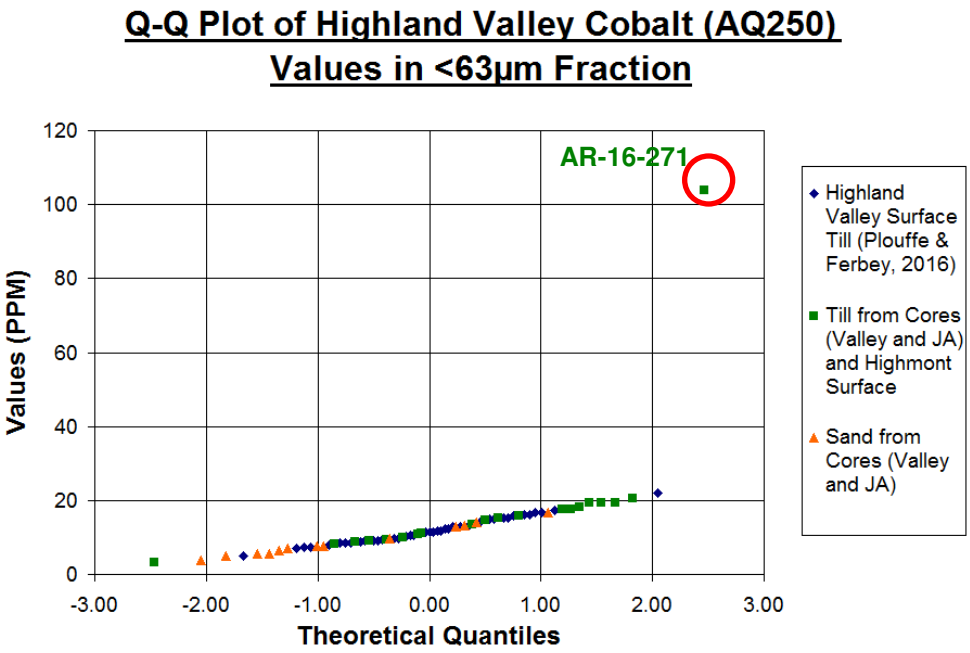

Figure C.85 Quantile-quantile plot of cobalt concentrations for this study and Plouffe and Ferbey's study (2016), with the till sample from core DH-15-GG highlighted.

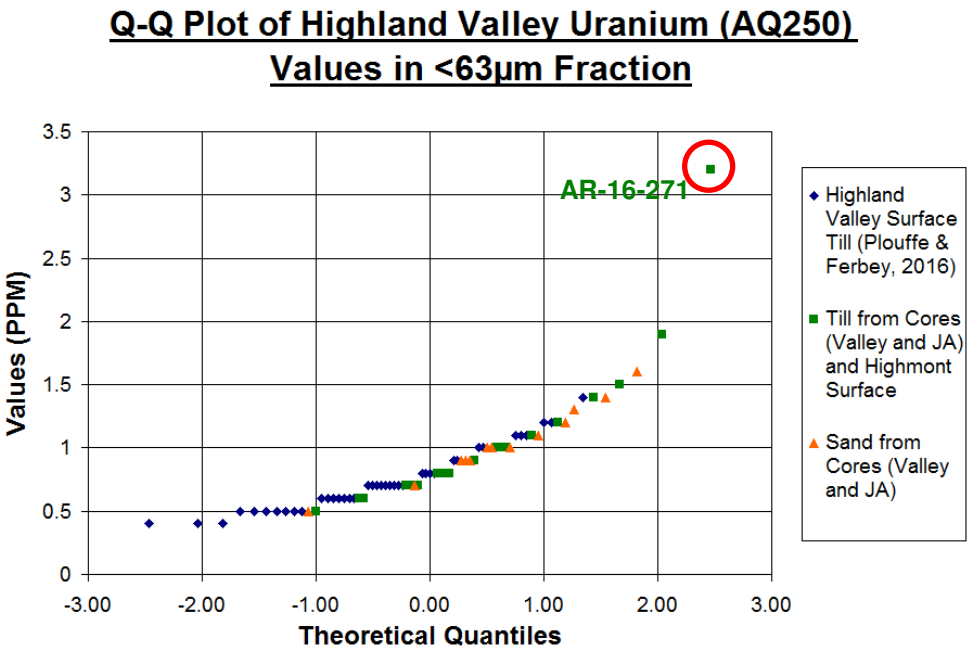

Figure C.86 Quantile-quantile plot of uranium concentrations for this study and Plouffe and Ferbey's study (2016), with the till sample from core DH-15-GG highlighted.

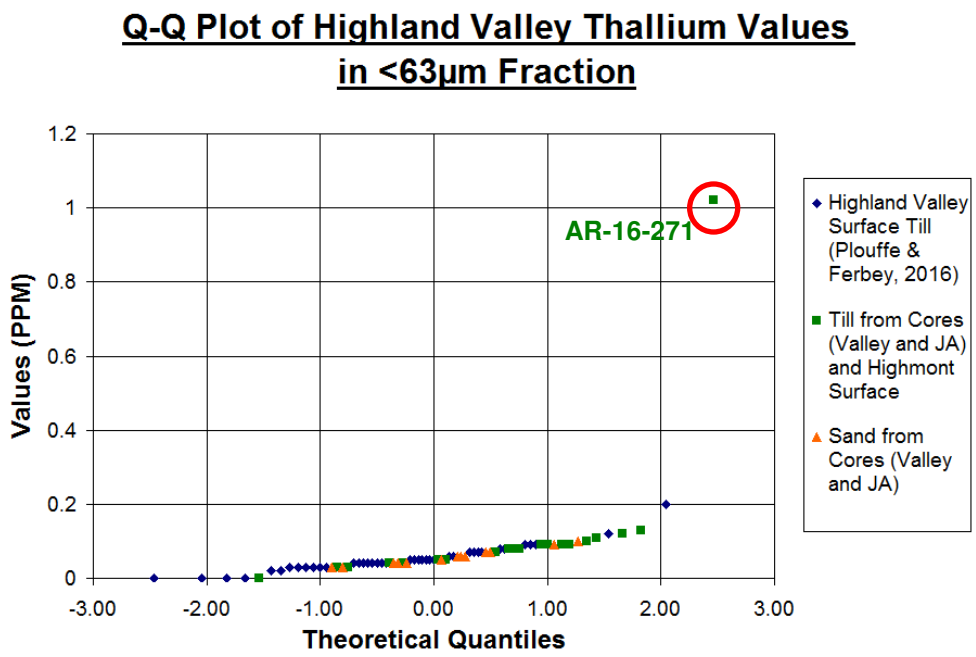

Figure C.87 Quantile-quantile plot of thallium concentrations for this study and Plouffe and Ferbey's study (2016), with the till sample from core DH-15-GG highlighted.

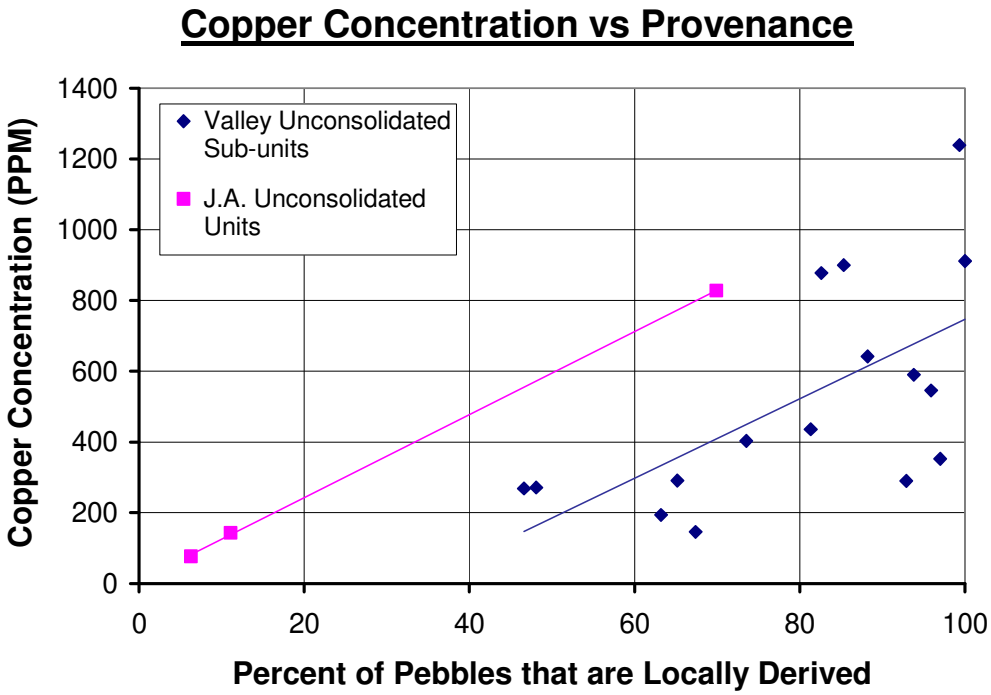

Figure C.88 Copper concentration vs proportion of sample that is locally (Guichon Creek batholith) derived.

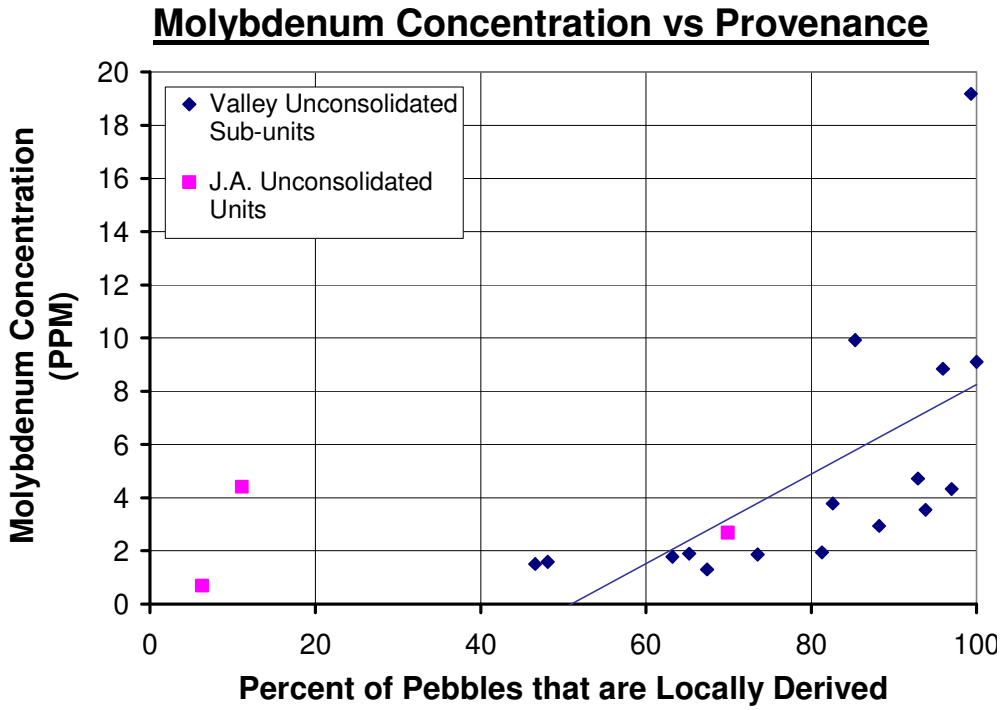

Figure C.89 Molybdenum concentration vs proportion of sample that is locally (Guichon Creek batholith) derived.

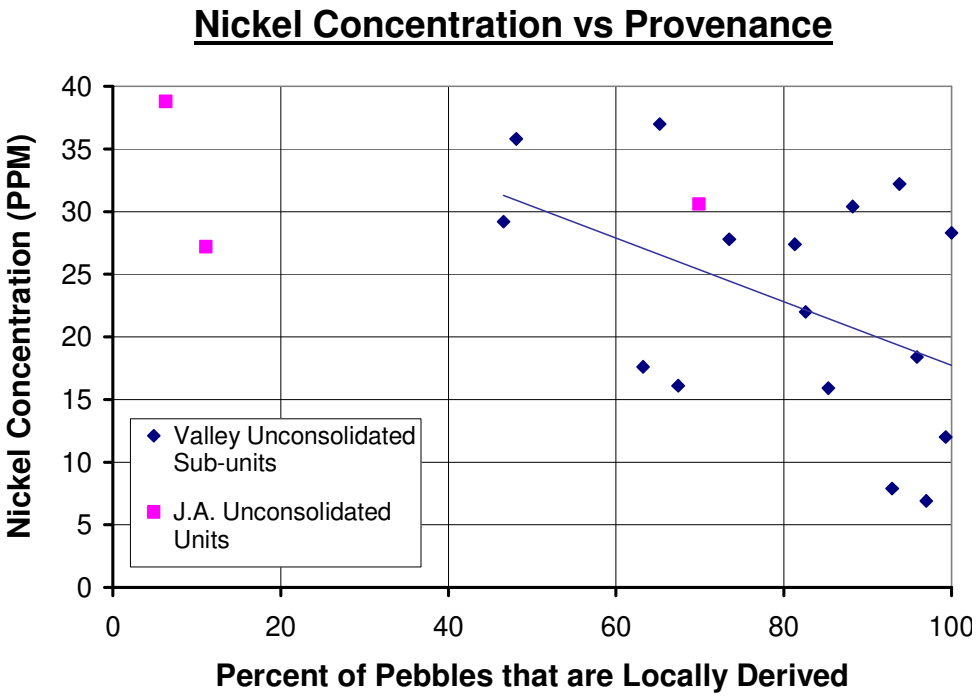

Figure C.90 Nickel concentration vs proportion of sample that is locally (Guichon Creek batholith) derived.

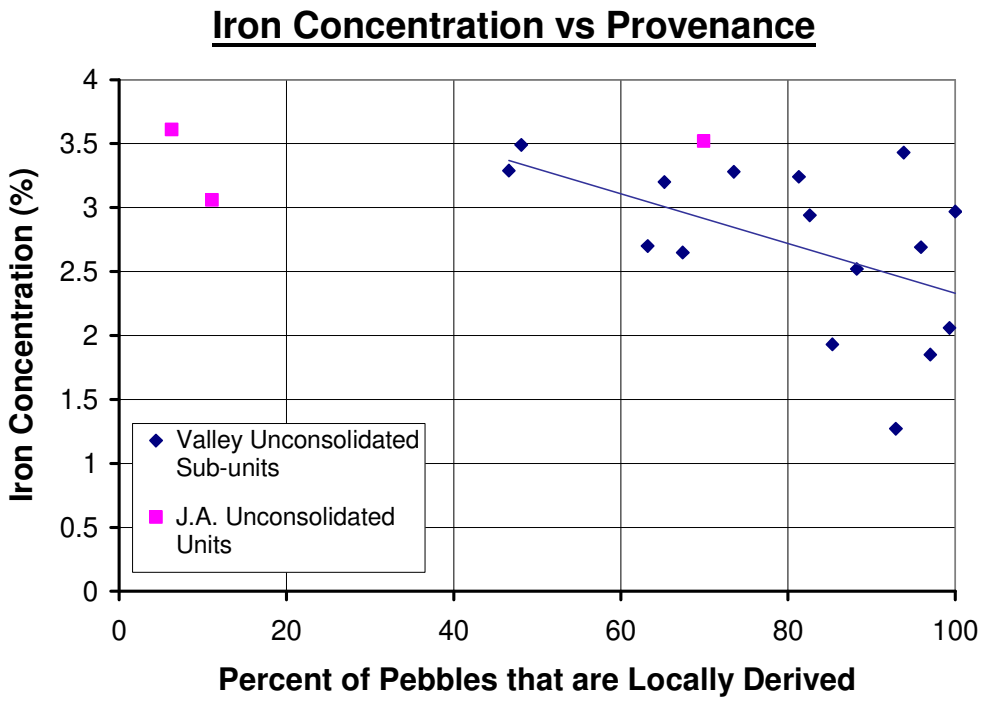

Figure C.91 Iron concentration vs proportion of sample that is locally (Guichon Creek batholith) derived.

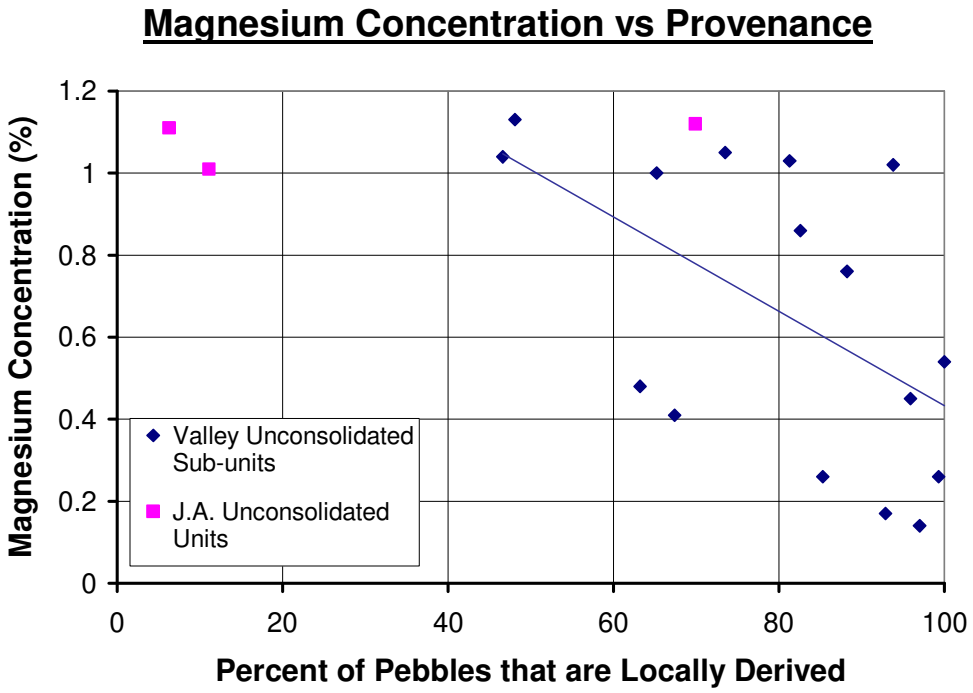

Figure C.92 Molybdenum concentration vs proportion of sample that is locally (Guichon Creek batholith) derived.

Table C.7 Indicator mineral results for tills from this study compared to average values and anomaly thresholds of Plouffe and Ferbey's shallow till samples (2016). Both datasets are normalized to five kilograms. Results for this study that are higher than Plouffe and Ferbey's threshold for anomaly are highlighted.

Dataset / Mineral	Plouffe and Ferbey shallow till samples (2016)	Sub-unit 5b	Sub-unit 4c	Thick till dominating top of J.A. stratigraphy	Surficial till at Highmont South
Visible Gold	Average = 1 grain Threshold for anomaly = 2 grains	VTH2014-10: 0 grains VTH2014-13A: 0 grains	VTH2014-10: 4 grains VTH2014-11: 3 grains	Both samples: 5 grains each	0 grains
Pyrite in 0.25-0.5mm Fraction	Average = 2 grains Threshold for anomaly = 12 grains	VTH2014-10: 23 grains VTH2014-13A: 5 grains	VTH2014-10: 56 grains VTH2014-11: 11 grains	Sample from middle of unit: 0 grains Sample from bottom of unit: 38 grains	1 grain
Chalcopyrite	Average = 3 grains Threshold for anomaly = 15 grains	VTH2014-10: 55 grains VTH2014-13A: 9 grains	VTH2014-10: 0 grains VTH2014-11: 13 grains	Sample from middle of unit: 10 grains Sample from bottom of unit: 0 grains	2 grains
Andradite	Average = 3 grains Threshold for anomaly = 6 grains	VTH2014-10: 5 grains VTH2014-13A: 5 grains	VTH2014-10: 0 grains VTH2014-11: 2 grains	Sample from middle of unit: 2 grains Sample from bottom of unit: 0 grains	1 grain
Mn-Epidote	Average = 3 grains Threshold for anomaly = 8 grains	VTH2014-10: 5 grains VTH2014-13A: 9 grains	VTH2014-10: 6 grains VTH2014-11: 25 grains	Sample from middle of unit: 2 grains Sample from bottom of unit: 0 grains	1 grain

Low-Cr Diopside	Average = 3 grains Threshold for anomaly = 5 grains	VTH2014-10: 0 grains VTH2014-13A: 0 grains	VTH2014-10: 4 grains VTH2014-11: 5 grains	Both samples: 0 grains each	0 grains
Red Rutile	Average = 1 grain Threshold for anomaly = 3 grains	VTH2014-10: 0 grains VTH2014-13A: 0 grains	VTH2014-10: 2 grains VTH2014-11: 2 grains	Both samples: 0 grains each	1 grain
Chromite	Average = 5 grains Threshold for anomaly = 20 grains	VTH2014-10: 5 grains VTH2014-13A: 16 grains	VTH2014-10: 11 grains VTH2014-11: 12 grains	Sample from middle of unit: 2 grains Sample from bottom of unit: 5 grains	1 grain

Table C.8 Geochemical results for tills from this study compared to average values and anomaly thresholds of Plouffe and Ferbey's shallow till samples (2016). Results for this study that are higher than Plouffe and Ferbey's threshold for anomaly are highlighted.

Dataset / Element	Plouffe and Ferbey shallow till samples (2016)	Sub-unit 5d	Sub-unit 5b	Sub-unit 4c	Sub-unit 4a	Thick till dominating top of J.A. stratigraphy	Surficial till at Highmont South	Till of DH-15-GG (12 kms to the northwest of Valley pit)
Copper	Average = 213.1 ppm Threshold for anomaly = ~250 ppm	VTH2014-07: 193.7 ppm VTH2014-08: 271.2 ppm VTH2014-10: 150.5 ppm VTH2014-11:	VTH2014-07: 123.9 ppm VTH2014-09: 589.8 ppm VTH2014-10: 268.5 ppm VTH2014-13A,	VTH2014-03: 416.8 ppm VTH2014-07: 254.1 ppm VTH2014-08: 1016.9 ppm VTH2014-09:	VTH2014-08: 911.3 ppm	Sample from middle of unit: 827.5 ppm Sample from bottom of unit: 76.8 ppm	184.3 ppm	164.4 ppm

		359.0 ppm	top: 116.5 ppm VTH2014-13A, bottom: 146.3 ppm	435.8 ppm VTH2014-10: 403.1 ppm VTH2014-11: 877.6 ppm				
Molybdenum	Average = 1.9 ppm Threshold for anomaly = ~2.0 ppm	VTH2014-07: 1.8 ppm VTH2014-08: 1.6 ppm VTH2014-10: 1.8 ppm VTH2014-11: 2.8 ppm	VTH2014-07: 0.9 ppm VTH2014-09: 3.6 ppm VTH2014-10: 1.5 ppm VTH2014-13A, top: 1.0 ppm VTH2014-13A, bottom: 1.3 ppm	VTH2014-03: 3.2 ppm VTH2014-07: 1.3 ppm VTH2014-08: 11.4 ppm VTH2014-09: 2.0 ppm VTH2014-10: 1.9 ppm VTH2014-11: 3.8 ppm	VTH2014-08: 9.1 ppm	Sample from middle of unit: 2.7 ppm Sample from bottom of unit: 0.7 ppm	1.3 ppm	1.0 ppm
Tungsten	Average = 0.2 ppm Threshold for anomaly = ~0.7 ppm	VTH2014-07: 0.0 ppm VTH2014-08: 0.7 ppm VTH2014-10:	VTH2014-07: 0.1 ppm VTH2014-09: 0.0 ppm VTH2014-10:	VTH2014-03: 2.5 ppm VTH2014-07: 0.0 ppm VTH2014-08:	VTH2014-08: 0.0 ppm	Sample from middle of unit: 0.3 ppm Sample from bottom of unit: 0.0	0.3 ppm	0.0 ppm

		0.5 ppm VTH2014-11: 0.1 ppm	0.0 ppm VTH2014-13A, top: 0.0 ppm VTH2014-13A, bottom: 0.0 ppm	4.0 ppm VTH2014-09: 0.0 ppm VTH2014-10: 0.0 ppm VTH2014-11: 0.0 ppm		ppm		
Gold	Average = 3.5 ppb Threshold for anomaly = ~6.0 ppb	VTH2014-07: 1.5 ppb VTH2014-08: 2.9 ppb VTH2014-10: 1.3 ppb VTH2014-11: 3.6 ppb	VTH2014-07: 4.0 ppb VTH2014-09: 3.6 ppb VTH2014-10: 2.0 ppb VTH2014-13A, top: 0.3 ppb VTH2014-13A, bottom: 0.7 ppb	VTH2014-03: 1.2 ppb VTH2014-07: 1.8 ppb VTH2014-08: 25.6 ppb VTH2014-09: 5.1 ppb VTH2014-10: 2.2 ppb VTH2014-11: 2.7 ppb	VTH2014-08: 0.3 ppb	Sample from middle of unit: 2.2 ppb Sample from bottom of unit: 1.4 ppb	0.5 ppb	12.0 ppb
Zinc	Average = 45.3 ppm Threshold for anomaly = ~80 ppm	VTH2014-07: 41.6 ppm VTH2014-08:	VTH2014-07: 35.1 ppm VTH2014-09:	VTH2014-03: 44.6 ppm VTH2014-07:	VTH2014-08: 83.1 ppm	Sample from middle of unit: 61.0 ppm	16.9 ppm	246.4 ppm

		73.3 ppm VTH2014-10: 47.2 ppm VTH2014-11: 89.8 ppm	105.4 ppm VTH2014-10: 64.4 ppm VTH2014-13A, top: 35.0 ppm VTH2014-13A, bottom: 37.8 ppm	66.2 ppm VTH2014-08: 85.9 ppm VTH2014-09: 77.5 ppm VTH2014-10: 76.6 ppm VTH2014-11: 68.8 ppm		Sample from bottom of unit: 64.4 ppm		
Lead	Average = 3.6 ppm Threshold for anomaly = ~5.6 ppm	VTH2014-07: 5.2 ppm VTH2014-08: 6.5 ppm VTH2014-10: 3.9 ppm VTH2014-11: 6.1 ppm	VTH2014-07: 4.7 ppm VTH2014-09: 11.1 ppm VTH2014-10: 8.0 ppm VTH2014-13A, top: 4.8 ppm VTH2014-13A, bottom: 4.4 ppm	VTH2014-03: 4.5 ppm VTH2014-07: 5.0 ppm VTH2014-08: 7.3 ppm VTH2014-09: 7.2 ppm VTH2014-10: 7.7 ppm VTH2014-11: 5.6 ppm	VTH2014-08: 8.9 ppm	Sample from middle of unit: 7.8 ppm Sample from bottom of unit: 4.9 ppm	2.0 ppm	22.3 ppm
Nickel	Average = 25.0 ppm	VTH2014-07:	VTH2014-07:	VTH2014-03:	VTH2014-08:	Sample from	7.7 ppm	101.9 ppm

	Threshold for anomaly = ~40.0 ppm	17.6 ppm VTH2014-08: 35.8 ppm VTH2014-10: 21.7 ppm VTH2014-11: 37.5 ppm	19.3 ppm VTH2014-09: 32.2 ppm VTH2014-10: 29.2 ppm VTH2014-13A, top: 14.8 ppm VTH2014-13A, bottom: 16.1 ppm	16.7 ppm VTH2014-07: 34.4 ppm VTH2014-08: 26.2 ppm VTH2014-09: 27.4 ppm VTH2014-10: 27.8 ppm VTH2014-11: 22.0 ppm	28.3 ppm	middle of unit: 30.6 ppm Sample from bottom of unit: 38.8 ppm		
Magnesium	Average = 0.7 % Threshold for anomaly = ~1.2 %	VTH2014-07: 0.5 % VTH2014-08: 1.1 % VTH2014-10: 0.6 % VTH2014-11: 1.3 %	VTH2014-07: 0.6% VTH2014-09: 1.0 % VTH2014-10: 1.0 % VTH2014-13A, top: 0.5 % VTH2014-13A, bottom: 0.4 %	VTH2014-03: 0.5 % VTH2014-07: 0.8 % VTH2014-08: 0.8 % VTH2014-09: 1.0 % VTH2014-10: 1.1 % VTH2014-11:	VTH2014-08: 0.5 %	Sample from middle of unit: 1.1 % Sample from bottom of unit: 1.1 %	0.2 %	1.3 %

				0.9 %				
Iron	Average = 2.9 % Threshold for anomaly = ~3.7 %	VTH2014-07: 2.7 % VTH2014-08: 3.5 % VTH2014-10: 2.8 % VTH2014-11: 3.5 %	VTH2014-07: 3.1% VTH2014-09: 3.4 % VTH2014-10: 3.3 % VTH2014-13A, top: 2.8 % VTH2014-13A, bottom: 2.7 %	VTH2014-03: 2.2 % VTH2014-07: 3.6 % VTH2014-08: 2.9 % VTH2014-09: 3.2 % VTH2014-10: 3.3 % VTH2014-11: 2.9 %	VTH2014-08: 3.0 %	Sample from middle of unit: 3.5 % Sample from bottom of unit: 3.6 %	1.7 %	4.1 %
Tin	Average = 0.4 ppm Threshold for anomaly = ~4 ppm	VTH2014-07: 2 ppm VTH2014-08: 1 ppm VTH2014-10: 1 ppm VTH2014-11: 0 ppm	VTH2014-07: 1 ppm VTH2014-09: 1 ppm VTH2014-10: 3 ppm VTH2014-13A, top: 2 ppm VTH2014-13A,	VTH2014-03: 0 ppm VTH2014-07: 1 ppm VTH2014-08: 0 ppm VTH2014-09: 1 ppm VTH2014-10: 2	VTH2014-08: 1 ppm	Sample from middle of unit: 2 ppm Sample from bottom of unit: 1 ppm	0 ppm	2 ppm

			bottom: 0 ppm	ppm VTH2014-11: 0 ppm				
Silver	Average = 117 ppb Threshold for anomaly = ~130 ppb	VTH2014-07: 69 ppb VTH2014-08: 103 ppb VTH2014-10: 55 ppb VTH2014-11: 164 ppb	VTH2014-07: 53 ppb VTH2014-09: 176 ppb VTH2014-10: 97 ppb VTH2014-13A, top: 42 ppb VTH2014-13A, bottom: 30 ppb	VTH2014-03: 100 ppb VTH2014-07: 39 ppb VTH2014-08: 219 ppb VTH2014-09: 144 ppb VTH2014-10: 134 ppb VTH2014-11: 237 ppb	VTH2014-08: 284 ppb	Sample from middle of unit: 287 ppb Sample from bottom of unit: 82 ppb	13 ppb	361 ppb
Arsenic	Average = 5.6 ppm Threshold for anomaly = ~7.0 ppm	VTH2014-07: 3.0 ppm VTH2014-08: 4.2 ppm VTH2014-10: 3.2 ppm VTH2014-11:	VTH2014-07: 2.9 ppm VTH2014-09: 10.9 ppm VTH2014-10: 3.9 ppm VTH2014-13A,	VTH2014-03: 1.8 ppm VTH2014-07: 4.9 ppm VTH2014-08: 7.9 ppm VTH2014-09:	VTH2014-08: 4.8 ppm	Sample from middle of unit: 5.9 ppm Sample from bottom of unit: 4.8 ppm	2.1 ppm	10.0 ppm

		4.6 ppm	top: 2.9 ppm VTH2014-13A, bottom: 2.8 ppm	4.5 ppm VTH2014-10: 4.8 ppm VTH2014-11: 4.6 ppm				
Antimony	Average = 0.3 ppm Threshold for anomaly = ~0.45 ppm	VTH2014-07: 0.2 ppm VTH2014-08: 0.3 ppm VTH2014-10: 0.2 ppm VTH2014-11: 0.3 ppm	VTH2014-07: 0.3 ppm VTH2014-09: 0.2 ppm VTH2014-10: 0.3 ppm VTH2014-13A, top: 0.3 ppm VTH2014-13A, bottom: 0.2 ppm	VTH2014-03: 0.3 ppm VTH2014-07: 0.4 ppm VTH2014-08: 0.3 ppm VTH2014-09: 0.2 ppm VTH2014-10: 0.2 ppm VTH2014-11: 0.3 ppm	VTH2014-08: 0.2 ppm	Sample from middle of unit: 0.3 ppm Sample from bottom of unit: 0.2 ppm	0.1 ppm	0.7 ppm
Barium	Average = 175.8 ppm Threshold for anomaly = ~330 ppm	VTH2014-07: 181.2 ppm VTH2014-08: 262.7 ppm VTH2014-10:	VTH2014-07: 114.6 ppm VTH2014-09: 346.8 ppm VTH2014-10:	VTH2014-03: 182.6 ppm VTH2014-07: 282.7 ppm VTH2014-08:	VTH2014-08: 636.3 ppm	Sample from middle of unit: 167.3 ppm Sample from bottom of unit:	117.6 ppm	2386.9 ppm

		177.8 ppm VTH2014-11: 282.1 ppm	203.5 ppm VTH2014-13A, top: 99.5 ppm VTH2014-13A, bottom: 116.2 ppm	427.6 ppm VTH2014-09: 300.9 ppm VTH2014-10: 266.2 ppm VTH2014-11: 251.4 ppm		170.8 ppm		
Tellurium	Average = 0.007 ppm Threshold for anomaly = ~0.06 ppm	VTH2014-07: 0.02 ppm VTH2014-08: 0.00 ppm VTH2014-10: 0.03 ppm VTH2014-11: 0.04 ppm	VTH2014-07: 0.00 ppm VTH2014-09: 0.04 ppm VTH2014-10: 0.02 ppm VTH2014-13A, top: 0.02 ppm VTH2014-13A, bottom: 0.03 ppm	VTH2014-03: 0.03 ppm VTH2014-07: 0.05 ppm VTH2014-08: 0.48 ppm VTH2014-09: 0.00 ppm VTH2014-10: 0.03 ppm VTH2014-11: 0.04 ppm	VTH2014-08: 0.00 ppm	Sample from middle of unit: 0.04 ppm Sample from bottom of unit: 0.02 ppm	0.02 ppm	0.11 ppm
Bismuth	Average = 0.10 ppm Threshold for anomaly = ~0.17 ppm	VTH2014-07: 0.10 ppm VTH2014-08:	VTH2014-07: 0.09 ppm VTH2014-09:	VTH2014-03: 0.14 ppm VTH2014-07:	VTH2014-08: 0.20 ppm	Sample from middle of unit: 0.35 ppm	0.10 ppm	0.44 ppm

		0.15 ppm VTH2014-10: 0.09 ppm VTH2014-11: 0.17 ppm	0.29 ppm VTH2014-10: 0.12 ppm VTH2014-13A, top: 0.06 ppm VTH2014-13A, bottom: 0.08 ppm	0.09 ppm VTH2014-08: 1.03 ppm VTH2014-09: 0.24 ppm VTH2014-10: 0.19 ppm VTH2014-11: 0.17 ppm		Sample from bottom of unit: 0.11 ppm		
Sulphur	Average = 0.002 % Threshold for anomaly = 0.01 %	VTH2014-07: 0.00 % VTH2014-08: 0.00 % VTH2014-10: 0.00 % VTH2014-11: 0.00 %	VTH2014-07: 0.00 % VTH2014-09: 0.00 % VTH2014-10: 0.00 % VTH2014-13A, top: 0.00 % VTH2014-13A, bottom: 0.00 %	VTH2014-03: 0.00 % VTH2014-07: 0.00 % VTH2014-08: 0.03 % VTH2014-09: 0.00 % VTH2014-10: 0.00 % VTH2014-11: 0.00 %	VTH2014-08: 0.00 %	Sample from middle of unit: 0.00 % Sample from bottom of unit: 0.00 %	0.00 %	0.04 %